Eva Mariasole Angelin

Mestre em Ciencias para Conservação e Restauro

The fate of colors in the 20th - 21st centuries: preserving the organic colorants in plastic artifacts

Dissertação para obtenção do Grau de Doutor em
Conservação e Restauro, especialidade em Ciências da Conservação

Orientador: Doutora Maria João Seixas de Melo, Professora Catedrática, Faculdade de Ciências e Tecnologia da Universidade Nova de Lisboa (Portugal)

Co-orientadores: Doutor Marcello Picollo, Researcher, Istituto di Fisica Applicata "Nello Carrara" – Consiglio Nazionale delle Ricerche (Italy)

Doutor Austin Benjamin Nevin, Head of the Department of Conservation, The Courtauld Institute of Art (UK)

Júri:

Presidente: Doutor Carlos Manuel Agra Coelho, Professor Catedrático, Faculdade de Ciências e Tecnologia da Universidade NOVA de Lisboa (Portugal)

Arguentes: Doutora Suzan de Groot, Senior Conservation Scientist, Cultural Heritage Agency (The Netherlands)

Doutora Catherine M. Schmidt Patterson, Associate Scientist, Getty Conservation Institute (USA)

Vogais: Doutor Peter Vandenabeele, Full Professor, Ghent University, Department of Archaeology (Belgium)

Doutor Marcello Picollo, Researcher, Instituto di Fisica Applicata "Nello Carrara" – Consiglio Nazionale delle Ricerche (Italy)

Doutora Marisa Pamplona, Head of Conservation Science Department, Deutsches Museum (Germany)

FACULDADE DE CIÊNCIAS E TECNOLOGIA
UNIVERSIDADE NOVA DE LISBOA

Maio 2021

Eva Mariasole Angelin

Mestre em Ciencias para Conservação e Restauro

The fate of colors in the 20th - 21st centuries: preserving the organic colorants in plastic artifacts

Dissertação para obtenção do Grau de Doutor em
Conservação e Restauro, especialidade em Ciências da Conservação

Orientador: Doutora Maria João Seixas de Melo, Professora Catedrática, Faculdade de Ciências e Tecnologia da Universidade Nova de Lisboa (Portugal)

Co-orientadores: Doutor Marcello Picollo, Researcher, Istituto di Fisica Applicata "Nello Carrara" – Consiglio Nazionale delle Ricerche (Italy)

Doutor Austin Benjamin Nevin, Head of the Department of Conservation, The Courtauld Institute of Art (UK)

Júri:

Presidente: Doutor Carlos Manuel Agra Coelho, Professor Catedrático, Faculdade de Ciências e Tecnologia da Universidade NOVA de Lisboa (Portugal)

Arguentes: Doutora Suzan de Groot, Senior Conservation Scientist, Cultural Heritage Agency (The Netherlands)

Doutora Catherine M. Schmidt Patterson, Associate Scientist, Getty Conservation Institute (USA)

Vogais: Doutor Peter Vandenabeele, Full Professor, Ghent University, Department of Archaeology (Belgium)

Doutor Marcello Picollo, Researcher, Instituto di Fisica Applicata "Nello Carrara" – Consiglio Nazionale delle Ricerche (Italy)

Doutora Marisa Pamplona, Head of Conservation Science Department, Deutsches Museum (Germany)

FACULDADE DE CIÊNCIAS E TECNOLOGIA
UNIVERSIDADE NOVA DE LISBOA

Maio 2021

THE FATE OF COLORS IN THE 20TH - 21ST CENTURIES: PRESERVING THE ORGANIC COLORANTS IN PLASTIC ARTIFACTS

Acknowledgements

My first acknowledgement goes to my supervisor Maria João Melo, for her inestimable help and tireless dedication in following this research work over the years. Especially, I would like to thank her for having passed on to me her passion for research, constantly pushing me to improve myself, my work, and develop my skillsets. I do believe I am a better researcher because of this. I am also deeply thankful to my co-supervisors Marcello Picollo and Austin Nevin, for being always present with their invaluable advice throughout this journey of personal and professional growth. Thanks again for believing in me. I would also thank my advisory committee: Anita Quye and César Laia, for providing inspiring and diverse food for thought and final feedback on the thesis.

My gratitude to Fundação para a Ciência e Tecnologia for funding my grant CORES Ph.D. programme (PD/BD/114412/2016), the project "The Triumph of Bakelite – Contributions for a History of Plastics in Portugal" (PTDC/IVC-HFC/5174/2014) and the Associated Laboratory for Green Chemistry-LAQV.

I arrived in Portugal on the 15th of February 2016 and, believe me, I never imagined the extent of this experience. The effects of moving to another country are countless. In the beginning, you feel lost and stressed. Then you start to meet new people, make new friends, and establish connections and your confidence starts to grow. In fear of forgetting someone, I thank all the people I met as they made this experience unique and priceless. Thank you, Portugal, for welcoming me with open arms, this place is like a second home now.

A thanks to professors and researchers from DCR FCT NOVA, Márcia Vilarigues, Ana Maria Ramos, Joana Lia Ferreira, Rita Macedo, Leslie Carlyle, Inês Coutinho, Isabel Pombo, Emanuela Sara Fragoso, who have always shown interest in my project. Special thanks go to Susana França de Sá and Élia Roldão. At the beginning as colleagues and later as professors, you always inspired me. I heartfully thank you both for listening to me and helping me, particularly to Susana França de Sá, without whom this thesis would not have the same success.

I also would like to thank the professors and seniors of the CHARM group of LAQV-Requimte NOVA, Jorge Parola, João Carlos Lima and Fernando Pina, for hearing my doubts with a broad and reassuring smile. Your valuable knowledge and firsthand experience have been a key contribution to this work. Additionally, I would like to thank all researchers of the photochemistry group with whom I shared many hours in the laboratories: Ambrosio Camuenho, Ana Lucia Pinto, David Souza, Hugo Cruz, Sandra Maria Nunes Gago, João Avó, Tiago Moreira, Patricia Máximo. My sincere gratitude to Artur Moro and Nuno Basílio, who have endlessly helped with never-ending patience with all my doubts, difficulties and troubles; thank you both. To Alfonso Armijo, who managed to make me smile with his contagious good mood. To Johan Mendoza, with whom, more than colleagues, become a sincere friend. I would also like to thank Miguel Santos and Zeljko Petrovski for their joyful company. Finally, to Alberto Trevisan, who has maintained the Italianness in the photochemistry group with his unmistakable Venetian spirit.

This work counted with the support of many people outside FCT NOVA, and I gratefully acknowledge professors and researchers from other national and international institutions. Many thanks to Mauro Bacci for sharing his vast knowledge and showed me the good way of diplomacy in the academic field and outside. My thanks to Daniela Comelli and Gianluca Valentini for receiving me at your laboratories at Politecnico of Milano and letting me work with on such intriguing topics as photoluminescence, and to Marta Ghirardello for having worked side by side with me with passion and shared laughs. I would also like to thank Laura Chelazzi, from University of Florence, who supported the powder X-ray diffraction and Rietveld analyses. To Professor Maria Conceição Oliveira, from Técnico, for her constant willingness to cooperate and precious time. To Professor

João de Almeida Lopes, from Universidade de Lisboa, for his incredible patience with my requests. I also thank Maria Elvira Callapez, from Centro de História das Ciências Universidade de Lisboa, for letting me take part in the project "The Triumph of Bakelite" from which I got most of my results and opportunities. Finally, to the team of Conservation and Science Department at Deutsches Museum, Anna Micheluz and Marisa Pamplona, who have supported me in many ways, making me feel confident. Lastly, I am thankful to Danilo Bersani and Peter Vandenabeele, who have always fueled my curiosity and had tips to give.

As PhD mates, I would like to thank those who arrived before, with and after me. I especially thank Tatiana Vitorino for being the first person who has welcomed me to Portugal and helped to settle in. A word of thanks to Marta Félix Campos, Sílvia Sequeira, Rita Araújo, Joana Silva and Susana Belchior. I thank Vanessa Otero for her unquestionable support and advice. I am grateful to my "PhD buddy" Paula Nabais for her help and encouragement in many points of this journey, especially in the most critical ones. Thank you, Sara Babo, for sharing with me part of this adventure and for the long talks we had. To Samaneh Sharif, Telma Ribeiro, Catarina Geraldes, Francisca Pulido Valente, Joana Devesa, Rute Chaves with whom I share many hours of seminars and workshops, always interacting as a team. A last word of thank to Sara Sá, Raquel Marques, Sofia Gomes, Hermine Grigoryan, Daniel Vega, Carla Machado, Artur Neves, Ângela Santos, Ailin Chen, Márcia Vieira.

I do not have enough words to express my gratitude to Ana Maria, Alexandra Paula Rodrigues, Mario Bandiera and Angelica Bartoletti. You have been my reference points in academia and outside. I am grateful for your friendship and unlimited support. You really made all the difference. I would like to thank Xavi (Rafael Díaz Hidalgo) for your endless friendship and kind words.

To my friends outside the faculty Giancarlo Bruno and Valentina Brunello who have been encouraging me for many many years. To Valentina Pintus who, in the last phase of the PhD, has believed in me and pushed me forward.

In closing, I thank my family. Your support has always been of paramount importance in undertaking every challenging decision. Even if I was moving in a farther place in the world in each stage of my academic path, you were always there. Even though it was difficult at times, you never told me to give up, on the contrary, you gave me all the support to make all of this come true. I must also include my cats Mimi and Pulce to have shared my desk with your joyful company for many hours.

To Paulo Bonifácio, for bringing new happiness to my life. I will never be able to repay your patience and care throughout the final months of writing.

Lastly, I dedicate this thesis to my mother and father. I am forever thankful, indebted for your love.

Resumo

Objectos modernos e contemporâneos feitos de plástico são amplamente encontrados no património cultural. Presentemente, a sua preservação levanta questões críticas aos conservadores e cientistas uma vez que estes objectos podem facilmente sofrer degradação num curto espaço de tempo. Um dos fenómenos que pode alterar significativamente a aparência de objectos em plástico é a alteração de cor (descoloração). De um modo geral, a descoloração é habitualmente associada à degradação dos polímeros, contudo, os pigmentos, que são parte integrante das formulações do plástico, também podem desvanecer devido à exposição à luz. A identificação de objetos de plástico com pigmentos sensíveis à luz é um exercício bastante exigente devido à sensibilidade dos mesmos a alterações na cor.

A caracterização dos corantes nos plásticos é normalmente realizada através de amostragem, métodos de extração e testagem destrutiva. Como alternativa, esta tese apresenta uma abordagem inovadora e multi-analítica baseada em espectroscopias que foi desenvolvida para a identificação in situ dos pigmentos em plásticos históricos. Esta metodologia compreendeu a utilização de microscopia ótica (MO), micro-espectrometria por fluorescência de raios X dispersiva de energias (μ-EDXRF), espectroscopia UV-Vis-NIR de reflectância, fotoluminescência (PL) e micro-espectroscopia de Raman (μ-Raman) na análise de obras de arte, objetos industriais e de uso diário, datados de 1950-2000s e pertencentes a coleções Portuguesas. Deste estudo resultou a identificação dos pigmentos comumente presentes na paleta de cor dos coloristas da indústria dos plásticos portuguesa: óxido de ferro (PR 101, α-Fe_2O_3), molibdato de cromato de chumbo (PR 104, $Pb(Cr,Mo,S)O_4$), vermelho de cádmio (PR 108, Cd(S,Se); PR 113, (Cd,Hg)S), amarelo de cádmio (PY 37, CdS; PY 35; (Cd,Zn)S), branco de titânio (PW 6, TiO_2 ambos rutilo e anátase), oxicloreto de bismuto (PW 14, BiOCl) e lacas do pigmento orgânico β-naftol (PR 48, PR 49, PR 53). Adicionalmente, foi também identificado um pigmento fora do comum, o pigmento perlascente plumbonacrite $Pb_5(CO_3)_3O(OH)_2$. Para todos os casos de estudo, μ-Raman foi a ferramenta chave para a caracterização dos pigmentos nos objetos de plástico, aportando dados conclusivos para a identificação dos mesmos. A impressão digital vibracional dos pigmentos orgânicos e inorgânicos foi adquirida com sucesso recorrendo à focagem do laser na superfície das partículas. A aquisição de dados espectrais de pigmentos com concentrações muito baixas (0.1 % a 5%, aproximadamente) à escala micro foi possível através de microscopia confocal, que faz parte do sistema do equipamento de μ-Raman. Adicionalmente, foi também possível obter informação sobre o polímero base (principalmente termoplásticos) e cargas. Os métodos analíticos desenvolvidos neste estudo deverão, em trabalhos futuros, facilitar a obtenção de informação complementar sobre estes objetos de plástico e permitir uma melhor identificação e avaliação do seu estado de conservação.

Esta tese foca particularmente objectos de plástico vermelhos visto que estes foram identificados como os mais severamente afetados por alterações de cor. O estado avançado de desvanecimento identificado no pigmento β-naftol PR 53 mostrou a sua fraca estabilidade à luz em formulações de plástico. Esta situação, junto com as alterações de cor descritas em literatura para o pigmento PR 48 em objetos de plástico, sugere uma sensibilidade dos pigmentos vermelhos da família dos β-naftol ao desvanecimento. O PR 53 e os pigmentos vermelhos da família dos β-naftóis são pigmentos históricos facilmente encontrados em objetos do património cultural. No entanto, o conhecimento acerca da sua estabilidade a longo prazo e resistência à foto-degradação é limitado, especialmente para os casos onde os mesmos se encontram em polímeros, sendo que este conhecimento é essencial para a sua preservação. Neste estudo, a quantificação da foto-estabilidade para uma série de pigmentos vermelhos da família dos β-naftol foi realizada pela primeira vez, através do cálculo do rendimento

quântico de fotodegradação (Φ_R). Os valores obtidos variaram entre $3x10^{-6}$ e $4x10^{-5}$, indicativo de uma estabilidade relativamente boa à luz por parte das moléculas. Tendo em consideração que a estabilidade dos pigmentos não se limita exclusivamente ao pigmento em si, mas também à sua interação com o meio envolvente, foram realizados ensaios de envelhecimento por exposição à luz ($\lambda \geqslant 300$ nm) do pigmento em solução, em pó e incorporado em polímeros de modo a avaliar o papel do meio na estabilidade à luz dos pigmentos e as vias pelas quais estes se degradam. Verificou-se que o ligante tem um impacto significativo na estabilidade do pigmento uma vez que se foi detetada uma maior sensibilidade à luz dos pigmentos PR 48 e PR 53 quando incorporados nos plásticos, comparativamente ao ensaio do pigmento em pó. Este novo conhecimento irá contribuir para o desenvolvimento de novas estratégias na conservação dos plásticos com estes pigmentos vermelhos fotossensíveis através da previsão do desvanecimento. Espectrometrias de massa (MS) por cromatografia em fase líquida e gasosa foram utilizadas na caracterização dos principais subprodutos da degradação. Observou-se uma fotodegradação significativa e a formação de compostos ftálicos e ftalatos nos pigmentos em solução e em pó.

Palavras-chave: Artefactos de plástico, Coleções portuguesas de polímeros históricos, Pigmentos, Caracterização in situ, Vermelhos β-naftol, Fotodegradação, Desvancecimento

Abstract

Modern and contemporary objects made of plastics are widely found in cultural heritage. Today, their preservation poses critical issues to conservators and scientists, as they can suffer from extensive degradation in a short time period. Color change (discoloration) is one of the alteration phenomena that can significantly affect their appearance. Discoloration is commonly associated with the degradation of polymers. However, pigments within plastics can also fade due to exposure to light. The identification of objects that contain light-sensitive pigments is demanding because of the sensitivity of plastics to color change.

Normally sampling, extraction methods and destructive testing are required for the characterization of colorants in plastics. In this work, an innovative multi-analytical spectroscopic approach for the in situ identification of pigments in historical plastics was developed. Optical microscopy (MO), micro-energy dispersive X-ray fluorescence (μ-EDXRF), UV-Vis-NIR reflectance, photoluminescence (PL) and Raman microscopy (μ-Raman), were used for the analysis of artworks, industrial and daily objects dated from 1950s-2000s from Portuguese collections. A common colorists' palette within the Portuguese plastics industry was identified: iron oxide (PR 101, α-Fe_2O_3), lead chromate molybdate (PR 104, $Pb(Cr,Mo,S)O_4$), cadmium red (PR 108, Cd(S,Se); PR 113, (Cd,Hg)S) and cadmium yellow (PY 37, CdS; PY 35; (Cd,Zn)S) pigments, titanium whites (PW 6, TiO_2 both rutile and anatase), bismuth oxychloride (PW 14, BiOCl) and organic β-naphthol lakes (PR 48, PR 49, PR 53). An exceptional pigment found was the pearlescent plumbonacrite pigment $Pb_5(CO_3)_3O(OH)_2$. In all the case studies, μ-Raman was the key analytical tool for pigment characterization in the plastic objects, providing conclusive data for their identification. The vibrational fingerprint of both inorganic and organic pigments was successfully recorded by focusing the laser beam on particle surfaces. The confocal microscopy system used in μ-Raman enabled the collection of spectral data from low concentrations of pigments (approximately 0.1%-5%) on the micro-scale. In addition to pigments, information on the base polymer (mainly thermoplastics) and fillers was obtained. The analytical methods developed will facilitate the acquisition of complementary data from plastics allowing material identification and condition assessment in the future.

This thesis focused on red pigmented plastic artifacts, as they were found to be severely faded among the studied objects. The identification of β-naphthol pigment lake PR 53 as a faded pigment highlighted its poor fastness in plastics, that together with the color change of PR 48 in plastic objects, reported in literature, suggests the particular susceptibility of β-naphthol red lakes to fading. PR 53, and the other β-naphthol reds, are historical pigments widely found in cultural heritage. However, little is known about their photodegradation and stability, especially when they are found in polymer media, and this knowledge is essential for their long-term preservation. For the first time, photodegradation quantum yields (Φ_R) were calculated for a series of red pigments based on β-naphthol in order to quantify their photo-stability. Φ_R values ranging from $3x10^{-6}$ to $4x10^{-5}$ were obtained, indicating relatively light-stable molecules. Bearing in mind that pigment fastness is not only related to the pigment itself, but also to its interaction with the confined environment, light-aging experiments ($\lambda \geqslant 300$ nm) were conducted in solution, on powders, and in polymers to assess the role of the medium on the lightfastness of the pigments and their degradation pathways. A significant impact of the binder on their stability was found. Indeed, a higher sensitivity to light of PR 48 and PR 53 pigments, when incorporated in plastics than in powder, was observed. This new knowledge will contribute to the prediction of plastic fading and inform effective preventive conservation strategies for objects containing light-sensitive β-naphthol red pigments. Liquid- and gas-chromatography mass spectrometry (MS) were used for the characterization of the main degradation products. Extensive photodegradation was observed with the

formation of phthalic compounds and phthalates in both solution and powder phases.

Keywords: Plastic artifacts, Portuguese polymer collections, Pigments, In situ characterization, β-naphthol reds, Photodegradation, Fading

Symbols and Notations

ε	Molar absorption coefficient
ε_{max}	Molar absorption coefficient at λ_{max}
λ_{irr}	Irradiation wavelength
λ_{max}	Maximum wavelength
μ-EDXRF	Micro- Energy Dispersive X-Ray Fluorescence Spectroscopy
μ-FTIR	Micro- Fourier Transform Infrared Spectroscopy
μ-Raman	Micro- Raman spectroscopy
Φ_R	Quantum yield of reaction

ATR	Attenuated Total Reflection
C.I.	Color Index
DCR FCT NOVA	Department of Conservation and Restoration of the NOVA School of Science and Technology, NOVA University Lisbon
DMF	Dimethylformamide
DRIFT	Diffuse Reflection Infrared Fourier Transform
EGA-MS	Evolved Gas Analysis-Mass Spectrometry
ER-FTIR	External Reflection Fourier-Transform Infrared Spectroscopy
ESiPT	Excited-State intramolecular Proton Transfer
EtOH	Ethanol
FORS	Fiber Optics Reflectance Spectroscopy
H_2O	Purified water with Millipore
HPLC-DAD	High Performance Liquid Chromatography coupled with a Diode Array Detector
HRMS	High Resolution Mass Spectrometry
I_0	Intensity of the incident light
I_{abs}	Total absorbed light
NIR	Near Infrared
OM	Optical Microscopy
PCA	Principal Components Analysis
PE	Polyethylene
PL	Photoluminescence spectroscopy
PMMA	Poly(methyl methacrylate)
PP	Polypropylene
PS	Polystyrene
Py-GC/MS	Pyrolysis-Gas Chromatography/Mass Spectrometry
TD-GC/MS	Thermal Desorption-Gas Chromatography/Mass Spectrometry
UV	Ultraviolet
Vis	Visible
XRD	X-Ray Diffraction

Contents

List of Figures

List of Tables

Synopsis

Since the invention of the first synthetic mauve dye in the second half of the 19th century [1,2], innovations in modern chemistry have introduced a staggering array of new colorants (i.e. pigment and dyes), and new colors for the artists' palette (modern paints) and polymer-based materials such as plastics. Unfortunately, colorants are susceptible to degradation following light exposure, a phenomenon that can lead to noticeable color changes (e.g. fading) in heritage collections [3]. As discoloration strongly affects the aesthetic, historical and material integrity of objects, light-induced alteration of synthetic colorants continues to be a subject of ongoing research within art conservation [3]. This thesis contributes to the study of pigments and their fading in one of the most challenging materials found in modern and contemporary museums: mass-colored plastics.

In the first part (**Part I**), the complexity of colorant degradation in plastic artifacts and the urgency in their study for conservation purposes are highlighted.
The environment in which objects are displayed and stored can have an impact on the lifespan of the constituent materials. As already stated [3], light is known to be the largest agent in fading colored plastics. However, the process by which light interacts with the objects and leads to colorant degradation is still poorly understood, especially when organic pigments are mixed within the constituents of plastics [4,5]. A colorant's ability to resist light (fastness) is considerably influenced by its chemical composition as well as the other ingredients of a plastic. Indeed, plastic objects are almost always made of a base polymer, functioning as a binder, and several organic and inorganic materials (additives), including colorants, that are homogeneously distributed in the blend in a wide range of formulations. As such, photodegradation is dependent on more than just the colorant itself.
The museum community has reported color changes in plastic objects (yellowing, darkening, and fading) [6-8] that serve as a warning of ongoing plastic deterioration. It is not only colorants that fade: polymers making up plastics are degraded by light exposure. The photodegradation and stability of polymers have been studied extensively [9,10], while only limited research is available on colorants [4]. The fading of colored plastics as a conservation issue was first approached in the international conference "Polymers in Conservation" as early as 1991 [11], but only recently it has been re-addressed in conservation science [12-15]. This thesis adds a valuable and innovative contribution to the evolving knowledge on colorants in plastics.

In undertaking this research, only pigmented plastics were considered. Objects were collected from Portugal, where the history, technology and material culture are less well researched than in other countries [16]. The selection of objects included rigid three-dimensional artifacts ranging from artworks, industrial and daily objects, some of which exhibit fading as a symptom of degradation which makes their study imperative for their preservation.
Managing mass-colored artifacts and planning their effective preventive conservation requires knowledge of their constituent ingredients (formulation) and the identification of objects that contain light-sensitive pigments. For these reasons, two steps in research were necessary. The first one involved material analysis of objects that lead to information on the history of plastics in Portugal. In parallel, a novel multi-analytical spectroscopic methodology for the in situ characterization of the plastic composition, with a special focus on the pigments and their nature, was developed. A second step involved the study of the photodegradation of a particularly susceptible red pigments that lead to new insights into the fading of plastic objects. The developed methodology is schematically presented in **Figure 0.1**.
Analytical methods for in situ analysis are usually preferred as sampling of cultural heritage objects may not be possible. The second part of this thesis (**Part II**) focuses on developing an innovative in situ multi-analytical approach for investigating the pigments found in plastic objects.
The wide availability of spectroscopy systems paves the way for their reliable applications. In this research, the following spectroscopic techniques were considered: optical microscopy (OM), micro X-ray fluorescence (μ-EDXRF), Fourier transform infrared (FTIR) working in attenuated total reflection (ATR)-FTIR, external

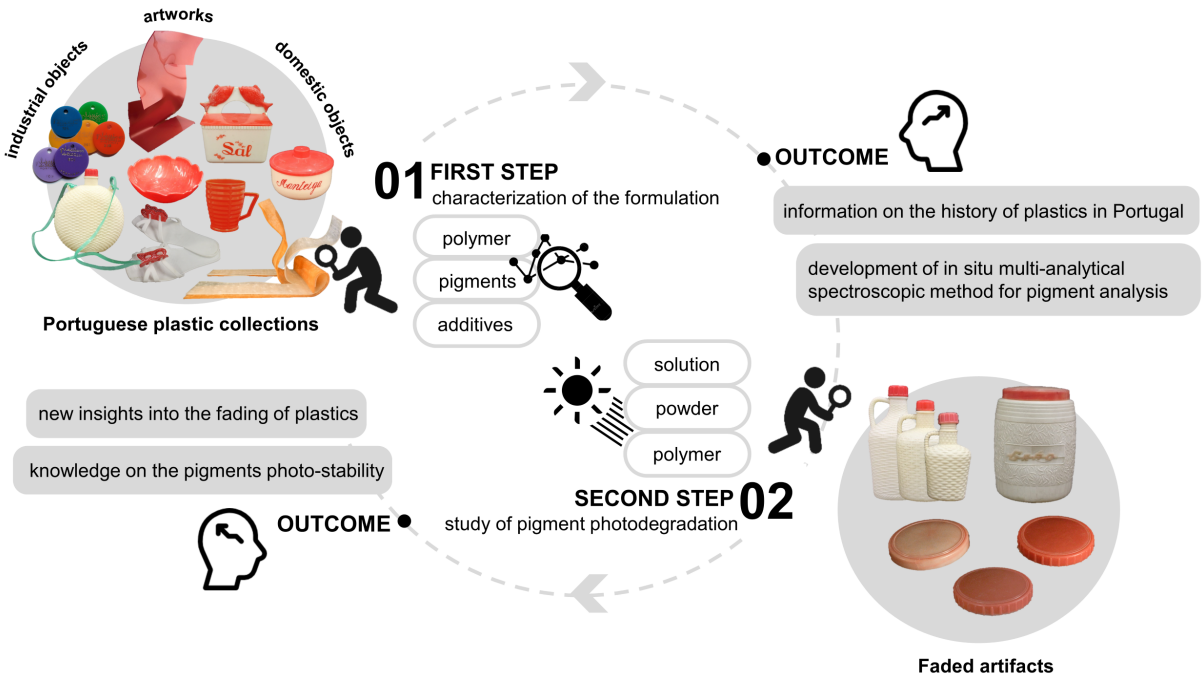

Figure 0.1.: The methodology developed in this research work for investigating mass-colored plastic artifacts.

reflection (ER)-FTIR and diffuse reflection (DRIFT), UV-Vis-NIR diffuse reflectance, laser-induced photoluminescence (PL), Raman microscopy (μ-Raman). The spectroscopic techniques enabled the identification of polymer types (mainly thermoplastics), fillers, and almost all pigments, such as special effect (i.e. pearlescent), conventional inorganic and organic pigments. Noting that pigments exist in very small concentrations (ca 0.1%-5%) and are constituted by micro-sized particles that are dispersed within the plastic, the analysis and identification of pigments was an analytical challenge. The integration of the information obtained through the elemental, optical and vibrational analyses is the result of the multi-analytical methodology used and, in all cases studied, μ-Raman enabled the unequivocal identification of embedded pigments.

Pigments commonly used to color plastics were found in historical objects [17-20], including hematite, lead chromate molybdate, red and yellow cadmium pigments, titanium whites and organic β-naphthol lakes (PR 48, PR 49, PR 53[1]). While bismuth oxychloride is commonly referenced as a pearlescent pigment in industrial applications, the discovery of basic lead carbonate, plumbonacrite, to imitate mother-of-pearl was never specifically reported before [21]. These results contribute with new information regarding Portuguese plastics industry and support the planning of better preventive and conservation strategies of collections.

Among the cases studied, fading was unequivocally observed in some red-pigmented plastics. In such objects, PR 53 organic pigment had almost completely lost its original color. The fading of PR 53 together with the color alteration of PR 48 in other historical objects [12], highlights a sensitivity to light of this family of organic pigments in plastics. β-naphthol reds have been used since the beginning of the 20th century [22], and their impact as artists' material is well-documented in modern and contemporary artworks [23]. Although their investigation is recognized in conservation literature [24], no comprehensive studies on their photostability are available [25]. This shows a general lack of knowledge of the chemistry of these species [24]. Hence, it was necessary to study the light-susceptibility of β-naphthol reds in the third part (**Part III**) of this work.

To understand the fading of β-naphthol reds, photodegradation studies were essential. Light-aging experiments were used to simulate the degradation that occurs during natural aging. The organic pigments PR 48 and PR 53 were aged in simple conditions, as solutions and in powder form, as well as within plastic matrices. The great advantage of working in solution is that both qualitative and quantitative understanding of the chemical

[1]PR is the acronym used for Color Index Pigment Red.

events can be obtained. As little is known on their photochemistry, the quantification and comparison of their photostability through photodegradation quantum yields (Φ_R) [26] provided new insights into their fastness properties, revealing that, despite the fading observed in plastics, β-naphthol reds are relatively stable pigments. The aging of the neat pigment powders was then compared with measurements collected on original plastic samples. Their severe fading suggested a higher sensitivity to light of pigments when incorporated in plastics rather than in powder form. Based on these results, it is hypothesized that the polymer medium influences the degradation of β-naphthol reds in plastics. This is consistent with published literature [27], which has ascribed a crucial role to the binding medium in the poor light stability of PR 49 organic pigment in paints. The research has demonstrated the impact of the binder on stability. This new awareness represents a novel and fundamental step in improving our comprehension of the lightfastness of β-naphthol reds and the prediction of their degradation in objects. In summary, fading of β-naphthol based pigments poses a serious threat to the historical plastic collections and, for their preservation, their sensitivity to light should be carefully considered during display and storage.
Other β-naphthol reds and similar dye molecules were included in the aging experiments in solutions for the photodegradation studies of the stability of this class of colorants. The identification of degradation products formed following aging is fundamental for the understanding of degradation mechanisms. However, degradation pathways are still not completely clear. The characterization of phthalates and phthalic derivatives in both solution and powder phases suggests important steps in degradation that will support further mechanistic studies.

This research work is the first comprehensive attempt at studying pigments in plastic artifacts and the photofading of β-naphthol based pigments within conservation science. New knowledge and methods will inform future studies in cultural heritage research and contribute important information for the conservation of plastics in collections.

References

[1] Travis AS. The rainbow makers: the origins of the synthetic dyestuffs industry in Western Europe. Bethlehem: Lehigh University Press; 1993.
[2] Finlay V. Mauve – Chemistry project gone wrong. In: The brilliant history of color in art. Los Angeles: Getty Publications; 2014. p. 84-85.
[3] Miliani C, Monico L, Melo MJ, Fantacci S, Angelin EM, Romani A, Janssens K. Photochemistry of artists' dyes and pigments: towards better understanding and prevention of colour change in works of art. Angew Chem Int Ed. 2018; 57: 7324-7334. DOI: 10.1002/anie.201802801.
[4] Allen NS, McKellar JF, editors. Photochemistry of dyed and pigmented polymers. London: Applied Science; 1980.
[5] Klemchuk PP. Influence of pigments on the light stability of polymers: a critical review. Polym Photochem. 1983; 3(1): 1-27. DOI: 10.1016/0144-2880(83)90042-8.
[6] Quye A, Williamson C, editors. Plastics: collecting and conserving. Edinburg: NMS Publishing Limited; 1999.
[7] Shashoua Y. Conservation of plastics. Oxford: Butterworth-Heinemann; 2008.
[8] Lavédrine B, Fournier A, Martin G, editors. Preservation of Plastic Artefacts in Museum Collections (POPART). Paris: Comité Des Travaux Historiques et Scientifiques (CTHS); 2012.
[9] Allen NS, Edge M. Fundamentals of polymer degradation and stabilization. London: Elsevier Applied Science Ltd.; 1992.
[10] Rabek JF. Polymer photodegradation: mechanisms and experimental methods. Dordrecht: Springer Science+Business Media; 1995.
[11] Allen NS. Action of light on dyes and pigmented polymers. In: Allen NS, Edge M, Horie CV, editors.

Polymers in conservation. Cambridge: The Royal Society of Chemistry; 1992. p. 193-213
[12] de Groot S, van Keulen H, Megens L, van Oosten T, Wiresma H. Discolouration of plastics objects: investigation into composition using various analytical techniques. In: Bechthold T, editor. Future Talks 013 – Lectures and workshops on technology and conservation of modern materials in design. Munich: Die Neue Sammlung – The Design Museum; 2015. p. 19-26.
[13] de Groot S, van Keulen H, van den Akker S, van Oosten T. Discoloration of plastics objects: the identification of yellow and orange synthetic pigment in plastic objects. In: Bechthold T, editor. Future Talks 015 – Processes. The making of design and modern Art. Materials, technologies and conservation strategies. Munich: Die Neue Sammlung - The Design Museum; 2017. p. 147-158.
[14] Maragno A, Schossler P, Rizzutto M. Challenges in the conservation of synthetic polymers: discolouration of plastic objects. In: Future Talks 019, Munich (Germany), 11-13 November 2019; Oral presentation.
[15] Angelin EM, França de Sá S, Picollo M, Nevin A, Callapez ME, Melo MJ. The identification of synthetic organic red pigments in historical plastics: developing an in situ analytical protocol based on Raman microscopy. J Raman Spectrosc. 2021; 52: 145-158. DOI: 10.1002/jrs.5985.
[16] França de Sá S, Marques da Cruz S, Callapez ME, Carvalho V. Plastics that made history – The contribution of conservation science for the history of the Portuguese Plastics Industry. Conservar Património 2020; 35: 85-100. DOI: 10.14568/cp2019017.
[17] Webber TG, editor. Coloring of plastics. New York: John Wiley & Sons Inc.; 1979.
[18] Harris RM. Coloring technology for plastics. Norwich: Plastics Design Library; 1999.
[19] Müller A. Coloring of plastics. Munich: Carl Hanser Verlag; 2003.
[20] Charvat RA, editor. Coloring of plastics: fundamentals. New Jersey: John Wiley & Sons Inc., second ed.; 2004.
[21] Angelin EM, Babo S, Ferreira JL, Melo MJ. Raman microscopy for the identification of pearlescent pigments in acrylic works of art. J Raman Spectrosc. 2019; 50: 232-241. DOI: 10.1002/jrs.5431.
[22] Society of Dyers and Colorists and American Association of Textile Chemists and Colorists. Color Index international. Bradford: Society of Dyers and Colorists and associates, Heritage ed. on DVD; 2014.
[23] Berrie BH, Lomax SQ. Azo Pigments: their history, synthesis, properties, and use in artists' materials. Studies in the History of Art 1997; 57: 8-33. URL: jstor.org/stable/42622254
[24] Micheluz A, Angelin EM, Almeida Lopes J, Melo MJ, Pamplona M. Discoloration of historical plastic objects: new insight into the degradation of β-naphthol pigment lakes. Polymers 2021; 13: 2278. DOI: 10.3390/polym13142278.
[25] Angelin EM, Conceição Oliveira M, Nevin A, Picollo M, Melo MJ. To be or not to be an azo pigment: chemistry for the preservation of historical β-naphthol reds in cultural heritage. Dyes Pigm. 2021; 190: 109244. DOI: 10.1016/j.dyepig.2021.109244.
[26] Montalti M, Credi A, Prodi L, Gandolfi MT. Handbook of photochemistry. Boca Raton: Taylor & Francis, third ed.; 2006.
[27] Stenger J, Kwan EE, Eremin K, Speakman S, Kirby D, Stewart H, Huang SG, Kennedy AR, Newman R, Khandekar N. Lithol red salts: Characterization and deterioration. e-Preservation Sci. 2010; 7: 147-157. URL: e-preservationscience/2010/Stenger-29-05-2010

This thesis is based on the following publications:

Part II. The color appearance of plastics: innovative multi-technique spectroscopic approaches for the identification of polymers, pigments and additives

Chapter 3. Application of infrared reflectance spectroscopy on plastics in cultural heritage collections: a comparative assessment of two portable mid-Fourier transform infrared reflection devices
Eva Mariasole Angelin, Susana França de Sá, Inês Soares, Maria Elvira Callapez, Joana Lia Ferreira, Maria João Melo, Mauro Bacci, Marcello Picollo, "Application of infrared reflectance spectroscopy on plastics in cultural heritage collections: a comparative assessment of two portable mid-Fourier transform infrared reflection devices", Appl Spectrosc. 2021; 75: 818-833.

Chapter 4. Raman microscopy for the identification of pearlescent pigments in acrylic works of art
Eva Mariasole Angelin, Sara Babo, Joana Lia Ferreira, Maria João Melo, "Raman microscopy for the identification of pearlescent pigments in acrylic works of art", J Raman Spectrosc. 2019; 50: 232-241.

Chapter 5. The multi-analytical in situ analysis of cadmium-based pigments in plastics
Eva Mariasole Angelin, Marta Ghirardello, Sara Babo, Marcello Picollo, Laura Chelazzi, Maria João Melo, Austin Nevin, Gianluca Valentini, Daniela Comelli, "The multi-analytical in situ analysis of cadmium-based pigments in plastics", Microchem J. 2020; 157: 105004.

Chapter 6. The identification of synthetic organic red pigments in historical plastics: developing an in situ analytical protocol based on Raman microscopy
Eva Mariasole Angelin, Susana França de Sá, Marcello Picollo, Austin Nevin, Maria Elvira Callapez, Maria João Melo, "The identification of synthetic organic red pigments in historical plastics: developing an in situ analytical protocol based on Raman microscopy", J Raman Spectrosc. 2021; 52: 145-158.

Part III. Photochemistry for the preservation of color change: study the lightfastness of β-naphthol reds and their fading in historical plastics

Chapter 7. Photochemistry of artists' dyes and pigments: towards better understanding and prevention of colour change in works of art[2]
Costanza Miliani, Letizia Monico, Maria João Melo, Simona Fantacci, Eva Mariasole Angelin, Aldo Romani, Koen Janssens, "Photochemistry of artists' dyes and pigments: towards better understanding and prevention of colour change in works of art", Angew Chem Int Ed. 2018; 57: 7324-7334.

Chapter 8. To be or not to be an azo pigment: chemistry for the preservation of historical β-naphthol reds in cultural heritage
Eva Mariasole Angelin, Maria Conceição Oliveira, Austin Nevin, Marcello Picollo, Maria João Melo, "To be or not to be an azo pigment: chemistry for the preservation of historical β-naphthol reds in cultural heritage", Dyes Pigm. 2021; 190: 109244.

Chapter 9. Discoloration of historical plastic objects: new insight into the degradation of β-naphthol pigment lakes[3]
Anna Micheluz, Eva Mariasole Angelin, João Almeida Lopes, Maria João Melo, Marisa Pamplona. "Discoloration of historical plastic objects: new insight into the degradation of β-naphthol pigment lakes", Polymers 2021; 13: 2278.

[2] The author of this doctoral dissertation participated in the discussion of the data and the working of the article.
[3] The author of this doctoral dissertation participated in the acquisition and discussion of the data and the working of the article.

Part I.

General Introduction

Since their introduction in the late 19th century, man-made polymers have become one of the most relevant materials in modern and contemporary ages, and today, museums contain an increasing number of plastic-based objects in their collections. In the last thirty years, conservators, restorers, and scientists have been confronted with their vulnerability. Indeed, plastics can suffer from extensive degradation, and at times, shortly after their production, an issue that can make their preservation a challenge.
Plastics are available in a wide range of formulations and generally, are made by mixing a base polymer together with property modifiers (additives) to improve its processing, end-use performance, and aging properties. This process also includes the coloring and consequently appearance of polymeric materials. Colorants (i.e. dyes and pigments) are commonly used for the mass coloration of plastics. The final color being determined by the superimposition of the individual contribution of the triad: colorant, polymer and additive packages (e.g. fillers).
Following exposure to light, polymers and/or colorants may degrade resulting in severe changes in color appearance. Fading of organic colorants is a visible alteration that is brought forth by light-induced chemical changes. Those take place at a molecular level and the understanding of these photochemical mechanisms is key for the preservation of colored plastic artifacts.
Color change (discoloration) of plastics like yellowing, darkening, and fading may occur over a few decades. Unfortunately, this subject has been unattended and only recently been revalued in the view of conservation science. Much attention has been focused on the impact and contribution of polymer degradation to discoloration and studies on colorants in plastics within collections are limited.

This dissertation intends to contribute and expand the knowledge on colorants, with an emphasis on particulate pigments, and fading of plastics within the Portuguese cultural heritage collections. The research work that was undertaken included the development of innovative multi-analytical methods for the in situ[4] characterization of pigments and the study of their lightfastness in rigid three-dimensional plastic-based artifacts. When evaluating the impacts of color change in the Portuguese collections, this thesis focuses on the photodegradation of red plastic objects which have been colored with synthetic hydrazone-azo organic pigment lakes based on β-naphthol (2-naphthol), a class of red pigments that has found widespread use in plastic coloring and in modern and contemporary artworks.
The review of the color appearance of plastic objects and color change in historical collections represents the starting point of this research. In the first part of this work (**Part I**, **Chapter 1**), the fundamental concepts related to plastics and colorants are presented, also included is a general description of the degradation phenomena that lead to color change in plastics collections, followed by an overview of the photochemistry of dyed and pigmented polymers. Finally, the end of this first part covers the description of the goals and methodology of the research that was conducted (**Chapter 2**).
By exploring the potential of multi-analytical spectroscopic methods, the second part of this work (**Part II**) aims to provide methods for in situ identification of pigments, gathering case studies from Portuguese heritage. This part of the research also focuses on the development and improvement of analytical procedures for characterizing polymeric materials and additives (e.g. fillers) in plastic artifacts. The application of in situ, rapid spectroscopic analytical methods for the investigation of plastic objects are discussed in **Chapters 3** to **6**. Additionally, in **Chapter 6**, the fading of historical plastics colored with β-naphthol reds in collections is highlighted.
The third part of the research (**Part III**) is allied to the study of the photodegradation of β-naphthol based pigments and their fading in historical plastics. In **Chapter 7**, a review of recent findings regarding the photochemistry and light-induced alterations of artists' dyes and pigments is presented. The results of photo-aging studies that explore the lightfastness of hydrazone-azo colorants based on β-naphthol are discussed in **Chapter 8**. Finally, **Chapter 9** presents the first results on the light stability of β-naphthol lakes in plastics

[4] In situ analysis means that the sampling is not required and the analysis is performed directly on the object [1].

and the influence of the plastic system on their fading.
Some conclusions and future perspectives are presented in the last **Chapter 10** - **Part IV**.

1. Plastics: coloring in industry and discoloring in cultural heritage collections

1.1. Fundamentals of plastic coloring

Color is perceived in the presence of visible light.
The fundamental science of coloring materials is based on the understanding of the basics of light – how light interacts with objects, and finally how humans respond to the stimulus interpreted by the brain. Color thus exists in the mind of the viewer and it is a subjective response to what we observe.
In determining the perceived color of an object, properties of the light source, the object itself and the human eye are equally important. In coloring of plastics, the plastic object is the most important matter.
The mass coloring of plastic materials is not a simple process; its color science involves many technological and scientific subjects, such as the selection of the components of the plastic formulation, the method used in the manufacturing and the color description of the plastic pieces (colorimetry). All of those are aimed to produce a final plastic product which matches the desired color appearance.
The main topic of this thesis are colorants, one of core ingredients in the formulation, which play a fundamental role in the color appearance of a plastic object. An overview of colorant properties, the physics and chemistry of color in plastic systems is discussed in **Sections 1.1.1** and **1.1.2**. A summary of color technology in the formulation work is given in **Section 1.1.3**. The topics treated in these sections serve as support for the subsequent chapters and provide the reader with an overview of the complex issues that are involved in the coloring of plastics.
This thesis does not aim to be an exhaustive examination on the coloring technology of plastics that is explored in more detail in key references [2-7][1]. Significant fields of color science commonly applied in plastic industry, such as colorimetry, color specifications and color matching, are beyond the scope of this work.

1.1.1. Introduction to colorants

Formulation of plastic materials consists in selecting the *polymeric*[2] or *resin material*[3] and *additives*[4]. *Colorants* are additives that may be used by color technologists or colorists, to adjust the color appearance of the final plastic product.
Due to their physical and chemical nature, colorants are able to impart a color to plastics when they are incorporated in the polymeric resin. Generally, polymers tend to be colorless, whitish, or pale yellow and the addition of colorants to the polymer masks the natural color of the resin, if it has one.
In terms of formulation, a colorant is the key part of the *colorant system*, as it represents the mixture of

[1] Those references were used as basis for writing Chapter 1.
[2] The polymer is a high-molecular-weight organic compound whose structure consists of one or more units repeated any number of times. It is the basic material for plastics.
[3] In a broad sense, the term "resin" is used to designate any polymer.
[4] Additives are supplementary chemical substances that are combined with the base material (i.e. polymer) to provide special properties to both formulation and final plastic product. The addition of additive packages to the polymer improves its processing, end-use performance and aging properties. The most commonly used additives are: plasticizers, flame retardants, antioxidants, acid scavengers, light and heat stabilizers, lubricants, colorants, antistatic agents and slip compounds. Wide literature on their properties and uses is available [8-12].

colorants with additives[5] and/or polymer. The *binder*, that holds colorants and additives forming the colorant system, is a polymer or plastic resin. When colorants are left out, the mixture of the base polymer and additives (if present), represents the *polymer system*.

Colorants are usually produced as fine dry powders with current technology giving the plastic color formulator a wide range of colorant systems[6]. These color preparations can be highly concentrated mixtures of colorants and additives and, in industrial applications, they allow the plastic manufacturer to color a raw polymer. In practice, for this application, the colorant system is mixed into the plastic resin resulting in the distribution and dispersion of the colorant and additives into the final product. The strategy of mixing depends on colorant system's form and processing method[7] used during the plastics manufacturing process.

In the world of plastic coloring there are hundreds of colorants to select from. Mainly synthetic, they comprise both *pigments* and *dyes*. Pigments are distinct particulate materials, which remain insoluble in the polymer system and are incorporated in the plastic by dispersion. On the other hand, dyes are instead soluble in the polymeric system, more precisely, they are soluble in at least one component of the polymeric system. Because they do not retain crystal or particulate structure, they are dissolved and not dispersed within the polymer matrix. Most dyes are organic compounds (i.e. they contain carbon), whereas pigments are classified as either organic or inorganic (i.e. they do not contain carbon).

To identify colorants, colorists usually use a system of nomenclature and classification promoted jointly by the Society of Dyers and Colorists (SDC) of UK and the American Association of Textile Chemists and Colorists (AATCC). This system is known as *Color Index* (*C.I.*) [17] and identifies each colorant by giving a unique name and number known as *C.I. Generic Name* and *C.I. Constitution Number*. The description of a pigment using the C.I. Generic Name and C.I. Constitution Number will identify the chemical composition and identity unequivocally. As an example, consider the commercially named "Toluidine Red" has the C.I. Generic name of C.I. Pigment Red 3 (PR 3) and C.I. Constitution Number 12120. Copper phthalocyanine blue becomes C.I. Pigment Blue 15 (PB 15), C.I. Constitution Number 74160. Orange dye "Sudan I", is classified as C.I. Solvent Yellow 14 (SY 14) with C.I. Constitution Number 12055. The designations "C.I. Pigment xxx", "C.I. Solvent xxx" are often omitted for brevity and their acronyms (e.g. PB, PR, SY) with the identification number are used.

Since its first edition published in 1924, the C.I. Color Index represents the most comprehensive guide to colorant and their application. Colorants which are not classified in the C.I., have not found their way to see widespread use in the industry. The *Heritage C.I. editions* represent a fundamental document because they trace all colorants available over the 20th century [18].

Metals may be part of the chemical formula of *organic pigments* as precipitating agents (formation of a complex or lake pigments)[8]. In **Figure 1.1** the most important families of organic pigments used in coloring of plastics and some examples are presented[9]. Classification for organic pigments according to their chemical constitution is universally accepted by all those involved in their manufacture and application. This classification system makes distinction between hydrazone[10] and nonhydrazone (polycyclic)[11] pigments [19]. Both sorts are found in plastics. Miscellaneous pigments, such as metal complexes[12], refer instead to organic pigments with different

[5] Generally speaking, colorants are additives. However, in this thesis whenever the expression "additive(s)" is used, it relates to designate all additives other than colorants.

[6] Several forms of colorant systems are available including dry powdery, liquid and granulated/pellets color preparations, this latter form is also known as *color masterbatch*.

[7] The type of process to be used in the plastic fabrication depends on a variety of factors, including the properties of both plastic material and final product. For an overview of the processing methods and plastic manufacturing see references [13-16].

[8] The C.I. identifies organic pigments that differ only in the metal used for the lake formation by the addition of number after the colon. Thus, for example, C.I. Pigment Red 48 (C.I. 15865) is the sodium salt, C.I. Pigment Red 48:1 (C.I. 15865:1) is the barium salt, C.I. Pigment Red 48:2 (C.I. 15865:2) is the calcium salt.

[9] Examples of organic pigments were selected on the basis of their impact in coloring of plastics and relevance in this dissertation.

[10] Hydrazone pigments owe their name to the hydrazone functional group (-NH-N=) that they carry. Formerly, hydrazone pigments were called 'azo pigments', because they were believed to contain the azo group (-N=N-).

[11] Polycyclic pigments are compounds featuring several closed rings of atoms and consist of condensed aromatic or heterocyclic ring systems.

[12] Metal complexes consist of hydrazone and azomethine compounds containing usually the coordinative tetravalent Cu^{2+}, Ni^{2+}

chemical structure that cannot be categorized in the other two groups. For a detailed description of each family (properties and structures) see reference [19].

Inorganic pigments are instead the combination of metallic or metalloid elements with oxygen, sulfur or selenium including metal oxides[13] and hydroxides[14], inorganic complexes[15] and metal salts[16] [20]. Outside of these families, pigments consisting of pure elements (e.g. C.I. Pigment Black (PBk) 7, C.I. n. 77266[17]) and silicate pigments of ultramarines (e.g. C.I. Pigment Blue (PB) 29, C.I. n. 7707) are classified as inorganic pigments. All pigment families presented in **Figure 1.2** and related examples have been used in plastic coloring[18].

Dyes cover a huge number of molecules. They may be classified according to the chemical structure or by their application method. The latter approach is used predominantly by the color technologist and it is the principal system adopted by the C.I. Following this classification, solvent[19], dispersed[20] and vat[21] dyes [21] are commonly used in the coloring of plastics.

To impart specific effect appearance to the polymer, *special colorant types* (*specialty colorants*) such as metallic, pearlescent, fluorescent, phosphorescent, thermochromic and photochromic colorants may be also used. Their physical and chemical properties determine the special effects that they are able to produce. In the most cases, environmental external inputs such as light and heat are the triggers of such "special" behaviors. Platelet-like particles may provide a metallic and pearl appearing surface by light scattering. Mostly inorganic, metallic pigments act as microscopic mirrors and reflect the light, while pearlescent pigments derive their effect thought light interference.

Luminescent colorants produce a brilliant "glow" of light of the material when exposed to light. In contrast to conventional pigments that only reflect a small portion of the visible light, luminescent pigments re-emit energy as light of a longer wavelength after absorption of higher energy radiation.

Thermochromic and photochromic colorants are instead capable to shift between two states that possess different absorption spectra. Creating an "interactive" plastic, the vivid color change is activated by temperature variations and absorption of electromagnetic radiation.

1.1.2. Understanding the "science of color" in plastics

Colorants are essential to ensure the phenomenon of color generation in plastics. The knowledge on the physical and chemical principles of color strongly supports the comprehension of colorants' properties and their role in coloring.

Colorants do not lose their appeal if the mechanism used to generate their color is explained, on the contrary, they become even more fascinating. But, as in so many other phenomena, everything starts in a very simple way, in this case it is visible light striking a colored object.

Electromagnetic radiation shows a wave-particle duality. It is considering the quantum nature (photons), that the origin of color in materials[22] can be described.

---

and Co^{2+} ions. Respect to the other complexes or lakes, their chemical structures are obtained from aromatic *o,o'*-dihydroxyazo and *o,o'*-dihydroxyazomethine.

[13] Metal oxides are chemical compounds that contain a metal and at least one oxygen atom O^{2-}.

[14] Metal hydroxides are chemical compounds made up from hydroxide ions (OH^-) and a cation of a particular metal.

[15] Inorganic complexes are solid solutions or compounds consisting of two or more metal oxides.

[16] Metal salts are inorganic binary ionic compounds containing metals with variable cation charge.

[17] There is still some difference of opinion as whether carbon black (PBk 7) is organic or inorganic. In the colorists' palette PBk 7 is considered inorganic. This is because its properties most closely align with general inorganic pigment.

[18] Examples of inorganic pigments were selected on the basis of their impact in coloring of plastics and relevance in this dissertation.

[19] Solvent dyes are water-insoluble but, as the name suggests, are instead solvent-soluble compounds.

[20] Dispersed dyes are water-insoluble nonionic compounds which were designed to be mixed ("dispersed") with a dispersant. In their disperse colloidal form, they are suitable for dying most of the substrates.

[21] Vat dyes are water-insoluble compounds that require reducing agents to solubilize. Following exhaustion onto the substrate, they are re-oxidized to their insoluble form.

[22] From this point on, only the color of non-luminous bodies, namely non-emitting, are considered.

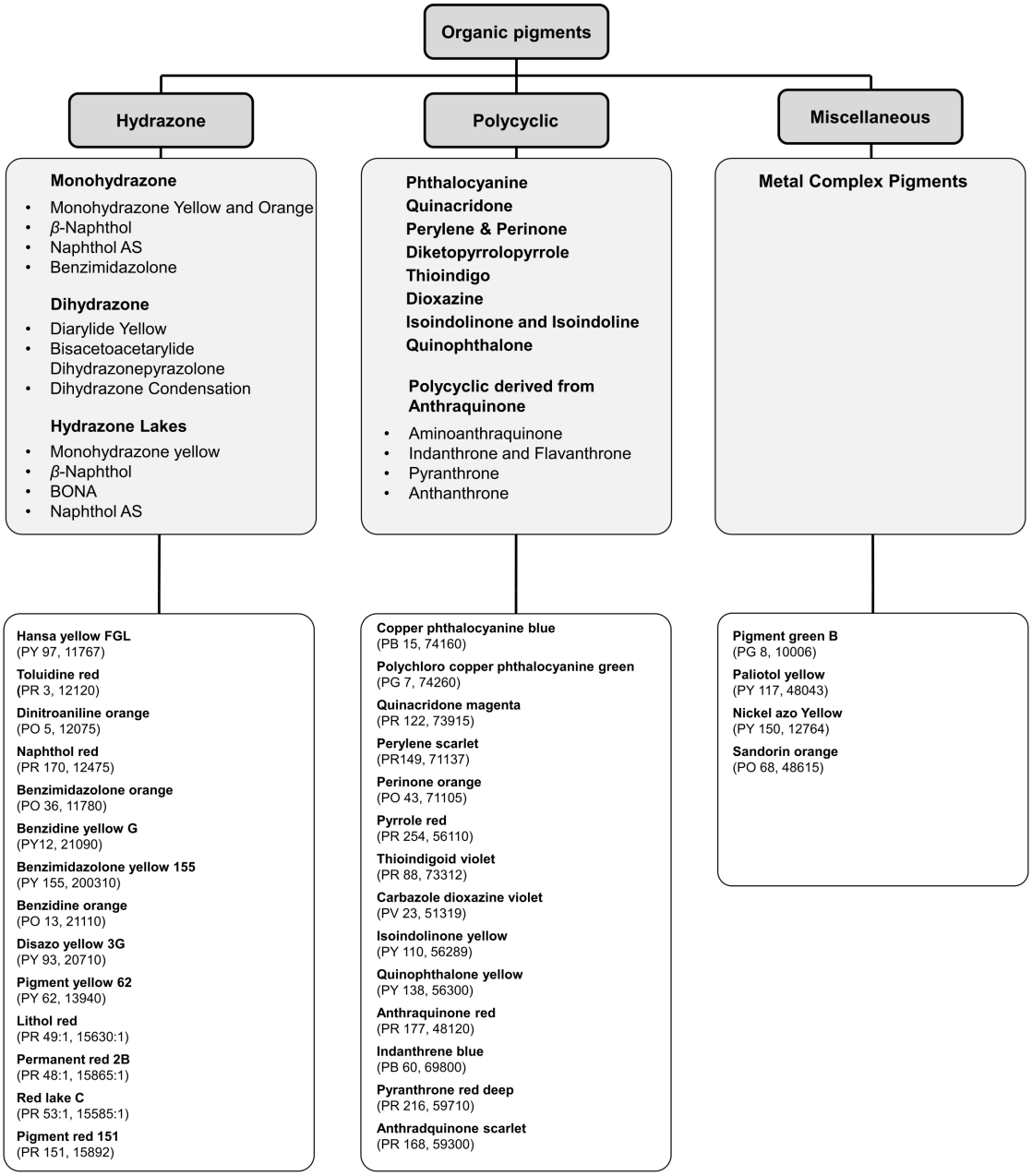

Figure 1.1.: Classification of organic pigments based on their chemical structure. Examples of pigments used in coloring of plastics are listed in the bottom part of the image. Common commercial name (in bold), Color Index C.I. Generic Name and Number (in parenthesis) are reported for each pigment.

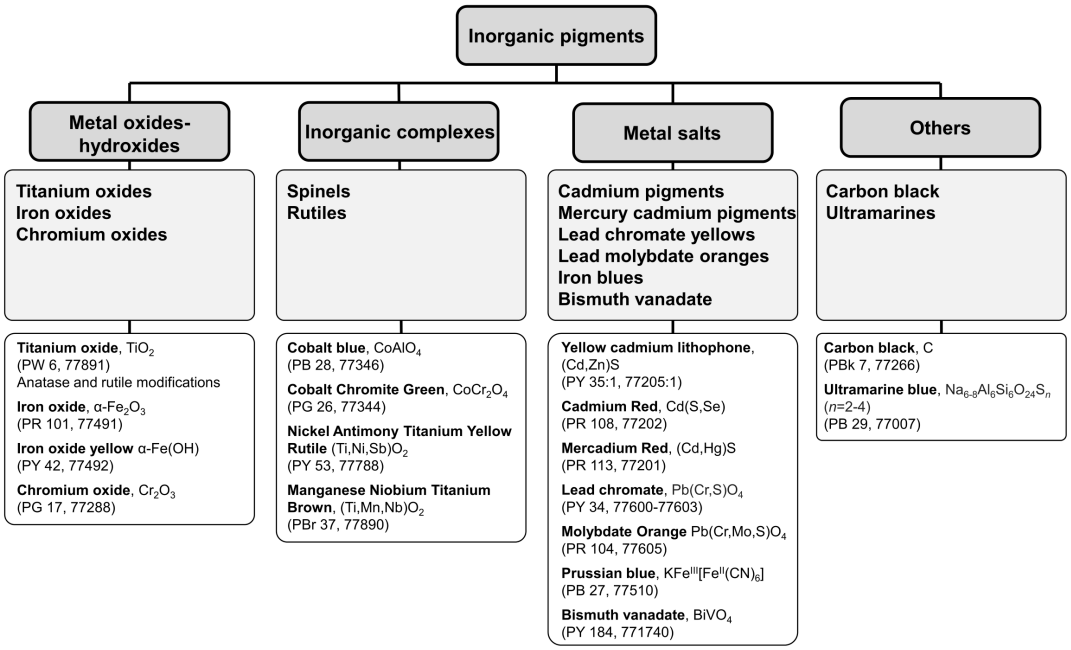

Figure 1.2.: Classification of inorganic pigments based on their crystalline structure. Examples of pigments used in coloring of plastics are listed in the bottom part of the image. Common commercial name (in bold), Color Index C.I. Generic Name and Number (in parenthesis) are reported for each pigment.

The electromagnetic spectrum covers all types of radiation, but only the visible spectrum is of chief interest to color. This consists of a range of photons (or wavelengths) between 3.1 eV (400 nm) to 1.55 eV (800 nm)[23], typically detectable by the human eye. From here, there is the definition "visible".
The phenomenon of color and color vision is complex with many intricacies [22], and a deep understanding of the way in which light interacts with matter and the human visual system is required to appreciate it.
The color of an object depends on its ability to absorb visible light. When white light[24] hits or passes through a colored substance, certain photons (mixed wavelengths) are selectively absorbed, resulting in the subtraction ("loss") of a portion of the incident radiation. The remaining light, being reflected or transmitted, can enter in the eye and producing a *color sensation*[25] [26]. This portion of visible radiation is called *color stimulus*[27] and arises from the absorption by the colored object. Now, the absorption of this color stimulus in the human retina determines the color vision phenomenon. Thus, light absorption is a fundamental process for the coloring. The selection of the photons being absorbed by the object and the photochemical process that stimulates the retina regards the quantum nature of light.

So, the existence of color is much devoted to the nature of the object. Bearing in mind this concept, polymers, colorants and additives and their superimposed contribution must be considered for plastics. The optical properties (color and opacity) of the materials are the results of both physical and chemical processes and the

[23] There are not precise limits for the visible spectral range considering the properties of the human eye system. Generally, the lower limit is taken between 360-400 nm and the upper limit between 760-830 nm [22]. Throughout this thesis the range of wavelengths from 400-800nm is considered.
[24] In this context, white light is composed of the broad range of all radiation wavelengths in the visible portion of the spectrum.
[25] Oleari clearly explains in "Standard colorimetry" [22] all the details of the complexity of the color vision phenomenon. Considering the description by Optical Society of America (OSA), he defined the color as a *"visual sensation which arises from the stimulation of the retina of the eye"*.
[26] The process explained is true for "colored" color sensation. The black and white color sensations are the two extreme cases. An object is seen as black because it absorbs all portions of the visible light (no photons reach the eye), and as if it reflects equally all portions of the visible light (no absorption occurs). The lack and the sum of all photons are respectively translated by the eye as black and white sensations.
[27] Color stimulus corresponds to the *"visible radiation entering the eye and producing a sensation of color, either chromatic or achromatic"* [22].

Table 1.1.: Classification of some plastics based on their optical clarity.

Transparent[a]	**Translucent/opaque**[b]	**Opaque**[c]
Polymethyl methacrylate (PMMA)	Cellulose acetate (CA)	Phenol-formaldehyde
Polystyrene (PS)	Cellulose nitrate (CN)	Urea- and thiourea-formaldehyde
Polycarbonate (PC)	Polyethylene (PE)	Melamine formaldehyde (MF)
Cellulose acetate butyrate (CAB)	Polypropylene (PP)	
	Polyamide (PA)	
	Polyvinyl chloride (PVC)	
	Polyethylene terephthalate (PET)	
	Acrylonitrile-butadiene-styrene (ABS)	
	Polytetrafluoroethylene (PTFE)	
	Polyurethane (PUR)	

[a] as sheets and molded plastics, [b] as molded plastics and clear as sheets, [c] always opaque as molded.

way they interact with visible light trough *absorption* and *scattering*. Summarizing the combination of the two effects, after light reaches the surface of the object, a portion is scattered (reflected) at the surface interface. The remaining wavelengths penetrate the surface and are changed through selective absorption and/or scattering by the colorants, polymer, and additives. The final color is thus determined by the accumulative amount of absorption and scattering that overall occurs. The manner by which light interacts with a material, both at the surface and inside, strongly influences its appearance.
Polymers, colorants, and additives are characterized by several properties. Not all of them playing a part in color. Below, the relevant properties that affect the color perception are summarized.

Polymers
The color phenomenon is strongly related to the light-matter interaction, the *refractive index* (n) is key in guiding this process. Indeed, transmission, surface and internal scattering are due to the refractive index of the material. As an example, two polymers possessing different n may appear differently even though they have been colored with the same colorant.
Besides surface scattering that always occurs, it is the property of the internal scattering that defines the opacity level of the resin. Plastics can be classified as *transparent* (no internal scattering), *translucent* (some scattering occurs, light is both reflected and transmitted) and *opaque* (so much scattering that no light is transmitted)[28]. In **Table 1.1** examples of transparent, translucent and opaque plastics are given[29].
Internal scattering is usually diffusely orientated, and considering only the polymer, it has a white color. This occurs because the change of n, that the incident light encounters when penetrates in the resin, causes the scattering of all portions of light with no absorption. On the other hand, both diffuse and specular reflections may occur at the surface and they will have the same color as light source (typically cold, neutral, or warm depending on the light source).
In addition to the optical clarity, another characteristic that influences overall color is the base color of the polymer. Most synthetic plastic resins are colorless (e.g. PMMA, PS, PC), but some show light, white-to-pale yellow with varying degrees of hue depending upon grade and manufacturer (e.g. PE, PP, ABS). This color appearance is the superimposition of both the absorption and scattering of the polymer.

[28] Optical clarity is closely linked to another material's properties, the degree of crystallinity of the polymer. Amorphous structure leads to transparency, while highly crystalline polymers scatter so high that the material looks opaque. Semi-crystalline polymers usually appear almost opaque because of the difference in refractive index of the amorphous and crystalline domains, which leads to internal scattering.
[29] Quantifying optical clarity can be difficult as it changes with the thickness. Even opaque material (e.g. PE, PP) can appear translucent or even transparent if sufficiently thin (e.g. sheets). Because three-dimensional objects are the focus of this dissertation, the classification of the optical clarity is based on molded plastics.

Both optical clarity and inherent color of the resin have effects on the final color. In transparent resins, the color is generated through transmitted or reflected light without the overlapping with the diffuse internal scattering component. In this way, bright, colors can be easily obtained. On the contrary, if the aim is to obtain an opaque polymeric resin issues arise and a scattering opacifier (such as a white pigment) is needed. In the case of yellowish and opaque resins, higher concentration of colorant is required. Its noteworthy that, these differences not only determine the choice of colorant and its amount, but also influence the resulting color. If the resin has its own natural color, the colorant should then mask it giving a new color sensation. Resins with a higher degree of translucency produce a visually more brilliant, higher chroma color than more opaque resins which, due to the higher white diffuse scattering, appear lighter and less saturated in color.

Colorants

There are many important factors that must be considered for colorants. The first one is that colorants do not "produce" color by the same mechanisms. Nassau in *"The Physics and Chemistry of Color"* described fifteen different causes [23]. From this work, it is clear that the reasons for the origin of color is obtained through different paths whether the colorant is organic or inorganic.

Colored compounds contain a characteristic grouping or arrangement of atoms called a *chromophore* (from the Greek chroma, phorós, "which brings color") which is the responsible for their colors. When visible light photons collide with an organic molecule, electrons in the molecular orbitals pertaining to the chromophoric part (e.g. π-bonding of double bonds and n-nonbonding on heteroatoms such as oxygen or nitrogen) are elevated from the ground state to an excited state by absorbing selected wavelengths [24], thereby giving the molecule the shade of the resulting complementary color. The observed color is thus modulated by the energy gap between the ground and excited electronic states which should fall in the visible part of the electromagnetic spectrum[30]. As such, the chromophore can promote an electronic transition in its molecular orbitals that is responsible for a spectral band. The type of chromophore depends on the chemistry of the colorant and it is influenced by modifying groups or substituents, *auxochromes*, which alter the primary hue of the colorant. Auxochromes have the capability to donate or accept one or more electrons through the molecular orbitals changing the extension and position of the conjugated system and consequently its color [23-27]. In inorganic colorants, the electrons (preferably from the outer electron shells) are elevated from the ground energy to a higher energy level, following other types of electronic transitions such as charge-transfer[31], ligand field[32] and valence-conduction band[33] [23,28-30].

These electronic transitions usually fall into the visible range and describe the mechanism by which the colorants absorb visible light. These aspects are not only important in the definition of the properties of colorants themselves, but also in the understanding of their physical and chemical behavior and the interactions when incorporated in the plastic material.

Colorants present other fundamental characteristics which should be considered as they are incorporated in the resin. Pigments are dispersed in the binder and their "coloring" properties include particle size, refractive index n, dispersibility, color and tinting strengths[34]. On the other hand, dyes are characterized only by color and tinting strengths, as they do not retain a particle structure. This characteristic has significant effects

[30] Among all possible electronic transitions, the $n \rightarrow \pi^*$ and $\pi \rightarrow \pi^*$ are usually achievable by the energies available in the 400 to 800 nm spectrum [24].

[31] Charge-transfer indicates transition between molecular orbitals which are localized in different sites of the molecule or crystal so that a real electron transfer occurs during the transition.

[32] Ligand field transitions involve metal ions characterized by unpair electrons in the d and f orbitals. The ligand ions (atoms or molecules), that surround the metal ion, are capable of resolving the degeneracy of the d and f orbitals of the transition-metal ion. When light is absorbed, electronic transitions between d or f orbitals localized mainly on the transition-metal ion at different energy level occurs.

[33] Being typical of semiconductor materials, in energy band transition electrons move from the valence band to the conducting band trough the band gap.

[34] Color and tinting strengths are two properties closely linked. The color strength of a colorant (dye or pigment) is related to its absorption property. Practically, it gives the color yield. Tinting strength refers to the relative ability of the colorant to color a resin and gives a reliable idea of the color strength.

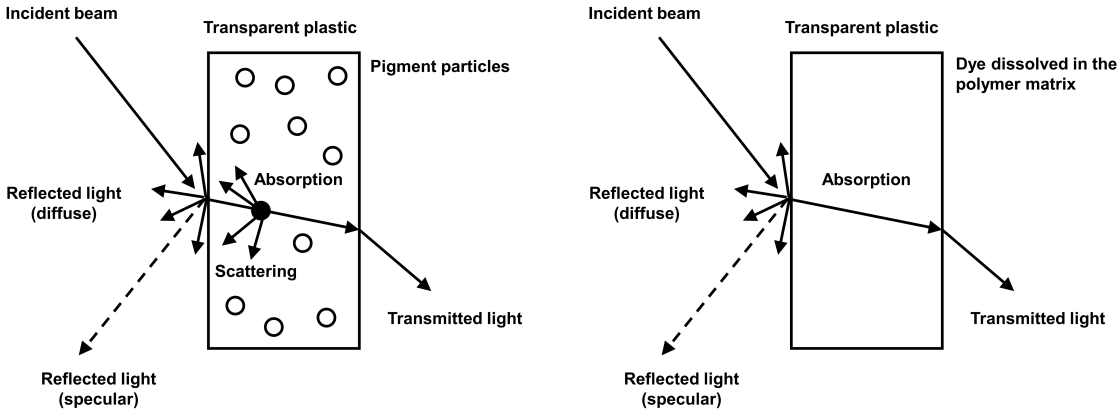

Figure 1.3.: Overview of different optical behavior of pigment (left) and dye (right) in transparent plastics.

Table 1.2.: Comparison of the properties of colorants in plastic applications.

Property	**Inorganic Pigments**	**Organic Pigments**	**Dyes**
Solubility	Totally insoluble	Partial solubility[b]	Totally soluble
Particle size	Mostly $> 1\mu m$	Mostly $< 1\mu m$	No particle size[a]
Tendency to form agglomerates/aggregates	Low	High	No agglomerates[a]
Refractive index n	1.5-3.0	1.3-2.5	No n[a]
Dispersibility	Good	Not very good (small particle size)	No dispersion required[a]
Transparency	Low, thereby high scattering power	High, thereby low scattering power	Very high, no scattering power
Color & tint strengths	Low, mostly not brilliant and often dull	High, good brilliance	Very high, good brilliance

[a] these properties cannot be quantified as dyes are dissolved in the resin. [b] generally, they are insoluble but can be partially soluble depending on concentration and formulation system.

in coloring. Indeed, pigments can produce color stimuli by both light absorption and scattering, while dyes only absorb light. **Figure 1.3** shows an overview of the optical behavior of a pigment and a dye highlighting their fundamental difference[35]. Organic and inorganic pigments also have differences and a comprehensive comparison between the properties of both those pigments and dyes is presented in **Table 1.2**.

Pigment scattering power and absorption strength (color strength) are dependent on particle size and the individual pigment refractive index, which may be explained by the Mie theory providing an excellent guide to their relative ratios [31,32]. As presented by Feller [33], colored organic and inorganic pigments present different relationship between absorption and scattering. Generally, it is noted that organics ($n < 2$) show the greatest absorption at the smallest particle size, while in inorganics ($n > 2$) the absorption and scattering can be both maximized at similar particle size. In plastics those behave likewise. However, the amount of scattering depends also on the magnitude of difference in refractive index between the polymer (commonly near 1.5) and the pigment ($n_{\text{pigment}} > n_{\text{polymer}}$, pigment scatters a relatively larger amount of light). Additionally, there is an optimum particle size for scattering[36], which is generally in the range of the half of the wavelength of the

[35] This example is given considering a transparent resin, as it better depicts the difference. If translucent/opaque resins were presented, the internal scattering of the polymer should be included for completeness, making the scheme more complex.

[36] Calculating the optimum particle size for scattering is tasking for any pigments. Besides the wavelength of light, it is dependent on the indexes of refraction of the substance and the medium.

incident light (< 1 μm). When significantly larger or smaller than this reference size, the pigment particles scatter less [33].

Generally, organic pigments usually have n closer to those of the resins and therefore do not scatter as much. Additionally, they have much smaller size than the wavelength of visible light, ensuring minimal light scattering and thus highly transparency. The colors of organic pigments are usually bright and intense, while weaker and duller colors are in general obtained using inorganic pigments. This difference is explained by the higher color strength that characterizes organic pigments and is a consequence of the different mechanisms in generating the color between organic and inorganic pigments, caused by the fundamental differences in their chemical structures [23]. Inorganic pigments are usually high refractive index materials and therefore highly scattering. So, when incorporated into plastics they provide opacity[37]. Organic and inorganic pigments present completely different properties and the particle size is a fundamental factor in influencing their tinting strength. Organic pigments have preferably very small size to increase their color strength, while many inorganic pigments have an optimum particle size at which the color strength and scattering reach their maximum.

If conventional pigments mostly interact with light by absorption and scattering, metallic and pearlescent specialty pigments work by light reflection and interference with minimal or even no absorption. Their lustrous or metallic appearance comes from the increase of the internal scattering which, due to the specific properties of both pigments, is partially oriented (spatially). In luminescent pigments, which can best take advantage of absorption of the illumination to re-emit photons of different wavelength, the scattering takes secondary importance.

Specific values of particle size are therefore the aim targeted by most manufacturers. However, in industrial applications, the optimum particle size is not always achieved. As reported by Charvat [5], the typically particle size ranges from between 0.02 μm to over 30 μm, with organic pigments usually characterized by smaller dimensions. Some inorganic pigments can reach particle sizes in the 30 μm range. However, they tend to present a higher percentage of single digit size particles (i.e. 4 to 10 μm). These values are approximate and much depends on the nature of the pigment and manufacturing process. Experimentally, it becomes clear that it is more convenient to separate organic and inorganic pigments at the 1 μm threshold (**Table 1.2**).

Different to dyes which molecule becomes a color site, a satisfactory dispersion of the pigments particles determines the uniformity of the plastic. However, pigments can form agglomerates and aggregates[38] and their breaking down to the minimum particle size enhances tinting strength[39], economizing on coloring material.

Thanks to the tinting strength of most pigments, they can be used in very small concentrations (0.1%-2% and up to 5% for special applications), this being considered suitable for coloring most plastic materials industry-wide.

Additives

If we consider a system made of colorant and polymeric resin only, the final color appearance will be determined by the cumulative contribution of both components. In practical applications, other factors must be considered such as additive packages.

When additives are incorporated in the polymer system, problems in coloring are usually related to the intrinsic whiteness of the compounds and the ensuing increase in scattering of the polymer system itself[40], which in

[37] Pigments, like other forms of particulate matter, have specific optical properties (n, absorption and scattering) different than those of the resin. When pigments are incorporate into the polymer system, interfaces between two optically different materials are created. This leads to new internal scattering (and absorption) and thus affects translucency and opacity.

[38] The two terms are frequently interchanged to describe assemblages of particles [34]. However, each term has a specific meaning in plastic coloring: "agglomerates" are loosely held clusters of particles, "aggregates" are very tightly held clusters [5].

[39] Breaking the clusters intensifies the color strength by creating numerous pigment-resin interfaces and thus, new absorption and scattering. Additionally, it increases the number of color sites. Both effects raise the tinting strength.

[40] The diffusely reflected light due to internal scattering has the color of whatever component is causing the scattering (e.g. colored pigments) with or without the added scattering of the plastic itself. In the case of white pigments or other whitish particulate materials (e.g. fillers), the plastics' white color derives from the properties of the particulate-crystal structures, which are purely reflective. Not providing any hue to the resin, they are added for pure white shades, lightening of the colored shades and opacifying the plastic product.

turn rises the diffuse reflection (white light). That is mixed with the colored reflected light generated by the pigment interactions. As a result, this mix provokes a dilution of the colorfulness and thus the color appears lighter and duller.
Increased light scattering can be caused by the presence of mineral particulate materials (e.g. fillers), cellular structure (e.g. foaming agents) or due to the characteristics of the additives; if those are characterized by a significantly different n compared to the base polymer (e.g. antioxidants, antistatics, coupling agents, flame retardants, heat stabilizers, impact modifiers, lubricants, etc.). In some few cases, a yellowish tint may be imparted to the polymer (UV stabilizers). The impact of the additives depends not only on the nature of the compounds but also on their concentration in the polymeric system, with higher quantities leading to greater scattering.
Some *fillers* commonly used in plastics to reinforce the polymeric resin or simply to reduce the cost are talc (PW 26, C.I. n. 77718), calcium carbonate (PW 18, C.I. n. 77220), barium sulfate (PW 21, C.I. n. 77120), and silica (PW 27, C.I. n. 77811). These have a strong influence on the colorability of the base polymer. They possess a particulate structure and in most cases behave as "weak" white pigments/scattering opacifies. Being characterized by low n (< 1.7[41]), they do not have the same scattering power as those white pigments ($n \geqslant 1.7$), such as titanium dioxide (anatase and rutile) (PW 6, C.I. n. 77891), zinc oxide (PW 4, C.I. n. 77947) and zinc sulfide (PW 7, C.I. n. 77995). But their presence is enough to scatter larger portions of incident light and so increase the scattering of the polymer system.

Any material may have unique characteristics that determine the color, and colorants are fundamental for the coloring of plastics. Pigments are capable of realizing hundreds of shades in opaque to translucent materials, while dyes color mainly transparent items. White pigments and/or fillers may be added to whitening and increase the opacity.
Color is one of the single characteristics that has made attractive the art we admire on our walls and in our museums throughout the ages. Following the same path, the vibrant and colorful surfaces of historical plastic objects have found their way to be appreciated. Interestingly, the making of the color in the field of art has not changed much over the centuries. As a *binder* held *colorants* and *additives* on the application of color on ancient, medieval, modern, and contemporary artifacts, so too a *polymer* carries all ingredients of a plastic formulation, *colorants* and *additives*.

1.1.3. Requirements and pitfalls in plastic formulation

It is possible to color plastics by several different methods, and frequently, the intricacies and potential problems related to plastic coloring are not considered. There is a science in this process and as in all sciences, there is a framework of fundamental knowledge about colorants that should be known to colorists.

Once such basic need is the avoidance of any *chemical incompatibility* between the chemistry of the polymer and the chemistry of the colorant system. The chemical stability is the "beating heart" of the color resistance in a plastic system.
When there is a perceived color change as a result of the colorant alteration, this implies that a chemical reaction has taken place, a situation that may occur during the processing or life cycle of the plastic. From a colorists' point of view, an observed color change indicates a failure of the coloring process, and although colorants are the first "actor" responsible for the failure, this issue may involve more components than just the colorants. They can degrade due to possible negative interactions with their microenvironment, in fact, polymers and additives are not chemically inert and their interaction with the colorants cannot be excluded. As a summary, it can be said that for a colorant to perform as expected, it *must* remain unaffected during the full cycle of plastic life.

[41] Strictly speaking, the limiting value of 1.7 is not constant because it depends also on the polymeric matrix and its n.

No *migration* of colorants should ever occur in the plastic, when it does, this is usually the result of a partial solubility, which leads to the mobility of colorants within the plastic matrix. Some examples are blooming[42] and bleeding[43] issues. Dyes are more susceptible to migration than pigments, due to the dye's intrinsic solubility. In practice some organic pigments can be partially soluble in the polymer system and these can also migrate.

An important criterion in the selection of colorants is *thermal stability*, as the colorant must be capable of surviving the temperatures at which the polymer is processed. This process temperature varies considerably (usually between 160 °C to 320 °C) and depends on the type of plastic. The colorant should remain stable not only during heat processing, but also during the fabrication and life cycle of the plastic. The method to assess the heat resistance of a colorant is through many combinations of time and temperature. In fact, the same colorant can behave differently if exposed for 90 seconds at 175 °C or 15 seconds at 300 °C.
The thermal and chemical stabilities are fully connected. Indeed, the chemical reactions at high temperatures can speed up and the colorant should be chemically stable here too.

Degradation of colorants may also occur due to environmental factors. Light, humidity, atmospheric oxygen (and other gasses), temperature, among others, can trigger or be part of chemical reactions resulting in visible color change and in extreme cases, in the collapse of the entire plastic. For this reason, the colorant *lightfastness* and *weatherability* are two important requirements in the colorists' work.
The fastness properties of the colorants are always related to the whole plastic system and depend on several factors: i) colorant's properties including its chemistry, crystal modification and concentration; ii) type and production method of the polymer; iii) presence of additives; iv) processing parameters; v) quality, intensity and duration of irradiation; vi) temperature during the use of the plastic object; vii) atmospheric condition of the surroundings.
In plastic applications, the light fastness/weather resistance of most of inorganic pigments is considered excellent. In contrast, fastness of organic pigments is strongly dependent on their chemical structure. Even different crystal modifications of the same organic pigment usually show differences in fastness properties [19]. The concentration of the colorant directly affects the ease of seeing color changes. In case of high concentration, the degradation of a single or a large number of molecules is not visually obvious. When in low concentrations, it is more noticeable if a single molecule is damaged. Colorants can be added in the formulation in pure form or as a mixture with other colorants and/or fillers. The fastness of the colorants should also be differently evaluated if applied in pure tone or in mixture, as an example, the addition of titanium dioxide (PW 6, C.I. n. 77891) to the colorant in white reductions may influence the colorant's resistance (**Section 1.4.3**).
Beside the intrinsic fastness properties of the colorant, the polymer and additives can affect the colorant's light and weather stability. Indeed, polymers and additives can trigger or be part of chemical reactions that cause colorant degradation. Unfortunately, the chemistry of all possible interactions has not yet been fully understood so currently exact predictions are not possible. A solution to meet industry requirements is to check the fastness of the whole formulation system including polymer, colorants and additives.
Issues with incorrect processing parameters may have an adverse effect on the colorant's fastness. An increase of temperature and/or cycle times may lead to a pre-damage of the colorants which may not be immediately detectable but, in the end, may affect the light fastness.
Polymers have different photoreactivity depending on their chemistry and structure. To start a photochemical reaction in a polymer chain, three fundamental steps must be fulfilled: 1) incident radiation is absorbed, 2) the

[42] Blooming is an alteration characteristic which consists in the formation of a powder or crystal-like deposit on the surface of the plastic. These can be colorants that have been dissolved and migrated from inside to the outside of the plastic and recrystallized on the surface.

[43] Bleeding can modify the appearance of the plastics in two ways: i) when a plastic contains a plasticizer in which a colorant is soluble, the plasticizer migrates to the surface of the polymer and so does the colorant; ii) when a plastic is in contact with a solvent which is capable of dissolving the colorant at the surface of the plastic. This latter may also result in the transfer of the color from one object to an another medium.

reactive group in the polymer is moved to an excited state, 3) finally the reaction starts before the absorbed radiation is released again. The absorption of radiation depends on chromophores of the polymer chain (ketones, aldehydes, double bonds, aromatic groups, etc.) as well as defects (double bonds, chain scissions, oxidized groups, etc.) and impurities (e.g. residues of catalyst) as a consequence of the production method. In plastic production, regardless of the effort and care placed in the manufacture, defects are unavoidable.
Only radiation absorbed by the system can lead to chemical changes. The absorption of photons with suitable energy creates excited states, wherein molecules can then dissipate the excess energy absorbed through several deactivation channels, including degradation pathways. Polyolefins (PO) are aliphatic polymers and can be used as a model to understand the fundamentals of polymer photodegradation [35]. Taking a structure containing single bonds like C-C, C-H, it should not absorb light of wavelength longer than 200 nm. This is far UV radiation and in practice does not reach the earth's surface. However, PO can undergo photodegradation as it contains extraneous groups (defects) and/or impurities which absorb light in the range of the solar light (ca $\lambda \geqslant$ 300nm) and form excited states. Extensive work has been devoted to the nature of these species. As it is well presented by Lemaire, Gardette and co-workers in a leading paper that summarizes decades of investigation [35], hydroperoxides are key light absorbing groups. Light absorption by these groups results in the formation of homolytic or heterolytic bond cleavage in the polymer chains, leading to chain scission, cross-linking and oxidation. The same concept can be applied to the remaining types of commercial polymers. But, unlike PO, their absorption can occur in longer wavelengths, in the middle UV (200-300 nm), as they contain chromophores in their structure (e.g. ketones, aldehydes, double bonds, aromatic groups) such as PS, PET, PUR, PMMA, etc. When pondering the light-induced polymer degradation, the near UV radiation (300-400 nm) is of particular interest. This is the most energetic sunlight radiation available on earth and it usually determines the lifetime of polymeric materials as being possibly absorbed by the admixtures present in the chains (i.e. defects and impurities) [36,37].
Photodegradation can also proceed via a complex sequence of reactions which may involve other species. Humidity (H_2O), atmospheric oxygen (O_2), nitric oxides (NO_x), sulfuric oxide (SO_2) and ozone (O_3) may be part and/or accelerate the light-induced aging. Temperature also speeds up the chemical reaction rate.
The colorants and polymer system properties along with the environmental factors determine the fastness of the colorant and consequently, of the whole system. To prolong the lifetime of colored plastic objects, colorants should remain stable during the fabrication, their lifetime in the hands of the consumer and even much longer for museum objects.

When pigments are incorporated in the polymer, a satisfactory dispersion of the pigment agglomerates and distribution of its particles is necessary. The *dispersability*[44] is one of the most important and problematic tasks for the success of the final product. The aim is that all pigment agglomerates are homogeneously distributed and broken into their individual particles, so that all end up coated by the polymer binder. Particle size together with the chemical composition of the colorant have a significant influence in this process and, consequently, in the final color appearance.

The typical colorant loading level in a finished plastic is low (0.1%-5%). This is the result of choices made by the colorist, who evaluates the colorant and polymer system compatibility. The concentration can vary depending on the end application of the plastic and specific colorant/polymer properties. A proper *pigment loading* (a limit to how much color can be added) guarantees good property retention before the material is negatively affected. Colorants, as all other additives, are contaminants and in low concentrations have no adverse effects on the formulation.

The *manner in which color is incorporated* into the base resin is also important. The plastic color formulator

[44] Dispersability should not be confused with *dispersibility*. The first interests the separation of pigment particles and agglomerates into their ultimate individual particles. The latter refers to the ease with which the desired degree of dispersion is achieved.

has a choice between many methods of mixing colorants into the plastic resin, including the use of several forms of colorant systems (e.g. powdery colorants, liquid color preparations and masterbatch) (**Section 1.1.1**). Each choice implies different technological requirements. As an example, the mix of a pigment powder in a thermoplastic resin requires a different method than the one used to color a thermoset resin with a liquid preparation. Significant literature on technological applications for this subject is readily available [38-42]. From early on, and until the 1970s [43], colorants were usually mixed in powdery form to the resin, while after that, the use of liquid and masterbatch color preparations became popular and achieved widespread use [43].

Today *toxicological* and *ecological considerations* have become a prime concern and colorants are no exception. In the formulation work the safety aspects of a plastic formulation must be considered, this implies not only the effects on human health, but also on animals and ecology. As the world becomes more safety conscious and environmentally aware, many colorants have stopped being used, are being gradually removed or have been simply banned from their utilization in plastic production in heavily industrialized countries. This is particularly evident for heavy metal compounds upon which many inorganics are based. Although legislation in major markets limits the presence of heavy metals, no worldwide restrictions exist. The plastic colorist's palette has become significantly smaller over years, although new organic colorant families are available. Considering current toxicological and ecological guidelines, today's colorants are for the most part, insoluble in water and biologically inert.

The colorant and additive selection is one of the more difficult steps in the designing process of the plastic formulation. There are hundreds of possible compounds and the colorists should follow some criteria in their choice. The identification of the *end application* for a plastic is the starting point for choosing colors. Colorant systems may be used in contact with food (as packing and warping materials), cosmetics, toys, automotive, pharmaceutical, medical applications, etc. each of those having specific requirements. Given the end application, the colorist can then predict to which environmental conditions and for how long the plastic will be exposed.

Polymer science and material chemistry offer guidelines to understand the cause and effect of molecular events in plastics during their production and use. As chemical reactions may occur during the fabrication, problems may also start during the life cycle of a plastic, although, plastics are tested to be stable during their established use time in the hands of the consumer. An example is the emerging 21st generation of biodegradable plastics which, after being used, fully decompose within a few months. Besides mechanical stresses (e.g. shear forces, tension, compression), *the aging of plastic articles during their usage time implies chemical reactions*. Colorists' considerations on the properties of colorants and whole plastic systems should support the knowledge of the coloring failure over years. When an object is acquired by a museum or cultural heritage collection, the science of conservation meets the science of the plastic coloring. Many of the concepts presented in this section may serve as a tool for the study of colorants and color change in historical plastics.

1.2. Plastics as cultural heritage and its conservation challenge

The development of man-made polymers from the mid-19th century [44,45] significantly changed the modern world. Those changes expanded to all the aspects of society, including technologies, lifestyle and art.
The significant developments in the polymer industry and its huge cultural and historical impact have turned plastic into one of the most relevant materials in modern and contemporary ages. Therefore, polymer-based objects are now increasingly common in cultural heritage collections as testimonies of our past and memories associated with their role and impact, among others, in the social context.
Nowadays, polymer-based objects are found in almost every type of museum worldwide in the form of foams, elastomers, films, fibers and rigid plastics. This includes mass-produced three-dimensional objects in science

and social history collections, digital media tapes in archives, textiles and fashion articles, and unique and valuable artworks, partially or completely made of plastic.

But, for all of those, *there is an intrinsic challenge in preserving plastic artifacts much longer than their intended lifespan*.

Industry and conservation science conceptualize durability and fate for the plastics differently. Forindustry: *"Testing is imperative to be sure a colored system will meet the demands [...] and finally ensuring that the finished product will perform as expected and as long as expected in the hands of the consumer"* [46]. This means that plastics are not designed to last forever. Form this point onwards is where the intrinsic challenge in the preservation of plastics starts. Conservators are trying to preserve a material with limited lifespan. While traditional artworks on parchment, paper, textiles, wall, canvas, panel paintings, etc., were conceived to last over time, in the case of plastics, they are designed to be *replaceable* in time.

Over the last thirty years, the dichotomy of plastics sturdiness has clearly emerged [47]. When their production started at the beginning of the 20th century, plastics were promoted as stable and durable materials [48,49]. In this way, a common belief of their everlasting stability was spread in society. With the conference "Saving the Twentieth Century: The Conservation of Modern Materials" organized by the Canadian Conservation Institute in 1991 [50], the susceptibility of plastic to degradation in museums and galleries was formally recognized. Since then, increasing attention has been focused on the challenges raised by the deterioration plastics in collections. In 1993, the Historical Plastics Research Scientists Group (HPRSG) was formed in the UK with the purpose of establishing the degradation pathways of plastics in museum collections. Three years later, in 1996, the International Council of Museums Committee for Conservation (ICOM-CC) established the working group "Modern Materials and Contemporary Art" to discuss conservation theory and practice for plastic materials. During the 1990s surveys of collections were made [51,52] and raised interest in plastic conservation, together with an increasing number of publications, conferences and multidisciplinary research projects [53-75]. An important step in the progress in conservation of plastics was made by the EU 7th Framework research project POPART (Preservation of Plastic Artifacts in Museum Collections)[45] [76]. Outputs from this project were the establishment of a damage ATLAS of nomenclature and guidelines in interventive conservation (especially cleaning) as well as suggestion of analytical methods for their studying in museums.

The conservation community is now aware that plastics cannot last forever. They have a short lifetime when compared to more traditional artistic materials and can exhibit various symptoms of degradation. As recognized by Quye [77], some plastics *"are unfortunately degrading faster than expected"* and *"the bad news is that once chemical degradation has started, it is almost impossible to reverse the process"* leading, at times, to the total collapse of the material. The preventive conservation and the detection of incipient degradation phenomena are thus key to the objects' safeguarding. The controlling factors in understanding degradation pathways include not only the object itself but also the environment in which it exists.
Considering these arguments, at present, the conservation of plastics is a critical issue in cultural heritage science. Even though advances in caring, conserving and studying of collections have been done mainly by the POPART project [76], very little scientific research is found on the colorants and their degradation. This situation highlights that the study of colorants is a priority, as the color is an integral part of the aesthetic, historical and material authenticity of historical plastics.

[45]The POPART project was a 42-month (2008-2011) international research project part funded by the European Commission; http://popart-highlights.mnhn.fr (accessed 07.10.2020).

1.3. Colorants in plastic artifacts, an unwritten story

From the production of the first colored Parkesine[46] objects in the 1860s, colorants used in plastics have changed over time. Modern chemistry has led to not only the production of colorants on the industrial scale, with innovative methods but also, to the worldwide introduction of hundreds of new synthetic colorants. The history of coloring in plastics goes together with the history of technological and industrial development from the 19th century onwards, being linked to both the plastic and colorant industries history.

The first mention of a colored plastic is by Alexander Park at the Great International Exhibition in Great Britain in 1862 with the display of the first man-made plastic, Parkesine moldings. Although they were dark colored or black, in the official exhibition catalogue Parkes claimed that Parkesine could be made "*hard as ivory, transparent or opaque, or any degree of flexibility, of the most brilliant colors; [...] the most perfect imitation of tortoiseshell, woods and an endless variety of effects can be produced*" [78,79].
From there on, plastics had an explosion of color.

Multi-colored Galalith[47] casein-formaldehyde buttons appeared on the dresses in the first half of the 20th century. The dark, deep color of telephones made of phenolic resins first Bakelite[48] in the 1920s, were followed by the light, gaudy colors of ureic resins. Kitchenware imitating marble effects started to appear in homes, and pink, green, and turquoise radio casings showed up in the offices by the 1930s [80]. Early plastics were also designed to imitate luxury materials which experienced an ever-growing demand and with a decreasing supply. Some notorious examples are celluloid – plasticized cellulose nitrate (CN) and cellulose acetate (CA) objects simulating ivory, tortoiseshell and mother-of-pearl [81-83].
Synthetic dyes and pigments have been used since the beginning of plastic production and, in the first half of the 20th century, objects covered already a wide range of color appearance [18]. Colorants, used in the first plastics to imitate ivory, tortoiseshell and mother-of-pearl are better documented in literature, although sometimes their exact characterization is missing. Zinc oxide, added as white pigment, was commonly used to make imitation ivory [84], mottled patterns in plastic imitations of tortoiseshell were caused by the addition of dyes to a clear polymer base [85], while basic lead carbonate became the pigment choice for simulating pearlescence [86].
Between 1930-1945 several new synthetic plastics were introduced, such as polyethylene (PE), polymethyl methacrylate (PMMA), polystyrene (PS), polyvinyl chloride (PVC), polyurethanes (PUR), polyamides (PA), and others. In the aftermath of this new formulation explosion, during the 1950s more types of synthetic plastics were developed, including acrylonitrile-butadiene-styrene (ABS), polypropylene (PP), polycarbonate (PC), polytetrafluoroethylene (PTFE) and polyethylene terephthalate (PET) [44,45]. The increased number of resins and the introduction of new colorants offered the birth of new trends coloring our daily life.
With the introduction of a such plethora of polymers and colorants, the reconstruction of the coloring history becomes even more difficult. Color can also tentatively be used as a guide to identify polymeric materials of the early plastics (e.g. cellulose esters, casein, phenolics, urea-thioureas) by simple visual inspection [87,88] while for the remaining synthetic plastics, there are still not clear guidelines.

Documenting the history of the coloring of plastics is thus not an easy task, considering that there are few sources of information about the topic. Besides the C.I. where the application of colorants in plastic is sometimes briefly mentioned [17,18], technical monographs for industrial practice only started to be published

[46] Patented in 1856 by Alexander Parkes (1813-1890), Parkesine is a tradename of the first semisynthetic celluloid-based plastic, cellulose nitrate.
[47] Under the tradename Galalith, casein-based plastics were successfully produced in the first half of the 20th century. This semisynthetic plastic material was manufactured by the interaction of casein, protein of milk (from the Greek word "Gala" = milk), with formaldehyde allowing the protein to become a hard material.
[48] Bakelite, trademark of thermosetting phenol formaldehyde resin, was patented in 1909 by Leo H. Baekeland. It is recognized as the world's synthetic plastic made.

from the 1960s onwards [2-5,89] and mainly in German [90]. National technical journals or magazines such as *"Kunststoffe"* in Germany [90], *"British Plastics"* in UK [91], *"DuPont Magazine"* in USA [92] would, sometimes, also report some information on coloring.

This thesis is focused on plastics and collections in Portugal, so it is important to consider the national context of the formulation and fabrication of plastics nationwide. If other nations (such as Germany, Great Britain, USA) can count on museums, archives and library collections on plastics and their industrial history, the information on Portuguese panorama is in its youth. Most of the knowledge on Portuguese plastic history can be attributed to Maria Elvira Callapez, who through an interdisciplinary approach, studied together the historical, technological and social perspectives of this modern material [93]. In her research, specialized documentary sources were collected and assessed. Those included magazines and other publications written by professional associations of the Portuguese processing plastics industry, such as *Associação Portuguesa da Indústria de Plásticos*[49] (APIP).

The APIP (first called *Grémio Nacional dos Industriais de Composição e Transformação de Matérias Plásticas*[50] in 1965 and later in 1975 APIP), published three main national bulletins: *"Plásticos: revista da indústria de matérias plásticas"*[51] (1967-1978), *"CNP plásticos: boletim informativo"*[52] (1980-1997) and *"Reviplast: revista da indústria de plásticos"*[53] (1997-present) [49,94,95]. Nevertheless, references to colorants and coloring applications are rarely found in the bulletins and periodic journals accessed in the APIP archives [96]. In detail, only one documented source on the subject was found, a dossier entitled *"Aditivos / Pigmentos – Sua Influência nas Características Finais dos Productos"*[54] that was part of APIP's seminars. APIP produced and used this monograph probably from 1995 until 1999, in the XVI seminar organized by the association for the education of engineers working in the field of plastics in Portugal. This specific monograph discusses the coloring of thermoplastic resins in addition to the fundamentals of colorimetry. It describes four *"tecnicas de coloração"*[55] with powdery colorants, liquid and solid preparations (masterbatch) reporting practical examples of PVC, PE and PP coloring. Surprisingly, families of dyes, organic and inorganic pigments are listed at the beginning of document. Iron oxide reds, lead chromate yellows, lead molybdate oranges, cadmium reds and yellows, ultramarine blues, chromium oxide greens, titanium whites and carbon blacks are part of the Portuguese colorist's palette. Referring to organic pigments, phthalocyanine greens, phthalocyanine blues, azo lakes, diazo and polycyclic compound are part of the list. As dyes, only the anthraquinone family is mentioned. Unfortunately, specific examples of organic colorants (such as C.I. Generic Name or Constitution Number) are not mentioned. The monograph also gives some notes on colorant stability, with no mention of technical literature or chemical studies. In the document, all inorganic pigments are considered heat and light resistant, with only the crystalline form anatase of titanium dioxide not matching the same fastness. All organic colorants show good heat stability up to ca 250 °C and polycyclic pigments are characterized by *"solidez boa"*[56] under exposure to light. The families of pigments mentioned in the monograph are some of those widely used in the coloring plastics. Interestingly, inorganic pigments containing heavy metals such as lead, chromium, cadmium, selenium, are still mentioned although they may be subject to restrictions due to toxicity and environmental reasons, a measure that has been enforced worldwide in the 1990s [97,98]. As such, this document presents some useful information on the coloring practices of the 1990s. But what about before that period?

There is almost no relevant data available before this period, so a colorant timeline of their historical development would resolve this issue, at least to some extent. Traditionally, paintings have always reflected the

[49] "Portuguese Association of the Plastics Industry". All translations found in this section were made by the author of this dissertation.
[50] "National Guild of the Industry for the Composition and Transformation of Plastics".
[51] "Plásticos: Magazine of the Compounds for Plastic Industry".
[52] "CNP plásticos: Divulgation Bulletin".
[53] "Reviplast: Magazine of the Plastic Industry".
[54] "Additive / Pigments – Their influence in the final characteristics of the products".
[55] "coloring techniques".
[56] "good lightfastness".

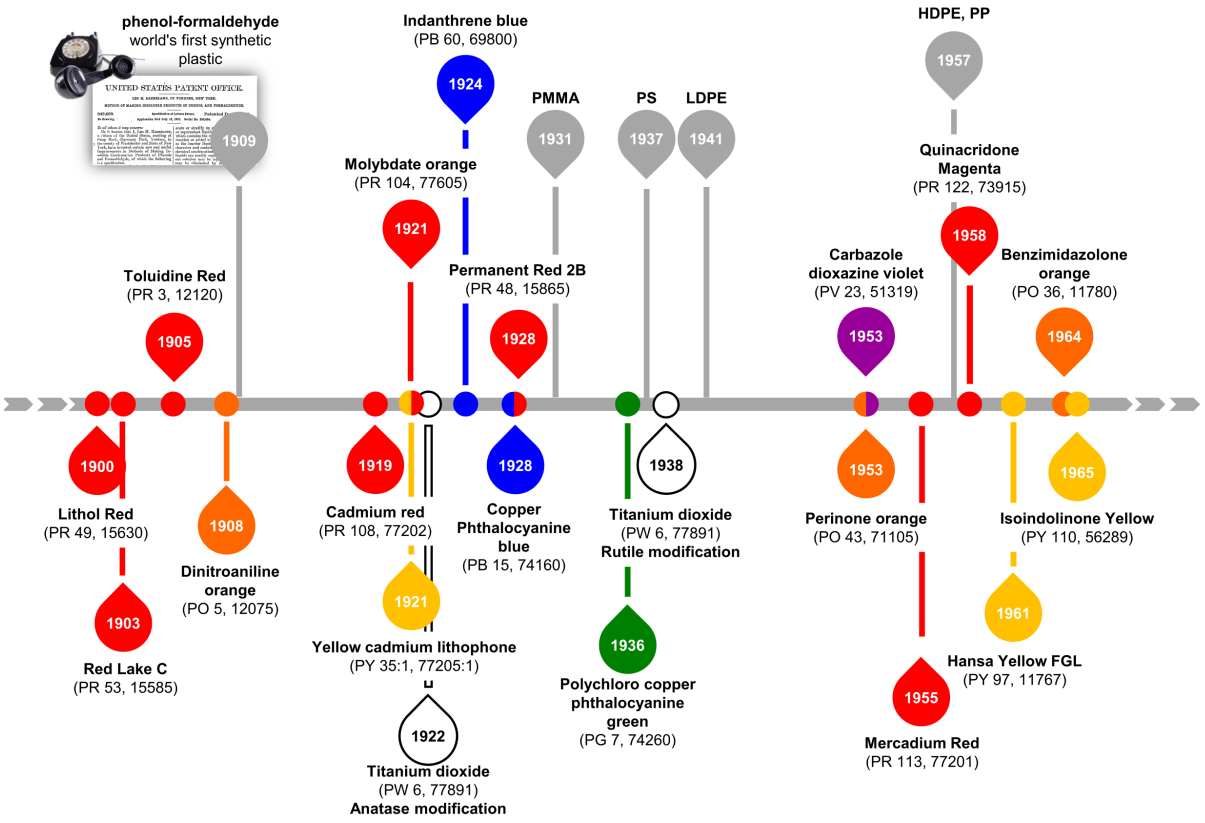

Figure 1.4.: Timeline showing the increasing availability of pigments parallel to the chronological development of some commercial polymers.

materials available to artists at the time of their inception, for the colorists, this is represented by pigments, their technical maturity and availability on the market.

Figure 1.4 presents a survey of the first recorded date of industrial production of some synthetic pigments in the 20th century[57] [99-101]. Chronological development of some commercial polymers is also reported for comparison[58] [45]. All the depicted pigments are mentioned for plastic applications [2-5,18]. Nevertheless, their effective use in time in coloring is still not widely documented. The author devoted a significant length of time in researching documentation on colorants alas, no comprehensive studies on the history of plastic coloring could be found in conservation literature. Additionally to this, very few studies have been found focusing on the scientific characterization of colorants [102-104] that could strongly support the knowledge on their use to color historical plastics.

1.4. Color change in plastic artifacts

There are many tell-tale signs that indicate the deteriorating of historical plastics. Besides physical changes, almost all of the degradation signs change the original objects' appearance. For instance, the development of a thin network of cracks (crazing) can turn a clear transparent PMMA opaque, the formation of a powder-like deposit due to plasticizer migration (blooming) on CN can hide its surface, the appearance of a lot of small bubble-like distortions (blistering) can locally change the gloss of CA. Many examples could be included in this list, but only few degradation signs can be strictly related to the alteration of the original color (*discoloration*) of bulk-colored plastic artifacts.

[57] Pigments were selected on the basis of their impact in coloring of plastics and relevance in this dissertation.
[58] Polymers were selected on the basis of their relevance in this dissertation.

Discoloration of plastic-based objects in museums and collections has been reported by the conservation community [87,105-107]. Following the POPART damage ATLAS [108], color change includes *darkening* (the material becomes dark or darker), *fading* (partial or complete loss of color and brightness) and *yellowing* (shifting toward yellowish tint/color).
For many collectors, the colorful image of the plastic is as important as the object itself. Thus, the color restoration of original plastic objects becomes a fully justifiable endeavor. Abrasive polishing and superficial recoloring are common practices [109], especially for mass-produced and easily available objects; however, historically important objects or unique pieces should not be subjected to such drastic actions. Currently, no single treatment to recover original color is known.

Some of the wear and tear effects responsible for plastic discoloration can be attributed to surface effects, degradation of the polymer, alongside modifications of the colorants. Each those effects will be here presented (**Sections 1.4.1** to **1.4.3**).

1.4.1. Surface effects

Grime, dust, and any particulate material deposited on the surface can change the apparent color of plastics. Surface cleaning can improve the look of the surface, and with some luck, the piece original color can be found neatly preserved under that initial grime layer.
Since the POPART project [110], the number of studies on cleaning procedures of plastics have exponentially grown. Plastic cleaning can be performed either using dry methods [111] or aqueous-based solutions or solvents applied with cotton swabs or microfiber cloths [112]. Confining systems, such as gels, have also been investigated for plastic cleaning [113-115], including some novel gels developed during the NANORESTART project (NANO materials for the RESToration of ART)[59] [116,117].
Plastics are not impermeable to gases, vapors, and liquids. Discoloration may result from the absorption of other compounds on the plastic's surface. As an example, many plastics are effective in absorbing oily liquids and can change pigmentation when in contact with food, a phenomenon that has been observed when some of those are used for the fabrication of food containers [106]. Another issue can be encountered when a plastic absorbs colored materials that are in close contact [102]. This process can be explained as a chemical and/or physical process where material is transferred from one surface to the other. Typically, the colored material can suffer substance migration, were the material concentrates on the surface of the original plastic, this is then transferred to the adjacent surface, causing color change.

1.4.2. Polymer degradation

It is sometimes very difficult to determine whether the discoloration is due primarily to the degradation of the polymer or the colorants, though in both cases, degradation occurs mainly due to light.
Photochemical action is a chemical change at the molecular level and results from reactions triggered by light exposure. The chemical reactions take place at the surface of the objects and cause the color to turn yellowish, darken, or fade, when compared with unexposed areas. Photochemical reactions can induce chemical changes in the polymer (e.g. cross-linking and chain scission) and colorants (e.g. chromophore loss) along with the formation some new chemical entities (photoproducts).

The effects of light exposure in the degradation of polymers have been a topic of study for decades, and publications in polymer science [118-129] and cultural heritage [105,106,130-132] provide useful background information on this subject.

[59] NANORESTART was a 42-month collaborative research project (2015-2018) funded under the EU Framework Programme for Research and Innovation Horizon 2020 (grant agreement number 646063); http://www.nanorestart.eu (accessed 07.10.2020).

The absorption of light by the polymer is followed by various chemical and physical interactions which result in the conversion of the excitation energy into chemical energy by photochemical reactions. Light-induced degradation usually proceeds via radical chain mechanism and could involve a complex sequence of reactions, including energy transfer, oxidation and even hydrolysis [133].
When focusing on discoloration, the primary consequence of polymer degradation is the formation of new chromophores, able to absorb radiant energy in the visible range. Yellowing is a common manifestation of this form of photodegradation. Almost all polymers suffer from yellowing [106,134], which is attributed, in most cases, to the formation of conjugated structures, including polyenes (alternate carbon-carbon double bonds and carbon-carbon single bonds), carbon-carbon double bonds conjugated to carbonyl or aromatic groups [135-138][60]. The development of carbonyls (C=O) and unsaturated carbon bonds (C=C) in the backbone of the polymer results in color formation in white opaque and transparent plastics.
The darkening phenomena is typically less common than yellowing and generally both occur in the outermost plastic layer. Deep brown coloration of degraded PVC is one of the few examples of darkening. Generally, it is accepted that yellowing and subsequently darkening are due to the formation of polyene structures. Depending on the extent of the conjugated polyene system, absorption from 400 nm upwards leads to a progressive color change from white, to yellow, to orange, to red, to brown, and lastly almost black [106,135].

Finally, discoloration is related not only to light-induced polymer's chemical changes but also to the presence of degradation products and their reactions with other components of the formulation (e.g. colorants). Some examples can be seen in the degradation of CN and CA that produce oxidizing and acidic gases. Indeed, light and moisture can cause CN and CA to produce nitrogen oxide gases (including nitrous oxide (N_2O), nitric oxide (NO), nitrogen dioxide (NO_2)) and acetic acid (CH_3COOH), respectively. N_2O has a brown hue, so when it is trapped in the polymeric matrix, it can darken the plastic. Mobile acidic vapors produced by deteriorating CA can catalyze the degradation of the other materials/components [105]. These reactions can occur both in the bulk and at the surface and are different from photooxidation.

Research on the mechanisms of photochemical aging, uncovered the fact that discoloration is often symptomatic of polymer photooxidation [120,124,153,154]. Historical plastics are constantly in contact with light and oxygen. As clearly presented by Lemaire et al. [35], the action of light in the presence of oxygen is *de facto*, the fundamental degradation mechanism of polymeric materials to which all plastics are subjected during their lifetime.
The chemical evolution of the degradation process can vary in complexity, depending on the type of polymer, formulation composition adding to environmental factors. Indeed, structural irregularities and impurities also contribute to the definition of polymer lightfastness (**see Section 1.1.3**).
Photodegradation pathways can involve solely the polymer or other chemical entities such as additives. In fact, additives may influence the chemistry of the reactions [11]. For colored polymers, the colorants can influence the photodegradation of the polymeric matrix. As colorants interact directly with light, they can stabilize or accelerate the photochemical reactions.

1.4.3. Colorant degradation

As mentioned in **Section 1.1.3**, the colorant's fastness in plastics depends on its chemical/physical properties and interactions with the polymer system. Besides the nature of the colorant, other three principal factors play a role in the definition of the photostability of the colored polymer system: i) the intrinsic chemical/physical nature of the polymer, ii) the presence of antioxidants and light stabilizers[61], and iii) the environment in which

[60] For studies on individual polymer types see references: PE [139], PP [140], PS [141,142], PMMA [143,144], PVC [145,146], ABS [147,148], PUR [149-152].
[61] Antioxidants and light stabilizers are the most important additives in the photoprotection of colorants in polymers. Antioxidants slow down oxidation degradation, while light stabilizers improve the resistant to light-induced changes. Exposure to UV light

the system is used.
For long-term stability, *the whole formulation lives as a chemical reactor* in which the components can react, and colorants may photodegrade.

Fading is usually ascribed to colorant degradation, which results of a chemical change of the molecules' structure that eventually leads to a change in color. This can be explained considering that pigments and dyes are the components that are most subjected to this type of decay for their ability to absorb light and lose their characteristic chromophore group. As a result, a plastic totally or partially loses color in favor of the natural polymer coloration. In addition to colorant change, the yellowing/darkening of the polymeric matrix can take place at the same or at a later time. Additionally, modification of the polymer texture (e.g., surface cracking and crazing[62]) can cause whitening[63] (**Section 1.1.2**).
While the impact and contribution of polymer degradation to discoloration have been widely studied (**Section 1.4.2**), considerably less research has been made focusing on the lightfastness of pigmented or dyed polymeric systems.
Fading of colorants in colored plastics is a very complex interplay of phenomena and mechanisms, many of which remain still unresolved. In literature, the photofading and light stability of colored polymers is usually discussed focusing on the colorant-polymer interaction, a mechanisms which seems better understood [155], while the nature of the interaction with additives is lesser explored [156].
Most of the research has been focused on the photosensitizing and photostabilization effects of colorants in polymer degradation [157-163]. Although colorants are primarily used to impart color to the polymer, pigments and dyes may not only undergo fading but also have a dramatic effect on the photostability of the polymer itself. In these photochemical processes, the colorant can remain unaffected by light exposure or eventually degrade into fading products [162].
A photoexcited dye chromophore is the starting point of the photo- catalyzed and stabilization mechanisms [164-166]. The dye can then sensitize the photochemical breakdown of the polymer or be involved in energy transfer and quenching with photoactive units or impurities giving rise to photosensitize and/or stabilization effects.
The mechanisms within which colored pigments may act as photosensitizes or photoprotectors require further clarification. As Allen comments [167], "*many workers have examined the effect of colored pigments on the light stability of polymers but the data may contain many discrepancies".* Indeed, certain colored pigments can be considered good stabilizers *"although other workers find the opposite effect"*. This scientific inconsistency is probably due to the pigment manufacturing history and other tainting pigments or impurities. It should be noted that the photochemical activity of pigments is dependent on the nature of their surface treatments[64].
From the available literature, it is difficult to make an exact prediction of whether a pigment will be photoactive or not and by which mechanism it will work, this being especially true for colored pigments. The photochemical activity of white and black pigments is better understood [167]. Pigments operate as stabilizers by either reflecting and/or absorbing incident light which, given the activation spectrum of polymers[65], corresponds

is damaging not only to the polymer but also to colorants. Thus, UV stabilizers received more interest for their ability in absorbing UV radiation and dissipating the associated energy in a harmless manner.

[62] Cracking and crazing are both degradation phenomena related to the physical changes. While crazing indicates the formation of a network of cracks, cracking describes a break without the complete separation of the parts. In the case of the complete separation of an objects into pieces or fragments, it is referred as break. Cracking and crazing can be the result of mechanical stresses and/or chemical reactions.

[63] As consequence of plastic degradation, the surface texture may change. The increase of surface roughness and imperfections (crack and crazing) leads to higher diffuse scattering of all wavelengths appearing lighter.

[64] The surface of organic and inorganic pigment particles can be treated and/or coated without having influence on the color to improve application properties according to its expected performance, such as light and weather fastness, rheology, dispersion, solvent fastness, etc. The surface treatment can consist of inorganic and organic or combined inorganic/organic compounds. The term "encapsulation" appears frequently in literature. It consists of a polymeric specific treatment which covers the entire surface of the pigment particle. The encapsulation procedure is performed not only to protect poor lightfast pigments from light exposure but it is also commonly to reduce the photoactivity of pigments known as reactive.

[65] The activation spectrum is an important representation of the wavelength sensitivity of a polymer to photodegradation as shows

to UV radiation. Inorganic white pigments (titanium oxide, zinc oxide, magnesium oxide, calcium oxide, lead carbonate, barium sulfate) possess a UV reflector property. However, their UV light reflectance varies very widely depending upon the nature and crystalline structure. For example, magnesium oxide and barium sulphate are very good UV screeners between 300 and 400 nm, whereas titanium white and zinc oxide show low UV reflectance[66]. Black pigments (carbon black) are excellent UV/Vis absorbers. Colored pigments, as a whole, show poor UV reflectance. Acting as absorbers, they must confine absorption of light by the polymer. However, the absorption spectrum of the colored pigments is unlikely to match the activation spectra maxima of all possible polymers.

Titanium dioxide is the preferred white pigment for plastics [169,170]. The different photoactivity between anatase and rutile crystalline forms, when incorporated into polymers, has been extensively studied [162,167,170-172]. In plastic applications, photochemically inactive rutile forms are usually preferred [97,170]. What is noticeable in this regard is the different UV reflectance that the two crystalline forms have. Although anatase is more photoactive than rutile, it is a better UV reflector [169]. Carbon black is considered one of the most effective pigments in the photostabilization of the polymer [167], besides its ability to efficiently screen the harmful UV-Visible radiation, other positive influences are recognized for this pigment [162,167,173-175].

Considering the mechanism of colorant photodegradation in plastics, a large portion of our knowledge on the factors that govern light-induced fading are owed to the work of Giles et al. [176]. The first paper on the subject only considered the effects of oxygen, water vapor and atmospheric contaminants [177]. Today, the relationship between colorant lightfastness and physical and chemical properties of the colorant system[67] is well-established. External[68] and internal[69] factors to the colored substrate are critical in the lightfastness properties of colorants [155,176].

Most of the knowledge is thanks to Allen [158,159,167,178,179] who provides the first comprehensive review of possible photochemical mechanisms of a large number of dyes. His papers discussed most of the dye classes, which were divided by chromophore type. Follow on reviews [180] and books [155,181,182] integrate new case studies on dyes and pigments.

Oxidation and reduction are proposed as dominant reactions in the photofading mechanism of dyes and their chemical evolution has been principally correlated to singlet oxygen reactions and hydrogen or electron abstraction from the polymer. The experimental results presented in the photodegradation of dyes are based on solution and polymeric material studies. In the experimental setup of exposure, short wavelengths of UV radiation ($\lambda < 300$ nm) frequently were employed as irradiation sources, especially in the earlier studies. However, care must be taken. The purely mechanistic understanding of photochemical reactions in simple model systems (such as solutions) provide useful fundamental knowledge on the photochemistry and degradation pathways of colorants (weaker chemical bonds, more light sensitive structures), but bear little, or may not have, relation to actual practical polymer situations. In fact, the medium (solvents or polymers) and colorants' state of aggregation have an important impact on stability. Considering the radiant energy, high energetic wavelengths ($\lambda < 300$ nm) can produce other disruptive pathways that do not simulate mechanisms that will take place under the near UV or visible ranges (300-800 nm) of chief interest to conservators[70]. Nevertheless, photodecomposition of synthetic dyes has been widely studied and some of its aspects are somewhat clearer

"the efficacy of different spectral regions of a specific source spectrum in causing a photoprocess" [35]. Individual polymers are sensitive to UV radiation (290-400nm) and exhibit activation spectra maxima within specific wavelengths. Selection of UV absorbers should take into account these maxima in order to provide the greatest level of protection [168].

[66] Considering the absorption edge in the reflectance spectra, the UV reflector property stops at 380 nm (zinc oxide), 400 nm (rutile), 370 nm (anatase).

[67] For convenience from this point of the thesis, the term "colorant system" refers to the combination of colorant and its environment (polymer and additives) in the final product.

[68] Spectral distribution of the incident light, atmospheric composition, humidity and temperature are examples of external factors.

[69] Internal factors are all those properties strongly linked with the colorant system such as concentration of the colorant, degree of dye aggregation or pigment particle size, chemical and physical structure of the substrate, and diffusion of volatile substances in the polymeric matrix.

[70] Works of art could be exposed not only to visible light (400-800 nm) but also to UV radiation filtered by glass windows ($\lambda \geqslant 300$ nm) of the sunlight depending on the museum environment and lighting system.

today. Tests of the lightfastness of dyed substrates such as animal- and plant-based fibers (such as cotton, wool, etc.), synthetic polymeric fibers and films (such as polyolefins, polyester, polyamide, acrylic, epoxy, cellulose, polystyrene, etc.) have been conducted pointing out the high complexity of the fading mechanism in polymeric systems. It is clear that different mechanisms of colorant decomposition may govern the fading of the same colorant on different substrates and in the presence of different radiant energies. Experiments on the lightfastness of colorants have been performed using polychromatic light sources such as daylight and unfiltered lamps. Although they better resemble exhibition and storage conditions, their use did not allow for fundamental photochemical research. Experiments on light stability performed with polychromatic light sources and comparative studies of the lightfastness of colorants are all qualitative, even if the experimental protocols and procedures are well-standardized. Results of fundamental photochemical research give both qualitative and quantitative rationalization of the chemical events.

Relatively little is known about the factors that determine the lightfastness of pigments. Most of the studies debate their photoprotector of photocatalyst role in polymer degradation without mentioning their photo-induced degradation mechanisms. Few significant studies on the photofading of pigments in plastics have been found by the author, including ultramarine blue [183], phthalocyanine [184], hydrazone-azo pigments [185-188] and TiO_2-pigment system [189,190]. In the mentioned papers, pigment photofading is solely presented in terms of color change without discussion of their mechanism of degradation. Unfortunately, this is not sufficient in providing a comprehensive insight into the principles of photodegradation of pigments in plastics.

The study of colorant fading in plastics has been predominantly based on empirical evidence without the support of photochemical studies, especially by color technologists [5]. At industrial level, when during product testing fading occurs over light exposure[71], the quick answer is to change the colorants, hoping for better performance. As a result, the chemical reactions that take place are never entirely understood. This is a significant limitation in the colorist's approach and may well explain why the photochemistry of dyed and pigmented polymers was started to be studied relatively late by polymer and color scientists.
In illustrating the problems of organic polymer systems encountered in art conservation, the first work "*Action of light on dyes and pigmented polymers*" on the discoloration issue was presented by Allen in the early 1990s [191]. Unfortunately, the subject has been only recently revalued in conservation science [102-104].
Although our scientific knowledge on dye photodegradation has constantly improved, photofading of pigmented plastics remains a little understood subject to this day. The photochemistry of dyes has captured more attention than pigments, likely due to the intense research activity in discoloration of textiles [180]. As described by Klemchuk, the photochemical behavior of pigments in polymer formulations is a *"tantalizing mystery"* [162]. Among all colorant classes, hydrazone-azo dyes constitute the largest and most varied class of dyestuffs and their polymer photochemistry captured most research activity since the 1980s [158,192]. Concerning hydrazone-azo pigments, a particular challenge is to provide a better understanding of why some orange, yellow, and red organic pigments exhibit poor lightfastness in polymeric systems [4,5,19]. β-naphthol (lake, non-lake forms) and BONA pigments are particularly considered due to their relevance in cultural heritage [193].
Radiation can be used to reproduce natural aging in photoaging experiments. A first comprehension of the photochemical processes in solution would be fundamental because basic knowledge in this area is also lacking. This new knowledge could then be used to plan fading experiments in polymeric media and allow scientific and industry community to gain insight into the degradation mechanisms.

[71] Tests are commonly used in industry to evaluate the characteristics of the plastic products, including its color durability. The fade resistance (ability of the plastic part to resist color change due to effects of irradiation exposure) can be evaluated in laboratory with using different systems (test chambers, fadeometers, etc.) in order to simulate a variety of environments and accelerating conditions.

1.5. References

[1] Melo MJ, Nevin A, Baglioni P. Special issue of pure and applied chemistry devoted to "Chemistry and cultural heritage". Pure Appl Chem. 2018; 90(3): 429-433. DOI: 10.1515/pac-2018-0106.
[2] Webber TG, editor. Coloring of plastics. New York: John Wiley & Sons Inc.; 1979.
[3] Harris RM. Coloring technology for plastics. Norwich: Plastics Design Library; 1999.
[4] Müller A. Coloring of plastics. Munich: Carl Hanser Verlag; 2003.
[5] Charvat RA, editor. Coloring of plastics: fundamentals. New Jersey: John Wiley & Sons Inc., second ed.; 2004.
[6] Christie RM. Pigments for plastics. In: Pritchard G, editor. Plastics additives – An A-Z reference. London: Chapman & Hall; 1998. p. 485-498; and references therein.
[7] Bente LA. Dyes for the mass coloration of plastics. In: Pritchard G, editor. Plastics additives – An A-Z reference. London: Chapman & Hall; 1998. p. 217-225.
[8] Pritchard G. Plastics additives – An A-Z reference. London: Chapman & Hall; 1998.
[9] Hummel DO. Atlas of plastics additives – Analysis by spectrometric methods. Berlin: Springer-Verlag; 2002.
[10] Stepek J, Daoust H. Additives for plastics. New York: Springer Science+Business Media; 1983.
[11] Murphy J. Additives for plastics handbook. Oxford: Elsevier Science, second ed.; 2001.
[12] Seymour RB, editor. Additives for plastics. New York: Academic Press, Vol 1; 1978.
[13] Painter PC, Coleman MM. Processing. In: Essentials of polymer science and engineering. Lancaster: DEStech Publications Inc.; 2009. p. 473-514.
[14] Rosato DV. Plastics processing data handbook. Cambridge: Chapman & Hall, second ed.; 1997.
[15] Muccio EA. Plastic processing technology. ASM International; 1994.
[16] Strong AB. Plastics: materials and processing. USA: Pearson Prentice Hall, third ed.; 2005.
[17] The Colour Index™. colour-index.compublished online by Society of Dyers and Colourists and American Association of Textile Chemists and Colorists.
[18] Society of Dyers and Colorists and American Association of Textile Chemists and Colorists. Color Index international. Bradford: Society of Dyers and Colorists and associates, Heritage ed. on DVD; 2014.
[19] Hunger K, Schmidt MU. Industrial organic pigments: production, crystal structures, properties, applications. Weinheim: Wiley-VCH, fourth completely revised ed.; 2018.
[20] Buxbaum G, Pfaff G, editors. Industrial inorganic pigments. Weinheim: Wiley-VCH, completely revised third ed.; 2005.
[21] Hunger K, editor. Industrial dyes: chemistry, properties, applications. Weinheim: Wiley-VCH; 2003.
[22] Oleari C. Standard colorimetry – Definitions, algorithms and software. Chichester: John Wiley & Sons; 2016.
[23] Nassau K. The physics and chemistry of color – The fifteen causes of color. USA: John Wiley & Sons. 1983.
[24] Valeur B, Berberan-Santos MN. Absorption of ultraviolet, visible, and near-infrared aadiation, in: Molecular fluorescence – Principles and applications. Weinheim: Wiley-VCH, second ed.; 2012. p. 33-52.
[25] Christie RM. The physical and chemical basis of colour. In: Colour chemistry. Cambridge: The Royal Society of Chemistry, second ed.; 2015. p. 21-71.
[26] Zollinger H. Color of organic compounds. In: Color chemistry – Syntheses, properties, and applications of organic dyes and pigments. Weinheim: Wiley-VCH. 2003. p. 15-66.
[27] Gürses A, Açıkyıldız M, Güneş K, Gürses MS. Dyes and pigments: their structure and properties. In: Dyes and pigments. Cham: Springer, SpringerBriefs in Molecular Science; 2016. DOI: 10.1007/978-3-319-33892-7_2.
[28] Tilley RJ. Colors of inorganic compounds. In: Scott RA, editor. Encyclopedia of inorganic and bioinorganic

chemistry; 2020. DOI: 10.1002/9781119951438.eibc2629.
[29] Burns RG. Mineralogical applications of crystal field theory. Cambridge: Cambridge University Press, Vol. 5., second ed.; 1993. DOI: 10.1017/CBO9780511524899.
[30] Brill TB. The origin of color in inorganic compounds. In: Light – Its interaction with art and antiquities. New York: Plenum Press; 1980. p. 197-216.
[31] Van de Hulst HC. Light scattering by small particles. New York: Dover; 1981.
[32] Bohren CF, Huffman DR. Absorption and scattering of light by small particles. New York: Wiley; 1983.
[33] Feller RJ. Color science in the examination of museum objects: nondestructive procedures. USA: The J. Paul Getty Trust; 2001.
[34] Nichols G, Byard S, Bloxham MJ, Botterill J, Dawson NJ, Dennis A, Diart V, North NC, Sherwood JD. A review of the terms agglomerate and aggregate with a recommendation for nomenclature used in powder and particle characterization. J Pharm Sci. 2002; 91(10): 2103-2109. DOI: 10.1002/jps.10191.
[35] Lemaire J, Gardette JL, Lacoste J, Delprat P, Vaillant D. Mechanisms of photooxidation of polyolefins: prediction of lifetime in weathering conditions. In: Clough RL, Billingham NC, Gillen KT, editors. Polymer durability: degradation, stabilization and lifetime predictions. Washington DC: American Chemical Society; 1996. p. 577-598. DOI: 10.1021/ba-1996-0249.ch035.
[36] Andrady AL. Wavelength sensitivity in polymer photodegradation. In: Polymer analysis Polymer physics. Berlin: Springer, Advances in Polymer Science, Vol. 128; 1997. p. 47-94. DOI: 10.1007/3-540-61218-1_6.
[37] Rånby B. Photodegradation and photo-oxidation of synthetic polymers. J Anal Appl Pyrolysis. 1989; 15: 237-247. DOI: 10.1016/0165-2370(89)85037-5.
[38] Muller B. Colorants for thermoplastic polymers. In: Kutz M, editor. Applied plastics engineering handbook. William Andrew Publishing; 2011. p. 435-440. DOI: 10.1016/B978-1-4377-3514-7.10043-1.
[39] Murphy J. Background information: equipment – Mixings compounding, and dosing. In: Additives for plastics handbook. Oxford: Elsevier Science, second ed.; 2001. p. 245-255.
[40] Stepek J, Daoust H. Colorants and brightening. In: Additives for plastics. New York: Springer Science+Business Media; 1983. p. 99-111.
[41] Brydson JA. Plastic materials. London: Butterworth-Heinemann, seventh ed.; 1999.
[42] Pritchard G. Practical methods of mixing additives with polymers. In: Plastics additives – An A-Z reference. London: Chapman & Hall; 1998. p. 16-25.
[43] Colin Williamson, personal communication May 29, 2019.
[44] Quye A, Williamson C, editors. Plastics in context. In: Plastics: collecting and conserving. Edinburg: NMS Publishing Limited; 1999. p. 1-33.
[45] Shashoua Y. Historical development of plastics. In: Conservation of plastics. Oxford: Butterworth-Heinemann; 2008. p. 19-37.
[46] Charvat RA, editor. Coloring of plastics: fundamentals. New Jersey: John Wiley & Sons Inc., second ed.; 2004. p. 98-99.
[47] Sharon B. An introduction to plastics and rubbers in collections. Stud Conserv. 1990; 35(2): 53-63. DOI: 10.1179/sic.1990.35.2.53.
[48] Waentig F. Plastics in art: a study from the conservation point of view. Petersberg: Imhof; 2008.
[49] Callapez ME. Os plásticos em Portugal: a origem da indústria transformadora. Lisbon: Editorial Estampa; 2000.
[50] Grattan DW, editor. Saving the Twentieth century, the conservation of modern materials: proceedings of a conference, Symposium '91, Saving the Twentieth Century, Ottawa, Canada, 15 to 20 September 1991. Ottawa: Canadian Conservation Institute; 1993.
[51] Morgan J. A survey of plastics in historical collections. London: Plastics Historical Society and The Conservation Unit, Museums and Galleries Commission; 1994.
[52] Then E, Oakley V. A survey of plastic objects at the Victoria and Albert Museum. V&A Conservation

Journal 1993; 6: 11-14.
[53] Morgan J. Conservation of plastics: an introduction to their history, manufacture, deterioration, identification and care. London: Plastics Historical Society; 1991.
[54] Allen NS, Edge M, Horie CV, editors. Polymers in conservation. Cambridge: The Royal Society of Chemistry; 1992.
[55] Quye A, Williamson C, editors. Plastics: collecting and conserving. Edinburg: NMS Publishing Limited; 1999.
[56] Winsor P. Conservation of plastic collections. Museums and galleries commission fact sheet. London: Museums and Galleries Commission; 1999.
[57] van Oosten T, Shashoua Y, Waentig F, editors. Plastics in art: history, technology, preservation. Munich: Siegl; 2002.
[58] Hummelen I, Sillé D, editors. Modern Art: Who cares?. Amsterdam: Archetype Publication; 2005.
[59] Chiantore O, Rava A. Conservare l'arte contemporanea. Milano: Electa; 2005.
[60] Shashoua Y. Conservation of plastics. Oxford: Butterworth-Heinemann; 2008.
[61] Keneghan B, Egan L, editors. Plastics: looking at the future and learning from the past. London: Archetype Publications; 2009.
[62] Martuscelli E. The chemistry of degradation and conservation of plastic artefacts. Firenze: Paideia; 2010.
[63] van Oosten T. PUR Facts: conservation of polyurethane foam in art and design. Amsterdam: Amsterdam University Press; 2011.
[64] Martuscelli E. Degradation and preservation of artefacts in synthetic plastics. Firenze: Paideia; 2012.
[65] Verteramo R. The age of plastic. Beni artistici e industriali. Saonara: Il prato; 2013.
[66] Cassese G, editor. The future of the contemporary. Conservation and restoration of design. Naples: PLART; 2015.
[67] Bechthold T, editor. Future Talks 009 – The conservation of modern materials in applied arts and design, 22/23 October 2009. Munich: Die Neue Sammlung – The Design Museum; 2011.
[68] Bechthold T, editor. Future Talks 011 – Technology and conservation of modern Materials in Design. 26/28 October 2011. Munich: Die Neue Sammlung – The Design Museum; 2013.
[69] Bechthold T, editor. Future Talks 013 – Lectures and workshops on technology and conservation of modern materials in design, 23/25 October 2013. Munich: Die Neue Sammlung – The Design Museum; 2015.
[70] Bechthold T, editor. Future Talks 015 – Processes. The making of design and modern Art. Materials, technologies and conservation strategies, Munich, 28/30 October 2015. Munich: Die Neue Sammlung - The Design Museum; 2017.
[71] Bechthold T, editor. Future Talks 017 – The Silver edition. Visions. Innovations in technology and conservation of the modern, 11/13 October 201. Munich: Die Neue Sammlung - The Design Museum; 2019.
[72] Future Talks 019 – Surfaces. Lectures and workshops on technology and conservation of the modern, 11/13 November 2019, Die Neue Sammlung - The Design Museum, Munich. in press
[73] e-plastory (accessed 08.03.2021).
[74] The Plastics Heritage Congress 2019 - History, Limits and Possibilities (accessed 08.03.2021).
[75] Plastics in Peril: Focus on Conservation of Polymeric Materials in Cultural Heritage (accessed 08.03.2021).
[76] Lavédrine B, Fournier A, Martin G, editors. Preservation of Plastic Artefacts in Museum Collections (POPART). Paris: Comité Des Travaux Historiques et Scientifiques (CTHS); 2012.
[77] Quye A, Williamson C, editors. Plastics: collecting and conserving. Edinburg: NMS Publishing Limited; 1999, p. 111.
[78] Inkster I. Highly fraught with good to man: patent organisation, agency, and useful and reliable knowledge in British machinofacture circa 1780-1851 and beyond. In: Inkster I, editor. History of technology. London: Bloomsbury Publishing Plc, Volume 31; 2012. p. 115-144.
[79] Commentary. Anti-Corros Method M. 1962; 9(6): 141-144. DOI: 10.1108/eb019966.

[80] Cecchini C, Petroni M, editors. Plastic Days – Materiali e design. Cinisello Balsamo: Silvana Editoriale; 2015.
[81] Quye A. Quality matters for historical plastics: the past-making of cellulose nitrates for future preservation. In: Teissier P, Mody CMC, Van Tiggelen B, editors. From bench to brand and back: the co-shaping of materials and chemists in the Twentieth century. Nantes: Cahiers Francois Viète; 2017. p. 45-68.
[82] Morgan J. Conservation of plastics: an introduction to their history, manufacture, deterioration, identification and care. London: Plastics Historical Society; 1991.
[83] Williams SR. Care of plastics: malignant plastics. WAAC Newsletter. 2002: 24(1). URL: cool.culturalheritage.org/waac/wn/wn24/wn24-1/wn24-102.html.
[84] Sachs AP, Oscar O. Camphor substitutes in the manufacture of celluloid. J Ind Eng Chem. 1921; 13(10): 893-90. DOI: 10.1021/ie50142a012.
[85] Hainschwang T, Leggio L. The characterization of tortoise shell and its imitations. Gems and Gemology. 2006; 42(1): 36-52. URL: 1615229594-404889908.1613127054.
[86] Greeinsten LM. Nacreous (pearlescent) pigments and interference pigments. In: Lewis PA, editor. Pigment handbook, properties and economics. New York: J. Wiley & Sons, Vol I, second ed.; 1988. p. 829-858.
[87] Quye A, Williamson C, editors. Identifying plastics. In: Plastics: collecting and conserving. Edinburg: NMS Publishing Limited; 1999. p. 54-83.
[88] Shashoua Y. Identification of plastics in collections. In: Conservation of plastics. Oxford: Butterworth-Heinemann; 2008. p. 113-149.
[89] Christensen I. Developments in colorants for plastics. Shawbury: Smithers Rapra Publishing; 2003.
[90] Biber A. Dipping into colours. Studies on the technological collection of plastics samples in the Technical Museum Vienna. In: Bechthold T, editor. Future Talks 015 – Processes. The making of design and modern art. materials, technologies and conservation strategies. Munich: Die Neue Sammlung - The Design Museum; 2017. p. 109-116. and referenced therein.
[91] Krimanm MM, Kriman M. The literature of resins and plastics. In: Gould RF, editor. Literature of chemical technology. Washington DC: American Chemical Society, Advances in Chemistry Series, Vol. 78; 1968. p. 387-399. DOI: 10.1021/ba-1968-0078.ch021.
[92] Fernández-Villa DG, San Andrés Moya M, Blasco S. Industrial development of plastics and 20th-century art: new synergies. In: Eyb-Green S, Townsend JH, Clarke M, Nadolny J, Kroustallis S, editors. The Artist's Process. Technology and Interpretation. London: Archetype Publications; 2012. p. 205-206.
[93] França de Sá S, Marques da Cruz S, Callapez ME, Carvalho V. Plastics that made history – The contribution of conservation science for the history of the Portuguese Plastics Industry. Conservar Património 2020; 35: 85-100. DOI: 10.14568/cp2019017.
[94] França de Sá S. The Portuguese landscape. In: What does the future hold for polyurethane fashion and design? Conservation studies regarding the 1960s and 1970s objects from the MUDE collection. Doctoral dissertation. Lisbon: Universidade Nova de Lisboa, Faculdade de Ciências e Tecnologia; 2017. p. 89-113.
[95] Callapez ME. História do PVC em Portugal: Cires – Um Caso de Sucesso. Lisbon: Escolar Editora; 2010.
[96] S. França de Sá, personal communication September 30, 2020.
[97] Müller A. Colorants for polymer. In: Coloring of plastics. Munich: Carl Hanser Verlag; 2003. p. 61-210
[98] Surgeon P. The environment and government regulations. In: Charvat RA, editor. Coloring of plastics: fundamentals. New Jersey: John Wiley & Sons Inc., second ed.; 2004. p. 358-379.
[99] de Keijzer M. The history of modern synthetic inorganic and organic artists' pigments. In: Mosk JA, Tennant NH, editors. Contributions to conservation: research in conservation at the Netherlands Institute for Cultural Heritage (ICN). London: James and James; 2001. p. 42-54.
[100] de Keijzer M. The delight of modern organic pigment creations. In: van den Berg KJ, Burnstock A, de Keijzer M, Krueger J, Learner T, Tagle A, Heydenreich G, editors. Issues in contemporary oil paint. Cham: Springer International Publishing; 2014. p. 45-73.

[101] Craddock P. Painting. In: Craddock P, editor. Scientific investigation of copies, fakes and forgeries. Oxford: Elsevier; 2008. p. 271-312.
[102] de Groot S, van Keulen H, Megens L, van Oosten T, Wiresma H. Discolouration of Plastics objects: investigation into composition using various analytical techniques. In: Bechthold T, editor. Future Talks 013 – Lectures and workshops on technology and conservation of modern materials in design. Munich: Die Neue Sammlung – The Design Museum; 2015. p. 19-26.
[103] de Groot S, van Keulen H, van den Akker S, van Oosten T. Discoloration of plastics objects: the identification of yellow and orange synthetic pigment in plastic objects. In: Bechthold T, editor. Future Talks 015 – Processes. The making of design and modern art. Materials, technologies and conservation strategies. Munich: Die Neue Sammlung - The Design Museum; 2017. p. 147-158.
[104] Maragno A, Schossler P, Rizzutto M. Challenges in the conservation of synthetic polymers: discolouration of plastic objects. In: Future Talks 019, Munich (Germany), 11-13 November 2019; Oral presentation.
[105] Quye A, Williamson C, editors. Degradation. In: Plastics: collecting and conserving. Edinburg: NMS Publishing Limited; 1999. p. 111-135.
[106] Shashoua Y. Degradation of plastics. In: Conservation of plastics. Oxford: Butterworth-Heinemann; 2008. p. 151-192.
[107] a) Keneghan B, van Oosten T, Laganà A, Wagenaar M, Barabant G, Balcar N, Bluzat H, Bollard C, Fayein J, Kuperholc S, Ramel S, Lattuati-Derieux A. In what condition are my artefacts? Case studies. In: Lavédrine B, Fournier A, Martin G, editors. Preservation of Plastic Artefacts in Museum Collections (POPART). Paris: Comité Des Travaux Historiques Et Scientifiques (CTHS); 2012. p. 109-137; b) Bacci M, Cucci C van Oosten T, Shahoua Y, Rychlý J. Surveying plastic artefacts collections in museums. In: Lavédrine B, Fournier A, Martin G, editors. Preservation of Plastic Artefacts in Museum Collections (POPART). Paris: Comité Des Travaux Historiques Et Scientifiques (CTHS); 2012. p. 139-149.
[108] POPART_List_of_terms (accessed 08.03.2021).
[109] Quye A, Williamson C, editors. Caring for plastics. In: Plastics: collecting and conserving. Edinburg: NMS Publishing Limited; 1999. p. 84-110.
[110] Balcar N, Barabant G, Bollard C, Kuperholc S, Keneghan B, Lagana A, van Oosten T, Segel K, Shashua Y. Studies in cleaning plastic. In: Lavédrine B, Fournier A, Martin G, editors. Preservation of plastic artefacts in museum collections (POPART). Paris: Comité des travaux historiques et scientifiques (CTHS); 2012. p. 225-269.
[111] Shashoua Y, Segel K, van Oosten T, Lagana A, Keneghan B, Barabant G, Bollard C, Kulperholc S. Wiping away the dirt – A safe option for plastics. In: Bridgland J, editor. ICOM-CC 16th Triennial Conference Preprints, Lisbon, 19-23 September 2011. Almada: Critério; 2011.
[112] Fricker AL, McPhail DS, Keneghan B, Pretzel B. Investigating the impact of cleaning treatments on polystyrene using SEM, AFM and ToF-SIMS. Herit Sci. 2017; 5(28): 1-9. DOI: 10.1186/s40494-017-0142-5.
[113] Kavda S, Golfomitsou S, Richardson E. The effect of gelling agents and solvents on PMMA surfaces: a comparative study. In: Angelova LV, Ormsby B, Townsend JH Wolbers R, editors. Gels in the Conservation of Art. London: Archetype Publications Ltd; 2017. p. 331-336.
[114] Kavda S, Richardson E, Golfomitsou S. The use of solvent-gel systems for the cleaning of PMMA. MRS Advances. 2017; 2(39-40): 2179-2187. DOI: 10.1557/adv.2017.249.
[115] Bollard C, Kuperholc S, Balcar N, Barabant G. Effects of cleaning gel systems on plastic. A preliminary study on plasticized poly(vinyl chloride). In: Bechthold T, editor. Future Talks 011 – Technology and conservation of modern materials in design. Munich: Die Neue Sammlung - The Design Museum; 2013. p. 119-126.
[116] Shashoua Y, Alterini M, Pastorelli G, Cone L. From microfibres to nanogels: conservation cleaning of plastics heritage. In: The Plastics Heritage Congress, Lisbon (Portugal), 29-31 May 2019; Oral presentation.
[117] Angelova LV, Sofer G, Bartoletti A, Ormsby BA. Comparative surface cleaning study of Op Structure,

an Op Art PMMA sculpture by Michael Dillon. *Forthcoming*.
[118] McKellar JF, Allen NS. Photochemistry of man-made polymers. London: Applied Science Publishers; 1979.
[119] Allen NS, editor. Degradation and stabilization of polyolefins. London: Applied Science Publishers Ltd.; 1983.
[120] Allen NS, Edge M. Fundamentals of polymer degradation and stabilization. London: Elsevier Applied Science Ltd.; 1992.
[121] Rånby B, Rabek JF. Photodegradation of polymer materials. In: Aggarwal SL, Russo S, editor. Comprehensive polymer science. Oxford: Pergamon Press; 1992. p. 253-283.
[122] Rabek JF. Photodegradation of polymers. In: Mechanisms of photophysical processes and photochemical reactions in polymers. Chichester, England: John Wiley & Sons; 1987. p. 510-20.
[123] Andrady AL. Polymer materials. In: Tevini M, editor. UV-B Radiation and ozone depletion: effects on humans, animals, plants, microorganisms and material. Ann Arbor: Lewis Publishers; 1993. p. 193-227.
[124] Rabek JF. Polymer photodegradation: mechanisms and experimental methods. Dordrecht: Springer Science+Business Media; 1995.
[125] Rabek JF. Photodegradation of polymers: physical characteristics and applications. Berlin: Springer-Verlag; 1996.
[126] Ravve A. Organic reactions of polymers. In: Principles of polymer chemistry. Springer, third ed.; 2000. p. 567-694.
[127] Andrady A.L. Ultraviolet radiation and polymers. In: Mark JE, editor. Physical properties of polymers handbook. New York: Springer; 2007. p. 857-886. DOI: 10.1007/978-0-387-69002-5_51.
[128] Halim Hamid S, editor. Handbook of polymer degradation. Marcel Dekker, second ed.; 2000.
[129] Allen NS. Photochemistry and photophysics of polymer materials. New Jersey: John Wiley & Sons Inc.; 2010.
[130] McNeill IC. Fundamental aspects of polymer degradation. In: Allen NS, Edge M, Horie MV, editors. Polymers in Conservation. Cambridge: Royal Society of Chemistry; 1992.
[131] Wiles DM. Changes in polymeric materials with time. In: Grattan DW, editor. Saving the Twentieth century, the conservation of modern materials: proceedings of a conference, Symposium '91, Saving the Twentieth Century, Ottawa, Canada, 15 to 20 September 1991. Ottawa: Canadian Conservation Institute; 1993. p. 105-112.
[132] May E, Jones M. Plastics. In: May E, Jones M., editors. Conservation Science: heritage materials. Cambridge: Royal Society of Chemistry; 2006. p. 185-211.
[133] Singh B, Sharma N. Mechanistic implications of plastic degradation. Polym Degrad Stab. 2008; 93(3): 561-584. DOI: 10.1016/j.polymdegradstab.2007.11.008.
[134] Rychlý J, Rychlá L. Introduction. In: Lavédrine B, Fournier A, Martin G, editors. Preservation of Plastic Artefacts in Museum Collections (POPART). Paris: Comité Des Travaux Historiques Et Scientifiques (CTHS); 2012. p. 159-160.
[135] Rabek JF. Photodegradation and photo-oxidative degradation of homochain polymers. In: Polymer photodegradation: mechanisms and experimental methods. Dordrecht: Springer Science+Business Media; 1995. p. 67-254.
[136] Rabek JF. Photodegradation and photo-oxidative degradation of heterochain polymers. In: Polymer photodegradation: mechanisms and experimental methods. Dordrecht: Springer Science+Business Media; 1995. p. 255-352.
[137] Rånby B. Basic reactions in the photodegradation of some important polymers. J Macromol Sci A 1993; 30(9-10): 583-594. DOI: 10.1080/10601329308021247.
[138] Fox RB. Photodegradation of high polymers. Prog Polym Sci. 1967; 1: 45-89. DOI: 10.1016/0079-6700(67)90002-0.

[139] Gardette M, Perthue A, Gardette JL, Janecska T, Földes E, Pukánszky B, Therias S. Photo- and thermal-oxidation of polyethylene: comparison of mechanisms and influence of unsaturation content. Polym Degrad Stab. 2013; 98(11): 2383-2390. DOI: 10.1016/j.polymdegradstab.2013.07.017.
[140] Philippart JL, Sinturel C, Arnaud R, Gardette JL. Influence of the exposure parameters on the mechanism of photooxidation of polypropylene. Polym Degrad Stab. 1999; 64(2): 213-225. DOI: 10.1016/S0141-3910(98)00191-8.
[141] Gardette JL, Mailhot B, Lemaire J. Photooxidation mechanisms of styrenic polymers. Polym Degrad Stab. 1995; 48(3): 457-470. DOI: 10.1016/0141-3910(95)00113-Z.
[142] Yousif E, Haddad R. Photodegradation and photostabilization of polymers, especially polystyrene: review. SpringerPlus 2013; 2(398): 1-32. DOI: 10.1186%2F2193-1801-2-398.
[143] Siampiringue N, Leca JP, Lemaire J. Mecanismes de photo-oxydation du poly(methacrylate de methyle). Eur Polym J. 1991; 27(7): 633-641. DOI: 10.1016/0014-3057(91)90148-H.
[144] Torikai A, Ohno M, Fueki K. Photodegradation of poly(methyl methacrylate) by monochromatic light: quantum yield, effect of wavelengths, and light intensity. J Appl Polym Sci. 1990; 41: 1023-1032. DOI: 10.1002/app.1990.070410513.
[145] Yousif E, Hasan A. Photostabilization of poly(vinyl chloride) – Still on the run. J Taibah Univ Sci. 2015; 9(4): 421-448. DOI: 10.1016/j.jtusci.2014.09.007.
[146] Decker C. Photodegradation of PVC. In: Owen ED, editor. Degradation and stabilisation of PVC. Dordrecht: Springer; 1984. DOI: 10.1007/978-94-009-5618-6_3.
[147] Jouan X, Gardette JL. Photo-oxidation of ABS: Part 2 – Origin of the photodiscoloration on irradiation at long wavelengths. Polym Degrad Stab. 1992; 36(1): 91-96. DOI: 10.1016/0141-3910(92)90054-9.
[148] Piton M, Rivaton A. Photo-oxidation of ABS at long wavelengths ($\lambda > 300$ nm). Polym Degrad Stab. 1997; 55(2): 147-157. DOI: 10.1016/S0141-3910(96)00116-4.
[149] Thapliyal BP, Chandra R. Advances in photodegradation and stabilization of polyurethanes. Prog Polym Sci. 1990; 15(5): 735-750. DOI: 10.1016/0079-6700(90)90010-X.
[150] Wilhelm C, Gardette JL. Infrared analysis of the photochemical behaviour of segmented polyurethanes: aliphatic poly(ether-urethane)s. Polymer 1998; 39(24): 5973-5980. DOI: 10.1016/S0032-3861(97)10065-9.
[151] Newman CR, Forciniti D. Modeling the ultraviolet photodegradation of rigid polyurethane foams. Ind Eng Chem Res. 2001; 40(15): 3346-3352. DOI: 10.1021/ie0009738.
[152] Rosu D, Rosu L, Cascaval CN. IR-change and yellowing of polyurethane as a result of UV irradiation. Polym Degrad Stab. 2009; 94(4): 591-596. DOI: 10.1016/j.polymdegradstab.2009.01.013.
[153] Scott G. Some fundamental aspects of the photooxidation and stabilisation of polymers. Br Polym J. 1984; 16(4): 271-283. DOI: 10.1002/pi.4980160421.
[154] Pospíšil J, Pilař J, Billingham NC, Marek A, Horak Z, Nešpůrek S. Factors affecting accelerated testing of polymer photostability. Polym Degrad Stab. 2006; 91(3): 417-422. DOI: 10.1016/j.polymdegradstab.2005.01.049.
[155] Zollinger H. Photo-, Thermo-, and electrochemical reactions of colorants. In: Color chemistry: syntheses, properties, and applications of organic dyes and pigments. Zürich: Wiley-VCH; 2003. p. 429-504.
[156] Moura JCVP, Oliveira-Campos AMF, Griffiths J. The effect of additives on the photostability of dyed polymers. Dyes Pigm. 1997; 33(3): 173-196. DOI: 10.1016/S0143-7208(96)00050-2.
[157] Egerton GS, Morgan AG. The photochemistry of dyes. IV – The role of singlet oxygen and hydrogen peroxide in photosensitised degradation of polymers. J Soc Dye Colour. 1971; 87: 268-277. DOI: 10.1111/j.1478-4408.1971.tb03027.x.
[158] Allen NS, McKellar JF, editors. Photochemistry of dyed and pigmented polymers. London: Applied Science; 1980.
[159] Allen NS. 20 – Effects of dyes and pigments. In: Allen G, Bevington JC, editors. Comprehensive polymer science and supplements. Pergamon Press Plc.; Vol 6; 1989. p. 579-595. DOI: 10.1016/B978-0-08-096701-

1.00200-7.
[160] Allen NS, Edge M. Effects of dyes and pigments. In: Fundamentals of polymer degradation and stabilization. London: Elsevier Applied Science Ltd.; 1992. p. 149-175.
[161] Norman NS, Edge M, Corrales T, Childs A, Liauw CM, Catalina F, Peinado C, Minihan A, Aldcroft D. Ageing and stabilisation of filled polymers: an overview. Polym Degrad Stab. 1998; 61(2): 183-199. DOI: 10.1016/S0141-3910(97)00114-6.
[162] Klemchuk PP. Influence of pigments on the light stability of polymers: a critical review. Polymer Photochemistry 1983; 3(1): 1-27. DOI: 10.1016/0144-2880(83)90042-8.
[163] Steinlin F, Saar W. Influence of pigments on the degradation of polypropylene fibers on exposure to light and weather. Melliand Textil Int. 1980; 61(11): 941-945.
[164] a) Egerton GS. The action of light on dyed and undyed cotton. J Soc Dye Colour. 1947; 63(6): 161-171. DOI: 10.1111/j.1478-4408.1947.tb02464.x. b) Egerton GS. The mechanism of the photochemical degradation of textile material. J Soc Dye Colour. 1949; 65: 764-780. DOI: 10.1111/j.1478-4408.1949.tb02558.x. c) Egerton GS. Action of light on dyes in polymer materials. Br Polym J. 1971; 3: 63-67. DOI: 10.1002/pi.4980030203. d) Egerton GS, Morgan AG. The photochemistry of dyes. J Soc Dye Colour. 1970; 86: 79-83. DOI: 10.1111/j.1478-4408.1970.tb02938.x. e) Egerton GS, Morgan AG. The photochemistry of dyes II – Some aspects of the fading Process. J Soc Dye Colour. 1970; 86: 242-249. DOI: 10.1111/j.1478-4408.1970.tb02954.x. f) Egerton GS, Morgan AG. The Photochemistry of dyes. III – Some general processes and techniques. J Soc Dye Colour. 1971; 87: 223-228. DOI: 10.1111/j.1478-4408.1971.tb03022.x. g) Egerton GS, Morgan AG. The photochemistry of dyes. IV – The role of singlet oxygen and hydrogen peroxide in photosensitised degradation of polymers. J Soc Dye Colour. 1971; 87: 268-277. DOI: 10.1111/j.1478-4408.1971.tb03027.x.
[165] a) Bamford CH, Dewar MJS. Photosensitisation and tendering by vat dyes. J Soc Dye Colour. 1949; 65: 674-681. DOI: 10.1111/j.1478-4408.1949.tb02544.x. b) Bamford CH, Dewar MJS. Photosensitization by vat dyes. Nature 1949; 163: 214. DOI: 10.1038/163214a0. c) Bamford CH, Dewar MJS. The autoxidation of tetralin. Proc R Soc A 1949; 198(1053): 252-267. DOI: 10.1098/rspa.1949.0099.
[166] a) Moran JJ, Stonehill HI. Fading and tendering activity in anthraquinonoid vat dyes. Part I. Electronic absorption spectra of dye solutions. J Chem Soc. 1957: 765-778. DOI: 10.1039/JR9570000765. b) Moran JJ, Stonehill HI. Fading and tendering activity in anthraquinonoid vat dyes. Part II. Fluorescence, absorption spectra, and stability to light of dyed films. J Chem Soc. 1957: 779-788. DOI: 10.1039/JR9570000779. c) Moran JJ, Stonehill HI. Fading and tendering activity in anthraquinonoid vat dyes. Part III. Free-radical production and probable reaction mechanisms. J Chem Soc. 1957: 788-795. DOI: 10.1039/JR9570000788.
[167] Allen NS. Photofading and light stability of dyed and pigmented polymers. Polym Degrad Stab. 1994; 44(3): 357-374. DOI: 10.1016/0141-3910(94)90095-7.
[168] Hawkins WL. Polymer degradation. In: Polymer degradation and stabilization. Berlin: Springer-Verlag; 1984. p. 3-34.
[169] Komar LC. Pigmentation of white plastics. In: Patton TC, editor. Pigment handbook, applications and markets. New York: J. Wiley & Sons, Vol II, second ed.; 1988. p. 253-276
[170] Holtzen DA, Reid AH. Titanium dioxide pigments. In: Charvat RA, editor. Coloring of plastics: fundamentals. New Jersey: John Wiley & Sons Inc., second ed.; 2004. p. 146-158.
[171] Allen NS, McKellar JF. Photosensitized degradation of polymers by dyes and pigments. In: Allen NS, McKellar JF, editors. Photochemistry of dyed and pigmented polymers. London: Applied Science; 1980. p. 247-278.
[172] Day RE. The role of titanium dioxide pigments in the degradation and stabilisation of polymers in the plastics industry. Polym Degrad Stab. 1990; 29(1): 73-92. DOI: 10.1016/0141-3910(90)90023-Z.
[173] Story WS. Pigmentation of black plastics. In: Patton TC, editor. Pigment handbook, applications and markets. New York: J. Wiley & Sons, Vol II, second ed.; 1988. p. 287-290
[174] Brewer SA. Carbon black pigments for plastics. In: Charvat RA, editor. Coloring of plastics: fundamen-

tals. New Jersey: John Wiley & Sons Inc., second ed.; 2004. p. 159-174.
[175] Allen NS, Pena JM, Edge M, Liauw CM. Behaviour of carbon black pigments as excited state quenchers in LDPE. Polym Degrad Stab. 2000; 67(3): 563-566. DOI: 10.1016/S0141-3910(99)00150-0.
[176] Giles CH, Forrester SD. Physical factors affecting the light stability of dyes and pigmented polymers. In: Allen NS, McKellar JF, editors. Photochemistry of dyed and pigmented polymers. London: Applied Science; 1980. p. 51-91.
[177] Egerton GS. Action of light on dyes in polymer materials. Br Polym J. 1971; 3: 63-67. DOI: 10.1002/pi.4980030203
[178] Allen NS. Photofading mechanisms of dyes in solution and polymer media. Rev Prog Coloration 1987; 17(1): 61-71. DOI: 10.1111/j.1478-4408.1987.tb03752.x.
[179] Allen NS, Edge M. Lightfastness of dyes and pigments. In: Fundamentals of polymer degradation and stabilization. London: Elsevier Applied Science Ltd.; 1992. p. 176-193.
[180] Feller RL. Accelerated aging: photochemical and thermal Aspects. Michigan: The J. Paul Getty Trust; 1994.
[181] Kuramoto K. The photodegradation of synthetic colorants. In: Peters AT, Freeman HS, editors. Physico-chemical principles of color chemistry. London: Chapman & Hall, Advances in Color Chemistry Series , Vol. 4; 1996. p. 196-244.
[182] Schaeffer TT. Effects of light on materials in collections – Data on photoflash and related sources. Los Angeles: The J. Paul Getty Trust; 2001.
[183] Factor A, Tomaja DL, Chu ML. The effect of molding conditions on resin, colorant, stabilizer interactions in bisphenol – A polycarbonate containing ultramarine pigments. Angew Makromol Chem. 1998; 261-262(1): 55-64. DOI: 10.1002/(SICI)1522-9505(19981201)261-262:1<55::AID-APMC55>3.0.CO;2-U.
[184] Saron C, Zulli F, Giordano M, Felisberti MI. Influence of copper-phthalocyanine on the photodegradation of polycarbonate. Polym Degrad Stab. 2006; 91(2): 3301-3311. DOI: 10.1016/j.polymdegradstab.2006.06.004.
[185] Mallet VN, Newbold BT. Fading of phenylazo-β-naphthol dyes on polypropylene. J Soc Dye Colour. 1974; 90(1): 4-7. DOI: 10.1111/j.1478-4408.1974.tb03167.x.
[186] Hafner O. Lightfastness of organic pigments as a function of their particle size distribution. J. Paint Technol. 1975; 47: 64-69.
[187] Saron C, Felisberti MI, Zulli F, Giordano M. Influence of diazo pigment on polycarbonate photodegradation. J Appl Polym Sci. 2008; 107: 1071-1079. DOI: 10.1002/app.27055.
[188] de Freitas Brito Cavalcanti RS, Silveira Rabello M. The effect of red pigment and photo stabilizers on the photo degradation of polypropylene Films. Mater Res. 2019; 22(3): e20180708. DOI: 10.1590/1980-5373-mr-2018-0708.
[189] Okamoto S, Ohya-Nishiguchi H. Fading mechanism of paint films composed of insoluble azo pigment and titanium dioxide. Bull Chem Soc Jpn. 1990; 63(8): 2346-2351. DOI: 10.1246/bcsj.63.2346.
[190] Shang J, Chai M, Zhu Y. Photocatalytic degradation of polystyrene plastic under fluorescent light. Environ Sci Technol. 2003; 37(19): 4494-4499. DOI: 10.1021/es0209464.
[191] Allen NS. Action of light on dyes and pigmented polymers. In: Allen NS, Edge M, Horie CV, editors. Polymers in conservation. Cambridge: The Royal Society of Chemistry; 1992. p. 193-213.
[192] Griffiths J. Solution and polymer photochemistry of azo dyes and related compounds. In: Allen NS, editor. Developments in polymer photochemistry. London: Applied Science Publishers, Vol 1; 1980. p. 145-190.
[193] Berrie BH, Lomax SQ. Azo pigments: their history, synthesis, properties, and use in artists' materials. Studies in the History of Art 1997; 57: 8-33. URL: jstor.org/stable/42622254.

2. Research aim and methodology

The available literature on the history of plastics and studies of the cultural plastic collections worldwide is increasing. Nevertheless, the Portuguese panorama is still poorly known [1].
The origin of the Portuguese plastic industry is placed in the 1930s [2] and since the beginning it has been focused as an *"indústria transformadora dos plásticos"*[1] for thermoplastics. PE, PP, PMMA, PS and other thermoplastics can be found in the national collections in various shapes, sizes, and color appearances.
Studies on Portuguese cultural plastics are scarce and no information is available concerning the colorants used as coloring agents. Also, their color stability has never been studied.

The purpose of this thesis is to investigate the color appearance in plastic artifacts gathered from Portuguese collections, focusing on the colorants and their alteration. Rigid three-dimensional plastics from artworks, industrial and social heritage collections were selected for this research in an attempt to fill the gaps of knowledge on their cultural material. This will allow covering most, if not all, the possible types of artifacts found in the Portuguese context.
Some of the plastic objects that were included in this research work show color changes as symptom of degradation (i.e. fading and yellowing), a situation that makes the identification and degradation study of the colorants imperative for their preventive conservation.

For studying the color appearance, the identification of colorants in plastics is the first logical step.
The characterization of the formulation's components is a routine task for the plastic industry, and to this end, *deformulation analysis*[2] is commonly employed. A conventional extraction method needs from hundreds of milligrams to tens of grams of plastic sample [3]. Analytical methods convenient for in situ analysis are usually preferred in art conservation science. Even if conservation scientists have access to sampling analytical techniques, they usually require a minimum amount of sample (e.g. 1-200 μg, micro-samples). In contrast to industrial protocols, sampling is inappropriate within plastic heritage collections. Plastic objects vary significantly in shape, size and fragility, and thus in situ and rapid approaches are increasingly demanded for their study, although often, these approaches are less specific than destructive testing.
The particles that characterize the pigments and their individual and agglomerate sizes (tens to few microns) justify the use of in situ analytical methods for their study. Those coupled with optical microscopy, or capable of measuring small spot size, allow for the observation and characterization of such pigments. Although pigments are usually used in very small concentrations, their scattering power encourages the application of techniques working in reflectance mode. Thus, pigments are good candidates for testing in situ approaches.
The study of dyes in plastics represents a different challenge in research, which is not covered in the present thesis. The fact that dyes are dissolved in the polymeric matrix raises the analytical degree of difficulty. Firstly, the use microscope- or imaging-based techniques is meaningless; secondly, the identification of dyes would imply testing of extraction/deformulation methods which are out of the scope of an in situ approach.

This first steps taken in pigment identification further supported the investigation of the faded plastic artifacts available for this research, providing new insight into the photosensitive pigments.

[1] "plastic processing industry".
[2] Polymer/additives deformulation is attempting to "reverse engineer" an existing product. It consists of a sequence of analytical instrumental techniques and extraction methods strategically designed to identify and quantify the ingredients in a plastic formulation. This implies the identification of the major component of the mixture (polymer) and of unknown additive package [3].

Among the pigments identified in the historical plastics, organic pigment lakes based on β-naphthol (2-naphthol) were found degraded, resulting in the color fading of the objects.
β-naphthol reds[3] are the most extensive family of organic red pigments [5-8] and their impact in the plastic coloring industry is well known [4,5,9,10][4]. Used as coloring agents for printing inks, paints, and artists' colors from the beginning of the 20th century, problems related to their lightfastness in historical collections are well documented [15-18], including in plastics [19]. Unfortunately, little is known about their photochemical behavior resulting in a general lack of knowledge of the chemistry of these species in modern/contemporary heritage. Their fading in the historical plastic collections is a conservation issue that until now has not been deeply studied.

It was within this framework that the research work was planned to fulfill the following objectives:

1. develop an innovative multi-analytical approach based on spectroscopic techniques for the in situ characterization of pigments,

2. study the lightfastness of β-naphthol reds and their fading in historical plastics.

As the pigments are intrinsic elements of the whole formulation, they were studied as part of plastic system, and in relation to its components. As such, the whole plastic's formulation was included in the research (i.e. polymers, fillers and other additives), this not only because it defines the color appearance (Section **1.1.2**), but also because it strongly influences the light stability of colorants (**Section 1.1.3** and **1.4.3**). The results of research of points 1 and 2 are presented, respectively, in **Part II** and **Part III** of this work.

This thesis is presented as compendium of research papers that originate from the work done by the author in the last four years. The presented research is split into seven chapters, each one corresponding to a published or forthcoming scientific article. **Part II** is constituted by **Chapters 3** to **6** while **Chapters 7** to **9** appear in **Part III**. The chapter order is based on two main points: i) the methodology of research and the logical sequence of the results, ii) advances made during the research work and the growing insight into the in situ identification methods of pigments in plastics and light stability of β-naphthol reds.

The research presented in **Part II** is focused on the development of innovative multi-technique approaches for the in situ characterization of the plastic formulation's components. **Chapter 3** is based on the identification of polymers and **Chapter 4** to **6** are focused on the study of pigments and other additives (e.g. fillers).

The study of polymers in plastics is a widely debated subject in the cultural heritage field, and both in situ and micro-sampling methods can be used to this end. Fourier transform infrared (FTIR) spectroscopy is probably the most well-established method in polymeric material analysis [20-23]. Within IR techniques, FTIR reflectance spectroscopy has found an increasing application in the survey of plastic heritage collections thanks to the development of portable instruments which allow rapid, in situ and contactless measurements [24-26]. While for the analysis of other materials found in artworks the use of FTIR reflectance devices is better understood [27-31], its application in the study of historical plastics needs further investigation. Complex IR signals are usually acquired in reflectance mode and the interpretation of reflectance spectra can be a difficult task as IR bands may be affected by distortions. Also, a drawback can be the lack of an extensive and readily available spectral databases for plastic characterization.

[3] This definition is retained throughout this dissertation and comprises hydrazone-azo pigments based on 1-arylazo-2-naphthol skeletal structure. This includes β-naphthol lake and non-lake pigments, and beta-oxynaphthoic acid (BONA)-based pigment lakes [4].

[4] β-naphthol pigments are one of the oldest groups of synthetic colorants and were one of the first molecules to be used in the coloring of plastics [5,6]. Later, the lake forms found application in the plastic industry and replaced the non-lake β-naphthol compounds, being characterized by higher migration resistance and good color strength [11-14].

In **Chapter 3**, a new insight into the analytical applications of FTIR reflectance spectroscopy in identifying polymers in cultural heritage collections is presented. This study was aimed at comparing two portable mid-IR devices, working in external reflection (ER-FTIR) and in diffuse reflection (DRIFT), for the analysis of plastics. The instrument performance of the two systems was systematically evaluated on a set of polymeric references, everyday and historical object from the Portuguese context. The spectral features were discussed in light of the two different optical geometries and analytes' properties.

Studies on the colorants in plastics are rare in cultural heritage [32]. Few works treat analytically the issue of the identification of pigments in plastics [19,33,34] and when results are presented, they are secondary to the investigation's purpose and sometimes presented without detail [35-39].
In the multi-analytical method proposed by de Groot et al. [19,33], FTIR and X-ray diffraction (XRD) were not suitable for the identification of low pigment concentrations, while X-ray fluorescence spectrometry (XRF) and scanning electron microscopy with energy-dispersive X-ray spectroscopy (SEM-EDX), gave a reliable indication of elemental composition of inorganic pigments and fillers. Although Raman microscopy (μ-Raman) provided identification of the organic pigments in some cases, pyrolysis-gas chromatography/mass spectrometry (Py-GC/MS) was adopted for precise identification, that requiring micro-sampling.
Summing up, in situ identification of pigments in historical plastics is an analytical challenge which, in heritage science, has not been systematically faced yet. As pigments can degrade, the testing of novel multi-technique approaches is a strongly demanding task and the present thesis is intent on this goal.
Organic and inorganic pigments display different features, including the particle size, tendency to form agglomerates and scattering power. Specialty pigments (e.g. metallic and pearlescent) have specific particle shapes, depending on the special effects that are aimed to produce. The characterization of pigments proposed in the **Chapters 4** to **6**, covers all categories of pigments used in the coloring of plastics, such as specialty, conventional inorganic and organic. This allows the assay of multi-analytical spectroscopic methods in the study of all pigment sorts.

At the beginning of the 20th century, it was noticeable the increasing demand of materials capable of imitating luxury materials such as mother of pearl. Thus, synthetic pearlescent pigments have found widespread application in many fields of the plastic industry and today, many artifacts containing those specialty pigments are displayed in museum and collections [40]. Used to simulate pearlescence, they have been employed in the production of artificial pearls, bijouterie, and acrylic and polyester buttons during the 20th century by the Portuguese industry. Besides the use of pearlescent pigments in the production of everyday objects, lustrous plastics have been found attractive by the artists, possibly due to their specific visual effect.
In **Chapter 4** a material study of five lustrous acrylic sheets, found in the studio of the artist Ângelo de Sousa (1938-2011)[5] is presented. These acrylic sheets were likely purchased by the artist from a small Portuguese company and used to produce a series of three-dimensional sculptures. The variety of the pearlescent pigments is not known, and attention must be given to them as they can be susceptible to degradation which will affect the sculpture's appearance. The objective of this work was to characterize the pearlescent pigments responsible for the lustrous effect of the acrylic sheets. To avoid sampling, several in situ spectroscopic techniques were used. The integration of the results drove to the characterization of the formulation's components of the acrylic sheets. The identification of the pearlescent pigments not only will lead to better informed strategies for the preservation of Ângelo's plastic sculptures, but also integrate the coloring technology literature which generalizes about the crystalline forms of possible luster pigments.

Cadmium-based pigments have been widely used for most plastic formulations due to their extraordinary performance properties [9,10,42]. From the 1950s, they started to appear in almost all colorists' palettes for plastic coloring [43]. Cadmium pigments are not identified by a fixed chemical formula. Solid solutions of

[5]For more details on the artist and his activity consider reference [41].

various composition (containing e.g., cadmium, sulfur, zinc, selenium, mercury) are available, tuning the color from yellow to deep brown hues. Their deep characterization implies the determination of the solid solution stoichiometry. The extrapolation of the elemental molar fractions of powder Cd-pigments with spectroscopic methods has already been successfully achieved [44,45]. However, their characterization by using in situ approaches in plastics can pose new challenges.
The research presented in **Chapter 5** was aimed at testing a novel multi-analytical spectroscopic approach for the in situ characterization of cadmium-based pigments in historical plastics. As methodology, all samples were analyzed with the same spectroscopic techniques, and their results compared to assess the differences in the elemental composition and stoichiometry of the pigments. The sample set included eighteen colored acrylic samples produced in the second half of the 20th century. in Portugal by the company *Plásticos do Sado*[6]. The colored acrylics covered almost all possible colors obtainable with cadmium-based pigments. This allowed the application of the new multi-analytical methodology on a wide range of cadmium-pigment compositions.

The research project *"The Triumph of Bakelite – Contributions for a History of Plastics in Portugal"*[7] [46] made available for study over two hundred historical plastic objects produced in Portugal. The objects cover all the color spectrum, but within those, fading was visible in some of the red plastic pieces. Under optical microscopy, a particulate material still red was observed. This suggests the use of pigments in their formulation. In plastic applications, inorganic and organic pigments are characterized by different lightfastness properties (**Section 1.1.3**). Both inorganic and organic pigments could have been used as colorings agents for the red plastics. The identification of the red pigments responsible for the color can contribute new information regarding technology and the history of the Portuguese plastics industry and insight into the fading phenomena. In **Chapter 6**, the results of the material study conducted on a selection of faded and non-faded historical objects gathered within the project is presented. This work intended to develop a new in situ multi-analytical protocol for the distinction of inorganic and organic pigments in historical plastics. Additionally, it aimed at the identification of the faded pigments. β-naphthol Lake Red C pigment (C.I. Pigment Red 53, C.I. n. 15585) was emphasized as photosensitive. Together with the identification of BONA Permanent Red 2B pigment (C.I. Pigment Red 48, C.I. n. 15865) as a faded colorant in a historical plastic object [19], the research work highlights the conservation problems of β-naphthol based pigments fading in plastics collections.

Photochemistry and photophysics studies are essential for understanding the color changes that occur in works of art. Color change of plastics is usually caused by prolonged exposure to harmful radiation (mainly near UV), and other materials found in artworks can share the same fate. While photophysics deals with the photoexcitation and any subsequent physical event, photochemistry explains the reactions caused by radiant energy. Both disciplines would support the understanding of the complex physical and chemical events in the excited states. Their importance in studying the color change in works of art is summarized in **Chapter 7**, reviewing the most relevant analytical investigations on the subject. Encompassing inorganic pigments and dyes, their photodegradation processes and chemistry of the excited states were presented.
This introductory chapter opens **Part III** which is dedicated to the photodegradation studies.

Information on β-naphthol reds in museum and historical collections is strongly in demand because of the color change to which cultural heritage objects, including plastics, are already susceptible.
The comprehension of the fundamental chemistry of light sensitive β-naphthol reds is critical, especially as much of their photochemical behavior is unclear. In fact, their photochemical stability and degradation mechanisms are still not thoroughly understood in heritage science.

[6] *Plásticos do Sado* was a small Portuguese company that produced acrylic sheets from c.1959-1960 until the beginning of the 21st century. For more details on its history and production see reference [38].
[7] The Triumph of Bakelite – Contributions for a History of Plastics in Portugal was a 36-month research project (2016-2018) funded by Fundação para a Ciência e Tecnologia (grant number PTDC/IVC-HFC/5174/2014); http://plasticos.ciuhct.org/ (accessed 02.02.2021).

In **Chapter 8**, the photostability and degradation mechanisms of β-naphthol reds and parent dyes molecules are reviewed. The first attempt of this work was to clarify their structures, which have been erroneously reported in the cultural heritage field. This new fundamental knowledge opens new perspectives in the comprehension of their chemistry. Calculation of the quantum yields of photodegradation (Φ_R) and accelerated photo aging experiments ($\lambda_{irr} \geqslant 300$ nm) of a selection of β-naphthol-based colorants were included to investigate their light-induced degradation. This was meant to lead to a better grasp of the photochemistry of these organic reds. The colorants were strategically chosen including β-naphthol lake and non-lake pigments, BONA pigments and parent dyes molecules, which share the 1-arylazo-2-naphthol skeletal structure. The study of parent molecules is a conceptual key to understand the photochemistry of the organic red pigments. As already state in **Section 1.4.3**, the insight into the fundamental photochemistry of these organic reds in homogenous media will help to comprehend the photodegradation and predict resulting color change in more complex systems, such as plastics.

Among the case studies treated in **Part II**, color fading was only observed in the red historical objects of **Chapter 6**. Thanks to the pigment characterization in the faded objects and literature data [19], the poor lightfastness of β-naphthol based pigments in plastics is acknowledged.
The plastic system could have played a role in the photo fading mechanism. The understanding of its influence on the degradation of the pigment lakes can add to the research on the color change of the historical objects. To this end, historical plastic samples containing the two organic pigment lakes (PR 48 and PR 53) were selected and artificially aged using xenon source ($\lambda_{irr} \geqslant 300$ nm). The results of the photo-aging experiment are discussed in **Chapter 9**. The rationale of this work was to provide a better understanding of the contribution of polymer and organic pigments photodegradation to the discoloration of the historical samples, with special emphasis on the fading of the β-naphthol pigment lakes. Neat PR 48:2 and PR 53:1 powder pigments and polymer references were included in the aging experiment. This allowed the study of the individual susceptibility of the organic pigment lakes and polymer to photooxidation and their combined effect on the historical plastic formulation. This newfound knowledge on the photochemistry of β-naphthol reds of **Chapter 8** supported the discussion of the light-induced changes of PR 48 and PR 53.
Relevant conclusions on the photodegradation of PR 48:2 and PR 53:1 considering the effect of the polymeric matrix (functioning as a binder) were made. No works are known or have been found to the best of the author's knowledge, discussing the relation between the polymer system and the fading of β-naphthol pigment lakes in cultural heritage plastics. The results obtained and methodology of research adopted in this work can inspire further photoaging studies.

2.1. References

[1] França de Sá S, Marques da Cruz S, Callapez ME, Carvalho V. Plastics that made history – The contribution of conservation science for the history of the Portuguese Plastics Industry. Conservar Património 2020; 35: 85-100. DOI: 10.14568/cp2019017.
[2] Callapez ME. Os plásticos em Portugal: a origem da indústria transformadora. Lisbon: Editorial Estampa; 2000.
[3] Bart JCJ. Additives in polymers – Industrial analysis and applications. Chichester: John Wiley & Sons Ltd; 2005.
[4] Hunger K, Schmidt MU. Industrial organic pigments: production, crystal structures, properties, applications. Weinheim: Wiley-VCH, fourth completely revised ed.; 2018.
[5] Society of Dyers and Colorists and American Association of Textile Chemists and Colorists. Color Index international. Bradford: Society of Dyers and Colorists and associates, Heritage ed. on DVD; 2014.
[6] Berrie BH, Lomax SQ. Azo pigments: their history, synthesis, properties, and use in artists' materials.

Studies in the History of Art 1997; 57: 8-33. URL: jstor.org/stable/42622254
[7] Lomax SQ, Learner T. A review of the classes, structures, and methods of analysis of synthetic organic pigments. J Am Inst Conserv. 2006; 45(2): 107-125. DOI: 10.1179/019713606806112540.
[8] de Keijzer M. A survey of red and yellow modern synthetic organic artists' pigments discovered in the 20th century and used in oil colours. In: Bridgland J, Brown J, editors. ICOM-CC 12th Triennial Conference Preprints, Lyon, 29 August - 3 September 1999. London: James and James (Science Publishers), Vol. I; 1999. p. 369-374.
[9] Müller A. Coloring of plastics. Munich: Carl Hanser Verlag; 2003.
[10] Charvat RA, editor. Coloring of plastics: fundamentals. New Jersey: John Wiley & Sons Inc., second ed.; 2004.
[11] Lewis PA, editor. Pigment handbook, properties and economics. New York: J. Wiley & Sons, Vol I, second ed.; 1988.
[12] Herbst W, Hunger K. Azo pigments. In: Industrial organic pigments. Weinheim: Wiley-VCH, third completely revised ed.; 2004. p. 184-421.
[13] Kaul BL. Coloration of plastics using organic pigments. Rev Prog Color Relat Top. 1993; 23: 19-35. DOI: 10.1111/j.1478-4408.1993.tb00093.x.
[14] Christie RM. Pigments, dyes and fluorescent brightening agents for plastics: an overview. Polym Int. 1994; 34: 351-361. DOI: 10.1002/pi.1994.210340401.
[15] Wise D, Wise A. Application of Raman microspectroscopy to problems in the conservation, authentication and display of fragile works of art on paper. J. Raman Spectrosc. 2004; 35: 710-718. DOI: 10.1002/jrs.1213.
[16] Hensick T, Whitmore P. Rothko's Harvard Murals. In: Cohn MB, editor. Mark Rothko's Harvard Murals. Cambridge: Harvard University Art Museums; 1988, p. 15-30.
[17] Standeven HAL. The history and manufacture of lithol red, a pigment used by Mark Rothko in his Seagram and Harvard Murals of the 1950s and 1960s. Tate Papers 2008; 10.
[18] Stenger J, Khandekar N, Wilker A, Kallsen K, Kirby DP, Eremin K. The making of Mark Rothko's Harvard Murals. Stud Conserv. 2016; 61(6): 331-347. DOI: 10.1179/2047058415Y.0000000009.
[19] de Groot S, van Keulen H, Megens L, van Oosten T, Wiresma H. Discolouration of Plastics objects: investigation into composition using various analytical techniques. In: Bechthold T, editor. Future Talks 013 – Lectures and workshops on technology and conservation of modern materials in design. Munich: Die Neue Sammlung – The Design Museum; 2015. p. 19-26.
[20] Lavédrine B, Fournier A, Martin G, editors. Preservation of Plastic Artefacts in Museum Collections (POPART). Paris: Comité Des Travaux Historiques et Scientifiques (CTHS); 2012.
[21] Quye A, Williamson C, editors. Identifying plastics. In: Plastics: collecting and conserving. Edinburg: NMS Publishing Limited; 1999. p. 54-83.
[22] Shashoua Y. Identification of plastics in collections. In: Conservation of plastics. Oxford: Butterworth-Heinemann; 2008. p. 113-149.
[23] Analytical Methods Committee, AMCTB No. 83. Identification of plastics in cultural heritage collections by Fourier transform infrared spectroscopy (FTIR). Anal Methods 2018; 10: 687-689. DOI: 10.1039/C8AY90010H.
[24] Cucci C, Bartolozzi G, Marchiafava V, Picollo M, Richardson E. Study of semi-synthetic plastic objects of historic interest using non-invasive total reflectance FT-IR. Microchem J. 2016; 124: 889-897. DOI: 10.1016/j.microc.2015.06.010.
[25] Saviello D, Toniolo L, Goidanich S, Casadio F. Non-invasive identification of plastic materials in museum collections with portable FTIR reflectance spectroscopy: Reference database and practical applications. Microchem J. 2016; 124: 868-877. DOI: 10.1016/j.microc.2015.07.016.
[26] Bell J, Nel P, Stuart B. Non-invasive identification of polymers in cultural heritage collections: evaluation, optimisation and application of portable FTIR (ATR and external reflectance) spectroscopy to three-dimensional polymer-based objects. Herit Sci. 2019; 7(95): 1-18. DOI: 10.1186/s40494-019-0336-0.

[27] Madariaga M. Applicability of a Diffuse Reflectance Infrared Fourier Transform handheld spectrometer to perform in situ analyses on Cultural Heritage materials. Spectrochim Acta, Part A 2014; 129: 259-267. DOI: 10.1016/j.saa.2014.03.096.
[28] Rosi F, Cartechini L, Sali D, Miliani C. Recent trends in the application of Fourier Transform Infrared (FT-IR) spectroscopy in Heritage Science: from micro- to non-invasive FT-IR. Phys Sci Rev. 2019; 4(11): 20180006. DOI: 10.1515/psr-2018-0006; and references therein.
[29] Izzo F, Germinario C, Grifa C, Langella A, Mercurio M. External reflectance FTIR dataset (4000-400 cm^{-1}) for the identification of relevant mineralogical phases forming Cultural Heritage materials. Infrared Phys Technol. 2020; 106: 103266. DOI: 10.1016/j.infrared.2020.103266.
[30] La Nasa J, Moretti P, Maniccia E, Pizzimenti S, Colombini MP, Miliani C, Modugno F, Carnazza P, De Luca D. Discovering Giuseppe Capogrossi: study of the painting materials in three works of art stored at Galleria Nazionale (Rome). Herit. 2020; 3(3): 965-984. DOI: 10.3390/heritage3030052.
[31] Moretti P, Rosi F, Miliani C, Daugherty M, van den Berg KJ, Cartechini L. Non-invasive reflection FT-IR spectroscopy for on-site detection of cleaning system residues on polychrome surfaces. Microchem J. 2020; 157: 105033. DOI: 10.1016/j.microc.2020.105033.
[32] Biber A. Dipping into colours. Studies on the technological collection of plastics samples in the Technical Museum Vienna. In: Bechthold T, editor. Future Talks 015 – Processes. The making of design and modern art. Materials, technologies and conservation strategies. Munich: Die Neue Sammlung - The Design Museum; 2017. p. 109-116.
[33] de Groot S, van Keulen H, van den Akker S, van Oosten T. Discoloration of plastics objects: the identification of yellow and orange synthetic pigment in plastic objects. In: Bechthold T, editor. Future Talks 015 – Processes. The making of design and modern art. Materials, technologies and conservation strategies. Munich: Die Neue Sammlung - The Design Museum; 2017. p. 147-158.
[34] Maragno A, Schossler P, Rizzutto M. Challenges in the conservation of synthetic polymers: discolouration of plastic objects. In: Future Talks 019, Munich (Germany), 11-13 November 2019; Oral presentation.
[35] Price BA, Melenks S, Surtherland K, Lins A, Carlson JH. Naum Gabo's Construction in Spaze: Two Cones: history and materials. In: Keneghan B, Egan L, editors. Plastics: looking at the future and learning from the past. London: Archetype Publications, 2009. p. 81-88.
[36] Littlejohn D, Pethrick RA, Quye A, Ballany JM. Investigation of the degradation of cellulose acetate museum artefacts. Polym Degrad Stab. 2013; 98(1): 416-424. DOI: 10.1016/j.polymdegradstab.2012.08.023.
[37] Paris C, Coupry C. Fourier transform Raman spectroscopic study of the first cellulose-based artificial materials in heritage. J Raman Spectrosc. 2005; 36: 77-82. DOI: 10.1002/jrs.1288.
[38] Babo S, Ferreira JL, Melo MJ, Ramos AM. Back to the origin: understanding the history of production and its influence on the properties of acrylic sheet. In: Bechthold T, editor. Future Talks 015 – Processes The making of design and modern art materials, technologies and conservation strategies. Munich: Die NeueSammlung – The Design Museum; 2015. p. 160-170.
[39] Reggio D, Saviello D, Lazzari M, Iacopino D. Characterization of contemporary and historical acrylonitrile butadiene styrene (ABS)-based objects: pilot study for handheld Raman analysis in collections. Spectrochim Acta Part A 2020; 242: 118733. DOI: 10.1016/j.saa.2020.118733
[40] Cwiertnia E. Do we need a new method for describing and analysing coatings with special effect pigments? a discussion and suggestions based on case studies. In: Future Talks 017, Munich (Germany), 11-13 October 2017; Oral presentation.
[41] Melo MJ, Ferreira JL, Babo S, Pereira AI, Callapez ME, Àvila MJ, Sarmento J. A new substance under the sun: how synthetic polymers were selected and transformed into works of art by Ângelo de Sousa, Julião Sarmento and Lourdes Castro. In: Sgamellotti A, Brunetti BG, Miliani C, editors. Science and art: the contemporary painted surface. Croydon: Royal Society of Chemistry; 2020. p. 225-248. DOI: 10.1039/9781788016384-00225.

[42] Webber TG, editor. Coloring of plastics. New York: John Wiley & Sons Inc.; 1979.
[43] Dunning P. Cadmium pigments. In: Faulkner EB, Schwartz RJ, editors. High performance pigments. Weinheim: Wiley-VCH, second ed.; 2009. p. 13-26.
[44] Rosi F, Grazia C, Gabrieli F, Romani A, Paolantoni M, Vivani R, Brunetti BG, Colomban P, Miliani C. UV-Vis-NIR and micro Raman spectroscopies for the non destructive identification of $Cd_{1-x}Zn_xS$ solid solutions in cadmium yellow pigments. Microchem J. 2016; 124: 856-867. DOI: 10.1016/j.microc.2015.07.025.
[45] Grazia C, Rosi F, Gabrieli F, Romani A, Paolantoni M, Vivani R, Brunetti BG, Colomban P, Miliani C. UV-Vis-NIR and microRaman spectroscopies for investigating the composition of ternary $CdS_{1-x}Se_x$ solid solutions employed as artists' pigments. Microchem J. 2016; 125: 279-289. DOI: 10.1016/j.microc.2015.11.008.
[46] Callapez ME. An interdisciplinary project on the history of plastics in Portugal. e-plastory 2017; 1: 1-8. URL: e-plastory/article/view/Callapez/34.

Part II.

The color appearance of plastics: innovative multi-technique spectroscopic approaches for the identification of polymers, pigments and additives

3. Application of infrared reflectance spectroscopy on plastics in cultural heritage collections: a comparative assessment of two portable mid-Fourier transform infrared reflection devices

Abstract

Plastics have been increasingly used to create modern and contemporary art and design, and nowadays, museum collections hold numerous objects completely or partially made of plastics. However, the preservation of these materials is still a challenging task in heritage conservation, especially because some plastics show signs of degradation shortly after their production. In addition, different degradation mechanisms can often take place depending on the plastic composition and appropriate environmental and packaging conditions should be adopted. Therefore, methods for in situ and rapid characterization of plastic artifacts' composition are greatly needed to outline proper conservation strategies. Infrared (IR) spectroscopy, such as attenuated total reflection Fourier transform infrared spectroscopy (ATR FT-IR), is a well-established method for polymeric material analysis. However, ATR FT-IR requires an intimate contact with the object, which makes its application less appropriate for the in situ investigation of fragile or brittle degraded plastic objects. Mid-FT-IR reflectance spectroscopy may represent a valid alternative as it allows in situ measurements with minimum or even no contact, and IR data can be acquired rapidly. On the other hand, spectral interpretation of reflectance spectra is usually difficult as IR bands may appear distorted with significant changes in band maximum, shape, and relative intensity, depending on the optical properties and surface texture of the material analyzed. Presently, mid-FT-IR reflection devices working in external reflection (ER FT-IR) and diffuse reflection infrared Fourier transform spectroscopy (DRIFTS) modes have been used in cultural heritage research studies. As the collected vibrational information depends on the optical layout of the measuring system, differences between ER FT-IR and DRIFT spectra are thus expected when the same polymer is analyzed. So far, ER FT-IR and DRIFT spectroscopy have been individually explored for the identification of plastic objects, but comparative studies between the application of two reflectance FT-IR modes have not been presented yet. In this work, the use of two portable FT-IR spectrometers equipped with ER FT-IR and DRIFTS modes were compared for plastics identification purposes for the first time. Both references of polymeric materials and historical plastic objects (from a Portuguese private collection) were studied and the differences between ER FT-IR and DRIFT spectra were discussed. The spectra features were examined considering the two different optical geometries and analytes' properties. This new insight can support a better understanding of both vibrational information acquired and practical aspects in the application of the ER FT-IR and DRIFTS in plastic analysis.

3.1. Introduction

Within cultural heritage materials, synthetic polymers can pose serious conservation challenges [1-4]. Environmental factors can affect their longevity and after degradation starts, the decay of the material is irreversible and fast. However, preventive conservation strategies can slow down the degradation process. As the lifespan of plastics is greatly related to their chemical nature and storage conditions, the identification and degradation study of plastic objects in collections, museums, and art galleries are priority tasks for their preservation. Infrared (IR) spectroscopy is the most commonly used analytical technique for characterizing polymeric materials in cultural heritage collections [5]. Within IR techniques, transmission and reflection modes can be selected. Transmission Fourier transform infrared spectroscopy (FT-IR), e.g., FT-IR microscopy (μFT-IR), and attenuated total reflection (ATR) FT-IR are well-established methods in polymeric material analysis. However, for transmission FT-IR sampling is required, while an intimate contact between the object and the sampling crystal is necessary in ATR FT-IR measurements. To overcome the practical limitations of sampling and contact, other analytical modes have been tested in the cultural heritage field, especially in the last 20 years with the development of portable reflection FT-IR spectrometers. These portable instruments allow an in situ and quick analysis with minimum or even no contact. Amongst portable molecular spectrometers [6], in situ non-destructive and contactless FT-IR reflectance spectroscopy has found an increasing application for the survey of plastic heritage collections, enabling better decision-making in choosing conservation, preservation, storage, and display strategies of plastic artifacts. In such context, the use of portable equipment operating in external reflection (ER FT-IR) mode has been mainly explored [7-11]. Relatively little research has instead been conducted in analyzing cultural plastic objects using a portable diffuse reflection infrared Fourier transform spectroscopy (DRIFTS) device [12]. Even though comparison between different IR acquisition modes is available in literature for the characterization of cultural heritage plastics [7], no systematic studies have been carried out assessing the application of both ER FT-IR and DRIFTS configurations. The present paper is framed in this research and compares two portable FT-IR spectrometers for plastic analysis: Alpha Bruker Optics and Agilent Handheld 4300 working in ER FT-IR and DRIFTS modes, respectively. The rationale was to provide a better understanding of the collected spectral signals from both spectrophotometers as well as discussing pros and cons of ER FT-IR over DRIFTS (or vice versa) use for material identification and condition assessment of historical plastic objects.

To contribute to this goal, over two-hundred historical plastic objects gathered within the funded research project, "The Triumph of Bakelite: Contributions for a History of Plastics in Portugal" [13], were available for research. A selection of these objects was displayed at the exhibition "Plasticity: A History of Plastics in Portugal" (Museum of Leiria, Portugal), started in 2019 [14] and awarded with the Dibner Award for Excellence in Museum Exhibit by the Society for the History of Technology. The displayed objects included items with different sizes and end uses (mostly domestic), covering all ages of the Portuguese plastics' industry (from 1930s to 2000s). Portable FT-IR reflectance spectroscopy was employed for polymer identification and condition assessment of the historical objects. Several plastic formulations were identified, including mostly thermoplastics such as polyethylene (PE), poly(methyl methacrylate) (PMMA), polypropylene (PP), and polystyrene (PS).

In this work, the performance of the ER FT-IR Alpha (Bruker) and DRIFTS Handheld 4300 (Agilent) devices was evaluated and compared in the in situ analysis of historical plastic objects (naturally aged, composite formulations) showing complex and irregular shapes, from a Portuguese private collection. References of polymeric materials (unaged and non-colored) and daily life objects (unaged and naturally aged, composite formulations) were also included in the investigation. The differences between the reflectance IR spectra collected by the two sampling modules were highlighted. The resulting spectral features were examined in light of the optical geometries of the two different measuring devices as well of the analytes' properties such as surface texture (roughness), optical constants, and plastic thickness. In the results discussion, spectral

acquisition conditions (position of the sample according to the sampling module and influence of backscattering materials) were also considered.
To have a better insight into the reflectance spectra acquired with ER FT-IR and DRIFTS devices, measurements with μFT-IR in transmission mode and ATR FT-IR with a single-reflection diamond crystal plate sampling accessory were also included. This work led to a more comprehensive comparison between different IR acquisition modes for the analysis of historical plastic objects.

3.1.1. Principles of reflection IR spectroscopy and instrumentations

Reflection techniques for IR analysis have been explored since the second half of the 20th century [15] and in these analytical methods, the intensity of the radiation reflected by the sample surface (its reflection response) is reported versus the frequency (or wavelength) at the desired angle of detection.
As described by Griffiths and de Haseth [16], there is an issue with the nomenclature used in reflection spectroscopy and over the years, different terms were used by various authors to define the IR beam reflection paths and their optical properties [16-19]. For example, external reflection and diffuse reflection are used sometimes to indicate the different degree of penetration of the IR beam in the medium (for external reflection, the radiation does not penetrate the medium prior to being reflected, while for diffuse reflection, the radiation has penetrated the front surface). However, the term diffuse is also used in a strictly geometrical sense to differentiate the IR beams which are not reflected at a specular angle. In addition, external reflection is at times used to refer to techniques that collect the radiation reflected from the sample surface, in contrast to total internal reflection (such as ATR FT-IR) where the electromagnetic radiation undergoes single or multiple internal reflections in a crystal element with higher refractive index placed into contact with the sample. To achieve the condition of total internal reflection, the incident angle of the radiation at the crystal/sample interface must be greater than the critical angle. Because confusion might occur, an overview of the most relevant reflection principles for the results discussion is presented by the authors. For a more detailed discussion, please see the references cited in this section.
In the cultural heritage field, the first work that applies mid-IR reflectance spectroscopy for the analysis of opaque or partially absorbing objects was presented by Fabbri et al. [20,21]. The paper focused on the limitations and issues involved in the application of mid-IR fiber optics coupled with a FT-IR bench system. Additionally, the same paper gave a comprehensive review of the necessary theoretical principles. Being the lead paper on the subject in cultural heritage, theoretical aspects and definitions for surface reflection (R_S), volume reflection (R_V), and total reflectance (R_T) were retained throughout this paper.
As previously stated [20,21], when opaque or partially absorbing objects are analyzed with FT-IR reflectance devices, both R_S and R_V contribute to the resulting R_T spectra. The extent of R_S and R_V depends on the optical layout of the measuring system but, primarily, on the analytes' properties including surface texture, concentration, and IR optical constants, mainly refractive (n) and absorption (k) indexes [22].
As clearly noted by Fabbri et al. [20], R_S and R_V show an angular distribution which includes specular and diffuse components. R_S comprises not only the specular reflection (defined as light reflected at the same angle of incidence) but can also contain surface reflected light coming from angles different from the incident one. Likewise, R_V can emerge from the sample, with an angle of reflection equal to the incident one as well as, coming from different angles, diffusely reflected by the sample. In this latter case, the IR beam penetrating into the sample passes through numerous reflections and refractions events and, as consequence, it scatters from numerous points over a wide angle. In summary, the difference of the specular and diffuse components between R_S and R_V is essentially on the degree of penetration, due to the optical properties of the surface.
The relative contribution of both specular and diffuse components of R_S can be influenced by the surface texture (roughness) of the material. For example, optically flat (compared with the wavelength of the incident beam) and shiny surfaces provide a greater amount of specular reflection, while rougher and matte textures

mostly generate diffuse reflection.

Concerning the configuration of the FT-IR devices, the geometrical layout of the detection system determines the collection of the specular and/or diffuse components, while the extent of both R_S and R_V depends on the analytes' properties. In the ER FT-IR configuration, both R_S and R_V components of the specular and diffuse reflected radiation are detected [7]. DRIFTS accessories are designed to eliminate the specular reflected radiation and to exclusively collect the diffusely scattered IR radiation [23,24]. They promote the detection of R_V but cannot completely eliminate R_S from the measurement.

The ER FT-IR and DRIFT spectra are usually and intrinsically more complex than those acquired in transmittance and ATR FT-IR modes. ER FT-IR and DRIFTS measurements can present large distortions in the spectra with changes in maximum, shape, and relative intensity of the IR bands. This is explained because both R_S and R_V lead to spectral distortions. The resulting reflection shapes are modeled according to the extent of the R_S and R_V contributions, which generally co-exist in reflectance IR measurements.

The R_S gives rise to derivative-like spectral features and/or inverted bands (reststrahlen effect) for absorption bands with $k<1$ (following the anomalous dispersion of n) and for strong oscillators with $k\gg1$ (strong absorbance coefficient), respectively [16,17,25,26]. For most organic molecules, including polymers, the presence of reststrahlen bands is uncommon due to their low k index (i.e., the average k for a reasonably strong absorption of an organic molecule is about 0.1 [27]), while for most inorganic salts containing nitrates, carbonates, sulfates, phosphates (with $k\gg1$), reststrahlen bands are usually evident. Thus, R_S is responsible for the main spectral distortions that appear in the reflectance spectra and the Fresnel's law explains its dependency on both k and n as follows [20]

$$R = \frac{(n-1)^2 + k^2}{(n+1)^2 + k^2} \qquad \textbf{(1)}$$

for a reflection (R) at normal incidence from the interface between air and the medium with complex refractive index $\widetilde{n} = n+ik$, where the real (n) and the imaginary (k) parts are the refractive and absorption indexes of the particulate medium, respectively.

As proved by Fabbri et al. [20,21], the specular component of R_S causes the major distortions in the analysis of powders and paint layers. Tested in off-line configuration for a portable fiber optic FT-IR system, a progressive reduction of the distortions caused by R_S is observed by inclining the fiber from the perpendicular incidence, as consequence of the decrease in detection of the specular reflection. The strongest distortions are thus found in the case of $0°/0°$ geometry, where the detection of the specular component is maximized.

Being the specular reflection the major responsible for the spectral distortions, in the last years, new optical configurations have been developed to minimize its contribution in the reflectance IR detection.

The R_V is basically originated from absorption processes and it gives similar spectra in terms of shape to those collected in transmission mode. Distortions such as broadening and change in the relative band intensities are usually observed [16].

The penetration depth (d_p) of the R_V diffusely reflected is inversely proportional to both absorption (k) and scattering (s) coefficients, as stated in **Eq. 2** [28]

$$d_p = \frac{1}{\sqrt{k(k+2s)}} \qquad \textbf{(2)}$$

From here, stronger scattering and absorbing coefficients result in shorter d_p, while the penetration becomes almost infinitive for very small k coefficients. This relationship justifies the extremely high sensitivity of R_V to weak absorbers for which the thickness of the sample appears greater. For those, the IR radiation penetrates deeper, and the repeated refraction and absorbance events enhance the intensity of their IR bands relatively compared to the bands of strong absorbers [28].

Other factors can also influence the relative intensities of the bands in diffuse R_V, such as the wavenumber of the incident radiation and the variation of scattering coefficient (s) in the mid-IR region. At low frequencies,

the beam penetrates deeper [29] and here, lower scattering coefficients occur [28,30]. Therefore, enhancements in the relative intensity for low wavenumber bands (relatively to conventional transmission FT-IR spectra) are usually observed.

Overtones (integral multiplies of fundamental absorption frequencies) and combination bands (addition and subtraction of fundamental absorption frequencies) can be found in IR reflectance spectra [31]. Usually overtones and combination bands are weakly intense (small k coefficients), and an increase in their relative intensity can be observed by measuring a longer travel distance in the sample (**Eq. 2**).

The spectra anomalies arising from R_S and R_V can be treated with Kramers-Kronig (KK) operation [32] and the Kubelka-Munk (KM) correction [29], respectively. Both methods can give reliable results when applied to spectra obtained on surfaces where R_S and R_V predominate, respectively. Because of the nature, morphology, and heterogeneity of the materials found in cultural heritage objects, R_S and R_V co-exist in the IR reflectance spectrum in unknown variable proportions. This makes the spectra interpretation not straightforward and the use of KK and KM limited. Also, biggest drawback is that R_V cannot be completely optically separated from R_S.

Infrared reflection process of optically thick cultural heritage materials is thus a very complex phenomenon resulting in IR spectra difficult to handle [33-41]. Some studies proved the efficiency of using the KK correction on derivative-like bands ($k<1$) [42-44], while not satisfactory results were obtained for this algorithm when applied to reststrahlen bands ($k\gg1$) [44-46].

As stated in the **Eq. 1**, derivative-shaped bands arise from the superposition of absorption k and refractive n indexes and their anomalous dispersions. This type of spectral distortion usually occurs at the frequency of maximum absorbance, when the refractive index of the material drastically changes due to its high absorption coefficient [47-49]. This overlay can be separated by subjecting the reflectance spectrum to KK correction, which yields both refractive index spectrum (index n against wavenumber) and more analytically useful absorption index spectrum (index k against wavenumber). In this way, KK algorithm makes possible to reconstruct a pseudo-absorption spectrum in index k (KK units) by extracting the complex refractive index accurately [32,50,51]. In the case of reststrahlen bands where the reflection maximum occurs in place of the absorption band, the KK correction cannot distinguish the contributions of k and n to the reflectance shapes. Thus, the application of KK to reststrahlen bands leads to a new distortion of the spectral features [20,31,45].

Therefore, the identification of the absorbance maxima of the derivative-like spectral features requires a lot of caution. In fact, these signals should not be directly compared with the bands of FT-IR spectra acquired in transmission or ATR modes because of their band shape distortions. KK is the most accurate data processing method for this type of spectral distortion. It can be used for defining the actual position of the absorption band location and allows the comparison between the corrected spectra and the ones obtained with conventional FT-IR modes (i.e., transmittance, ATR). Calculating the first derivative can also help in locating the IR bands maxima of derivative-shaped bands, particularly when one decides to examine the raw spectrum without the application of KK. Although the derivative method is considered mathematically valid, it presents limitations, first, by not considering the anomalous dispersion of refractive n and absorption k indexes and, second, by not delivering the absorbance index spectrum, as KK does.

The KM theory has been widely used to describe diffuse reflection [16,17]. The conversion allows a comparison with the transmission spectra because it converts reflectance (which is a nonlinear function of absorbance) to a quantity (KM units) by a scaling factor that is linear relative to absorbance and thus, to the concentration of the analyte. However, KM model incorporates several requirements regarding the sample [22,52], making difficult its application on cultural heritage objects.

In summary, KK operation deals with the band shape (R_S main distortion), while KM function essentially treats the band intensity (R_V main distortion). Until now, no mathematical functions have been developed to treat the reststrahlen bands.

An IR reflectance spectrum can be thus presented in KK or KM units. Reflectance can be also transformed into

pseudo-absorbance A' = log(1/R) (R = reflectance), which allows the processing of the reflectance information without any correction of the bands.

3.2. Experimental

3.2.1. Materials

Polymer references. Polymer reference samples (unaged) were obtained from non-colored and non-plasticized formulations of high-density polyethylene (HDPE) (from Repsol Polímeros), PP (from EPSI, Empresa de Polímeros de Sines), PS and PMMA (both from Plexicril, Lda.). With a JCS Shinha press and mold plates, pellets of HDPE and PP were molded into circular disks of 2.5 cm diameter by the application of heat and pressure.

Daily life objects. Samples of commercial and composite formulations were also collected from everyday plastic objects. This selection included unaged and naturally aged objects considering the polymers under study.

Plastic historical objects. Naturally aged historical objects from a Portuguese private collection, showing composite formulations and complex shapes, were also selected to compare the potential of using both acquisition devices in the in situ analysis of plastic objects.

3.3. Instrumentation

3.3.1. External reflection Fourier transform infrared and diffuse reflection infrared Fourier transform spectroscopies

Infrared reflectance analyzes in ER FT-IR and DRIFTS modes were performed using two different portable reflection FTIR devices, both intended for in situ analysis.

The ER FT-IR spectra were acquired by means of the portable Alpha FT-IR spectrophotometer (Bruker Optics), equipped with a silicon carbide (SiC) globar source and temperature stabilized deuterated triglycine sulfate (DTGS) detector. All measurements were performed positioning the samples in front of the instrument using the external reflectance module with a measurement spot of 10 mm in diameter. The spectral range investigated was 4000-650 cm^{-1}, with 8 cm^{-1} resolution; 128 scans were acquired for the background using a gold flat mirror as reference, and 128 scans were recorded on the samples in order to optimize the signal to noise ratio (S/N) (Opus 7.0.122 software, Bruker Optics).

The DRIFTS measurements were performed using the Agilent Handheld 4300 FT-IR spectrophotometer, equipped with wire wound IR source and a thermoelectrically cooled DTGS detector, coupled to a diffuse reflectance sampling module with a measuring spot of 10 mm diameter. The DRIFT spectra were acquired between 4000 and 650 cm^{-1}, with a resolution of 8 cm^{-1} and 128 scans. A coarse silver reference cap was used for the background calibration every 10 min.

According to the type of reflection desired to be collected, different optical geometries can be designed. **Figure 3.1** shows the configuration of the two portable devices as proposed in this publication.

The Alpha (Bruker) is equipped with a working optical layout for reflection measurements where the IR radiation is incident at 25° and the reflected signal is collected inside an imaginary cone of 25° around the emission beam. On the other hand, in the Handheld 4300 (Agilent), the IR beam impinges upon the surface at 0° and the reflected signal is collected inside an angle range from 24° to 60° from normal. For both modules, a set of mirrors/lens focuses the reflected IR signal to the detector.

Given the optical detection geometry of the ER FT-IR mode of the Alpha instrumentation (Bruker), both diffuse and specular components of reflection are collected, although the specular is favored. On the other

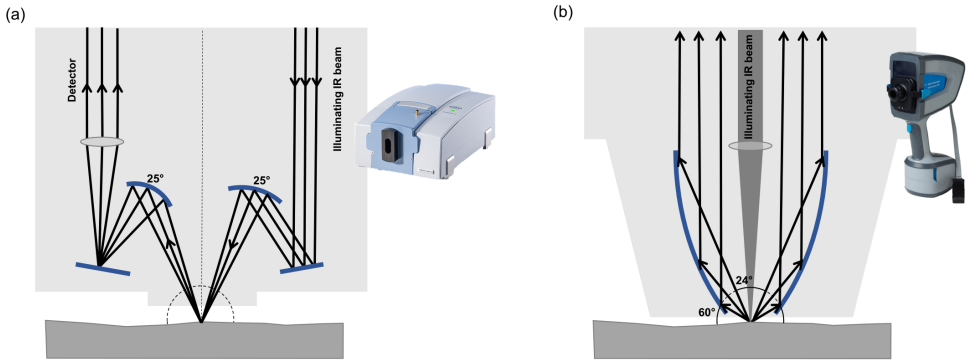

Figure 3.1.: Schematic representation of the two tested reflectance sampling modules: (a) ER FT-IR module (Bruker Alpha) and (b) DRIFTS module (Agilent Handheld 4300).

hand, the specular component is expected to be excluded with the DRIFTS module of the Handheld 4300 (Agilent), and a higher proportion of diffuse reflection is measured. With this DRIFTS optical configuration, the penetration of the IR beam into the sample is strongly promoted because of the incident ray normal at the surface (θ_i=0°). In this geometry, the Fresnel equations for reflectance (R) and transmittance (T) coefficients reduce to [53,54]

$$R = \left(\frac{n_t - n_i}{n_t + n_i}\right)^2 \qquad \textbf{(3)}$$

$$T = \frac{4 n_t n_i}{(n_t + n_i)^2} \qquad \textbf{(4)}$$

resulting, for an air-plastic interface with refractive indexes $n_i = 1$ and $n_t = 1.5$ [1], in a total percentage of reflectance (R%) and transmittance (T%) of 4% and 96%, respectively.
The ER FT-IR and DRIFT spectra were processed by using Omnic (v.7.3, Thermo Fisher Scientific) and OriginPro 8 (OriginLab Corporation) software, without basic corrections or normalizations. The IR reflectance spectra were reported as pseudo-absorbance (A' = log(1/R); R = reflectance). The maxima of the pseudo-absorbance bands were considered at the points with the highest relative intensity, as commonly done for the true absorption bands. For derivative-like bands, the same band locating process was followed. This allowed the identification of the maxima graphically depicted, and although these points did not represent the real maximum absorbance values, they were chosen for spectral comparison purposes. For one case study, the ER FT-IR spectrum was found distorted to high extent; hence KK transform was applied to correct the derivative-shaped bands using Omnic software. For all the other spectra, no corrections were applied.

3.3.2. Fourier transform infrared microspectroscopy

Infrared analyses were performed using a Nicolet Nexus spectrophotometer coupled to a Continuμm microscope (15× objective) in transmission mode with MCT-A detector cooled by liquid nitrogen. The spectra were collected in transmission mode in a measuring spot of about 50 μm, with 4 cm^{-1} resolution and 128 scans, using a Thermo diamond anvil compression cell. The CO_2 absorption at circa 2400-2300 cm^{-1} was removed from all the acquired spectra (4000-650 cm^{-1}). Background spectra were acquired before each acquisition.

3.3.3. Attenuated total reflection Fourier transform infrared spectroscopy

Infrared spectroscopy in ATR FT-IR was carried out with the Handheld Agilent 4300 spectrophotometer, equipped with a ZnSe beam splitter, a Michelson interferometer, and a thermoelectrically cooled DTGS detector. Spectra were acquired with a diamond ATR module, 128 scans and 4 cm^{-1} resolution. This ATR

module allows the analysis of samples with a minimum size of 200 microns. Background spectra were collected between every acquisition. The OriginPro 8 software was used for the analysis of the spectra, which were shown as acquired, without baseline corrections or normalizations.

3.3.4. Energy dispersive X-ray fluorescence microspectroscopy

Elemental analysis of the historical objects was performed to detect the possible presence of inorganic compounds in the plastics formulation (such as fillers, pigments, and processing aids). This approach was followed to assess the influence of inorganic compounds in the IR reflectance spectra of the plastic object as inorganic compounds are expected to promote the appearance of spectral distortions such as reststrahlen (inverted) bands. Energy dispersive X-ray fluorescence microspectroscopy (μEDXRF) results were obtained using an Art-TAX spectrometer (Intax GmbH) with a Mo anode, X-flash detector refrigerated by the Peltier effect (Sidrift), sustained by a mobile arm. The low-power Mo X-ray tube attains a microspot with a spatial resolution of about 70 μm. The accuracy of the incident beam position on the sample is achieved through three beams crossing diodes controlled by an integrated charge-coupled device camera. The characteristic Xrays emitted by the sample (at 40°) were detected by a silicon drift electrothermally cooled detector. The experimental parameters used were: 25 kV of voltage, 300 μA of intensity, for 360 s, under helium gas flux. The experimental parameters used permitted the reduction of the bremsstrahlung effect ("braking radiation") due to the polymeric (organic) matrix.

3.4. Results and Discussion

3.4.1. Reflection response of the reference materials

Figure 3.2 shows the FT-IR spectra of HDPE plastic reference in several acquisition modes: transmission (μFT-IR), ATR FTIR, DRIFTS, and ER FT-IR. The DRIFT and ER FT-IR spectra were acquired by placing the reference samples closer (1 mm gap) and parallel to the reflectance modules as shown in **Figure A.1A** (**Appendix A**). Spectra of PP, PS, and PMMA plastic references are reported in **Figures A.2** to **A.4**. The assignments of the most characteristic bands in the IR spectra are listed in **Table A.1** (**Appendix A**).
As observed in the acquired spectra of the HDPE reference (**Figure 3.2**), the different optical geometries of ER FT-IR and DRIFTS modules were mirrored in the collected reflectance spectra. Compared to ATR FT-IR and μFT-IR (transmission) spectra, the HDPE ER FT-IR and DRIFT spectra featured more bands, and the fundamental ones were found distorted with change in position, shape, and relative intensity. These resulting reflection shapes are modeled according to the extent of the R_S, R_V, specular, and diffuse contributions. All fundamental bands such as $-CH_2$ stretching (circa 2918 and 2850 cm^{-1}) and bending (circa 1466 and 718 cm^{-1}) [55,56] appeared as derivative thshaped bands in both ER FT-IR and DRIFT spectra due to the R_S contribution. These spectral distortions can be related to the anomalous dispersion in both absorption (k) and refractive indexes (n), which show abrupt changes when approaching resonance frequencies [47]. Due to the characteristic profiles of such distortions in HDPE reflectance spectra, these bands and their specific spectral shapes can be used as markers to identify PE in plastic objects, as already proposed by Soares et al. [12].
In addition to the fundamental bands, overtones and combination bands were also found (2500-1800 cm^{-1}) [57,58] which might be associated with the semi-crystallinity of HDPE spherulites [59,60]. Above 3500 cm^{-1}, fundamental OH stretching modes of free water (unbound to the polymer chain, likely water sorbed in HDPE) were also detected [61]. Overtones and combinations signals are shaped as common absorption bands (without spectral distortions) in both ER FT-IR and DRIFT spectra, even though these bands are better visible and more intense in the DRIFT spectrum. This can be explained by a higher penetration depth of the IR beam promoted by the DRIFTS module, and a consequent enhancement of the R_V, which increases the intensity

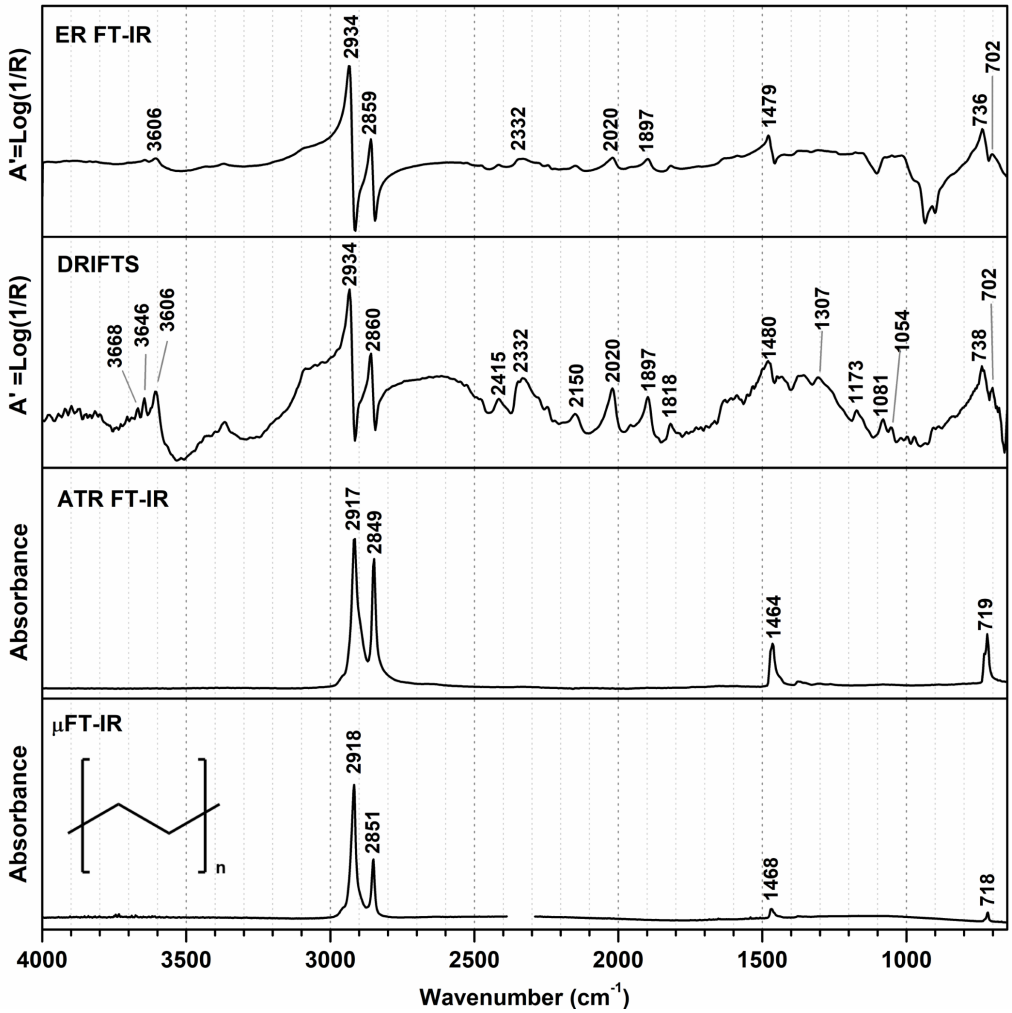

Figure 3.2.: FT-IR spectra of the HDPE polymer reference using several acquisition modes. From bottom to top: μFT-IR, ATR FT-IR, DRIFTS and ER FT-IR.

of the bands and justifies the lack of bands shape distortion. Because plastics generally present smooth and polished textures, the specular component is expected to play a fundamental role in the resulting spectra acquired with both ER FT-IR and DRIFTS modes. The S/N of the DRIFT spectrum is likely related to the lower quantity of signal diffusely reflected by the sample. Additionally, the instrumental performance of the DRIFTS system (e.g., source, interferometer, optical components, detector) may have played an important role in the S/N result.

For the PP reference, the same conclusions can be generally made (**Figure A.2**). Considering these observations, a similar optical behavior of HDPE and PP can be thus suggested.

For the PS and PMMA plastic references, a higher contribution of the specular component in both ER FT-IR and DRIFT spectra was observed, as consequence of their more pristine and neat surfaces. As shown in **Figures A.3** and **A.4**, the increased number of bands due to the R_V contribution was not detected, especially in the region between 2500 and 2200 cm^{-1}. As for HDPE and PP, the fundamental absorption bands appeared as derivative-shaped bands in the reflectance spectra as a consequence of the strong contribution of the R_S component.

Due to the lack of diffuse contribution from PMMA, it was not possible to collect any reflectance FT-IR spectrum using the DRIFTS module (**Figure A.4**). In fact, with the PMMA sample parallel to the DRIFTS module, no signal reached the detector, and consequently, no spectrum was acquired. As PMMA shows a neat and pristine surface, its diffuse reflectivity is low (or even absent), justifying the weak (or absent) reflected signal collected with this reflection mode and angular distribution. This result confirms that the optical geometry of the DRIFTS module favors the collection of diffuse reflection and there is a predominance of the specular R_S component in the reflection response of the PMMA sample. A DRIFT spectrum of the PS sample was instead measured (**Figure A.3**). This suggests a slightly different reflection response of the PS material compared to PMMA in which few diffuse and major specular reflection portions are present.

When the PMMA reference was placed in an oblique angle to the sampling module (as shown in **Figure A.1B**), enough signal reached the detector so that a satisfactory DRIFT spectrum was acquired (**Figure 3.3**). Nonetheless, the acquired spectrum continues to be the result of the specular reflection response of R_S of the material, as first derivative-shaped bands were detected. Therefore, even though the angle of incidence can be easily changed by tilting the position of the sample surface in relation to the sampling module, the reflection response of the PMMA sample did not change. Based on these results, one can infer that more than the angle of incidence, it is the absorption and refractive indexes of PMMA that mostly dictate the extent of specular and diffuse, and R_S and/or R_V response. This is even more evident when the two different optical geometries (ER FT-IR and DRIFTS sampling modules) resulted in identical reflectance spectra.

3.4.2. Influence of the surface texture

Because the specular component prevailed in the reflection response of PS and PMMA, the influence of the surface texture to the reflection response of the materials was investigated. Reflectance spectra of abraded and non-abraded surfaces of the references were acquired with both ER FT-IR and DRIFTS modes, following a strategy already adopted [12].

Both ER FT-IR and DRIFT spectra of the non-abraded and abraded PS reference (**Figure 3.4a**) showed significant differences in 3100-2850 cm^{-1}, approximately 1600 cm^{-1} and 1500-1450 cm^{-1} regions. In fact, the abraded sample resulted in a larger diffuse reflection giving rise to more "regular" absorption bands (without band distortions).

In the case of PMMA (**Figure 3.4b**), the difference between the abraded and non-abraded DRIFT spectra was even more clear. While it was not possible to acquire a spectrum for the non-abraded sample, the spectrum of the abraded surface exhibited similar shape to those acquired with transmission and ATR FT-IR modes, proving that roughness has an influence on the reflection response of the material. On the other hand, the

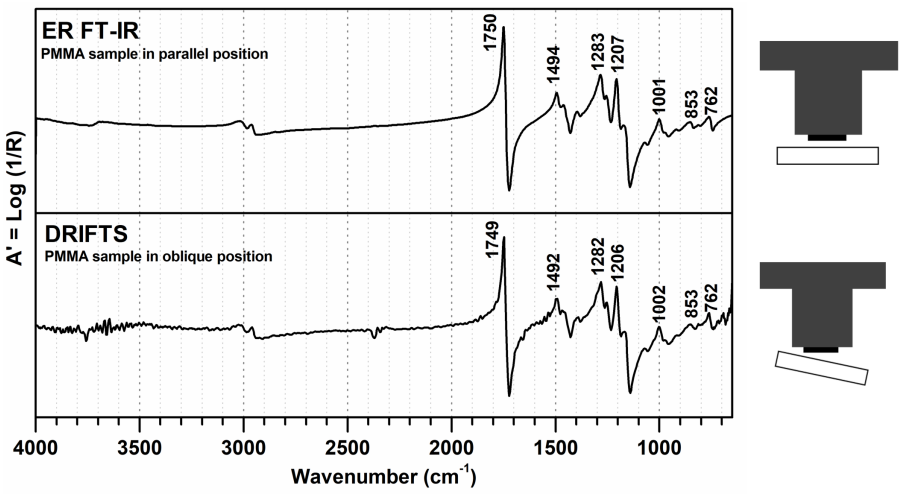

Figure 3.3.: FT-IR spectra of the PMMA reference using ER FT-IR and DRIFTS modes. The spectra were acquired with the sample in parallel (ER FT-IR) and placed in an oblique (DRIFTS) position to the sampling modules, as represented in the scheme on the right.

ER FT-IR spectra of the abraded and non-abraded surfaces were not significantly different, showing both derivative-shaped like bands.
Since surface abrasion is a damage commonly found in historical plastic objects, the analysis of such areas could be used to collect vibrational spectra would appear alike to conventional transmission FT-IR spectra. This would allow for a more straightforward spectral interpretation [12], especially when devices which favor the collection of diffuse reflection are used.

3.4.3. Penetration depth of the IR beam according to the acquisition mode

Polymers are characterized by small k coefficients in the mid-IR region [62]. Thus a higher penetration depth (d_p) of the IR beam is expected in comparison to other materials found in artworks such as paintings (e.g., pigments and fillers). Therefore, as plastics can be more "transparent" to IR beams, the disclose of their optical behavior under IR reflection measurements is fundamental. Assessing the influence of both plastic thickness and optical properties in the reflectance response is also crucial, as well as evaluating the probability of a transflection occurrence.
In order to assess the d_p of the mid-IR incidence beam, an aluminum foil was placed on the back of the reference samples prior to the spectra collection with both ER FT-IR and DRIFTS modes. For comparison purposes, spectra were collected with (**Figure A.1C**) and without (**Figure A.1A**) the aluminum foil on the back (**Figure 3.5**). To clearly show the increase in intensity of the reflected signal when the aluminum foil was placed behind the samples, the spectra were reported as reflectance. Here, it is important to mention that all plastic references showed a thickness of 1.5 or 2 mm and were all non-colored samples.
It was observed that depending on the plastic type, the penetration depth of the IR incidence beams was higher or lower, favoring a more R_V or R_S response, respectively. For instance, while the presence of the aluminum foil in the back of the PMMA reference (2mm thickness) did not influence its reflection response (**Figure 3.5d**); in the case of PS (2mm thickness), HDPE and PP (both 1.5 mm thickness), the aluminum foil promoted the back reflection of the transmitted beams (**Figures 3.5a** to **3.5c**). This double transmission through the samples produced a "back-reflection" spectra, resulting in a sort of transflection spectra. The analyzed plastic samples made of PP, HDPE, and PS proved to be not optically thick in the mid-IR as back scattering was observed. As a result of transmission and then back scattering, the intensity of the reflectance signal increased, especially when the DRIFTS module was used. On the contrary, PMMA proved to be optically

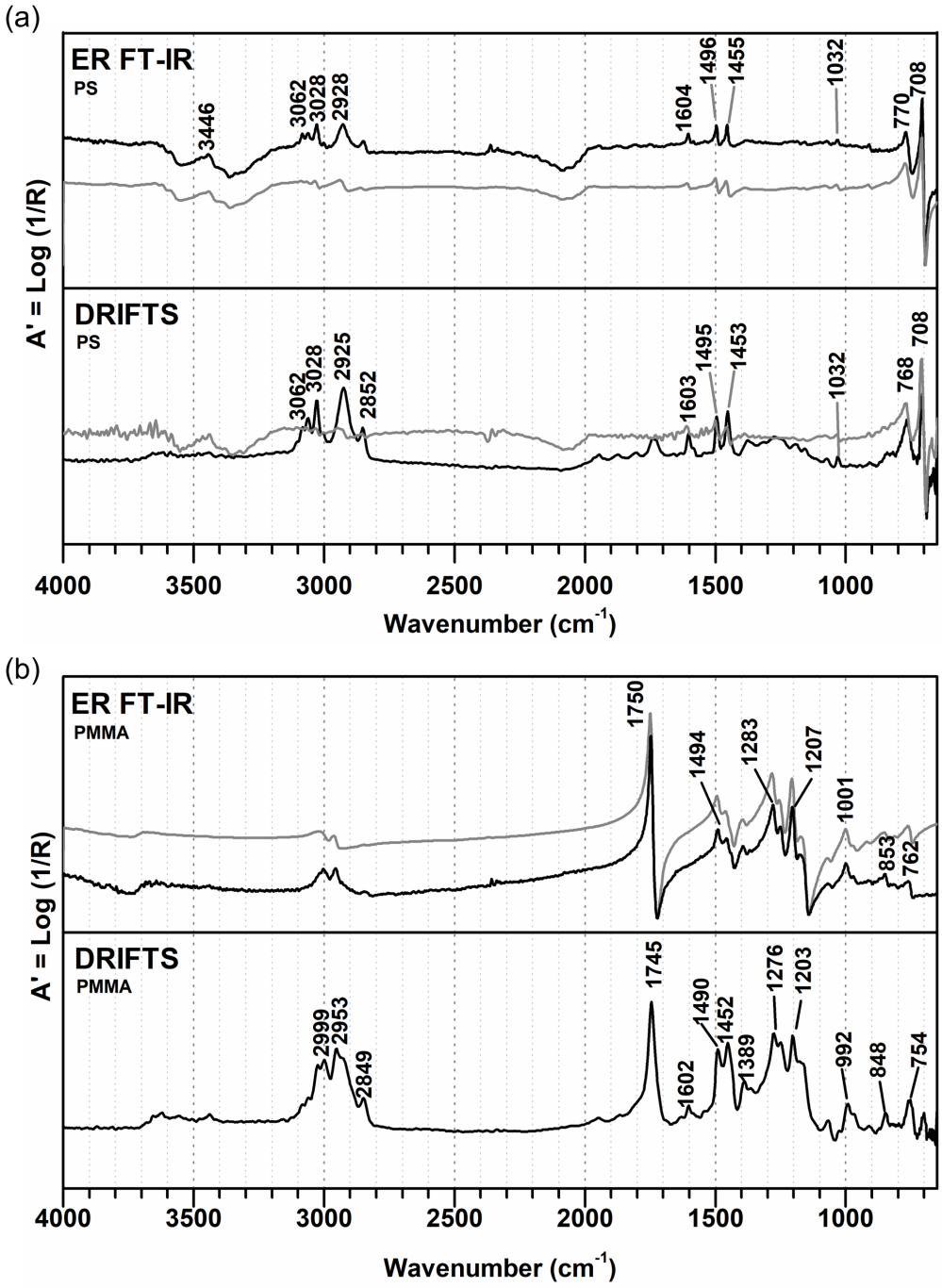

Figure 3.4.: FT-IR spectra of (a) PS and (b) PMMA references using ER FT-IR and DRIFTS modes: abraded (black line) and non-abraded (grey line). All spectra were acquired with the sample in parallel position to the sampling module.

thick (no transmission occurs) when the IR beam stroked onto its surface
The same approach was followed in colored and visually opaque HDPE commercial objects (**Figure 3.6**), both with an approximate 2 mm thickness. For these objects, the same tendency was observed, e.g., the reflectance signal increased due to back scattering caused by the aluminum foil. This confirms that not all plastics are optically thick and therefore, transmission can occur even with thickness such as 2 mm. The presence of highly scattering materials on the back of plastics should be taken into consideration in midIR spectra analysis and when in situ analyzes are performed on plastic-based objects
As clearly presented in **Figures 3.5** and **3.6**, the different penetration depths between plastic references depend on the IR optical properties of the samples. Additionally, the transparency to the incident IR beam varies with the wavenumber, and at the frequency of stronger oscillators (fundamentals IR bands) there is a prominence of the specularly R_S as a consequence of minor degree of penetration.

3.4.4. Historical plastics objects

Both ER FT-IR and DRIFTS modules allowed the analysis of a large number of areas in the same object without contact or sampling. This enabled a quick and more complete molecular characterization of the whole items, contrary to μFT-IR or even ATR FT-IR, which are more time-consuming approaches. Even so, the complexity of the collected ER FT-IR and DRIFTS signals highlight the importance of developing spectral databases for an accurate data interpretation
The example of two key historical plastic objects among the ones analyzed is here discussed: a naturally aged white telephone made of acrylonitrile butadiene styrene (ABS) showing yellowed and non-yellowed areas; and a food container with a red lid, both made of PE, with the printed red lettering inscription, *Açúcar* (sugar). For both case studies, ER FT-IR and DRIFTS measurements enabled the identification of the polymers and the assignment of their corresponding IR marker bands. Also, both IR reflectance modes displayed a higher sensitivity compared to ATR FT-IR in detecting possible degradation signals.
In both ER FT-IR spectra, IR reflectance markers for the acrylonitrile (ν(C≡N) at 2246 cm^{-1}), butadiene (δ(C-H) 992 and 958 cm^{-1}) and styrene (δ(C-C) aromatic ring at 774 and 712 cm^{-1}) monomers were detected with a derivative-shaped band profile [12,56] (**Figure 3.7**).
Compared to ATR FT-IR, the ER FT-IR module was more effective in the detection of minor molecular changes between yellowed and non-yellowed areas of the telephone. The most significant spectral differences were observed in the C=O stretching (1755 cm^{-1}), C=O and/or C=C stretching (1680 cm^{-1}) and C-H bending (between 1000-900 cm^{-1}) regions [63-65], suggesting the formation of carbonyl groups, the degradation of the butadiene unit, and the formation of early degradation products such as new chromophores responsible for the superficial phone yellowing.
The DRIFTS analysis of the sugar container also enabled the detection of the IR reflectance markers for PE at 2933 and and 2863 cm^{-1} (**Figure 3.8a**). While ATR FT-IR spectra of the body and lid were mostly identical, evident spectral differences between the two plastic parts were observed in the DRIFT spectra, especially in the 1750-1400 cm^{-1} region, possibly related to the photo-oxidation of PE [66-68].
When the lettering *Açúcar* was analyzed using the ER FT-IR module, spectral information mainly from the red printing ink (upper layer) were detected (**Figure 3.8b**). Distorted with a derivative-like shape, fingerprint bands of the organic binder such as cyclohexanone polycondensation resin were identified in the ER FT-IR spectra after being processed with KK correction: ketone ν(C=O) (1717 cm^{-1}), in-plane δ_{as}(C-H) (1453 cm^{-1}), in-plane δ(O-H) (1255 cm^{-1}), out of-plane δ(C-H) (1122 cm^{-1}) and hydroxyl ν(C-O) (1042 cm^{-1}) [69]. The identification was possible by the positive match with the reference IR ISR00045 spectrum of the IR and Raman users group (IRUG) 2007 spectral database [15,70]. In the region of the aliphatic (–CH_2, –CH_3) stretching vibration (2800-3000 cm^{-1}), the lack of bands' definition might be related to the overlay of organic resin and PE vibrational information. While overtones and combinations bands typical of PE were still

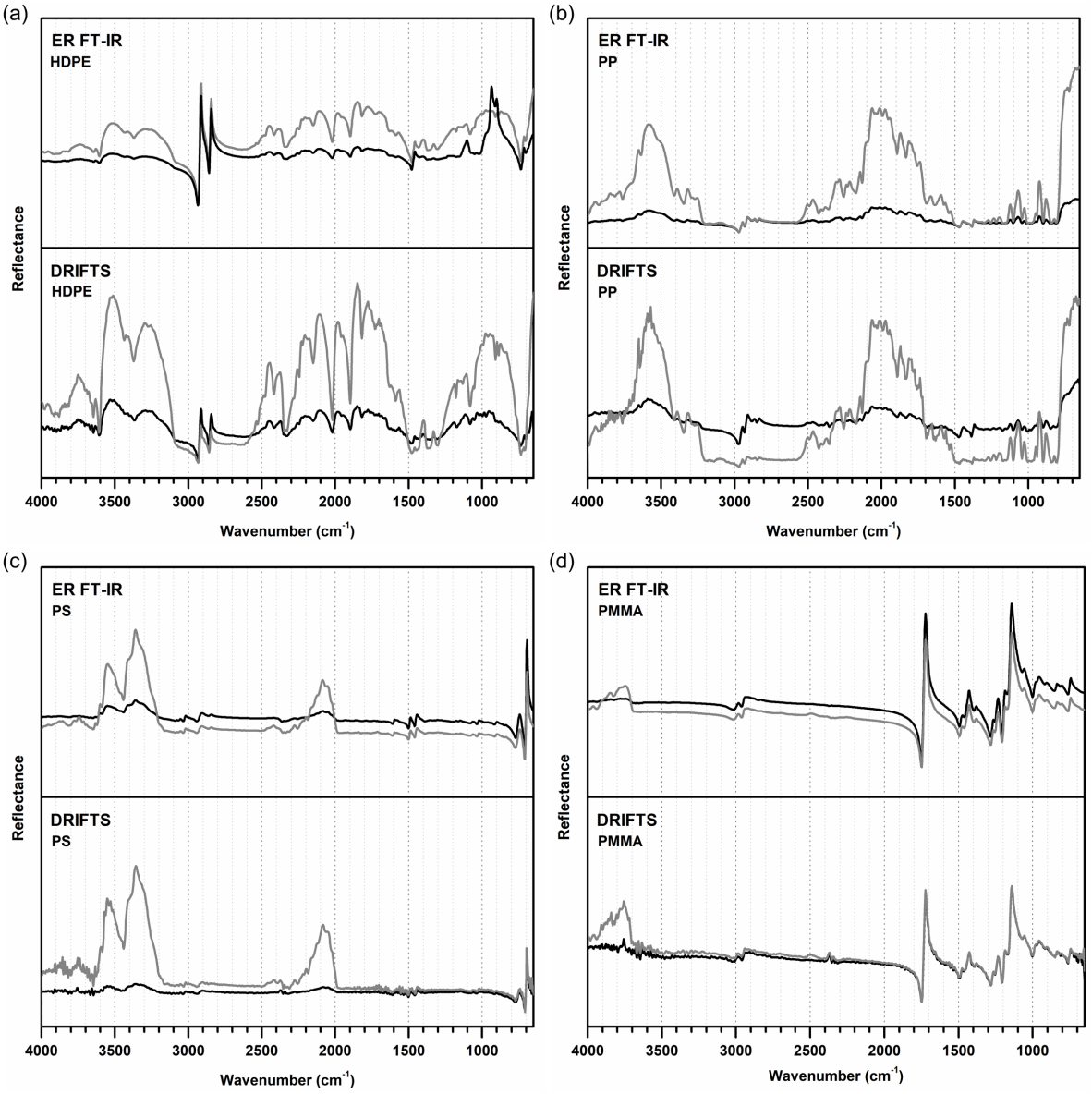

Figure 3.5.: Reflectance FT-IR spectra of plastic references using ER FT-IR and DRIFTS modes with (grey line) and without (black line) the aluminum foil in the back: (a) HDPE, (b) PP, (c) PS, and (d) PMMA. All spectra were acquired with the sample in parallel position to the sampling module despite the DRIFTS measurement of PMMA which was collected in oblique position.

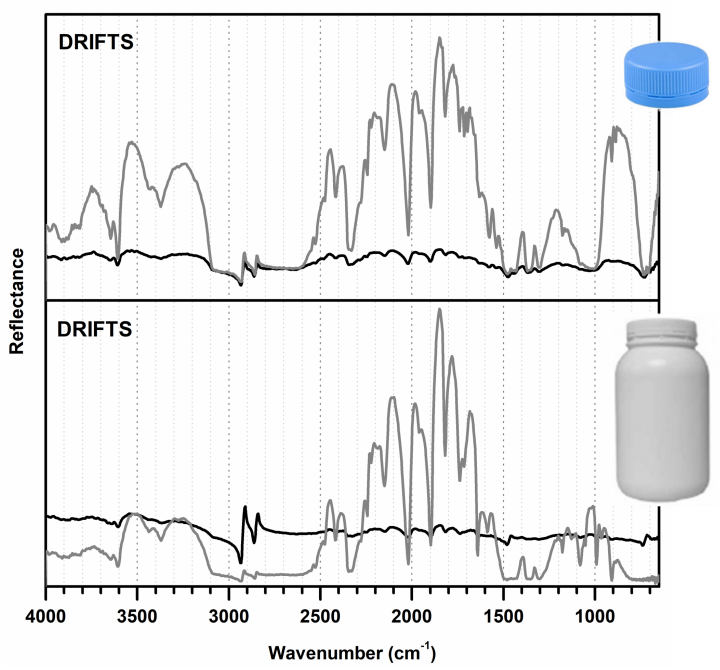

Figure 3.6.: Reflectance FT-IR spectra of PE colored and opaque commercial objects using DRIFTS mode with (grey line) and without (black line) the aluminum foil in the back: blue bottle cap (top) and white plastic bottle (bottom).

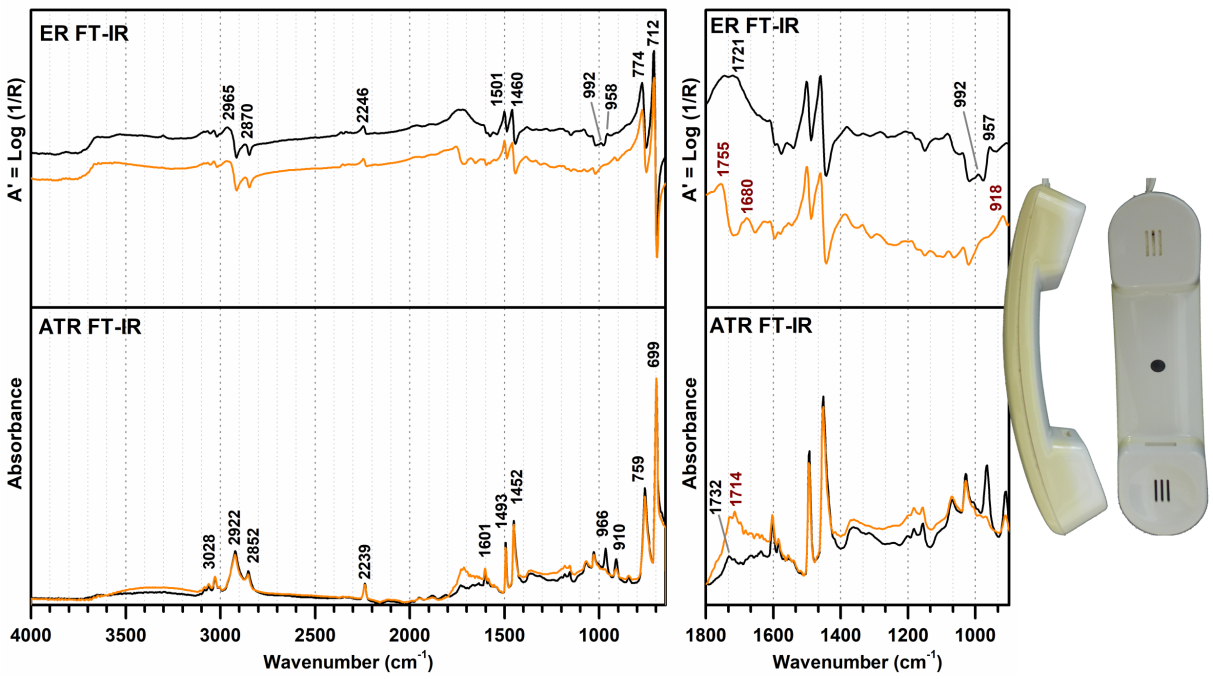

Figure 3.7.: FT-IR spectra of ABS historical telephone using ER FT-IR and ATR FT-IR modes: yellowed (orange line) and non-yellowed (black line) areas. Detail of the 1800-900 cm^{-1} region is shown, pointing to the most significant spectral differences between yellowed and non-yellowed areas.

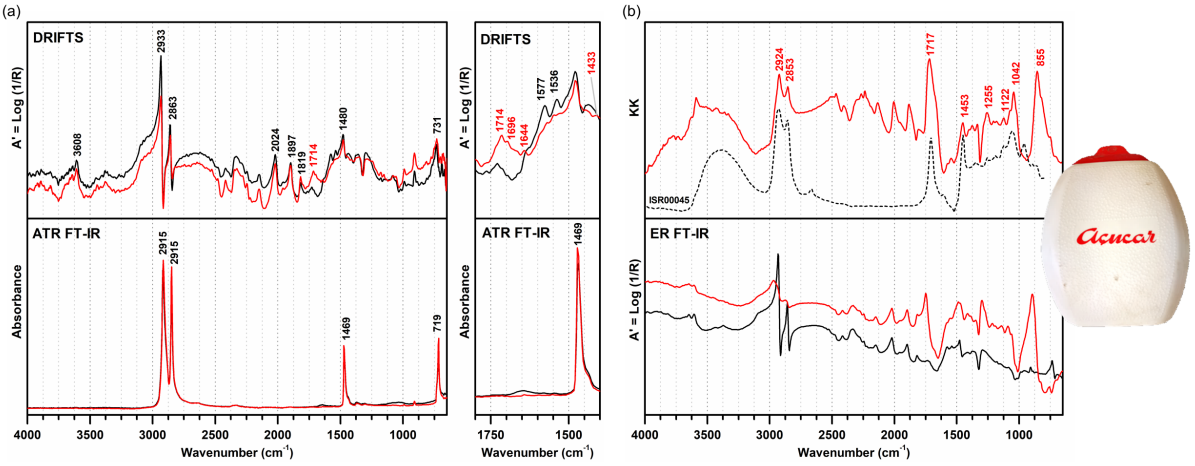

Figure 3.8.: FT-IR spectra of PE historical sugar recipient (*Açúcar*). (a) lid (red line) and body (black line) using DRIFTS and ATR FT-IR modes. Detail of the 1800-1400 cm^{-1} region is shown, pointing to the most significant spectral differences between the body and the lid. (b) Lettering (red line) and body (black line) using ER FT-IR mode. Reference IR spectrum of ketone resin (cyclohexanone polymer) ISR00045 from IRUG 2007 database (black dashed line) is reported for comparison.

observed from 2500 to 1800 cm^{-1}, the strong band at 855 cm^{-1} can be assigned to Cr–O stretching of a lead chromate-based pigment [71] possibly molybdenum red $Pb(CrMoS)O_4$ [72], generally used as a colorant for the lettering [73]. This hypothesis was supported with the detection of lead (Pb) and chromium (Cr) counts by μEDXRF analysis (**Figure A.5**). Although reststrahlen bands are commonly found for most inorganic salts, the vibrational band related to the chromate anion CrO_4^{2-} was found here as a derivative shaped band, possibly due to the very low concentration of the pigment and its combination with organic resin and PE information. The ER FT-IR measurement allowed the in situ identification of both printing ink composition (binder and colorant) and polymer of the food container. In this case, positive results were obtained for the correction of derivative-like spectral features when KK algorithm was applied.

3.5. Conclusion

In this study, two portable reflection FT-IR spectrometers equipped with ER FT-IR and DRIFTS modules were extensively compared for the first time for the polymer identification of several plastic samples and historical objects. For this comparison, different sample characteristics (plastic surface texture, optical thickness) and spectral acquisition conditions (position of the sample according to the sampling module and influence of backscattering materials) were taken into consideration, as well as the different optical geometries of the two modules.

While the ER FT-IR device collects all the reflected IR beams from a material surface (even though it favors acquisition of the specular contribution), the DRIFTS accessory is designed to maximize the detection of the diffuse reflection component and to avoid the specular contribution. Accordingly, in the analysis of plastics, ER FT-IR showed more advantages for the characterization of objects with smooth and pristine surfaces (i.e., higher specular component), whereas DRIFTS showed a better application for the analysis of objects with more rough and matte surfaces (i.e., higher diffuse component).

R_S and R_V (and related distortions) co-existed in both ER FT-IR and DRIFTS measurements. Regarding the polymers under study, R_S was found in much higher proportion than R_V in both PS and PMMA reflectance spectra. In the specific case of PMMA, the specular component ruled the resulting IR reflectance spectra feature. The different optical behavior observed between the polymeric samples was related to the surface texture (roughness) and IR optical constants (mainly refractive (n) and absorption (k) indexes) of the materials. Also,

a correlation between optical behavior and degree of crystallinity is suggested for semicrystalline (HDPE, PP) and amorphous (PS, PMMA) morphologies. From these observations, it can be inferred that the determining factors in the resulting IR spectra were the surface texture and the optical properties of the analyzed plastics rather than the instrument optical layout.

Contrary to other cultural heritage materials such as paintings, this study proves that plastics (both colored and uncolored) cannot be considered opaque materials to IR radiation for 1.5-2 mm of thickness. In fact, transflection or "back-reflection" spectra were acquired with a reflecting material placed on the back of the plastic during acquisition, independently of its transparency or apparent opacity. This indicates that care must be taken in the analysis of plastic heritage with ER FT-IR and DRIFT spectroscopies, as the presence of highly scattering materials underneath (or closer) may influence the collected signal.

The larger diffuse reflection due to the abrasion of the plastic surface allowed the collection of less distorted vibrational spectra, especially with the DRIFTS device. Thus, the analysis of abraded areas with instruments which favor the collection of diffuse reflection (such as DRIFTS) is advisable.

Thanks to the in situ approach offered by the two devices, a quick and a more complete overview of molecular characterization was possible without compromising the physical integrity of the historical plastic objects and with no limitations correlated to micro-sampling (required in transmission, μFT-IR) or pressure (required in ATR FT-IR). Additionally, the spectral acquisition provided substantial data for plastics' molecular characterization and degradation assessment. ER FT-IR and DRIFTS measurements succeeded in detecting molecular changes related to ABS yellowing and PE photooxidation on historical plastic objects, which were not clearly identified by other IR acquisition modes (μFT-IR an ATR FT-IR). This emphasized the applicability and effectiveness of ER FT-IR and DRIFTS techniques for the analysis of plastics in cultural heritage collections.

The findings of this study aimed to assist the development of an IR spectral database, which are strongly required considering the complexity of IR reflectance spectra one can obtain. As recently stated by Rosi et al. [74], some efforts have been made to improve the analytical power of FT-IR reflection spectroscopy for the investigation of the chemical properties of cultural heritage materials. The present study contributed to this objective by providing new and deeper insights into the use of ER FT-IR and DRIFTS as complementary techniques to characterize heritage plastic objects.

3.6. References

[1] Shashoua Y. Conservation of plastics. Oxford: Butterworth-Heinemann; 2008.

[2] Quye A, Williamson C, editors. Plastics: collecting and conserving. Edinburg: NMS Publishing Limited; 1999.

[3] Lavédrine B, Fournier A, Martin G, editors. Preservation of Plastic Artefacts in Museum Collections (POPART). Paris: Comité Des Travaux Historiques et Scientifiques (CTHS); 2012.

[4] van Oosten T. PUR Facts: conservation of polyurethane foam in art and design. Amsterdam: Amsterdam University Press; 2011.

[5] Analytical Methods Committee, AMCTB No. 83. Identification of plastics in cultural heritage collections by Fourier transform infrared spectroscopy (FTIR). Anal Methods 2018; 10: 687-689. DOI: 10.1039/C8AY90010H.

[6] Crocombe RA. Portable spectroscopy. Appl Spectrosc. 2018; 72(12): 1701-1715. DOI: 10.1177/2818809719

[7] Picollo M, Bartolozzi G, Cucci C, Galeotti M, Marchiafava V, Pizzo B. Comparative study of Fourier transform infrared spectroscopy in transmission, attenuated total reflection, and total reflection modes for the analysis of plastics in the cultural heritage field. Appl Spectrosc. 2014; 68(4): 389-397. DOI: 10.1366/13-07199.

[8] Cucci C, Bartolozzi G, Marchiafava V, Picollo M, Richardson E. Study of semi-synthetic plastic objects of historic interest using non-invasive total reflectance FT-IR. Microchem J. 2016; 124: 889-897. DOI: 10.1016/j.microc.2015.06.010.

[9] Saviello D, Toniolo L, Goidanich S, Casadio F. Non-invasive identification of plastic materials in museum collections with portable FTIR reflectance spectroscopy: reference database and practical applications. Microchem J. 2016; 124: 868-877. DOI: 10.1016/j.microc.2015.07.016.
[10] Bell J, Nel P, Stuart B. Non-invasive identification of polymers in cultural heritage collections: evaluation, optimisation and application of portable FTIR (ATR and external reflectance) spectroscopy to three-dimensional polymer-based objects. Herit Sci. 2019; 7(95): 1-18. DOI: 10.1186/s40494-019-0336-0.
[11] Carter EA, Swarbrick B, Harrison TM, Ronai L. Rapid identification of cellulose nitrate and cellulose acetate film in historic photograph collections. Herit Sci. 2020; 8(51): 1-13. DOI: 10.1186/s40494-020-00395-y.
[12] Soares I, França de Sá S, Ferreira JL. A first approach into the characterisation of historical plastic objects by in situ diffuse reflection infrared Fourier transform (DRIFT) spectroscopy. Spectrochim Acta Part A 2020; 240: 118548. DOI: 10.1016/j.saa.2020.118548.
[13] Callapez ME. An interdisciplinary project on the history of plastics in Portugal. e-plastory 2017; 1: 1-8. URL: e-plastory/article/view/Callapez/34.
[14] França de Sá S, Marques da Cruz S, Callapez ME, Carvalho V. Plastics that made history – The contribution of conservation science for the history of the Portuguese Plastics Industry. Conservar Património 2020; 35: 85-100. DOI: 10.14568/cp2019017.
[15] Derrick MR, Stulik D, Landry JM. Infrared spectroscopy in conservation science. Los Angeles: Getty Publications; 1999.
[16] Griffiths PR, de Haseth JA. Fourier transform infrared spectrometry. Hoboken: Wiley, second ed.; 2007.
[17] Korte EH, Röseler A. Foundations and features of infrared reflection techniques. In: Schrader B, editor. Infrared and Raman spectroscopy: methods and applications. Weinheim: Wiley-VCH; 1995. p. 572-602.
[18] Everall NJ, Chalmers JM, Griffiths PR. Vibrational spectroscopy of polymers: principles and practice. Chichester: Wiley; 2007.
[19] Chalmers JM, Everall NJ. Qualitative and quantitative analysis of plastics, polymers and rubbers by vibrational spectroscopy. In: Chalmers JM, Griffiths PR, editors. Handbook of vibrational spectroscopy. Chichester: Wiley, Vol. 1; 2007. DOI: 10.1002/9780470027325.s6101.pub2.
[20] Fabbri M, Picollo M, Porcinai S, Bacci M. Mid-infrared fiber-optics reflectance spectroscopy: a noninvasive technique for remote analysis of painted layers. Part I: technical setup. Appl Spectrosc. 2001; 55(4): 420-427. DOI: 10.1366/0003702011952172; and references [3-6] therein.
[21] Fabbri M, Picollo M, Porcinai S, Bacci M. Mid-infrared fiber-optics reflectance spectroscopy: A noninvasive technique for remote analysis of painted layers. Part II: statistical analysis of spectra. Appl Spectrosc. 2001; 55(4): 428-433. DOI: 10.1366/0003702011952181.
[22] Kortüm G. Reflectance spectroscopy: principles, methods, applications. New York: Springer Verlag; 1969.
[23] Blitz JP. Diffuse reflectance spectroscopy. In: Mirabella FM, editor. Modern techniques in applied molecular spectroscopy. New York: John Wiley & Sons, Techniques in Analytical Chemistry Series, Vol. 14; 1998. p. 185-219.
[24] Mitchell MB. Fundamentals and applications of diffuse reflectance infrared Fourier transform (DRIFT) spectroscopy. In: Urban MW, Craver CD, editors. Structure property relation in polymers, spectroscopy and performance. Washington: ACS Publications, Advances in Chemistry Series, Vol. 236; 1993. p. 351-375. DOI: 10.1021/ba-1993-0236.ch013.
[25] Korte EH, Röeseler A. Infrared reststrahlen revisited: commonly disregarded optical details related to $n<1$. Anal Bioanal Chem. 2005; 382: 1987-1992. DOI: 10.1007/s00216-005-3407-x.
[26] Miljkovic M, Bird B, Diem M. Line shape distortion effects in infrared spectroscopy. Analyst 2012; 137: 3954-3964. DOI: 10.1039/C2AN35582E.
[27] Kattner J, Hoffmann H. External reflection spectroscopy of thin films on dielectric aubstrates. In: Chalmers JM, Griffiths PR, editors. Handbook of vibrational spectroscopy. Chichester: Wiley, Vol. 2; 2002. p. 1009-

1027.
[28] Milosevic M, Berets SL. A review of FT-IR diffuse reflection sampling considerations. Appl Spectrosc Rev. 2002; 37(4): 347-364. DOI: 10.1081/ASR-120016081.
[29] Allen TJ. Paint sample presentation for Fourier transform infrared microscopy. Vib Spectrosc. 1992; 3(3): 217-237. DOI: 10.1016/0924-2031(92)87004-Y.
[30] Fraser DJJ, Griffiths PR. Effect of scattering coefficient on diffuse reflectance infrared spectra. Appl Spectrosc. 1990; 44(2): 193-199. DOI: 10.1366/0003702904085561.
[31] Arrizabalaga I, Gómez-Laserna O, Aramendia J, Arana G, Madariaga JM. Applicability of a diffuse reflectance infrared Fourier transform handheld spectrometer to perform in situ analyses on cultural heritage materials. Spectrochim Acta Part A 2014; 129: 259-267. DOI: 10.1016/j.saa.2014.03.096.
[32] Lucarini V, Peiponen K-E, Saarinen JJ, Vartiainen EM. Kramers-Kronig relations in optical materials research. Berlin: Springer Verlag, Optical Sciences, Vol. 110; 2005.
[33] Rampazzi L, Brunello V, Corti C, Lissoni E. Non-invasive techniques for revealing the palette of the Romantic painter Francesco Hayez. Spectrochim Acta Part A 2017; 176: 142-154. DOI: 10.1016/j.saa.2017.01.011.
[34] Invernizzi C, Rovetta T, Licchelli M, Malagodi M. Mid and near-infrared reflection spectral database of natural organic materials in the cultural heritage field. Int J Anal Chem. 2018; 1-16. DOI: 10.1155/2018/7823248.
[35] Zuena M, Pensabene Buemi L, Stringari L, Legnaioli S, Lorenzetti G, Palleschi V, Nodari L, Tomasin P. An integrated diagnostic approach to Max Ernst's painting materials in his *Attirement of the Bride*. J Cult Herit. 2020; 43: 329-337. DOI: 10.1016/j.culher.2019.10.010.
[36] McClelland A, Bulat E, Bernier B, Murphy EL. Specular reflection FTIR: a non-contact method for analyzing coatings on photographs and other cultural materials. J Am Inst Conserv. 2020; 59(2): 123-136. DOI: 10.1080/01971360.2019.1660546.
[37] Moretti P, Rosi F, Miliani C, Daugherty M, Jan van den Berg K, Cartechini L. Non-invasive reflection FT-IR spectroscopy for on-site detection of cleaning system residues on polychrome surfaces. Microchem J. 2020; 157: 105033. DOI: 10.1016/j.microc.2020.105033.
[38] Invernizzi C, Fiocco G, Iwanicka M, Kowalska M, Targowski P, Blümich B, Rehorn C, Gabrielli V, Bersani D, Licchelli M, Malagodi M. Non-invasive mobile technology to study the stratigraphy of ancient Cremonese violins: OCT, NMR-MOUSE, XRF and reflection FT-IR spectroscopy. Microchem J. 2020; 155: 104754. DOI: 10.1016/j.microc.2020.104754.
[39] Izzo F, Germinario C, Grifa C, Langella A, Mercurio M. External reflectance FTIR dataset (4000-400 cm^{-1}) for the identification of relevant mineralogical phases forming cultural heritage materials. Infrared Phys Technol. 2020; 106: 103266. DOI: 10.1016/j.infrared.2020.103266.
[40] Monico L, Cartechini L, Rosi F, Chieli A, Grazia C, De Meyer S, Nuyts G, Vanmeert F, Janssens K, Cotte M, De Nolf W, Falkenberg G, Crina Anca Sandu I, Storevik Tveit E, Mass J, Pereira de Freitas R, Romani A, Miliani C. Probing the chemistry of CdS paints in *The Scream* by in situ noninvasive spectroscopies and synchrotron radiation x-ray techniques. Sci Adv. 2020; 6(20): eaay3514. DOI: 10.1126/sciadv.aay3514.
[41] Legan L, Leskovar T, Črešnar M, Cavalli F, Innocenti D, Ropret P. Non-invasive reflection FTIR characterization of archaeological burnt bones: reference database and case studies. J Cult Herit. 2020; 41: 13-26. DOI: 10.1016/j.culher.2019.07.006.
[42] Ploeger R, Scalarone D, Chiantore O. Non-invasive characterisation of binding media on painted glass magic lantern plates using mid-infrared fibre-optic reflectance spectroscopy. J Cult Herit. 2010; 11(1): 35-41. DOI: 10.1016/j.culher.2009.01.005.
[43] Invernizzi C, Daveri A, Vagnini M, Malagodi M. Non-invasive identification of organic materials in historical stringed musical instruments by reflection infrared spectroscopy: a methodological approach. Anal Bioanal Chem. 2017; 409: 3281-3288. DOI: 10.1007/s00216-017-0296-8.
[44] Monico L, Rosi F, Miliani C, Daveri A, Brunetti BG. Non-invasive identification of metal-oxalate complexes on polychrome artwork surfaces by reflection mid-infrared spectroscopy. Spectrochim Acta A 2013; 116: 270-

280. DOI: 10.1016/j.saa.2013.06.084.
[45] Buti D, Rosi F, Brunetti BG, Miliani C. In-situ identification of copper-based green pigments on paintings and manuscripts by reflection FTIR. Anal Bioanal Chem. 2013; 405: 2699-2711. DOI: 10.1007/s00216-013-6707-6.
[46] Poli T, Elia A, Chiantore O. Surface finishes and materials: fiber-optic reflectance spectroscopy (FORS) problems in cultural heritage diagnostics. e-Preserv Sci. 2009; 6: 174-179. URL: e-preservationscience/2009/Poli-03-07-2008.
[47] Bouchard J, Douek M. Structural and concentration effects on the diffuse reflectance FTIR spectra of cellulose, lignin and pulp. J Wood Chem Technol. 2006; 13(4): 481-499. DOI: 10.1080/02773819308020530.
[48] Claybourn M. Infrared reflectance spectroscopy of polymers: analysis of films, surfaces and interfaces. Moorhead: Global Press; 1998.
[49] Lipson SG, Lipson H, Tannhauser DS. Optical physics. Cambridge: Cambridge University Press, third ed.; 1995.
[50] Chalmers JM, Everall NJ, Ellison S. Specular reflectance: a convenient tool for polymer characterization by FTIR-microscopy?. Micron 1996; 27(5): 315-328. DOI: 10.1016/S0968-4328(96)00021-2.
[51] Yamamoto K, Ishida H. Optical theory applied to infrared spectroscopy. Vib Spectrosc. 1994; 8(1): 1-36. DOI: 10.1016/0924-2031(94)00022-9.
[52] Kubelka P, Munk F. An article on optics of paint layers. Z Tech Phys. 1931; 12: 593-609.
[53] Goldstein D. Mueller matrices for reflection and transmission. In: Polarized light. New York: Marcel Dekker Inc., second ed.; 2003. p. 133-164.
[54] Milosevic M. Fresnel equations. In: Milosevic M, editor. Internal reflection and ATR spectroscopy. Hoboken: John Wiley & Sons Inc.; 2012. p. 39-54.
[55] Krimm S, Liang CY, Sutherland GBBM. Infrared spectra of high polymers. II. Polyethylene. J Chem Phys. 1956; 25(3), 549-562. DOI: 10.1063/1.1742963.
[56] Noda I, Dowrey AE, Haynes JL, Marcott C. Group frequency assignments for major infrared bands observed in common synthetic polymers. In: Mark JE, editor. Physical properties of polymers handbook. New York: Springer, second ed.; 2007. p. 395-406.
[57] Read BE, Stein RS. Polarized Infrared studies of amorphous orientation in polyethylene and some ethylene sopolymers. Macromolecules 1968; 1(2): 116-126. DOI: 10.1021/ma60002a004.
[58] Krimm S. Infrared spectra of high polymers. In: Fortschritte Der Hochpolymeren-Forschung. Berlin: Springer, Advances in Polymer Science, Vol 2/1; 1960. Vol 2/1, pp. 51-172. DOI: 10.1007/BFb0050351.
[59] Gedde UW, Mattozzi A. Polyethylene morphology. In: Albertsson AC, editor. Long term properties of polyolefins. Berlin: Springer, Advances in Polymer Science, Vol. 169; 2004. p. 29-74. DOI: 10.1007/b94176.
[60] Woo EM, Lugito G. Origins of periodic bands in polymer spherulites. Eur Polym J. 2015; 71: 27-60. DOI: 10.1016/j.eurpolymj.2015.07.045.
[61] De Oliveira MG, Pessoa OJr, Vargas H, Galembeck F. Low-density polyethylene depth profile analysis by photoacoustic spectroscopy. J Appl Polym Sci. 1988; 35: 1791-1802. DOI: 10.1002/app.1988.070350707.
[62] Wang Y, Abe Y, Matsuura Y, Miyagi M, Uyama H. Refractive indices and extinction coefficients of polymers for the mid-infrared region. Appl Opt. 1998; 37(30): 7091-7095. DOI: 10.1364/ao.37.007091.
[63] Boldizar A, Möller K. Degradation of ABS during repeated processing and accelerated ageing. Polym Degrad Stab. 2003; 81(2): 359-366. DOI: 10.1016/S0141-3910(03)00107-1.
[64] Salman SR, Al-Shama'a ND. Effect of thermal aging on the optical properties of ABS plastics. Polym Plast Technol Eng. 1991; 30(4): 343-349. DOI: 10.1080/03602559108021000.
[65] Saviello D, Pouyet E, Toniolo L, Cotte M, Nevin A. Synchrotron-based FTIR microspectroscopy for the mapping of photo-oxidation and additives in acrylonitrile-butadiene-styrene model samples and historical objects. Anal Chim Acta 2014; 843: 59-72. DOI: 10.1016/j.aca.2014.07.021.
[66] Gardette JL. Fundamental and technical aspects of the photooxidation of polymers. In: Hamid SH, editor.

Handbook of polymer degradation. New York: Marcel Dekker, second ed.; 2000. p. 671-689.
[67] Gulmine JV, Janissek PR, Heise HM, Akcelrud L. Degradation profile of polyethylene after artificial accelerated weathering. Polym Degrad Stab. 2003; 79(3): 385-397. DOI: 10.1016/S0141-3910(02)00338-5.
[68] Gardette M, Perthue A, Gardette JL, Janecska T, Földes E, Pukánszky B, Therias S. Photo- and thermal-oxidation of polyethylene: comparison of mechanisms and influence of unsaturation content. Polym Degrad Stab. 2013; 98(11): 2383-2390. DOI: 10.1016/j.polymdegradstab.2013.07.017.
[69] Doménech-Carbó MT, Doménech-Carbó A, Gimeno-Adelantado JV, Bosch-Reig F. Identification of synthetic resins used in works of art by Fourier transform infrared spectroscopy. Appl Spectrosc. 2001; 55(12): 1590-1602. DOI: 10.1366/0003702011954152.
[70] Spectral database Infrared & Raman Users Group (IRUG) (accessed 30.11.2020).
[71] Monico L, Janssens K, Cotte M, Sorace L, Vanmeert F, Brunetti BG, Miliani C. Chromium speciation methods and infrared spectroscopy for studying the chemical reactivity of lead chromate-based pigments in oil medium. Microchem J. 2016; 124: 272-282. DOI: 10.1016/j.microc.2015.08.028.
[72] Castro K, Pérez-Alonso M, Rodríguez-Laso MD, Fernández LA, Madariaga JM. On-line FT-Raman and dispersive Raman spectra database of artists' materials (e-VISART database). Anal Bioanal Chem. 2005; 382: 248-258. DOI: 10.1007/s00216-005-3072-0.
[73] Cowley ACD. Molybdate orange. In: Lewis PA, editor. Pigment handbook, properties and economics. New York: John Wiley & Sons Inc., Vol. I, second ed.; 1988. p. 327-345.
[74] Rosi F, Cartechini L, Sali D, Miliani C. Recent trends in the application of Fourier Transform Infrared (FT-IR) spectroscopy in heritage science: from micro- to non-invasive FT-IR. Phys Sci Rev. 2019; 4(11): 20180006. DOI: 10.1515/psr-2018-0006

This is an Accepted Manuscript of an article published by John Wiley and Sons Ltd in Journal of Raman Spectroscopy, on 20/07/2018, available online:

Angelin EM, Babo S, Ferreira JL, Melo MJ. Raman microscopy for the identification of pearlescent pigments in acrylic works of art. J Raman Spectrosc. 2019; 50: 232-241. DOI: 10.1002/jrs.5431.

4. Raman microscopy for the identification of pearlescent pigments in acrylic works of art

Abstract

In this work, pearlescent pigments used to create luster in poly(methyl methacrylate) artworks by Ângelo de Sousa (1938-2011) were identified in an effort to predict their possible degradation. Raman microscopy was used, in situ, to identify plumbonacrite and bismuth oxychloride. Unequivocal characterization of plumbonacrite and bismuth oxychloride was made possible by comparison with reference materials, synthesized for this study. The vibrational pattern (infrared and Raman) of both pigments is discussed. Based on their Raman ν_1 stretching mode at around 1050 cm^{-1}, we show that it is possible to differentiate between the two basic lead carbonates that are both reported in the literature to be pearlescent: hydrocerussite $Pb_3(CO_3)_2(OH)_2$ and plumbonacrite $Pb_5(CO_3)_3O(OH)_2$. Raman microscopy was thus, for the first time, used as fingerprint tool for the molecular identification of pearlescent pigments in plastic materials. Based on these findings, better-informed conservation strategies for the acrylic sculptures will be developed.

4.1. Introduction

Pearlescent pigments have been used since the beginning of the 20th century to imitate mother-of-pearl. Mostly synthetic, they consist of flakes or thin platelet-like particles which partially reflect and partially transmit light. The pearlescent effect results from a high refractive index, smooth surfaces, optimum platelet thickness and diameter, and in addition, to a specific alignment of the platelets in the resin [1,2]. Pearlescent pigments confer a sense of depth due to the simultaneous reflection from many layers of platelets in a parallel orientation within the resin. The effect is referred to as *nacreous luster* or *pearl luster*, distinguished from *metallic luster* where the material's surface mostly reflects incident light [3,4].

In museum collections, pearlescent pigments may be present in paints, inks, ceramics, and especially, plastic objects (buttons, bijouterie, etc.). The identification of pearlescent pigments in plastic articles is challenging owing to the small size of the particles (between 1 and 200 μm) and the low amount of pigment dispersed in the resin matrix (between 0.5% and 2%) [5]. Given this scale, Raman microscopy can be explored as a possible analytical tool for their characterization in situ.

An important Portuguese artist, Ângelo de Sousa (1938-2011), explored the properties of poly(methyl methacrylate) (PMMA) in a series of acrylic sculptures executed between 1965 and 1967. These included six artworks made with white, yellow, and orange lustrous sheets [6,7]. Two later works using yellow and red acrylic sheets appear to have been made by the artist in the early 2000s for a retrospective exhibition in 2006 [8]. It was important to distinguish these sculptures from his earlier work, particularly because they presented different surface effects to those from the 1960s. Ângelo de Sousa explored the thermoplastic properties of PMMA by heating, cutting, and then modelling the sheets into three dimensional forms. His sculptures have various sizes, from 18 to 65 cm in height. Those made in the 1960s are characterized by a strong pearlescent luster, whereas the ones thought to be more recent appear more brilliant but not with the same luster.

The identification of dyes and pigments in plastic artifacts is a recent line of research in conservation [9,10],

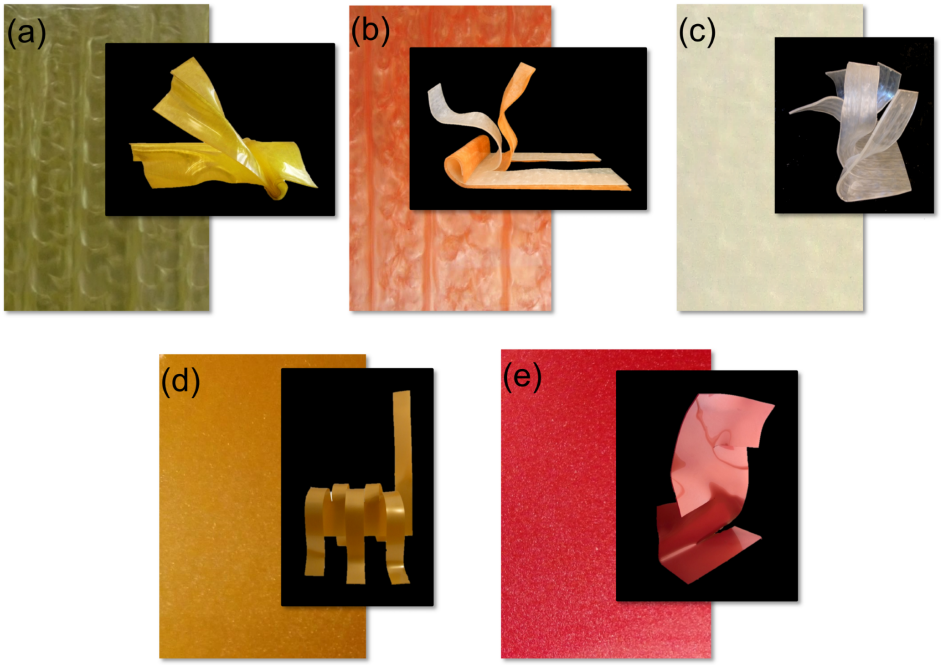

Figure 4.1.: Pictures of the five pearlescent acrylic sheets found in the studio of Ângelo de Sousa (Porto, Portugal) probably made in 1960s (a-c) and 2000s (d-e). A possible match with the original acrylic sculptures by the artist is presented for each acrylic sheet.

and to date, no publications regarding the identification of pearlescent pigments by Raman spectroscopy have been found. Understanding the original materials used by the artist is important in the interpretation of their work over time, because some materials can be susceptible to degradation which will affect their appearance. For Ângelo de Sousa's sculptures, the difference between the original works and those thought to be from a later date was intriguing, and an explanation was sought. Furthermore, establishing the nature of the materials used allows future research into the possible mechanisms for their degradation. Therefore, in this work, the use of Raman microscopy as fingerprint tool for the in situ molecular investigation of pearlescent pigments in plastic materials was explored.

The investigation was carried on lustrous acrylic sheets found in the studio of Ângelo de Sousa (Porto, Portugal), possibly the same that were used in the actual artworks [11]. These acrylic sheets, one white, one yellow, and one orange, were likely purchased by Ângelo de Sousa from a small company active in the 1960s, *Plásticos do Sado*, which produced pearlescent acrylic sheets for the button industry [11]. Two other sheets, one yellow and one red, were also found and thought to be produced in the early 2000s. In **Figure 4.1**, these five sheets are displayed with possible dates and correlation with the original sculptures.

Based on a literature survey and preliminary results from X-ray fluorescence analysis, hydrocerussite (lead white), plumbonacrite, and bismuth oxychloride were considered most likely to be the pigments used [2,11].

These monocrystalline pearlescent pigments were produced in the 20th century and used in plastics [5,11,12]. The basic lead carbonates, which are described as being pearlescent, include hydrocerussite $Pb_3(CO_3)_2(OH)_2$ and the more basic plumbonacrite $Pb_5(CO_3)_3O(OH)_2$ [13-15]. In modern manufacture, the basic lead carbonate pigments both take the form of regular thin hexagonal platelets [13], making the distinction between the two different pigments by optical observation extremely difficult.

Basic lead carbonates with pearlescent properties were manufactured in the 1930s [16,17] and, by the 1950s and 1960s, represented the most common synthetic pearlescent pigments employed in the production of artificial pearls, bijouterie, and acrylic and polyester buttons. From the late 1960s, they started to be replaced by other pigments, such as bismuth oxychloride BiOCl due to growing concerns regarding the toxicity of lead based

materials [2-4,18].
The formula $Pb_3(CO_3)_2(OH)_2$ (or $2PbCO_3 \cdot Pb(OH)_2$) is generally reported in descriptions of the basic lead carbonates used as pearlescent pigments [3-5,18,19]. This corresponds to hydrocerussite, also known as lead white. As a mineral, hydrocerrusite crystallizes in the trigonal system $R3m$ space group [20], whereas synthetic plumbonacrite crystallizes in the trigonal system $P3c1$ space group and is represented as pentaleadtricarbonatedihydroxide oxide, $Pb_5(CO_3)_3O(OH)_2$ (or $3PbCO_3 \cdot Pb(OH)_2 \cdot PbO$) [14]. The currently accepted structure was proposed by Krivovichev and Burns [21], instead of $Pb_{10}(CO_3)_6O(OH)_6$ (or $6PbCO_3 \cdot Pb(OH)_2 \cdot PbO$) as proposed originally by Olby [22]. Nevertheless, $Pb_{10}(CO_3)_6O(OH)_6$ is still used in the literature, possibly due the fact that the experimental X-ray diffraction (XRD) pattern obtained by Olby and the calculated XRD pattern based on crystallographic data from Krivovichev and Burns are similar.
In the conservation literature, plumbonacrite was reported for the first time in the early 1970s by Feller et al. [13] with the formula proposed by Olby [22]. Although plumbonacrite has been reported as corrosion product of lead in an acidic environment [23-25]; a degradation product in stone conservation [26]; an alteration in red lead [27]; and a conversion product between different lead species in lead soap formation in paintings [28-30]; its use as a pigment is rarely reported [14]. Even though both hydrocerussite and plumbonacrite are both basic lead(II) carbonate compounds, their stability may be quite different [31-33].
Bismuth oxychloride is a rare example of a nontoxic heavy metal compound, in use since the early 1960s in cosmetics and only in the late 1960s in the plastic industry [2]. It is a pearlescent pigment currently used in coatings for cars and in cosmetics, printing, buttons, and bijouterie [5,34]. As a mineral, bismoclite crystallizes in the tetragonal system $P4/nmm$ space group and is characterized by thin octagonal/square platelets. BiOCl monocrystal platelets are formed by hydrolysis of acid bismuth salt solutions in the presence of chlorine ions (e.g., $BiCl_3$) in water [2,5].
In order to confirm the nature of the pigments responsible for the pearlescent luster in the acrylic sheets found in Ângelo de Sousa's studio and those in his sculptures, an investigation of the pigments in the acrylic sheets was carried out in situ using Raman microscopy within a multianalytical approach which included observation under the microscope and micro-energy dispersive X-ray fluorescence (EDXRF) analysis. Reference materials were required for comparison, therefore crystals of plumbonacrite and bismuth oxychloride were synthesized for this research and their composition confirmed with XRD, Fourier-transform infrared spectroscopy, and Raman analyses. An analytical grade basic lead(II) carbonate without any further purification was used as the reference for the hydrocerussite.

4.2. Experimental

4.2.1. Reference materials

All reagents used in the synthesis of the pigments were analytical grade, and Millipore water was used.

4.2.1.1. Plumbonacrite

Plumbonacrite is no longer commercially available [35]. Several different methods of synthesis described in the literature were tested without success [22,31,36]. Therefore, we adapted the method reported by Krivovichev and Burns [36] which involved heating a mixture of 0.10 g of PbO and 0.10 g of K_2CO_3 in 5 ml of H_2O, in a Teflon-lined Parr bomb. This was heated to 230 °C for 36 hr. The white powder which remained in the bottom of the Teflon-lined Parr bomb was then collected by filtration and washed several times with Millipore water before being left to dry.

4.2.1.2. Hydrocerussite

A few milligrams of basic lead(II) carbonate were used without further purification.

4.2.1.3. BiOCl

Based on **Equation (1)** proposed by Brauer, but not on his method, crystals of BiOCl were synthetized [37]

$$BiCl_3 + H_2O \rightarrow BiOCl + 2HCl \qquad \textbf{(1)}$$

The 0.5 g ($1.55x10^{-3}$ mol) of bismuth (II) chloride ($BiCl_3$) were dispersed in 100 ml of water and stirred at room temperature for 30 min. The precipitate was collected by filtration and washed several times with Millipore water. The powder obtained was dried under vacuum for 4 hr. Reagent grade $BiCl_3$ was used without further purification.

4.2.2. Characterization methods

4.2.2.1. Optical microscopy (OM)

Optical microscopy (OM) was used to identify the shape, size, orientation, and distribution of the pearlescent pigments in the plastic sheets from Ângelo's studio. OM was also used to characterize the physical and optical properties of the pearlescent reference pigments. Images were acquired using a Zeiss Axioplan 2 Imaging system (HAL 100) coupled to a Nikon DXM1200F digital camera and ACT-1 software. Different illumination modes (brightfield and darkfield) were used.

4.2.2.2. Infrared spectroscopy (FTIR)

Infrared analysis was performed with a Nexus spectrophotometer in transmission mode, from 4000 to 400 cm^{-1}, with KBr pellets, 128 coadded scans and 4 cm^{-1} spectral resolution. Omnic E.S.P.5.2 software was used to perform the spectral analysis of the products. All spectra are presented as acquired without any baseline correction or other treatment.

4.2.2.3. Raman microscopy

Raman microscopy was carried out using a Labram 300 Jobin Yvon spectrometer, equipped with a He-Ne 17-mW laser and a 100-mW diodes laser operating at 632.8 and 785 nm, respectively. Spectra were recorded as an extended scan. The system was calibrated using a silicon standard. The laser beam was focused either with a 50× or a 100× Olympus objective lens. The laser power at the surface of the samples was controlled with neutral density filters (optical densities 0.3 and 0.6). Raman data analysis was performed using LabSpec 5 software. All spectra are presented as acquired without any baseline correction or other treatment.

4.2.2.4. X-ray diffraction (XRD)

X-ray powder diffractograms were acquired with a Benchtop X-Ray Diffractometer RIGAKU MiniFlex II, using CuK_α radiation with a current intensity of 15 mA and a 30 kV voltage in the 2Θ range between 2° and 60° (step size of 0.01°). The ICDD PDF-2 reference database (2007) was used to interpret the XRD patterns. The Powder Cell software package was used to simulate diffractograms to compare with the experimental data [38].

4.2.2.5. Micro-EDXRF

Micro-EDXRF results were obtained using an ArtTAX spectrometer (Intax GmbH) equipped with a molybdenum (Mo) anode and Xflash detector. The experimental parameters used were 25 kV voltage and 300 μA of

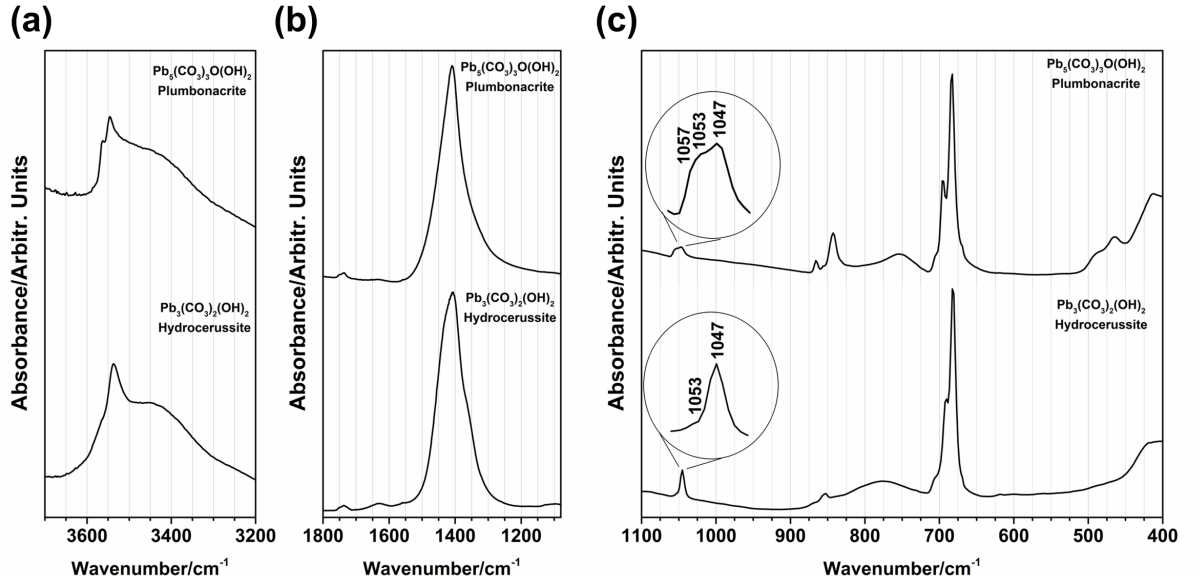

Figure 4.2.: FTIR of plumbonacrite $Pb_5(CO_3)_3O(OH)_2$ and hydrocerussite $Pb_3(CO_3)_2(OH)_2$.

intensity for 360s acquisition time, under a Helium gas flux. The experimental parameters used permitted the reduction of the *bremsstrahlung* effect ("braking radiation") due to the polymeric (organic) matrix.

4.3. Results and Discussion

4.3.1. Characterization of the synthesized pigments

The synthesized plumbonacrite was observed in OM and consisted of hexagonal crystals with various diameters and thickness (**Figure B.1**). The lamellar aggregation of the hexagonal crystals was also visible in OM, and iridescent surface colors were observed. In the case of BiOCl, no crystals were seen with OM due to their very small dimension (<1 μm).

The composition of the crystals synthesized in this study was confirmed through XRD analysis (**Figures B.2** and **B.3**). The XRD patterns of both pigments match simulations from published crystallographic data [21,39] and database information for plumbonacrite $Pb_5(CO_3)_3O(OH)_2$ (ICDD PDF 73-8925) and bismoclite BiOCl (ICDD PDF 06-0249), respectively. Differences of relative intensities between their diffractograms and XRD simulations are associated with the preferred orientation of the crystals.

The XRD pattern of the plumbonacrite we synthesized also corresponds to $Pb_{10}(CO_3)_6(OH)_6$ as prepared by Olby [22] (ICDD PDF 19-0680). Therefore, we assume that the plumbonacrite reported by Olby is the same basic lead carbonate that was studied by Krivovichev and Burns, although described by different formulas by the two authors [21,22].

The infrared and Raman spectra of plumbonacrite are shown in **Figures 4.2** and **4.3**, together with the spectra of hydrocerussite for comparison. Raman shift values and infrared wavenumbers for the spectral features with their respective assignments are listed in **Table 4.1**.

In the Raman spectra, it is possible to distinguish plumbonacrite by its ν_1 stretching mode, characterized by three strong different sub-bands (1048, 1052, and 1056 cm^{-1}) whereas hydrocerussite has only two sub-bands (1048 and 1051 cm^{-1}) [26,40,41]; this reflects the three and two independent sites for the carbonate ion in plumbonacrite and hydrocerussite, respectively. In the infrared spectra, the two carbonates are distinguished by low intensity but well resolved in-plane and out-of-plane bending absorptions of CO_3^{2-} between 680 and 710 cm^{-1} and 840 and 870 cm^{-1}, respectively. OH stretching frequencies at 3545 and 3562 cm^{-1} and at 3536

Table 4.1.: Raman and infrared assignments of hydrocerussite $Pb_3(CO_3)_2(OH)_2$ and plumbonacrite $Pb_5(CO_3)_3O(OH)_2$.

Hydrocerussite		**Plumbonacrite**		
Raman ($\Delta\nu$/cm^{-1})	**Infrared (ν/cm^{-1})**	**Raman ($\Delta\nu$/cm^{-1})**	**Infrared (ν/cm^{-1})**	**Assignments**
73m		73m		Lattice modes
		86sh		
105s		105s		
		113s		
126sh		126s		
		170m		
		273m,br		
324w,br		306m		
415m	415m	398m		ν_{PbO}
		427sh	414m	
		461m	465mw	
		490w		
677w	681s	678w	683s	ν_4 (in-plane δCO_3^{2-})
693vw	690m	691vw	695m	
	706sh	705 w	706w	
	775br		754w,br	δ_{PbOH}
		845w	842w	ν_2 (out-of-plane δCO_3^{2-})
	855w		856vw	
863vw	869vw	865 w	866w	
	1045m			ν_1 (ν_s CO_3^{2-})
1048vvs		1048vvs	1047vw	
1051vs	1053vw	1052vs	1053vw	
		1056s	1057sh	
1362m,br	1360sh			ν_3 (ν_{as} CO_3^{2-})
1396sh	1406vs	1384m	1409vs	
		1690vw		$2\nu_2$
1733vw		1731vw		
	1736w		1736w	$\nu_1 + \nu_4$
			1748vw	
	3536w		3545w	ν_{OH}
			3562w	

Note. m: medium; s: strong; w: weak; v: very; sh: shoulder; br: broad; ν: stretching (a: symmetric; as: asymmetric); δ: bending

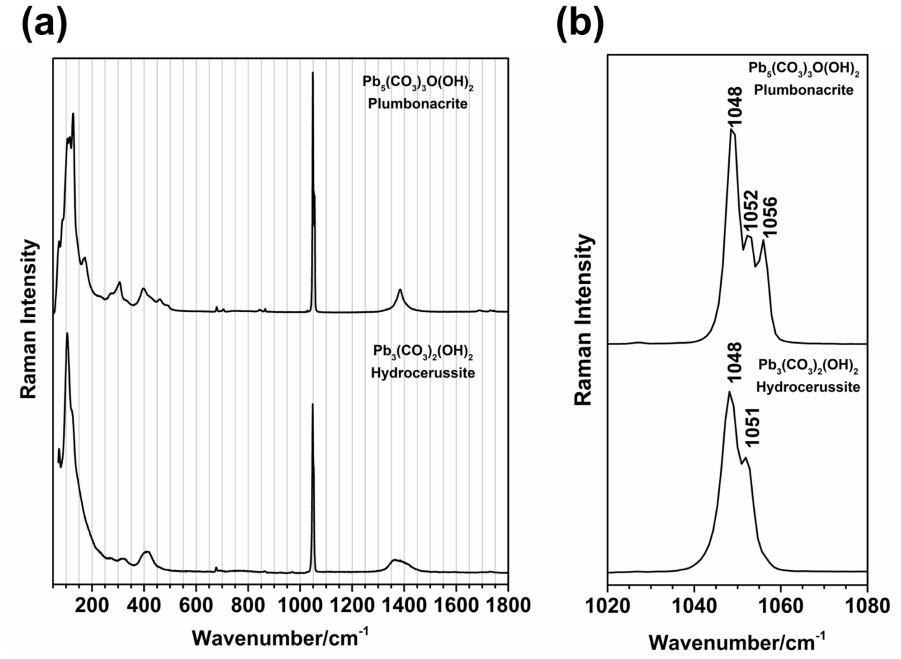

Figure 4.3.: (a) Raman spectra of plumbonacrite $Pb_5(CO_3)_3O(OH)_2$ and hydrocerussite $Pb_3(CO_3)_2(OH)_2$. (b) Detail of the ν_1 stretching mode of the carbonate ion from 1020 to 1080 cm^{-1} (632.8 nm excitation).

Table 4.2.: Raman and infrared assignments of bismuth oxychloride BiOCl

BiOCl		
Raman ($\Delta\nu/cm^{-1}$)	**Infrared (ν/cm^{-1})**	**Assignments**
60m		A_{1g}
142vs		A_{1g}
198s		E_g
394m		B_{1g}+ E_g
	528	A_{2u}

Note. m: medium; s: strong; v: very

cm^{-1} in plumbonacrite and hydrocerussite, respectively, support this observation [42] (**Table 4.1**).

The assignments for the normal modes of vibration of carbonate ion are well established, and all fundamental internal vibrations of the carbonate ion are detected between 1800 and 600 cm^{-1} [43-45]. Both spectra are dominated by the strong stretching associated with the carbonate ion: although a strong band associated to ν_3 mode is observed in the infrared spectra (1406 and 1409 cm^{-1} in hydrocerussite and plumbonacrite, respectively; **Figure 4.2**), the ν_1 mode rises to a very strong and sharp band at around 1050 cm^{-1} in the Raman spectra (**Figure 4.3**).

The vibrational spectra of bismuth oxychloride is due to its isostructure (D^7_{4h} space group) characterized by two molecular formulas per unit cell with A_{1g}, B_{1g}, E_g Raman active modes, and E_u, A_{2u} infrared-active modes. In the Raman spectra of synthetized BiOCl, which is reported in **Figure 4.4**, both halogen sensitive and halogen insensitive bands are observed, whereas only the A_{2u} vibration mode is detected at 528 cm^{-1} [46,47]. The vibration bands with related assignments are listed in **Table 4.2**.

For bismuth oxychloride, six Raman bands would be expected ($2A_{1g}$ + B_{1g} + $3E_g$), however only three resolved Raman bands were found for the synthetized BiOCl. The Raman bands below 200 cm^{-1} are halogen

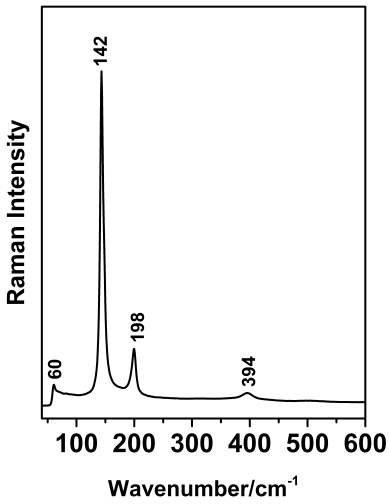

Figure 4.4.: Raman spectrum of synthetized bismuth oxychloride BiOCl (632.8 nm excitation).

sensitive including the A_{1g} external Bi–Cl mode (60 cm^{-1}), E_g internal Bi–Cl stretching mode (198 cm^{-1}), and the strongest A_{1g} internal Bi–Cl stretching mode (142 cm^{-1}). At around 400 cm^{-1}, the E_g and B_{1g} halogen insensitive bands are not resolved resulting in a broad Raman band (394 cm^{-1}). The remnant E_g external Bi–Cl stretching mode is likely masked by the strongest peak at 142 cm^{-1}. The Raman shifts observed in the present work are similar to the reported values [46,48-50]. No other peaks were observed at higher Raman shifts.

4.3.2. In situ characterization of the pearlescent pigments

By means of Raman microscopy analysis, the identification of the polymer as PMMA was confirmed in all plastic sheets. The Raman spectrum of the polymer is presented in **Figure B.4**, and the most important absorption frequencies are listed in **Table 4.3**. Assignments of vibration bands were based on the literature [51].

Regular thin hexagonal platelet-like particles (~10 μm of diameter and <1 μm of thickness) were observed with OM in the yellow and orange PMMA sheets which corresponded to the 1960s artworks (**Figure 4.5a,b**). In the case of the nacreous white sample, only a few hexagonal platelets were observed (~5 μm of diameter; **Figure 4.5c**), and these appeared to be very small and not well formed. Regular thin octagonal and square platelets were seen in the acrylic samples considered to be more recent (**Figure 4.5d,e**). These were larger (~15 μm of diameter), and although individual platelets were well formed, there were more broken fractions dispersed throughout the acrylic matrix.

The majority of the platelets in all of the plastic sheets were oriented parallel to each other and to the surface of the acrylic sheets thus producing the lustrous effect. Consequently, in cross-section, only the thin sections of the platelets could be observed, and the hexagonal and octagonal/square shapes of the particle faces were only visible from the surface of the sheets. Platelets were distributed differently in the sheets dating from the 1960s versus those thought to be from the early 2000s. A greater sense of depth in the 1960s sheets was achieved by the highly irregular dispersion of pigment platelets (**Figure B.5a,b**). As reported by Babo et al. [11], this final appearance had been designed intentionally by the Portuguese company *Plásticos do Sado*. In contrast, the completely homogeneous appearance of the more recent sheets was achieved by a uniform distribution of the platelets (**Figure B.5c,d**).

Focusing the Raman laser beam on the hexagonal platelets in the acrylic sheets, a peak centered at around 1050 cm^{-1} was observed (**Figure 4.6a**). This peak, not assignable to the vibrational fingerprint of PMMA, suggests

Table 4.3.: Raman bands (cm^{-1}) and assignments of poly(methyl methacrylate).

Raman shift (cm^{-1})	Mode	Assignments
1725	ν(C=O)	Stretching vibration of the C=O
1485	$\delta_{as}(CH_3)$	Asymmetric bending vibration of the CH_3
1450	$d(CH_2)$	Deformation of the CH_2
1389	$\delta_s(CH_3)$	Symmetric bending vibration of the CH_3
1241	ν(C–C)	Degenerate stretching of CC_4
1183	ν(C–C)	Degenerate stretching of CC_4
1159	ν(C–O) + $\rho(CH_3)$	Stretching vibration of C–O coupled with rocking vibration of the CH_3
1121	ν(C–O) + $\rho(CH_3)$	Stretching vibration of C–O coupled with rocking vibration of the CH_3
1063	$\omega(CH_2)$	Wagging vibration of the CH_2
986	ν(C–C)	Stretching vibration C–C of the main chain
967	ν(C–C)	Stretching vibration C–C of the main chain
837	d(C=O) + $\rho(CH_3)$	Deformation of C=O coupled with rocking vibration of the CH_3
811	ν_s(C–C)	Symmetric stretching vibration of CC_4
732	d(O–C=O) + $\rho(CH_3)$	Deformation O–C=O coupled with rocking vibration of the CH_3
600	δ(O–C=O)	In-plane bending O–C=O in hydrogen bonding
552	δ(O–C=O)	In-plane bending O–C=O in hydrogen bonding
482	d(C–C)	Skeletal deformation of CC_4
362	d(C–C)	Skeletal deformation of CC_4
300	d(C–C)	Skeletal deformation of CC_4

Note. ν: stretching (a: symmetric; as: asymmetric); ρ: rocking; δ: bending; τ: twisting; ω: wagging; d: deformation

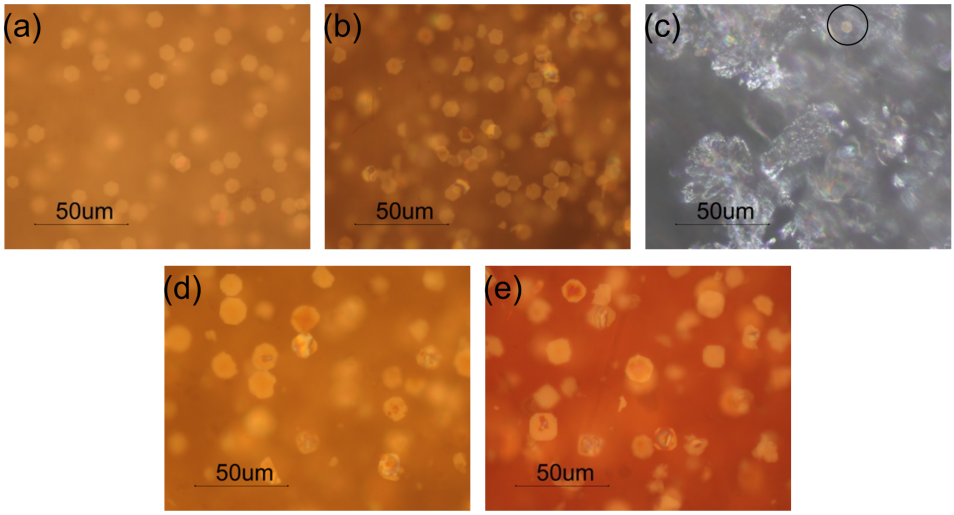

Figure 4.5.: Microscopy images of the platelets in (a,d) yellow, (b) orange, (c) white and (e) red pearlescent acrylic sheet probably made in 1960s (a-c) and 2000s (d-e). A small hexagonal platelet-like particle is underlined in the pearlescent white sample (c).

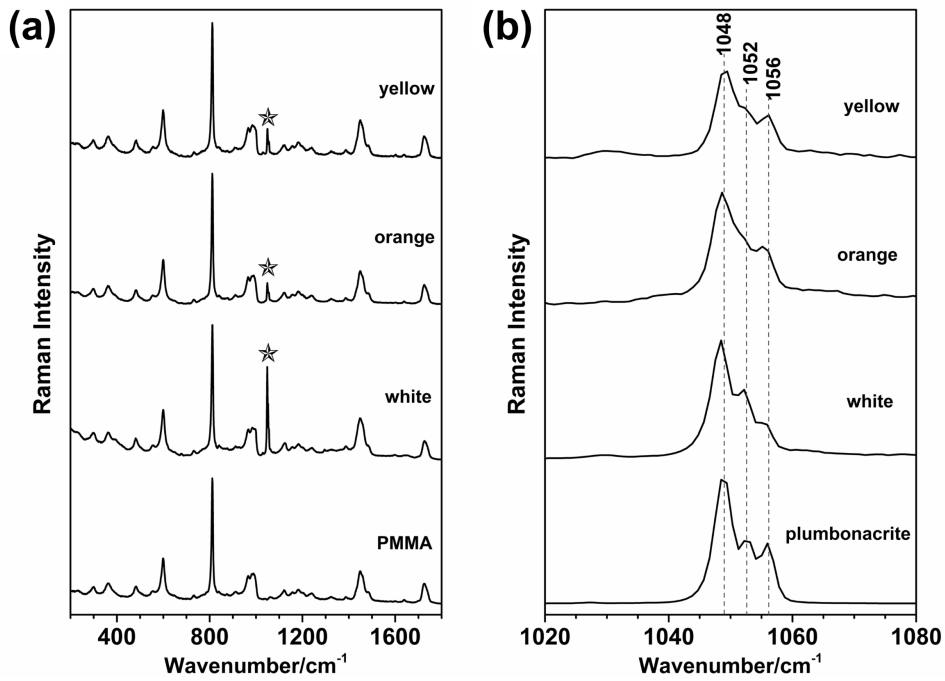

Figure 4.6.: Raman spectra of the hexagonal platelets in yellow, orange, and white pearlescent acrylic sheets dated from 1960s. The Raman spectra of poly(methyl methacrylate) (PMMA) and synthesized plumbonacrite are also reported for comparison. Peaks centered at around 1050 cm^{-1} are marked with a star in (a) and seen in detail in (b). These bands are associated to ν_1 symmetric stretching mode of the CO_3^{2-} ion (632.8 nm excitation).

the presence of the crystal phase of plumbonacrite due to the factor-group splitting of the ν_1 symmetric stretching mode of the CO_3^{2-} ion. A division in three different subbands (1048, 1052, and 1056 cm^{-1}) is also observed in the Raman spectrum of the synthesized plumbonacrite (**Figure 4.6b**) supporting its identification in situ in the acrylic sheets.

Bismuth oxychloride was identified in the more recent acrylics by the detection of three bands (142, 198, and 394 cm^{-1}) in the region between 100 and 400 cm^{-1} (**Figure 4.7a**) which matches the position and relative intensity of the Raman bands for synthesized bismoclite BiOCl (**Figure 4.7b**). To perform Raman microscopy analysis on the yellow acrylic sheet, the 785-nm excitation wavelength was used to avoid florescence which occurred at 628.3 nm likely due to the dye present as colorant in the acrylic sheet.

The identification of plumbonacrite and bismuth oxychloride is also supported by micro-EDXRF results. Lead (Pb) was detected in the hexagonal platelets, whereas bismuth (Bi) and chlorine (Cl) were detected and associated in the octagonal/square platelets.

4.4. Conclusions

Raman microscopy proved to be a valuable technique for the identification of pearlescent pigments in plastic materials. For the first time, plumbonacrite $Pb_5(CO_3)_3O(OH)_2$ and bismuth oxychloride BiOCl were identified in situ using Raman microscopy. Despite the low amount of pearlescent pigment dispersed in the acrylic polymeric matrix (max 2%), it was possible to obtain molecular information at the micrometer-scale by focusing the laser beam on the platelets' surfaces, taking advantage of the confocal system associated with the Raman equipment. The vibrational fingerprint of the pigments was obtained by observing some Raman bands not assignable to the PMMA Raman spectrum. These were identified using synthesized pigments to provide the reference bands. The identification of the two different pearlescent pigments supports the dating of the acrylic sheets and the artworks. In fact, the pigment identification agrees with the literature, since as

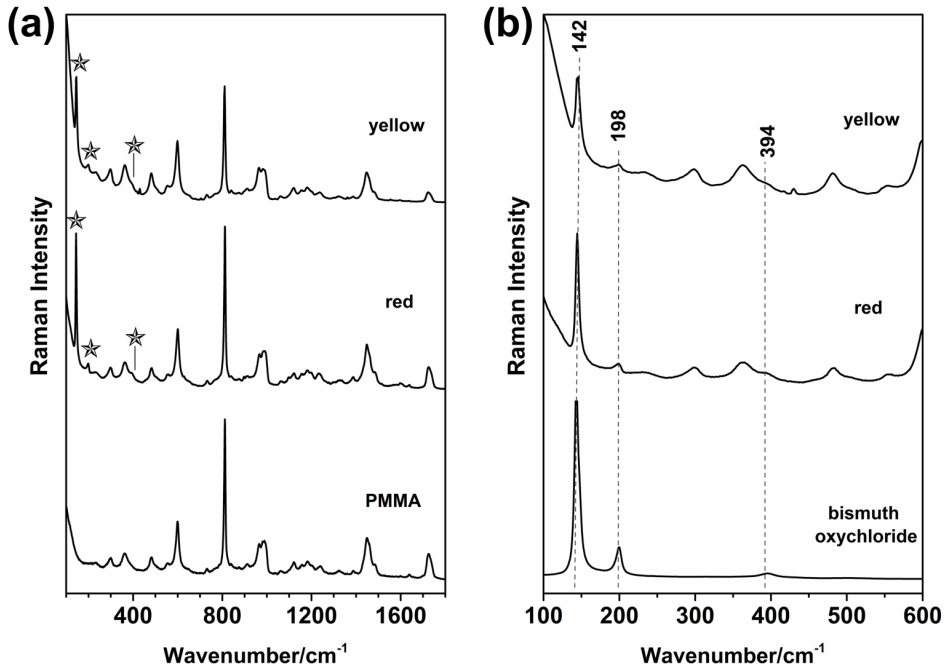

Figure 4.7.: Raman spectra of the square/octagonal platelets in yellow and red pearlescent acrylic sheets dated from the 2000s. The Raman spectra of the square/octagonal platelets in the red and yellow sheets are acquired in situ with 632.8 and 785 nm excitation, respectively. The Raman spectra of poly(methyl methacrylate) (PMMA) and synthetized bismuth oxychloride are also reported for comparison. Peak at 142, 198, and 394 cm^{-1} are underlined.

previously stated, from the second half of the 20th century, basic lead carbonates were progressively replaced by BiOCl due to the toxicity problems associated with lead compounds [2,3].

This work clarifies that the basic lead carbonate used in the 1960s acrylic sheets studied was plumbonacrite $Pb_5(CO_3)_3O(OH)_2$, rather than hydrocerussite $Pb_3(CO_3)_2(OH)_2$. This identification evidences the use of plumbonacrite as pearlescent pigment by the plastic industry, which was never specifically reported in the coloring technology literature. In fact, pearlescent lead pigments are simply referred as basic lead carbonate defined by the formula for hydrocerrusite. The presence of plumbonacrite in the sheets dated from 1960s, and bismuth oxychloride in those thought to date from 2000s also explains the difference in their appearance. Although plumbonacrite is recognized to be a nacreous pigment, bismuth oxychloride is considered to be more metallic and brilliant in appearance (due to its higher refractive index, $n = 2.15$) [2]. The differences between the two in terms of pigment distribution in the acrylic matrix also accounts for the different visual effects.

The use of Raman microscopy to identify the two pigments in situ will lead to better informed strategies for the preservation of Ângelo's plastic sculptures. The limited chemical stability of basic lead carbonates [52] and the low light stability of BiOCl to UV radiation [2,5] will inform the design of new guidelines for their storage and exhibition.

4.5. References

[1] Greeinsten LM. Pearlascent – The optical behavior of nacreous and interface pigments. In: Patton TC, editor. Pigment handbook, characterization and physical relationships, New York: J. Wiley & Sons, Vol III, second ed.; 1973. p. 357-390.

[2] Greeinsten LM. Nacreous (pearlascent) pigments and interface pigments. In: Lewis PA, editor. Pigment handbook, properties and economics. New York: J. Wiley & Sons, Vol I, second ed.; 1988. p. 829-858.

[3] Pfaff G, Franz K-D, Emmert R, Nitta K. Luster pigments. In: Buxbaum G, editor. Industrial inorganic pigments. Weinheim: Wiley-VCH, second ed.; 1998. p. 211-231.
[4] Pfaff G. Special effect pigments. In: Faulkner EB, Schwartz RJ, editors. High performance pigments. Weinheim: Wiley-VCH, second ed..; 2009. p. 77-104.
[5] Pfaff G, Weitzel J. Pearlascent pigments/flakes. In: Charvat RA, editor. Coloring of plastics: fundamentals. New Jersey: John Wiley & Sons Inc., second ed.; 2004. p. 226-241.
[6] Araujo A, Catalogue coord. Ângelo: 1993 Uma Antológica. Porto: Fundação de Serralves; 1993.
[7] de Almeida BP. Ângelo de Sousa Esculturas 66 67 – A Imaginação da Matéria. Porto: Galeria Quadrado Azul; 1992.
[8] Faria N, Catalogue coord. Ângelo de Sousa Escultura. Lisbon: CAM – Fundação Calouste Gulbenkian; 2006.
[9] de Groot S, van Keulen H, Megens L, van Oosten T, Wiresma H. Discolouration of plastics objects: investigation into composition using various analytical techniques. In: Bechthold T, editor. Future Talks 013 – Lectures and workshops on technology and conservation of modern materials in design. Munich: Die Neue Sammlung – The Design Museum; 2015. p. 19-26.
[10] de Groot S, van Keulen H, van den Akker S, van Oosten T. Discoloration of plastics objects: the identification of yellow and orange synthetic pigment in plastic objects. In: Bechthold T, editor. Future Talks 015 – Processes. The making of design and modern art. Materials, technologies and conservation strategies. Munich: Die Neue Sammlung - The Design Museum; 2017. p. 147-158.
[11] Babo S, Ferreira JL, Melo MJ, Ramos AM. Back to the origin: understanding the history of production and its influence on the properties of acrylic sheet. In: Bechthold T, editor. Future Talks 015 – Processes. The making of design and modern art materials, technologies and conservation strategies. Munich: Die NeueSammlung-The Design Museum; 2015. p. 160-170.
[12] Webber TG. Pigments for plastics. In: Webber TG, editor. Coloring of plastics. New York: John Wiley & Sons Inc.; 1979. p. 37-55.
[13] Feller R, Keisch B, Curran M. Notes on modern pigments. Bulletin of the American Group-IIC 1971; 12(1): 60-62. DOI: stable/3178996.
[14] Corbeil M-C, Sirois PJ. A note on a modern lead white, also known as 'synthetic plumbonacrite'. Stud Conserv. 2007; 52(4): 281-288. DOI:10.1179/sic.2007.52.4.281.
[15] Eastaugh N, Walsh V, Chaplin T, Siddall R. Pigment compendium – A dictionary and optical microscopy of historical pigments. Amsterdam: Elsevier Butterworth-Heinemann; 2008.
[16] Brossman PB. U.S. Patent 2,097,269. E. I. to du Pont de Nemours and Co. October 1937.
[17] Thompson GW, Stewart A. U.S. Patent 2,218,940. October 1940.
[18] Müller A. Coloring of plastics. Munich: Carl Hanser Verlag; 2003.
[19] Ostertag W, Mronga N. Properties and application of luster pigments. Macromol Symp. 1995; 100: 63-168. DOI: 10.1002/masy.19951000127
[20] Martinetto P, Anne M, Dooryhée E, Walter P, Tsoucaris G. Synthetic hydrocerussite, $2PbCO_3 \cdot Pb(OH)_2$, by X-ray powder diffraction. Acta Crystallogr C 2002; 58(6): i82-i84. DOI: 10.1107/S0108270102006844
[21] Krivovichev SV, Burns PC. Crystal chemistry of basic lead carbonates. II. Crystal structure of synthetic 'plumbonacrite'. Mineral Mag. 2000; 64(6): 1069-1075. DOI: 10.1180/002646100549887.
[22] Olby JK. The basic lead carbonates. J Inorg Nucl Chem. 1966; 28(11): 2507-2512. DOI: 10.1016/0022-1902(66)80373-1.
[23] Tétreault J, Sirois J, Stamatopoulou E. Studies of lead corrosion in acetic acid environments. Stud Conserv. 1998; 43(1): 17-32. DOI: 10.1179/sic.1998.43.1.17.
[24] Tétreault J, Cano E, van Bommel M, Scott D, Dennis M, Barthés Labrousse M-G, Minel L, Robbiola L. Corrosion of copper and lead by formaldehyde, formic and acetic acid vapours. Stud Conserv. 2003; 48(4): 237-250. DOI: stable/1506913.

[25] Niklasson A, Johansson L-G, Svensson J-E. The influence of relative humidity and temperature on the acetic acid vapour-induced atmospheric corrosion of lead. Corros Sci. 2008; 50(11): 3031-3037. DOI: 10.1016/j.corsci.2008.08.009.
[26] Bersani D, Campani E, Casoli A, Lottici PP, Marino I-G. Spectroscopic study of the degradation products in the holy water fonts in Santa Maria della Steccata Church in Parma (Italy). Anal Chim Acta 2008; 610(1): 74-79. DOI: 10.1016/j.aca.2008.01.041.
[27] Aze S, Vallet J-M, Detalle V, Grauby O, Baronnet A. Chromatic alterations of red lead pigments in artworks: a review. Ph Transit. 2008; 81(2-3): 145-154. DOI: 10.1080/01411590701514326.
[28] Boon JJ, van der Weerd J, Keune K, Noble P, Wadum J. Mechanical and chemical changes in Old Master paintings: dissolution, metal soap formation and remineralization processes in lead pigmented ground/intermediate paint layers of 17th century paintings. In: Vontobel R, editor. ICOM-CC 13th Triennial Meeting Preprints, Rio de Janeiro, 22-27 September 2002. London: Earthscan ltd., Vol. I; 2002. p. 401-406.
[29] Vanmeert F, Van der Snickt G, Janssens K. Plumbonacrite identified by X-ray powder diffraction tomography as a missing link during degradation of red lead in a Van Gogh painting. Angew Chem Int Ed. 2015; 54: 3607-3610. DOI: 10.1002/anie.201411691.
[30] Cotte M, Checroun E, De Nolf W, Taniguchi Y, De Viguerie L, Burghammer M, Walter P, Rivard C, Salomé M, Janssens K, Susini J. Lead soaps in paintings: friends or foes? Stud Conserv. 2016; 62: 2-23. DOI: 10.1080/00393630.2016.1232529.
[31] Taylor P, Lopata VJ. Stability and solubility relationships between some solids in the system PbO–CO_2–H_2O. Can J Chem. 1984; 62(3): 395-402. DOI: 10.1139/v84-070.
[32] Flemming NJ, Lopata VJ, Sanipelli BL, Taylor P. Thermal decomposition of basic lead carbonates: a comparison of hydrocerussite and plumbonacrite. Thermochim Acta 1984; 81: 1-8. DOI: 10.1016/0040-6031(84)85104-7.
[33] Haacke DF, Williams PA. Stability of plumbonacrite. J Inorg Nucl Chem. 1981; 43(2): 406. DOI: 10.1016/0022-1902(81)90036-1.
[34] Suzuki EM. Infrared Spectra of U.S. Automobile original finishes (1998-2000). IX. Identification of bismuth oxychloride and silver/white mica pearlescent pigments using extended range FT-IR spectroscopy, XRF spectrometry, and SEM/EDS analysis. J Forensic Sci. 2014; 59(5): 1205-1225. DOI: 10.1111/1556-4029.12414.
[35] Franz KD, Emmert R, Nitta K. Interference pigments. Kontakte (Darmstadt). 1992; 2: 3-14.
[36] Krivovichev SV, Burns PC. Crystal chemistry of basic lead carbonates. I. Crystal structure of synthetic shannonite, $Pb_2O(CO_3)$. Mineral Mag. 2000; 64(6): 1063-1068. DOI: 10.1180/002646100550065.
[37] Schenk PW. Bismuth oxide chloride. In: Brauer G, editor. Handbook of preparative inorganic chemistry. New York: Academic Press, Vol 1, second ed.; 1963. p. 622-623.
[38] Nozle G, Kraus W. Powder Cell for Windows Version 2.4. Berlin, Germany: Federal Institute for Materials Research and Testing, 2000, available at powdcell/a_v/v_1/powder/e_cell.html.
[39] Keramidas KG, Voutsas GP, Rentzeperis PI. The crystal structure of BiOCl. Z Kristallogr Cryst Mater. 1993; 205(1): 35-40. DOI: 10.1524/zkri.1993.205.Part-1.35.
[40] Brooker HM, Sunder S, Taylor P, Lopata VJ. Infrared and Raman spectra and X-ray diffraction studies of solid lead(II) carbonates. Can J Chem. 1983; 61(3): 494-502. DOI: 10.1139/v83-087.
[41] Bouchard M, Smith DC. Catalogue of 45 reference Raman spectra of minerals concerning research in art history or archaeology, especially on corroded metals and coloured glass. Spectrochim Acta A 2003; 59(10): 2247-2266. DOI: 10.1016/S1386-1425(03)00069-6.
[42] Chukanov NV, Chervonnyi AD. Infrared spectroscopy of minerals and related compounds. Switzerland: Springer International Publishing; 2016.
[43] Nakamoto K. Infrared and Raman spectra of inorganic and coordination compounds – Part A: theory and applications in inorganic chemistry. New Jersey: J. Wiley and Sons, sixth ed.; 2009.

[44] Herzberg G. Molecular spectra and molecular structure. II. Infrared and Raman spectra of polyatomic Molecules. New York: D. van Nostrand Co. Inc.; 1962.
[45] Nyquist RA, Putzig CL, Leugers MA, editors. Infrared and Raman spectral atlas of inorganic compounds and organic salts: text and explanations. San Diego: Academic press, Vol 1; 1997.
[46] Davies JED. Solid state vibrational spectroscopy – III[1] The infrared and Raman spectra of the bismuth(III) oxide halides. J Inorg Nucl Chem. 1973; 35(5): 1531-1534. DOI: 10.1016/0022-1902(73)80242-8.
[47] Rulmont A. Spectre infra-rouge de quelques oxyhalogénures de bismuth et de terres rares. Spectrochim Acta A. 1972; 28(7): 1287-1296. DOI: 10.1016/0584-8539(72)80098-9.
[48] Rulmont A. Raman spectra of a single crystal of BiOCl. Spectrochim Acta A. 1974; 30(1): 311-313. DOI: 10.1016/0584-8539(74)80235-7.
[49] Tripathi GK, Saini KK, Kurchania R. Synthesis of nanoplate bismuth oxychloride – A visible light active material. Opt Spectrosc. 2015; 119(4): 656-663. DOI: 10.1134/S0030400X15100136.
[50] Ascencio-Aguirre FM, Bazán-Díaz L, Mendoza-Cruz R, Santana-Vázquez M, Ovalle-Encinia O, Gómez-Rodríguez A, Herrera-Becerra R. Chemical synthesis and characterization of bismuth oxychloride BiOCl nanoparticles. Appl Phys A. 2017; 123: 155. DOI: 10.1007/s00339-017-0797-5.
[51] Ren Y, Matsushita A, Matsukawa K, Inoue H, Minami Y, Noda I, Ozaki Y. Two-dimensional Fourier-transform-Raman and near-infrared correlation spectroscopy studies of poly(methyl methacrylate) blends: 2. Partially miscible blends of poly(methyl methacrylate) and poly(4-vinylphenol). Vib Spectrosc. 2000; 23(2): 207-218. DOI: 10.1016/S0924-2031(00)00063-1.
[52] Pfaff G, Franz KD, Emmert R, Nitta K, Besold R. Pigments, inorganic. 6. Luster pigments. In: Ullmann's Encyclopedia of industrial chemistry. Weinheim: Wiley-VCH, Vol. 27; 2012. p. 359-373. DOI: 10.1002/14356007.n20_n05.

This is an Accepted Manuscript of an article published by Elsevier Inc. in Microchemical Journal, on 23/05/2020, available online:

Angelin EM, Ghirardello M, Babo S, Picollo M, Chelazzi L, Melo MJ, Nevin A, Valentini G, Comelli D. The multi-analytical in situ analysis of cadmium-based pigments in plastics. Microchem J. 2020; 157: 105004. DOI: 10.1016/j.microc.2020.105004.

5. The multi-analytical in situ analysis of cadmium-based pigments in plastics

Abstract

Colorants are present in trace concentration in objects made of plastic and their identification is a methodological and analytical challenge. In conservation, the identification of colorants may allow a better understanding of colorant degradation (such as color change and fading) and provide information about the historical development, production and processing of plastics. Although micro-destructive analytical protocols are well established for the analysis of colorants, in cultural heritage, where in situ methodologies are preferred and, in some cases, mandatory, new approaches are greatly needed. In this work, an in situ multi-analytical approach is used to specifically study inorganic cadmium-based pigments that were commonly used for coloring plastics during the 20th c. First introduced as vivid artists' pigments, cadmium-based additives were used for coloring plastics because of their exceptional performance properties. Eighteen colored polymethyl methacrylate (PMMA) samples, produced in the second half of the 20th c. by the company Plásticos do Sado (Portugal), were studied with a combination of optical microscopy, colorimetry, UV-Vis-NIR diffuse reflectance, laser-induced photoluminescence, vibrational (μ-Raman) and elemental (μ-EDXRF) spectroscopies. On the basis of complementary data, the chemical composition of most of the coloring agents employed in the acrylic samples were identified without any micro-sampling.

5.1. Introduction

Plastics are increasingly becoming part of our cultural heritage, and as design objects and works of art they are found widely in collections, museums and art galleries. Broadly, plastics are formulated by adding chemicals to polymers to improve both processing and end-use performance. Small quantities (0.1%-5%) of colorants may be added to provide color to the polymer formulation. Following the literature of coloring technology for plastics [1], colorants compromise both soluble dyes and finely divided insoluble pigments. Additives such as fillers and extenders can be part of the colorant formulation or can be incorporated into the plastic matrix to improve processing, physical, mechanical properties or reduce cost [2-4]. While much attention has focused on polymer identification and on its degradation in cultural heritage [5-22], few studies have been devoted to the investigation of colorants. The low concentration and the fact that additives are dissolved or dispersed within the polymeric matrix make their characterization an analytical challenge.

Following exposure to light, colorants may degrade resulting in fading or color change, dramatically affecting the appearance and perception of objects and works of art made of plastic [5,23,24]. The chemical structure of chromophores and their micro-environment play a key role in assessing the colorant stability and lightfastness [25]. Hence, their identification in plastic objects becomes essential for understanding and supporting conservation studies, and recommendations regarding suitable display or storage. In addition, it contributes to achieve new insights into the historical development, production and processing of plastics formulation.

To identify colorants in plastics, analytical micro-destructive protocols (i.e. polymer/additives analysis), employed in industry are standard and require the treatment of a sample and its deformulation via extraction,

dissolution and precipitation [2,26]. Nonetheless, in situ methods, which allow bulk analysis directly on plastics, are required for many fields including conservation science where sampling is intrinsically limited [27-30]. Only few studies, mainly based on Raman spectroscopy, have attempted to identify colorants in historical plastics [31-33].

This work presents an in situ multi-analytical approach to identify cadmium-based coloring agents in plastics. Cadmium-based pigments were widely used by artists since their introduction during the 19th century [34] and were employed as colorants in plastics [1,35-42]. While some cadmium pigments found in works of art have faded [25,43-45], modern cadmium pigments have exceptional performance properties. In plastic industry, these pigments are considered opaque, highly saturated, strong in tint, lightfast, chemically stable and heat resistant to above 400 °C. In addition, they are easy-to-disperse and have good migration resistance. As such, they are technically usable in any virtually polymer formulation. While common in the 20th c., the current use of cadmium pigments in the plastic industry is limited nationally by specific regulations and restrictions owing to potential toxicological and environmental issues [36-38,46] and very recently a ban of cadmium from all plastic products has been suggested in the EU [47].

The basic composition of cadmium pigments is cadmium sulfide (CdS), co-precipitated with increasing amounts of zinc ($Cd_{1-x}Zn_xS$), to achieve greener hues of yellow, or with increasing amounts of selenium ($CdS_{1-x}Se_x$) to produce tonalities from orange to deep red. Another variant substitutes mercury for some of the cadmium in the crystal lattice to yield mercury-cadmium sulfide ($Cd_{1-x}Hg_xS$), tuning the color from deep orange to maroon hues. Interestingly, this latter pigment is the first American-born pigment developed in the early 1950s in specific response to the adverse economic condition in the supply of selenium [40,42,48] – and patented in 1955 by Ciba-Geigy Corporation as Mercadium® [49]. Its production was discontinued in the 1980s with the falling price of selenium [50]. While optical, electronic and vibrational properties of CdS, $Cd_{1-x}Zn_xS$ and $CdS_{1-x}Se_x$ pigments are already studied [51-54], no information specifically related to $Cd_{1-x}Hg_xS$ solid solutions are present, to the best of authors' knowledge.

The introduction of yellow cadmium lithophones (a co-precipitate of $Cd_{1-x}Zn_xS$ and $BaSO_4$) in the 1920s was the most important factor bringing cadmium-based pigments into widespread industrial use [55-57] and, in coloring technology for plastics, they started to be predominantly used since the 1950s [38]. In fact, the physical mixture of cadmium sulfide with barium sulfate, used as an extender in concentrations up to 60%, produced a wide range of shades, comparable tinting strength, heat and chemical resistance to the pure form, lowering the cost of production.

The Color Index (C.I.) designations for the cadmium yellows, oranges and red, along with their lithopone varieties are reported in **Table 5.1**. All C.I. designations have been used in plastic colorings and are usually based on the more stable hexagonal crystal form (wurtzite) of CdS.

A swatch of eighteen colored polymethyl methacrylate (PMMA) samples produced in the second half of the 20th c. by the company Plásticos do Sado (Portugal) [60] was selected for this study. The set of samples, made of yellow, orange, red and maroon shades, was analyzed using a multi-analytical approach, comprising optical microscopy, colorimetry, UV-Vis-NIR diffuse reflectance, laser-induced photoluminescence, μ-Raman and μ-EDXRF spectroscopies. The advantages and limitations of the approach is discussed, including the important influence of the acrylic polymeric matrix in which the pigments are dispersed.

5.2. Materials and methods

5.2.1. Plastic samples

A total of eighteen acrylic samples produced by the Portuguese company Plásticos do Sado (see **Appendix C**, **Background: PMMA and Plásticos do Sado products**) in the 1960s-1970s and 1990s were analyzed (**Figure 5.1**). With similar thickness between 2 and 3 mm, the acrylic swatches from 1960s-1970s are round

Table 5.1.: Color Index (C.I.) classification, color and chemical composition of the cadmium-based pigments.

C. I. Generic Name[a]	C. I. Constitution number[a]	Color	Chemical composition[a]
PY 35	77205	Yellow	$Cd_{1-x}Zn_xS$ cadmium-zinc sulfide
PY 35:1	77205:1	Yellow	$Cd_{1-x}Zn_xS$ + BaSO4 lithopone
PY 37	77199	Yellow	CdS cadmium sulfide
PY 37:1	77199:1	Yellow	CdS + $BaSO_4$ lithopone
PO 20	77202	Orange	$CdS_{1-x}Se_x$ cadmium sulfo-selenide (Se $< 10\%$)[b]
PO 20:1	77202:1	Orange	$CdS_{1-x}Se_x$ + $BaSO_4$ lithopone
PO 23	77201	Orange	$Cd_{1-x}Hg_xS$ mercury-cadmium sulfide
PO 23:1	77201:1	Orange	$Cd_{1-x}Hg_xS$ + $BaSO_4$ lithopone
PR 108	77202	Red	$CdS_{1-x}Se_x$ cadmium sulfo-selenide (Se$>10\%$)[b]
PR 108:1	77202:1	Red	$CdS_{1-x}Se_x$ + $BaSO_4$ lithopone
PR 113	77201	Red	$Cd_{1-x}Hg_xS$ mercury-cadmium sulfide
PR 113:1	77201:1	Red	$Cd_{1-x}Hg_xS$ + $BaSO_4$ lithopone

[a] [58]
[b] [59]

(3.2 cm Ø), while those dated to the 1990s are rectangular (8.9 cm × 4.2 cm). Golden lettering of the company name and printed identification numbers identified each sample. For this work, samples were divided into three groups: yellows, reds, and orange/brown. A list of the acrylic samples is reported in **Table 5.2**.

5.2.2. Reference powder compounds

Five powder pigments were analyzed as reference materials: "Cadmium yellow dark" pigment (catalog number 21060, Kremer Pigmente GmbH & Co., Germany) was used as reference of pure hexagonal cadmium sulfide [*h-CdS*], cadmium selenide [*CdSe*] (Aldrich, electronic grade, 99.99%), mercury sulfide (Aldrich, Mercury(II) sulfide, red, 99%) as a reference of pure trigonal cinnabar [α-*HgS*], a commercial pigment labelled as "Cinabro del Monte Amiata" (Zecchi, Italy) as an example of mercury-cadmium sulfide [*(Cd,Hg)S*] and zinc sulfide in hexagonal form [*h-ZnS*] (catalog number 46350 Kremer Pigmente GmbH & Co., Germany). Owing to the lack of experimental knowledge for $Cd_{1-x}Hg_xS$ solid solutions, powder X-ray diffraction (PXRD) was performed on the *(Cd,Hg)S* sample to determine its crystalline phase and chemical composition. The employed PXRD set-up is described in **Appendix C**, **Powder X-ray diffraction (PXRD)**.
The proposed in situ multi-analytical protocol for the investigation of cadmium-based coloring agents in plastics is schematically depicted in **Figure 5.2**, together with the typical information provided by each technique.

5.2.3. Color measurements

A Konica Minolta (Minolta Co. Ltd., Japan) CM-700d spectro-colorimeter (spectral range: 400-700 nm, wavelength pitch 10 nm, d/8° geometry) was employed for measuring the visible reflectance spectrum of the acrylic samples and for extracting their colorimetric coordinates. The reflected specular component was excluded in the measurements (SCE mode). CIELAB color coordinates were calculated considering the D65 standard illuminant and the 10° colorimetric observer (CIE 1964) on the basis of the average of three repeated measurements (analysis area = Ø 8 mm).

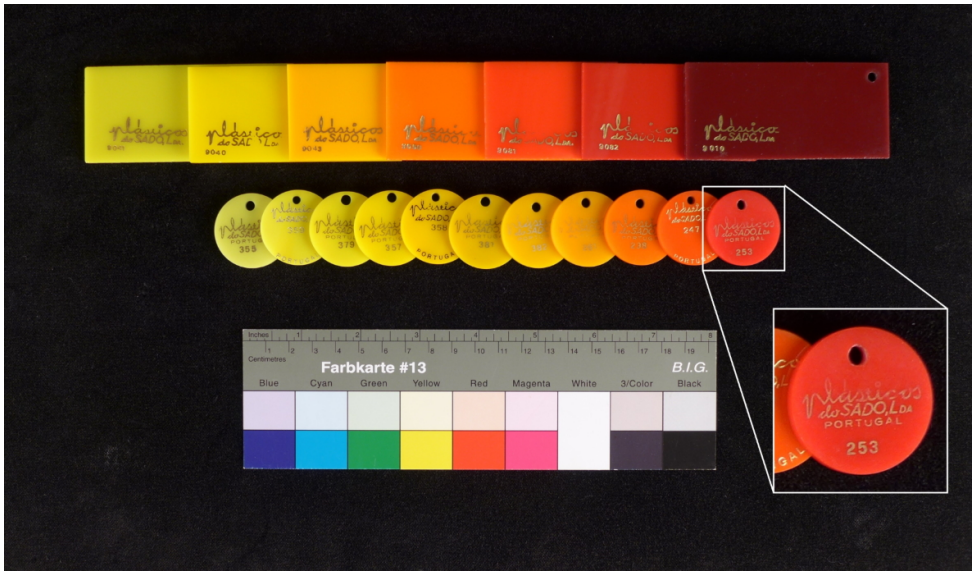

Figure 5.1.: Color picture of the analyzed acrylic samples produced by the Portuguese company Plásticos do Sado in the 1990s (top) and in the 1960s-1970s (bottom).

Table 5.2.: List of the eighteen acrylic samples in terms of identification code, color and period of production.

Sample	Color	Dating
9041	Light yellow	1990s
9040	Yellow	
9043	Deep yellow	
9050	Orange	
9081	Scarlet red	
9082	Deep red	
9010	Brown	
355	Lemon yellow	1960s-1970s
359	Very light yellow	
379	Light yellow	
357	Yellow	
358	Deep yellow	
381	Deep yellow	
382	Deep yellow	
261	Light orange	
238	Deep orange	
247	Light red	
253	Deep red	

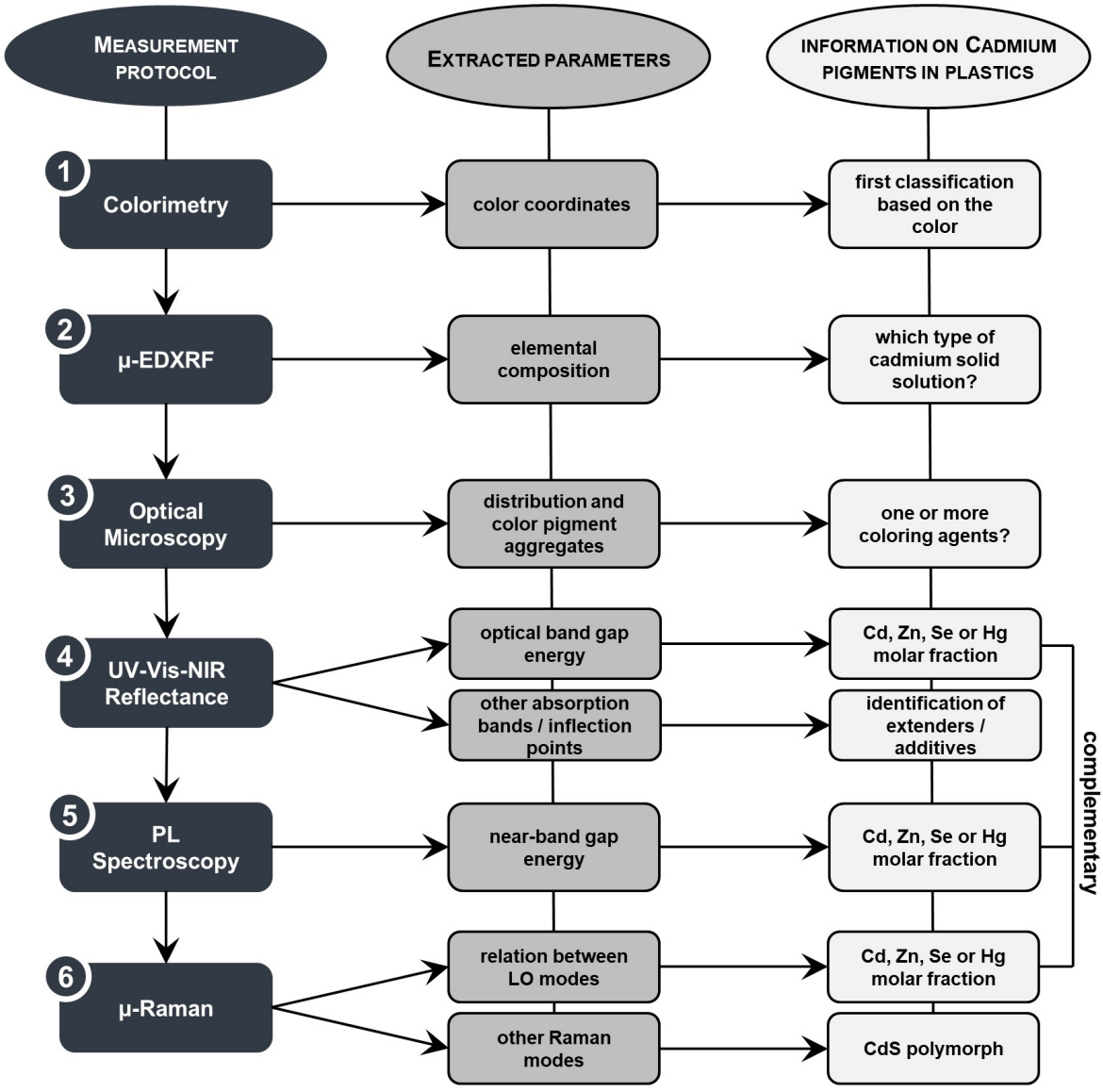

Figure 5.2.: Flow-chart of the in situ multi-analytical protocol and following data analysis for the determination of the chemical composition of cadmium-based coloring agents in plastics.

5.2.4. Micro-energy dispersive X-ray fluorescence spectrometry (μ-EDXRF)

μ-EDXRF was carried out to confirm the elemental composition of plastic samples and test for the presence of possible fillers/additives. Measurements were performed with an ArtTAX spectrometer (Intax GmbH) equipped with a molybdenum (Mo) anode and Xflash detector (Sidrift). The experimental parameters used were 25 kV and 300 μA for 180s, under a He flux.

5.2.5. Optical microscopy (OM)

Optical microscopy (OM) was used to assess the distribution of cadmium pigments in the plastic samples. Images were acquired in bright-field and dark-field illumination using a Zeiss Axioplan 2 Imaging system (HAL 100) coupled to a Nikon DXM1200F digital camera.

5.2.6. UV-Vis-NIR diffuse reflectance spectroscopy

Diffuse reflectance spectra were recorded between 200 and 1000 nm using a bench-top spectrophotometer (Lambda 1050, PerkinElmer) equipped with an integrating sphere (Ø 60 mm). The instrument has a spectral resolution of 2 nm between 200 and 860 nm, providing greater confidence in the estimation of the optical band gap energies. However, at longer wavelengths (860-1000 nm), the spectral resolution is variable. 0°/d measurement geometry with the specular component excluded was used. Calibration of the spectrophotometer was carried out using a diffuse reflectance standard (99% Labsphere Spectralon, Labsphere, Inc. North Sutton, NH, US). Because of the partial transparency of the acrylic samples, the diffuse reflectance standard was placed behind samples during their measurements.
Optical band gap energies (E_g/eV, λ_g/nm) were calculated from diffuse reflectance spectra according the method proposed in the literature (Tauc plot) [61,62] and summarized by Rosi et al. [51]. The Zn, Se and Hg molar fractions in the $Cd_{1-x}Zn_xS$, $CdS_{1-x}Se_x$, $Cd_{1-x}Hg_xS$ solid solutions were extrapolated by using a linear relationship between optical band gap energies and elemental molar fractions that have been derived from X-ray diffraction studies [51,52,63,64].

5.2.7. Laser-induced photoluminescence spectroscopy

Photoluminescence (PL) spectroscopy was performed through excitation with a Q-switched pulsed laser (excitation wavelength 355 nm, 1 ns pulse, 100 Hz repetition rate, FTSS 355-50, CryLas GmbH) focused on a 1-mm spot on samples. This high-fluence laser excitation (power density = 0.4 W/cm^2, fluence energy per pulse = 4 mJ/cm^2) promotes emission from Near Band Edge (NBE) in semiconductor materials as CdS, as a consequence of trap state saturation phenomena [65].
PL spectra of samples were recorded with a compact spectrometer (TM-CCD C10083CA-2100, Hamamatsu Photonics, Japan) between 350 and 1000 nm with a resolution of 6 nm. The PL spectra were corrected for background, system efficiency and sample self-absorption [66]. Optical band gap energies were then extracted from NBE emission spectra in terms of wavelength of the emission peaks (λ_{NBE}/nm, E_{NBE}/ eV), where conversion from wavelength (nm) to energy units (eV) and scaling of the PL data have been performed through the Jacobian transformation [67]. Following this, the chemical composition of colorants, in terms of Zn and Se molar fraction, was calculated as for reflectance data [51,52].

5.2.8. Raman microscopy (μ-Raman)

μ-Raman was carried out using a Labram 300 Jobin Yvon spectrometer equipped with three laser sources: a He-Neon laser (operating at 632.8 nm, 17 mW), a 100-mW diodes laser operating at 785 nm and a solid state 50-mW laser operating at 532 nm. The three excitation lines were employed to explore the resonance Raman

spectra of red samples, identify CdS polymorphs (cubic or hexagonal) [68] and enhance the resonance profile of the yellow cadmium pigments. The selected laser beam was focused either with a 50× or a 100× objective with a maximum power density of 8 W/cm^2. We exclude laser induced temperature effect since measurements were performed on the sample with an increasing laser power and no spectral modifications were observed.
All spectra are presented as acquired without baseline correction or other treatment. To calculate the composition of the solid solution $Cd_{1-x}Zn_xS$, the relation $x = \Delta R/R_0$ is used [51]. In this expression $\Delta R_0 = 50$ cm^{-1} considering the values of the longitudinal optical (LO) phonons obtained in this work for *h-CdS* and *h-Zn*S references (298 cm^{-1} CdS-LO, 348 cm^{-1} ZnS-LO, 532 nm excitation). The analogous relation for the 2LO modes could not be considered because of the in-plane bending O–C=O in hydrogen bonding from PMMA at approximately 600 cm^{-1} [33]. The molar fraction in $CdS_{1-x}Se_x$ was obtained by using the calibration curve presented by Grazia et al. [52] of the CdS-LO and CdSe-LO difference with 632.8 laser excitation.

5.3. Results

Results of analysis in terms of colorimetric coordinates (L*, a*, b*), elemental (μ-EDXRF), optical (Vis reflectance, Vis photoluminescence (PL)) and vibrational (μ-Raman) characterization of the yellow, red, and brown-orange samples are summarized in **Table 5.3**, **Table 5.4** and **Table 5.5**. Data from colorimetry (CIELAB 76 color space) and optical microscope observations are reported in **Appendix C**.
For all historical samples, the PMMA matrix was confirmed by μ-Raman (**Figure C.1**). The Raman assignments of historical PMMA are listed in **Table C.1**.

5.3.1. Yellow samples

All samples contained Cd and Zn. In some cases, Ba and S in traces were also detected. When evaluating the Vis-NIR reflectance spectra, the sigmoidal curve characteristic of semiconductor materials is observed (**Figure 5.3a**) [72]. The lack of secondary bands or shoulders in the first derivative spectra suggests the presence of only one CdS-based phase (**Figure 5.3b**).
Vis reflectance, Vis PL and resonance Raman data (532 nm excitation) suggest cadmium-zinc sulfide solid solutions with an increasing amount of Zn in different paler yellow hues. Experimentally determined band gap energies from reflectance profiles change from around 512 nm (2.42 eV) to around 472 nm (2.63 eV). Different yellow tones as consequence of the Zn contents is also confirmed by colorimetry: while negative values of a* characterize Zn-rich pale/lemon yellow samples, increase redness (>a*) is found for Zn-poor yellow samples (**Figure C.2**). In PL data (**Figure 5.3c**) a faint PMMA contribution to the emission (broad shoulder below 450 nm) can be seen in samples from the 1960s-1970s and this may be due to the accumulation of oxidation products or other additives.
As previously indicated, μ-Raman spectra acquired in resonance conditions (532 nm excitation) provide spectral profiles compatible with Zn-modified CdS pigments (**Figure 5.4a**). With increasing concentration of Zn, the intense LO and 2LO modes of $Cd_{1-x}Zn_xS$ solid solutions change continuously from the frequency of CdS ($LO(A_1/E_1) = 298$ cm^{-1}) [73] to that of ZnS ($LO(A_1/E_1) = 348$ cm^{-1}) [74]. Further, a gradual broadening of both LO and 2LO modes become detectable [51], as a consequence of the increased compositional disorder. It is noted that in the analyzed plastic samples while the shift of first order LO is easily visible, the second order LO is masked by the in-plane δ(O–C=O) vibration at 600 cm^{-1} of PMMA [33]. In addition to both LO and 2LO modes, E_2 (ca. 252 cm^{-1}), transverse optical (TO) phonon (A_1/E_1) (ca. 240 cm^{-1}) and multi-phonon (213 cm^{-1}) modes of CdS [68,75] become detectable when the conditions for the Raman resonance are not perfectly matched (samples from 9040 to 355).
When considering the off-resonance spectra (785 nm excitation), all fundamental long-wavelength optical phonon frequencies of CdS are detectable (see **Table C.2**) [51,68,75]. With the gradual increase of Zn

Table 5.3.: Results of the measurements on yellow acrylics (μ-EDXRF, Vis reflectance, Vis PL and μ-Raman) and pigment chemical composition. Data for h-ZnS and h-CdS are reported for comparison.

Sample	Colorimetric coordinates			μ-EDXRF	Reflectance		PL		μ-Raman		Identified solid solution
									@532 nm	@785 nm	
	L*	a*	b*	Elemental composition	λ_g (nm)	Zn molar fraction (x)	λ_{NBE} (nm)	Zn molar fraction (x)	Zn molar fraction (x)	Crystalline composition / polymorphs	
h-ZnS	–	–	–	Zn,S	329[a]	1 (ZnS)	317[c]	1 (ZnS)	1 (h-ZnS)	–	–
355	75.00	-13.53	75.46	Cd, S(tr), Zn, Ba(tr)	472	0.24	470	0.24	0.24	h-CdS	$Cd_{1-x}Zn_xS$
359	80.98	-6.21	96.27	Cd, S(tr), Zn, Ba	479	0.20	481	0.19	0.21		$Cd_{1-x}Zn_xS$
9041	80.36	-6.51	105.22	Cd, Zn, Ba	483	0.18	486	0.16	0.18		$Cd_{1-x}Zn_xS$
379	77.67	-2.21	103.25	Cd, S(tr), Zn, Ba	489	0.15	484	0.17	0.16		$Cd_{1-x}Zn_xS$
357	75.20	5.38	101.21	Cd, Zn	502	0.07	502	0.07	0.06		$Cd_{1-x}Zn_xS$
9040	75.21	6.68	109.68	Cd, S(tr), Zn, Ba	505	0.06	504	0.06	0.04		$Cd_{1-x}Zn_xS$
358	72.54	17.20	98.08	Cd, Zn, Ba	510	0.03	506	0.05	0.02		$Cd_{1-x}Zn_xS$
381	66.51	14.34	86.82	Cd, Zn, Ba	512	0.02	506	0.05	0.01		$Cd_{1-x}Zn_xS$
h-CdS	–	–	–	Cd, S(tr)	514[b]	0 (CdS)	513	0 (CdS)	0 (CdS)		–

(tr) traces
[a]Calculated from [69]
[b][51], sample 21060 according to the Kremer catalog, bench top analysis
[c][70]

Table 5.4.: Results of the measurements on red acrylics (μ-EDXRF, Vis reflectance, Vis PL and μ-Raman) and pigment chemical composition. Data for h-CdS, CdSe and α-HgS are also reported for comparison.

	Colorimetric coordinates			μ-EDXRF	Reflectance		PL		μ-Raman		Identified solid solution
									@632.8 nm	@785 nm	
Sample	L*	a*	b*	Elemental composition	λ_g (nm)	Hg or Se molar fraction (x)	λ_{NBE} (nm)	Se molar fraction (x)	Hg or Se molar fraction (x)	Crystalline composition / polymorphs	
α-HgS	–	–	–	Hg, S	563[a]	1 (HgS)	–	–	1 (α-HgS)	α-HgS	–
9082	30.07	52.55	40.20	Cd, Ba, Hg	580	0.16 (Hg)	593	–	–	–	$Cd_{1-x}Hg_xS$
CdSe	–	–	–	Cd, Se	738[b]	1 (CdSe)	717	1 (CdSe)	1 (CdSe)	CdSe	–
253	31.84	57.33	41.19	Cd, Se	592	0.34 (Se)	593	0.37 (Se)	0.32 (Se)	–	$CdS_{1-x}Se_x$
9081	39.77	62.64	51.75	Cd, S(tr), Ba, Se	580	0.29 (Se)	585	0.33 (Se)	0.27 (Se)	–	$CdS_{1-x}Se_x$
247	43.70	60.58	57.62	Cd, Ba, Se	571	0.25 (Se)	571	0.26 (Se)	0.23 (Se)	–	$CdS_{1-x}Se_x$
h-CdS	–	–	–	Cd, S(tr)	514[c]	0 (CdS)	512	0 (CdS)	0 (CdS)	h-CdS	CdS

(tr) traces
[a]Calculated from [71]
[b][52]
[c][51]

Table 5.5.: Results of the measurements on orange and brown acrylics (μ-EDXRF, Vis reflectance, Vis PL and μ-Raman) and pigment chemical composition.

Sample	Colorimetric coordinates			μ-EDXRF	Reflectance		PL		μ-Raman			Identified solid solution
									@532 nm	@632.8 nm	@785 nm	
	L*	a*	b*	Elemental composition	λ_g (nm)	Zn or Se molar fraction (x)	λ_{NBE} (nm)	Zn or Se molar fraction (x)	Zn or Se molar fraction (x)	Zn or Se molar fraction (x)	Crystalline composition / polymorphs	
9043	70.57	33.97	104.66	Cd, S(tr), Zn, Ba, Se	526	0.04 (Se)	523	0.02 (Se)	–	0.09 (Se)	–	$CdS_{1-x}Se_x$
					523	0.03 (Se)	–	–	CdS	CdS	h-CdS	CdS
					500	0.08 (Zn)	502	0.07 (Zn)	0.06 (Zn)	–	h-CdS	$Cd_{1-x}Zn_xS$
382	68.17	20.98	89.25	Cd, Zn, Ba	566	0.22 (Se)	556	0.18 (Se)	–	0.23 (Se)	–	$CdS_{1-x}Se_x$
					508	0.04 (Zn)	508	0.04 (Zn)	0.04 (Zn)	–	h-CdS	$Cd_{1-x}Zn_xS$
9050	52.92	58.60	79.83	Cd, Ba, Se	555	0.17 (Se)	561	0.21 (Se)	–	0.21 (Se)	–	$CdS_{1-x}Se_x$
					526	0.04 (Se)	544	0.12 (Se)	CdS	CdS	h-CdS	CdS
238	49.15	51.90	61.57	Cd, Zn, Ba, Se	566	0.22 (Se)	564	0.22 (Se)	–	0.23 (Se)	–	$CdS_{1-x}Se_x$
					520	0.01 (Se)	502	0.07 (Zn)	0.03 (Zn)	–	h-CdS	$Cd_{1-x}Zn_xS$
261	60.10	30.12	78.61	Cd, Zn, Ba	568	0.23 (Se)	564	0.22 (Se)	–	0.23 (Se)	–	$CdS_{1-x}Se_x$
					508	0.04 (Zn)	506	0.05 (Zn)	0.04 (Zn)	–	h-CdS	$Cd_{1-x}Zn_xS$
9010	13.15	22.36	12.48	Cd, Ba, Se	616	0.45 (Se)	608	0.45 (Se)	–	0.39 (Se)	–	$CdS_{1-x}Se_x$
					–	–	508	0.04 (Zn)	0.08 (Zn)	–	h-CdS	$Cd_{1-x}Zn_xS$

(tr) traces

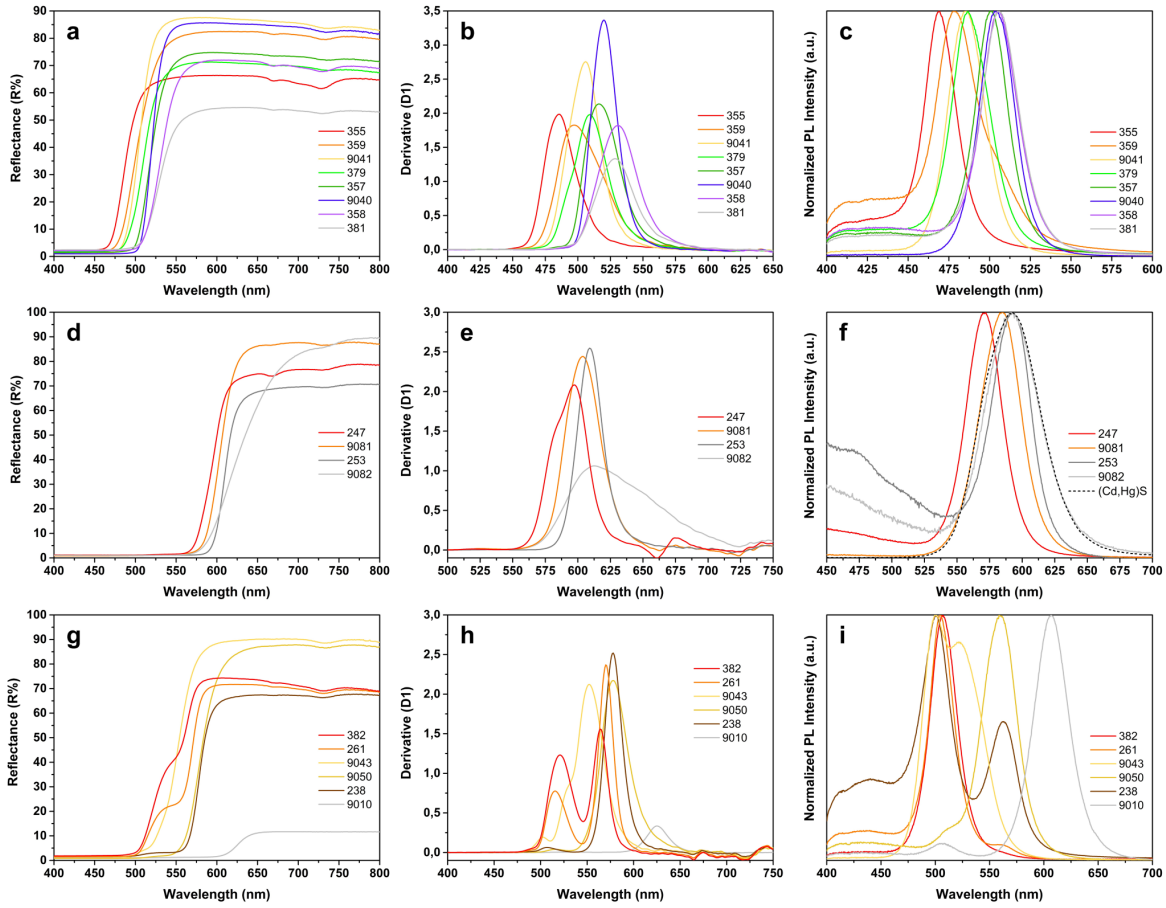

Figure 5.3.: Vis-NIR reflectance (a, d, g), first derivative (b, e, h) and NBE emission (c, f, i) spectra of historical yellow (upper), red (middle) and orange-brown samples (bottom). In (f) the NBE emission spectrum of sample *(Cd,Hg)S* pigment is reported for comparison (black dashed line).

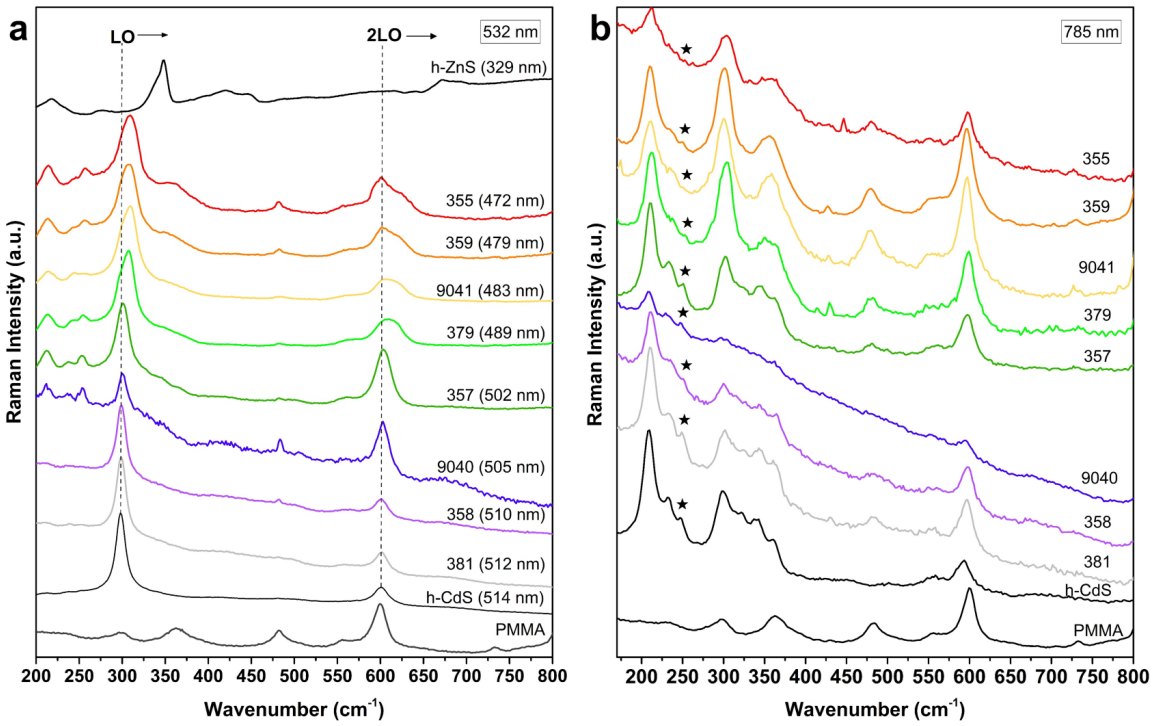

Figure 5.4.: μ-Raman spectra of the yellow samples recorded under (a) resonance and (b) out-of-resonance conditions. In (a) extrapolated λ_g(nm) are reported in parenthesis. The band at ca 252 cm^{-1} typical of h-CdS is marked with an asterisk. References of PMMA, *h-CdS* and *h-ZnS* are also reported for comparison.

(**Figure 5.4b** from *h-CdS* to sample 355), TO modes (at 232-242 cm^{-1}) and the multi-phonon modes (at 213 cm^{-1} and between 320 and 560 cm^{-1}) progressively disappear probably due to the increase in structural defects. The wurtzite-specific Raman signature at ca. 252 cm^{-1} is observed in all acrylic samples, indicating the presence of the hexagonal CdS polymorph.
Beside the Cd-based phases, other additives are detected by μ-Raman and reflectance measurements. Samples 9040 and 9041 from the 1990s show Raman scattering characteristic of barium sulfate $BaSO_4$ (448m, 456m, 613w, 624w, 642w, 985vs cm^{-1}) [76,77]. Considering the UV-Vis-NIR reflectance spectra, very weak composite absorption bands between 650 and 750 nm suggest the presence of trace Co(II) as expected for its pseudo tetrahedral sulfur coordination in ZnS (**Figure C.3a**). Additional evidence of ZnS presence is revealed by the detection of its inflection point at 340 nm in the Zn-richest sample 355 (**Figure C.3b**) [78,79].

5.3.2. Red samples

Only four samples are red and show high positive a* values (>50) in the CIELab 1976 color space (**Figure C.2**). The presence of cadmium sulfo-selenide $CdS_{1-x}Se_x$ (all red samples apart for sample 9082) and of mercury-cadmium sulfide $Cd_{1-x}Hg_xS$ (sample 9082) mixed with barium sulfate is hypothesized based on elements detected with μ-EDXRF.
The inflection points in the sigmoidal shape of the Vis-NIR reflectance spectra (**Figure 5.3d,e**) are found at higher wavelengths with respect to yellow samples [34,80,81]. While all samples containing Se show a relatively close to idealized spectral reflectance curve for semiconductive materials, sample 9082 is characterized by a reduced slope of the rising edge, probably due to the distortion of the crystal lattice [82]. While no Zn was detected by μ-EDXRF, Co(II) in ZnS could account for the multiband system (650-750 nm) observed samples in 9081 and 247 [78,79].
Given the experimentally determined band gap energies extrapolated from both Vis reflectance and Vis PL data, solid solutions of $CdS_{1-x}Se_x$ with different Se content are suggested for samples 253, 9081 and 247, where Se molar fractions around 0.34, 0.29 and 0.25 are estimated from reflectance data.
Sample 9082 is characterized by an optical band gap λ_g of 580 nm (2.14 eV) from reflectance data. Considering the linear correlation reported by Kremheller et al. [63] and Adachi [64], a Cd molar fraction of 0.84 is estimated, suggesting the presence of a $Cd_{0.84}Hg_{0.16}S$ solid solution. Interestingly, this sample has an NBE PL emission that perfectly matches the emission of the reference *(Cd,Hg)S*, suggesting the same degree of substitution of Cd in the crystal lattice (**Figure 5.3f**).
As seen in Raman spectra depicted in **Figure 5.5a**, the resonance LO modes of CdSe and non-resonance CdS-LO modes (first and second order) shift continuously with increasing Se molar fraction: in particular, as the Se content increases the CdSe-LO band at 194 cm^{-1} shifts to higher wavenumbers, while the first and second order of CdS-LO modes at 302 and 600 cm^{-1} shift to lower wavenumbers. It is noted that the band 484 cm^{-1} is attributed to the skeletal deformation C–C in CC_4 from PMMA [33]. In sample 9082, the $Cd_{1-x}Hg_xS$ phonon frequencies is reported for the first time (**Figure 5.5b,c**). The Raman spectra of pure *h-CdS*, pure *α-HgS* (trigonal) and the *(Cd,Hg)S* reference sample are reported for comparison. When exciting in resonance conditions (632.8 nm excitation), the two $Cd_{1-x}Hg_xS$ pigments are characterized by a similar Raman signature: as Hg is introduced in the crystal lattice, the LO and 2LO-CdS modes shift towards lower wavenumbers, with the frequency of CdS ($LO(A_1/E_1)$ = 302 cm^{-1}) likely changing continuously to that of HgS (LO(E) = 288 cm^{-1}). Assignments of the firstorder Raman lines of *α-HgS* [83-85] are reported in **Table C.3**. The multi-phonon band around 214 cm^{-1} of CdS is also detected, probably due to the lack of perfect match of resonance condition. When employing the out-of-resonance excitation (785 nm) (**Figure 5.5c**) other Raman bands of both h-CdS and α-HgS become detectable: multi-phonon modes at 212 cm^{-1} and better structured multi-bands at 320-370 cm^{-1} for CdS, TO(E) at 280 cm^{-1} for α-HgS.

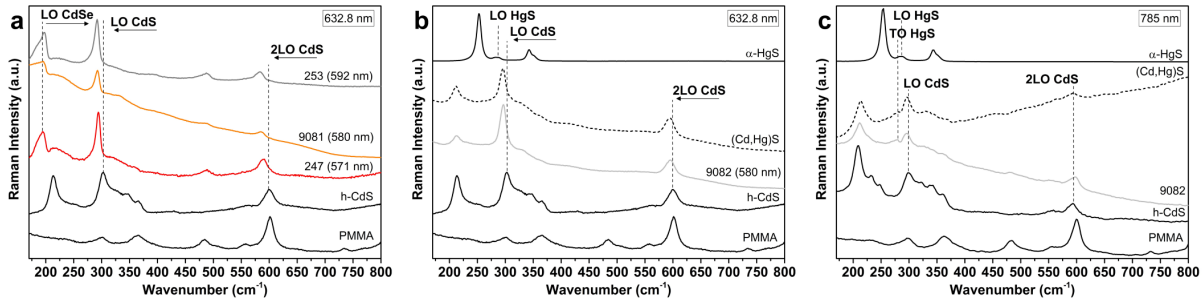

Figure 5.5.: μ-Raman spectra of the red samples recorded under (a, b) resonance and (c) out-of-resonance conditions. In (a, b) extrapolated λ_g(nm) are reported in parenthesis. References of PMMA, *h-CdS*, *α-HgS* and *(Cd,Hg)S* pigments are also reported for comparison.

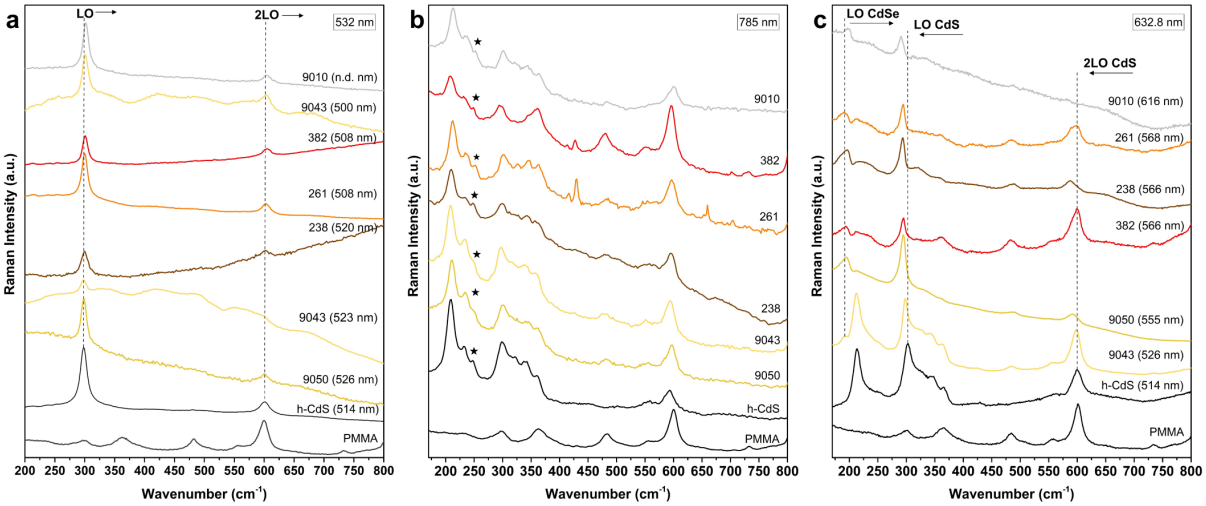

Figure 5.6.: μ-Raman spectra of the orange-brown samples recorded under (a, c) resonance and (b) out-of-resonance conditions. In (a, c) extrapolated λ_g(nm) are reported in parenthesis. The band at ca 252 cm^{-1} typical of h-CdS is marked with an asterisk. References of PMMA, *h-CdS* and *h-ZnS* are also reported for comparison.

5.3.3. Orange & brown samples

Colorimetric coordinates (**Figure C.2**) reflect the three different shades of the last set of samples: deep yellow (samples 9043, 382), orange (9050, 238, 261) and brown (9010).

The use of more than one Cd-based pigment is indicated by optical microscope observations (**Figure C.4**), where differently colored agglomerates are observed. The presence of mixtures is confirmed by reflectance measurements, with the detection of more than one inflection point (visible region) in the Vis-NIR reflectance (**Figure 5.3g**) and first derivative spectra (**Figure 5.3h**).

Given the Vis reflectance and Vis PL data (**Figure 5.3i**), it is possible to infer that all samples are mixtures of $Cd_{1-x}Zn_xS$ and $CdS_{1-x}Se_x$ pigments. In particular, solid solutions with low (or zero) Zn and variable Se molar fractions are suggested on the basis of the estimated optical bandgap energies.

In **Figure 5.6** the Raman spectra of the Cd-based pigments used in mixture are shown.

In samples 9043, 382, 238, 261, 9010 the presence of $Cd_{1-x}Zn_xS$ with trace Zn ($\leqslant$0.08) is suggested by resonance Raman spectra, where only small shifts towards higher wavenumbers of the LO-CdS mode are observed (first and second order). The result is confirmed by Vis PL and Vis reflectance data for all samples, except for samples 9010 and 238. Raman spectra acquired from sample 9010 indicate a $Cd_{1-x}Zn_xS$ solid solution with the higher Zn content (0.08), although no optical band gap related to the solid solution is identified from

reflectance data. Instead, the presence of $Cd_{1-x}Zn_xS$ pigment is confirmed by PL measurements (NBE emission of 508 nm / 2.44 eV). Similarly, Raman spectra from sample 238 suggest a composition of $Cd_{0.97}Zn_{0.03}S$, even if the optical band gap (520 nm / 2.38 eV) extrapolated from reflectance data suggests a cadmium sulfo-selenide solid solution (with a very low Se molar fraction). Elemental analysis and NBE emission support the conclusive identification of a Zn-modified cadmium pigment with NBE emission centered at 502 nm.
The identification of the selenium molar fraction in the cadmium sulfo-selenide coloring agents is less problematic and only slightly different compositions are reported between the extrapolated optical band gap energies and Raman spectra. In sample 9043, while resonance Raman spectra (532 nm laser line) suggest the presence of pure CdS as one of the plastic coloring agents, its presence is not detected by Vis PL data, while Vis reflectance data indicates a cadmium sulfo-selenide solid solution with 0.03 Se molar fraction. Similarly, in sample 9050 the presence of pure CdS is inferred from resonance Raman data, while the optical band gaps calculated from Vis reflectance and Vis PL data indicate a cadmium sulfo-selenide solid solution. Interestingly, samples 261 and 382 are made of a mixture of chemically similar yellow and red Cd-pigments. The presence of different proportions of the two components of the mixture justifies their different color properties ranging from a deep yellow (for sample 382) to light orange (for sample 261). This issue is confirmed by optical microscope observation where few red agglomerated are observed in sample 382 resulting in a more yellowish shade (**Figure C.4**).
Finally, traces of cobalt in ZnS are suggested for sample 261 and 382 due to the absorption bands in the 650-750 nm in Vis-NIR reflectance spectra. As found for the yellow acrylic samples, the Raman spectra in off-resonance condition (785 nm) of the yellow coloring agents in these complex mixtures show the typical signature of h-CdS at ca 252 cm^{-1} (**Figure 5.6b**).

5.4. Discussion

5.4.1. General observations

This study confirms that the extrapolation of molar fraction of the solid solution is extremely useful for the identification of Cd-based pigments in plastics. The obtained values are similar to the concentrations of Zn, Se and Hg proposed for commercial pigments being 25, 50 and 26 the maximum respectively mole % used [39,40,42].
The proposed analytical protocol employs three different spectroscopy techniques (UV-Vis-NIR diffuse reflectance, laser-induced photoluminescence and μ-Raman) to estimate the concentration of substitutional ions in the cadmium-based solid solutions. A comparison between the results achieved with the three methods is provided in **Figure 5.7** for the yellow acrylic samples and in **Figure C.5** for red and brown-orange samples. In general, small and reasonable variations between the results of the three techniques are observed, with problematic discrepancies only when considering complex samples made of multiple coloring agents. For example, in the case of brown sample 9010, no optical band gap of the yellow Cd-pigment is extrapolated from Vis reflectance data, probably due to the superposition of the reflectance profile of the more abundant red $CdS_{1-x}Se_x$ component. Similarly, for samples 9043 and 9050, while Raman measurements suggest the presence of pure CdS, NBE emission and Vis reflectance data are not able of detecting this component owing to the overlay with the more intense $Cd_{1-x}Zn_xS$ and $CdS_{1-x}Se_x$ signals. In the case of red sample 9082, a strong match with the luminescence properties and Raman signature of reference *(Cd,Hg)S* is found. Similar solid solution composition is thus suggested, where the Hg content proposed by Vis reflectance spectroscopy (16%) is within that estimated by PXRD and Rietveld refinement (21(± 6)%).
Considering optical measurements, although the Cd-based pigments are dispersed in the polymeric matrix, chemical compositions of the solid solutions are efficiently characterized by UV-Vis-NIR diffuse reflectance spectroscopy. Indeed, beside the specular reflection from the sample surface, little internal scattering can be

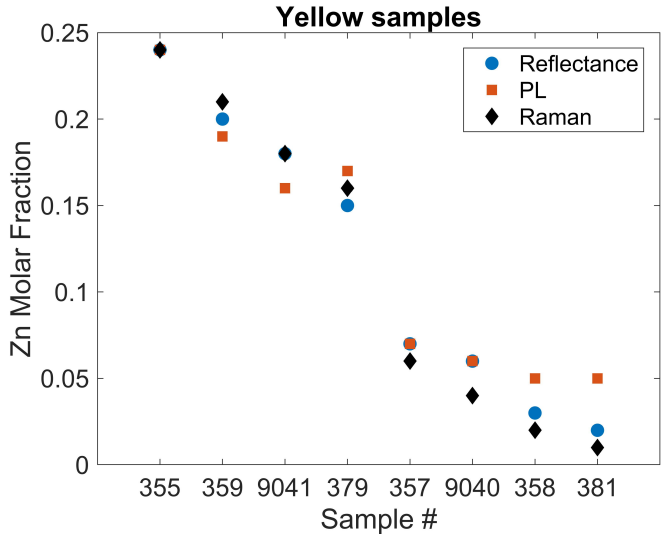

Figure 5.7.: Extrapolated Zn molar fraction of the yellow acrylic samples obtained on the basis of reflectance (blue circles), PL (red squares) and μ-Raman (black diamonds) data.

associated with transparent, amorphous PMMA. Hence, the color of the acrylic samples depends mainly on the accumulative scattering and absorption from the pigment particles. Similarly, PL data are little affected by the PMMA matrix that gives rise only to a faint emission. In μ-Raman spectroscopy, even if a small contribution of some Raman bands associated with PMMA is observed, the molecular characterization of the dispersed colorants is successfully obtained focusing the laser beam only on the colored grains.

Based on the results from the applied multi-analytical methods suggested in this work, the identified cadmium pigments and additives are listed in **Table 5.6**. The results of this study show clear differences in the chemical composition of the acrylic samples. Whereas yellow samples are characterized by $Cd_{1-x}Zn_xS$ pigments (PY 35), red samples are found to contain $CdS_{1-x}Se_x$ (PR 108, Se>10%) and $Cd_{1-x}Hg_xS$ (PR 113). To provide intermediate orange and brown shades, one or two yellow-based cadmium pigments ($Cd_{1-x}Zn_xS$ - PY 35 and CdS - PY 37) have been mixed with a red cadmium-based pigment ($CdS_{1-x}Se_x$ - PR 108, PO 20).

Both PMMA and cadmium-based pigments do not show degradation at molecular level. Most important absorption frequencies of PMMA were detected and no differences are observed in comparison with the Raman spectra of an unaged PMMA reference. Concerning the cadmium-based pigments, the proper encapsulation in the acrylic matrix likely accounts for their preservation and, so far, no degradation seems to be triggered by the polymeric matrix (including the components of the whole formulation).

As cadmium pigments were produced for the plastic industry from the 1950s [38], the same yellow and red coloring agents are identified in samples from the 1960s-1970s and 1990s. It is of interest that PR 113 (mercury-cadmium sulfide) was identified in swatches, as it is a very rarely used pigment [86]. Mainly used for plastic applications [34,42], the identification of PR 113 in one sample from the 1990s prolongs its use as a plastic colorant, although its production was limited after the 1980s [50].

5.4.2. The band gap

As the optical properties of semiconductor materials is due to the band gap, a shift of the absorption edge in the reflectance spectra indicates a change in crystal structure and related chemical composition. The blue shift of the optical band gap observed for of $Cd_{1-x}Zn_xS$ pigments reflects the progressive decrease of the unit cell dimensions. In fact, $Cd_{1-x}Zn_xS$ pigments fall between hexagonal wurtzite CdS (space group $P6_3mc$ with $a_0 = 4.136$ Å, $c_0 = 6.713$ Å) and hexagonal wurtzite ZnS (space group $P6_3mc$ with $a_0 = 3.820$ Å and $c_0 = 6.260$ Å), showing greener and lighter hues of yellow as Zn is introduced in the CdS lattice. The red shift for

Table 5.6.: Cadmium pigments and additives identified in the historical acrylic samples through the in situ multi-analytical approach.

	Sample		Color	Dating	Colorants	Additives
Yellow	355		yellow, lemon	1960s-1970s	$Cd_{1-x}Zn_xS$ (PY 35)	$BaSO_4$[a] ZnS[b]
	359		yellow, very light	1960s-1970s	$Cd_{1-x}Zn_xS$ (PY 35)	$BaSO_4$[a] ZnS[b]
	9041		yellow, light	1990s	$Cd_{1-x}Zn_xS$ (PY 35)	$BaSO_4$[a] ZnS[b]
	379		yellow, light	1960s-1970s	$Cd_{1-x}Zn_xS$ (PY 35)	$BaSO_4$[a] ZnS[b]
	357		yellow	1960s-1970s	$Cd_{1-x}Zn_xS$ (PY 35)	ZnS (PW 7)
	9040		yellow	1990s	$Cd_{1-x}Zn_xS$ (PY 35)	$BaSO_4$[a] ZnS[b]
	358		yellow, deep	1960s-1970s	$Cd_{1-x}Zn_xS$ (PY 35)	$BaSO_4$[a] ZnS[b]
	381		yellow, deep	1960s-1970s	$Cd_{1-x}Zn_xS$ (PY 35)	$BaSO_4$[a] ZnS[b]
Red	9082		red, deep	1990s	$Cd_{1-x}HgxS$ (PR 113:1)	$BaSO_4$
	253		red, deep	1960s-1970s	$CdS_{1-x}Se_x$ (PR 108)	
	9081		red, scarlet	1990s	$CdS_{1-x}Se_x$ (PR 108)	$BaSO_4$[a] ZnS[b]
	247		red, light	1960s-1970s	$CdS_{1-x}Se_x$ (PR 108)	$BaSO_4$[a] ZnS[b]
Orange & brown	9043		yellow, deep	1990s	$CdS_{1-x}Se_x$ + CdS + $Cd_{1-x}Zn_xS$ (PO 20 + PY 37 + PY 35)	$BaSO_4$[c]
	382		yellow, deep	1960s-1970s	$CdS_{1-x}Se_x$ + $Cd_{1-x}Zn_xS$ (PR 108 + PY 35)	$BaSO_4$[a,c] ZnS[b]
	9050		orange	1990s	$CdS_{1-x}Sex$ + CdS (PR 108 + PY 37)	$BaSO_4$[c]
	238		orange, deep	1960s-1970s	$CdS_{1-x}Se_x$ + $Cd_{1-x}Zn_xS$ (PR 108 + PY 35)	$BaSO_4$[c]
	261		orange, light	1960s-1970s	$CdS_{1-x}Se_x$ + $Cd_{1-x}Zn_xS$ (PR 108 + PY 35)	$BaSO_4$[a,c] ZnS[b]
	9010		brown	1990s	$CdS_{1-x}Se_x$ + $Cd_{1-x}Zn_xS$ (PR 108 + PY 35)	$BaSO_4$[c]

[a] As PW 5 ($ZnS/BaSO_4$) or lithophone extension of the cadmium-based pigments (:1)
[b] As PW 5 ($ZnS/BaSO_4$) or PW 7
[c] As lithophone extension of the cadmium-based pigments (:1) is not possible to be associated to a specific phase of the mixture

$CdS_{1-x}Se_x$ pigments is instead correlated to deeper red hues as mutual expansion of a_0 and c_0 from hexagonal wurtzite CdS (space group $P6_3mc$ with $a_0 = 4.136$ Å, $c_0 = 6.713$ Å) to hexagonal CdSe modification (space group $P6_3mc$ with $a_0 = 4.299$ Å, $c_0 = 7.\ 010$ Å) occurs [42,87].

5.4.3. Raman spectra

Raman spectroscopic analysis is performed using an excitation slightly above the band gaps (532 and 632.8 laser lines) to record, with resonant enhancement via electronic transitions, the Raman signature of $Cd_{1-x}Zn_xS$, $CdS_{1-x}Se_x$ and $Cd_{1-x}Hg_xS$ as function of the Zn, Se and Hg contents respectively.
The observed linear correlation between the Zn content and peak shifts of the LO and 2LO modes of CdS phase in $Cd_{1-x}Zn_xS$ solid solution is well discussed in literature [88-90]. Because a single set of longwavelength optical phonons appears and the phonon spectra vary in energy as the alloy composition is varied from one member to another, in hexagonal $Cd_{1-x}Zn_xS$ II-VI ternary alloys the vibrational bands exhibit one-mode behavior following the definition of the zone-center optical phonon modes in $A_{1-x}B_xC$ ternary alloys by Brodsky et al. [91]. The one-mode behavior is also consistent with the MREI model of Chang and Mitra [92,93] due to the significant mass difference between cadmium (A_{1-x}), zinc (B_x) and sulfur (C) [94]. The influence of ZnS as an additive in the resonance Raman of the yellow samples is excluded because it is an incompatible crystallographic mixture with Cd-based pigments.
Considering the resonance Raman spectra obtained for $CdS_{1-x}Se_x$ solid solution, two distinct sets of optical modes with frequencies characteristic of each end member (CdS-LO and CdSe-LO) are observed. CdS-LO frequencies move towards the local mode and CdSe-LO frequencies move from the gap mode. This is in accordance with the twomode type of compositional behavior as experimental and theoretically proposed for hexagonal $CdS_{1-x}Se_x$ II-VI ternary alloy semiconductors [93,95-100].
As predicted by MREI model and given the masses of the end members Cd and Hg [92-94], one-mode behavior of the vibrational modes might likely explain the red shift of the CdS-LO to HgS-LO for $Cd_{1-x}Hg_xS$ solid solution, proposed here for the first time.
Out of resonance, the Raman fingerprint of the hexagonal CdS polymorph is identified. This finding is consistent with the production methods of Cd-modified pigments following calcination [37,38] to convert the cubic structure to more stable wurtzite hexagonal crystals [42] recommended for plastic coloring [1,36].

5.4.4. Additives

Additives are identified in the samples, such as barium sulfate $BaSO_4$ and zinc sulfide ZnS. The presence of ZnS is suggested by UV-Vis-NIR reflectance measurements, thanks to the detection of specific cobalt(II) absorption bands; it was added in small quantities from the mid-1920s in the ZnS production to achieve improved lightfastness, high brightness and pure whiteness [78,79,101]. Barium sulfate and zinc sulfide can be used respectively as extender ($BaSO_4$, PW 21) and lightener (ZnS, PW 7) or as an intimate mixture to produce lithopone ($ZnS/BaSO_4$, PW 5) for plastic coloring [34,35]. On the basis of the achieved results, the exact use of the both additives cannot be determined. ZnS could have been physically mixed as a lightener with the $Cd_{1-x}Zn_xS$ pigments to achieve greenish lemon and primrose types of cadmium yellow [34,102], while $BaSO_4$ was used as an extender in the yellow samples as cadmium lithopone varieties. The lack of Ba and the identification of ZnS in sample 357 supports this hypothesis. For sample 9082 the presence of mercury-cadmium sulfide lithopone can be proposed (PR 113:1). Instead, $BaSO_4$ may be both present as PW 5 and cadmium lithopone for 247 and 9081 red samples. Less probably, ZnS could have been added as lightener for the red cadmium pigments.
Lowering the production cost, the presence of $BaSO_4$ does not affect the variety of shades available retaining a close similarity in masstone to the pure form. In terms of optical properties, $BaSO_4$ does not affect the spectral reflectance curve due to the lower refractive index ($\eta = 1.64$ [35]) compared to hexagonal cadmium sulfide

(η = 2.5) [103] cadmium-zinc sulfide (η = 2.3-2.5) [34,103] cadmium sulfoselenide (η = 2.6-2.8) [37,103], mercury-cadmium sulfide (η = 2.5-2.9) [103].
On the other hand, ZnS is considered in plastic industry a white pigment owing to its high refractive index (η = 2.37) [35] and, when it is used, an increase of the reflectance values in the visible range may be observed. The optical band gap position of the Cd-based pigments should not be affected owing to the lack of crystallographic mixture.

5.5. Conclusion

A multi-analytical in situ approach for the identification of cadmium-based coloring agents in plastics is here presented. Although the cadmium pigments are dispersed in the polymeric matrix, the proposed method is suitable to satisfactorily determine the unknown pigment composition without any micro-sampling.
CdS (PY 37), $Cd_{1-x}Zn_xS$ (PY 35) $CdS_{1-x}Se_x$ (PR 108, PO 20), $Cd_{1-x}Hg_xS$ (PR 113) pigments have been identified based on their optical and vibrational properties. In some samples, mixtures of more than one coloring agent are easily revealed by their diffuse reflectance spectra containing more inflection points in the visible range, and the use of optical microscopy and μ-Raman spectroscopy is of great value for supporting this finding. The presence of two additives, barium sulfate and zinc sulfide, is also inferred from complementary techniques in many of the samples. Generally, the results obtained from the different analytical techniques agree in the definition of the chemical composition of the coloring agents and additives in the analyzed plastics. The integration of the information achievable by elemental, optical and vibrational in situ analysis represent the great value of the multi-analytical methodology used.
A band gap calculation method (Tauc plot) well-suited for semiconductor materials has been used to estimate the band gap energies of the cadmium-based pigments. Because the method makes use of the Vis reflectance spectra, the optical band gap position of the Cd-based pigments should not be affected by the other components of the plastic formulation. In the current case studies, no influence of both acrylic medium and additives in the diffuse reflectance measurements is found, thus validating the results obtained. PL spectroscopy also supports the investigation by providing a cross-verification of the band gap estimation. Vibrational analysis and identification of specific semiconductors was achieved by recorded Raman scattering directly from pigment particles within the polymer matrix.
Cadmium pigments have been widely studied in paint. This article reports the first analytical study on their identification in plastics as colorants. For the first time, experimental data from mercury-cadmium sulfide ($Cd_{1-x}Hg_xS$) is reported along with a review of its use in plastics. Given the reliable results obtained with the proposed in situ multitechnique method, this work opens new avenues for in situ research on modern and contemporary heritage made of plastics containing colorants. While the present study has been performed in the laboratory, in principle the proposed approach could be performed with compact portable instrumentation directly on design plastic objects in museums or private collections, but care is needed in the application of techniques without microscopic selection of pigment particles. In this sense, the availability of common portable instruments and mounting different spectroscopy techniques on the same detection head is of great interest, as is combined XRF and Raman spectrometers [104] and combined diffuse reflectance and photoluminescence spectroscopy devices [105].

5.6. References

[1] Charvat RA, editor. Coloring of plastics: fundamentals. New Jersey: John Wiley & Sons Inc., second ed.; 2004.
[2] Bart JCJ. Additives in polymers – Industrial analysis and applications. Chichester: John Wiley & Sons Ltd;

2005.
[3] Harper CA, Petrie EM. Plastics materials and processes – A concise encyclopedia. New Jersey: John Wiley & Sons Inc.; 2003.
[4] Rosato DV, Rosato MG, Rosato DV. Concise encyclopedia of plastics. New York: Springer Science & Business Media; 2000.
[5] Lavédrine B, Fournier A, Martin G, editors. Preservation of Plastic Artefacts in Museum Collections (POPART). Paris: Comité Des Travaux Historiques et Scientifiques (CTHS); 2012.
[6] Grattan DW, editor. Saving the Twentieth century, the conservation of modern materials: proceedings of a conference, Symposium '91, Saving the Twentieth Century, Ottawa, Canada, 15 to 20 September 1991. Ottawa: Canadian Conservation Institute; 1993.
[7] Allen NS, Edge M, Horie CV, editors. Polymers in conservation. Cambridge: The Royal Society of Chemistry; 1992.
[8] van Oosten T. PUR facts: conservation of polyurethane foam in art and design. Amsterdam: Amsterdam University Press; 2011.
[9] França de Sá S, Ferreira JL, Pombo Cardoso I, Macedo R, Ramos AM. Shedding new light on polyurethane degradation: assessing foams condition in design objects. Polym Degrad Stab. 2017; 144: 354-365. DOI: 10.1016/j.polymdegradstab.2017.08.028.
[10] Quye A, Littlejohn D, Pethrick RA, Stewart RA. Investigation of inherent degradation in cellulose nitrate museum artefacts. Polym Degrad Stab. 2011; 96(7): 1369-1376. DOI: 10.1016/j.polymdegradstab.2011.03.009.
[11] Neves A, Angelin EM, Roldão É, Melo MJ. New insights into the degradation mechanism of cellulose nitrate in cinematographic films by Raman microscopy. J Raman Spectrosc. 2019; 50(2): 202-212. DOI: 10.1002/jrs.5464.
[12] Littlejohn D, Pethrick RA, Quye A, Ballany JM. Investigation of the degradation of cellulose acetate museum artefacts. Polym Degrad Stab. 2013; 98(1): 416-424. DOI: 10.1016/j.polymdegradstab.2012.08.023.
[13] Toja F, Saviello D, Nevin A, Comelli D, Lazzari M, Levi M, Toniolo L. The degradation of poly(vinyl acetate) as a material for design objects: a multi-analytical study of the effect of dibutyl phthalate plasticizer. Part 1. Polym Degrad Stab. 2012; 97(11): 2441-2448. DOI: 10.1016/j.polymdegradstab.2012.07.018.
[14] Toja F, Saviello D, Nevin A, Comelli D, Lazzari M, Valentini G, Toniolo L. The degradation of poly(vinyl acetate) as a material for design objects: a multi-analytical study of the Cocoon lamps. Part 2. Polym Degrad Stab. 2013; 98(11): 2215-2223. DOI: 10.1016/j.polymdegradstab.2013.08.021.
[15] Ferreira JL, Melo MJ, Ramos AM. Poly(vinyl acetate) paints in works of art: a photochemical approach. Part 1. Polym Degrad Stab. 2010; 95(4): 453-461. DOI: 10.1016/j.polymdegradstab.2010.01.015.
[16] Saviello D, Pouyet E, Toniolo L, Cotte M, Nevin A. Synchrotron-based FTIR microspectroscopy for the mapping of photo-oxidation and additives in acrylonitrile-butadiene-styrene model samples and historical objects. Anal Chim Acta 2014; 843: 59-72. DOI: 10.1016/j.aca.2014.07.021.
[17] Chiantore O, Trossarelli L, Lazzari M. Photooxidative degradation of acrylic and methacrylic polymers. Polymer 2000; 41(5): 1657-1668. DOI: 10.1016/S0032-3861(99)00349-3.
[18] Melo MJ, Bracci S, Camaiti M, Chiantore O, Piacenti F. Photodegradation of acrylic resins used in the conservation of stone. Polym Degrad Stab. 1999; 66(1): 23-30. DOI: 10.1016/S0141-3910(99)00048-8.
[19] Schilling MR, Learner T. Evolved gas analysis as a tool for characterizing plastics. In: Bridgland J, editor. ICOM-CC 16th Triennial Conference Preprints, Lisbon, 19-23 September 2011. Almada: Critério; 2011.
[20] Degano D, Modugno F, Bonaduce I, Ribechini E, Colombini MP. Recent advances in analytical pyrolysis to investigate organic materials in heritage science. Angew Chem Int Ed. 2018; 57: 7313-7323. DOI: 10.1002/anie.201713404.
[21] La Nasa J, Biale G, Ferriani B, Colombini MP, Modugno F. A pyrolysis approach for characterizing and assessing degradation of polyurethane foam in cultural heritage objects. J Anal Appl Pyrol. 2018; 134:

562-572. DOI: 10.1016/j.jaap.2018.08.004.
[22] La Nasa J, Biale G, Sabatini F, Degano I, Colombini MP, Modugno F. Synthetic materials in art: a new comprehensive approach for the characterization of multimaterial artworks by analytical pyrolysis. Herit Sci. 2019: 7: 1-14. DOI: 10.1186/s40494-019-0251-4.
[23] Shashoua Y. Conservation of plastics. Oxford: Butterworth-Heinemann; 2008.
[24] Quye A, Williamson C, editors. Plastics: collecting and conserving. Edinburg: NMS Publishing Limited; 1999.
[25] Miliani C, Monico L, Melo MJ, Fantacci S, Angelin EM, Romani A, Janssens K. Photochemistry of artists' dyes and pigments: towards better understanding and prevention of colour change in works of art. Angew Chem Int Ed. 2018; 57: 7324-7334. DOI: 10.1002/anie.201802801.
[26] Pritchard G. Plastics additives – An A-Z reference. London: Chapman & Hall; 1998.
[27] Invernizzi C, Fiocco G, Iwanicka M, Kowalska M, Targowski P, Blümich B, Rehorn C, Gabrielli V, Bersani D, Licchelli M, Malagodi M.Non-invasive mobile technology to study the stratigraphy of ancient Cremonese violins: OCT, NMRMOUSE, XRF and reflection FT-IR spectroscopy. Microchem J. 2020; 155: 104754. DOI: 10.1016/j.microc.2020.104754.
[28] Micheletti F, Orsilli J, Melada J, Gargano M, Ludwig N, Bonizzoni L. The role of IRT in the archaeometric study of ancient glass through XRF and FORS. Microchem J. 2020; 153: 104388. DOI: 10.1016/j.microc.2019.104388.
[29] Tibúrcio C, Valadas S, Cardoso A, Candeias A, Barreira C, Miguel C. On the use of EDXRF and UV-Vis FORS to unveil the production of two illuminated manuscripts from the fifteenth century portuguese royal court. Microchem J. 2020; 153: 104455. DOI: 10.1016/j.microc.2019.104455.
[30] Amanatiadis S, Tsardaka E-C, Karamanos T, Karagiannis G. Infrared spectroscopic mapping imaging for depth analysis of artworks. Microchem J. 2020; 156: 104869. DOI: 10.1016/j.microc.2020.104869.
[31] de Groot S, van Keulen H, Megens L, van Oosten T, Wiresma H. Discolouration of plastics objects: investigation into composition using various analytical techniques. In: Bechthold T, editor. Future Talks 013 – Lectures and workshops on technology and conservation of modern materials in design. Munich: Die Neue Sammlung – The Design Museum; 2015. p. 19-26.
[32] de Groot S, van Keulen H, van den Akker S, van Oosten T. Discoloration of plastics objects: the identification of yellow and orange synthetic pigment in plastic objects. In: Bechthold T, editor. Future Talks 015 – Processes. The making of design and modern art. Materials, technologies and conservation strategies. Munich: Die Neue Sammlung - The Design Museum; 2017. p. 147-158.
[33] Angelin EM, Babo S, Ferreira JL, Melo MJ. Raman microscopy for the identification of pearlescent pigments in acrylic works of art. J Raman Spectrosc. 2019; 50: 232-241. DOI: 10.1002/jrs.5431.
[34] Fiedler I, Bayard M. Cadmium yellows, oranges and reds. In: Feller RL, editor. Artists' pigments: a handbook of their history and characteristics. Washington: National Gallery of Art, Vol 1; 1986. p. 65-108
[35] Müller A. Coloring of plastics. Munich: Carl Hanser Verlag; 2003.
[36] Webber TG, editor. Coloring of plastics. New York: John Wiley & Sons Inc.; 1979.
[37] Buxbaum G, editor. Industrial inorganic pigments. Weinheim: Wiley-VCH Verlag GmbH, second completely revised ed.; 1998.
[38] Dunning P. Cadmium pigments. In: Faulkner EB, Schwartz RJ, editors. High performance pigments. Weinheim: Wiley-VCH, second revised expanded ed.; 2009. p. 13-26.
[39] Loya JE. Cadmium sulfide pigments. In: Lewis PA, editor. Pigment handbook, properties and economics. New York: John Wiley & Sons Inc., Vol. I, second ed.; 1988. p. 347-352.
[40] Daly JE. Cadmium-mercury sulfides. In: Lewis PA, editor. Pigment handbook, properties and economics. New York: John Wiley & Sons Inc., Vol. I, second ed.; 1988. p. 353-356.
[41] Murray BG. Pigmentation of colored plastics. In: Lewis PA, editor. Pigment handbook, applications and markets. New York: John Wiley & Sons Inc., Vol. II, second ed.; 1988. p. 277-290.

[42] Huckle WG, Swigert GF, Wiberley SE. Cadmium pigments. Structure and composition. Ind Eng Chem Prod Res Dev. 1966; 5: 362-366. DOI: 10.1021/i360020a016.
[43] Mass JL, Opila R, Buckley B, Cotte M, Church J, Mehta A. The photodegradation of cadmium yellow paints in Henri Matisse's *Le Bonheur de vivre* (1905-1906). Appl Phys. A 2013; 111: 59-68. DOI: 10.1007/s00339-012-7418-0.
[44] Mass J, Sedlmair J, Patterson CS, Carson D, Buckley B, Hirschmugl C. SR-FTIR imaging of the altered cadmium sulfide yellow paints in Henri Matisse's *Le Bonheur de vivre* (1905-6) – examination of visually distinct degradation regions. Analyst 2013; 138: 6032-6043. DOI: 10.1039/C3AN00892D.
[45] Comelli D, MacLennan D, Ghirardello M, Phenix A, Patterson CS, Khanjian H, Gross M, Valentini G, Trentelman K, Nevin A. Degradation of cadmium yellow paint: new evidence from photoluminescence studies of trap states in Picasso's *Femme* (*Époque des "Demoiselles d'Avignon"*). Anal Chem. 2019; 91: 3421-3428. DOI: 10.1021/acs.analchem.8b04914.
[46] Turner A. Cadmium pigments in consumer products and their health risks. Sci Total Environ. 2019; 657: 1409-1418. DOI: 10.1016/j.scitotenv.2018.12.096.
[47] European Chemicals Agency. Europe considers total ban on cadmium in plastics. Addit Polym. 2013; 2013: 10-11.
[48] de Keijzer M. A brief survey of the synthetic inorganic artists' pigments discovered in the 20th century. In: Grimstrad K, editor. ICOM-CC 9th Triennial Conference Preprints, Dresden, 26-31 August 1990. Los Angeles: ICOM Committee for Conservation, Vol I; 1990. p. 214-219.
[49] Gagliano LJ, Falls G, Daly JE, Falls H. Pigments and process of making them. US patent 2.878.134; 1955; Modified cadmium sulphide colours or pigments, US patent 813.952; 1956.
[50] de Keijzer M. The history of modern synthetic inorganic and organic artists' pigments. In: Mosk JA, Tennent NH, editors. Contributions to conservation: research in conservation at the Netherlands Institute for Cultural Heritage (ICN). London: James & James (Science Publishers); 2002. p. 42-54.
[51] Rosi F, Grazia C, Gabrieli F, Romani A, Paolantoni M, Vivani R, Brunetti BG, Colomban P, Miliani C. UV-Vis-NIR and micro Raman spectroscopies for the non destructive identification of $Cd_{1-x}Zn_xS$ solid solutions in cadmium yellow pigments. Microchem J. 2016; 124: 856-867. DOI: 10.1016/j.microc.2015.07.025.
[52] Grazia C, Rosi F, Gabrieli F, Romani A, Paolantoni M, Vivani R, Brunetti BG, Colomban P, Miliani C. UV-Vis-NIR and microRaman spectroscopies for investigating the composition of ternary $CdS_{1-x}Se_x$ solid solutions employed as artists' pigments. Microchem J. 2016; 125: 279-289. DOI: 10.1016/j.microc.2015.11.008.
[53] Ghirardello M, Mosca S, Marti-Rujas J, Nardo L, Burnstock A, Nevin A, Bondani M, Toniolo L, Valentini G, Comelli D. Time-resolved photoluminescence microscopy combined with X-ray analyses and Raman spectroscopy sheds light on the imperfect synthesis of historical cadmium pigments. Anal Chem. 2018; 90: 10771-10779. DOI: 10.1021/acs.analchem.8b01666.
[54] Ghirardello M, Valentini G, Toniolo L, Alberti R, Gironda M, Comelli D. Photoluminescence imaging of modern paintings: there is plenty of information at the microsecond timescale. Microchem J. 2020; 154: 104618. DOI: 10.1016/j.microc.2020.104618.
[55] Marston JR. Manufacture of cadmium pigment. U.S. patent 1.399.506; 1921.
[56] Ward HWD. New cadmium pigments, the chemical trade journal and chemical. Engineer 1927; 80: 59-60.
[57] O'Brien WJ. Pigment and method of producing the same. US patent 1.894.931; 1933.
[58] Society of Dyers and Colorists and American Association of Textile Chemists and Colorists. Color Index international. Bradford: Society of Dyers and Colorists and associates, third ed. on CD; 1995.
[59] Buxbaum G, Pfaff G, editors. Industrial inorganic pigments. Weinheim: Wiley-VCH, third completely revised ed.; 2005.
[60] Babo S, Ferreira JL, Melo MJ, Ramos AM. Back to the origin: understanding the history of production and its influence on the properties of acrylic sheet. In: Bechthold T, editor. Future Talks 015 – Processes. The making of design and modern art materials, technologies and conservation strategies. Munich: Die

NeueSammlung-The Design Museum; 2015. p. 160-170.
[61] Tauc J, Grigorovici R, Vancu A. Optical properties and electronic structure of amorphous germanium. Phys Status Solidi B 1966; 15: 627-637. DOI: 10.1002/pssb.19660150224.
[62] Murphy AB. Band-gap determination from diffuse reflectance measurements of semiconductor films, and application to photoelectrochemical water-splitting. Sol Energy Mater Sol Cells 2007; 91(14): 1326-1337. DOI: 10.1016/j.solmat.2007.05.005.
[63] Kremheller A, Levinea AK, Gashurov G. Hydrothermal preparation of two component solid solutions from II–VI compounds. J Electrochem Soc. 1960; 107: 12-15. DOI: 10.1149/1.2427590.
[64] Adachi S. Properties of semiconductor alloys: group-IV, III–V and II–VI semiconductors. Chichester: John Wiley & Sons Ltd.; 2009.
[65] Cesaratto A, D'Andrea C, Nevin A, Valentini G, Tassone F, Alberti R, Frizzi T, Comelli D. Analysis of cadmium-based pigments with time-resolved photoluminescence. Anal Methods 2014; 6: 130-138. DOI: 10.1039/C3AY41585F.
[66] Verri G, Clementi C, Comelli D, Cather S, Piqué F. Correction of ultravioletInduced fluorescence spectra for the examination of polychromy. Appl Spectrosc. 2008; 62: 1295-1302. DOI: 10.1366/000370208786822296.
[67] Mooney J, Kambhampati P. Correction to "get the basics right: Jacobian conversion of wavelength and energy scales for quantitative analysis of emission spectra". J Phys Chem Lett. 2014; 5: 3497. DOI: 10.1021/jz502066v.
[68] Chi TTK, Gouadec G, Colomban P, Wang G, Mazerolles L, Liem NQ. Off-resonance Raman analysis of wurtzite CdS ground to the nanoscale: structural and size-related effects. J Raman Spectrosc. 2011; 42: 1007-1015. DOI: 10.1002/jrs.2793.
[69] Ong HC, Chang RPH. Optical constants of wurtzite ZnS thin films determined by spectroscopic ellipsometry. Appl Phys Lett. 2001; 79: 3612-3614. DOI: 10.1063/1.1419229.
[70] Bellei S, Nevin A, Cesaratto A, Capogrosso V, Vezin H, Tokarski C, Valentini G, Comelli D. Multianalytical study of historical luminescent lithopone for the detection of impurities and trace metal ions. Anal Chem. 2015; 87: 6049-6056. DOI: 10.1021/acs.analchem.5b00560.
[71] Wood BJ, Strens RGJ. Diffuse reflectance spectra and optical properties of some sulphides and related minerals. Mineral Mag. 1979; 43: 509-518. DOI: 10.1180/minmag.1979.043.328.11.
[72] Bacci M. UV-VIS-NIR, FT-IR, and FORS spectroscopies. In: Ciliberto E, Spoto G, editors. Modern analytical methods in art and archeology. New York: John Wiley & Sons Inc., Chemical Analysis Series, Vol. 155; 2000. p. 321-361.
[73] Rossetti R, Nakahara S, Brus LE. Quantum size effects in the redox potentials, resonance Raman spectra, and electronic spectra of CdS crystallites in aqueous solution. J Chem Phys. 1983; 79: 1086-1088. DOI: 10.1063/1.445834.
[74] Brafman O, Mitra SS. Raman effect in wurtzite- and zinc-blende-type ZnS single crystals. Phys Rev. 1968; 171: 931-934. DOI: 10.1103/PhysRev.171.931.
[75] Tell B, Damen TC, Porto SPS. Raman effect in cadmium sulfide. Phys Rev. 1966; 144 771-774. DOI: 10.1103/PhysRev.144.771.
[76] Bell IM, Clark RJH, Gibbs PJ. Raman spectroscopic library of natural and synthetic pigments (pre- ≈ 1850 AD). Spectrochim Acta Part A 1997; 53(12): 2159-2179. DOI: 10.1016/S1386-1425(97)00140-6.
[77] Burgio L, Clark RJH. Library of FT-Raman spectra of pigments, minerals, pigment media and varnishes, and supplement to existing library of Raman spectra of pigments with visible excitation. Spectrochim Acta Part A 2001; 57(7): 1491-1521. DOI: 10.1016/S1386-1425(00)00495-9.
[78] Bacci M, Picollo M, Trumpy G, Tsukada M, Kunzelman D. Non-invasive identification of white pigments on 20th-century oil paintings by using fiber optic reflectance spectroscopy. JAIC 2007; 46: 27-37. DOI: 10.1179/019713607806112413.
[79] Picollo M, Bacci M, Magrini D, Radicati B, Trumpy G, Tsukada M, Kunzelman D. Modern white pigments:

their Identification by means of noninvasive ultraviolet, visible, and infrared fiber optic reflectance spectroscopy. In: Learner TJS, Smithen P, Krueger JW, Schilling MR, editors. Modern paints uncovered. Los Angeles: Getty Conservation Institute; 2007. p. 118-128.

[80] Paulus J, Knuutinen U. Cadmium colours: composition and properties. Appl Phys A 2004; 79: 397-400. DOI: 10.1007/s00339-004-2646-6.

[81] Barnes NF. Color characteristics of artists' pigments. J Opt Soc Am. 1939; 29(5): 208-214. DOI: 10.1364/JOSA.29.000208.

[82] Tsunashima M, Sorimachi M, Mohri K. Evaluation of cadmium pigments for plastics use. Color Res Appl. 1979; 4: 66-70. DOI: 10.1111/j.1520-6378.1979.tb00091.x.

[83] Zallen R, Lucovsky G, Taylor W, Pinczuk A, Burstein E. Lattice vibrations in trigonal HgS. Phys Rev B 1970; 1: 4058-4070. DOI: 10.1103/PhysRevB.1.4058.

[84] Nusimovici MA, Meskaoui A. Raman scattering by α-HgS (cinnabar). Phys Status Solidi B 1973; 58: 121-125. DOI: 10.1002/pssb.2220580112.

[85] Cardona M, Kremer RK, Siegle G, Muñoz A, Romero AH, Schmidt M. Electronic and phononic properties of cinnabar: *ab initio* calculations and some experimental results. Phys Rev B 2010; 82(8): 085210. DOI: 10.1103/PhysRevB.82.085210.

[86] Bacci M, Baronti S, Casini A, Lotti F, Picollo M, Casazza O. Non-destructive spectroscopic investigations on paintings using optical fibers. MRS Proceedings, Symposium J – Materials Issues in Art and Archaeology III 1992; 267: 265-283. DOI: 10.1557/PROC-267-265.

[87] Anglos D, Solomidou M, Zergioti I, Zafiropulos V, Papazoglou TG, Fotakis C. Laser-induced fluorescence in artwork diagnostics: an application in pigment analysis. Appl Spectrosc. 1996; 50(10): 1331-1334. DOI: 10.1366/0003702963904863.

[88] Lucovsky G, Lind E, Davis EA. Infrared active lattice modes of the mixed system $Cd_{(1-x)}Zn_{(x)}S$. In: Thomas DG, editor. Proceedings International Conference: II-VI Semiconducting Compounds. New York: Benjamin Inc.; 1967. p. 1150-1163.

[89] Ichimura M, Usami A, Wada T, Funato M, Ichino K, Fujita Sz, Fujita Sg. Raman spectra of cubic $Zn_{1-x}Cd_xS$. Phys Rev B 1992; 46: 4273-4276. DOI: 10.1103/PhysRevB.46.4273.

[90] Shi J, Yan H, Wang W, Feng Z, Lei Z, Li C. Composition-dependent optical properties of $Zn_xCd_{1-x}S$ synthesized by precipitable-hydrothermal process. Solid State Commun. 2008; 146(5-6): 249-252. DOI: 10.1016/j.ssc.2008.02.016.

[91] Brodsky MH, Lucovsky G, Chen MF, Plaskett TS. Infrared reflectivity spectra of the mixed crystal system $Ga_{1-x}In_xSb$. Phys Rev B 1970; 2: 3303-3311. DOI: 10.1103/PhysRevB.2.3303.

[92] Chang IF, Mitra SS. Long wavelength optical phonons in mixed crystals. Adv Phys. 1971; 20: 359-404. DOI: 10.1080/00018737100101271.

[93] Chang IF, Mitra SS. Application of a modified random-element-isodisplacement model to long-wavelength optic phonons of mixed crystals. Phys Rev. 1968; 17: 924-933. DOI: 10.1103/PhysRev.172.924.

[94] Oh E, Ramdas AK. Multi-mode behavior of optical phonons in II-VI ternary and quaternary alloys. J Electron Mater.1994; 23: 307-312. DOI: 10.1007/BF02670640.

[95] Parrish JF, Perry CH, Brafman O, Chang IF, Mitra SS. Phonons in mixedcrystal system CdS_xSe_{1-x}. In: Thomas DG, editor. Proceedings International Conference: II-VI Semiconducting Compounds. New York: Benjamin Inc.; 1967. p. 1164-1185.

[96] Beserman R. Zone edge phonons in $CdS_{1-x}Se_x$. Solid State Commun. 1977; 23: 323-327. DOI: 10.1016/0038-1098(77)91338-2.

[97] Sussman SS, Alben R, Selders M, Chang RK, Callender RH. Wavelength and concentration dependence of Raman scattering from $CdS_{1-x}Se_x$. Solid State Commun. 1973; 13(7): 799-802. DOI: 10.1016/0038-1098(73)90370-0.

[98] Tu A, Persans PD. Raman scattering as a compositional probe of II-VI ternary semiconductor nanocrystals.

Appl Phys Lett.1991; 58: 1506-1508. DOI: 10.1063/1.105160.
[99] Bersani D, Lottici PP. Confinement effects on the LO-phonons in $CdSe_xS_{1-x}$ doped glasses. Phys Status Solidi B 1992; 174: 575-582. DOI: 10.1002/pssb.2221740227.
[100] Adachi S. Optical constants of crystalline and amorphous semiconductors. New York: Springer Science & Business Media; 1999.
[101] Clausen H. Zinc-based pigments. In: Lewis PA, editor. Pigment handbook, properties and economics. New York: John Wiley & Sons Inc., Vol I, second ed.; 1988. p. 43-56.
[102] Curtis PJ, Wright RB. Cadmium pigments. JOCCA 1954; 37: 26-43.
[103] Eastaugh N, Walsh V, Chaplin T, Siddall R. Pigment compendium – A dictionary and optical Mmcroscopy of historical pigments. Oxford: Elsevier Butterworth-Heinemann; 2008.
[104] Guerra M, Longelin S, Pessanha S, Manso M, Carvalho ML. Development of a combined portable x-ray fluorescence and Raman spectrometer for *in situ* analysis. Rev Sci Instrum. 2014; 85: 063113-63121. DOI: 10.1063/1.4883188.
[105] Romani A, Grazia C, Anselmi C, Miliani C, Brunetti BG. New portable instrument for combined reflectance, time-resolved and steady-state luminescence measurements on works of art. Proc. SPIE 8084, O3A: Optics for Arts, Architecture, and Archaeology III 2001; 8084: 808403. DOI: 10.1117/12.889529.

This is an Accepted Manuscript of an article published by John Wiley and Sons Ltd in Journal of Raman Spectroscopy, on 13/09/2020, available online:

Angelin EM, França de Sá S, Picollo M, Nevin A, Callapez ME, Melo MJ. The identification of synthetic organic red pigments in historical plastics: developing an in situ analytical protocol based on Raman microscopy. J Raman Spectrosc. 2021; 52: 145-158.DOI: 10.1002/jrs.5985.

6. The identification of synthetic organic red pigments in historical plastics: developing an in situ analytical protocol based on Raman microscopy

Abstract

The identification of colorants in historic plastics is a methodological and analytical challenge. Although deformulation is performed by the plastics industry, in the case of historical objects, sampling is often impossible, and in situ protocols are needed. The accurate identification of colorants provides insights into historical plastic formulations, supports planning of conservation studies, and critical data for objects that already exhibit color change (e.g. fading). Indeed, colorants may degrade following exposure to light, and color changes have been reported for plastic objects. The analysis of colorants remains a challenge, and microsampling is usually required. Successful identification of red pigments from thirty historical plastics is reported following a new in situ analytical protocol based on Raman microscopy. Information about other pigments, fillers and plastic polymers are reported. Fading has been observed in the historical plastic objects containing Pigment Red 53.

6.1. Introduction

The exhibition "Plasticity – A History of Plastics in Portugal," displayed in the *Museu de Leiria* (2019–2020, Portugal) and awarded with the Dibner Award for Excellence in Museum Exhibit by the Society for the History of Technology (SHOT), was designed in the framework of the research project, "The Triumph of Bakelite – Contributions to a History of Plastics in Portugal" [1]. This exhibition, along with the project, created the perfect opportunity for an in-depth material study of plastic collections – especially useful for the preparation of the objects for display (e.g. planning of conservation and restoration procedures) and for the study of Portuguese Plastics History [2]. Studies on the material cultural of plastics are scarce, and especially so in the Portuguese context. Thus, the material analysis carried out within this project contributed new information regarding technology and the history of the Portuguese plastics industry.

Infrared (IR) spectroscopy (in ATR-FTIR and FTIR reflectance) is a well-established method for the identification of polymer type that is critical for conservation research [3-8]; but methods for the in situ characterization of colorants (pigments and dyes) in plastics are limited, motivating the present study. Indeed colorants play a key role in the appearance of plastic objects, and the wide range of colors, shades and transparencies offered have been exploited extensively within the industry since the introduction of Bakelite. Still, colorants and plastics can degrade, especially following exposure to light and the identification of sensitive colorants is key for preservation of historic objects [9]. Color change like fading might occur over only few decades, resulting in severe changes in the appearance of plastic heritage [10,11]. Methods for the identification of colorants in plastics are urgently required, as data will support the definition of aging studies and conservation procedures that could lead to better understanding of photodegradation mechanisms.

In plastics, colorants are used in very small concentrations (0.1%-5%) that can vary depending on the plastic formulation, intended color and tinting strength [12]. Colorants can be used in the form of soluble dyes or as finely divided insoluble pigments. In the resulting polymer blend, dyes are completely dissolved in the matrix while pigments are dispersed.
In the industrial context, the analysis of plastic colorants requires destructive testing, usually consisting of sample treatment and deformulation [13]. After initial examination (e.g. by optical microscopy) of the solid plastic, dye(s) are separated from the bulk via extraction/dissolution, and solid residues of inorganic pigment(s) can be obtained via precipitation. Both strategies may also be used for organic pigments, depending on their chemical nature and solubility. Spectroscopic, separation, and mass spectrometric techniques of colorants may provide molecular identification.
In contrast to industrial materials, within heritage collections sampling and deformulation are inappropriate, and in situ approaches are increasingly common if often less specific than destructive testing. For the in situ characterization of inorganic pigments in historical plastics, Raman microscopy (μ-Raman) is an established tool [14,15]. The situation is more complex for organic pigments; although μ-Raman was proposed by de Groot et al. [16,17], pyrolysis-gas chromatography/mass spectrometry (Py-GC/MS) was adopted for precise identification, requiring microsampling. Also, from de Groot et al. [16,17], it is clear that the successful identification of organic pigments in plastics is an analytical challenging task that requires extensive spectral databases. This is mostly because many synthetic organic pigments have been used in industry. Due to their general small size (approximately 0.02-30 μm [12]), micro-scale analysis is needed for their in situ identification. Given the resolution of μ-Raman system, it can represent a valid alternative for the in situ identification of organic pigments in plastics.
In this work, the use of μ-Raman as a part of a multianalytical approach for the in situ identification of organic pigments on historical plastic objects is tested. The red color has been specifically selected for an indepth study because some of the objects exhibit color changes (mostly fading), which is hypothesized to be related to colorant degradation.
The multi-analytical investigation is based on complementary optical microscopy (OM) and attenuated total reflectance Fourier transform infrared (ATR-FTIR), μ-Raman, and energy dispersive X-ray fluorescence (μ-EDXRF) spectroscopies. A primary aim is to identify the chemical nature of the red organic pigments. Analytical results also yield information about the formulation of some of the historical plastic objects, such as polymer type and other additives (white pigments and fillers).

6.2. Experimental

6.2.1. Historical plastic objects

Within the Portuguese private collection gathered by Isabel Florentino (more than three hundred objects), thirty-six objects containing red plastic components have been selected for this study (**Figure 6.1**). A detailed description of each object as well as a number code that will be used in the entire study are provided in **Table D.1**. Except for two sandals (object n. 4 and 5), the remaining objects are everyday objects for domestic use (food containers).
In eleven cases, the manufacturing brands are visible on the bottom of the objects (**Figure D.1**), supporting their dating and place of production in Portugal. On the remaining objects, no labels or brands were found. Portuguese inscriptions such as "Açúcar" (sugar), "Farinha" (flour), "Feijão" (beans), and "Alhos" (garlic) suggest that these were also produced in Portugal Also, based on both França de Sá et al. [2] and the oral testimony of the private collector, a tentative dating between the 1950s and 1970s can be proposed for the production of the objects. In the case of objects with multicomponent elements (e.g. lid, three-dimensional (3D) lettering), only the red plastic components were analyzed.

Figure 6.1.: Thirty-six historical plastic objects under study, identified with numbers.

6.2.2. Instrumentation

6.2.2.1. Optical microscopy (OM)

Optical microscopy (OM) was used to identify the color and distribution of the pigments in the polymeric matrixes. Images were acquired using a Zeiss Axioplan 2 Imaging system (HAL 100) coupled to a Nikon DXM1200F digital camera and ACT-1 software. Brightfield and darkfield illumination were used. Microsampling was carried out only when the object (or red plastic component) could not be placed on the OM stage due to the shape and size of the object.

6.2.2.2. Energy dispersive X-ray fluorescence microspectroscopy (μ-EDXRF)

μ-EDXRF results were obtained using an ArtTAX spectrometer (Intax GmbH) equipped with a molybdenum (Mo) anode and Xflash detector cooled by the Peltier effect (Sidrift). The primary X-ray beam is focused to a diameter of 70 μm. The experimental parameters were 25 kV voltage and 300 μA of intensity for 360 s acquisition time, under a Helium flux, reducing the bremsstrahlung effect from the polymeric (organic) matrix. Software Spectra ARTAX 7.2.5.0 (Bruker Nano GmbH) was used to interpret data.

6.2.2.3. Attenuated total reflection Fourier transform infrared spectroscopy (ATR-FTIR)

Infrared spectroscopy in attenuated total reflection (ATR-FTIR) was carried out with the Handheld Agilent 4300 spectrophotometer, equipped with a ZnSe beam splitter, a Michelson interferometer and a thermoelectrically cooled DTGS detector. Spectra were acquired from 4000 to 650 cm^{-1} with a diamond ATR crystal (requiring a minimum sample size of 200 μm), 128 co-added scans, and 4 cm^{-1} spectral resolution. Background acquisition was carried out between every acquisition. Spectral analysis was performed using EZ OMNIC 7.3 software (Thermo Electron Corporation). The spectra are shown as acquired, without baseline corrections or normalization.

6.2.2.4. Raman microscopy (μ-Raman)

The plastic objects or plastic components were placed on the stage of Olympus BXFM-ILHS microscope coupled to Jobin Yvon LabRam 300 confocal Raman spectrometer. The μ-Raman study was carried out using both the 632.8 and 785 nm lines of He-Ne (17 mW) and diode laser (100 mW), respectively, for Raman excitations. The apparatus includes an air cooled multichannel CCD detector. Gratings of 600 and 1800 groves/mm were used to collect spectra between 100 and 4000 cm^{-1} (785 nm) and 100-2000 cm^{-1} (632.8, 785 nm), respectively. The system was calibrated by using the 520.7 cm^{-1} band of standard silicon (1 0 0) wafer. The confocal pinhole was maintained at a minimum aperture (200 μm) to reduce the thickness of the focal plane. The laser beam was focused on the sample by a ×100 objective lens to give a spot size

of approximately 1 μm. The laser power at the surface of the samples was controlled using neutral density filters (optical densities 0.3, 0.6, 1, and 2). Spectra were recorded as an extended scan. Choice of integration time and accumulations was noted for each colorant and plastic polymer to achieve an acceptable s/n ratio. Raman data analysis was performed using LabSpec 5 software (Horiba Jobin Yvon). All spectra are presented as acquired without baseline correction or other treatment.

6.3. Results

The results of analysis of the bulk plastic and colorants in terms of elemental and molecular composition are summarized in **Table 6.1**. In the case of more than one red plastic component for each object, the component is specified. Both inorganic and organic red pigments were identified through the combination of different analytical techniques.

6.3.1. Polymer identification on red plastic components

Both ATR-FTIR and μ-Raman measurements show that from the total set of red plastic objects, seventeen plastic components are made of polyethylene (PE), one object is entirely made of polypropylene (PP), and twenty-four plastic components are made of polystyrene (PS). Thus, mainly PE and PS plastics are identified, in accordance with the literature [2]. Also, as observed in **Figure 6.1**, there are objects containing more than one red plastic component (e.g. red lid and red 3D lettering). From their characterization, different plastics have been identified. For instance, objects number 28, 29, and 34 have a PS lid and PE 3D lettering. In addition, no polymer mixtures (blends) or copolymers have been detected in these objects.

The characteristic vibrational bands of each polymer and their tentative assignments are reported as supporting information (**Table D.2** and **Figure D.2**).

Given the simple chemical structure of PE (linear chain of methylene groups $–(CH_2)_n–$), the main stretching vibrations (asymmetric/symmetric) and bending modes of CH_2 groups are found in the IR and Raman spectra. The presence of only two bands (1368 and 1353 cm^{-1}) in the IR region 1400-1330 cm^{-1} and the lack of a band at approximately 1377 cm^{-1}, specifically assigned to the $CH_3–$ groups terminating the short- and long-chain branching [18], suggests that these objects are high-density polyethylene (HDPE) [19]. A high degree of crystallinity (small degree of branching) was also supported by Raman data, where a narrow band at 1294 cm^{-1}, as well as two groups of distinct bands centered at 1463, 1439, and at 1128, and 1063 cm^{-1} are observed [18].

Mainly frequencies involving $–CH_2–$ and $CH_3–$ groups are observed in vibrational spectra of PP. The characteristic bands of isotactic polypropylene (iPP) were detected by ATR-FTIR at 1166, 998, 899, and 841 cm^{-1}, while the Raman band at 1152 cm^{-1} can be assigned to the methyl groups of the regular head-to-tail (HT) sequence, also corroborating the tacticity of iPP [18,20].

Aliphatic CH_2 stretching (2950-2800 cm^{-1}) and aromatic C–H stretching vibrations (3100-3000 cm^{-1}) of PS are observed as bands characteristic of monosubstitution. Respectively, IR and Raman spectra show distinctive doublets at 1493-1451 cm^{-1}, 751-695 cm^{-1}, and 1603-1584 cm^{-1}, 1031-1001 cm^{-1}, related to in-plane and out-of-plane ring-mode vibrations of monosubstituted aromatic compound [21-23]. Bands that may be related to the atactic nature of PS are detected at 1372 (IR), 1330 (Raman), and 1068 cm^{-1} (IR) [18,24].

6.3.2. Red colorants

Red particles/aggregates dispersed in the polymeric matrix are observed under magnification for all plastic components in this study. Thus, red pigments in the plastic formulation are the main colorants. Examples of microscopic images are reported in supporting information (**Figures D.3** and **D.4**).

Table 6.1.: Summary of multi-analytical analysis of polymer, colorants and additives.

Object n.	Red plastic part	Plastic polymer	Elemental composition	Red organic pigments	Red inorganic pigments	Additives
1	3D fish decoration	PS	Ti, Ca, Zn, Ba	PR 53	-	-
2	3D fish decoration	PS	Ti, Ca, Ba, S (tr), Se, Cd	-	PR 108	-
3	lid[a]	PS	Ti, Ca, Zn, Fe, Ba	PR 53	-	PW 6 (A)
4	footwear	PE	Ti, Ca, Cr, Zn, Fe, K (tr), Ba, Se, Cd (tr), Pb	PR 53	PR 108, PR 104	PW 6 (A,R)
5	3D butterfly decoration	PE	Ti, Ca, Cr, Zn, Fe, Ba (tr), Pb	-	PR 104	-
6	knob	PS	Ti, Ca, Zn Fe, K (tr), Ba	PR 53	-	-
7	knob	PS	Ti, Ca, Zn, Fe, K (tr), Ba	PR 53	-	-
8	knob	PS	Ti, Ca, Zn, Fe, K (tr), Ba	PR 53	-	-
9	knob	PS	Ti, Ca, Zn, Fe, Ba (tr)	PR 53	-	-
10	lid[a]	PE	Ti, Ca, Zn, Fe (tr), Ba (tr)	PR 53	PR 101	PW 6 (A)
11	lid[a]	PE	Ti, Ca, Zn, Fe, K (tr), Cl (tr), Ba (tr)	PR 53	-	PW 6 (A)
12	lid[a]	PE	Ti, Ca, Zn, Ba (tr)	PR 53	-	PW 6 (A)
13	bowl	PS	Ti, Ca, Zn, Fe, Ba	PR 49, PR 53	-	-
14	lid	PS	Ti, Ca, Zn, Fe (tr), Ba, Se, Cd	PR 48	PR 108	-
15	cup	PS	Ti, Ca, Zn, Fe	PR 48, PR 53	-	-
16	dish	PP	Ca, Cr, Pb	PR 48	PR 104	-
17	lid	PS	Ti, Ca, Zn, Ba	PR 53	-	PW 6 (R)
18	lid	PS	Ti, Ca (tr), Zn, Fe, Ba, S (tr), Se, Cd (tr)	PR 53	PR 108	PW 6 (A)
19	cup	PS	Ti, Zn, Ba	PR 53	-	PW 6 (R)
20	lid	PS	Ti, Ca (tr), Zn, Ba, Se, Cd	-	PR 108	-
21	lid	PS	Ti, Ca (tr), Zn, Fe, Ba, S (tr), Se, Cd (tr)	PR 53	PR 108	PW 6 (A)
22	lid	PS	Ti, Ca, Zn, Fe, Ba	PR 53	-	-
23	lid	PS	Ti, Ca, Zn, Fe, Ba, S (tr), Se, Cd	PR 53	PR 108	PW 6 (A)
24	lid	PS	Ti, Ca, Zn, Ba	PR 53	-	PW 6 (A,R)
25	lid	PE	Ti, Ca, Zn, Fe, Ba	PR 49, PR 53	-	PW 6 (A)
26	lid	PE	Ti, Ca, Zn, Fe, K, Cl, Si	PR 48	PR 101	-
27	lid	PE	Ti, Ca, Zn, Fe	PR 48	-	-
28	lid	PS	Ti, Ca, Zn, Fe, Ba, S (tr), Se, Cd (tr)	PR 53	PR 108	PW 6 (A,R)
	lettering	PE	Ti, Ca, Zn, Fe, Ba	PR 53	-	-
29	lid	PS	Ti, Ca (tr), Zn, Fe (tr), Ba, S (tr), Se, Cd (tr)	PR 53	PR 108	PW 6 (A)
	lettering	PE	Ti, Ca, Zn (tr), Fe	organic pigment n.i.	PR 101	-
30	lid	PS	Ti, Ca, Zn, Fe, Ba (tr)	PR 53	-	PW 6 (A)
31	lid[a]	PE	Ti, Ca, Zn, Fe, Ba	PR 53	-	PW 6 (R)
	lettering[a]	PE	Ti, Ca, Zn, Fe, Ba	PR 53	-	PW 6 (A)
32	lid[a]	PE	Ti, Ca, Zn, Fe (tr), Ba	PR 53	-	PW 6 (A)
33	lid[a]	PE	Ti, Ca, Zn, Ba	PR 53	-	PW 6 (A)
	lettering[a]	PE	Ti, Ca, Zn, K (tr), Cl (tr), Ba	PR 53	-	PW 6 (A)
34	lid	PS	Ti, Ca, Zn, K, Cl, Ba	PR 53	-	PW 6 (A)
	lettering	PE	Ti, Ca, Fe, Se, Cd	-	PR 108	-
35	lid	PS	Ti, Ca, Zn, Fe, Ba, Se, Cd	-	PR 108	-
	lettering	PS	Ti, Ca, Zn, Ba, Se, Cd	-	PR 108	-
36	lid	PE	Ti, Ca, Cr, Fe, K, Pb	PR 53	PR 104	-

Abbreviations: A, anatase crystalline form; n.i., not identified; PR, Pigment Red; PW, Pigment White; R, rutile crystalline form; tr, traces
[a]Objects showing fading

6.3.2.1. Inorganic red pigments

Cd, Se, Cr, Pb, and Fe detected by μ-EDXRF are ascribed to red inorganic pigments cadmium sulfo-selenite, lead chromate, and iron oxide. This hypothesis is unequivocally confirmed by μ-Raman analysis identifying Pigment Red (PR) 108 (cadmium sulfo-selenide Cd(S,Se), C.I. no. 77202), PR 104 (lead chromate/molybdate/sulphate $Pb(Cr,Mo,S)O_4$, C.I. no. 77605), and PR 101 (hematite α-Fe_2O_3, C.I. no. 77491).
Cadmium-based and lead chromate pigments have already been identified in plastics [15,25]. In this study, PR 108 is identified in eleven plastic objects (n. 2, 4, 14, 18, 20, 21, 23, 28, 29, 34, and 35) with PR 104 and PR 101 in only three plastic objects (n. 5, 16 and 36) and (n. 10, 26 and 29), respectively.
In resonance conditions, there is an enhancement of Raman signal of $CdS_{1-x}Se_x$ as a function of the Se content (**Figure 6.2a**). By using 632.8 nm excitation, there is a progressive shift of the resonance longitudinal optical (LO) mode of CdSe and non-resonance CdS-LO modes (first and second order) that increases with Se content [26-31]. Within the plastics examined, from the lowest Se content (object n. 14) to the highest (object n. 34 lettering), the CdSe-LO band at 192 cm^{-1} shifts to higher wavenumbers, while the first and second order of CdS-LO modes at 297 and 593 cm^{-1}, respectively, shift to lower wavenumbers. In addition, the broad band at approximately 215 cm^{-1} related to the CdS phase (multiphonon mode) is progressively reduced. Following the calibration curve presented by Grazia et al. [32] of the CdSLO and CdSe-LO difference with 632.8 laser excitation, molar fractions ranging from 0.09 to 0.43 can be estimated (**Table D.3**). The Se content is below the maximum recommended value of 0.5 [33,34].
$Pb(Cr_{1-x-y}Mo_yS_x)O_4$ is identified by comparison with published data [35-37] and by exclusion of other lead chromate phases $PbCrO_4$ [38,39], $PbCr_{1-x}S_xO_4$ [40], $PbCrO_4 \cdot xPbO$ [41] (**Figure 6.2b**). With respect to the Raman spectra of crocoite $PbCrO_4$ (monoclinic, $P2_{1/n}$ space group, $C^5{}_{2h}$) where five bands (approximately 327vw, 339w, 360m, 379w, and 402vw cm^{-1}) and three bands (approximately 825w, 841vs, and 856vw cm^{-1}) accurately describe the Cr–O bending and stretching region respectively [42,43], only two distinct bands at approximately 337m and 357m cm^{-1} in the bending $\nu_2/\nu_4(CrO_4{}^{2-})$ region are observed, with the most intense band in the Cr–O stretching region at 823vs cm^{-1}. In object n. 4, two additional bands at 376w and 400vw cm^{-1} and shoulder at 839s cm^{-1} are also visible. The change in the relative intensity of bands in the Cr–O stretching and bending regions is recorded for the first time and is ascribed to the partial replacement of Cr with Mo and S in the crystal lattice.
Although iron oxides are poor light scatters, six of the seven phonon lines expected from hematite α-Fe_2O_3 (trigonal, $R\bar{3}C$ space group, $D^6{}_{3d}$) $2A_{1g} + 5E_g$ [44] are detected: 225m (A_{1g}), 245w (E_g), 292s (E_g), 410m (E_g), 497w,br (A_{1g}), and 611m cm^{-1} (E_g) [45-47] (**Figure 6.2c**).

6.3.2.2. Organic red pigments

PR 48 (C.I. no. 15865), PR 49 (C.I. no. 15630) and PR 53 (C.I. no. 15585) are unequivocally identified by μ-Raman. The Raman spectra of the three red pigment lakes and their molecular structures are shown in **Figure 6.3**. The organic pigments have distinct spectral features that allow their exact identification by comparison with reference compounds, databases and published spectra [48].
All three red organic pigments identified here are based on β-naphthol (2-naphthol) and characterized by common a 1-arylazo-2-naphthol basic skeleton. Owing to the aromatic rings, Raman bands in the fingerprint region between 1800 and 1000 cm^{-1} can be assigned to CH deformations and aromatic CC stretching vibrations, while, at lower wavenumbers, skeletal vibrations such as δ(CCC) and ring deformations are excepted. Specifically bands at around 1600 cm^{-1} and 600 cm^{-1} are related to quadrant stretching and ring deformation of the benzene ring. Bands at 1550, 950 and 720 cm^{-1} are tentatively ascribed to the naphthalene moiety [49-51].
The ionic character of the lakes and their successful metal complexation is guaranteed by the presence of "salt-forming" groups ($–SO_3^-$ and/or $–CO_2^-$) [52]. Sulfonate SO_3^- groups generate a weak band due to the

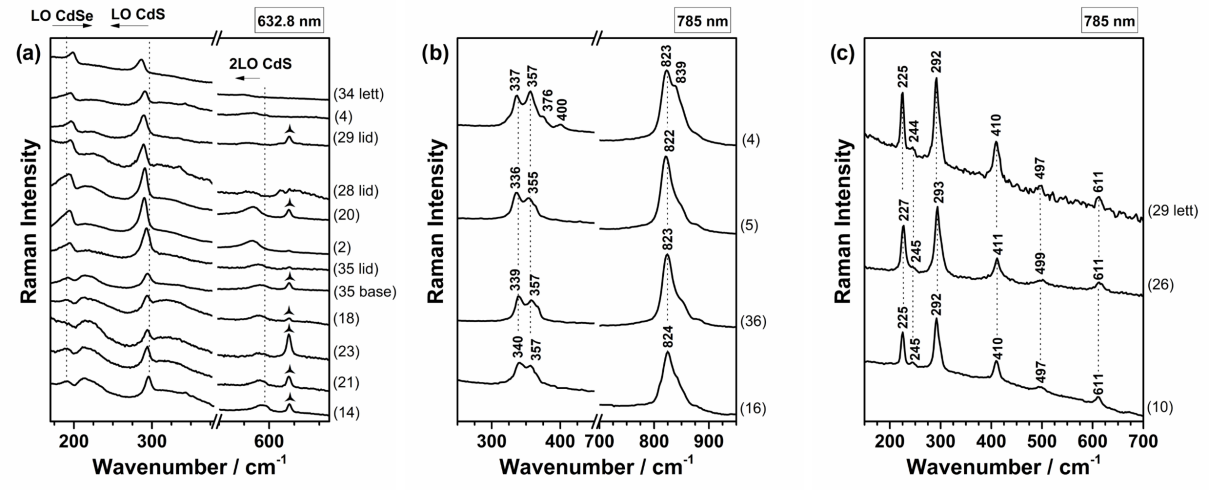

Figure 6.2.: Raman spectra of PR 108 Cd(S,Se) (a), PR 104 $Pb(Cr,Mo,S)O_4$ (b), and PR 101 α-Fe_2O_3 (c). In (a) band at 620 cm^{-1} of PS contribution is underlying (▲). The object number is given in parenthesis.

symmetric SO_2 stretch that may give rise the band at 1160 cm^{-1} [50]. As for all the beta-oxynaphthoic acid (BONA)-based pigment lakes, PR 48 has a characteristic carboxylate group Ar-COO^-. The position of the symmetric CO_2 stretch falls between 1450 and 1335 cm^{-1} depending on the counter ion [23,53].
BONA (PR 48) and β-naphthol (PR 49 and PR 53) pigment lakes are usually described as azo pigments as they are believed to contain an azo group (–N=N–). However, rather than containing azo groups, these pigments have a hydrazone function (–NH–N=) [54-59]. Each tautomer is characterized by specific Raman-active functional group vibrations [50,55,60-62] and specific Raman bands are recognized in the spectra. Considering the azo/enol form, a characteristic band ν(N=N) stretching vibration of the trans azo functionality is expected between 1450 and 1380 cm^{-1}. Instead the hydrazone/keto tautomer presents a band at 1550 cm^{-1} ν_s(C=O) that may increase due to contributions of the δ(NH) mode.

6.3.3. White pigments and fillers

Ti, Ca, Zn, and Ba signals are detected in most of the objects. These elements are not specifically related to red inorganic pigments, and instead could be from Pigment White (PW) 6 (titanium dioxide TiO_2, C.I. no. 77891), PW 7 (zinc sulfide ZnS, C.I. no. 77975), PW 18 (calcium carbonate $CaCO_3$, C.I. no. 77220) and PW 21 (barium sulphate $BaSO_4$, C.I. no. 77120). Only PW 6 is identified by μ-Raman. Titanium oxide as rutile (tetragonal, $P4_{2/mnm}$ space group, $D^{14}{}_{4h}$) and anatase (tetragonal, $I4_{1/amd}$ space group, $D^{19}{}_{4h}$) crystalline forms is found (**Figure 6.4**). In the Raman spectra of rutile (R), three bands at 223m,br (multi-photon process), 444m,br (E_g), and 619m,br (A_{1g}) cm^{-1} are observed. While five Raman-active optical phonon modes at 141vs (E_g), 194vw (E_g), 393w (B_{1g}), 513w (A_{1g} + B_{1g}), and 636w (E_g) characterize the Raman spectrum of anatase (A) [63-66]. In object n. 24, overlapping signals from the two crystalline Raman signatures are observed.

6.4. Discussion

6.4.1. General considerations

The identification of three thermoplastic polymers (PE, PP and PS) is in agreement with the few documental sources about the Portuguese plastic industry. In fact, the processing industry prevailed in Portugal from the 1950s, and thermoplastics were favored for domestic applications [2,67]. Injection molding could have been

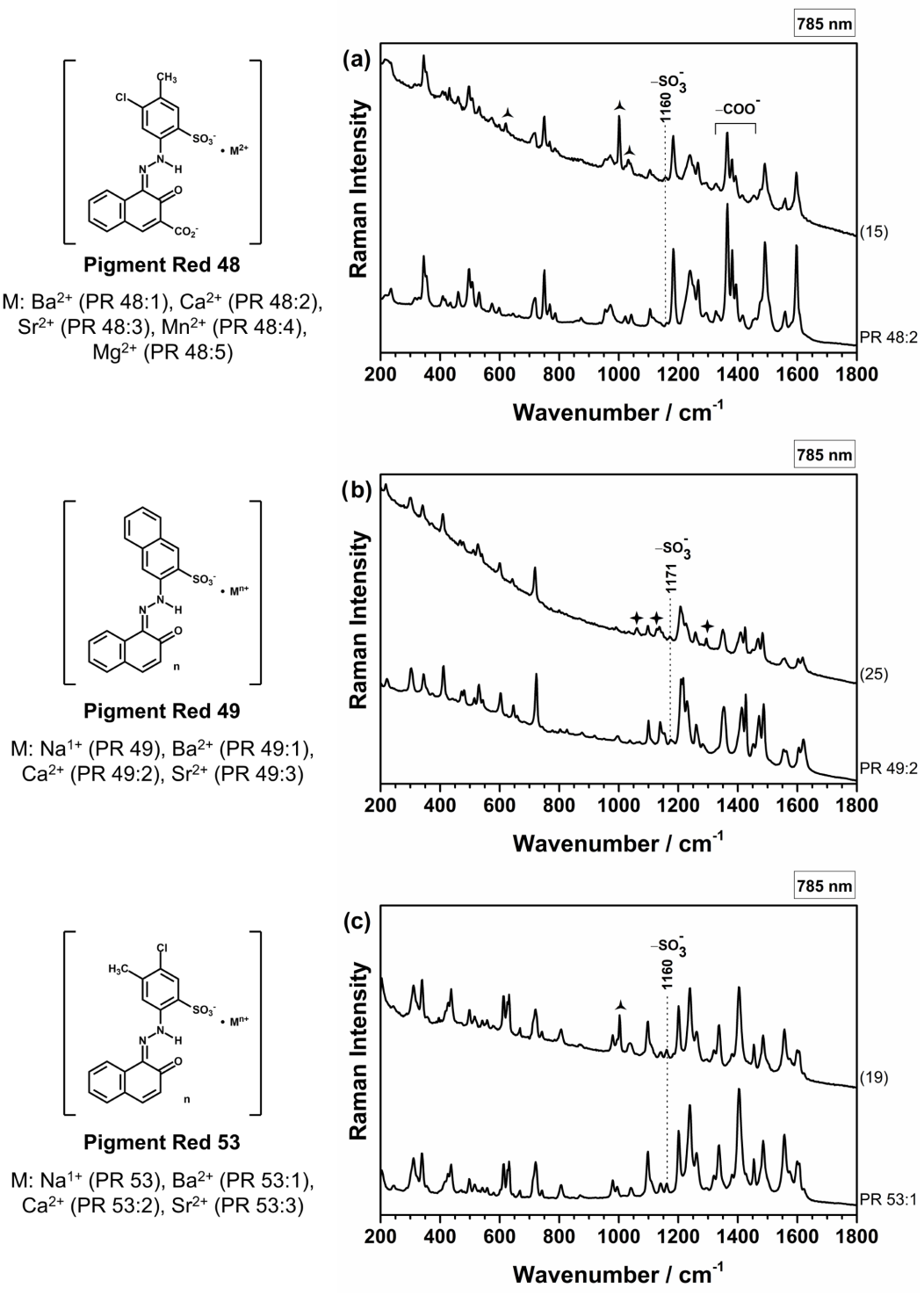

Figure 6.3.: Raman spectra of PR 48 (a), PR 49 (b) and PR 53 (c). The object number is reported in parenthesis. Bands of PS (▲) and PE (✦) are indicated. On the left, molecular structures of the organic red pigment in the hydrazone/keto form are depicted. Raman spectra of reference compounds are also reported for comparison: PR 48:2 (Clariant), PR 49:2 (SunChemical), PR 53:1 (Clariant).

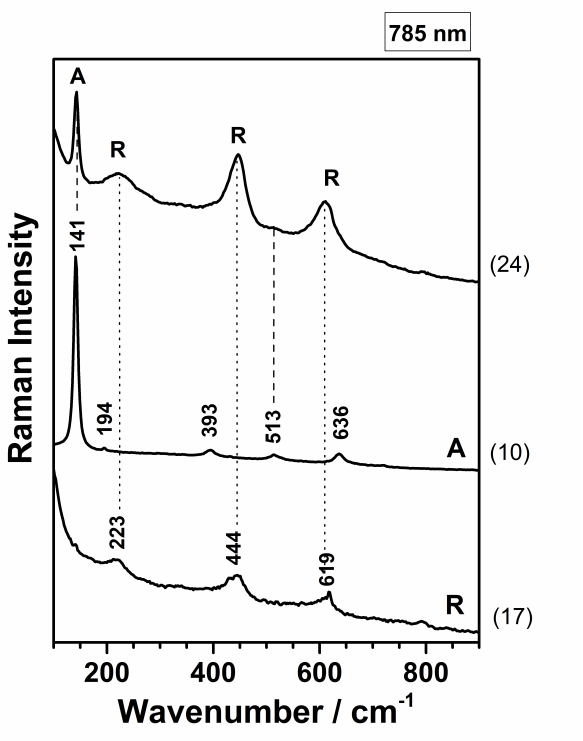

Figure 6.4.: Raman spectra of PW 6 in rutile (R) and anatase (A) crystalline forms. The object number is given in parenthesis.

used for processing as the objects have sprues and junction pointlines in their format/design.

Considering that the polymers are in fair condition (suggested by a visual examination), molecular information about the polymer degree of crystallinity and tacticity might be tentatively extracted from vibrational spectroscopic data. However, to date only few studies on this subject have been published, these assignments should be carefully considered.

In this study, both inorganic (PR 101, 104 and 108) and organic red pigments (PR 48, 49 and 53) are successfully identified in the plastic components. Synthetic organic pigments are found in 24/42 plastic components, 6/42 have inorganic pigments, and in 12/42 have a mixture of organic and inorganic pigments. Of the mixtures, PR 53 and PR 108 are found together, except for in object n. 4, where PR 104 is also detected.

The inorganic and organic red pigments identified in the historical plastic objects are consistent with published literature [12,68-73] and are the most important categories of red pigments for the plastic coloring technology. In detail, their use is recommended for PE, PP and PS plastics as they are thermally stable and chemically resistant [68,69]. This also suggests that the Portuguese plastic industry was up to date with production and processing knowledge of these raw materials. As the worldwide plastic industry was already using these red pigments after the 1950s [74-76], pigment identification in this work supports the date proposed for the objects studied.

Cadmium sulfo-selenide and lead chromate/molybdate/sulphate pigments represent an almost ideal choice for plastic coloration due to their exceptional performance [12-68]. These pigments do not have a fixed chemical formula, and the composition of the solid solutions can be varied to meet specific requirements, although their use today is limited due to their toxicity and environmental impact.

Synthetic organic red pigments such as BONA (e.g. PR 48) and β-naphthol (e.g. PR 49 and PR 53) pigment lakes are considered an industrial replacement of the previously used category of β-naphthol pigments (e.g. PR 1, 3 and 4). The ionic character of this class of chemical compounds increases their solvent and migration

fastness [77] allowing a better dispersion in the polymer blends. PR 48 and PR 53 are two of the most important red lakes used for plastic coloring today. The detection of PR 49 in some of the plastic objects is of interest as this colorant has only limited applications within plastics and is mainly used in inks for printing. However, in this study, this pigment is always found in mixtures, probably with the intent to reduce the formulation cost [12].
Offering UV protection and color, PR 101 is identified only in three objects by μ-Raman even though Fe is detected in most of them. The presence of other iron content compounds cannot be excluded, although iron is usually associated with pigments, or as an impurity associated with residues of catalysts [13]. In this study, PR 101 was found in combination with an organic red pigment which, as suggested by Charvat [12], would yield a shade formally produced by red cadmium-based pigments. This finding suggests specific color research and matching by Portuguese companies.
Pigments based on titanium dioxide are the preferred white pigment for polymer use. They are added for pure white shades, lightening of the colored shades and opacifying the plastic product. In the plastic components, both rutile and anatase polymorphs are found even if rutile is more common due to its higher optical properties and lightfastness [68].
Concerning the other additives, although only PW 6 is identified in the plastic objects, the use of PW 7, 18 and 21 is suggested by elemental analysis and published data [12,68,69]. PW 7 is the second most important white pigment, and the presence of PW 4 (zinc oxide ZnO, C.I. no. 77947) could be excluded because it does not play a role in coloring of thermoplastic resins [68]. PW 18 and PW 21 would be added to the formulation as fillers to reinforce the plastics and/or in processing. PW 21 in the lithopone variety (PW 5, ZnS + $BaSO_4$, C.I. no. 77115) and red cadmopone (PR 108:1, Cd(S,Se) + $BaSO_4$, C.I. no. 77202:1) cannot be excluded.

6.4.2. Methodology for organic red pigment identification

The observation of red particulate materials by optical microscopy validates the use of μ-Raman as the main analytical tool for the organic pigment characterization. Focusing the laser beam onto the surface of the red particles, the vibrational fingerprint of both inorganic and organic red pigments was successfully recorded. The main advantage of the Raman instrument used in this study is the associated confocal system, which allows the selection of the plane of focus and the thickness of the focal plane on the micrometer scale. Although some contributions of the polymeric matrix are observed, the system sufficiently eliminates the radiation coming from the out of focus planes. Based on the molecular/crystalline structure, different excitation lines can be also used to enhance specific vibrational features of the pigments. Information of the polymer type was obtained by focusing the laser beam onto the plastic object surface.
Even if μ-Raman proved to be experimentally the most powerful technique for the identification of the synthetic organic red pigments in situ, few limitations in the spectra interpretation were also detected.
The vibrational analysis of the individual organic pigment is challenging owing to the numerous vibrational bands observed, and their identification is usually supported by a comparison with databases. In fact, the distinction between organic pigments is rarely straightforward because they may only differ in chemical structure by the position and nature of substituents. As Raman spectroscopy is sensitive to the molecular structure and conformation, spectra of lakes that differ only in their counter ion may display only subtle differences in position and relative intensity of the bands [48,51]. In addition, these differences are small and may remain undetected due to the influence of the micro-environment. In this study, no differences were observed that could support the identification of counter ions.
Based only on the vibrational investigation, the definition of the predominant tautomeric form of organic pigments cannot be addressed. In fact, due to the high number of vibrational bands, specific Raman structural fingerprint bands of each tautomeric form cannot be easily recognized. Few vibrational studies report the assignments of the two tautomers in conservation science (especially for the hydrazone/keto form) and the

definition in the condensate state of the most abundant tautomeric specie would support future in-depth studies on their vibrational features.
In addition, although preliminary and complementary information related to red pigments, polymer and additives was also extracted from the other techniques here applied, some analytical limitations were found for the identification of the synthetic organic pigments.
ATR-FTIR spectra allow the identification of the polymer type but no bands related to the red pigments and other additives were observed, possibly because of the low pigment concentration, well below the detection limit of the technique (around $<3\%$) [78].
Elemental analysis supports a preliminary discrimination of the plastic components possibly containing inorganic red pigments by detecting Cd, Se, Cr, and Pb, while no definitive information related to organic pigments is found. In fact, the detection of Ca and Ba by μ-EDXRF cannot be directly related to the counter ion of the organic pigment due to superimposition with the signals of other inorganic additives. Cl was detected in four objects and may relate to the coloring agents PR 48 and PR 53. Still, chlorine-containing additives (e.g. flame retardants) might be present in the formulation making its attribution to PR 48 and PR 53 more complex.
Elemental data suggests the presence of inorganic additives. Because of the ca 100-200 ppm detection limit of μ-EDXRF (for $Z > 11$ depending on the matrix and element) [13], if Ti, Zn, Ba, and Ca are detected, inorganic pigment/fillers can be suggested. Other inorganic components of the polymeric matrices should not be detectable due to their very low concentration level (ppm to ppb range).
Based on the results obtained, an in situ multianalytical protocol for the investigation of red organic pigments in plastics is schematically proposed in **Figure 6.5**. Information on inorganic pigments can also be obtained. Of great value in the use of this multi-analytical methodology here proposed is the experimental sequence and the integration of the information achievable by elemental and vibrational in situ analysis.

6.4.3. Degradation assessment

For the PE plastic objects where PR 53 is identified alone, fading of the plastic components is observed. Particles dispersed in the polymeric matrix are still visible (**Figure 6.6b**), although they have completely or partially lost their color. For comparison, **Figure 6.6a** shows an optical image of PR 53 which completely preserved its color.
The presence of defined particles might be an important indication of the condition of the object, making possible the in situ characterization of degradation products. While Raman signals ascribed to PR 53 are detected on the reddish part (less degraded) of the particle, no Raman signals have been detected on lighter part (more degraded) particles due to the strong fluorescence background.
Fading of the plastic components could be related to the poor lightfastness of the organic pigments as well as the influence of the polymeric matrix and/or additives (antioxidants, heat stabilizers, plasticizers, etc.) on its degradation. As PR 53 is also found in a good condition in plastic components made of PS, more complete characterization of the PE plastic formulation is fundamental to assess the degradation mechanism of the colorants.
In addition to the identification of PR 48 as a faded colorant in a historical plastic object [16], this study also highlights PR 53 as a photosensitive pigment. Because Raman and ATR spectra of PE did not show spectral changes due to polymer degradation, fading of PR 53 is ascribed to photodegradation. Chemical compounds of the same pigment lake class, PR 49 are also found in a faded condition in contemporary paintings [79,80]. This evidence highlights the poor light fastness of the β-naphthol lakes and BONA pigments, but the photochemical stability and degradation mechanisms of the pigments in paintings and plastic are not thoroughly understood.
In the case of the object n. 3, the inhomogeneous color observed is likely related to a technical problem during the injection molding process where the organic pigment was not efficiently mixed in the polymer formulation, or an intended aesthetic effect (**Figure D.5**).

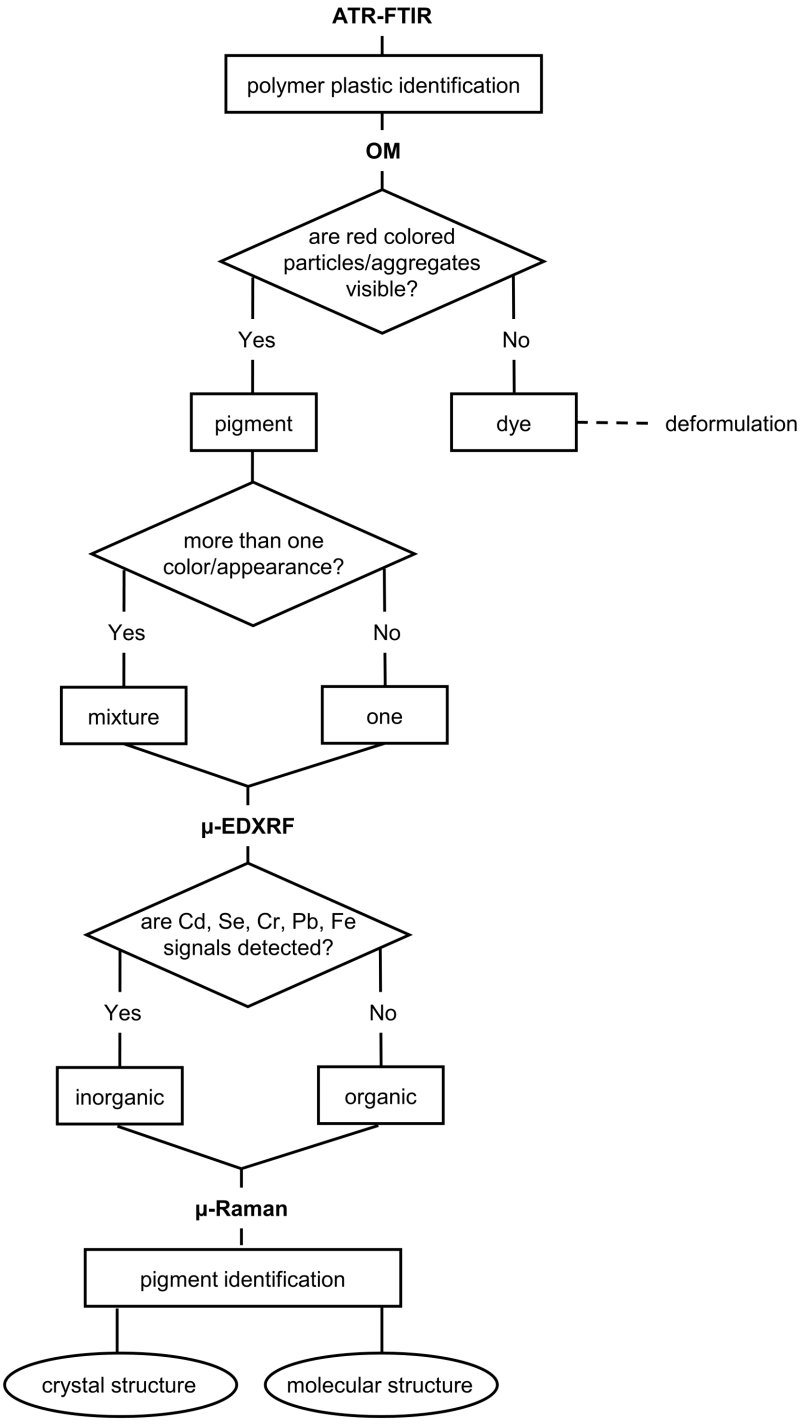

Figure 6.5.: Flowchart of the in situ multi-analytical methodology for red colorant identification.

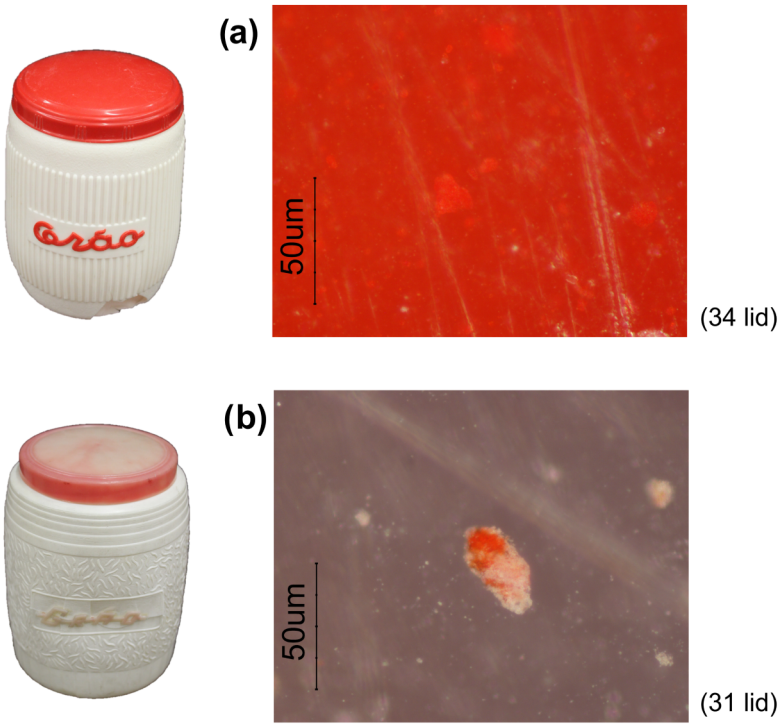

Figure 6.6.: Microscopy images of the red particles under reflected visible light (50× magnification, dark field).

6.5. Conclusions

This study demonstrates μ-Raman for the identification of synthetic organic red pigments in historical plastic objects. Taking advantages of the confocal micro Raman system, information from pigment particles were selectively collected. PR 48, 49 and 53 were identified as coloring agents in red historical plastic objects in combination with inorganic red pigments (PR 101, 104 and 108) and PW 6. The presence of other additives was suggested by complementary elemental analysis and supported by published literature.

Based on results, an in situ multi-analytical protocol for the study of organic red pigments is also proposed. The novelty of the protocol is the analytical sequence of techniques, integration of the information achievable by elemental and vibrational in situ analysis and the final molecular characterization of organic red pigments. Organic red pigments were identified as coloring agents in historical plastic objects, and the results of the pigment identification allow new insights into the cultural material of plastics used in Portugal, as well as new information that is essential for conservation and collection care. For example, the identification of PR 53 in faded plastic components will inform the planning of better conservation strategies for historical plastic objects as well as the initiation of aging studies on photodegradation mechanisms. In addition, red plastic components made of PE seem to be more susceptible to fading than the ones made of PS when PR 53 was identified.

This work also highlights the conservation problems of fading in plastics in collections. It represents a starting point to develop new analytical methods and strategies for in situ characterization of faded pigments, perhaps with a combination of fluorescence spectroscopy and Raman analysis. Different excitation lasers in the NIR might be used to reduce the fluorescence background. The influence of the microenvironment should be removed as much as possible, for instance, by the preparation of cross sections that might help the selection of an area with more pigment particles at the surface. To the best of authors' knowledge, no attempts have been devoted to the identification of dyes in plastics in conservation science. Extraction/deformulation methods

could also be tested, and given the promising results obtained by μ-Raman, SERS and SORS combined with microscopy [81] might be useful in analyzing the extracted material from the polymer matrices.

6.6. References

[1] Callapez ME. An interdisciplinary project on the history of plastics in Portugal. e-plastory 2017; 1: 1-8. URL: e-plastory/article/view/Callapez/34.

[2] França de Sá S, Marques da Cruz S, Callapez ME, Carvalho V. Plastics that made history – The contribution of conservation science for the history of the Portuguese Plastics Industry. Conservar Património 2020; 35: 85-100. DOI: 10.14568/cp2019017.

[3] Mitchell G, Fenella F, Alison N, Leung Tang P, Gibson LT. Assessment of historical polymers using attenuated total reflectance-Fourier transform infra-red spectroscopy with principal component analysis. Herit Sci. 2013; 1(28): 1-10. DOI: 10.1186/2050-7445-1-28.

[4] Lazzari M, Ledo-Suárez A, López T, Scalarone D, López-Quintela MA. Plastic matters: an analytical procedure to evaluate the degradability of contemporary works of art. Anal Bioanal Chem. 2011; 399: 2939-2948. DOI: 10.1007/s00216-011-4664-5.

[5] Cucci C, Bartolozzi G, Marchiafava V, Picollo M, Richardson E. Study of semi-synthetic plastic objects of historic interest using non-invasive total reflectance FT-IR. Microchem J. 2016; 124: 889-897. DOI: 10.1016/j.microc.2015.06.010.

[6] Saviello D, Toniolo L, Goidanich S, Casadio F. Non-invasive identification of plastic materials in museum collections with portable FTIR reflectance spectroscopy: reference database and practical applications. Microchem J. 2016; 124: 868-877. DOI: 10.1016/j.microc.2015.07.016.

[7] Picollo M, Bartolozzi G, Cucci C, Galeotti M, Marchiafava V, Pizzo B. Comparative study of Fourier transform infrared spectroscopy in transmission, attenuated total reflection, and total reflection modes for the analysis of plastics in the cultural heritage field. Appl Spectrosc. 2014; 68(4): 389-397. DOI: 10.1366/13-07199.

[8] Bell J, Nel P, Stuart B. Non-invasive identification of polymers in cultural heritage collections: evaluation, optimisation and application of portable FTIR (ATR and external reflectance) spectroscopy to three-dimensional polymer-based objects. Herit Sci. 2019; 7(95): 1-18. DOI: 10.1186/s40494-019-0336-0.

[9] Miliani C, Monico L, Melo MJ, Fantacci S, Angelin EM, Romani A, Janssens K. Photochemistry of artists' dyes and pigments: towards better understanding and prevention of colour change in works of art. Angew Chem Int Ed. 2018; 57: 7324-7334. DOI: 10.1002/anie.201802801.

[10] Shashoua Y. Conservation of plastics. Oxford: Butterworth-Heinemann; 2008.

[11] Quye A, Williamson C, editors. Plastics: collecting and conserving. Edinburg: NMS Publishing Limited; 1999.

[12] Charvat RA, editor. Coloring of plastics: fundamentals. New Jersey: John Wiley & Sons Inc., second ed.; 2004.

[13] Bart JCJ. Additives in polymers – Industrial analysis and applications. Chichester: John Wiley & Sons Ltd; 2005.

[14] Angelin EM, Babo S, Ferreira JL, Melo MJ. Raman microscopy for the identification of pearlescent pigments in acrylic works of art. J Raman Spectrosc. 2019; 50: 232-241. DOI: 10.1002/jrs.5431.

[15] Angelin EM, Ghirardello M, Babo S, Picollo M, Chelazzi L, Melo MJ, Nevin A, Valentini G, Comelli D. The multi-analytical in situ analysis of cadmium-based pigments in plastics. Microchem J. 2020; 157: 105004. DOI: 10.1016/j.microc.2020.105004.

[16] de Groot S, van Keulen H, Megens L, van Oosten T, Wiresma H. Discolouration of plastics objects: investigation into composition using various analytical techniques. In: Bechthold T, editor. Future Talks 013 – Lectures and workshops on technology and conservation of modern materials in design. Munich: Die Neue

Sammlung – The Design Museum; 2015. p. 19-26.
[17] de Groot S, van Keulen H, van den Akker S, van Oosten T. Discoloration of plastics objects: the identification of yellow and orange synthetic pigment in plastic objects. In: Bechthold T, editor. Future Talks 015 – Processes. The making of design and modern art. Materials, technologies and conservation strategies. Munich: Die Neue Sammlung – The Design Museum; 2017. p. 147-158.
[18] Nishikida K, Coates J. Infrared and Raman analysis of polymers. In: Lobo H, Bonilla JV, editors. Handbook of plastics analysis. New York: Marcel Dekker Inc.; 2003. p. 186-316.
[19] Gulmine JV, Janissek PR, Heise HM, Akcelrud L. Polyethylene characterization by FTIR. Polym Test. 2002; 21(5): 557-563. DOI: 10.1016/S0142-9418(01)00124-6.
[20] Andreassen E. Infrared and Raman spectroscopy of polypropylene. In: Karger-Kocsis J, editor. Polypropylene: an A-Z reference. Dordrecht: Springer, Polymer Science and Technology Series, Vol. 2; 1999. p. 320-328.
[21] Painter PC, Koenig JL. A normal vibrational analysis of isotactic polystyrene. J Polym Sci Polym Phys Ed. 1977; 15: 1885-1903. DOI: 10.1002/pol.1977.180151102.
[22] Liang CY, Krimm S. Infrared spectra of high polymers. VI. Polystyrene. J Polym Sci. 1958; 27: 241-254. 10.1002/pol.1958.1202711520.
[23] Lin-Vien D, Colthup NB, Fateley WG, Grasselli JG. The handbook of infrared and Raman characteristic frequencies of organic molecules. San Diego: Academic Press; 1991.
[24] Nyquist RA, Putzig CL, Leugers MA, McLachlan RD, Thill B. Comparison of the vibrational spectra and assignments for α-syndiotactic, β-syndiotactic, isotactic, and atactic polystyrene and toluene. Appl Spectrosc. 1992; 46(6): 981-987. DOI: 10.1366/0003702924124321.
[25] Paris C, Coupry C. Fourier transform Raman spectroscopic study of the first cellulose-based artificial materials in heritage. J Raman Spectrosc. 2005; 36: 77-82. DOI: 10.1002/jrs.1288.
[26] Parrish JF, Perry CH, Brafman O, Chang IF, Mitra SS. Phonons in mixedcrystal system CdS_xSe_{1-x}. In: Thomas DG, editor. Proceedings International Conference: II-VI Semiconducting Compounds. New York: Benjamin Inc.; 1967. p. 1164-1185.
[27] Chang IF, Mitra SS. Application of a modified random-element-isodisplacement model to long-wavelength optic phonons of mixed crystals. Phys Rev. 1968; 17: 924-933. DOI: 10.1103/PhysRev.172.924.
[28] Bersani D, Lottici PP. Confinement effects on the LO-phonons in $CdSe_xS_{1-x}$ doped glasses. Phys Status Solidi B 1992; 174: 575-582. DOI: 10.1002/pssb.2221740227.
[29] Beserman R. Zone edge phonons in $CdS_{1-x}Se_x$. Solid State Commun. 1977; 23: 323-327. DOI: 10.1016/0038-1098(77)91338-2.
[30] Sussman SS, Alben R, Selders M, Chang RK, Callender RH. Wavelength and concentration dependence of Raman scattering from $CdS_{1-x}Se_x$. Solid State Commun. 1973; 13(7): 799-802. DOI: 10.1016/0038-1098(73)90370-0.
[31] Tu A, Persans PD. Raman scattering as a compositional probe of II-VI ternary semiconductor nanocrystals. Appl Phys Lett.1991; 58: 1506-1508. DOI: 10.1063/1.105160.
[32] Grazia C, Rosi F, Gabrieli F, Romani A, Paolantoni M, Vivani R, Brunetti BG, Colomban P, Miliani C. UV-Vis-NIR and microRaman spectroscopies for investigating the composition of ternary $CdS_{1-x}Se_x$ solid solutions employed as artists' pigments. Microchem J. 2016; 125: 279-289. DOI: 10.1016/j.microc.2015.11.008.
[33] Huckle WG, Swigert GF, Wiberley SE. Cadmium pigments. Structure and composition. Ind Eng Chem Prod Res Dev. 1966; 5: 362-366. DOI: 10.1021/i360020a016.
[34] Loya JE. Cadmium sulfide pigments. In: Lewis PA, editor. Pigment handbook, properties and economics. New York: John Wiley & Sons Inc., Vol. I, second ed.; 1988. p. 347-352.
[35] Castro K, Pérez-Alonso M, Rodríguez-Laso MD, Fernández LA, Madariaga JM. On-line FT-Raman and dispersive Raman spectra database of artists' materials (e-VISART database). Anal Bioanal Chem. 2005; 382: 248-258. DOI: 10.1007/s00216-005-3072-0.

[36] Chua L, Hoevel C, Smith GD. Characterization of Haku Maki prints from the "Poem" series using light-based techniques. Herit Sci. 2016; 4(25): 1-11. DOI: 10.1186/s40494-016-0096-z.
[37] Zięba-Palus J, Michalska A, Wesełucha-Birczynska A. Characterisation of paint samples by infrared and Raman spectroscopy for criminalistic purposes. J Mol Struct. 2011; 993(1-3): 134-141. DOI: 10.1016/j.molstruc.2010.12.016.
[38] Scheuermann W, Ritter GJ. The vibrational spectra of strontium chromate ($SrCrO_4$) and lead chromate ($PbCrO_4$). Zeitschrift für Naturforschung A 1970; 25(12): 1856-1862. DOI: 10.1515/zna-1970-1212.
[39] Errandonea D, Muñoz A, Rodríguez-Hernández P, Proctor JE, Sapiña F, Bettinelli M. Theoretical and experimental study of the crystal structures, lattice vibrations, and band structures of monazite-type $PbCrO_4$, $PbSeO_4$, $SrCrO_4$, and $SrSeO_4$. Inorg Chem. 2015; 54: 7524-7535. DOI: 10.1021/acs.inorgchem.5b01135.
[40] Monico L, Janssens K, Hendriks E, Brunetti BG, Miliani C. Raman study of different crystalline forms of $PbCrO_4$ and $PbCr_{1-x}S_xO_4$ solid solutions for the noninvasive identification of chrome yellows in paintings: a focus on works by Vincent van Gogh. J Raman Spectrosc. 2014; 45: 1026-1033. DOI: 10.1002/jrs.4548.
[41] Roncaglia DI, Botto IL, Baran EJ. Vibrational spectrum of Pb_2CrO_5. J Mater Sci Lett. 1985, 4: 1427-1428. DOI: 10.1007/BF00720120.
[42] Wilkins RWT. The Raman spectrum of crocoite. Mineral Mag. 1971; 38(294): 249-250. DOI: 10.1180/minmag.1971.038.294.15.
[43] Frost RL. Raman microscopy of selected chromate minerals. J Raman Spectrosc. 2004; 35: 153-158. DOI: 10.1002/jrs.1121.
[44] de Faria DLA, Venâncio Silva S, de Oliveira MT. Raman microspectroscopy of some iron oxides and oxyhydroxides. J Raman Spectrosc. 1997; 28: 873-878. DOI: 10.1002/(SICI)1097-4555(199711)28:11<873::AID-JRS177>3.0.CO;2-B.
[45] Bell IM, Clark RJH, Gibbs PJ. Raman spectroscopic library of natural and synthetic pigments (pre- ≈ 1850 AD). Spectrochim Acta Part A 1997; 53(12): 2159-2179. DOI: 10.1016/S1386-1425(97)00140-6.
[46] Burgio L, Clark RJH. Library of FT-Raman spectra of pigments, minerals, pigment media and varnishes, and supplement to existing library of Raman spectra of pigments with visible excitation. Spectrochim Acta Part A 2001; 57(7): 1491-1521. DOI: 10.1016/S1386-1425(00)00495-9.
[47] Bouchard M, Smith DC. Catalogue of 45 reference Raman spectra of minerals concerning research in art history or archaeology, especially on corroded metals and coloured glass. Spectrochim Acta Part A 2003; 59(10): 2247-2266. DOI: 10.1016/S1386-1425(03)00069-6.
[48] Scherrer NC, Stefan Z, Francoise D, Annette F, Renate K. Synthetic organic pigments of the 20th and 21st century relevant to artist's paints: Raman spectra reference collection. Spectrochim Acta Part A 2009; 73(3): 505-524. DOI: 10.1016/j.saa.2008.11.029.
[49] Vandenabeele P, Moens L, Edwards HGM. Raman spectroscopy of modern art: classification and identification of azo-pigments. Proc. SPIE 4098, Optical Devices and Diagnostics in Materials Science 2000; .4098: 301-310. DOI: 10.1117/12.401642.
[50] Vandenabeele P, Moens L, Edwards HGM, Dams R. Raman spectroscopic database of azo pigments and application to modern art studies. J Raman Spectrosc. 2000; 31: 509-517. DOI: 10.1002/1097-4555(200006)31:6<509::AID-JRS566>3.0.CO;2-0.
[51] Fremout W, Saverwyns S. Identification of synthetic organic pigments: the role of a comprehensive digital Raman spectral library. J Raman Spectrosc. 2012; 43: 1536-1544. DOI: 10.1002/jrs.4054.
[52] Christie RM, Mackay JL. Metal salt azo pigments. Color Technol. 2008; 124: 133-144. DOI: 10.1111/j.1478-4408.2008.00133.x.
[53] Socrates G. Infrared and Raman characteristic group frequencies: tables and charts. Chichester: John Wiley & Sons Ltd., third ed.; 2001.
[54] Hunger K, Schmidt MU. Industrial organic pigments: production, crystal structures, properties, applications. Weinheim: Wiley-VCH, fourth completely revised ed.; 2018.

[55] Ferreira GR, Garcia HC, Couri MRC, Dos Santos HF, de Oliveira LFC. On the azo/hydrazo equilibrium in Sudan I azo dye derivatives. J Phys Chem A 2013; 117: 642-649. DOI: 10.1021/jp310229h.
[56] Olivieri AC, Wilson RB, Paul IC, Curtin DY. Carbon-13 NMR and x-ray structure determination of 1-(arylazo)-2-naphthols. Intramolecular proton transfer between nitrogen and oxygen atoms in the solid state. J Am Chem Soc. 1989; 111: 5525-5532. DOI: 10.1021/ja00197a003.
[57] Aiken S, Gabbutt CD, Gillie LJ, Heywood JD, Jacquemin D, Rice CR, Heron BM. The remarkable hyperchromicity of ketohydrazone dyes and pigment lakes derived from 4-morpholino-2-naphthol. Eur J Org Chem. 2013; 36: 8097-8107. DOI: 10.1002/ejoc.201390103.
[58] Kennedy AR, Stewart H, Eremin K, Stenger S. Lithol red: a systematic structural study on salts of a sulfonated azo pigment. Chem Eur J. 2012; 18: 3064-3069. DOI: 10.1002/chem.201103027.
[59] Gorelik T, Schmidt MU, Brüning J, Beko S, Kolb U. Using electron diffraction to solve the crystal structure of a laked azo pigment. Cryst Growth Des. 2009; 9: 3898-3903. DOI: 10.1021/cg801099r.
[60] Munro CH, Smith WE, Armstrong DR, White PC. Assignments and mechanism of SERRS of the hydrazone form for the azo dye Solvent Yellow 14. J Phys Chem 1995; 99: 879-885. DOI: 10.1021/j100003a008.
[61] Abbott LC, Batchelor SN, Oakes J, Gilbert BC, Whitwood AC, Lindsay Smith JR, Moore JN. Experimental and computational studies of structure and bonding in parent and reduced forms of the azo dye Orange II. J Phys Chem A 2005; 109: 2894-2905. DOI: 10.1021/jp045216s.
[62] Kunov-Kruse AJ, Kristensen SB, Liu C, Berg EW. Experimental and *ab initio* DFT calculated Raman spectrum of Sudan I, a red dye. J Raman Spectrosc. 2011; 42: 1470-1478. DOI: 10.1002/jrs.2876.
[63] Ma HL, Yang JY, Dai Y, Zhang YB, Lu B, Ma GH. Raman study of phase transformation of TiO_2 rutile single crystal irradiated by infrared femtosecond laser. Appl Surf Sci. 2007; 253(8): 7497-7500. DOI: 10.1016/j.apsusc.2007.03.047.
[64] Balachandran U, Eror NG. Raman spectra of titanium dioxide. J Solid State Chem. 1982; 42(3): 276-282. DOI: 10.1016/0022-4596(82)90006-8.
[65] Porto SPS, Fleury PA, Damen TC. Raman spectra of TiO_2, MgF_2, ZnF_2, FeF_2, and MnF_2. Phys Rev. 1967; 154(2): 522-526. DOI: 10.1103/PhysRev.154.522.
[66] Ohsaka T, Izumi F, Fujiki Y. Raman spectrum of anatase, TiO_2. J Raman Spectrosc. 1978; 7: 321-324. DOI: 10.1002/jrs.1250070606.
[67] Callapez ME. Os plásticos em Portugal: a origem da indústria transformadora. Lisbon: Editorial Estampa; 2000.
[68] Müller A. Coloring of plastics. Munich: Carl Hanser Verlag; 2003.
[69] Webber TG, editor. Coloring of plastics. New York: John Wiley & Sons Inc.; 1979.
[70] Herbst W, Hunger K. Industrial organic pigments. Weinheim: Wiley-VCH, third completely revised ed.; 2004.
[71] Buxbaum G, editor. Industrial inorganic pigments. Weinheim: Wiley-VCH Verlag GmbH, second completely revised ed.; 1998.
[72] Lewis PA, editor. Pigment handbook, properties and economics. New York: John Wiley & Sons Inc., Vol. I, second ed.; 1988.
[73] Murray BG. Pigmentation of colored plastics. In: Lewis PA, editor. Pigment handbook, applications and markets. New York: John Wiley & Sons Inc., Vol. II, second ed.; 1988. p. 277-290.
[74] de Keijzer M. The history of modern synthetic inorganic and organic artists' pigments. In: Mosk JA, Tennent NH, editors. Contributions to conservation: research in conservation at the Netherlands Institute for Cultural Heritage (ICN). London: James & James (Science Publishers); 2002. p. 42-54.
[75] de Keijzer M. A brief survey of the synthetic inorganic artists' pigments discovered in the 20th century. In: Grimstrad K, editor. ICOM-CC 9th Triennial Conference Preprints, Dresden, 26-31 August 1990. Los Angeles: ICOM Committee for Conservation, Vol I; 1990. p. 214-219.
[76] de Keijzer M. A survey of red and yellow modern synthetic organic artists' pigments discovered in the

20th century and used in oil colours. In: Bridgland J, Brown J, editors. ICOM-CC 12th Triennial Conference Preprints, Lyon, 29 August - 3 September 1999. London: James and James (Science Publishers), Vol. I; 1999. p. 369-374.

[77] Berrie BH, Lomax SQ. Azo pigments: their history, synthesis, properties, and use in artists' materials. Studies in the History of Art 1997; 57: 8-33. URL: jstor.org/stable/42622254

[78] Lavédrine B, Fournier A, Martin G, editors. Preservation of Plastic Artefacts in Museum Collections (POPART). Paris: Comité Des Travaux Historiques et Scientifiques (CTHS); 2012.

[79] Stenger J, Khandekar N, Wilker A, Kallsen K, Kirby DP, Eremin K. The making of Mark Rothko's Harvard Murals. Stud Conserv. 2016; 61(6): 331-347. DOI: 10.1179/2047058415Y.0000000009.

[80] Stenger J, Kwan EE, Eremin K, Speakman S, Kirby D, Stewart H, Huang SG, Kennedy AR, Newman R, Khandekar N. Lithol red salts: characterization and deterioration. e-Preservation Sci. 2010; 7: 147-157. URL: e-preservationscience/2010/Stenger-29-05-2010

[81] Bersani D, Conti C, Matousek P, Pozzi F, Vandenabeele P. Methodological evolutions of Raman spectroscopy in art and archaeology. Anal Methods 2016; 8: 8395-8409. DOI: 10.1039/C6AY02327D.

Part III.

Photochemistry for the preservation of color change: study the lightfastness of β-naphthol reds and their fading in historical plastics

7. Photochemistry of artists' dyes and pigments: towards better understanding and prevention of colour change in works of art

Abstract

The absorption of light gives a pigment its colour and its reason for being, but it also creates excited states, that is, new molecules with an energy excess that can be dissipated through degradation pathways. Photodegradation processes provoke long-term, cumulative and irreversible colour changes (fading, darkening, blanching) of which the prediction and prevention are challenging tasks. Of all the environmental risks that affect heritage materials, light exposure is the only one that cannot be controlled without any impact on the optimal display of the exhibit. Light-induced alterations are not only associated with the pigment itself but also with its interactions with support/binder and, in turn, are further complicated by the nature of the environmental conditions. In this Minireview we investigate how chemistry, encompassing multi-scale analytical investigations of works of art, computational modelling and physical and chemical studies contributes to improve our prediction of artwork appearance before degradation and to establish effective preventive conservation strategies.

7.1. Introduction

The harmful effect of light on artworks has been recognized for centuries. In the late 1880s, following the introduction of artificial lighting in the South Kensington Museum (now the Victoria and Albert Museum, London UK), a public controversy arose over the fading of watercolours in English national collections [1]. Two preeminent chemists, Dr. W. J. Russell and Capt. W. de W. Abney were commissioned by the Committee of Council on Education "to investigate as a scientific question the action of light on the various pigments used in painting". Using spectrophotometric measurements, for the first time they assembled compelling evidence that exposure to light was a cause of fading [2].

Today modern chemistry has gained a crucial role in heritage science, a research field, spanning humanities and natural sciences, that focuses on the understanding, conservation and management of cultural heritage. In this vivid context, a renewed cross-disciplinary interest for the impact of light on artists' materials has recently been triggered by technical innovations in museum lighting and artwork restoration [3]. A deep comprehension of the photochemical processes underpinning changes in artists' materials is sought to offer: 1) a solid framework to develop preventive conservation strategies through the selection of optimal lighting conditions [4]; 2) (semi)quantitative compositional data to predict the original artistic intended appearance of an artwork before discoloration and propose its digital reconstructions [5]. On the other hand, heritage materials with their often unknown and heterogeneous compositions and unmonitored long-term modifications represent highly complex systems. Understanding and disclosing their behaviour under visible light exposure is an intriguing challenge for chemical sciences.

In the following we review recent findings regarding different types of inorganic pigments belonging to the class of semiconductors and charge-transfer compounds of which the photoredox properties in paint layers have been

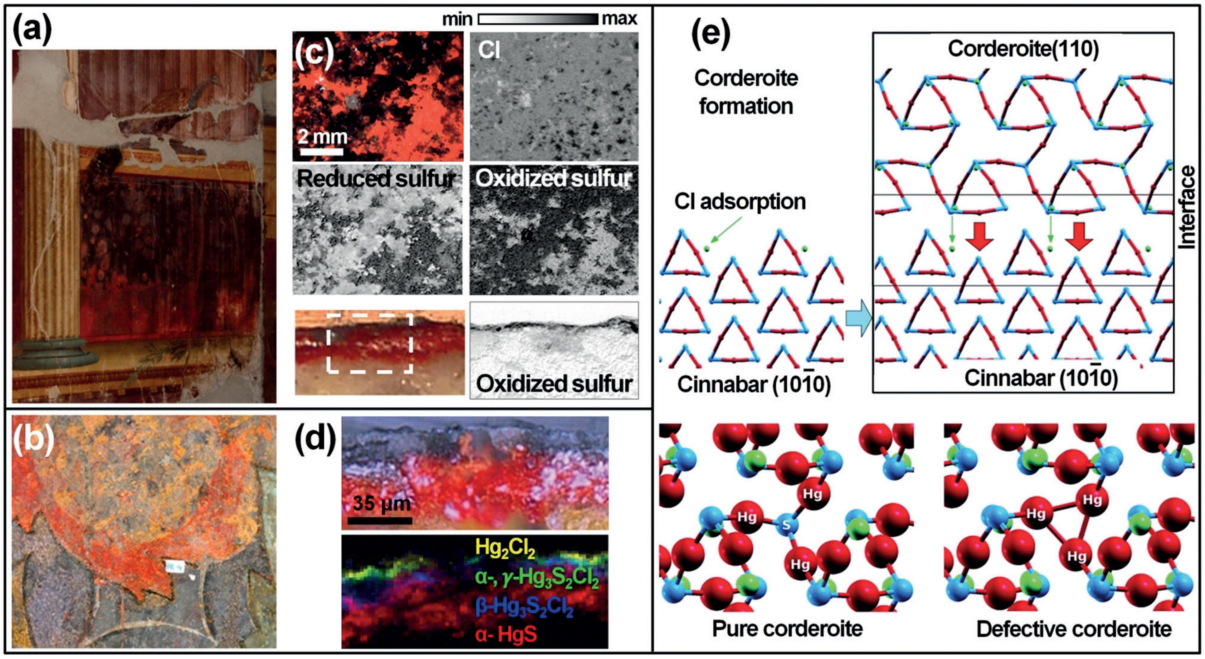

Figure 7.1.: Photographs of discolored α-HgS paints of a) a Roman fresco of *Oplontis* excavation sites (Torre Annunziata, IT) (credits: M. Pagano) and b) a wall painting of Pedralbes Monastery (Barcelona, ES). c) Photomicrograph and Cl and S speciation maps of a (top) fragment and (bottom) cross-section from a Roman fresco of *Villa Sora* (Torre del Greco, IT). d) Photomicrograph and synchrotron radiation (SR) μ-XRD maps of a cross-section from (b). e) (top) Proposed mechanism of α-$Hg_3S_2Cl_2$ formation; (bottom) local atomic structure for pure α-$Hg_3S_2Cl_2$ (left) and defective α-$Hg_3S_2Cl_2$ with a S vacancy (right). Adapted from Refs. [9,12,13].

investigated through a phenomenological approach starting from the identification of secondary products on artificially aged mock-ups and/or original artworks. A specific section is dedicated to natural organic dyes, the degradation issues of which have been addressed by studying the photophysics of parent molecules as a conceptual key to understand their photochemistry and to predict resulting colour changes in artworks.

7.2. Light-Induced Redox Behaviour of Inorganic Pigments in Paint Layers

7.2.1. Semiconductor Pigments

Several artists' pigments are semiconductors, the excited states of which can cause the self-redox reaction of the pigment (i.e. photocorrosion) as well as promote redox reactions of other paint components (i.e. photocatalysis).

The n-type semiconductor red cinnabar or vermilion (α-HgS) is known since the Neolithic period. Used worldwide in various kind of artefacts [6,7], under certain conditions it tends to develop lilac-gray/black crusts, disfiguring Old Masters' easel paintings [3,6,8] as well as wall paintings of archaeological sites and cathedrals (**Figure 7.1a,b**) [9,10]. While in the past the α-HgS blackening was ascribed a priori to the photoinduced structural change to black cubic β-HgS [6], recent analyses of microsamples from artworks [8-10,11,12] proved that the process is associated with Hg-Cl secondary products, such as $Hg_3S_2Cl_2$ polymorphs, Hg_2Cl_2 and $HgCl_2$ (**Figure 7.1c,d**). In fresco samples, calcium sulfates were also usually detected (**Figure 7.1c**).

Artificial aging of α-HgS mock-ups by UVA-Vis light, NaClO and O_2-rich conditions reproduced the conversion of α-HgS to Hg_2Cl_2 (with α-$Hg_3S_2Cl_2$ as intermediate) and sulfates [11].

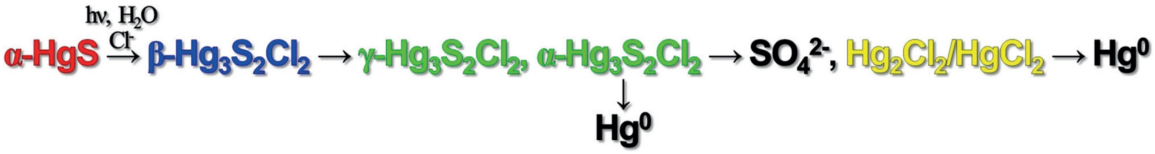

Figure 7.2.: Overall photodegradation mechanism of α-HgS based on the literature (cf. also **Figure 7.1**) [9-14].

Theoretical calculations allowed a scheme for the formation/decomposition paths of Hg-Cl secondary compounds to be proposed (**Figure 7.1e**) [13]. Upon light and humidity exposure, environmental Cl chemisorbs onto the α-HgS surface. The structure of Cl@HgS favours the growth of various Hg-S-Cl phases, before finally ending up as the more stable α-$Hg_3S_2Cl_2$. At the α-HgS/α-$Hg_3S_2Cl_2$ interface, significant lattice mismatch occurs, likely promoting the formation of structural instabilities within α-$Hg_3S_2Cl_2$, with the release of black Hg^0 (identified by electrochemistry experiment) [14]. The formation of whitish Hg_2Cl_2/$HgCl_2$ can take place as well, which may undergo further light-induced alteration (e.g., via disproportionation) providing a second path for Hg^0 precipitation.

Integrating the information gained through computational modelling studies, artificial aging experiments and phenomenological observations from case studies, the mechanism depicted in **Figure 7.2** can be proposed.

Cadmium yellows (CdYs) are n-type semiconductor pigments, comprising CdS and $Cd_{1-x}Zn_xS$ in different crystalline structure (hexagonal/cubic) [15a]. For their vibrant hues, 19th-20th century painters often employed CdYs, which only in some of their artworks appear discoloured today. A multianalytical approach was employed to study three of these masterpieces [16-18]. In *Flowers in a blue vase* by Van Gogh, amorphous $CdSO_4$, CdC_2O_4 and $PbSO_4$ were identified in the grayish alteration crust [16]. In *Still Life with Cabbage* by Ensor, $CdSO_4 \cdot nH_2O$ and $(NH_4)_2Cd(SO_4)_2$ were revealed in the white globules at the paint surface (**Figure 7.3a,d**) [17]. In *Joy of Life* and *Flower Piece* by Matisse, the blanched CdY paints resulted in products composed of $CdSO_4 \cdot nH_2O$, CdC_2O_4 and $CdCO_3$, while the darkened areas were enriched with Cd-Cl compounds (**Figure 7.3b,c,e-g**) [18].

The photo-oxidation of CdS-based compounds to $CdSO_4$, that is the most likely degradation pathways in the presence of O_2 and moisture [19], has been confirmed by electrochemical measurements on CdS powder [20]. Computational simulations of the interaction of CdS with O_2 and/or H_2O also showed that structural defects (i.e., Cd/S vacancies) at pigment surface are reasonably linked to the more complex photo-oxidation reactions observed in paintings [21]. Nevertheless, for the following reasons we are still far from a thoroughly understanding of the reactivity of CdS in paint layer: 1) both $CdSO_4$ and other compounds, identified as secondary products, could instead already be present in the original paint formulations, as synthesis residues or additives [15a]; 2) it is not clear whether or not Cd–Cl species (likely the residues of the CdS synthesis) can promote self-oxidation; 3) it is not clear how the stability of CdY is affected by their differences in crystal structure and stoichiometry. Moreover, also the possible activity of CdY as photocatalyst deserves further investigation since the chalking phenomenon visible in *Joy of Life* [18,22] and in CdY mock-ups exposed to light and humidity [23] might be ascribed to the oxidative degradation of the binding medium.

Minium or red lead (Pb_3O_4) and titanium white (TiO_2) are two other semiconductor pigments both recognized as photocatalysts [24-26]. Investigations of a blanched Pb_3O_4 sample from a Van Gogh's painting led to formulate the following mechanism [24]. The Pb_3O_4 excited conduction band can both reduce Pb^{IV} to Pb^{II} and induce decarboxylation of the oil binder at the pigment surface with the release of CO_2. The latter in turn reacts with Pb^{II} to form various white lead carbonates as final alteration products.

TiO_2-pigmented oil paints can experience the photooxidation of the binder into volatile low-molecular weight species. The process ultimately manifests as chalking, being more pronounced with increasing humidity and in the presence of O_2 [25,26]. Modelling studies of TiO_2 for photocatalysis are a well-established and pointed to

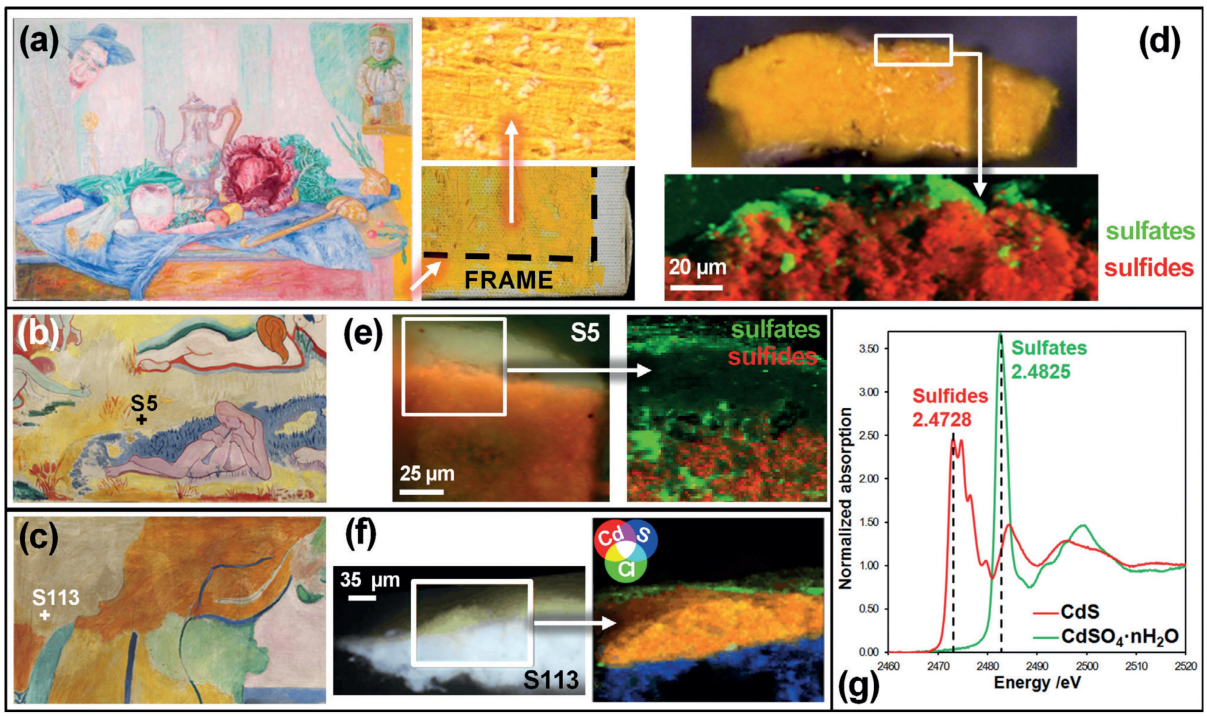

Figure 7.3.: Photographs of discolored CdY paints of: a) *Still Life with Cabbage* (James Ensor, ca. 1921; Kröller-Müller Museum, Otterlo, NL) and (b,c) *Joy of Life* (Henri Matisse, 1905-1906; The Barnes Foundation, Philadelphia, USA). d-f) Photomicrographs of cross-sections taken from (a-c) and corresponding RGB SR µ-XRF sulfides/sulfates and Cd/Cl/S maps. g) S-K edge XANES spectra of CdS (red) and $CdSO_4 \cdot nH_2O$ (green). Adapted from Refs. [17,18].

the prominent influence of crystal facets and defects on the reactivity of organic pollutants [27]. The insights obtained here may be directly transferred to the cultural heritage context along with dedicated analyses of different TiO_2 paint formulations and specific reaction media.

7.2.2. Charge-Transfer Pigments

The colour of many artists' pigments arises from charge transfer (CT) optical transitions of metal–ligand complexes, which, differently from d–d transitions, are not spin-forbidden and are thus very intense. Depending on the direction of CT, they are classified as either ligand-to-metal (LMCT) or metal-to-ligand (MLCT) charge transfer; the metal center can be photoreduced by the first and photo-oxidated by the second charge-transfer process.

Frequently used among impressionist and postimpressionist masters [15b], chromate-based yellows are characterized by an intense absorption band, due to a LMCT from the oxygen nonbonding to unoccupied Cr antibonding d orbitals.

The origin of the darkening of zinc yellow ($K_2O \cdot 4ZnCrO_4 \cdot 3H_2O$) observed in *A Sunday at La Grande Jatte* by Seurat was studied by investigating both microsamples obtained from the painting and artificially aged mock-ups using Cr-speciation methods [28,29]. Here light and sulfur gaseous pollutants promote the formation of Cr^{III} and dichromate compounds as secondary products.

An extended multi-technique study on microsamples from Van Gogh's paintings [30-33] as well as historical and inhouse synthesized powders [34-38] allowed the stability of various chrome yellows (CYs) to be assessed (**Figure 7.4**). It has been proved that the darkening is due to a $Cr^{VI} \rightarrow Cr^{III}$ photoreduction with long-lived Cr^{V}-species that are thermally formed through the interaction with the oil binder [36,37]. Cr^{III}-alteration products were usually found as a 3-5 mm thick layer (**Figure 7.4b,c**) and/or micrometric particles at the

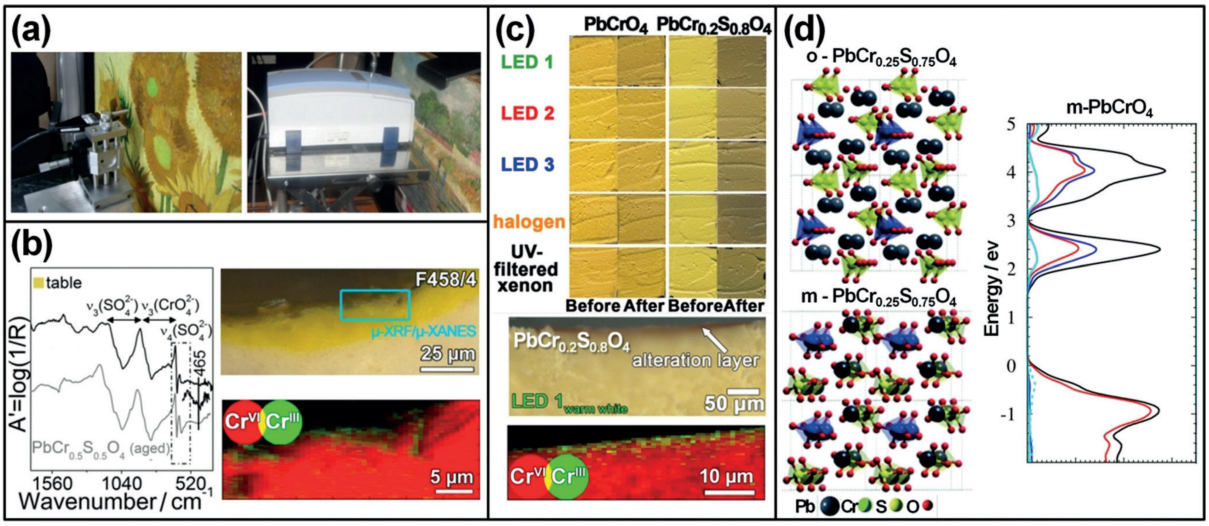

Figure 7.4.: a) Portable devices in front of *Sunflowers* and *Bank of the Seine* by Van Gogh (Van Gogh Museum, Amsterdam, NL). b) (left) Reflection FTIR spectrum (black) with reference (gray) obtained from the table area of *Sunflowers* and (right) photomicrograph of a cross-sections obtained from the same region where SR μ-XRF/μ-XANES analysis were performed. c) (from top) CY mock-ups before and after exposure to various white lamps, microphotograph of a LED-exposed CY thin section and corresponding RG Cr^{VI}/Cr^{III} maps. d) (left) Optimized structures of orthorhombic (o) and monoclinic (m) $PbCr_{0.25}S_{0.75}O_4$ and electronic structure for *m*-$PbCrO_4$. Adapted from Refs. [33,36,42].

surface [30-38]. A series of aging experiments on oil mock-ups allowed the following information to be gained: 1) monoclinic and/or orthorhombic $PbCr_{1-x}S_xO_4$ ($0<x\leqslant0.8$) more readily undergo darkening than monoclinic S-free $PbCrO_4$ [35]; 2) the degradation path depends on the environmental conditions: the formation of Cr^V-compounds is favoured under exposure to moisture, while that of Cr^{III}-species upon light irradiation [37]; 3) different lighting sources have different effects on the CY stability (**Figure 7.4c**) [36].

In recent investigations of *Sunflowers* (**Figure 7.4a**) [33,39], the sensitivity of reflection FTIR spectroscopy to detect at the painting surface not only different CY types but also Cr^{III} oxides (**Figure 7.4b**, left) was exploited, opening up the possibility of using this technique, along with Raman and MA-XRPD mapping, as a non-invasive tool for monitoring the CY stability at the macroscale length.

Pigment reconstructions following 19th century methods of synthesis used by Winsor & Newton colourmen were also spectroscopically characterized and photochemically aged allowing a better understanding of its manufacturing processes and how they impact on CY stability [40].

More recently the relationship of structure and electronic properties of different CY varieties have been examined by computational methods for better understanding their behaviour [41-43]. DFT methods have been employed to describe the electronic structure of $PbCrO_4$ and $PbCr_{1-x}S_xO_4$ (**Figure 7.4d**, left). All theoretical investigations have shown that the valence band (VB) of $PbCrO_4$ is mainly constituted of O 2p states, while its conduction band (CB) is mainly due to Cr 3d states (**Figure 7.4d**, right). The optical, electronic and structural modifications occurring within $PbCr_{1-x}S_xO_4$ solid solutions have revealed a general trend of increasing band gap upon increasing the SO_4^{2-} content. Since the increase in band gap is generally attributed to a lower photoreactivity, additional explanations for the SO_4^{2-}-induced pigment degradation have been put forward. Munoz-Garcia et al. [41] described that $PbCrO_4$ and $PbSO_4$ tend to segregate into separate phases, with the $PbCrO_4$-rich phase mainly undergoing degradation. Amat et al. [42] proposed degradation due to therelease CrO_4^{2-} anions into the paint matrix, thus pointing at an extrinsic degradation pathway. Rahemi et al. [43] instead reported that Cr reduction increased in SO_4^{2-}-rich phases, in relation to the calculated photoabsorption current. Although these three theoretical studies reached different conclusions, in this context

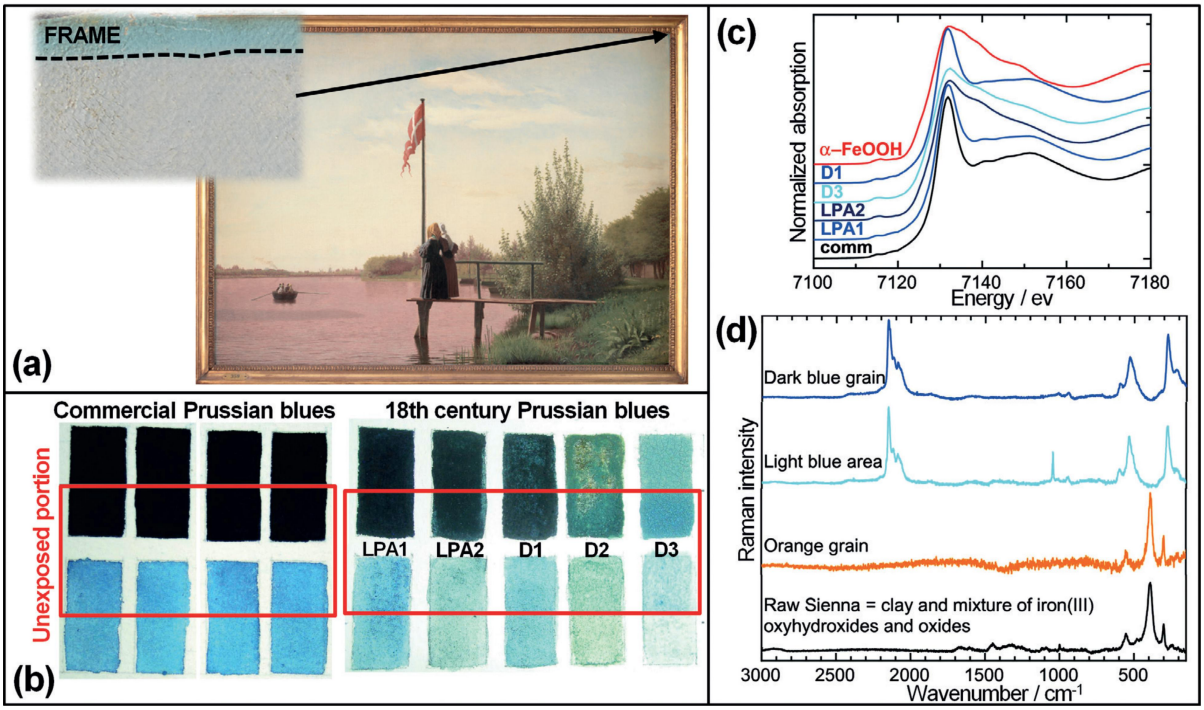

Figure 7.5.: a) Photograph and detail of a faded PB area of *View of Lake Sortedam from Dosseringen Looking Towards the Suburb Nørrebro outside Copenhagen* (Christen Købke, 1838; Statens Museum for Kunst, Copenhagen, DK). b) Photochemically aged PB watercolors mock-up paints and c) corresponding Fe K-edge XANES spectra compared to that of α-FeOOH. d) Raman spectra recorded from a cross-section of the *Guardian angel* (polychrome linden wood sculpture, Assumption church, La Gleize, BE) and a raw Sienna reference. Adapted from Refs. [45,50].

modelling was shown to provide valuable insights into the pigment properties, which may represent the basis for future targeted experimental investigations.

The intense blue colour of Prussian blue (PB; $KFe^{III}[Fe^{II}(CN)_6] \cdot xH_2O$ and $Fe^{III}_4[Fe^{II}(CN)_6]_3 \cdot xH_2O$) arises from a metal-to-metal charge transfer (MMCT) between Fe^{II} and Fe^{III} mediated by the CN moiety [44]. The fading of PB endangers various heritage artefacts, including textiles, prints, blueprints, watercolours, and oil paintings (**Figure 7.5a**) [45,46]. The extension of the phenomenon is variable and depends on the presence of white extenders [47,48], the type of environment and substrate [49], as well as the PB manufacture procedures [44,50]. The presence of Fe^{III} oxyhydroxide as by-product of eighteenth century PB-synthesized powders (**Figure 7.5c,d**) may contribute to enhance the tendency of the paint layer towards discoloration (**Figure 7.5b**) [50]. Studies on photochemically aged mock-ups by different spectroscopic techniques have proved that the PB fading is due to a $Fe^{III} \rightarrow Fe^{II}$ photoreduction [48-50], most likely activated through the LMCT Fe^{III}–CN transition.

7.3. Photophysics of Organic Dyes: A Key for Understanding Their Colour Change in Artworks

Indigo blues and anthraquinone reds are among the most important natural dyes used in various works of art, such as textiles, woods, or paints [51]. As other natural dyes, they are generally considered prone to photodegradation, and yet in many cases they display an almost pristine aspect. For instance, anthraquinone reds may undergo fading in paintings [3], while they may be incredibly resilient as showcased in millenary Andean textiles or medieval illuminated manuscripts [52]. In order to be lightfast, a molecule must absorb

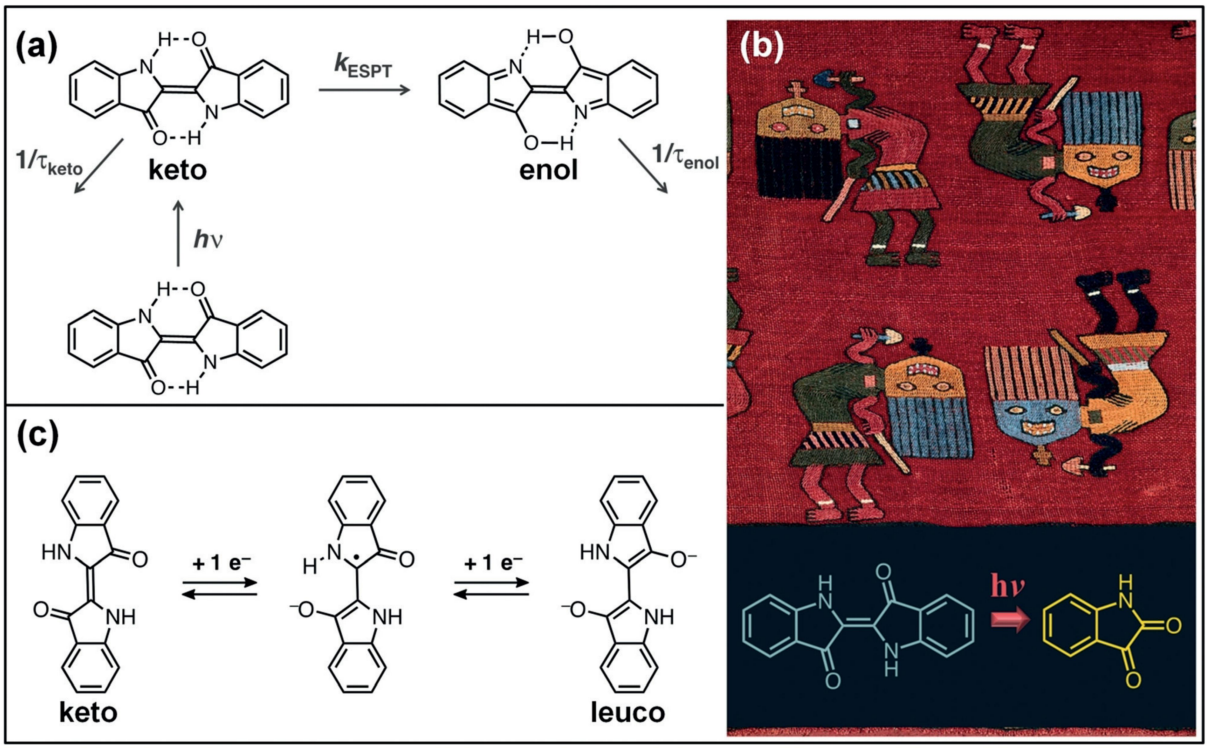

Figure 7.6.: a) The high stability of indigo has its mechanism associated with a fast ESPT: the keto excited species is converted into its enol isomer. b) (top) Photographic detail of an Andean textile (Man's poncho mfa31.496, 100B.C.-0; Museum of Fine Arts, Boston, USA) and (bottom) photoconversion reaction of indigo (blue, keto form) to isatin (yellow, leuco species). c) Scheme for the reduction of indigo in non-acidic media. Adapted from Ref. [60].

damaging radiation and safely dissipate it before irreversible chemical reactions can take place. The excess of absorbed energy may be dissipated through radiative or non-radiative decay pathways. These safe processes for returning to the ground state compete with unsafe electron-transfer reactions that usually are responsible of irreversible photochemistry.

7.3.1. Indigo

Indigo's intense blue colour is an intriguing feature for a relatively small molecule [53,54]. Resonance cannot explain it [55], thus the chromophore is best described as a donor-acceptor dye, where the amino groups act as the electron donors, while the carbonyl groups as the electron acceptors. DFT calculations supported this description, showing that the HOMO is essentially located in the central C=C bond and the nitrogen atoms, whereas the LUMO is located in the central C=C bond and the oxygen atoms [56]. In a simplified approximation, the absorption of visible light may be explained by a narrow HOMO-LUMO separation [56]; the donor groups raise the π orbital (HOMO) of the C=C double bond, while the acceptor groups lower the π^* orbital (LUMO). This favours an efficient coupling between the S_0 and S_1 vibrational modes, offering efficient radiationless conversion of the absorbed energy. In the excited state, the excess of energy of indigo may also be dissipated through excited-state proton transfer (ESPT, **Figure 7.6a**) [53,57-59]. These two very efficient deactivation channels allow for 99.99% of the quanta to be lost, protecting indigo from chemical modification [53,58,59].

Acquiring knowledge about indigo's photophysics is relevant for understanding its light-induced degradation. Experiments have shown that the central double bond is at the same time a photoprotector and a weak point [52a]. Based on the behaviour of indigo in *N,N*-dimethylformamide (DMF) solutions and solid matrixes, it

was proposed that the major colourless degradation product, isatin (**Figure 7.6b**), is produced from a reaction between indigo and a radical, resulting from an attack to the central double bond. The double bond and, in turn, indigo may be very stable under certain conditions, displaying photodegradation quantum yields with values either below 10^{-6} (reflecting stable environments) or ranging from 10^{-4} to 10^{-3} (that are representative of media where oxygen-based radicals or reducing species are present). Stable environments are represented by the blues from Andean textiles, dated from BC 200 to 200 AD (**Figure 7.6b**). These objects were kept for millennia in a very dry environment in Paracas (a region in South Peru) [52a]. In the blue indigo-coloured fibres, isatin was found as main photodegradation product, but in low-moderate relative amounts ($\leqslant$10%-20%). The mechanism of disruption of the central double bond connecting the two indole moieties is based on a two-step reduction and the reduction potential is pH-dependent [52a,60,61]. First, a radical is formed in one of the carbon atoms of the central double bond, that, in turn, reacts very promptly with other radicals present in solution. The destruction of the double bond creates a species that is like the *leuco* form (**Figure 7.6c**). The comparison between the photophysical properties of the *leuco* and *keto* forms revealed that the radiationless rate constants of all the studied *keto* forms are lower by about one order of magnitude than those found for the *leuco* forms [53]. Consequently, fluorescence and triplet-state formation are, in the case of the *leuco* forms, alternatives to the internal conversion deactivation channels for the singlet excited state. In fact, it seems reasonable to associate the larger fluorescence quantum yield (ϕ_F) values in the *leuco* forms with some degree of rotation around the central C=C bond. The remarkable stability of indigo is, in part, the result of intramolecular hydrogen bonding between the two-adjacent carbonyl and N–H groups, which keeps the molecule in a *trans* planar configuration, preventing the photochemical *cis-trans* isomerization, that in turn will led to irreversible photochemical fading. The differences observed between the two forms suggest that the well-known photostability of the *keto* forms of indigo is not present with the reduced species, *leuco* [53]. These same redox properties of indigo have been used in the past to dye textiles, by converting the insoluble *keto* species into the water-soluble *leuco* species. Indigo photophysics is shared with two other important historic dyes, Maya blue and Tyrian purple, being central for the understanding of their reactivity.

7.3.2. Anthraquinone Reds

The most common reds used in antiquity to dye textiles are based on hydroxy anthraquinone chromophores (**Figure 7.7**) [51,62]. They were extracted from the roots of a variety of plant from the *Rubiaceae* family, being alizarin and purpurin the major occurring species in *Rubia tinctoria L.* [51]. The red extracts were also prepared for use as a pigment for painting, by precipitation with aluminium salts (known as madder lake pigments). The structure of these metal–dye complexes is still a matter of controversy. Systematic phenomenological studies on the fading of various anthraquinone-lake paints, including cochineal lake pigments, indicated differences in colour fading [62,63]. Considering the lack of knowledge about accurate structures of lake pigments, we will focus on the photophysics of alizarin and purpurin and how it relates to their photostability.

During the last decades of the 20th century there has been a comprehensive body of published articles on the physicochemical and chemical properties of hydroxy, amino and acylamino derivatives [64-66]. The acidochromic effects in the excited state properties of purpurin and alizarin have been more recently studied [67,68]. From these studies it has been concluded that the substitution pattern of hydroxy anthraquinones is determinant for their excited state properties, where efficient radiationless processes play a determinant role in the overall stability of the molecules. The excited-state surface can be sensitively controlled by substituents, permitting the formation of a 1,10-keto tautomer, the ratio of which (compared to the excited 9,10) can be varied at least by two orders of magnitude (**Figure 7.7a**).

Advances in the fundamental photophysical processes enabled to gain further insights into the stability of this dye by single-molecule spectroscopy [69]. Authors proposed that the existence of a dark radical cation state formed by electron transfer (ET) would promote irreversible chemical transformation of the molecule

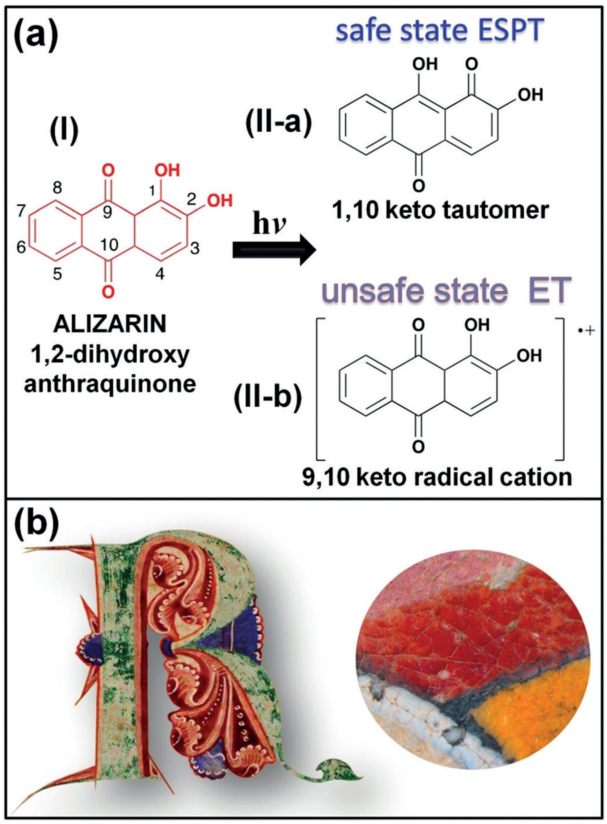

Figure 7.7.: a) Photoconversion pathways of (I) alizarin either into (II-a) 1,10-keto tautomer form or (II-b) a semioxidized 9,10-keto radical cation. The first species is formed through ESPT and will allow a safe return into the ground state. The latter is the result of an ET and will react, converting into degradation products. b) 12th century illuminated initial, where the anthraquinone-based red (lac dye) has preserved its original colour, whereas the Cu-based green is almost completely lost.

when returning to the ground state, resulting in the colour fading. In the excited state there will be a kinetic competition between an unsafe ET deactivation pathway and a safe ESPT process that will decay with recovery of the initial ground-state molecule (**Figure 7.7a**). Since the relative stabilities of alizarin and purpurin are best understood in the context of this kinetic competition in the excited state, we anticipate that the relative photostability of alizarin and purpurin–Al^{III} complexes will be maintained [70].

7.4. Summary and Outlook

The understanding and prevention of light-induced colour change in artworks are depending on the chemical comprehension of the excited-state behaviour of pigments and dyes in relation with the matrix and the environmental surrounding.

We have described how a phenomenological approach based on the identification of secondary products on a series of paintings has been pivotal in enabling us to understand the colour change of some pigments. The approach relies on the exploitation of advanced analytical methods which need to range from the nano- to the macro-scale yet ensuring high chemical speciation.

The use of computational modelling as interpretative tool of data from case studies and accelerated aging experiments has proved successful. The access to excited state properties through the time-dependent extension of DFT further opens up the possibility of simulating the evolution of the artists' materials after light absorption while interacting with chemicals possibly related to the degradation process. This is still a challenge, though potentially similar to related modelling studies in photocatalysis.

As for organic dyes, a more conceptual approach has been discussed which relies on fundamental knowledge on ultrafast reactions in the excited state of parent molecules. The comprehension of how the kinetic competition between safe proton transfer and disruptive electron transfer is affected by the substitution pattern of hydroxy anthraquinones as well as by chemistry of the support and the environmental surrounding may give an explanation of different lightfastness properties of anthraquinone reds in artworks.

As a necessary trend in chemistry for heritage science, we can envision physicochemical research addressing the structural, electronic and reactive properties of cultural heritage materials nourished by phenomenological studies unravelling the rich information enclosed in a work of art.

7.5. References

[1] Lambert S. The early history of preventive conservation in Great Britain and the United States (1850-1950). CeROArt. 1994. DOI: 10.4000/ceroart.3765.

[2] Druzik J, Eshøj B. Museum lighting: its past and future development. In: Padfield T, Borchersen K, editors. Museum microclimates. Copenhagen: National Museum of Denmark; 2007. p. 51-56.

[3] Clarricoates R, Dowding H, Gent A, editor. Colour change in paintings. London: Archetype Publications; 2016.

[4] Garside D, Curran K, Korenberg K, MacDonald L, Teunissen K, Robson S. How is museum lighting selected? An insight into current practice in UK museums. J Inst Conserv. 2017; (40)1: 3-14. DOI: 10.1080/19455224.2016.1267025.

[5] a) Berns RS, Byrns S, Casadio F, Fiedler I, Gallagher C, Imai FH, Newman A, Taplin LA. Rejuvenating the color palette of Georges Seurat's *A Sunday on La Grande Jatte* – 1884: a simulation. Color Res Appl. 2006; 31(4): 278-293. DOI: 10.1002/col.20223; b) Kirchner E, van der Lans I, Ligterink F, Geldof M, Megens L, Meedendorp T, Pilz K, Hendriks E. Digitally reconstructing Van Gogh's *Field with Irises near Arles* part 3: determining the original colors. Color Res Appl. 2018; 43(3): 311-327. DOI: 10.1002/col.22197; and references therein.

[6] Getterns RJ, Feller RL, Chase WT. Vermilion and cinnabar. In: Roy A, editor. Artists' pigments: a handbook of their history and characteristics. London: Archetype Publications, Vol 2; 1993. p. 159-182.
[7] Nöller R. Cinnabar reviewed: characterization of the red pigment and its reactions. Stud Conserv. 2015; 60(2): 79-87. DOI: 10.1179/2047058413Y.0000000089; and references therein.
[8] Keune K, Boon JJ. Analytical imaging studies clarifying the process of the darkening of vermilion in paintings. Anal Chem. 2005; 77(15): 4742-4750. DOI: 10.1021/ac048158f.
[9] Cotte M, Susini J, Metrich N, Moscato A, Gratziu C, Bertagnini A, Pagano M. Blackening of Pompeian cinnabar paintings: X-ray microspectroscopy analysis. Anal Chem. 2006; 78(21): 7484-7429. DOI: 10.1021/ac0612224.
[10] Radepont M, de Nolf W, Janssens K, Van der Snickt G, Coquinot Y, Klaassen L, Cotte M. The use of microscopic X-ray diffraction for the study of HgS and its degradation products corderoite (α-$Hg_3S_2Cl_2$), kenhsuite (γ-$Hg_3S_2Cl_2$) and calomel (Hg_2Cl_2) in historical paintings. J Anal At Spectrom. 2011; 26: 959-968. DOI: 10.1039/C0JA00260G; and references therein.
[11] Radepont R, Coquinot Y, Janssens K, Ezrati JJ, de Nolf W, Cotte M. Thermodynamic and experimental study of the degradation of the red pigment mercury sulfide. J Anal At Spectrom. 2015; 30: 599-612. DOI: 10.1039/C4JA00372A.
[12] Da Pieve F, Hogan C, Lamoen D, Verbeeck J, Vanmeert F, Radepont M, Cotte M, Janssens K, Gonze X, Van Tendeloo G. Casting light on the darkening of colors in historical paintings. Phys Rev Lett. 2013; 111: 208302. DOI: 10.1103/PhysRevLett.111.208302.
[13] Hogan C, Da Pieve F. Colour degradation of artworks: an *ab initio* approach to X-ray, electronic and optical spectroscopy analyses of vermilion photodarkening. J Anal At Spectrom. 2015; 30: 588-598. DOI: 10.1039/C4JA00327F.
[14] Anaf W, Janssens K, De Wael K. Formation of metallic mercury during photodegradation/photodarkening of α-HgS: electrochemical evidence. Angew Chem Int Ed. 2013; 52: 12568-12571. DOI: 10.1002/anie.201303977.
[15] a) Fiedler I, Bayard M. Cadmium yellows, oranges and reds. In: Feller RL, editor. Artists' pigments: a handbook of their history and characteristics. Washington: National Gallery of Art, Vol 1; 1986. p. 65-108; b) Kühn H, Curran M. Chrome yellow and other chromate pigments. In: Feller RL, editor. Artists' pigments: a handbook of their history and characteristics. Washington: National Gallery of Art, Vol 1; 1986. p. 187-217.
[16] Van der Snickt G, Janssens K, Dik J, De Nolf W, Vanmeert F, Jaroszewicz J, Cotte M, Falkenberg G, van der Loeff L. Combined use of synchrotron radiation based micro-X-ray fluorescence, micro-X-ray diffraction, micro-X-ray absorption near-edge, and micro-Fourier transform infrared spectroscopies for revealing an alternative degradation pathway of the pigment cadmium yellow in a painting by Van Gogh. Anal Chem. 2012; 84: 10221-10228. DOI: 10.1021/ac3015627.
[17] Van der Snickt G, Dik J, Cotte M, Janssens K, Jaroszewicz J, De Nolf W, Groenewegen G, van der Loeff L. Characterization of a degraded cadmium yellow (CdS) pigment in an oil painting by means of synchrotron radiation based X-ray techniques. Anal Chem. 2009; 81: 2600-2610. DOI: 10.1021/ac802518z.
[18] a) Mass J, Opila R, Buckley B, Cotte M, Church J, Mehta A. The photodegradation of cadmium yellow paints in Henri Matisse's *Le Bonheur de vivre* (1905-1906). Appl Phys A 2013; 111: 59-68. DOI: 10.1007/s00339-012-7418-0; b) Mass J, Sedlmair J, Patterson CS, Carson D, Buckley B, Hirschmugl C. SR-FTIR imaging of the altered cadmium sulfide yellow paints in Henri Matisse's *Le Bonheur de vivre* (1905-6) – examination of visually distinct degradation regions. Analyst 2013; 138: 6032-6043. DOI: 10.1039/C3AN00892D; c) Pouyet E, Cotte M, Fayard B, Salomè M, Meirer F, Mehta A, Uffelman ES, Hull A, Vanmeert F, Kieffer J, Burghammer M, Janssens K, Sette F. 2D X-ray and FTIR micro-analysis of the degradation of cadmium yellow pigment in paintings of Henri Matisse. J Mass Appl Phys A 2015; 121: 967-980. DOI: 10.1007/s00339-015-9239-4.
[19] Liu H, Gao H, Long M, Fu H, Alvarez PJ, Li Q, Zheng S, Qu X, Zhu D. Sunlight promotes fast release of hazardous cadmium from widely-used commercial cadmium pigment. Environ Sci Technol. 2017; 51:

6877-6886. DOI: 10.1021/acs.est.7b00654.
[20] Anaf W, Trashin S, Schalm O, van Dorp D, Janssens K, De Wael K. Electrochemical photodegradation study of semiconductor pigments: influence of environmental parameters. Anal Chem. 2014; 86: 9742-9748. DOI: 10.1021/ac502303z.
[21] Giacopetti L, Satta A. Reactivity of Cd-yellow pigments: role of surface defects. Microchem J. 2018; 137: 502-508. DOI: 10.1016/j.microc.2017.12.013; and references therein.
[22] Voras E, deGhetaldi K, Wiggins MB, Buckley B, Baade B, Mass JL, Beebe TB. ToF-SIMS imaging of molecular-level alteration mechanisms in *Le Bonheur de vivre* by Henri Matisse. Appl Phys A 2015; 121: 1015-1030. DOI: 10.1007/s00339-015-9508-2.
[23] Leone B, Burnstock A, Jones C, Hallebeek P, Boon J, Keune K. The deterioration of cadmium sulphide yellow artists' pigments. In: Verger I, editor. ICOM-CC 14th Triennial Conference Preprints, The Hague, 12-16 September 2005. London: James and James/Earthscan, Vol. II; 2005. p. 803-813.
[24] Vanmeert F, Van der Snickt G, Janssens K. Plumbonacrite identified by X-ray powder diffraction tomography as a missing link during degradation of red lead in a Van Gogh painting. Angew Chem Int Ed. 2015; 54: 3607-3610. DOI: 10.1002/anie.201411691; and references therein.
[25] a) Van Driel BA, Wezendonk TA, Van den Berg KJ, Kooyman PJ, Gascon J, Dik J. Determination of early warning signs for photocatalytic degradation of titanium white oil paints by means of surface analysis. Spectrochim Acta Part A 2017; 172; 100-108. DOI: 10.1016/j.saa.2016.04.026; b) Morsch S, van Driel BA, van den Berg KJ, Dik J. Investigating the photocatalytic degradation of oil paint using ATR-IR and AFM-IR. ACS Appl Mater Interfaces 2017; 9: 10169-10179. DOI: 10.1021/acsami.7b00638.
[26] Christensen PA, Dilks A, Egerton TA, Temperley J. Infrared spectroscopic evaluation of the photodegradation of paint Part II: the effect of UV intensity & wavelength on the degradation of acrylic films pigmented with titanium dioxide. J Mater Sci. 2000; 35: 5353-5358. DOI: 10.1023/A:1004898913140; and references therein.
[27] Setvin M, Shi X, Hulva J, Simschitz T, Parkinson GS, Schmid M, Di Valentin C, Selloni A, Diebold U. Methanol on anatase TiO_2 (101): mechanistic insights into photocatalysis. ACS Catal. 2017; 7: 7081-7091. DOI: 10.1021/acscatal.7b02003; and references therein.
[28] Casadio F, Xie S, Rukes SC, Myers B, Gray KA, Warta R, Fiedler I. Electron energy loss spectroscopy elucidates the elusive darkening of zinc potassium chromate in Georges Seurat's *A Sunday on La Grande Jatte – 1884.* Anal Bioanal Chem. 2011; 399: 2909-2920. DOI: 10.1007/s00216-010-4264-9.
[29] Zanella L, Casadio F, Gray KA, Warta R, Ma Q, Gaillard J-F. The darkening of zinc yellow: XANES speciation of chromium in artist's paints after light and chemical exposures. Anal At Spectrom. 2011; 26: 1090-1097. DOI: 10.1039/C0JA00151A.
[30] Monico L, Van der Snickt G, Janssens K, De Nolf W, Miliani C, Dik J, Radepont M, Hendriks E, Geldof M, Cotte M. Degradation process of lead chromate in paintings by Vincent van Gogh studied by means of synchrotron X-ray spectromicroscopy and related methods. 2. Original paint layer samples. Anal Chem. 2011; 83: 1224-1231. DOI: 10.1021/ac1025122.
[31] Monico L, Janssens K, Vanmeert F, Cotte M, Brunetti BG, Van der Snickt G, Leeuwestein M, Plisson JS, Menu M, Miliani C. Degradation process of lead chromate in paintings by Vincent van Gogh studied by means of spectromicroscopic methods. Part 5. Effects of nonoriginal surface coatings into the nature and distribution of chromium and sulfur species in chrome yellow paints. Anal Chem. 2014; 86: 10804-10811. DOI: 10.1021/ac502841g.
[32] Monico L, Janssens K, Alfeld M, Cotte M, Vanmeert F, Ryan CG, Falkenberg G, Howard DL, Brunetti BG, Miliani C. Full spectral XANES imaging using the Maia detector array as a new tool for the study of the alteration process of chrome yellow pigments in paintings by Vincent van Gogh. J Anal At Spectrom. 2015; 30: 613-626. DOI: 10.1039/C4JA00419A.
[33] Monico L, Janssens K, Hendriks E, Vanmeert F, Van der Snickt G, Cotte M, Falkenberg G, Brunetti

BG, Miliani C. Evidence for degradation of the chrome yellows in VanGogh's *Sunflowers*: a study using noninvasive insitu methods and synchrotron-radiation-based X-ray techniques. Angew Chem Int Ed. 2015; 54: 13923-13927. DOI: 10.1002/anie.201505840.

[34] Monico L, Van der Snickt G, Janssens K, De Nolf W, Miliani C, Verbeeck J, Tian H, Tan HY, Dik J, Radepont M, Cotte M. Degradation process of lead chromate in paintings by Vincent van Gogh studied by means of synchrotron X-ray spectromicroscopy and related methods. 1. Artificially aged model samples. Anal Chem. 2011; 83: 1214-1223. DOI: 10.1021/ac102424h.

[35] Monico L, Janssens K, Miliani C, Van der Snickt G, Brunetti BG, Guidi MC, Radepont M, Cotte M. Degradation process of lead chromate in paintings by Vincent van Gogh studied by means of spectromicroscopic methods. 4. Artificial aging of model samples of co-precipitates of lead chromate and lead sulfate. Anal Chem. 2013; 85: 860-867. DOI: 10.1021/ac3021592.

[36] Monico L, Janssens K, Cotte M, Romani A, Sorace L, Grazia C, Brunetti BG, Miliani C. Synchrotron-based X-ray spectromicroscopy and electron paramagnetic resonance spectroscopy to investigate the redox properties of lead chromate pigments under the effect of visible light. J Anal At Spectrom. 2015; 30: 1500-1510. DOI: 10.1039/C5JA00091B.

[37] Monico L, Janssens K, Cotte M, Sorace L, Vanmeert F, Brunetti BG, Miliani C. Chromium speciation methods and infrared spectroscopy for studying the chemical reactivity of lead chromate-based pigments in oil medium. Microchem J. 2016; 124: 272-282. DOI: 10.1016/j.microc.2015.08.028.

[38] Tan H, Tian H, Verbeeck J, Monico L, Janssens K, Van Tendeloo G. Nanoscale investigation of the degradation mechanism of a historical chrome yellow paint by quantitative electron energy loss spectroscopy mapping of chromium species. Angew Chem Int Ed. 2013; 52: 11360-11363. DOI: 10.1002/anie.201305753.

[39] Vanmeert F, Hendriks E, Van der Snickt G, Monico L, Dik J, Janssens K. Chemical mapping by macroscopic X-ray powder diffraction (MA-XRPD) of Van Gogh's *Sunflowers*: identification of areas with higher degradation risk. Angew Chem Int Ed. 2018; 57: 7418. DOI: 10.1002/anie.201713293.

[40] a) Otero V, Carlyle L, Vilarigues M, Melo MJ. Chrome yellow in nineteenth century art: historic reconstructions of an artists' pigment. RSC Adv. 2012; 2: 1798-1805. DOI: 10.1039/C1RA00614B; b) Otero V, Pinto JV, Carlyle L, Vilarigues M, Cotte M, Melo MJ. Nineteenth century chrome yellow and chrome deep from Winsor & Newton^{TM}. Stud Conserv. 2016; 62(3): 123-149. DOI: 10.1080/00393630.2015.1131478; c) Otero V, Vilarigues M, Carlyle L, Cotte M, De Nolf W, Melo MJ. A *little key* to oxalate formation in oil paints: protective patina or chemical reactor? Photochem Photobiol Sci. 2018; 17: 266-270. DOI: 10.1039/C7PP00307B.

[41] Muñoz-García AB, Massaro A, Pavone M. *Ab initio* study of $PbCr_{(1-x)}S_xO_4$ solid solution: an inside look at Van Gogh Yellow degradation. Chem Sci. 2016; 7: 4197-4203. DOI: 10.1039/C5SC04362J.

[42] Amat A, Miliani C, Fantacci S. Structural and electronic properties of the $PbCrO_4$ chrome yellow pigment and of its light sensitive sulfate-substituted compounds. RSC Adv. 2016; 6: 36336-36344. DOI: 10.1039/C6RA01444E.

[43] Rahemi V, Sarmadian N, Anaf W, Janssens K, Lamoen D, Partoens B, De Wael K. Unique optoelectronic structure and photoreduction properties of sulfur-doped lead chromates explaining their instability in paintings. Anal Chem. 2017; 89: 3326-3334. DOI: 10.1021/acs.analchem.6b03803.

[44] Grandjean F, Samain L, Long GJ. Characterization and utilization of Prussian blue and its pigments. Dalton Trans. 2016; 45: 18018-18044. DOI: 10.1039/C6DT03351B; and references therein.

[45] Vila A, Monard K, Filtenborg T, Wadum J. As time passed by came sunset. Christen Købke's view of lake sortedam, its genesis and colour changes. In: Sgamellotti A, Brunetti BG, Miliani C, editors. Science and art: the painted surface. Londond: The Royal Society of Chemistry; 2014. p. 354-372. DOI: 10.1039/9781839161957-00354.

[46] Berrie BH. Prussian blue. In: West FitzHugh E, editor. Artists' pigments: a handbook of their history and characteristics. Washington: National Gallery of Art, London: Archetype Publications, Vol. 3; 2000. p.

191-217.
[47] Kirby J, Saunders D. Fading and colour change of Prussian blue: methods of manufacture and the influence of extenders. Nat Gallery Tech Bull. 2004; 25: 73-99. DOI: kirby_saunders2004.
[48] Samain L, Gilbert B, Grandjean F, Long GJ, Strivaya D. Redox reactions in Prussian blue containing paint layers as a result of light exposure. J Anal At Spectrom. 2013; 28: 524-535. DOI: 10.1039/C3JA30359D; and references therein.
[49] a) Gervais C, Languille MA, Reguer S, Garnier C, Gillet M. Light and anoxia fading of Prussian blue dyed textiles. Herit Sci. 2014; 2: 26. DOI: 10.1186/s40494-014-0026-x; b) Gervais C, Languille MA, Moretti G, Reguer S. X-ray photochemistry of Prussian blue cellulosic materials: evidence for a substrate-mediated redox process. Langmuir 2015; 31: 8168-8175. DOI: 10.1021/acs.langmuir.5b00770.
[50] Samain L, Grandjean F, Long GJ, Martinetto P, Bordet P, Sanyova J, Strivay D. Synthesis and fading of eighteenth-century Prussian blue pigments: a combined study by spectroscopic and diffractive techniques using laboratory and synchrotron radiation sources. J Synchrotron Radiat. 2013; 20: 460-473. DOI: 10.1107/S0909049513004585.
[51] Melo MJ. History of natural dyes in the ancient Mediterranean world. In: Bechtold T, Mussak R, editors. Handbook of natural colorants. Chichester: Wiley; 2009. p. 3-18; and references therein.
[52] a) Sousa MM, Miguel C, Rodrigues I, Parola AJ, Pina F, Seixas de Melo JS, Melo MJ. A photochemical study on the blue dye indigo: from solution to ancient Andean textiles. Photochem Photobiol Sci. 2008; 7: 1353-1359. DOI: 10.1039/B809578G; b) Melo MJ, Claro A. Bright light: microspectrofluorimetry for the characterization of lake pigments and dyes in works of art. Acc Chem Res. 2010; 43: 857-866. DOI: 10.1021/ar9001894; c) Melo MJ, Araffljo R, Castro R, Casanova C. Colour degradation in medieval manuscripts. Microchem J. 2016; 124: 837-844. DOI: 10.1016/j.microc.2015.10.014.
[53] Seixas de Melo JS, Moura AP, Melo MJ. Photophysical and spectroscopic studies of indigo derivatives in their keto and leuco forms. J Phys Chem. A 2004; 108: 6975-6981. DOI: 10.1021/jp049076y.
[54] Wyman GM. Reminiscences of an accidental photochemist. EPA Newsl. 1994; 50: 9-13.
[55] a) Wille E, Lgttke W. 4,4,4,4-Tetramethyl-^{2,2}-bipyrrolidin-3,3-dion, eine verbindung mit dem grundchromophorsystem des indigos. Angew Chem. 1971, 83, 853-854. DOI: 10.1002/ange.19710832112; b) Klessinger M. Captodative substituent effects and the chromophoric system of indigo. Angew Chem Int Ed Engl. 1980; 19: 908-909. DOI: 10.1002/anie.198009081; and references therein.
[56] Melo MJ, Ferreira JL, Parola AJ, de Melo JS. Photochemistry for cultural heritage. In: Bergamini G, Silvi S, editors. Applied photochemistry: when light meets molecules. Berlin: Springer, Berlin; Lecture Notes in Chemistry Vol. 92; 2016. p. 499-530. DOI: 10.1007/978-3-319-31671-0_13; and references therein.
[57] Miliani C, Romani A, Favaro G. A spectrophotometric and fluorimetric study of some anthraquinoid and indigoid colorants used in artistic paintings. Spectrochim Acta Part A. 1998; 54(4): 581-588. DOI: 10.1016/S1386-1425(97)00240-0.
[58] Seixas de Melo JS, Serpa C, Burrows HD, Arnaut LG. The triplet state of indigo. Angew Chem Int Ed. 2007; 46: 2094-2096. DOI: 10.1002/anie.200604679.
[59] a) Nagasawa Y, Taguri R, Matsuda H, Murakami M, Ohama M, Okada T, Miyasaka H. The effect of hydrogen-bonding on the ultrafast electronic deactivation dynamics of indigo carmine. Phys Chem Chem Phys. 2004; 6: 5370-5378. DOI: 10.1039/B409443C; b) Iwakura I, Yabushita A, Kobayashi T. Transition state in a prevented proton transfer observed in real time. Bull Chem Soc Jpn. 2011; 84: 164-171. DOI: 10.1246/bcsj.20100269.
[60] Srividya N, Paramasivan G, Seetharaman K, Ramamurthy P. Two-step reduction of indigo carmine by dithionite: a stopped-flow study. J Chem Soc Faraday Trans. 1994; 90: 2525-2530. DOI: 10.1039/FT9949002525.
[61] Bond AM, Marken F, Hill E, Compton RG, Hügel H. The electrochemical reduction of indigo dissolved in organic solvents and as a solid mechanically attached to a basal plane pyrolytic graphite electrode immersed in aqueous electrolyte solution. J Chem Soc Perkin Trans. 2 1997; 1735-1742. DOI: 10.1039/A701003F.

[62] Berrie BH, Strumfels Y. Change is permanent: thoughts on the fading of cochineal-based watercolor pigments. Herit Sci. 2017; 5(30): 1. DOI: 10.1186/s40494-017-0143-4.
[63] Saunders D, KirbyJ. Light-induced colour changes in red and yellow lake pigments. Nat Gallery Tech Bull. 1994; 15: 79-97. DOI: saunders_kirby1994.
[64] El Ezaby MS, Salem TM, Zewail AH, Issa R. Spectral studies of some hydroxy-derivatives of anthraquinones. J Chem Soc. B 1970; 7: 1293-1296. DOI: 10.1039/J29700001293 .
[65] a) Van Benthem MH, Gillispie GD. Intramolecular hydrogen bonding. 4. Dual fluorescence and excited-state proton transfer in 1,5-dihydroxyanthraquinone. J Phys Chem. 1984; 88: 2954-2960. DOI: 10.1021/j150658a008; b) Marasinghe PAB, Gillispie GD. Intramolecular hydrogen bonding. IX. Theoretical geometries of substituted anthraquinones relevant to proton transfer studies. Chem Phys. 1989; 136(2): 249-257. DOI: 10.1016/0301-0104(89)80050-3.
[66] a) Smith TP, Zaklika KA, Thakur K, Walker GC, Tominaga K, Barbara PF. Spectroscopic studies of excited-state intramolecular proton transfer in 1-(acylamino)anthraquinones. J Phys Chem. 1991; 95: 10465-10475. DOI: 10.1021/j100178a038; b) Denny RA, Bagchi B, Barbara PF. Effects of vibrational energy relaxation and reverse reaction on electron transfer kinetics and fluorescence line shapes in solution. J Chem Phys. 2001; 115: 6058. DOI: 10.1063/1.1398591.
[67] Miliani C, Romani A, Favaro G. Acidichromic effects in 1,2-di- and 1,2,4-tri- hydroxyanthraquinones. A spectrophotometric and fluorimetric study. J Phys Org Chem. 2000; 13: 141-150. DOI: 10.1002/(SICI)1099-1395(200003)13:3<141::AID-POC220>3.0.CO;2-J.
[68] Amat A, Miliani C, Romani A, Fantacci S. DFT/TDDFT investigation on the UV-vis absorption and fluorescence properties of alizarin dye. Phys Chem Chem Phys. 2015; 17: 6374-6382. DOI: 10.1039/C4CP04728A.
[69] Tan JA, Garakyaraghi S, Tagami KA, Frano KA, Crockett HM, Ogata AF, Patterson JD, Wustholz KL. Contributions from excited-state proton and electron transfer to the blinking and photobleaching dynamics of alizarin and purpurin. J Phys Chem. C 2017; 121: 97-106. DOI: 10.1021/acs.jpcc.6b09818.
[70] Grazia C, Clementi C, Miliani C, Romani A. Photophysical properties of alizarin and purpurin Al(iii) complexes in solution and in solid state. Photochem Photobiol Sci. 2011; 10: 1249-1254. DOI: 10.1039/C1PP05039G.

This is an Accepted Manuscript of an article published by Elsevier in Dyes and Pigments, on 26/02/2021, available online:

Angelin EM, Conceição Oliveira M, Nevin A, Picollo M, Melo MJ. To be or not to be an azo pigment: chemistry for the preservation of historical β-naphthol reds in cultural heritage. Dyes Pigm. 2021; 190: 109244. DOI: 10.1016/j.dyepig.2021.109244.

8. To be or not to be an azo pigment: chemistry for the preservation of historical β-naphthol reds in cultural heritage

Abstract

Naphthol reds are historical pigments widely found in cultural heritage, characterized by 1-arylhydrazone-2-naphthol basic skeleton. Little is known about their degradation mechanisms, and this knowledge is essential for their long-term preservation. In this research, for the first time, the photodegradation quantum yields (Φ_R) were calculated for a series of pigment reds selected based on published literature, in order to evaluate the effects of the electron-withdrawing and donating groups present in C(4'), in particular the effect of sulfonate groups on the stability of these compounds. Φ_R values in homogeneous media, ranging from $3x10^{-6}$ to $4x10^{-5}$, are difficult to obtain in these systems, but provide the quantification of the stability of naphthol reds. One of the main conclusions is that the sulfonate groups have a stabilizing effect and that the keto forms are generally more stable. Another important piece of information is that the solvent, and as such the medium predictably, has a major impact on stability. For Sudan I and Orange II irradiation was also carried with a xenon source ($\lambda_{irr} \geqslant$ 300 nm), allowing characterizing the main degradation products by HPLC-DAD-MS and UHPLC-HRMS. For the dyes characterized by higher Φ_R, extensive degradation was observed with the formation of volatile compounds as phthalates.

8.1. Introduction

A key part of art conservation is the understanding of constituent materials, very few of which are simple [1]. Contemporary art poses challenges to conservators and scientists due to the intrinsic susceptibility of materials to degradation, much of which remains poorly understood. For this reason, chemistry has a central role to play in the conservation of these works of art, making them accessible, and ensuring the preservation of cultural heritage to future generations.

This work focus on fundamental aspects of the degradation mechanisms of modern colorants based on β-naphthol (2-naphthol), more specifically, on 1-arylhydrazone-2-naphthol, **Figure 8.1** [2-6]. Reds that have been applied to create icons of our modern art such as the Rothko murals in Harvard [7,8], design pieces and everyday objects, all testimonies of our material culture [9,10]. The study of the factors affecting β-naphthol reds fading is achieved by measuring the quantum yields of degradation, at 313 nm, for 9 selected parent dyes and pigments as well as by characterizing the main degradation products for Sudan I and Orange II by HPLC-DAD-MS and UHPLC-HRMS, in homogeneous media. Monochromatic irradiation at 313 nm, which allows selective excitation of the keto form, and polychromatic irradiation ($\lambda_{irr} \geqslant$ 300 nm) are carried out to understand the effects of substituents on the stability of these reds [2-6]. In **Tables 8.1-8.2** and **E.1** the molecular structures together with acronyms based on the international color index, name and common names of the colorants are listed, covering the most important categories of β-naphthol pigments found in contemporary heritage, in paint and plastic formulations, as well as reference compounds [11]. The reference

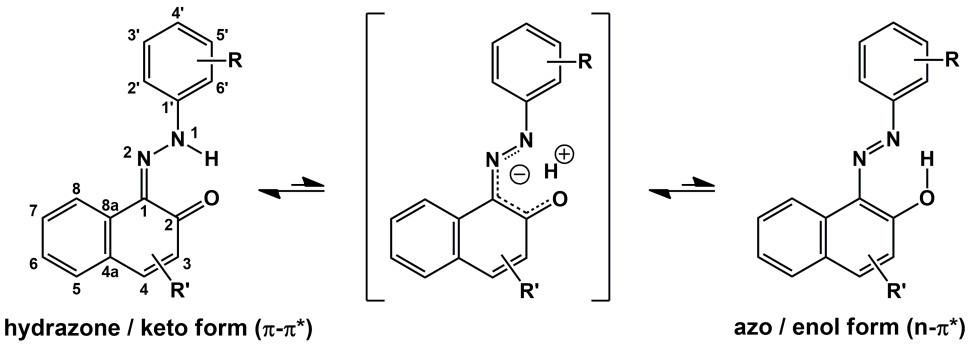

Figure 8.1.: For the naphthol reds studied in this work, the tautomeric equilibrium is shifted towards the hydrazone, which is further stabilized by electron-withdrawing groups in the para position of the phenyl ring, C(4'). The main absorption band in the visible is based on π-π* transition for the keto and n-π* for the enol forms.

Table 8.1.: Molecular structures and acronyms of the colorants studied in this work.

SY14 Sudan I	AO7 Orange II	AO10 Orange G	PR1 Para Red	PR3 Toluidine Red
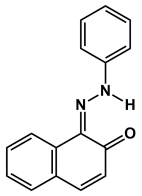	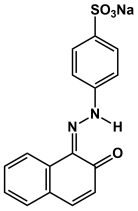	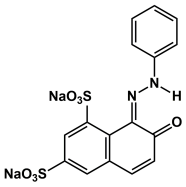	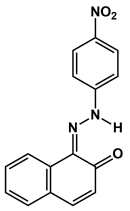	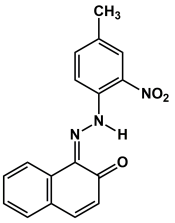

series includes water-soluble dyes Acid Orange 7 (AO7) and 10 (AO10) and the dye Solvent Yellow 14 (SY14). These will support the study of the more complex systems based on Pigment Red 1 (PR1), PR3, PR49:2, PR53:1, PR48:2, PR57:1.

In this introduction, we first discuss the experimental evidence that shows that these colorants should be represented as hydrazones and not as azo tautomers, and then proceed to an overview of their photophysics, concluding with the degradation mechanism and main degradation products identified in literature.

8.1.1. To be an azo or an hydrazone pigment: the main tautomer for pigment reds in cultural heritage

The pigment reds in **Tables 8.1-8.2** are usually described as azo pigments and depicted as such, within the heritage field [2,7,12]. However, for these β-naphthol reds, in the ground state the azoenol form is the minor tautomer, **Figure 8.1** [4,5,13-16]. Thus the name "hydrazone pigments", in these cases, is more appropriate than the traditional expression "azo pigments" [5]. For this reason thorough this paper, we will refer to these compounds as ketohydrazone colorants, hydrazone form, or keto species.

These enol and keto systems can be described as hydrogen-bonded, where intramolecular proton transfer occurs between nitrogen and oxygen atoms [17], establishing a tautomeric equilibrium that is modulated by the substituents in the phenyl and naphthol rings, **Figure 8.1**. An elegant analysis on the azoenol/ketohydrazone tautomerism in these systems, and how it is influenced by both substitution pattern and environment, has been reviewed by Heron et al. [13]. In brief, NMR studies and crystal structures have disclosed the effects of substituents on the equilibria [13,17] and theoretical simulations have provided some rationale for the observed experimental data [18,19]. A summary of the main experimental data based on X-Ray studies is reported in **Table E.2**.

Table 8.2.: Molecular structures and acronyms of the pigment lakes studied in this work. The possible metal ion pairs, M^{n+}, are described in the third row.

PR48 **Permanent Red 2B**	**PR49** **Lithol Red**	**PR53** **Lake Red C**	**PR57:1** **Lithol Rubine**
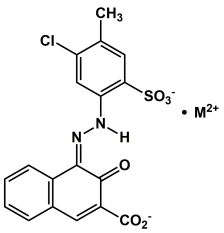	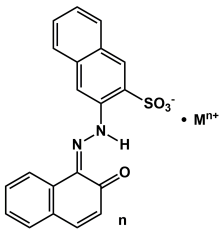	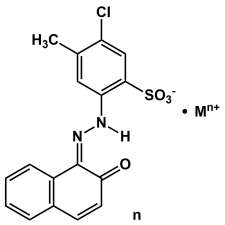	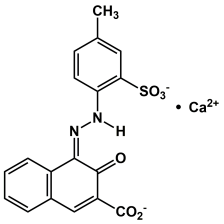
Ba^{2+}; PR 48:1 Ca^{2+}; PR 48:2 Sr^{2+}; PR 48:3 Mn^{2+}; PR 48:4 Mg^{2+}; PR 48:5	Na^{+}; PR 49 Ba^{2+}; PR 49:1 Ca^{2+}; PR 49:2 Sr^{2+}; PR 49:3	Na^{+}; PR 53 Ba^{2+}; PR 53:1 Ca^{2+}; PR 53:2 Sr^{2+}; PR 53:3	

NMR spectroscopy, in particular ^{13}C NMR, provides quantitative data on the relative concentration of the azo and hydrazone forms present in the equilibrium, both in solution and in the solid state [17,20]. It was also possible to prove that "equilibrium compositions in the solid materials are similar to those measured in solution" [17]. In this research, Sudan I that may be regarded as the common structure in our study, is "a rapidly exchanging mixture of ca 70% of the hydrazone form and 30% azo" [17], **Figure 8.1**. Substituents in the *para* position in the phenyl ring affect the position of the equilibrium; with strong electron-withdrawing groups the equilibrium shifts almost completely to the ketohydrazone tautomer [13,17], whereas electron-donating groups tend to favor the azo form [17,21]. For example, when R=NO_2 or SO_3Na, the equilibrium is mainly dominated by the keto species, while for R=OMe is approximately equimolar [17]. In these 2-naphthol based systems, the chemical shift of the C=O function (C-2) has been used as a probe to calculate the ratio of the ketohydrazone/azoenol tautomers [13,17].

The analysis of crystal structures yields crucial information on the chemical networks of these colorants and, corroborated the influence of the substitution pattern in the tautomeric equilibrium. Pigment lakes such as PR48 are obtained by complexation of sulfonated or carboxylate groups with Ba (PR48:1), Ca (PR48:2) or Sr ions (PR48:3). A series of systematic studies on the crystal structures of these type of dyes and pigment lakes have been published recently [3-5,7,22,23]. Kennedy et al. proved that dyes, with the same functional groups, could act as model for "sulfonated azo pigments" [3]. As dyes are water soluble and have better crystal growth properties than pigments, it was possible to discuss 87 related crystal structures, by-passing the difficulty in growing pigments crystals [3]. This essential information guided our selection, **Tables 8.1-8.2**. The systematical analysis of 87 structures, confirmed the sole presence of hydrazone tautomer, in sulfonated dyes; in this case, the keto form is stabilized through two intramolecular hydrogen bonds formed by interactions between the N-H donor and the O acceptor of the ketone and sulfonate groups [3]. It also proved that the most common ions (Ca, Sr, Ba) were associated with crystal structures that were defined as one-dimensional coordination polymers. The few crystal structures for pigments lakes that were published confirmed these observations. For example, for *ortho*-sulfonated lake pigments such as calcium salts of pigment reds 53 and 57 [4,5], the dye acts as a bidentate ligand and coordinates to the calcium ion through sulfonate and carbonyl oxygen atoms in a trans geometry, whereas the central calcium ion adopts a nearly octahedral geometry. In pigment lakes of this type, the sulfonate group bridges two calcium ions to give a molecular arrangement in a double-layer structure. The polar /ionic layer contains the calcium ions, keto and sulfonate groups and water molecules, whereas the non-polar layer consists of both aromatic rings. For pigments lakes with carboxylate

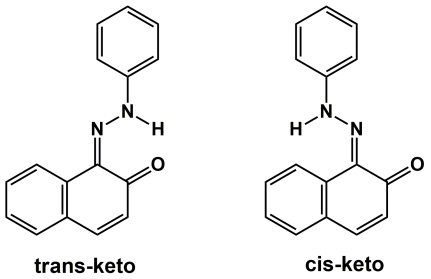

Figure 8.2.: Sudan I (SY14) in its thermodynamically stable *trans* conformer and in the *cis*-keto / hydrazone form that is available upon light absorption. For more details please see text.

groups, metal bonding to sulfonate plays a minor role, with chain propagation largely through carboxylate and the metal ions [5].

Further insight into the tautomeric equilibrium was achieved by Gilli and Gilli [14,15]. Analyzing structures assembled on the Cambridge Crystallographic Database, a comparison of selected bond lengths for the azoenol/ketohydrazone was used to detect the ketohydrazone or azoenol tautomers, and to discuss the type of substitution pattern that favors it [15]. The reasoning of the authors in assessing the position of the equilibrium is as follows: "from an analysis of the C-O, C-C, C-N and N-N distance, the simplest indicator being the C-O bond distance which is in the approximate ranges 1.20-1.25 Å and 1.31-1.36 Å for the keto and enol configurations, respectively. (...) A similar kind of reasoning can be applied to the N-N distances, which fall in the ranges 1.31-1.35 Å for keto and 1.28-1.31 Å for enol". In section 2.7 of this publication, the authors analyze 33 crystal structures of 1-arylazo-2-naphthols and conclude that 27 are "pure keto-hydrazo tautomers", in agreement with the conclusion obtained by NMR spectroscopy. This was a result of the nature of the substitution in the phenyl ring: "with the progressive change from electron-withdrawing to electron-donating substituents, the H-bond changes from pure keto (*p*-NO2, *m*-OMe and H) towards an intermediate region of tautomeric disorder where the enol fraction systematically increases with the increasing of the electron-donating nature of the substituent (*p*-Cl, *p*-F, *o*-F, *p*-NMe_2)" [15].

In summary, in β-naphthol reds, the *keto* form is largely preferred as acknowledged in the reference book " Industrial Organic Pigments" [24]. Contrarily to the robust understanding gathered for the fundamental state, the general physical and chemical principles that underlie its photostability are still poorly understood. We will briefly review them in next section.

8.1.2. Photostability mechanisms in pigment reds in cultural heritage

β-naphthol was the compound elected by Alfred Weller to illustrate the concept of excited state proton transfer and its kinetics [25]. The large electron delocalization in the naphthalene moiety was used by Weller to explain various excited state phenomena observed for β-naphthol such as catalysis by buffers and molecular fluorescence quenching [26]. It is this large π-electron delocalization in the naphthol ring that makes the difference between the chromophores based on a benzene or naphthalene ring. This delocalization can "pay" for the stronger hydrogen bond with the N atom, **Figure 8.2**. This is the case for the pigment reds depicted in **Tables 8.1-8.2**, in which the proton is not found as an OH group, but bond to the atom that displays a higher affinity to it, nitrogen [14], through the creation of a pseudo six-member ring (*trans*-keto in **Figure 8.2**). In the photophysic studies it is also necessary to consider that both keto and enol forms may be found as *trans* or *cis* conformers, **Figure 8.2**.

Most studies on the photophysics of β-naphthol reds have assumed that they were azo compounds, and the enol was considered the major species in the ground state. This, in part, undermines the rational that was proposed for the deactivation mechanisms in the excited state. Exceptions can be found, for example in the studies carried out by Antonov that have shown that only the keto form emits and with very small Stoke

shifts and extremely low quantum yields of fluorescence (0.05 at low temperatures, decreasing sharply with temperature increase) [16]. On the other hand, some other researchers as Rentzepis et al. designed their experiments to excite mainly the keto form [27]. This is possible because the absorption spectrum of Sudan I (SY14) is characterized by two main transitions, $n\pi^*$ at 350-400 nm which is allocated to the enol form and the stronger $\pi\pi^*$ transition at 450-550 nm of the keto species (which in part overlaps the enol band) [27,28]. In the seminal work by Rentzepis et al., excitation was carried out at 532 nm and the trans-cis isomerization between the two *cis* and *trans* keto conformers, depicted in **Figure 8.2**, was proposed as the main deactivation mechanism for the "hydrazone form" of Sudan I. Eight *trans* and *cis* conformers for the keto and enol forms were considered, **Figure 8.2** [27]. More recently, Douhal et al. published fluorescence lifetimes of Sudan I in solution and in confined environments in the fs to ns range, **Figure 8.2** [29,30]. In confined media, the excited state population decays with three time components; the shorter lifetime, in the range of 20 ps and similar to that in solution, was attributed to the isomerization of *trans*-hydrazone: "a twisting motion of the two aromatic parts along –N=N– (or =N–NH–) bonds leading to a *cis*-type form of Sudan I" [29], that decays from an "hot" vibrational excited state in 110-185 ps. Finally, the relaxed vibrational *cis* conformer decays with a lifetime in the 0.4-0.9 ns range recovering the *trans*-hydrazone. This isomerization mechanism in the excited state promotes a safe, non-radiative, deactivation of the excess energy absorbed. Excited state proton transfer was excluded as a deactivation mechanism. This proposal, can be reviewed following computational studies published in 2015 by Guan, Cui and Fang [18]. Although these researchers have chosen 2-hydrazonebenzene as model compound, i.e, a benzene based chromophore in which the enol form is the thermodynamically stable form in the ground state, their detailed analysis gives new insight into the excited-state deactivation mechanism. Guan, Cui and Fang predict four main ground-state conformers: *cis*-enol and -keto as well as *trans*-enol and -keto. The *trans* conformers display lower relative energies, and from the two, the *trans*-enol was calculated as the most stable species, as expected. Based on changes in bond lengths associated with the $^1\pi\pi^*$ and $^1n\pi^*$ transitions from the first excited singlet (S_1), they found that hydrogen-bonding strength is augmented in the excited keto forms and weakened in the enol species. This agrees with the finding that "excited-state intramolecular proton transfer (ESiPT) along the bright diabatic $^1\pi\pi^*$ state is barrierless and ultrafast", being proposed as one to the two uncovered deactivation channels. For the excited keto form, the second deactivation pathway consists in the decay from the first excited state to the ground state via a conical intersection region, which on reaching the ground state, "will bifurcate into *trans*-keto and *cis*-keto conformers, of which the former is preferred" [18].
In summary, for 2-hydrazonebenzene the computational results predicted that the excited-state decay into the ground state was, most probably, initiated by the rotation about the C1=N2 double bond which plays a photoprotective role. However, excited-state intramolecular proton transfer was also predicted as a deactivation channel.

8.1.3. Degradation mechanisms and main degradation products

The information on the degradation mechanisms of naphthol reds is in its infancy, and many studies offer significant data without in depth interpretation of analytical results [7,31,32]. The few studies published focused mainly on the tentative identification of degradation products [7,31]. Meetani et al. discussed possible photodegradation pathways for Acid Orange 10, however irradiation was carried out at 254 nm, in the presence of TiO_2 mixed with 20% chromium oxide as a catalyst [32]. Photocatalysis produced using UV light (254 nm) is not aimed at reproducing the mechanisms at play in natural conditions, but to produce an efficient total degradation of the molecule. For this reason, although common compounds can be identified, the data discussed cannot be used to extrapolate degradation mechanisms in less aggressive conditions, like those selected in this work. The same applies to a recent publication on the degradation of Acid Red 14 by microorganisms, in which, as in the previous work, products were identified by HPLC-MS, but in this case by

HRMS [33].

The first publication about degradation in the field of cultural heritage was focused on PR49:2 used by Rothko to paint the Harvard Murals in 1962 [7]. Light aging experiments, using a Xenon lamp, were performed both on the pigment applied as a powder and as a paint prepared with a collagen binding medium. XRD clearly shown that the pigment exists as the hydrazone tautomer. Molecular characterization of the products formed during irradiation was followed by infrared spectroscopy; the formation of sodium sulfate and a ring opening photoreaction are proposed [7]. Micro fading experiments were also carried suggesting that the binder increases the reaction rate. PR49:2 paints admixed with ultramarine blue were also tested and the authors concluded that it had no influence on the photodegradation rate.

More recently, a "systematic and comprehensive survey on the lightfastness properties of several pure synthetic artists' pigments, performed thanks to artificial ageing" [31], investigated keto-hydrazone colorants, applied as paints or spread as powders: PO5 (oil paint), PR3 (oil paint), PR48:1, PR49:2, PR53:1 (oil paint) and PR57:1 (gouache). Colorants were spread onto a glass slide, to be irradiated at $\lambda_{irr} > 300$ nm with a Xenon lamp, and aged samples were analyzed by infrared spectroscopy and pyrolysis coupled with GC/MS. Authors considered these ketohydrazone colorants as azo pigments. Py-GC/MS show the loss of SO_3^- group for PO46, PO49:2 and PR53:1, but not for PR48:1 and PR57:1. Analysis of the infrared spectra show the appearance of a broad band at 1710 and 1725 cm^{-1} ascribed to the formation of "carbonyl moieties in the aged samples, which may arise as a consequence of desulfonation and hydroxylation at the aromatic ring, followed by subsequent oxidation reactions". For PR48:1 and 49:2 additional formation of a band assigned to the O-H stretching, in the range between 3000 and 3500 cm^{-1}, was attributed to the formation of carboxylic acids. Color measurements were also performed based on reflectance spectra; the more drastic color changes were observed for PR48:1 and 53:1 [31].

Another important piece of information comes from the work of Worrall et al. [11], in their study of the effect of singlet molecular oxygen in the photodegradation of 1-arylhydrazone-2-naphthols. Irradiation was carried out at 450 nm in methanol, but I_0 values were not provided. Quantum yields of reactions are presented for AO7 and AO10 together with the contribution of singlet oxygen mechanism to the photodegradation: 11% for AO7 and 21% for AO10. The authors conclude that the predominant photooxidation pathways take place other than by singlet oxygen attack.

8.2. Experimental section

In this work, photodegradation studies of colorants listed in **Tables 8.1-8.2** were performed in homogeneous organic and aqueous solutions. At first, quantum yields of photodegradation, Φ_R, were obtained with monochromatic excitation at 313 nm to quantify and compare the photostability of colorants. Secondly, accelerated aging with polychromatic excitation (xenon-arc light source, $\lambda \geqslant 300$ nm) was included to investigate the degradation mechanisms by simulating exposure to light. Reaction kinetics was monitored by UV-VIS spectroscopy and the degradation products characterized by HPLC-DAD and UHPLC-HRMS.

8.2.1. Materials

SY14 (Sigma-Aldrich, dye content $\geqslant$95 %), AO7 (TCI chemicals, dye content >97.0%), AO10 (Alfa Aesar, Electrophoresis Grade), PR1 (Alfa Aesar, dye content 98.6 %), PR3, PR48:2, PR53:1, PR57:1 (Clariant), PR49:2 (Sun Chemicals), were used without further purification or recrystallization. All solvents used were spectrophotometric or HPLC grade. The absence of impurities in the commercial colorants was checked by HPLC-DAD.

8.2.2. Sample preparation

Two sets of samples were prepared for this work. To calculate Φ_R, solutions at concentrations in the range 7-10×10^{-5} M in H_2O, EtOH, 9:1 v/v EtOH-DMF mixture were prepared. Accelerated aging was instead performed on aqueous and ethanol solutions of SY14, AO7, AO10, PR1 at concentrations of approximately 1x10^{-3} M. For the preparation of the EtOH-DMF mixtures, PR3, PR48:2, PR53:1, PR49:2, PR57:1 were previously dissolved in DMF. Solutions were left to equilibrate for about two days at room temperature. Calculated volumes of DMF colorant solutions, pure DMF and EtOH were then mixed in order to reach the desired colorant concentration having 9:1 v/v volume ratio between solvents. DMF was found to be the most suitable solvent among various tested due to the scarce solubility of the colorants in organic solvents.

8.2.3. Determination of quantum yields of photodegradation

Solutions (2.5mL) were irradiated at 313 nm in the presence of O_2 (atmospheric conditions). Continuous magnetic stirring was avoided because of the formation of aggregates due to agitation. 2.5mL of each solution were kept in the dark for control. Initial absorbance at the 313-excitation wavelength of all solutions was around 0.6. This offered a better comparison of the calculated Φ_R values.
The intensity of the incident light (I_0) at 313 nm was measured using the potassium hexacyanocobaltate(III) ($K_3[Co(CN_6)]$) as chemical actinometer [34] at concentrations of 10^{-2} M (H_2O, pH=2). The I_0 was calculated, with correction for the absorbed light according to eqn (1):

$$I_0 = V_{sol}(\Delta A/\Delta\varepsilon)/(1000\Phi_R\Delta t) \qquad (1)$$

where, V_{sol} is the volume of irradiated solution in mL (2.5 mL); ΔA is the change in absorbance at the monitoring wavelength during irradiation (380 nm), Δt; $\Delta\varepsilon$ is the difference between ε of the reagent and product at the monitoring wavelength, 270 $Lmol^{-1}cm^{-1}$. The quantum yield, Φ_R, for the formation of pentacyanocobaltate (II) is 0.31. The calculated value of I_0 was 1.2x10^{-6} Einstein min^{-1}, obtained with a 15% estimated error.
The Φ_R were determined by monitoring colorant loss, at initial times, at the maximum absorption wavelengths of the colorants. The $\Delta\varepsilon$ calculated at the monitoring wavelength only considers the ε of the reagent as experimentally calculated for each solvent as the main products formed are colorless. Measurement of Φ_R were calculated with eqn (1) rearranged:

$$\Phi_R = V_{sol}(\Delta A/\Delta\varepsilon)/(1000I_{abs}\Delta t) \qquad (2)$$

where, I_{abs} is the light absorbed by the solution at the irradiation wavelength (313 nm); I_{abs} was made equal to I_0 x (1 - 10^{-A}) when $A < 2$. For more details please see Ref. [35].

8.2.4. Accelerated aging

Quartz cells containing solutions were placed inside the aging chamber. To avoid evaporation and loss of material, the polytetrafluoroethylene (PTFE) lids of the quartz cell were sealed with acrylic ester / PVC copolymer transparent glue, UHU. The quartz cells were irradiated for a maximum period of 100 hours. Small aliquots of the irradiated solutions were taken and analyzed with UV-Vis absorbance spectroscopy and HPLC-DAD and UHPLC-HRMS every 20 hours.

8.2.5. Apparatus

Monochromatic irradiations were performed, at 298 K, using a custom built set-up with an 200-W mercury-xenon lamp (Newport) from which the samples were placed at a distance of approximately 40 cm. A 313-nm bandpass filter (BrightLine® 315/15, nominal FWHM 20.4 nm) was placed between the lamp and quartz cell.

Table 8.3.: Absorption maxima in the visible (λ_{max}), molar extinction coefficients (ε) and quantum yields of reaction Φ_R (@λ_{irr} 313 nm); ε are also presented for 313 nm. (estimated error for the values presented $\leqslant$ 10%).

Colorant	Solvent	λ_{max} / nm	ε_{max} / Mol^{-1}cm^{-1}	ε_{313} / Mol^{-1}cm^{-1}	Φ_R
SY14	EtOH	478	13 200	6 530	3.1 x 10^{-5}
AO7	H_2O	484	16 600	7 140	2.6 x 10^{-5}
	EtOH	481	15 100	7 130	3.1 x 10^{-6}
AO10	H_2O	478	18 400	8 300	5.5 x 10^{-6}
	EtOH	498	16 800	9 280	5.1 x 10^{-6}
PR1	EtOH	483	15 500	6 690	2.4 x 10^{-5}
PR3	9:1 v/v EtOH-DMF	504	21 900	7 300	4.2 x 10^{-5}
PR48:2	9:1 v/v EtOH-DMF	526	22 200	7 120	3.8 x 10^{-5}
PR49:2	9:1 v/v EtOH-DMF	500	40 700	22 100	6.7 x 10^{-6}
PR53:1	9:1 v/v EtOH-DMF	486	37 800	17 100	7.3 x 10^{-6}
PR57:1	9:1 v/v EtOH-DMF	530	18 800	5 010	3.0 x 10^{-5}

Accelerating aging with polychromatic irradiation was carried out in a CO.FO.ME.GRA apparatus (SolarBox 3000e) (Milano, Italy) equipped with a xenon-arc light source ($\lambda \geqslant 300$ nm) with constant irradiation of 800 W/m^2. Temperature inside the apparatus was maintained at approximately 318K.

The UV-Vis absorption spectra were recorded on a Varian-Cary 100 Bio spectrophotometer, at room temperature.

HPLC-DAD-MS and UHPLC-High Resolution MS/MS (LC-HRMS/MS) analyses were conducted on a Dionex Ultimate 3000SD system with a diode array detector with a detection range between 220-800 nm, coupled inline to a LCQ Fleet ion trap mass spectrometer equipped with an ESI source (Thermo Scientific^{TM}, Waltham, MA, USA), and on an UHPLC Elute interfaced with a QqTOF Impact II mass spectrometer equipped with an ESI source (Bruker Daltoniks), respectively. The mass spectrometers were operated in the ESI positive and negative modes. The separation chromatographic was performed on a CORTECS RP18 column (Waters) using a gradient elution of 0.1% formic acid in water and as organic phase, acetonitrile or methanol. For details about LC-DAD-MS and LC-HRMS/MS settings, see Franca et al. [33].

8.3. Results and discussion

8.3.1. UV-VIS spectra

The absorption maxima (λ_{max}) and respective molar absorption coefficients (ε_{max}) are listed in **Table 8.3** together with the reaction quantum yields, Φ_R, obtained by irradiation at 313 nm. The experimental data used to calculate the ε_{max} is available in **Table E.1**.

For the reference compounds AO7 and AO10 it was possible to obtain these values in aqueous solutions, the solvent of choice for determining quantum yields of reaction. However, it was only possible to dissolve pigment reds in ethanol (EtOH) and, for most of the cases, they needed to be previously dissolved in dimethylformamide (DMF). For the pigment reds, ε_{max} ranges between 15000 and 41000 Mol^{-1}cm^{-1}, with a majority around 20000 Mol^{-1}cm^{-1} in agreement with a π-π* transition [36]. The reference compounds SY14, AO7 and AO10 also display values of characteristic of a π-π* transition. A comparison with published values is available in **Appendix E** (**Table E.3**).

For Sudan I in ethanol, the absorption maxima is at 478 nm, with a shoulder at 420 nm that cannot be attributed to the enol contribution, based on the following evidence. The sole presence of hydrazone tautomer

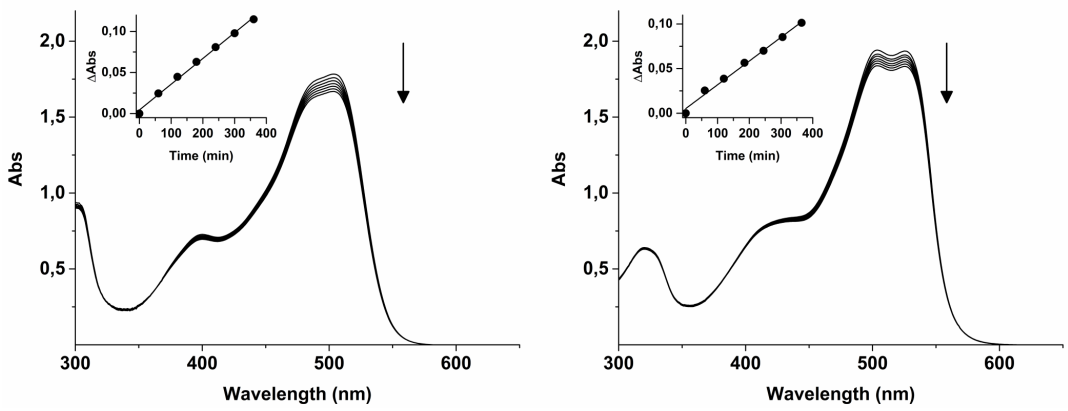

Figure 8.3.: UV-Vis absorption spectra in 9:1 v/v EtOH-DMF, irradiated at 313 nm, for *left*, PR3, in the inset is plotted the variation in absorbance at 504 nm, from which $\Phi_R = 4.2 \times 10^{-5}$ is calculated; *right*, PR48:2, in the inset, absorbance at 526 nm and $\Phi_R = 3.8 \times 10^{-5}$.

in sulfonated dyes has been confirmed [3], and in the spectrum of Orange II (AO7, a sulfonated dye), a similar shoulder at 424 nm is also observed. On Figure 4 in the work by Antonov, Stoyanov and Stoyanova published in 1995 [37], the maximum for the enol form in ethanol is predicted at 429 nm.
As a general trend, electron-donator groups in C(4') shift the absorption maxima to higher wavelengths (ca. 500-507 nm), whereas electron-withdrawing display spectra similar to Sudan I. Furthermore, substituents to the naphthalene ring also shift the absorption maxima to higher wavelengths, where carboxylate groups at C(3) lead to the appearance of a second maxima between 525-530 nm (PR48:2, PR57:1).

8.3.2. Quantum yields of photodegradation for naphthol reds

To the best of our knowledge, for the first time quantum yields of photodegradation, Φ_R, will be measured for the pigment reds listed in **Table 8.3**. For an accurate determination of reaction quantum yields we should ensure measurement accuracy for a single phenomenon as well as for the light absorbed. For this reason, values of Φ_R have been calculated at initial times to guarantee that a single event is being measured per photon absorbed at a specific wavelength, in this case, the degradation of the colorant at 313 nm, **Figure 8.3**.
Φ_R values ranging from $3x10^{-6}$ to $4x10^{-5}$ were obtained for the colorants studied, **Table 8.3**. Φ_R values bellow or equal to 10^{-6} are comparable to the lightfast pigment indigo, one of the most stable natural dyes and pigment [35,38]. In our study, the more stable chromophores are the sulfonated reference dyes, AO7 ($\Phi_R \approx 3x10^{-6}$) in EtOH, and AO10 both in water and ethanol solutions ($\Phi_R \approx 5x10^{-6}$). For AO7 in water an, unexplainable, tenfold increase in Φ_R is observed. For AO10, the SO_3 substituents are attached to the naphthalene moiety, whereas for AO7 they are found in the para position of the phenyl ring, C(4'), **Figure 8.1**. In literature [11], values closer to what obtained in water were calculated in methanol, irradiating at 450 nm: $5x10^{-5}$ for AO7 and $2x10^{-5}$ for AO10. For the moment, we cannot justify the fact that for AO10 no solvent effect is observed whereas for AO7 changing from ethanol to water dramatically affects Φ_R. This solvent effect will be discussed in more detail in the next section.
The first striking observation is that the lowest photodegradation quantum yields are obtained when electron-withdrawing groups are present at C(4') such as NO_2 and SO_3, **Figure 8.1**. As already detailed in the introduction, these groups lead to the sole presence of the hydrazone tautomer. Griffith ad Hawkins [39], in photo-oxidation experiments sensitized by Methylene blue, observed this same effect of "rate decreasing with the increasing electron-withdraw strength" of 1-arylhydrazone-2-naphthols substituted in the *para*-position.
For AO7, PR49:2 and PR53:1, quantum yields of photodegradation fall in the range of 10^{-6}, with the lowest value ascribed to the sulfonated dye AO7 in ethanol ($3x10^{-6}$). The exception in this series is PR1. On the

other hand, for electron-donating groups, a ten-fold increase is observed, with values similar to the calculated Φ_R values, 3-4x10^{-5}. PR3, PR48:2 and PR57:1 integrate this series, displaying a methyl group in the *para*-position, C(4'), **Figure 8.1**. Sudan I (SY14) is also included in this series, with Φ_R of 3x10^{-5}. In these pigments, it is possible that a certain amount of the azo form is present, although not as the major tautomer. In our experimental conditions, we assume that we will be exciting essentially the keto-form [40]. However, in literature the tautomeric equilibrium has been found as a rapidly exchanging mixture, so it is possible that in this series the enol form is present in the excited state, **Figure 8.1**. The data collected allow us to propose that the keto form is more stable to light with safer excited state deactivation channels that compete with photoreactions, and that this a result of electron withdraw groups that stabilize the keto-hydrazone form. Based on the available literature it is not possible to anticipate if it is based on a excited state cis-trans isomerization of conformers in S_1, **Figure 8.2**, an excited state proton transfer or both.

8.3.3. New insights into the degradation mechanisms of the basic structures of naphthol reds

To better understand the fundamental degradation mechanism at play, aging experiments irradiating with a Xenon lamp ($\lambda \geqslant 300$ nm) were carried out in two basic structures, AO7 and SY14. These studies allow the simulation, in much shorter times, of degradation that occurs during natural aging and can be used to obtain information on the products present on faded artworks. The results obtained irradiating until the color disappeared in AO7 and up to ca. 60% loss for SY14 are summarized in **Tables 8.4-8.6**. The concentration of the dye molecules decreased over time, with the formation of several intermediates, in very low yields, which were beyond the detection limit of the UV-VIS diode array. The proposed molecular structures for the main intermediates and final products are based on LC-DAD (**Figures E.1-E.3**) and HRMS/MS data (**Figures E.4-E.6**). Only cationic species were detected in this study. The ion formula for each proposed chemical structure was assessed based on accurate mass measurements of the precursor ion taking into account the accuracy and precision of the measurement parameters, such as error (ppm) and mSigma, **Tables 8.4-8.6**. The molecular formulae were validated through the fragmentation patterns, supporting the respective proposed chemical structure (**Figures E.7-E.15**). The identification of the degradation products is consistent with the shape of the UV-VIS spectrum, indicating the presence of conjugated benzene or naphthalene systems. The colorants were also analyzed by HRMS/MS (**Table E.5**) and the product ion spectra agree with what published in literature, Degano et al. [41] and Holcapek et al. [42] as well as [43].

The degradation of AO7 in ethanol and water has distinct intermediates and final products, in agreement with the difference in quantum yields calculated, **Table 8.3**. The products formed are, in both cases, colorless, **Tables 8.4** and **8.5**. In ethanol, as a result of the cleavage of the N-N bond, three compounds are formed which are derivatives of 2-methylnaphtho[1,2-d][1,3]oxazole, sharing common naphthol and oxazole moieties, **Table 8.4**. The major compound (m/z 184, t_R 26.2) and the cationic species with m/z 256 are formed via different mechanisms, involving addition reactions with ethanol. The cationic species m/z 256 results from an intermediate with m/z 228, $[C_{14}H_{13}NO_2]^+$, which was only detected in the full HR mass spectra, with a very low intensity. With the decrease in concentration of AO7, the major intermediate competes for light and possibly transforms into the product with m/z 212 and a t_R 29.5 min, **Table 8.4**. Thus, intermediates and final products elute after AO7. It is possible that desulfonation also occurs in the benzene moiety, but these intermediates were not detected. The UV-VIS spectra acquired agree very well with the spectra of a benzoic acid derivative.

On the other hand, in water, only two final products have been detected, phthalates, which are based on a keto-phenol ring and therefore elute before AO7. The major compound is characterized by m/z 167 and t_R 10.4 min; the other product by m/z 151 and t_R 9.9 min, **Table 8.5**. In this case, degradation is more extensive and in addition to the oxidative cleavage of the N-N bond, there is also a total loss of nitrogen

Table 8.4.: AO7 in ethanol, main degradation products identified by HPLC-DAD-MS and characterized by LC-HRMS/MS.

Proposed molecular structures	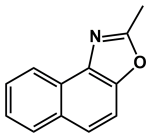	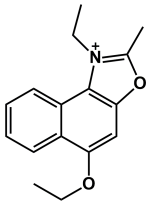	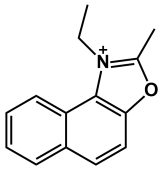
ESI(+)/MS (*m/z*)	184.0759	256.1332	212.1075
Ion formula Δ ppm; mSigma	$[C_{12}H_{10}NO]^+$ -0.1; 8.8	$[C_{16}H_{18}NO_2]^+$ -0.1; 13.3	$[C_{14}H_{14}NO_2]^+$ -0.4; 11.0
t_R/ min	26.2	28.9	29.5
λ_{max} / nm	222; 276; 320	226; 282; 324	226; 278; 324
Obs	major compound, appears at 40h of irr.	minor compound, appears at 60h of irr.	minor compound, appears at 80h of irr.

Table 8.5.: Main degradation products of A07 in water identified by HPLC-DAD-MS and characterized by LC-HRMS/MS.

Proposed molecular structures	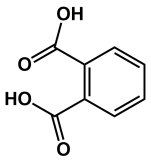	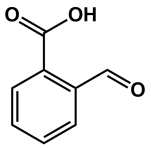
ESI(+)/MS (*m/z*)	167.0345	151.0382
Ion formula Δ ppm; mSigma	$[C_8H_7O_4]^+$ -3.9; 28.1	$[C_8H_7O_3]^+$ -4.7; 29.9
t_R / min	10.7	10.2
λ_{max} / nm	226; 278	232; 274
Obs	major compound, appears at 40h of irr.	minor compound, appears at 40h of irr.

Table 8.6.: Main degradation products of SY14 in ethanol identified by HPLC-DAD-MS and characterized by LC-HRMS/MS. The major degradation products were detected at 80h of irradiation.

Proposed molecular structures	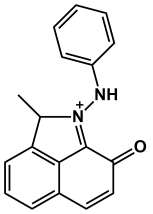	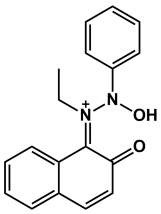	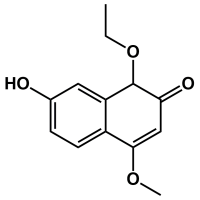	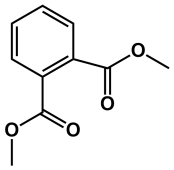
ESI(+)/MS (*m/z*)	275.1184	293.1290	235.0974	195.0663
Ion formula Δ ppm; mSigma	$[C_{18}H_{15}N_2O]^+$ -1.7; 14.1	$[C_{18}H_{17}N_2O_2]^+$ -1.5; 3.4	$[C_{13}H_{15}O_4]^+$ -2.9; 24.1	$[C_{10}H_{11}O_4]^+$ -4.9; 19.2
t_R / min	23.8	22.7	22.1	11.1
λ_{max} / nm	234; 312; 480	234; 316; 480	260; 414	234; 278
Obs	major compound, appears at 80h of irr.	major compound, appears at 80h of irr.	minor compound, appears at 80h of irr.	detected only at 100h irr.

atoms and ring opening with formation of carboxylic groups. This type of functional groups was also detected by Degano et al. [31]. Thus, in water degradation is so extensive that it almost reaches the degree in which small volatile fragments are produced, which again agrees with the higher quantum yield of reaction calculated in water, **Table 8.3**. Meetani et al. [32] also observed this kind of extensive degradation, leading to the formation of intermediate products that include "substituted phenols, aromatic hydroxyl amine, nitroso compounds and dicarboxylic aromatic compounds". In their conditions, irradiation at 254 nm in the presence of catalysts, different intermediates and products are observed, which allow us to propose that different mechanistic pathways occur when irradiating at 254 nm or at wavelengths lower than 300 nm.

The two major products identified during the degradation of SY14 in ethanol (*m/z* 275 and *m/z* 293), displayed an UV-VIS spectrum still showing the absorption band related to the azo-group conjugated with naphthalene. It is proposed that *m/z* 275 arises from an intermediate (not identified in the mass spectra) formed by reaction with ethanol, whereas *m/z* 293 results from hydroxylation of a nitrogen in the azo group. The two other compounds include a phthalate as the minor degradation product with *m/z* 195, **Table 8.6**. Reflecting a lower and higher degradation of the original molecule, as observed for AO7 in ethanol and water, respectively.

The stability of the final products identified for AO7 and SY14 should be investigated in future work. However, the results obtained for AO7 clearly show that the solvent, representing the dye environment, plays a crucial role in degradation, which explains one of the main conclusions obtained by Stenger et al. [7], when studying the degradation of Lithol Red pigments, "that the binding medium facilitates the photodegradation". Indeed, pigments dispersed in media can lead to almost total color loss in artificial ageing conditions. The in-depth study of basic structures like AO7 and SY14 are crucial to provide a complete rational of the reaction mechanisms at play in more complex systems that should include pigment reds in polymer networks within paints and plastics. Work currently in progress will allow to verify how electron-withdrawing groups enhance dye lightfastness [40], and to provide a consistent picture of the substituent effects on the lightfastness of these class of dyes.

8.4. Conclusions

β-naphthol reds studied in this work are better described as 1-arylhydrazone-2-naphthol systems. Based in this knowledge, we investigated the effect of substituents on fading. Φ_R values ranging from $3x10^{-6}$ to $4x10^{-5}$ were obtained and show that keto forms are generally more stable and that the sulfonate groups have a stabilizing effect. Considering the importance of the sulfonate groups, in future work, two other compounds can be added to the list in **Tables 8.1-8.2**, AO7 structure with SO_3Na in *orto*-position and a dye in which the NO_2 group in PR3 is substituted by SO_3Na.

This research has demonstrated the impact of solvent on stability, that has wider implications for the role of polymer medium on the lightfastness of colourants. A tenfold increase in the stability of Orange II (AO7) in ethanol was observed when compared to water. This was confirmed by the extent of degradation obtained through the final products characterized by LC-HRMS. The N-N bond is possibly the weak link in these systems and this allows us to predict that, in addition to the influence of the solvent, pH will also influence the stability of these colors. Future experiments should test the effect of pH and medium on the disappearance of color. Ongoing research will verify how electron-withdrawing groups enhance dye stability, and will provide a consistent picture of the substituent effects on the lightfastness of these class of dyes [40]. In future work, Φ_R values using visible light (for example with irradiation at 436 nm) should be calculated to verify the trend obtained using 313 nm.

In summary, the knowledge gathered in this work provides a major advance in our understanding of the stability of 1-arylhydrazone-2-naphthol systems. Quantum yields of photodegradation allow us to identify the most unstable structures and HRMS data reveals the evolution of photodegradation products. The methodology developed in this investigation can now be used to investigate substituent effects on the lightfastness of azo dyes, to understand how colourants in plastics may age in museum collections where UV light is excluded.

8.5. References

[1] Melo MJ, Nevin A, Baglioni P. Special issue of pure and applied chemistry devoted to "Chemistry and cultural heritage". Pure Appl Chem. 2018; 90(3): 429-433. DOI: 10.1515/pac-2018-0106.

[2] Berrie BH, Lomax SQ. Azo pigments: their history, synthesis, properties, and use in artists' materials. Studies in the History of Art 1997; 57: 8-33. URL: jstor.org/stable/42622254

[3] Kennedy AR, Stewart H, Eremin K, Stenger S. Lithol red: a systematic structural study on salts of a sulfonated azo pigment. Chem Eur J. 2012; 18: 3064-3069. DOI: 10.1002/chem.201103027.

[4] Gorelik T, Schmidt MU, Brüning J, Beko S, Kolb U. Using electron diffraction to solve the crystal structure of a laked azo pigment. Cryst Growth Des. 2009; 9: 3898-3903. DOI: 10.1021/cg801099r.

[5] Bekö SL, Hammer SM, Schmidt MU. Crystal Structures of the hydration states of Pigment Red 57:1. Angew Chem Int Ed. 2012; 51: 4735-4738. DOI: 10.1002/anie.201109082.

[6] de Keijzer M. The delight of modern organic pigment creations. In: van den Berg K, Burnstock A, de Keijzer M, Krueger J, Learner T, de Tagle A, Heydenreich G, editors. Issues in contemporary oil paint, Cham: Springer; 2014, p. 45-73.

[7] Stenger J, Kwan EE, Eremin K, Speakman S, Kirby D, Stewart H, Huang SG, Kennedy AR, Newman R, Khandekar N. Lithol red salts: characterization and deterioration. e-Preservation Sci. 2010; 7: 147-157. URL: e-preservationscience/2010/Stenger-29-05-2010

[8] Standeven HAL. The history and manufacture of lithol red, a pigment used by Mark Rothko in his Seagram and Harvard Murals of the 1950s and 1960s. Tate Papers 2008; 10.

[9] de Groot S, van Keulen H, Megens L, van Oosten T, Wiresma H. Discolouration of plastics objects: investigation into composition using various analytical techniques. In: Bechthold T, editor. Future Talks 013 – Lectures and workshops on technology and conservation of modern materials in design. Munich: Die Neue

Sammlung – The Design Museum; 2015. p. 19-26.
[10] Angelin EM, França de Sá S, Picollo M, Nevin A, Callapez ME, Melo MJ. The identification of synthetic organic red pigments in historical plastics: developing an in situ analytical protocol based on Raman microscopy. J Raman Spectrosc. 2021; 52: 145-158. DOI: 10.1002/jrs.5985.
[11] Jansen LMG, Wilkes IP, Wilkinson F, Worrall DR. The role of singlet molecular oxygen in the photodegradation of 1-arylazo-2-naphthols in methanol and on cotton. J Photochem Photobiol A 1999; 125(1-3): 99-106. DOI: 10.1016/S1010-6030(99)00095-7.
[12] Eastaugh N, Walsh V, Chaplin T, Siddall R. Pigment compendium – A dictionary and optical microscopy of historical pigments. Oxford: Elsevier Ltd; 2008.
[13] Aiken S, Gabbutt CD, Gillie LJ, Heywood JD, Jacquemin D, Rice CR, Heron BM. The remarkable hyperchromicity of ketohydrazone dyes and pigment lakes derived from 4-morpholino-2-naphthol. Eur J Org Chem. 2013; 36: 8097-8107. DOI: 10.1002/ejoc.201390103.
[14] Gilli P, Bertolasi V, Pretto L, Antonov L, Gilli G. Variable-temperature X-ray crystallographic and DFT computational study of the N-H$\cdots$O/N$\cdots$H-O tautomeric competition in 1-(arylazo)-2-naphthols. Outline of a transiton-state hydrogen-bond theory. J Am Chem Soc. 2005; 127(13): 4943-4953. 10.1021/ja0453984.
[15] Bertolasi V, Gilli P, Gilli G. Crystal chemistry and prototropic tautomerism in 2-(1-Iminoalkyl)- phenols (or naphthols) and 2-diazenyl-phenols (or naphthols). Curr Org Chem. 2009; 13(3): 250-268. DOI: 10.2174/138527209787314841.
[16] Joshi H, Kamounah FS, Gooijer C, van der Zwan G, Antonov L. Excited state intramolecular proton transfer in some tautomeric azo dyes and schiff bases containing an intramolecular hydrogen bond. J Photochem Photobiol A 2002; 152(1-3): 183-191. DOI: 10.1016/S1010-6030(02)00155-7.
[17] Olivieri AC, Wilson RB, Paul IC, Curtin DY. Carbon-13 NMR and x-ray structure determination of 1-(arylazo)-2-naphthols. Intramolecular proton transfer between nitrogen and oxygen atoms in the solid state. J Am Chem Soc. 1989; 111(15): 5525-5532. DOI: 10.1021/ja00197a003.
[18] Guan PJ, Cui G, Fang Q. Computational photochemistry of the azobenzene scaffold of Sudan I and Orange II dyes: excited-state proton transfer and deactivation via conical intersections. ChemPhysChem. 2015; 16(4): 805-811. DOI: 10.1002/cphc.201402743.
[19] Savarese M, Brémond É, Antonov L, Ciofini I, Adamo C. Computational insights into excited-state proton-transfer reactions in azo and azomethine dyes. ChemPhysChem. 2015; 16(18): 3966-3973. DOI: 10.1002/cphc.201500589.
[20] Harris RK, Jonsen P, Packer KJ, Campbell CD. Carbon-13 NMR of solid phenylazo-2-naphthols: tautomerism and (13C, 14N) residual dipolar coupling. Magn Reson Chem. 1986; 24: 977-983. DOI: 10.1002/mrc.1260241110.
[21] Ferreira GR, Costa Garcia H, Couri MRC, Dos Santos HF, de Oliveira LFC. On the azo/hydrazo equilibrium in Sudan I azo dye derivatives. J Phys Chem A 2013; 117(3): 642-649. DOI: 10.1021/jp310229h.
[22] Kennedy AR, McNair C, Smith WE, Chisholm G, Teat SJ. The first red azo lake pigment whose structure is characterized by single crystal diffraction. Angew Chem Int Ed. 2000; 39 :638-640. DOI: AID-ANGE652%3E3.0.CO;2-N.
[23] Schmidt MU, Buchsbaum C, Schnorr JM, Hofmann DWM, Ermrich M. Pigment Orange 5: crystal structure determination from a non-indexed X-ray powder diagram. Z Kristallogr. 2007; 222: 30-33. DOI: 10.1524/zkri.2007.222.1.30.
[24] Hunger K, Schmidt MU. Hydrazone pigments (formerly called azo pigments). In: Industrial organic pigments: production, crystal structures, properties, applications. Weinheim: Wiley-VCH, fourth completely revised ed.; 2018. p. 193-195.
[25] Weller A. Quantitative untersuchungen der fluoreszenzumwandlung bei naphtholen. Z Elektrochem. 1952; 56(7): 662-668. DOI: 10.1002/bbpc.19520560714.
[26] Weller A. Allgemeine basenkatalyse bei der elektrolytischen dissoziation angeregter naphthole. Z Elektrochem. 1954; 58(10): 849-853. DOI: 10.1002/bbpc.19540581006.

[27] Kobayashi T, Degenkolb EO, Rentzepis PM. Picosecond spectroscopy of 1-phenylazo-2-hydroxynaphthalene. J Phys Chem. 1979; 83(19): 2431-2434. DOI: 10.1021/j100482a001.
[28] Kobayashi T, Saito T. 2 – Ultrafast dynamics in the excited states of azo compounds. In Sekkat Z, Knoll W, editors. Photoreactive organic thin films, USA: Elsevier Science; 2002, p. 49-62.
[29] Gil M, Organero JA, Peris E, García H, Douhal A. Confinement effect of nanocages and nanotubes of mesoporous materials on the keto forms photodynamics of Sudan I. Chem Phys Lett. 2009; 474(4-6): 325-330. DOI: 10.1016/j.cplett.2009.05.002.
[30] Douhal A, Sanz M, Tormo L. Femtochemistry of orange II in solution and in chemical and biological nanocavities. Proc Natl Acad Sci. 2005; 102(52): 18807-18812. DOI: 10.1073/pnas.0507459102.
[31] Ghelardi E, Degano I, Colombini MP. Mazurek J, Schilling M, Khanjian H, Learner T. A multi-analytical study on the photochemical degradation of synthetic organic pigments. Dyes Pigm. 2015; 123: 396-403. DOI: 10.1016/j.dyepig.2015.07.029.
[32] Meetani MA, Rauf MA, Hisaindee S, Khaleel A, AlZamly A, Ahmad A. Mechanistic studies of photoinduced degradation of Orange G using LC/MS. RSC Adv. 2011; 1: 490-497. DOI: 10.1039/C1RA00177A.
[33] Franca RDG, Conceição Oliveira M, Pinheiro HM, Lourenço ND. Biodegradation products of a sulfonated azo dye in aerobic granular sludge sequencing batch reactors treating simulated textile wastewater. ACS Sustainable Chem Eng. 2019; 7(17): 14697-14706. DOI: 10.1021/acssuschemeng.9b02635.
[34] Pina F, Moggi L, Manfrin M, Balzani V, Hosseini M, Lehn JM. Photochemistry of supramolecular systems-size and charge effects in the photoaquation of adducts of the hexacyanocobaltate (III) anion with polyammonium macrocyclic receptors. Gazz Chim Ital. 1989; 119(1): 5-67.
[35] Sousa MM., Miguel C, Rodrigues I, Parola AJ, Pina F, de Melo JSS, Melo MJ. A photochemical study on the blue dye indigo: from solution to ancient Andean textiles. Photochem Photobiol Sci 2008; 7: 1353-1359. DOI: 10.1039/B809578G.
[36] Valeur B, Berberan-Santos MN. Molecular fluorescence: principles and applications. Weinheim: Wiley-VCH, second ed.; 2012. p. 33-52.
[37] Antonov L, Stoyanov S, Stoyanova T. Tautomeric equilibrium in 1-phenylazo-2-naphthol – A quantitative study. Dyes Pigm. 1995; 27(2): 133-142. DOI: 10.1016/0143-7208(94)00042-Z.
[38] Miliani C, Monico L, Melo MJ, Fantacci S, Angelin EM, Romani A, Janssens K. Photochemistry of artists' dyes and pigments: towards better understanding and prevention of colour change in works of art. Angew Chem Int Ed. 2018; 57: 7324-7334. DOI: 10.1002/anie.201802801.
[39] Griffiths J, Hawkins C. Oxidation by singlet oxygen of arylazonaphthols exhibiting azo-hydrazone tautomerism. J Chem Soc Perkin Trans 2 1977: 747-752. DOI: 10.1039/P29770000747.
[40] Allen NS. Photofading mechanisms of dyes in solution and polymer media. Rev Prog Coloration 1987; 17(1): 61-71. DOI: 10.1111/j.1478-4408.1987.tb03752.x.
[41] Sabatini F, Degano I. Investigating the fragmentation pathways of β-naphthol pigments using liquid chromatography/electrospray ionization quadrupole time-of-flight mass spectrometry. Rapid Commun Mass Spectrom. 2020; 34: e8789. DOI: 10.1002/rcm.8789.
[42] Holčapek M, Volná K, Vaněrková D. Effects of functional groups on the fragmentation of dyes in electrospray and atmospheric pressure chemical ionization mass spectra. Dyes Pigm. 2007; 75(1): 156-165. DOI: 10.1016/j.dyepig.2006.05.040.
[43] Lech K, Wilicka E, Witowska-Jarosz J, Jarosz M. Early synthetic dyes – A challenge for tandem mass spectrometry. J Mass Spectrom. 2013; 48(2): 141-147. DOI: 10.1002/jms.3090.

This is an Accepted Manuscript of an article published by MDPI AG in Polymers, on 12/07/2021:

Micheluz A, Angelin EM, Almeida Lopes J, Melo MJ, Pamplona M. Discoloration of historical plastic objects: new insight into the degradation of β-naphthol pigment lakes. Polymers 2021; 13: 2278. DOI: 10.3390/polym13142278.

9. Discoloration of historical plastic objects: new insight into the degradation of β-naphthol pigment lakes

Abstract

Light is a determining factor in the discoloration of plastics, and photodegradation processes can affect the molecular structures of both the polymer and colorants. Limited studies focused on the discoloration of heritage plastics in conservation science. This work investigated the discoloration of red historical polyethylene (PE) objects colored with PR 48:2 and PR 53:1. High-density and low-density PE reference polymers, neat pigment powders, and historical samples were assessed before and after accelerated photoaging. The applied methodology provided insight into the individual light-susceptibility of polyethylenes, organic pigment lakes, and their combined effect in the photoaging of historical plastic formulations. After light exposure, both PE references and historical samples yellowed, PR53:1 faded, and PR 48:2 darkened; however, both organic pigments faded severely in the historical samples. This highlights the role played by the plastic binder likely facilitating the pigment photofading. Fourier transform infrared spectroscopy and mass spectrometry techniques – EGA-MS, PY-GC/MS, and TD-GC/MS – were successfully employed for characterizing the plastic formulations and degradation. The identification of phthalic compounds in both aged β-naphthol powders opens new venues for studies on their degradation. This work's approach and analytical methods in studying the discoloration of historical plastics are novel, proving their efficacy, reliability, and potentiality.

9.1. Introduction

Museums are traditionally dedicated to collecting, investigating, preserving, and exhibiting testimonies from the past and portraying memories associated with their role and impact, among others, in the social context. The development of man-made polymers from the mid-19th century significantly changed the modern world. Those changes cover all the aspects of society, including the lifestyle. Therefore, polymer-based objects are now increasingly common in heritage collections as testimonies of our past. Today, plastic objects are found in every type of museum worldwide, ranging from designer pieces and unique and valuable artworks to mass-produced objects, partially or entirely made of plastic.

Since the first Parkesine plastics became popular [1], semi-synthetic and synthetic plastic objects have been made in all different shapes, sizes, and colors, thanks to the versatility of these materials and the manufacturing development from the early 20th century onwards. Between the visible characteristics, color is the property that made plastics so attractive, especially in modern plastic-based objects generally characterized by vibrant and colorful surfaces [2].

Additives are often mixed/blended with the basic polymer in the plastic formulation. The addition of these chemicals (e.g., plasticizers, flame retardants, antioxidants, acid scavengers, light and heat stabilizers, lubricants, antistatic agents, colorants, etc.) in plastic manufacturing improves the processing, end-use performance, and aging properties of the polymer. Since most plastic resins are weakly colored (white-to-pale

yellow) or colorless, colorants can be added to the polymer resin in the manufacturing process to internally color the formulation and impart a visible color to the plastic objects [3-5]. This will influence the aesthetics of plastic objects, such as the color appearance, turning a commodity plastic into a more visually pleasing product [6-8].

In the world of plastics, hundreds of synthetic colorants appear in the colorists' palette. Following the literature of plastic coloring technology [3-5], colorants are used in very small concentrations (0.1-5%), in the form of soluble organic dyes or as finely divided insoluble organic/inorganic pigments. They offer a wide range of colors for standard coloration, and the use of specific colorant types (e.g., metallic, pearlescent, fluorescent, phosphorescent, thermochromic, and photochromic) can impart a "special effects" appearance. Colorants can be used in pure tone or mixed to achieve the desired color appearance. Often additives such as fillers and extenders are incorporated into the plastic resin, together with the colorants, to improve processing, physical and mechanical properties, or to reduce cost.

Plastics in collections are challenging to preserve, as they tend to degrade faster than other materials found in artworks [9-17]. Synthetic organic/inorganic pigments also have stability issues [18-25] and their alteration in modern polymeric paints continues to be a subject of ongoing research in art conservation [26-31]. Both polymers and pigments are known to be sensitive towards aging, which can lead to color change.

Discoloration (alteration of original color) of plastic materials dramatically affects the perception of a wide range of polymer-based objects [1,32,33], making its study a research priority in conservation science of cultural heritage. When a color change is visible in aged plastic, a chemical reaction has already taken place. Discoloration is usually a symptom of photo-induced damage, where light caused chemical changes at the molecular level in the polymer matrix and/or colorants. Free radicals and atmospheric oxygen can also be involved in the chemical reactions.

The photodegradation of polymer resins and its contribution to discoloration (yellowing and darkening) has been widely studied [34-38], while only recently, the fading of organic pigments has been evaluated in conservation science, focusing mainly on the identification of the faded organic pigments in historical plastic objects [39-41]. Although few key research studies from the polymer science community discussed the degradation of pigmented polymers [42-44], they were not comprehensive enough in describing the photo-fading mechanisms of the organic pigments.

The study of the organic pigments and their fading phenomena in historical plastics represents a methodological and analytical challenge, firstly because of technical difficulties in their identification [41], secondly due to the complexity of their degradation pathways [43], and thirdly due to the often-unknown exposure (duration and intensity) to the agents of degradation (environmental factors). Once the decay mechanism starts, it is usually irreversible, and the pigment modification results in a chemical change of the molecule's pigment structure that causes a color shift or loss. The light-resistance of organic pigments is always related to the whole plastic system. Therefore, besides the intrinsic fastness properties of the pigment, the properties of polymer and additives can affect the organic pigments' light stability. Polymers have different photo-reactivity depending on their chemistry and structure. Their role is key in pigment photodegradation as they constitute the major component of the pigment environment. Indeed, the polymeric matrix can trigger or be part of the chemical reactions that cause the pigment degradation. So far, most of the studies about the interaction between polymers and synthetic organic pigments in heritage science were focused on the conservation of modern polymeric paints with synthetic binders [45-52]. Additives play a two-fold role in the photo-fading mechanism: (i) on one hand, chemicals such as light stabilizers and antioxidants improve the color stability and prolong the objects' longevity by protecting the plastic against harmful environmental factors (e.g., light and oxygen); (ii) on the other hand, the chemistry of all possible interactions in the triad polymer-pigment-additives has not been fully understood and so estimations of the process outcome are difficult.

β-naphthol pigment reds, substituted 1-arylhydrazone-2-naphthols, are the most extensive family of organic red colorants [53]. Their impact is well-documented in historical sources [54-57]. They were one of the first

pigment categories used in the coloring of plastics [54,55] and the subject of relevant publications [55,58-67]. In historical collections, problems related to their fading in printing inks [68], modern and contemporary paintings [69], as well as plastic artifacts [39,41] are well-documented. Nevertheless, little is known about their photochemistry in cultural heritage collections because few studies have focused on their degradation [70-72]. C.I. Pigment Red (PR) 48 (C.I. no. 15865) and C.I. PR 53 (C.I. no. 15585) pigment-type lakes were highlighted as photosensitive in polyolefin plastics [39,41]. However, their fading has not been studied yet, nor the influence of the formulation components on their degradation.

In this work, the discoloration of red historical polyethylene (PE) objects colored with PR 48:2 and PR 53:1 was investigated by a novel stepwise approach. The aim was to characterize the light-induced alterations of the polymer and organic pigments. To this end, the analytical strategy was planned to firstly identify the formulations' constituents of the historical samples, secondly analyze separately the discoloration of the polymer matrix and β-naphthol pigment lakes due to photodegradation, and thirdly observe their combined effect on a plastic formulation. As PE can display different amounts of chain branching, high-density (HD) and low-density (LD) PE polymer references were considered. PR 48:2 and PR 53:1 in powder form served as references for the pigments in the study. Formulations of PE with organic pigments were chosen to be taken from real historical objects, although being naturally aged to an unknown extent, because they were industrially produced with methods from the past, likely similar to those implemented in other cultural objects. Within the timeframe of this study, unaged reference formulations reproducing historical production methods were not achievable, remaining therefore a topic for future research. Samples were assessed before and after photoaging experiments by means of Fourier transform infrared spectroscopy (FTIR) and mass spectrometry (MS) techniques. Colorimetric measures and microscope observations were made to characterize the color changes. An accelerated aging test was used to simulate the discoloration process. As wavelengths no longer than ca. 290 nm reach the earth's surface, radiation at $\lambda \geqslant 300$ nm would probably be absorbed by the chromophores present in the plastics, reproducing a real exposure scenario. The PE polymer was selected as its photochemistry is well-known [73,74] and because β-naphthol pigments were widely used in the past to color polyolefins [3-5,54]. This study also led to exploring the applicability and effectiveness of MS-based techniques in the molecular characterization and degradation assessment of both polymer and organic pigments. To these ends, the performance of evolved gas analysis-mass spectroscopy (EGA-MS) and thermal desorption-gas chromatography/mass spectrometry (TD-GC/MS), combined with pyrolysis-gas chromatography/mass spectrometry (Py-GC/MS), were tested. Unsupervised modeling principal component analysis (PCA) was applied to help with the interpretation of multivariate thermographic datasets.

9.2. Materials and Methods

9.2.1. Samples

Historical plastic objects: The selection includes two food containers with a white body and red lid from the 1950s-1970s, gathered from a Portuguese private collection. One container has a printed red lettering inscription reading "*Açucar*" ("sugar", all the translations in the paper were made by the authors) and the other a three-dimensional (3D) red lettering inscription reading "*GRÃO*" ("chickpea") (**Figure 9.1, top**). No color alterations were observed for lid 1, while lid 2 showed an inhomogeneous color as a consequence of discoloration (**Figure 9.1, bottom**). In a previous study, Angelin et al. [41] characterized lid 1 and lid 2 as made of PE, and identified PR 48 and PR 53 as the main red coloring agents of lids 1 and 2, respectively. Further results on their elemental and molecular characterization are summarized in **Table F.1** [41]. Both PR 48 and PR 53 pigment-type lakes can be complexed by more than one cation type [53]. Since only Ca was detected as a possible counter ion in lid 1, the presence of calcium salt type PR 48:2 is suggested. Lid 2 is most likely colored with the barium PR 53:1 type, considering that all the other salts do not or have little

Figure 9.1.: The historical plastic objects under study, lid 1 made of PE with PR 48:2 (bottom left), lid 2 made of PE with PR 53:1 (bottom right).

value in plastic applications [4,5].

HDPE and LDPE Polymers: Polymer reference samples (unaged) were obtained from non-colored and additive-free formulations of high-density polyethylene (HDPE) and low-density polyethylene (LDPE) (Repsol Polímeros, Sines, Portugal). With a JCS Shinha press and mold plates, pellets of HDPE and LDPE were molded into circular disks of 2.5 cm diameter by the application of heat (160 °C) and pressure (400 psi) for 3 to 5 min. Samples of ca. 1 mm of thickness were obtained. Samples No. 25 (HDPE) and 24 (LDPE) from the ResinKit^{TM} collection [33] also served as reference materials. In this study, these samples were exclusively used to facilitate interpretation of the PCA results.

Synthetic organic pigments: PR 48:2 and PR 53:1 (Clariant, Muttenz, Switzerland) pigments were used as reference pigment powders without purification or recrystallization. Molecular structures of the red synthetic organic pigments are reported in **Table F.2**.

9.2.2. Artificial aging

Accelerating aging with polychromatic irradiation was carried out in a CO.FO.ME.GRA apparatus (SolarBox 3000e) (Milan, Italy) equipped with a Xenon-arc light source ($\lambda \geqslant 300$ nm) with constant irradiation of 800 W/m^2. Temperature inside the apparatus was maintained at approximately 40 °C. The experimental setup for artificial aging is shown in **Figure F.1**. The reference and historical plastic samples were cut in two different sizes (ca. $5 \times 5 \times 1$ mm^3, ca. $12 \times 12 \times 1$ mm^3), then placed in 10×10 quartz cuvettes (type-110 QS, cutoff $\lambda = 190$ nm, Hellma GmbH, Müllheim, Deutschland) and under a Pyrex glass (cutoff $\lambda = 280$ nm). The quartz cells were not closed with a cap during the aging experiment and, after monitoring measurements, the same surface of the samples was exposed to irradiation. Approximately 10 mg of organic pigment powders were placed onto a glass slide (single concavity) and covered with a Pyrex glass. Samples were irradiated for 110h (t_1), 220h (t_2), 550h (t_3), 770h (t_4). Another set of samples was kept in the dark for control, 0h (t_0). Historical lids and polymer references samples were considered homogenous having a uniformly dispersed composition of the plastic material. During the aging experiment, the historical lids (ca. $12 \times 12 \times 1$ mm^3) were analyzed by ATR-FTIR. At each irradiation time one sample (ca. $5 \times 5 \times 1$ mm^3) for each lid was taken and analyzed by EGA-MS and Py-GC/MS. To compare the results of the aged historical samples, ATR-FTIR and EGA-MS analysis were carried out on the HDPE and LDPE samples following the same experimental procedure in order to characterize the photo-induced molecular changes of the polymer references. All samples were observed under the stereomicroscope and color variation of the plastic samples

was monitored by colorimetry. Organic pigment powders were characterized before (t_0) and after (t_4) artificial aging by EGA-MS and Py-GC/MS. Sampling of the samples at the uppermost layer of the exposed surface was performed for MS measurements.

9.2.3. Attenuated Total Reflection Fourier-Transform Infrared Spectroscopy (ATR-FTIR)

The exposed surfaces of the historical and polymer reference samples were characterized by IR spectroscopy in attenuated total reflection (ATR-FTIR) with the Handheld 4300 FTIR spectrophotometer (Agilent Technologies Inc., Santa Clara, CA, USA), equipped with a ZnSe beam splitter, a Michelson interferometer, and a thermoelectrically cooled DTGS detector. Spectra were acquired with a diamond ATR module, 128 scans, and 4 cm^{-1} resolution, between 4000 and 650 cm^{-1}. This ATR module allows the analysis of samples with a minimum size of 200 μm. Background spectra were collected between every acquisition. The OriginPro 8 (OriginLab Corportation, Northampton, MA, USA) software was used to analyze the spectra, which are shown as acquired, without baseline corrections or normalizations. The same spot of the plastic surface was analyzed at each of the artificial aging intervals to guarantee monitoring accuracy.

9.2.4. Color measurements

A Microflash mobile colorimeter (DataColor International, Lucerne, Switzerland) was employed for measuring and monitoring the color of the historical and polymer reference samples during the artificial aging. The colorimeter was equipped with a Xenon lamp. The 1976 CIELAB color coordinates (L*, a*, b*) were calculated over an 8 mm diameter measuring area, considering the D65 standard illuminant and the 10° colorimetric observer (CIE 1964). The reflected specular component (SCE mode) was excluded from the measurements. The instrument was calibrated with a white (100% reflective) and black (0% reference) balance, in accordance with the DataColor calibration procedure. The white (porcelain) and black trap standards were provided by the manufacturer. Both the equipment measuring head and the sample were placed in a custom-made positioning mask, which allowed to obtain color measurements on the same area at each artificial aging interval. The reported values are the average of three measurements collected on the measurement area of the exposed plastic surfaces, which proved to be sufficient to guarantee reproducibility. Total color variation was calculated according to CIELAB 1976 (ΔE^*_{ab}) and CIEDE 2000 (ΔE_{00}) expressions [75].

9.2.5. Optical Microscopy (OM)

OM was used to identify the color and distribution of the pigment particles in the historical plastic samples before and during artificial aging. Images were acquired using a Axioplan 2 Imaging system (HAL 100) (Zeiss, Oberkochen, Germany) coupled to a DXM1200F digital camera (Nikon Corporation, Tokyo, Japan) and ACT-1 software (Nikon Corportation, Tokyo, Japan). Dark-field illumination was used.

9.2.6. Stereomicroscope

All samples were observed before and at the different irradiation times under a MZ16 stereomicroscope (Leica Microsystems GmbH, Wetzlar, Germany) (7.1× to 115× zoom range), and images were acquired using a Leica ICD digital camera and a fiber-optic light Leica system (Leica KI 1500 LCD) coupled with the stereomicroscope.

9.2.7. Evolved Gas Analysis-Mass Spectroscopy (EGA-MS)

The exposed surfaces of the historical and polymer reference samples as well as the pigments in powder were analyzed by EGA-MS. Around 200 μg of each sample was added directly into an 80 μL stainless-steel Eco-cup

sample holder (Frontier Laboratories Ltd., Koriyama, Japan) and analyzed by a Multi-shot Pyrolyzer EGA/PY-3030D (Frontier Laboratories Ltd.). The temperature program was set up from 100 to 700 °C (hold for 5 min) at a ramp of 20 °C/min. Evolved gas was transferred directly into the 5977B MSD mass spectrometer (Agilent Technologies Inc., Santa Clara, CA, USA) through a deactivated and uncoated stainless-steel transfer Frontier Ultra Alloy® EGA tube (UADTM 2.5N-2.5m-I.D. 0.15 mm, O.D. 0.47 mm, Frontier Laboratories Ltd.) maintained at 300 °C in the 7890B GC system oven (Agilent Technologies Inc.), with helium as carrier gas at a flow rate of 1.2 mL/min and a split ratio of 25:1. Ion detection was carried out in the *m/z* range of 25-550. The thermogram interpretations and the volatile identifications were performed by comparison and selective *m/z* extraction with the software and database F-Search 3.5.0 (Frontier Laboratories Ltd.) and literature data [76]. At each irradiation interval, the EGA-MS analysis was performed twice for all samples.

9.2.8. Single-Shot Pyrolysis-Gas Chromatography/Mass Spectrometry (Py-GC/MS)

Pyrolysis was performed on the pigments' powders for the characterization of their markers and their subsequent detection in the exposed surfaces of the historical PE lids. Around 100 μg of sample was placed into an 80 μL stainless-steel Eco-cup and pyrolyzed at 600 °C for 6 s using the same instrument described in the EGA-MS section. The pyrolysis interface was maintained at 300 °C. GC separations were performed using a Frontier UA5 capillary column (30m-0.25F, 30 m × 250 μm × 0.25 μm, Frontier Laboratories Ltd.), using helium as a carrier gas at flow rate of 1.2 °C/min and a split ratio of 15:1. The column temperature was programmed from 35 °C (hold for 1 min), increasing the rate at 16 °C/min to 220 °C, then at 10 °C/min to 315 °C (hold for 2 min). The MS parameters were: electron impact ionization (EI, 70 eV) in positive mode, transfer line at 280 °C, ion source at 230 °C, quadrupole at 150 °C, and scanning mass range 20-600 *m/z*. Data interpretation was performed by MassHunter Workstation Ver. B.0700 SP2 (Agilent Technologies Inc.) software and compound identification was accomplished by interpretation of their EI mass spectra, in comparison to NIST MS Search 2.2, F-Search 3.5.0 (Frontier Laboratories Ltd.) databases and literature data [39,76,77].

9.2.9. Thermal Desorption-Gas Chromatography/Mass Spectrometry (TD-GC/MS)

The thermal desorption analysis was performed on the basis of the previous EGA-MS results, analyzing the exposed surfaces of the historical polymeric matrices, focusing only on the volatile fractions for the additive's characterization. Around 200 μg of sample was added directly into an 80 μL stainless-steel Eco-cup sample to be analyzed with the same instrument described in the previous EGA-MS section. The temperature program started from 50 °C (hold for 30 s) to 320 °C (hold for 3 min), with an increasing ratio of 20 °C/min. The volatile focalization was obtained by a cryo-trap at -180 °C at the beginning of the GC column. GC separations were performed using a Frontier UA5 capillary column (see previous section), with helium as a carrier gas at a flow rate of 1.2 mL/min and a split ratio of 15:1. The injector temperature was set at 300 °C. The column temperature program ran from 40 °C (hold for 2 min), increasing at a rate of 20 °C/min until 280 °C (hold for 15 min). The MS parameters were: EI (70 eV) in positive mode, transfer line at 280 °C, ion source at 230 °C, quadrupole at 150 °C, and scanning mass range 29-550 *m/z*. Data interpretation was performed by MassHunter Workstation Ver. B.0700 SP2 (Agilent Technologies Inc.) software and compound identification was accomplished by interpretation of their EI mass spectra, in comparison to NIST MS Search 2.2, F-Search 3.5.0 (Frontier Laboratories Ltd.) databases and literature data [76].

9.2.10. Chemometric method

The PCA method was employed to analyze the EGA thermograms, namely, to recognize differences at a multivariate level between the high-density and low-density PE polymers, as well as to identify similarities with the historical samples. The PCA was performed on the EGA curves collected from unaged and artificially aged HDPE and LDPE polymer references, as well as historical lids. Sets of two replicas for each sample at the different irradiation doses were considered in the PCA model. The mass spectrometric data were excluded from the PCA. The first test of the PCA (Method A) included EGA thermograms preprocessed with normalization by unit area. The second test (Method B) was performed on a dataset of descriptors generated directly from EGA results, including signal area, peak maximum time, maximum and minimum peak slopes, and peak width at half height. For method A, the dataset was mean-centered before the application of PCA. For Method B, autoscaling was used. Matlab R2016b (Mathworks, Natick, MA, USA) and the PLS toolbox version 8.2.1 (Eigenvector, Manson, WA, USA) were used for PCA modeling. To address the robustness of the PCA calibration, reference ResinKit^{TM} samples No. 24 and 25 were considered.

9.3. Results

9.3.1. Colorimetric measures and microscope observations

After 770 h of irradiation, both PE reference samples and historical lids showed significant changes in color, surface texture, and cohesion. In accordance with the colorimetric results in **Figure F.2**, yellowing was observed in HDPE and LDPE samples, while the historical lids faded considerably. Indeed, all ΔE^*_{ab} values indicate a visible color change ($\Delta E^*_{ab} > 2.3$ [78]), with the highest difference for the historical lids 1 and 2 (**Table F.3**). A detailed description of the colorimetric measurements is available in **Appendix F**. Besides color change, both HDPE and LDPE samples cracked all over the exposed surfaces, as visible under the stereomicroscope (**Figure F.3**). On the other hand, the historical lids became brittle and broken with a network of tiny cracks on the top surface and alongside their entire thickness (**Figures F.3** and **F.4**), suggesting the occurrence of important light-induced chemical and physical modifications on the polymer molecular structure. Observing the side view of the lids' samples (thickness ca. 1 mm, **Figures F.4**), it can be inferred that fading took place at the surface of the plastic samples. A color gradient between the uppermost layers (whitish) and the middle-bottom areas (reddish) of the samples is clearly visible. Pigment particles dispersed in the polymeric matrix are still visible under the optical microscope after 220 h of artificial aging in the faded sample from lid 2 (**Figure F.5**), although many particles entirely or partially lost their color.
A color change was also observed for both pigment powders. In the aged sample PR 53:1, the formation of a pinkish superficial layer was seen, while PR 48:2 became slightly darker after 770 h (**Figure F.6**).

9.3.2. Polymer matrix: reference polymers and historical plastic samples

ATR-FTIR and EGA-MS analyses were performed to characterize the polymer and its degradation. Particular attention was given to the identification of aging markers, which can be correlated to significant changes in the polymer structures and yellowing.

9.3.2.1. ATR-FTIR results

The ATR-FTIR spectra of the PE reference samples and historical lids presented the same main absorption bands (**Figure F.7**), with characteristic aliphatic stretching vibrations at 2916, 2848 cm^{-1}, methylene-bending at 1472, 1463 cm^{-1}, and methylene-rocking at 730, 719 cm^{-1} bands [79,80]. The two doublet bands correspond to the PE crystalline (1474 and 730 cm^{-1}) and amorphous (1463 and 719 cm^{-1}) contents [81].

Polyethylenes with different degrees of chain branching (i.e., HDPE and LDPE types [82]) can be distinguished by IR analysis. The presence of the band at ca. 1377 cm^{-1} can be used as a marker for LDPE identification as being specifically associated with the vibration of the $–CH_3$ terminating groups of the short- and long-chain branching [83,84]. The ATR-FTIR spectra of the plastic samples prior to aging in the spectral range 1300-1430 cm^{-1} are depicted in **Figure F.8**. The PE reference samples match literature spectra [83,84] as respectively HD and LD. Lid 1 would be classified as HDPE, as previously suggested by Angelin et al. [41]. However, using the presence/absence of that marker for identifying the PE type of lid 2 could be misleading, because the plastic was naturally degraded, as observed by visual inspection and confirmed by the presence of bands at 1735 and 1714 cm^{-1} (**Figure F.7**), which indicate the formation of esters and carbonyl compounds (mainly carboxylic acids) respectively, characteristic of PE photooxidation [85]. This reflects the occurrence of the polymeric chain scission, which altered the degree of branching (extent of $–CH_3$ terminating groups) of lid 2. Yellowing (**Figure F.2**) and embrittlement (**Figure F.3**) are both characteristic symptoms of PE photo-oxidation [36,86-88]. The light-induced degradation of PE was identified by means of ATR-FTIR spectroscopy (**Figure F.9**) and involved the formation of oxidative products such as carboxylic acids (1714 cm^{-1}), esters (1733 cm^{-1}), lactones (1780 cm^{-1}), ketones (1410 cm^{-1}), vinyl (995 and 909 cm^{-1}), and *t*-vinylene (965 cm^{-1}) [85,89-91]. At ca. 1167 cm^{-1}, a strong band was also observed, for which controversial assignments have been proposed, including branching [89,92], esters [90,93], and vinyl groups [94]. The same photo-oxidation products were identified in the ATR-FTIR spectra of reference and historical plastic samples.

After 770 h of irradiation, the accumulation of the carbonylic species, vinylenic and vinyl un-saturations, became more significant for LDPE reference and historical lid 2 samples (**Figure F.9b,d**). This indicates a higher degree of photo-oxidative degradation of both samples. LDPE is known to be more susceptible to undergo photooxidation reaction than HDPE due to the greater number of tertiary carbons present at the branch points [35,86], as observed experimentally in [95,96]. Before irradiation, lid 2 exhibited photo-oxidation already at early stages (**Figure F.7**) and, after 550 h of exposure, a broad and strong band centered at 1640 cm^{-1} also appeared, suggesting the formation of new unsaturated species (**Figure F.9d**) [85,89-92]. These structures are strong chromophores and, depending on the extent of the conjugated unsaturated system, they can be responsible for the deeper yellowing of lid 2 [36]. In the LDPE reference sample, this broad absorbance band is only hinted at (**Figure F.9b**).

Dramatic changes in the 1400-1300 cm^{-1} spectral region were also detected with aging (**Figure F.10**). After 110 h, scission of the HDPE reference polymer chain occurred, as indicated by the appearance of the $–CH_3$ chain end groups (1374 cm^{-1}). This increase of end methyl groups in HDPE due to thermo-photo-oxidation processes had already been observed and reported [89,90,92]. In contrast, the marker band for LDPE, at ca. 1377 cm^{-1}, disappeared with aging. Both vibrational spectra of HDPE and LDPE reference samples were characterized by the emergence of a new band, at ca. 1360 cm^{-1}, assigned to photo-induced un-saturations (ketone structures) [89].

9.3.2.2. EGA-MS results

The results of EGA-MS analysis confirmed that lids 1 and 2 are made of PE, with their average maximum peaks at 492 and at 488 °C, respectively (**Figure 9.2**).

In **Figure 9.2**, the thermograms of lids 1 and 2 are compared with LDPE and HDPE reference samples before and after aging. At 0 h, the EGA curves of lid 1 and HDPE were similar, with the maximum peak located at 492 °C and slightly narrower than the broader curves of lid 2 and LDPE, which have the maximum peak at 488 °C. Lid 1 is likely made of HDPE; however, since the sample of lid 2 was previously naturally aged, it is not possible to draw conclusions by comparing it with unaged PE reference samples. After aging (770 h), lid 1 and HDPE showed similar curves (their maximum decreased by 5 °C to 487 °C), the curve of lid 2 was kept almost constant, and the curve of the LDPE sample became even broader and shifted its peak to less

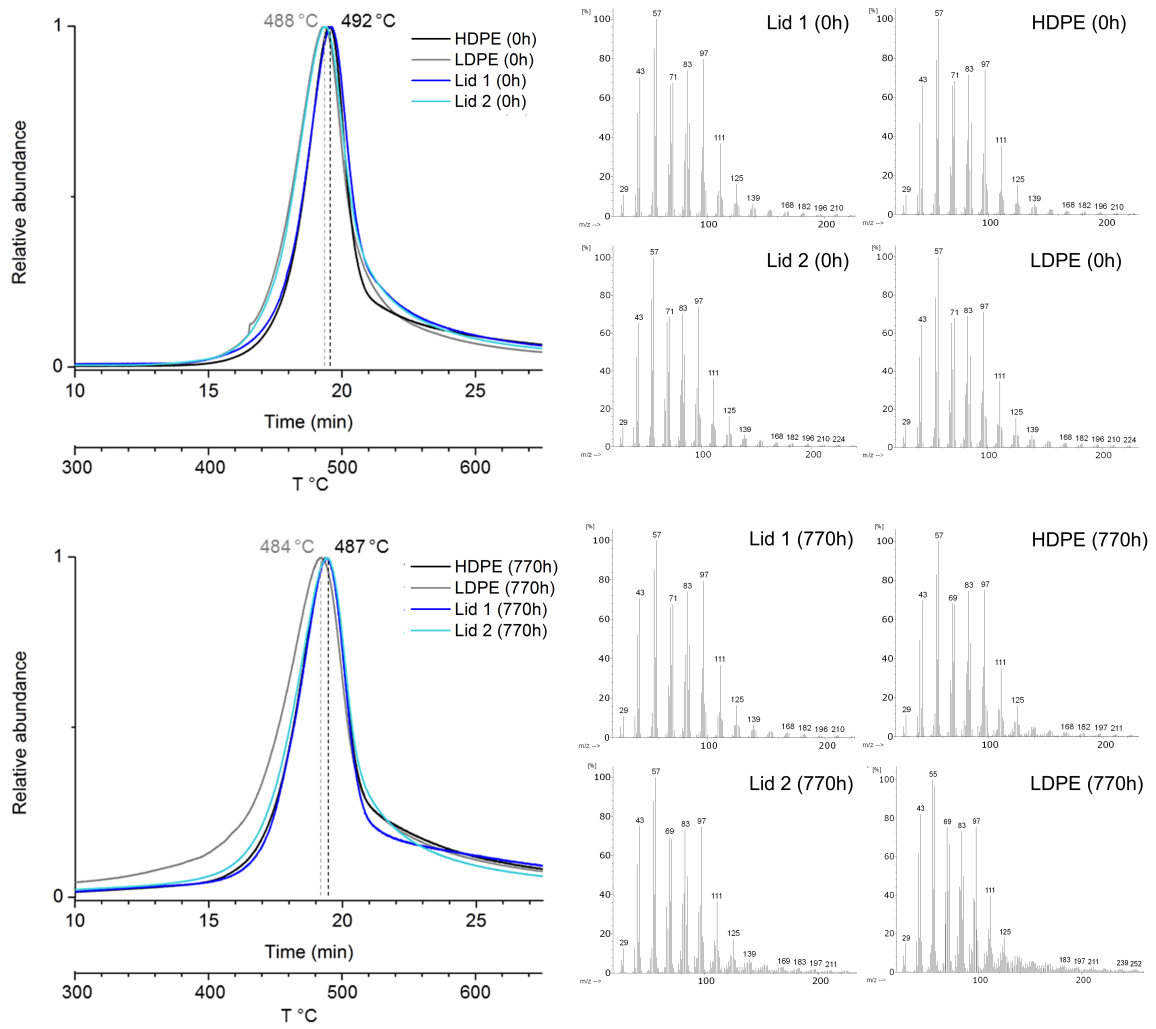

Figure 9.2.: Comparison of the EGA chromatograms of the four PE samples at 0 h (up) and 770 h (bottom) with the related average mass spectra. On the top: at 0 h, the curves of lid 1 and HDPE overlay, the curves of lid 2 and LDPE overlay. On the bottom: at 770 h, the curves of both lids and HDPE overlay. All intensities are normalized.

than 4 °C (maximum at 484 °C). The distinction between unaged LDPE and HDPE by EGA-MS analysis is not simple because their temperature range of decomposition overlays (between 480 and 490 °C [97]) and the distinction between their maximums is 4 °C apart. However, the polymer nature of the historical lid 1 became recognizable after aging, as EGA-MS analysis was sensitive enough for detecting the higher susceptibility of LDPE to undergo photo-oxidation reaction than HDPE [35,86]. The shift to lower temperatures of the maximum of both EGA-curves after aging is associated with degradation – shorter polymer chains – which happens for both LDPE and HDPE. The broadening of the LDPE indicates a higher degree of degradation with the formation of various lengths of polymer chains. Thus, the HD nature of lid 1 can be suggested considering that it exhibits similar curves to those of HDPE. However, the curve of lid 2 remained almost constant (from 488 to 487 °C). Considering the maxima of the curves, it is not possible to make suggestions about the type of polyethylene. To fully grasp these results, further investigation was performed in the next section.

9.3.2.3. PCA model

To support the polymer type identification made with evolved gas analysis for lid 1 and clarify the nature for lid 2, the EGA thermograms were analyzed by PCA (**Figure 9.3**). Note that the PCA model was calibrated using

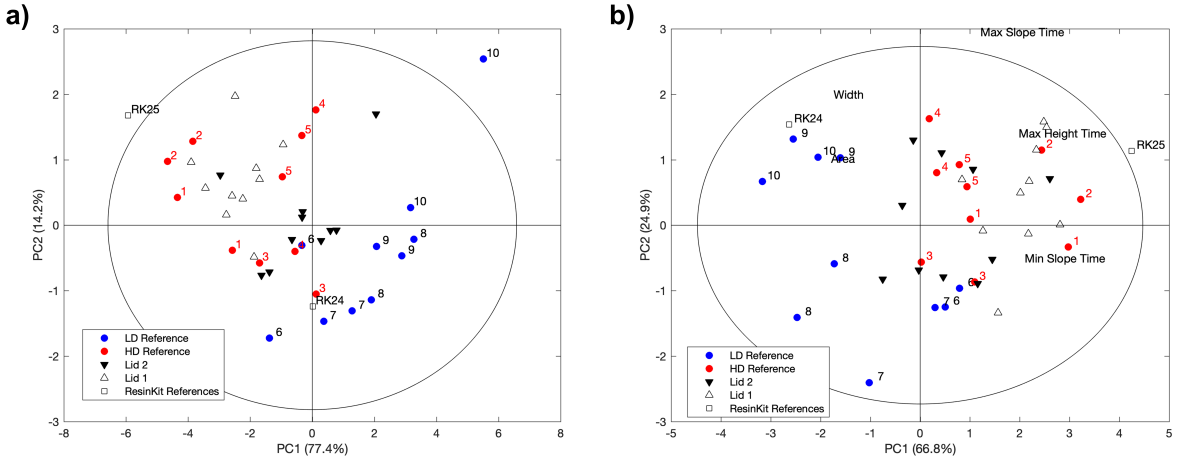

Figure 9.3.: PCA for normalized EGA curves (Method A) (a) and curve parameters (Method B) (b). Two replicates for each irradiation time were considered, numbered for LDPE and HDPE references, unnumbered for lid 1 and lid 2. Projection of ResinKit^{TM} No. 24 and 25 is also reported.

the HDPE and LDPE samples during the several aging steps (numeration is 1(0 h)–2(110 h)–3(220 h)–4(550 h)–5(770 h) for HDPE, and 6(0 h)–7(110 h)–8(220 h)–9(550 h)–10(770 h) for LDPE). Lid 1 and lid 2 samples at the same aging intervals were then projected onto the model to observe the relative positions against the reference polymer samples. Initially considering Method A, the two first principal components accounting for more than 98% of the total EGA signal variance were examined regarding the ability for separating HDPE and LDPE reference samples. A scatter plot of the two components shows a separation between HDPE and LDPE, confirming that EGA patterns are indeed different for both polymer types, unaged and aged (Method A). In the score plot, the HDPE and LDPE samples formed two separate clusters, indicating not only differences between them but also that each type of polymer may yield slightly varied profiles, thus explaining the observed scatter of projections/data/results. The samples' projection showed that lid 1 matched the HDPE sample, while lid 2 is placed in the middle of the graph with a closer match with HDPE than LDPE (**Figure 9.3a**). Considering the analysis using the extracted descriptors from EGA signals (Method B), LDPE is characterized by broader bands at lower temperatures (higher area and width, on the left of the graph), while HDPE bands are narrower, located at higher temperatures (max, min slope time, and time at maximum peak height are shorter, on the right) (**Figure 9.3b**). The same conclusions concerning the polymer nature of lid 1 and 2 can be drawn, as the sample projections of both lids over time are closer to the HDPE cluster. Although a low repeatability of the EGA method was observed (replicates for each irradiation time do not in general overlap in the score plot), the information extracted from the PCA method consolidates the interpretation by EGA for lid 1 and suggests that lid 2 is also made of HDPE. The Projection of ResinKit^{TM} samples No. 24 and 25 fits well with types of PE reference samples, ensuring the robustness of the PCA model.

9.3.3. β-naphthol synthetic pigments: reference powders and historical plastic samples

In this study, both EGA-MS and Py-GC/MS were used: (1) to characterize the thermal decomposition and the Py-markers of the reference pigment powders before and after aging, and (2) to investigate the presence of these markers in the historical samples, and eventually identify degradation products due to aging.

9.3.3.1. EGA-MS results

The EGA-MS analysis of the powder pigments at 0 h showed their different molecular structures, presenting different TIC thermograms and volatile products evolved in the temperature range 100-700 °C. In addition, the shift and appearance/disappearance of EGA peaks between the unaged and aged pigment powders indicate the occurrence of light-induced molecular changes (**Figures 9.4** and **9.5**).

Before aging (0 h), PR 48:2 is characterized by three main peaks: the first at 269 °C, the second at 394 °C, and the third at 465 °C. After aging (770 h), the first peak disappeared, the second shifted to 396 °C, and the third remained at the same temperature. Considering the average mass spectra, before and after aging, the samples did not show significant differences (**Figure 9.4a,c**). However, focusing on the zone A between 240 and 300 °C, at 0 h, several compounds evolved in this temperature range (**Figure 9.4b**), while after 770 h, the majority of those were lost, but the typical ions of phthalic anhydride ($C_8H_4O_3$: *m/z* 50, 76, 104, 148) [98] could be identified (**Figure 9.4d**).

From [77], the main Py-markers of PR 48:2 are *p*-toluidine,3-chloro, β-naphthol, and 8-chloro-5,6-dihydronaphthol[1,2-c]cinnoline. Moreover, it is also known that during the thermal degradation of sulfonated organic compounds, CO_2 and SO_2 are produced [99,100]. Therefore, to better understand the light-induced changes in the pigment composition, the specific ions of the aforementioned reference compounds, including phthalic anhydride, were extracted from the EGA-curves before (0 h) and after aging (770 h) (**Figure 9.4e,f**), in particular: *m/z* 44 for CO_2, *m/z* 64 for SO2, *m/z* 104 for phthalic anhydride, *m/z* 140 for *p*-toluidine,3-chloro, *m/z* 144 for β-naphthol, and *m/z* 266 for 8-chloro-5,6-dihydronaphthol[1,2-c]cinnoline. The extracted thermograms for the CO_2, SO_2, and pigment-markers before and after aging showed similarities. The two major bands of the TIC trends were associated with the pigment Py-markers, while SO_2 was mainly found at 465 °C. The TIC trends were also characterized by a constant CO_2 emission prolonged until 700 °C. The most significant difference was observed in the extracted thermograms of phthalic anhydride. The appearance of a broad band between 160 and 320 °C after aging clearly indicates that this phthalic compound is a degradation product.

By contrast, PR 53:1 at 0 h was mainly characterized by one peak at 402.5 °C, and a shoulder around 417 °C. After aging (770 h), the peak moved to higher temperatures (407 °C), with the shoulder disappearing, and a small band appearing around 480 °C (**Figure 9.5**).

Since PR 53:1 and PR 48:2 share the same basic skeleton structure with exchange of the –chlorine and –methyl substituents on the benzene ring (**Table F.2**), the ion extraction of PR 53:1 considered similar compounds to those selected for the interpretation of PR 48:2, however *m*-toluidine,4-chloro (*m/z* 141) and 9-chloro-5,6-dihydronaphthol[1,2-c]cinnoline (*m/z* 266) [77] were included. Comparing the extracted thermograms of PR 53:1 before and after aging, subtle differences were observed (**Figure 9.5**). The thermal evolutions of *m*-toluidine,4-chloro and β-naphthol did not present substantial changes, in contrast to 9-chloro-5,6-dihydronaphthol[1,2-c]cinnoline, which showed the disappearance of the shoulder at 417 °C after 770 h of aging (**Figure 9.5c,d**). Also associated with aging, a small increase of CO_2 emission at higher temperatures (550-700 °C) and a SO_2 emission responsible for the new broad and weak band at 480 °C were detected. The emission of phthalic anhydride at around 200 °C, as also detected for PR 48:2 in the same temperature range after aging, suggests the formation of the same degradation product for both β-naphthol pigments.

No evidence of the red pigments was visible in the thermograms of the historical lids (**Figure 9.2**), although this method is suitable for their identification, as showed in **Figures 9.4** and **9.5** for organic pigments' characterization. The very abundant contribution of the polymer to the thermogram could probably mask the pigment's EGA peaks. Normally, in plastic coloring, pigments are used in very small concentrations (0.1-2.0% and up to 5% for special requests) depending on the plastic formulation and end use application [5].

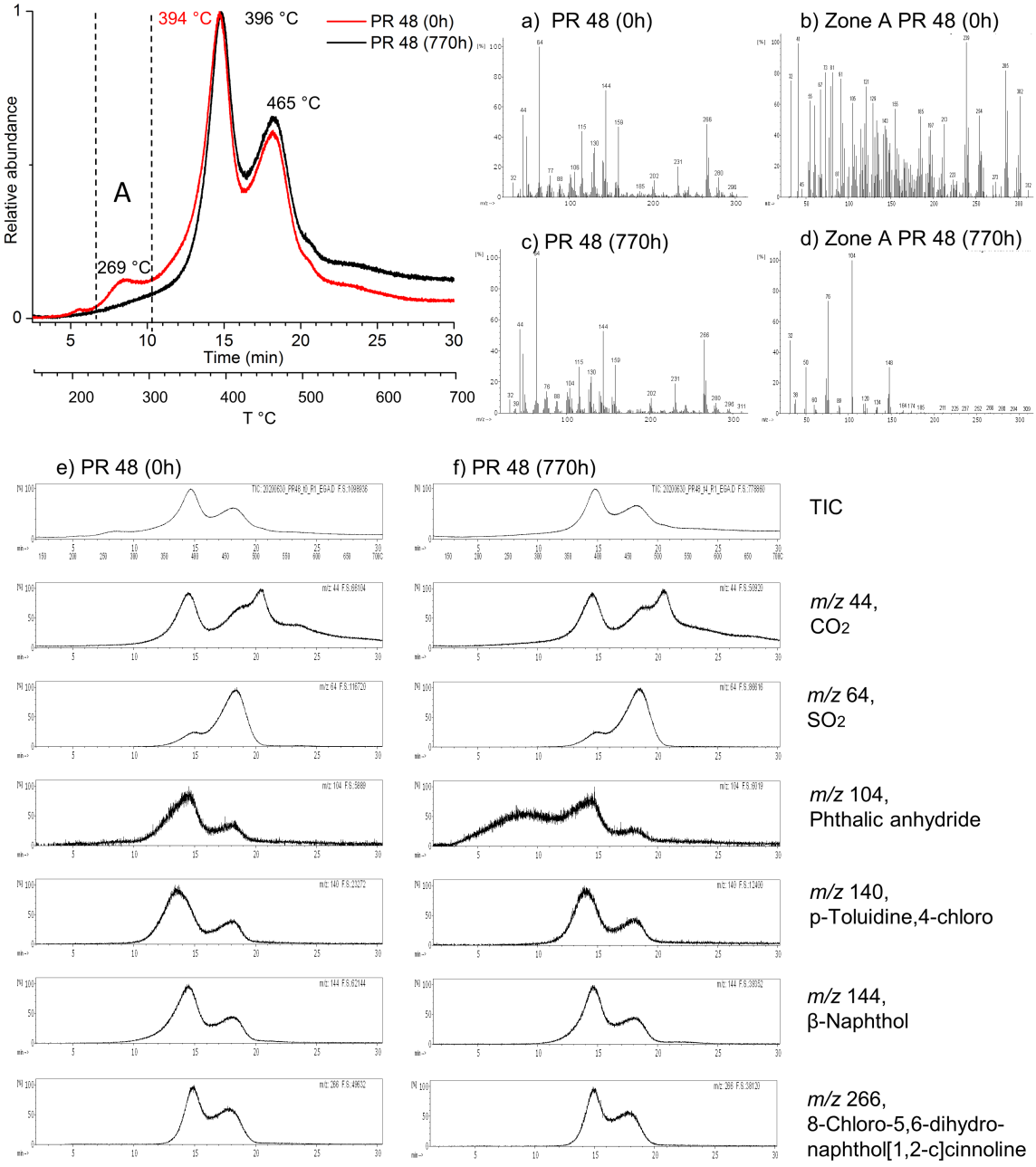

Figure 9.4.: EGA-curves of the pigment PR 48:2 at 0 h (no aging) and at 770 h and related mass spectra: (a) average mass spectrum of PR 48:2 at 0 h, (b) average mass spectrum of zone A for PR 48:2 at 0 h, (c) average mass spectrum of PR:2 48 at 770 h, (d) average mass spectrum of zone A for PR 48:2 at 770 h, (e) total ion current (TIC) and extracted ions for PR 48:2 at 0 h, and (f) total ion current (TIC) and extracted ions for PR 48:2 at 770 h. The ion trends are scaled to the largest peak in each plot.

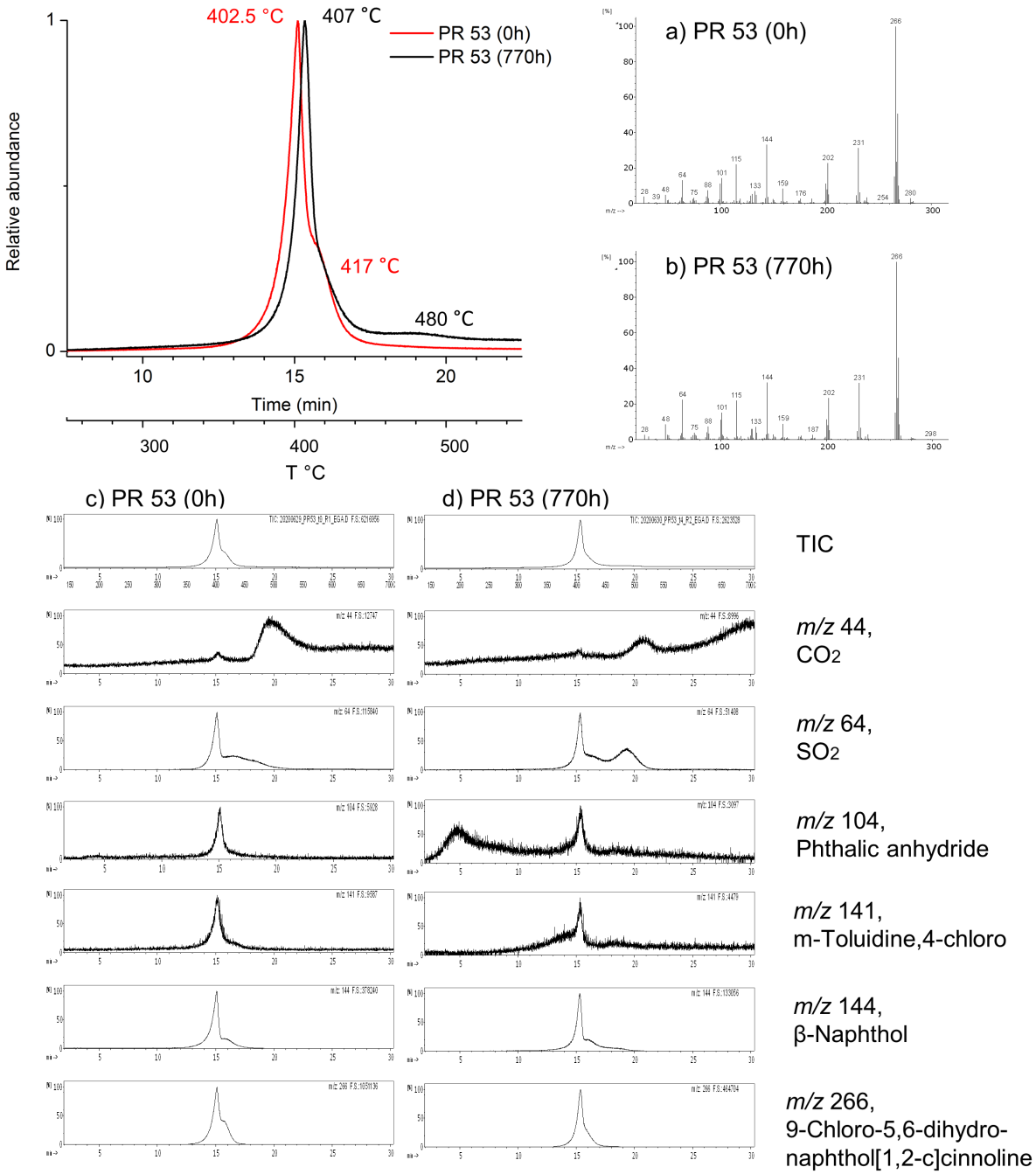

Figure 9.5.: EGA-MS curves of the pigment PR 53:1 at 0 h (no aging) and 770 h and related mass spectra: (a) average mass spectrum of PR 53:1 at 0 h, (b) average mass spectrum of PR 53:1 at 770 h, (c) total ion current (TIC) and extracted ions for PR 53:1 at 0 h, (d) total ion current (TIC) and extracted ions for PR 53:1 at 770 h. The ion trends are scaled to the largest peak in each plot.

Table 9.1.: Main pyrolysis products of the red azo-pigments PR 48:2 and PR 53:1 [77]. The degradation products are numbered and marked in *italic*.

Type	Pigment	t_R / min	Pyrolysis products	Main *m/z*
BONA	PR 48:2	9.5	*p*-Toluidine,3-chloro	77, 106, 140
pigment lakes		11.4	β-Naphthol	115, 144
		18.8	8-Chloro-5,6-dihydro-naphthol[1,2-c]cinnoline	202, 231, 266
		9.6	**(1)** *Phthalic anhydride*	*76, 104, 148*
		9.9	**(2)** *1,3-indandione*	*76, 104, 146*
		10.9	**(3)** *Phthalimide*	*76, 104, 147*
β-Naphthol	PR 53:1	9.6	*m*-Toluidine,4-chloro	77, 106, 141
pigment lakes		11.4	β-Naphthol	115, 144
		18.7	9-Chloro-5,6-dihydro-naphthol[1,2-c]cinnoline	202, 231, 266
		9.6	**(1)** *Phthalic anhydride*	*76, 104, 148*
		10.9	**(3)** *Phthalimide*	*76, 104, 147*

9.3.3.2. Py-GC/MS results

The Py-GC/MS analysis on the reference pigment powders detected the same principal Py-markers [77] previously identified by EGA-MS, confirming the presence of phthalic anhydride **(1)** as a photodegradation product in both pigments (**Table 9.1**). Further photodegradation compounds were detected: phthalimide **(3)** in both pigments, and 1,3-indandione **(2)** only in PR 48:2. The complete list of the pyrolysis products of the red pigments is presented in **Table F.4**.

Figures 9.6 and **9.7** show the pyrograms of the pigment powders before (0 h) and after aging (770 h). The main pyrolysis products of both pigments (**Figures 9.6a-c** and **9.7a-c**) decreased with irradiation.

Since no information related to the organic pigments could be extracted from EGA-MS analysis of the historical samples (possibly due to very low concentrations), their presence in the lids 1 and 2 was investigated by Py-GC/MS analysis

Considering the pyrolysis results obtained for the reference pigments, **Figures 9.8** and **9.9** show the pyrograms of the two lids, highlighting the extracted ions *m/z* 140, 144, 266, and *m/z* 141, 144, and 266 for PR 48:2 (**Figure 9.8a-c**) and PR 53:1 (**Figure 9.9a-c**), respectively. In lid 1 and lid 2, the signals of the three main Py-products from both pigments are relatively low when compared to those of the polymer. The ion *m/z* 140 deriving from PR 48:2 was easily detectable before and after aging (**Figure 9.8a**), while *m/z* 144 (**Figure 9.8b**) and 266 **Figure 9.8c**) appeared in very small amount or even in traces. In lid 2, the three main Py-products were visible before aging, *m/z* 141 was still detectable afterwards (**Figure 9.9a**), whereas *m/z* 144 (**Figure 9.9b**) and 266 (**Figure 9.9c**) were less recognizable. No signals of the degradation products were recognized in the plastic lids.

9.3.4. Additives: historical samples

Considering the EGA-MS analysis, both historical samples showed no clear signal of any significant amounts of additives in the temperature range between 100 and 350 °C (**Figure 9.2**). Polymer additives are usually present at concentrations in the order of 0.1-1 % w/w [101] and, other than fillers, antioxidants, stabilizers, and UV light protectors are key and typically used for polyolefins.

The investigation of the presence of additives in the lids 1 and 2 was additionally performed by TD-GC/MS analysis. TD-chromatograms are depicted in **Figure F.11** and the summary of the related volatile organic compounds is reported in **Table 9.2**. No additives were identified in the historical samples, confirming the EGA-MS results, while few compounds, mainly deriving from the PE chains (similar to unsaturated chains

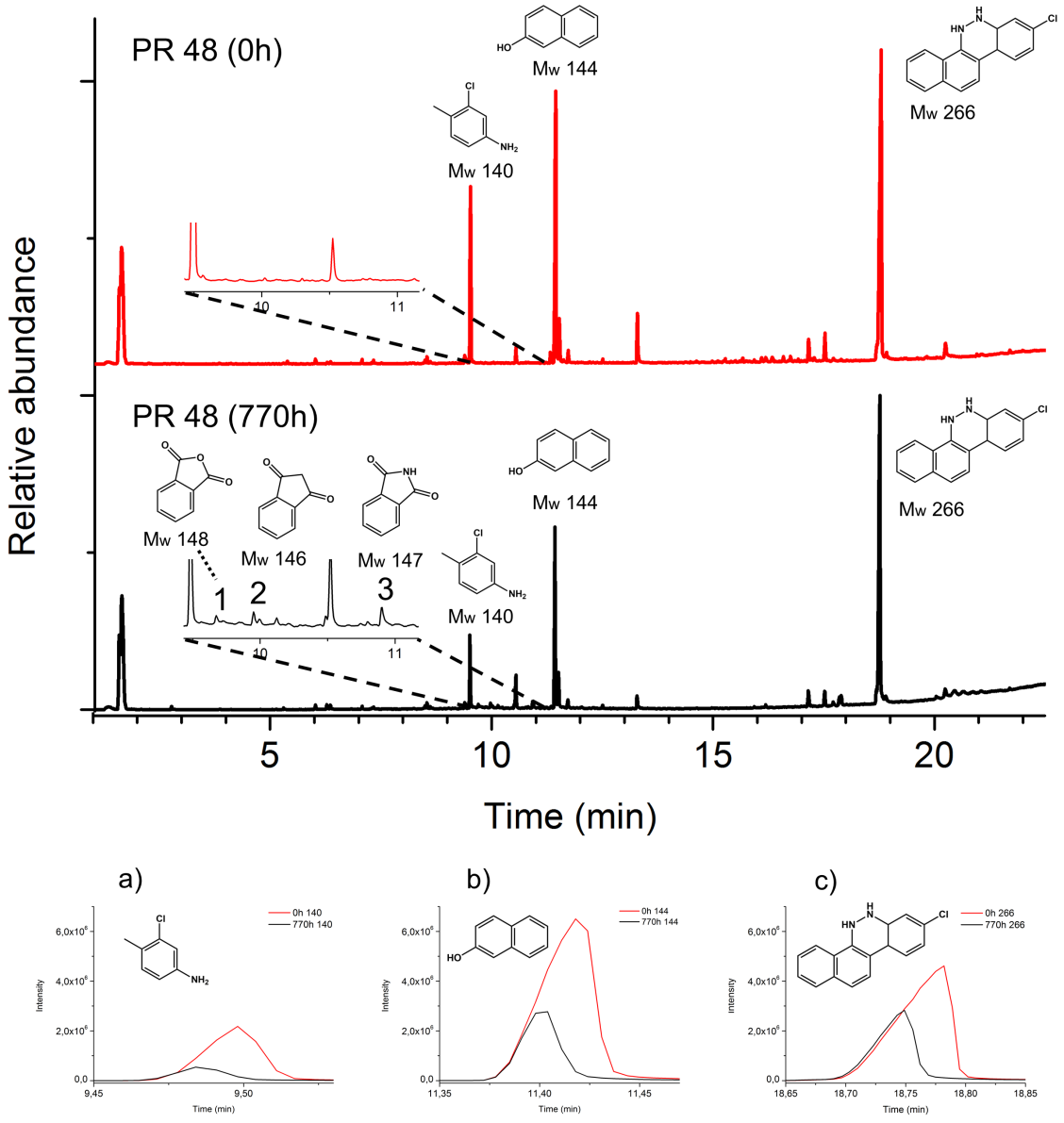

Figure 9.6.: Top: normalized pyrograms of the red powder pigment PR 48:2. At 0 h, the main pyrolysis structures (M_w 140, M_w 144, and M_w 266) are observed; after aging (770 h), decay products (M_w 148, M_w 146, and M_w 147) are formed (**Table 9.1**). Bottom (a-c): principal extracted ions (base peaks) of the main pyrolysis products.

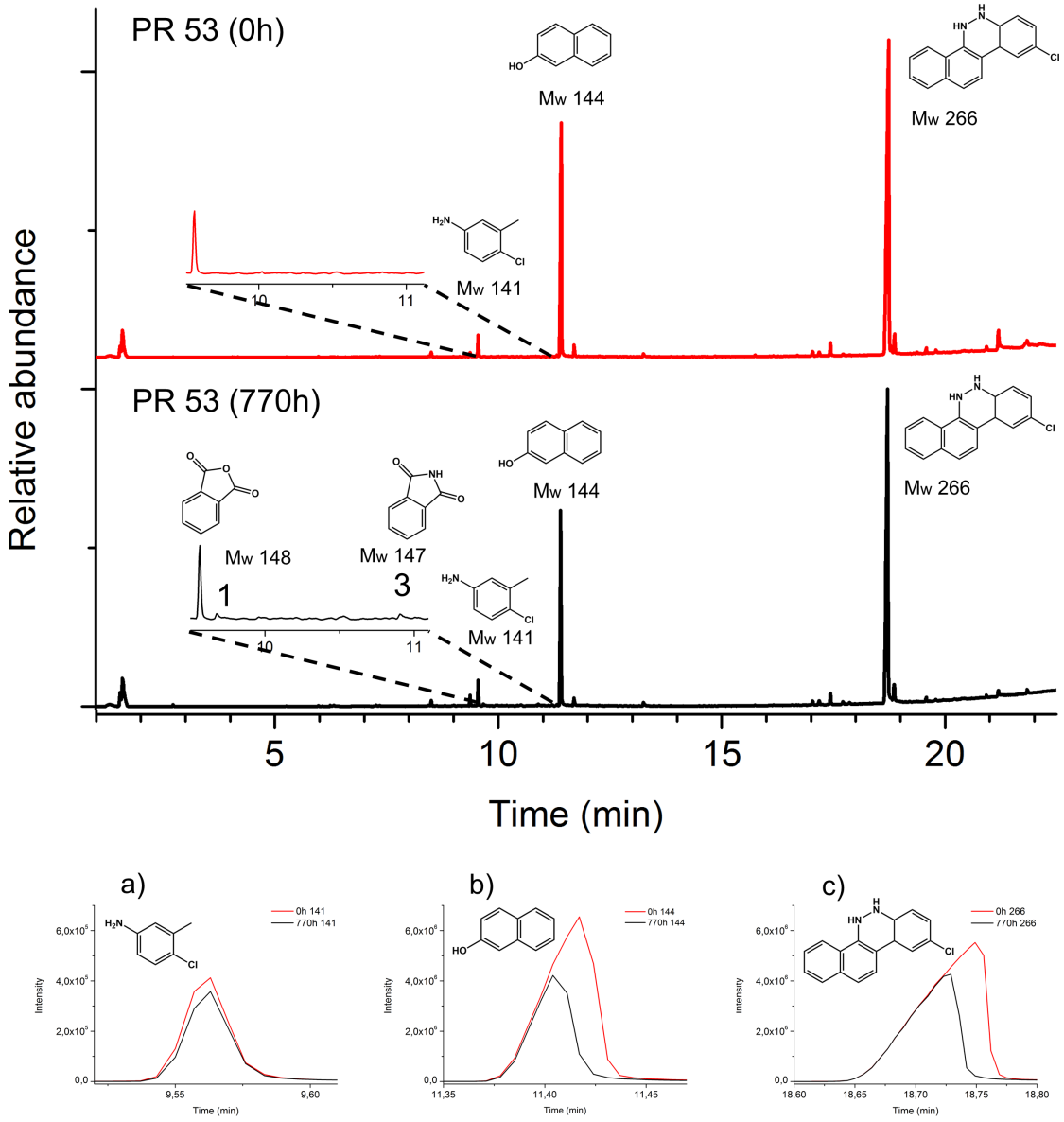

Figure 9.7.: Top: normalized pyrograms of the red powder pigment PR 53:1. At 0 h, the main pyrolysis structures (M_w 141, M_w 144, and M_w 266) are observed; after aging (770 h), decay products (M_w 148 and M_w 147) are formed (**Table 9.1**). Bottom (a-c): principal extracted ions (base peaks) of the main pyrolysis products.

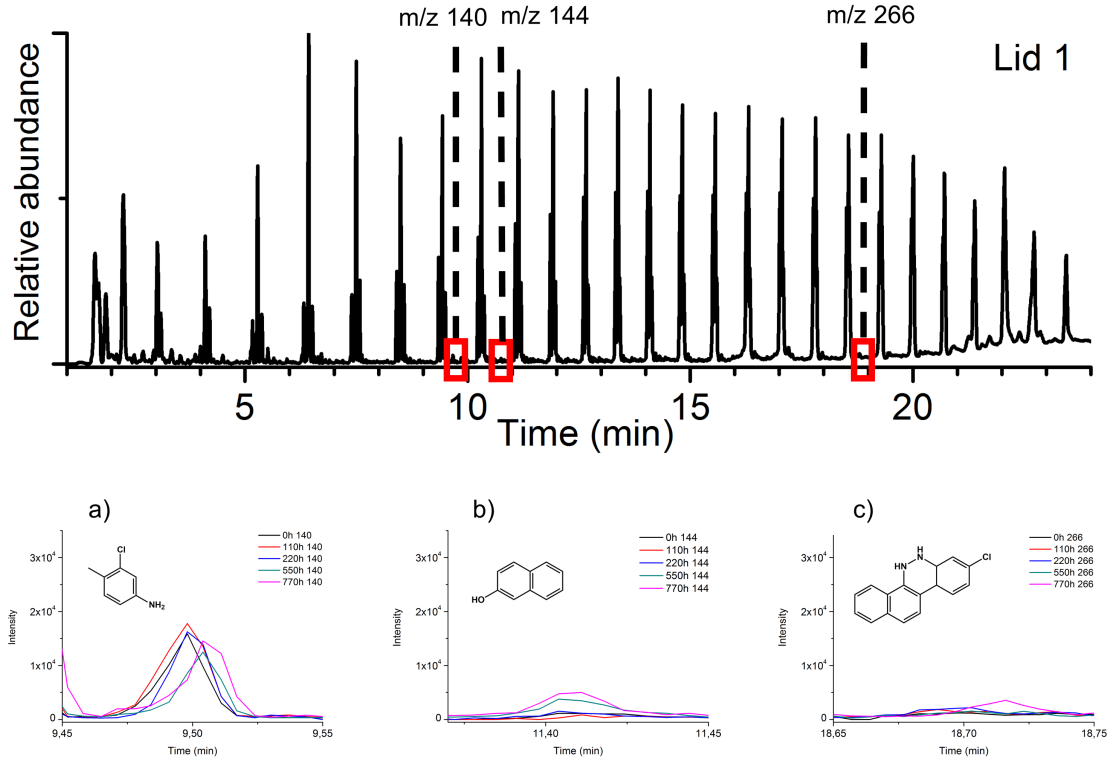

Figure 9.8.: Normalized pyrogram of lid 1 at 0 h and related extracted ions (base peaks) of the main pyrolysis products of the pigment PR 48:2, M_w 140 (a), M_w 144 (b), and M_w 266 (c), during the several aging steps (0–110–220–550–770 h).

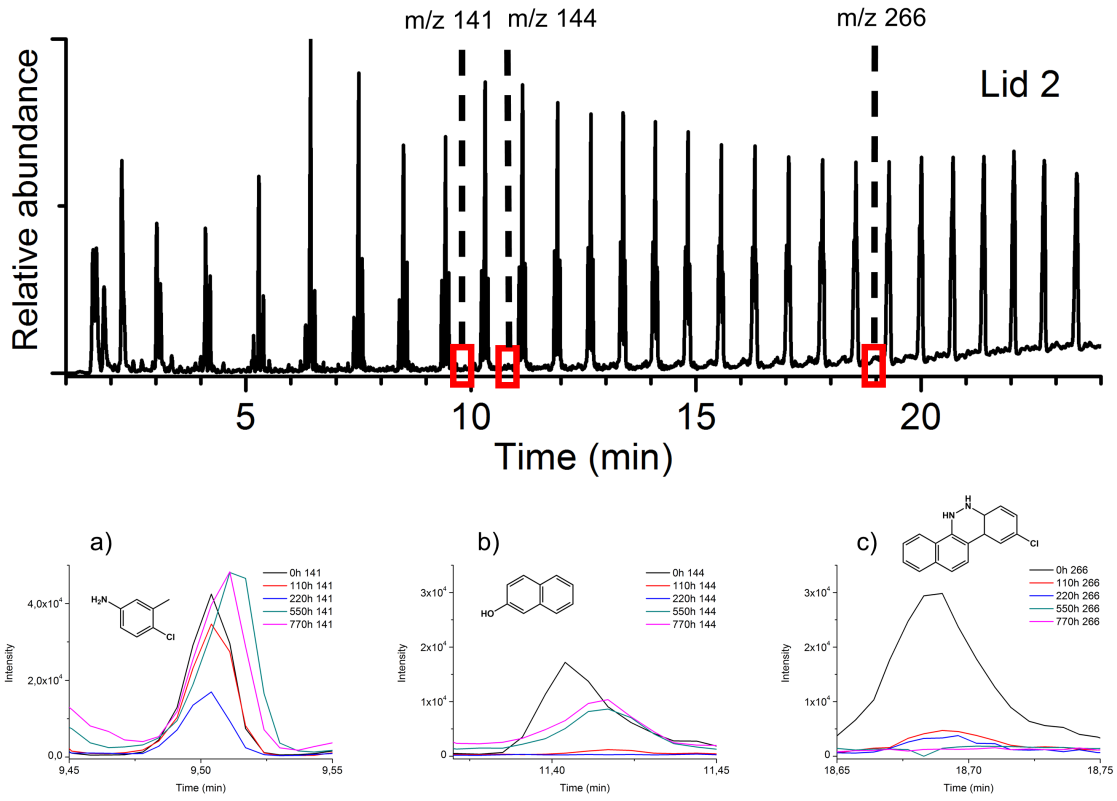

Figure 9.9.: Normalized pyrogram of lid 2 at 0 h and related extracted ions (base peaks) of the main pyrolysis products of the pigment PR 53:1, M_w 141 (a), M_w 144 (b), and M_w 266 (c), during the several aging steps (0–110–220–550–770 h).

Table 9.2.: Volatile organic compounds detected in the red lids 1 and 2 (characteristic ions in mass spectra: molecular weight, M_w, in bold and base peak underlined).

Peak number	Compound	*m/z*
1	1-Octadecene ($C_{18}H_{36}$)	41, 55, 69, 83, 97, 111, 125, **252**
2	Similar to n-eicosene ($C_{20}H_{40}$)	43, 55, 69, 83, 97, 111, 125, **280**
3	Similar to 1-docosene ($C_{22}H_{44}$)	43, 57, 69, 83, 97, 111, 125, **308**
4	Similar to 1-tetracosene ($C_{24}H_{48}$)	43, 57, 69, 83, 97 ,111, 125, **336**
5	Similar to 1-hexacosene ($C_{26}H_{52}$)	43, 57, 69, 83, 97, 111, 125, **364**
6	Similar to 1-octacosene ($C_{28}H_{56}$)	43, 57, 69, 83, 97, 111, 125, **392**
7	Similar to 1-triacontene ($C_{30}H_{60}$)	43, 57, 69, 83, 97, 111, 125, **420**
8	Similar to 1-dotriacontene ($C_{32}H_{64}$)	43, 57, 69, 83, 97, 111, 125, **448**

C18–C32 from Py analysis of PE) [76], were detected. As for the other additives, no signals concerning the presence of red pigments were found in the TD-chromatograms.

9.4. Discussion

9.4.1. Polymer reference matrix

HD- and LD-PE samples tended to yellow and crack as a consequence of the artificial aging. Both ATR-FTIR and EGA-MS measurements corroborated the occurrence of the polymer chain scission, which can be considered the main transformation of the macromolecular PE chain with aging. In detail, ATR-FTIR identified the vibrational markers of carboxylic acids, esters, lactones, vinyl, and *t*-vinylene functional groups. Additionally, the $-CH_3$ end groups were observed for HDPE. The broadening and shift towards lower temperatures of the EGA-MS curves highlighted the creation of shorter polymer chains with photo-oxidation.
Both polyethylenes were susceptible to photo-oxidation, with LDPE to a higher extent, due to its molecular structure (branching). The identification of the PE type is thus considered key in providing reliable predictions of possible color change in PE plastics following exposure to light, as yellowing is more likely to occur in LDPE. In pristine condition, the distinction between HD and LD polyethylenes was proved possible by IR analysis. However, in aged samples, the identification of the polymer type is challenging because of the light-induced modification in the microstructure (i.e., chain scission and formation of carbonyl and vinyl groups). The application of the PCA method on the EGA signals enabled the extrapolation of useful data for the PE type identification. The two methods used to create the PCA model led to the identification of HDPE in both the historical lids.

9.4.2. β-naphthol pigment powders

It has been proven that EGA-MS and Py-GC/MS can be effective techniques for the identification and characterization of the synthetic organic pigments PR 48:2 and PR 53:1, as well as their light-induced alterations. In the EGA-MS measurements, the two β-naphthol pigments were characterized by different thermal zones of interest (both in number and position), which made them discernible. In addition, EGA-MS was able to detect differences in the pigment composition after aging (i.e., identification of phthalic anhydride as a degradation product, appearance/disappearance and shift of the signals). The application of EGA-MS analysis in the characterization of organic pigment is mostly unexplored in the cultural heritage field, and the EGA-MS profiles of pure β-naphthol pigment lakes were presented for the first time. As used for other heritage materials [102-105], EGA-MS in combination with multi-shot pyrolysis may represent a valid method

for studying synthetic organic pigments. Besides the identification, their combination would allow the selective characterization of specific volatile fractions, such as additives and degradation products.
Between the MS techniques, Py-GC/MS is one of the most accepted analytical methods for the study of synthetic organic pigments, including hydrazone-azo pigments [77,106-108]. This technique does not require sample preparation and overcomes some practical limitations that organic pigments can present using liquid chromatography (LC) approaches, such as pigment extraction and the scarce solubility in organic solvents. In this study, the Py-GC/MS procedure enabled the identification of the pyrolysis products characteristic of the individual pigments, which were used as markers for the fading study in the historical plastics: *p*-toluidine,3-chloro (*m/z* 140) and 8-chloro-5,6-dihydronaphthol[1,2-c]cinnoline (*m/z* 266) for PR 48:2, *m*-toluidine,4-chloro (*m/z* 141) and 9-chloro-5,6-dihydronaphthol[1,2-c]cinnoline (*m/z* 266) for PR 53:1, and common β-naphthol (*m/z* 144) for both pigments.
Thanks to EGA-MS and Py-GC/MS analyses, phthalic derivatives, such as phthalic anhydride, 1,3-indandione, and phthalimide, were observed in small concentrations as degradation products after 770 h of artificial aging. These organic compounds were already detected as reaction intermediates in the photodegradation studies of the parent dye C.I. Acid Orange 7 [109-111]. However, these studies used conditions for the photoaging (presence of catalysts and/or $\lambda_{irr} < 300$ nm) far from conventional artificial aging performed in the cultural heritage field.
From a recent review [72], it is clear that little is known about the photodegradation mechanisms of β-naphthol pigments. The study of two parent dyes [72] allowed a preliminary insight into the factors affecting the β-naphthol fading. After irradiation of solutions under a polychromatic source ($\lambda_{irr} \geqslant 300$ nm), phthalic acid and phthalates were detected as degradation products. Phthalic acid can be converted into its anhydride by a condensation reaction, and the two compounds were already detected in the light-induced degradation of certain dyes [110,112,113]. Information on the degradation mechanism of the β-naphthol pigments still needs clarification. Nevertheless, the fact that the photodegradation of both parent dyes and β-naphthol pigments includes the formation of phthalic derivatives and phthalates as decay products can inspire further mechanistic studies.
Based on the MS measurements, no significant concentrations of additives were detected in the reference pigment powders. This confirms that the degradation products identified after aging are mainly formed from the light-induced degradation of the organic pigment molecules, without the influence of other components (i.e., additives).
PR 53:1 seemed more sensitive to the light aging condition tested in this study than PR 48:2. This hypothesis is posited based on the dramatic color change (red to pale pink) of the neat PR 53:1 powder. Fading of PR 53:1 was also detected by Ghelardi et al. [70]. The identification of whitish phthalic derivatives [114] agrees with the brightening of the pigment powder color.
Darkening of PR 48 pigment-type lakes and other β-naphthol red lakes as a consequence of UV exposure was already observed [70,71]. The loss of the chromophore in favor of colorless degradation products may account for the fading of the pigment; however, its darkening needs further clarification. The formation of phthalic derivatives can be a valid indicator of photodegradation at the early stages.

9.4.3. Discoloration of the plastic samples

The historical lids degraded severely during artificial aging, reaching an average value of the total color difference of $\Delta E^*_{ab} \approx 45$ (**Table F.3**). Chemical and physical degradation resulted from a combination of several processes: yellowing of the PE polymer, fading of the red organic β-naphthol pigment, and embrittlement of the samples, which, in turn, led the material to collapse. Both yellowing and fading determined severe changes in the color appearance of the aged historical samples. The action of light in the presence of oxygen is *de facto* the fundamental degradation mechanism to which plastics are subjected during their lifetime [34,74].

Considering that the formulation of both lids is based on a polymer that yellows and pigments that fade with photo-oxidation, their photodegradation involved chemical changes of both polymer and organic pigments. Only the absorbed radiation can lead to chemical changes. This is a complex mechanism and the likely interplay between the polymer and organic pigment behavior still needs to be further explained. To rationalize the polymer photodegradation, the absorption of the organic pigments should be clarified with further research, as radiation $\lambda \geqslant 300$ nm most probably would be absorbed by the lakes [72].

Compared to the aging of the reference polymers, similar conclusions can be generally made on the photodegradation of the PE historical matrices. This indicates that the degradation pathway and chromophores responsible for the PE yellowing would be comparable.

The aging experiments highlighted PR 48:2 and PR 53:1 as photosensitive pigments in PE. Fading of the historical lids can be related to the partial or total color loss of the pigment particles inside of the plastics, turning into a whitish or much lighter color (**Figures F.3-F.5**). Fading of the PR 53:1-containing lid is in accordance with the brightening of the neat pigment powder. Although the solely PR 48:8 darkened, this was not observed in lid 1 (**Figures F.3** and **F.4**). This discrepancy between the neat powder and the plastic system may be associated with different mechanism(s) and/or rate(s) of degradation, which lead to the formation of colorless degradation products.

After only 770 h, a noticeable color change was visible for the pigment powders, while, dispersed in the plastic matrix, at 110 h, some particles had already lost the red color under the OM. This can indicate a greater degree of sensitivity to light by the pigment lakes in the plastic samples. The polymer matrix of both lids could either have increased the reaction rate or induced other degradation mechanisms that led to severe fading in a shorter time. This evidence will have to be confirmed in future research, wherein the light absorbed by the pigments should be quantified, or at least guarantee the similar absorbance values prior to irradiation, in order to provide a better rationalization of the chemical events.

Fading was also observed as a superficial phenomenon which, to a high extent, can induce the total color loss of the plastics. In the aged mock-ups studied by Stenger [71], the same observation was made.

The use of Py-GC/MS for the identification of organic pigments in plastics was already tested [39,40,115]. Py-GC/MS was recommended for the precise identification of the organic pigments in the plastic objects, although the discrimination of the pigment peak fragments in the complex pyrograms was challenging and it required an extensive spectral database. In this work, small component peaks originating from the pigment were detected between the large range and abundant peaks (mainly deriving from the pyrolysis of the polymer). The use of Py-GC/MS enabled the unequivocal identification of the red organic pigments in the historical lids.

To study the fading mechanisms, a relevant aspect to consider is the decrease of the Py-markers' peaks. This demonstrated the consumption of the pigments in favor of the formation of the degradation products. Unfortunately, a clear decrease of the Py-markers' peaks in the historical lids with aging was not observed, probably as a consequence of the sampling procedure. Each sample was taken on the surfaces exposed to irradiation under stereomicroscope. As observed with the OM (**Figure F.5**), the red pigment particles progressively lost their color with aging, making their sampling extremely difficult under the stereomicroscope. For the same reason and considering the relatively little Py-peaks of the organic pigments compared to PE signals (**Figures 9.8** and **9.9**), degradation products such as phthalic anhydride and/or other intermediates were not recognized in the plastic lids. The relative abundance of the polymer with its several fractions, with high intensity, probably masked the degradation products present in small amounts, making the analysis of the MS signals unsatisfactory. To collect the discolored pigment particles in the PE matrix, the use of OM could have probably better supported the sampling procedure.

No organic and organometallic additives were detected in the historical lids, at least with a detectable concentration. Usually, few additives in relatively low concentration levels are required in the PE formulation, compared to other polymers [7,116,117]. Unfortunately, no historical documents on the formulation procedure are available from the Portuguese producer [118] to support our finding.

Nevertheless, it is important to mention that titanium dioxide, zinc sulfide, iron oxide-based pigments, and inorganic additives such as fillers (i.e., calcium carbonate, barium sulphate, silica) could have played a role in the plastic discoloration (**Table F.1**) [41]. Extensive literature is available concerning the photosensitizing and photoprotective influence of the two crystalline modifications of titanium dioxide (rutile and anatase) on the polymer degradation, including polyolefins [43,44,119-122], while little research was conducted on the photoactivity of the other inorganic compounds in polymeric systems [43,44,121].
Considering the private collection from where the historical lids were gathered, PR 53 was not found discolored in all the plastic objects [41]. Preliminary investigation on historical lid 3 (**Figure F.12**) by EGA-MS and TD-GC/MS identified a polystyrene (PS) matrix (**Figure F.13**) and some additives (**Figure F.14**). In detail, the light stabilizer drometrizol (peak n° 8), and the lubricants palmitic acid butyl ester and stearic acid butyl ester (peaks n° 9 and 10), were detected (**Table F.5**).
Further studies on the combined effect of polymer-additives on organic pigment degradation (and consequent plastic fading) are needed, and the methodology followed in this research is further suggested: (1) obtain the single reference materials: polymer, pigment(s), additive(s), and their mixed formulation in a plastic, (2) artificially age both sets of samples, and (3) characterize their color and molecular changes. For preparing adequate plastic samples, both historical and tailored formulations can be considered.

9.5. Conclusions

In this work, the discoloration of historical polyethylene (PE) samples colored with PR 48:2 and PR 53:1, with special emphasis on the fading of the β-naphthol pigment lakes, was studied for the first time. The study considered the individual susceptibility of (i) polymers and (ii) pigments to photooxidation, and their combined effect on a historical plastic formulation.
Light induced visible alterations in the reference polymers, reference pigments, and historical plastic samples. Particularly, the absorption of light caused long-term, cumulative, and irreversible chemical and physical changes in the historical plastics samples, visible through color variation and embrittlement, respectively. The artificial aging helped in simulating the mechanism(s) that induced severe fading – the ultimate effect of light exposure in the natural aging of pigmented plastics.
β-naphthol PR 48:2 and PR 53:1 pigment lakes proved to be light-sensitive in the historical PE objects. Isolated neat pigment powders showed a lower level of degradation than in the plastic environment. This leads to the interpretation that the plastic matrix (functioning as a binder) could have promoted the degradation of the pigments, even if their higher sensitivity due to natural aging cannot be excluded. The photo-oxidation and consequent fading of both organic pigments pose threats to museum and plastic heritage collections. As for other cultural heritage materials [123], light presents a duality in its interaction with plastics: it is essential for the perception and appreciation of the artifacts, but it, too, contributes to their degradation and damage. Considering our understanding of degradation mechanisms of this polymeric system [73,74], namely the fact that although PE does not directly absorb the UV-Vis radiation that reaches earth, it can overcome homolytic scission due to the existence of hydroperoxide groups that are formed during its synthesis, processing, etc. [74], one can infer that the hydroperoxide groups are the chromophores responsible for the formation of carbonyl-based functions and double bonds resulting from main- and side-chain scission. During these degradation processes, which can lead to scission and crosslinking, powerful oxidizing groups such as OH· are also formed. Thus, we can predict that these types of radical groups have a profound impact on the degradation of organic colorants present in the polymer matrix, as exemplified in the degradation of anthraquinone- and indigo-based systems [123,124].
The implemented analytical strategy used to investigate the individual sensitivity of (i) polymers (i.e., yellowing) and (ii) pigments to light-induced discoloration (i.e., fading of PR53:1 and darkening of PR 48:2), allowed to conclude that their combined influence in the historical plastic formulation resulted in the fading of both

organic pigments to a severe degree, dramatically affecting the appearance of the historical plastic samples. This strategy is therefore recommended for further heritage science investigations on the discoloration of historical plastics.

The combined effect of the plastic formulation was studied on historical samples. The fact that they were naturally aged might have influenced the results obtained, however, they provided the match with real plastic artifacts. To overcome this impasse, the results should be verified, for example, on well-preserved historical samples or recently made tailored formulations for investigating the chemical reactivity of both naphthol reds in PE matrix.

The analytical methods adopted in undertaking this research were found suitable for the study of plastic fading. Microscopy observations and MS analysis enabled the new insight into plastic discoloration and β-naphthols degradation, providing useful information on the changes at the molecular level of both reference samples and historical lids. In detail, EGA-MS clearly characterized the photoaging of the polymer, and PyGC/MS was the most valid method in studying the organic pigment, both in powder and in historical plastic matrixes. The unequivocal identification of phthalic derivatives as degradation products by Py-GC/MS opens new routes for studying the photodegradation mechanism(s) of both organic pigments. The application of TD-GC/MS in analyzing plastic heritage has been explored only recently. Here, it was effective in identifying the plastic additives of lid 3 and excluding their presence in lid 1 and lid 2.

The characterization of degradation products by means of Py-GC/MS originating from the artificially aged organic pigments in the historical lids was not conclusive. Future work includes the improvement of the sampling procedure, the preparation of tailored formulations reproducing historical production methods, and the application of a more specific analysis, such as the compound's selective heart-cut/pyrolysis-gas chromatography/mass spectrometry (HC/Py-GC/MS), to be performed with higher amounts of sample (e.g., 500 μg). This will support a deeper understanding of the fading mechanism through the application of Py-GC/MS.

9.6. References

[1] Quye A, Williamson C, editors. Plastics: collecting and conserving. Edinburg: NMS Publishing Limited; 1999.

[2] Cecchini C, Petroni M, editors. Plastic Days – Materiali e design. Cinisello Balsamo: Silvana Editoriale; 2015.

[3] Webber TG, editor. Coloring of plastics. New York: John Wiley & Sons Inc.; 1979.

[4] Müller A. Coloring of plastics. Munich: Carl Hanser Verlag; 2003.

[5] Charvat RA, editor. Coloring of plastics: fundamentals. New Jersey: John Wiley & Sons Inc., second ed.; 2004.

[6] Pritchard G. Plastics additives – An A-Z reference. London: Chapman & Hall; 1998.

[7] Murphy J. Additives for plastics handbook. Oxford: Elsevier Science, second ed.; 2001.

[8] Stepek J, Daoust H. Additives for plastics. New York: Springer Science+Business Media; 1983.

[9] Lazzari M, Reggio D. What Fate for Plastics in Artworks? An Overview of Their Identification and Degradative Behaviour. Polymers 2021; 13: 883. DOI: 10.3390/polym13060883.

[10] Pintus V, Piccolo A, Vetter W, Moretto LG, Sterflinger K, Schreiner M. What about Phenol Formaldehyde (PF) Foam in Modern-Contemporary Art? Insights into the Unaged and Naturally Aged Material by a Multi-Analytical Approach. Polymers 2021; 13: 1964. DOI: 10.3390/polym13121964.

[11] Neves A, Melo MJ, Ramos AM, Callapez ME, Friedel R, Réfrégiers M, Thoury M. Novel Markers to Map and Quantify Degradation on Cellulose Nitrate-Based Heritage: At the Submicrometer Level Using Synchrotron UV-Visible Multispectral Luminescence. Sci. Rep. 2021. DOI: 10.21203/rs.3.rs-505353/v1.

[12] Rijavec T, Strlic M, Cigic IK. Plastics in Heritage Collections: Poly(vinyl chloride) Degradation and Characterization. Acta Chim Slov. 2020; 67: 993-1013. DOI: 10.17344/acsi.2020.6479.

[13] King R, Grau-Bové J, Curran K. Plasticiser loss in heritage collections: Its prevalence, cause, effect, and methods for analysis. Herit Sci. 2020; 8: 1-17. DOI: 10.1186/s40494-020-00466-0.
[14] Nunes S, Ramacciotti F, Neves A, Angelin EM, Ramos AM, Roldão É, Wallaszkovits N, Armijo AA, Melo MJ. A diagnostic tool for assessing the conservation condition of cellulose nitrate and acetate in heritage collections: Quantifying the degree of substitution by infrared spectroscopy. Herit Sci. 2020; 8: 1-14. DOI: 10.1186/s40494-020-00373-4.
[15] Kammer J, Truong F, Boissard C, Soulié A-L, Dupont A-L, Simon L, Gros V, Lavédrine B. Quantitative and qualitative assessment of VOCs emitted from cellulose acetate movie films by PTR-ToF-MS. J Cult Herit. 2021; 47: 50-58. DOI: 10.1016/j.culher.2020.09.004.
[16] Jia Z, Li Y, Qi Y, Zhou Y, Hu D, Chao X, Xing H, Li J. Study on microbubble of cellulose acetate microfilm of the Republic of China (AD 1912-1949) collected in the Second Historical Archives of China. Herit Sci. 2020; 8: 1-10. DOI: 10.1186/s40494-020-00374-3.
[17] Royaux A, Apchain E, Fabre-Francke I, Balcar N, Barabant G, Bollard C, Lavédrine B, Fichet O, Cantin S. Conservation of plasticized PVC artifacts in museums: Influence of wrapping materials. J Cult Herit. 2020; 46: 131-139. DOI: 10.1016/j.culher.2020.07.002.
[18] Cato E, Scherrer N, Ferreira ESB. Raman mapping of the S_3^- chromophore in degraded ultramarine blue paints. J Raman Spectrosc. 2017; 48: 1789-1798. DOI: 10.1002/jrs.5256.
[19] René de la Rie E, Michelin A, Ngako M, Del Federico E, Del Grosso C. Photo-catalytic degradation of binding media of ultramarine blue containing paint layers: A new perspective on the phenomenon of "ultramarine disease" in paintings. Polym Degrad Stab. 2017; 144: 43-52. DOI: 10.1016/j.polymdegradstab.2017.08.002.
[20] Monico L, Cartechini L, Rosi F, Chieli A, Grazia C, De Meyer S, Nuyts G, Vanmeert F, Janssens K, Cotte M, De Nolf W, Falkenberg G, Anca Sandu IC, Storevik Tveit E, Mass J, Pereira de Freitas R, Romani A, Miliani C. Probing the chemistry of CdS paints in the Scream by in situ noninvasive spectroscopies and synchrotron radiation X-ray techniques. Sci Adv. 2020; 6: eaay3514. DOI: 10.1126/sciadv.aay3514.
[21] Comelli D, MacLennan D, Ghirardello M, Phenix A, Schmidt Patterson C, Khanjian H, Gross M, Valentini G, Trentelman K, Nevin A. Degradation of Cadmium Yellow Paint: New Evidence from Photoluminescence Studies of Trap States in Picasso's Femme (Époque des "Demoiselles d'Avignon"). Anal Chem. 2019; 91: 3421-3428. DOI: 10.1021/acs.analchem.8b04914.
[22] Monico L, Sorace L, Cotte M, de Nolf W, Janssens K, Romani A, Miliani C. Disclosing the Binding Medium Effects and the Pigment Solubility in the (Photo)reduction Process of Chrome Yellows ($PbCrO_4$/$PbCr_{1-x}S_xO_4$). ACS Omega 2019; 4: 6607-6619. DOI: 10.1021/acsomega.8b03669.
[23] Monico L, Cotte M, Vanmeert F, Amidani L, Janssens K, Nuyts G, Garrevoet J, Falkenberg G, Glatzel P, Romani A, Miliani C. Damages Induced by Synchrotron Radiation-Based X-ray Microanalysis in Chrome Yellow Paints and Related Cr-Compounds: Assessment, Quantification, and Mitigation Strategies. Anal Chem. 2020; 92: 14164-14173. DOI: 10.1021/acs.analchem.0c03251.
[24] Sabatini F, Eis E, Degano I, Thoury M, Bonaduce I, Lluveras-Tenorio A. The issue of eosin fading: A combined spectroscopic and mass spectrometric approach applied to historical lakes. Dyes Pigment. 2020; 180: 108436. DOI: 10.1016/j.dyepig.2020.108436.
[25] Chieli A, Miliani C, Degano I, Sabatini F, Tognotti P, Romani A. New insights into the fading mechanism of Geranium lake in painting matrix. Dyes Pigment. 2020; 181: 108600. DOI: 10.1016/j.dyepig.2020.108600.
[26] Grzesiak-Nowak M, Oszajca M, Rafalska-Łasocha A, Goszczycki P, Ostrowska K, Łasocha W. Crystal structure studies of selected lithol red salts with the use of powder diffraction data. Dyes Pigment. 2019; 160: 252-258. DOI: 10.1016/j.dyepig.2018.08.002.
[27] Jovanovic V, Eric S, Colomban P, Kremenovic A. Identification of Lithol Red Synthetic Organic Pigment Reveals the Cause of Paint Layer Degradation on the Lazar Vozarevic Painting "Untitled" with Copper Plates. Heritage 2019; 2: 2612-2624. DOI: 10.3390/heritage2030160.
[28] Papliaka ZE, Andrikopoulos KS, Varella EA. Study of the stability of a series of synthetic colorants applied

with styreneacrylic copolymer, widely used in contemporary paintings, concerning the effects of accelerated ageing. J Cult Herit. 2010; 11: 381-391. DOI: 10.1016/j.culher.2010.02.003.
[29] Sabatini F, Manariti A, di Girolamo F, Bonaduce I, Tozzi L, Rava A, Colombini MP, Lluveras-Tenorio A. Painting on polyurethane foam: "Composizione-Superficie Lunare" by Giulio Turcato. Microchem J. 2020; 156: 104872. DOI: 10.1016/j.microc.2020.104872.
[30] Bosi A, Ciccola A, Serafini I, Guiso M, Ripanti F, Postorino P, Curini R, Bianco A. Street art graffiti: Discovering their composition and alteration by FTIR and micro-Raman spectroscopy. Spectrochim Acta A 2020; 225: 117474. DOI: 10.1016/j.saa.2019.117474.
[31] La Nasa J, Campanella B, Sabatini F, Rava A, Shank W, Lucero-Gomez P, De Luca D, Legnaioli L, Palleschi V, Colombini MP, Degano I, Modugno F. 60 years of street art: A comparative study of the artists' materials through spectroscopic and mass spectrometric approaches. J Cult Herit. 2021; 48: 129-140. DOI: 10.1016/j.culher.2020.11.016.
[32] Shashoua Y. Conservation of plastics. Oxford: Butterworth-Heinemann; 2008.
[33] Lavédrine B, Fournier A, Martin G, editors. Preservation of Plastic Artefacts in Museum Collections (POPART). Paris: Comité Des Travaux Historiques et Scientifiques (CTHS); 2012.
[34] Allen NS, Edge M. Fundamentals of polymer degradation and stabilization. London: Elsevier Applied Science Ltd.; 1992.
[35] Hawkins WL. Polymer degradation. In: Polymer degradation and stabilization. Berlin: Springer-Verlag; 1984. p. 3-34.
[36] Rabek JF. Polymer photodegradation: mechanisms and experimental methods. Dordrecht: Springer Science+Business Media; 1995.
[37] Fox RB. Photodegradation of high polymers. Prog Polym Sci. 1967; 1: 45-89. DOI: 10.1016/0079-6700(67)90002-0.
[38] Andrady A.L. Ultraviolet radiation and polymers. In: Mark JE, editor. Physical properties of polymers handbook. New York: Springer; 2007. p. 857-886. DOI: 10.1007/978-0-387-69002-5_51.
[39] de Groot S, van Keulen H, Megens L, van Oosten T, Wiresma H. Discolouration of plastics objects: investigation into composition using various analytical techniques. In: Bechthold T, editor. Future Talks 013 – Lectures and workshops on technology and conservation of modern materials in design. Munich: Die Neue Sammlung – The Design Museum; 2015. p. 19-26.
[40] de Groot S, van Keulen H, van den Akker S, van Oosten T. Discoloration of plastics objects: the identification of yellow and orange synthetic pigment in plastic objects. In: Bechthold T, editor. Future Talks 015 – Processes. The making of design and modern art. Materials, technologies and conservation strategies. Munich: Die Neue Sammlung - The Design Museum; 2017. p. 147-158.
[41] Angelin EM, França de Sá S, Picollo M, Nevin A, Callapez ME, Melo MJ. The identification of synthetic organic red pigments in historical plastics: developing an in situ analytical protocol based on Raman microscopy. J Raman Spectrosc. 2021; 52: 145-158. DOI: 10.1002/jrs.5985.
[42] Allen NS, McKellar JF, editors. Photochemistry of dyed and pigmented polymers. London: Applied Science; 1980.
[43] Klemchuk PP. Influence of pigments on the light stability of polymers: a critical review. Polym Photochem. 1983; 3(1): 1-27. DOI: 10.1016/0144-2880(83)90042-8.
[44] Allen NS. Photofading and light stability of dyed and pigmented polymers. Polym Degrad Stab. 1994; 44(3): 357-374. DOI: 10.1016/0141-3910(94)90095-7.
[45] La Nasa J, Di Marco F, Bernazzani L, Duce C, Spepi A, Ubaldi V, Degano I, Orsini S, Legnaioli S, Tiné MR, De Luca D, Modugno F. Aquazol as a binder for retouching paints. An evaluation through analytical pyrolysis and thermal analysis. Polym Degrad Stab. 2017; 144: 508-519. DOI: 10.1016/j.polymdegradstab.2017.09.007.
[46] Melchiorre Di Crescenzo M, Zendri E, Sánchez-Pons M, Fuster-López L, Yusá-Marco DJ. The use of water-

borne paints in contemporary murals: Comparing the stability of vinyl, acrylic and styrene-acrylic formulations to outdoor weathering conditions. Polym Degrad Stab. 2014; 107: 285-293. DOI: 10.1016/j.polymdegradstab.2013.12.034.
[47] Duce C, Bernazzani L, Bramanti E, Spepi A, Colombini MP, Tiné MR. Alkyd artists' paints: Do pigments affect the stability of the resin? A TG and DSC study on fast-drying oil colours. Polym Degrad Stab. 2014; 105: 48-58. DOI: 10.1016/j.polymdegradstab.2014.03.035.
[48] Anghelone M, Jembrih-Simbürger D, Schreiner M. Influence of phthalocyanine pigments on the photodegradation of alkyd artists' paints under different conditions of artificial solar radiation. Polym Degrad Stab. 2016; 134: 157-168. DOI: 10.1016/j.polymdegradstab.2016.10.007.
[49] Anghelone M, Jembrih-Simbürger D, Pintus V, Schreiner M. Photostability and influence of phthalocyanine pigments on the photodegradation of acrylic paints under accelerated solar radiation. Polym Degrad Stab. 2017; 146: 13-23. DOI: 10.1016/j.polymdegradstab.2017.09.013.
[50] Anghelone M, Stoytschew V, Jembrih-Simbürger D, Schreiner M. Spectroscopic methods for the identification and photostability study of red synthetic organic pigments in alkyd and acrylic paints. Microchem J. 2018; 139: 155-163. DOI: 10.1016/j.microc.2018.02.029.
[51] Ciccola A, Guiso M, Domenici F, Sciubba F, Bianco A. Azo-pigments effect on UV degradation of contemporary art pictorial film: A FTIR-NMR combination study. Polym Degrad Stab. 2017; 140: 74-83. DOI: 10.1016/j.polymdegradstab.2017.04.004.
[52] Ciccola A, Serafini I, Guiso M, Ripanti F, Domenici F, Sciubba F, Postorino P, Bianco A. Spectroscopy for contemporary art: Discovering the effect of synthetic organic pigments on UVB degradation of acrylic binder. Polym Degrad Stab. 2019; 159: 224-228. DOI: 10.1016/j.polymdegradstab.2018.11.027.
[53] Hunger K, Schmidt MU. Industrial organic pigments: production, crystal structures, properties, applications. Weinheim: Wiley-VCH, fourth completely revised ed.; 2018.
[54] Society of Dyers and Colorists and American Association of Textile Chemists and Colorists. Color Index international. Bradford: Society of Dyers and Colorists and associates, third ed. on CD; 1995.
[55] Berrie BH, Lomax SQ. Azo pigments: their history, synthesis, properties, and use in artists' materials. Studies in the History of Art 1997; 57: 8-33. URL: jstor.org/stable/42622254
[56] de Keijzer M. A survey of red and yellow modern synthetic organic artists' pigments discovered in the 20th century and used in oil colours. In: Bridgland J, Brown J, editors. ICOM-CC 12th Triennial Conference Preprints, Lyon, 29 August - 3 September 1999. London: James and James (Science Publishers), Vol. I; 1999. p. 369-374.
[57] de Keijzer M. The history of modern synthetic inorganic and organic artists' pigments. In: Mosk JA, Tennent NH, editors. Contributions to conservation: research in conservation at the Netherlands Institute for Cultural Heritage (ICN). London: James & James (Science Publishers); 2002. p. 42-54.
[58] Lomax SQ, Learner T. A review of the classes, structures, and methods of analysis of synthetic organic pigments. J Am Inst Conserv. 2006; 45(2): 107-125. DOI: 10.1179/019713606806112540.
[59] Fremout W, Saverwyns S. Identification of synthetic organic pigments: the role of a comprehensive digital Raman spectral library. J Raman Spectrosc. 2012; 43: 1536-1544. DOI: 10.1002/jrs.4054.
[60] Lomax SQ, Lomax JF, de Luca-Westrate A. The use of Raman microscopy and laser desorption ionization mass spectrometry in the examination of synthetic organic pigments in modern works of art. J Raman Spectrosc. 2014; 45: 448-455. DOI: 10.1002/jrs.4480.
[61] Vandenabeele P, Moens L, Edwards HGM, Dams R. Raman spectroscopic database of azo pigments and application to modern art studies. J Raman Spectrosc. 2000; 31: 509-517. DOI: 10.1002/1097-4555(200006)31:6<509::AID-JRS566>3.0.CO;2-0.
[62] Kennedy AR, Stewart H, Eremin K, Stenger S. Lithol red: a systematic structural study on salts of a sulfonated azo pigment. Chem Eur J. 2012; 18: 3064-3069. DOI: 10.1002/chem.201103027.
[63] Gorelik T, Schmidt MU, Brüning J, Beko S, Kolb U. Using electron diffraction to solve the crystal structure

of a laked azo pigment. Cryst Growth Des. 2009; 9: 3898-3903. DOI: 10.1021/cg801099r.
[64] Bekö SL, Hammer SM, Schmidt MU. Crystal structures of the hydration states of Pigment Red 57:1. Angew Chem Int Ed. 2012; 51: 4735-4738. DOI: 10.1002/anie.201109082.
[65] Whitaker A. Crystal structure analysis of azo pigments involving β-naphthol: a review. J Soc Dye Colour. 1978; 94: 431-435. DOI: 10.1111/j.1478-4408.1978.tb03377.x.
[66] Lomax SQ. The application of x-ray powder diffraction for the analysis of synthetic organic pigments. Part 1: dry pigments. J Coat Technol Res. 2010; 7: 331-346. DOI: 10.1007/s11998-009-9206-0.
[67] Sabatini F, Degano I. Investigating the fragmentation pathways of β-naphthol pigments using liquid chromatography/electrospray ionization quadrupole time-of-flight mass spectrometry. Rapid Commun Mass Spectrom. 2020; 34: e8789. DOI: 10.1002/rcm.8789.
[68] Wise D, Wise A. Application of Raman microspectroscopy to problems in the conservation, authentication and display of fragile works of art on paper. J Raman Spectrosc. 2004; 35: 710-718. DOI: 10.1002/jrs.1213.
[69] Stenger J, Khandekar N, Wilker A, Kallsen K, Kirby DP, Eremin K. The making of Mark Rothko's Harvard Murals. Stud Conserv. 2016; 61(6): 331-347. DOI: 10.1179/2047058415Y.0000000009.
[70] Ghelardi E, Degano I, Colombini MP. Mazurek J, Schilling M, Khanjian H, Learner T. A multi-analytical study on the photochemical degradation of synthetic organic pigments. Dyes Pigm. 2015; 123: 396-403. DOI: 10.1016/j.dyepig.2015.07.029.
[71] Stenger J, Kwan EE, Eremin K, Speakman S, Kirby D, Stewart H, Huang SG, Kennedy AR, Newman R, Khandekar N. Lithol red salts: characterization and deterioration. e-Preservation Sci. 2010; 7: 147-157. URL: e-preservationscience/2010/Stenger-29-05-2010.
[72] Angelin EM, Conceição Oliveira M, Nevin A, Picollo M, Melo MJ. To be or not to be an azo pigment: chemistry for the preservation of historical β-naphthol reds in cultural heritage. Dyes Pigm. 2021; 190: 109244. DOI: 10.1016/j.dyepig.2021.109244.
[73] Allen NS, editor. Degradation and stabilization of polyolefins. London: Applied Science Publishers Ltd.; 1983.
[74] Lemaire J, Gardette JL, Lacoste J, Delprat P, Vaillant D. Mechanisms of photooxidation of polyolefins: prediction of lifetime in weathering conditions. In: Clough RL, Billingham NC, Gillen KT, editors. Polymer durability: degradation, stabilization and lifetime predictions. Washington DC: American Chemical Society; 1996. p. 577-598. DOI: 10.1021/ba-1996-0249.ch035.
[75] Oleari C. Standard colorimetry – Definitions, algorithms and software. Chichester: John Wiley & Sons; 2016.
[76] Tsuge S, Ohtani H, Watanabe C. Pyrolysis-GC/MS data book of synthetic polymers – programs, thermograms and MS of pyrolyzates. Oxford: Elsevier; 2011.
[77] Ghelardi E, Degano I, Colombini MP, Mazurek J, Schilling M, Learner T. Py-GC/MS applied to the analysis of synthetic organic pigments: characterization and identification in paint samples. Anal Bioanal Chem 2015; 407; 1415-1431. DOI: 10.1007/s00216-014-8370-y.
[78] Mahy M, Van Eycken L, Oosterlinck A. Evaluation of uniform color spaces developed after the adoption of CIELAB and CIELUV. Color Res Appl. 1994; 19: 105-121. DOI: 10.1111/j.1520-6378.1994.tb00070.x.
[79] Krimm S, Liang CY, Sutherland GBBM. Infrared spectra of high polymers. II. Polyethylene. J Chem Phys. 1956; 25(3): 549-562. DOI: 10.1063/1.1742963
[80] Noda I, Dowrey AE, Haynes JL, Marcott C. Group frequency assignments for major infrared bands observed in common synthetic polymers. In: Mark JE, editor. Physical properties of polymers handbook. New York: Springer, second ed.; 2007. p. 395-406.
[81] Zerbi G, Gallino G, Del Fanti N, Baini L. Structural depth profiling in polyethylene films by multiple internal reflection infra-red spectroscopy. Polymer 1989; 30(12): 2324-2327. DOI: 10.1016/0032-3861(89)90269-3.
[82] Morelly SL, Alvarez NJ. Characterizing long-chain branching in commercial HDPE samples via linear viscoelasticity and extensional rheology. Rheol Acta 2020; 59: 797-807. DOI: 10.1007/s00397-020-01233-5.

[83] Gulmine JV, Janissek PR, Heise HM, Akcelrud L. Polyethylene characterization by FTIR. Polym Test. 2002; 21(5): 557-563. DOI: 10.1016/S0142-9418(01)00124-6.
[84] Nishikida K, Coates J. Infrared and Raman analysis of polymers. In: Lobo H, Bonilla JV, editors. Handbook of plastics analysis. New York: Marcel Dekker Inc.; 2003. p. 186-316.
[85] Gardette M, Perthue A, Gardette JL, Janecska T, Földes E, Pukánszky B, Therias S. Photo- and thermal-oxidation of polyethylene: comparison of mechanisms and influence of unsaturation content. Polym Degrad Stab. 2013; 98(11): 2383-2390. DOI: 10.1016/j.polymdegradstab.2013.07.017.
[86] Feldman D. Polymer weathering: photo-oxidation. J Polym Environ. 2002; 10: 163-173. DOI: 10.1023/A:1021148205366.
[87] Pinter G, Haager M, Wolf C, Lang RW. Thermo-oxidative degradation during creep crack growth of PE-HD grades as assessed by FT-IR spectroscopy. Macromol Symp. 2004; 217: 307-316. DOI: 10.1002/masy.200451327.
[88] Yang R, Liu Y, Yu J, Zhang D. Spatial heterogeneity of photo-oxidation and its relation with crack propagation in polyethylene composites. Polym Eng Sci. 2008; 48: 2270-2276. DOI: 10.1002/pen.21177.
[89] Carrasco F, Pagès P, Pascual S, Colom X. Artificial aging of high-density polyethylene by ultraviolet irradiation. Eur Polym J. 2001; 37(7): 1457-1464. DOI: 10.1016/S0014-3057(00)00251-2.
[90] Costa L, Luda MP, Trossarelli L. Ultra high molecular weight polyethylene – II. Thermal- and photo-oxidation. Polym Degrad Stab. 1994; 58(1-2): 41-45. DOI: 10.1016/S0141-3910(97)00010-4.
[91] Tidjani A. Comparison of formation of oxidation products during photo-oxidation of linear low density polyethylene under different natural and accelerated weathering conditions. Polym Degrad Stab. 2000; 68(3): 465-469. DOI: 10.1016/S0141-3910(00)00039-2.
[92] Pagès P, Carrasco F, Surina J, Colom X. FTIR and DSC study of HDPE structural changes and mechanical properties variation when exposed to weathering aging during canadian winter. J Appl Polym Sci. 1996; 60: 153-159. DOI: 10.1002/(SICI)1097-4628(19960411)60:2<153::AID-APP2>3.0.CO;2-R.
[93] Küpper L, Gulmine JV, Janissek PR, Heise HM. Attenuated total reflection infrared spectroscopy for micro-domain analysis of polyethylene samples after accelerated ageing within weathering chambers. Vib Spectrosc. 2004; 34(1): 63-72. DOI: 10.1016/j.vibspec.2003.05.002.
[94] Martínez-Romo A, González Mota R, Soto Bernal JJ, Frausto Reyes C, Rosales Candelas I. Effect of ultraviolet radiation in the photo-oxidation of high density polyethylene and biodegradable polyethylene films. J Phys: Conf Ser. 2015; 582(1): 012026. DOI: 10.1088/1742-6596/582/1/012026.
[95] Ojeda T, Freitas A, Birck K, Dalmolin E, Jacques R, Bento F, Camargo F. Degradability of linear polyolefins under natural weathering. Polym Degrad Stab. 2011; 96(4): 703-707. DOI: 10.1016/j.polymdegradstab.2010.12.004.
[96] Martínez-Romo A, González-Mota R, Soto-Bernal JJ, Rosales-Candelas I. Investigating the degradability of HDPE, LDPE, PE-BIO, and PE-OXO films under UV-B radiation. J Spectrosc. 2015; 2015: 1-6. DOI: 10.1155/2015/586514.
[97] NETZSCH - Thermal Properties of the polymers (accessed 29.08.2020).
[98] National Institute of Standardisation (NIST) The NIST Mass Spectral Search Program, Version 2.2, Entry No. 133911 (phthalic anhydride, $C_8H_4O_3$).
[99] Rehorek A, Plum A. Characterization of sulfonated azo dyes and aromatic amines by pyrolysis gas chromatography/mass spectrometry. Anal Bioanal Chem. 2007; 388: 1653-1662. DOI: 10.1007/s00216-007-1390-0.
[100] Germinario G. Rigante ECL, van der Werf ID, Sabbatini L. Pyrolysis gas chromatography-mass spectrometry of triarylmethane dyes. J Anal Appl Pyrolysis 2017; 127: 229-239. DOI: 10.1016/j.jaap.2017.08.001.
[101] Hunt TP. Polymer additives: supercritical fluid chromatography. In: Wilson ID, editor. Encyclopedia of separation science. Academic Press; 2000. p. 3901-3906. DOI: 10.1016/B0-12-226770-2/03351-2.
[102] La Nasa J, Biale G, Sabatini F, Degano I, Colombini MP, Modugno F. Synthetic materials in art: a new comprehensive approach for the characterization of multi-material artworks by analytical pyrolysis. Herit Sci.

2019; 7(8): 1-14. DOI: 10.1186/s40494-019-0251-4.
[103] La Nasa J, Biale G, Ferriani B, Trevisan R, Colombini MP, Modugno F. Plastics in heritage science: analytical pyrolysis techniques applied to objects of design. Molecules 2020; 25(7): 1705. DOI: 10.3390/molecules25071705.
[104] Degano I, Modugno F, Bonaduce I, Ribechini E, Colombini MP. Recent advances in analytical pyrolysis to investigate organic materials in heritage science. Angew Chem Int Ed. 2018; 57(25): 7313-7323. DOI: 10.1002/anie.201713404.
[105] Mattonai M, Watanabe A, Shiono A, Ribechini E. Degradation of wood by UV light: a study by EGA-MS and Py-GC/MS with on line irradiation system. J Anal Appl Pyrolysis 2019; 139: 224-232. DOI: 10.1016/j.jaap.2019.02.009.
[106] Sonoda N. Characterization of organic azo-pigments by pyrolysis-gas chromatography. Stud Conserv. 1999; 44(3): 195-208. URL: jstor.org/stable/1506705.
[107] Learner TJS. Analysis of modern paints. Los Angeles: The J. Paul Getty Trust; 2004.
[108] Russell J, Singer BW, Perry JJ, Bacon A. The identification of synthetic organic pigments in modern paints and modern paintings using pyrolysis-gas chromatography-mass spectrometry. Anal Bioanal Chem. 2011; 400: 1473-1491. DOI: 10.1007/s00216-011-4822-9.
[109] Stylidi M, Kondarides DI, Verykios XE. Pathways of solar light-induced photocatalytic degradation of azo dyes in aqueous TiO_2 suspensions. Appl Catal B 2003; 40(4): 271-286. DOI: 10.1016/S0926-3373(02)00163-7.
[110] Stylidi M, Kondarides DI, Verykios XE. Visible light-induced photocatalytic degradation of Acid Orange 7 in aqueous TiO_2 suspensions. Appl Catal B 2004; 47(3): 189-201. DOI: 10.1016/j.apcatb.2003.09.014.
[111] Konstantinou IK, Albanis TA. TiO_2-assisted photocatalytic degradation of azo dyes in aqueous solution: kinetic and mechanistic investigations: A review. Appl Catal B 2004; 49(1): 1-14. DOI: 10.1016/j.apcatb.2003.11.010.
[112] Ahn C, Obendorf SK. Dyes on archaeological textiles: analyzing alizarin and its degradation products. Text Res J. 2004; 74(11): 949-954. DOI: 10.1177/004051750407401102.
[113] Zhong H, Shaogui Y, Yongming J, Cheng S. Microwave photocatalytic degradation of Rhodamine B using TiO_2 supported on activated carbon: mechanism implication. J Environ Sci. 2009; 21(2): 268-272. DOI: 10.1016/S1001-0742(08)62262-7.
[114] Lorz PM, Towae FK, Enke W, Jäckh R, Bhargava N, Hillesheim W. Phthalic acid and derivatives. In: Ullmann's Encyclopedia of industrial chemistry. Wiley-VCH, Vol. 27; 2012. p. 131-180. DOI: 10.1002/14356007.a20_181.pub2.
[115] Maragno A, Schossler P, Rizzutto M. Challenges in the conservation of synthetic polymers: discolouration of plastic objects. In: Future Talks 019, Munich (Germany), 11-13 November 2019; Oral presentation.
[116] Tolinski M. Additives for polyolefins. Oxford: Elsevier Inc., second ed.; 2015.
[117] Wypych G, editor. Handbook of plasticizers. Ontario: ChemTec Publishing, third ed.; 2017.
[118] França de Sá S, Marques da Cruz S, Callapez ME, Carvalho V. Plastics that made history – The contribution of conservation science for the history of the Portuguese Plastics Industry. Conservar Património 2020; 35: 85-100. DOI: 10.14568/cp2019017.
[119] Holtzen DA, Reid AH. Titanium dioxide pigments. In: Charvat RA, editor. Coloring of plastics: fundamentals. New Jersey: John Wiley & Sons Inc., second ed.; 2004. p. 146-158.
[120] Day RE. The role of titanium dioxide pigments in the degradation and stabilisation of polymers in the plastics industry. Polym Deg Stab. 1990; 29(1): 73-92. DOI: 10.1016/0141-3910(90)90023-Z.
[121] Norman NS, Edge M, Corrales T, Childs A, Liauw CM, Catalina F, Peinado C, Minihan A, Aldcroft D. Ageing and stabilisation of filled polymers: an overview. Polym Degrad Stab. 1998; 61(2): 183-199. DOI: 10.1016/S0141-3910(97)00114-6.
[122] Lemaire J. The photocatalyzed oxidation of polyamides and polyolefins. Pure Appl Chem. 1982; 54(9):

1667-1682. DOI: 10.1351/pac198254091667.
[123] Miliani C, Monico L, Melo MJ, Fantacci S, Angelin EM, Romani A, Janssens K. Photochemistry of artists' dyes and pigments: towards better understanding and prevention of colour change in works of art. Angew Chem Int Ed. 2018; 57: 7324-7334. DOI: 10.1002/anie.201802801.
[124] Sousa MM, Miguel C, Rodrigues I, Parola AJ, Pina F, Seixas de Melo JS, Melo MJ. A photochemical study on the blue dye indigo: From solution to ancient Andean textiles. Photochem Photobiol Sci. 2008; 7: 1353-1359. DOI: 10.1039/B809578G.

Part IV.

Conclusions

10. Final remarks and future perspectives

10.1. Discussion

Plastic coloring: pigments palette and practices used by the Portuguese industry

The study of cultural heritage made of Portuguese plastics is a current research focus at the Department of Conservation and Restoration (DCR) at FCT NOVA. In the last five years, considerable progress has been made in terms of their analysis and conservation [1-5]. This thesis sits within this framework and presents novel insights into the study of the color of Portuguese plastic artifacts, with a focus on pigments and their alteration.

Artworks, industrial and domestic objects made entirely of plastic were taken as examples of the modern and contemporary cultural heritage. The material analysis conducted as part of this research provided useful information on their composition, especially with respect to the coloring agents employed in Portuguese industry for daily, iconic, design and art objects in the historical collections.

The selection of historical objects studied for this PhD thesis was produced between the 1950s to the 2000s and made of thermoplastic polymers (e.g. PE, PP, PS, PMMA) [6]. All pigments identified are consistent with those reported in the literature [7-10]. The color palette of the investigated cultural heritage objects matches pigments cited in the dossier on the coloring of the APIP archives (**Section 1.3**), namely iron oxide, lead chromate molybdate, cadmium reds and yellows, titanium whites and hydrazone lakes [11,12]. An exception is pearlescent pigments which are not mentioned in the APIP's dossier. The Portuguese industry adopted plumbonacrite pigment instead of hydrocerussite, possibly due to economical convenience and/or supply availability. Plumbonacrite is a rare compound, even as an artists' material, and this discovery highlights its importance as a specialty pigment for plastics [13].

Concerns about the toxicologic and environmental issues of using heavy metal compounds in plastics arose worldwide in the 1990s with national restrictions being enforced on their use [14,15]. The identification of inorganic pigments containing mercury, lead, chromium, cadmium and selenium in plastics until the 1990s mirrors Portuguese restrictions, which to best of the author's knowledge, date from the late 1990s as a result of the implementation of European legislation on the national level [16]. In this context, it is indicative the identification of bismuth oxychloride in the acrylics found in the Ângelo de Souza's studio of the early 2000s [13]. This inorganic compound is one of the few rare examples of nontoxic heavy metal pigments and its use reflects the toxicological and environmental concerns by the Portuguese industry in contemporary times.

In summary, the Portuguese colorists' strategies and choices are aligned with the coloring technology generally adopted elsewhere. Additionally, the Portuguese plastic industry was up to date with production and processing knowledge of raw materials, as the identified pigments are all recommended for the coloring of thermoplastics covering the most relevant categories [7-10].

Challenges of pigments identification: an in situ multi-analytical approach

Low pigment concentration (ca 0.1%-5%) and the fact that they are particles dispersed in the polymer matrix with a micro-size (ca 0.02-30 μm) make their characterization an analytical challenge. This thesis demonstrates the reliability of multi-analytical spectroscopic methods for the in situ identification of pigments in historical plastics [11-13]. Generally, optical microscopy (OM) and micro X-ray fluorescence (μ-EDXRF) were used as preliminary investigation tools, and Raman microscopy (μ-Raman) provided complementary data for conclusive

identification. The specific advantage of Raman spectroscopy is the confocal microscopy system associated with the equipment for the in situ measurements, which enabled the collection of spectral data from pigment particles on the micro-scale by focusing the laser beam on particle surfaces. A more comprehensive multi-technique approach was considered in identifying the cadmium pigments [11], as data from Raman analysis was integrated with the optical characterization (Vis reflectance, Vis photoluminescence) exploiting the scattering, absorbance and luminescence properties of the pigments.

Fourier-transform infrared spectroscopy (FTIR) did not provide meaningful information on pigments within polymer matrices, possibly due to their concentration being below the detection limit of the technique (around >3% [17]). However, it efficiently identified the polymer medium. External reflection (ER)-FTIR and diffuse reflection (DRIFT) systems showed significant potential for the in situ analysis of plastic collections for both polymer characterization and the assessment of polymer degradation [18].

For the characterization of additives, additional considerations are required. Fillers can be used up to 50 % w/w for plastic formulation [19,20]. In this study, their elemental composition was characterized using X-ray fluorescence spectroscopy (μ-EDXRF) [11,12]. Furthermore, thanks to their particulate structure (and consequent scattering properties), fillers were detectable via μ-Raman, and in macro analysis with UV-Vis reflectance spectroscopy [11]. Additives other than fillers (e.g. flame retardants, antioxidants, light and heat stabilizers, lubricants, etc.) can have significantly lower concentration levels, in the range of 0.1-1 % w/w [21][1], making their situ identification with spectroscopic analytical protocols in the plastic artifacts unfeasible. For those, micro-sampling and analysis through more sophisticated methods (i.e. chromatographic and mass spectrometry systems) were required [22].

This thesis has developed an analytical methodology for investigating cultural heritage plastics, which permits the material identification and condition assessment considering the pigments contents. The knowledge gathered in this work together with the results have led to the proposal of a multi-technique spectroscopic approach built on two analytical steps: the first is preliminary, and the measurements can be performed directly on the object (in situ); the second is conclusive and may require micro-sampling depending on the object's mobility, size and shape. **Figure 10.1** shows the conceptual scheme of the analytical protocol which includes FTIR reflectance, optical microscope (digital) (OM), micro X-ray fluorescence spectrometry (μ-XRF), UV-Vis-NIR fiber optics reflectance spectroscopy (FORS), photoluminescence (PL) (1st step) and μ-Raman spectroscopy (2nd step). The selection of spectroscopic techniques was made considering their individual contribution to the investigation of plastics and empathizes the importance of using complementary analytical methods.

In situ spectroscopic measurements can be performed reliably as compact, portable and handled FTIR, X-ray, UV-Vis-NIR and PL spectrometers are available or, alternatively, custom-built set-ups can be made. Some devices can also use optical fibers and probe-heads for working in reflectance (e.g. FORS). Recent handheld digital Optical Microscopes (e.g. Dino-lite, Hirox), features high-resolution optics (magnification over 500 ×) that can reveal details on the micro-scale (approximately 3 μm), in the range typically found for pigments. The first step is designed to provide substantial data on the for the characterization of the plastic and facilitates a preliminary screening of the polymer type and decay problems. As the sampling of cultural heritage collections is limited, this initial inspection facilitates the selection of representative areas for subsequent collection of micro-samples and further analysis using μ-Raman and/or other techniques, if necessary. The amount of sample necessary will depend on the analytical method adopted. When sampling is an issue, complementary FTIR and Raman microscopy techniques are particularly relevant to the analysis of extremely small samples (usually around a fraction of millimeter of approximately 1 μg). The micro-sample is typically preserved after the measurements allowing for the utilization of complementary analytical methods. Chromatographic techniques coupled with mass spectrometry detectors instead require a larger amount of material (100-200 μg) and the

[1] The additives concentrations strongly depend on the additive type and plastic polymer. Usually ranging between 0.1-1 % w/w, the concentration levels can also reach ca 80% w/w for special applications and specific formulation (e.g. plasticized PVC) [19,20].

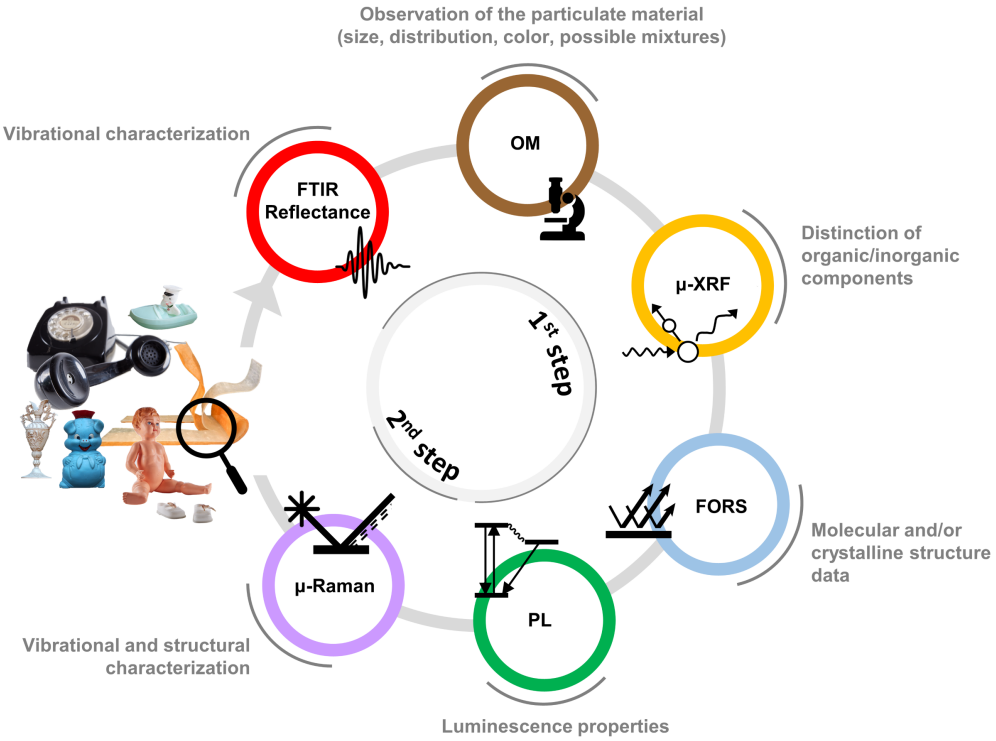

Figure 10.1.: Workflow proposed of the multi-analytical protocol for the investigation of cultural plastic collections.

analyte is destroyed during the analysis. Destructive testing methods usually yield more detailed information than in situ techniques and could be necessary for the full characterization of the plastic formulation. For this reason, the proposed protocol presents limitations in the identification of additives other than fillers.

β-naphthol reds: lightfastness and fading in historical plastics

Photodegradation processes provoke irreversible color changes in works of art [23]. Colored plastics share the same fate, a conclusion supported by both literature and the experimental evidence collected during this research [22].

The understanding of photo-induced color change in artworks implies the chemical comprehension of the excited-state behavior of colorants in relation to their environmental surroundings. Comparison between preliminary laboratory data and measurements collected on original artifacts is usually needed to achieve such a goal. As photochemical tools, several analytical techniques and light experiments are available for photodegradation studies. Those include accelerated aging tests capable of simulating degradation, used in this work to study the fading of β-naphthol pigments in plastic artifacts.

As little is known on the photochemical behavior of β-naphthol reds [24], the study of their fundamental chemistry in simple systems (in solution) was employed as a fundamental tool for their comprehension. Parent dyes used as model structures were also included as their analysis supported a better rational of 1-arylhydrazone-2-naphthol systems [24]. Results from the accelerated fading experiments of PR 48:2 and PR 53:1 shed light on their photo susceptibility in polymer situations [22].

Reaction quantum yields (Φ_R) are reliable parameters for quantifying the photo-stability [25] and their calculation provided insight and comparison of the fastness of the organic pigments and parent dyes studied. Φ_R values ranging from 3×10^{-6} to 4×10^{-5} were obtained, indicating relatively light-stable molecules. Indeed, Φ_R values below or equal to 10^{-6} are comparable to the lightfast pigment indigo, one of the most stable natural dyes and pigments [23,26], as well as lightfast alizarin (lakes, non-lake forms) which maintains its color with

$\Phi_R \approx 10^{-5}$ [27].
Light-induced alteration cannot be associated only with the colorant itself, but also with its interaction with the binder/medium that, in turn, may influence the colorant lightfastness [23]. A stabilization effect was observed in ethanolic solution in contrast to water for the parent dye Orange II (AO7) [24]. Higher sensitivity to light of PR 48:2 and PR 53:1 in plastics was suggested by the severe photofading of the historical samples when compared to the neat powders [22]. This research demonstrates how solvent and polymer media, representing the colorant environments, impact the lightfastness of colorants.
Mass spectrometry (MS) data revealed the evolution and extent of photodegradation. Even though distinctive intermediates and final products such as phthalic compounds and phthalates were identified [22,24], photofading mechanisms of the β-naphthol pigments require additional research. The characterization of degradation products originating from the artificially aged organic pigments from the historical plastics demands further research and will be able to draw from insights provided in this dissertation.

Conclusion
The diverse historical plastics studied for this PhD thesis enabled a good overview of Portuguese manufacturing. The material characterization supports new comprehensions into the coloring practices which, in turn, contributes with original information regarding technology and the history of the Portuguese plastics industry, enabling the planning of better preventive and conservation strategies of collections. Objects representative of the first generation of Portuguese plastic production (1930s-1940s) could be considered for further studies using the protocol adopted in this work.
In situ methods are usually preferred in the study of cultural heritage objects. Another significant outcome of this thesis is the proposal of an in situ multi-analytical approach based on spectroscopic techniques for the analysis of historical artifacts that, up to now, did not consider pigments within plastics. The analysis of a broader range of artifacts presenting different color and polymer types could corroborate its applicability and effectiveness.
The characterisation of the photo-stability of β-naphthol reds is of paramount importance to preserve the appearance of the modern and contemporary cultural heritage, including paintings and plastic artifacts. The information collected in this research provides a significant advance in understanding the stability of β-naphthol-based organic pigments, which is strongly dependent on the binding medium. The sensitivity to light of PR 48:2 and PR 53: 1 in plastics should be carefully considered in the managing of the cultural heritage artifacts. This thesis raises the awareness of the risk of the light exposure of historical plastics colored with β-naphthol reds as color fading can occur. As such, preventive conservation strategies should be adopted for their safety. The methodology developed in this investigation can now be used to study the lightfastness of β-naphthol pigments in polymeric media, also considering other formulations, where UV light is excluded. Further research can be conducted on the identification of the degradation products in fade plastics. This would support the insight into the implications of the role of the polymer in pigment degradation, such as reaction rate and mechanism.
In summary, this research work provides a major advance in understanding colorants and their degradation in cultural heritage plastics. As a subject only recently pursued within conservation science, the information it offers could be useful and inspire further studies in cultural heritage research.

10.2. Future research

The material analysis of other Portuguese artifacts will support the cataloguing of national cultural heritage collections and industrial production. The selection should be strategic considering both the date of production and manufacturer of the objects.
During the funded research project "The Triumph of Bakelite – Contributions for a History of Plastics in

Portugal" over two hundred historical plastic artifacts were available for study. It is a superb collection including items with different sizes, end-uses (mostly domestic) covering all ages of the Portuguese plastics' industry (from the 1930s to 2000s) and thermoplastic polymer types [28]. Although the project ended in December 2019, the artifacts are still accessible for study as many were donated to the DCR FCT NOVA. Their material analysis as future research will likely provide new insights and validation of the new multi-analytical approach.

Among the analytical methods used in this thesis, reflectance (FORS) and PL spectroscopies can be considered the most promising analytical methods for the investigation of the colorants and their alteration. Thanks to the scattering, absorbance, and luminescence properties of the pigments, FORS and PL make it possible to characterize their chemical composition and detect modifications due to degradation. Both techniques successfully supported the identification of cadmium pigments [11]. However, they have seen limited use in the analysis of colored plastics.
The lack of an experimental protocol in studying colored plastics by reflectance spectroscopy was first addressed by the author of this dissertation in 2018 [29,30]. Additional research work can include interpreting the compositional information gathered from the ultraviolet-visible-near infrared (UV-Vis-NIR) spectral range[2]. Indeed, each spectral region provides different information related to the identification of the formulations' components (e.g. colorants and pigments).
FORS can be used as a preliminary investigation tool to highlight of possible degradation trends by collecting data at regular intervals and monitoring spectral changes. In previous studies on plastic artifacts, the incipient degradation and color change (i.e. yellowing) of the polymers were successfully detected by reflectance spectroscopy [30,33]. Continuing along this line of research, the potential of FORS in the characterization of the pigment degradation and consequent fading can be investigated.
As molecular changes following degradation can be reflected in luminescence modifications, PL spectroscopy was mainly used as a tool for the condition assessment of the polymers in plastic collections [34-36]. Even if many pigments and dyes are luminescent, their properties were not used as a tool for the identification in plastics. In further research, PL methods[3] can be tested more systematically in the analysis of pigmented plastics as they offer highly sensitivity and selectivity. The luminescent characteristics of pigments may be affected by the microenvironment. As such, the implications of the polymer binder to the pigment emissions should be clarified. In undertaking this work a step learning curve will probably be necessary. Comparison between the emission signals of references pigments with those collected from tailored formulations and historical objects can be part of a starting methodology.

The knowledge on the photochemical behavior of β-naphthol reds is still limited. This thesis opens several routes of investigation, some of which can be considered in conservation strategies for polymer-based objects. The universal character of the photodegradation quantum yields (Φ_R) enables the comparison of the photostability properties of compounds with different structures in various media under diverse wavelengths. As such, future studies should be focused on the calculation of Φ_R using visible monochromatic excitation wavelength in solid polymer matrix. Those Φ_R could better assess the fastness properties of the pigments in practical polymer situations verifying their greater light susceptibly and, in turn, highlight the influence play by the polymeric medium on the pigment degradation.
Additional effort should be dedicated to the identification of the degraded products in faded historical plastics. To this end, the application of more specific analysis, like selective heart-cut/pyrolysis-gas chromatography/mass spectrometry (HC/Py-GC/MS) can be tested. Compared to solutions and powders, the composi-

[2]Despite FORS being a spot analytical technique, diffuse reflectance multispectral and hyperspectral imaging, i.e. the imaging version of reflectance spectroscopy [31,32], may also be used to obtain maps of the materials distributions (e.g. pigments in the polymeric matrix) and spectral differences (e.g. due to degradation).
[3]PL analysis can be performed by a variety of methods, those include the detection of emission spectra [37-39], both fluorescence and excitation spectra (spectrofluorimetry) [40,41], and emission lifetimes [42-44]. The PL spectroscopy can also be coupled with multispectral, lifetime and time-resolved photoluminescence imaging techinques [45-48].

tional information of the intermediates and final products will support the proposal of photoreaction pathways. In addition, tailored formulations can be prepared and aged artificially to simulate the photofading process.
Micro-fadeometry is a common technique used in conservation studies [49]. This test focuses on a tiny spot of very intense light and, because the color change is usually simultaneously monitored, it enables a better resolution of light-induced aging processes, including early-stage photo-degradation. Micro-fadeometry can be tested on historical plastics in order to measure the color change in light-sensitive materials such as β-naphthol reds. However, these micro-fading experiments cannot rationalize the chemical events as Φ_R does. Their comparison would be particularly relevant in light of the photo-stability results from this work and to aid prediction of future pigment fading in real objects. The characterization of the photodegradation products formed in the accelerated micro-fading can verify that a similar degradation pathway has occurred. If the results are comparable, micro-fadeometry could aid future photodegradation studies.

10.3. References

[1] França de Sá S. What does the future hold for polyurethane fashion and design? Conservation studies regarding the 1960s and 1970s objects from the MUDE collection. Doctoral dissertation. Lisbon: Universidade Nova de Lisboa, Faculdade de Ciências e Tecnologia; 2017.
[2] de Silva J. Ângelo de Sousa's photographic and film collection: strategies for the preservation of colour slide-based artworks. Doctoral dissertation. Lisbon: Universidade Nova de Lisboa, Faculdade de Ciências e Tecnologia; 2019.
[3] Roldão É. Unveiling the colours of cellulose nitrate black and white film-based negatives in colonial photography. Doctoral dissertation. Lisbon: Universidade Nova de Lisboa, Faculdade de Ciências e Tecnologia; 2020.
[4] Babo S. From object to shadow: conservation studies on acrylic artworks by Ângelo de Sousa and Lourdes Castro. Doctoral dissertation. Lisbon: Universidade Nova de Lisboa, Faculdade de Ciências e Tecnologia. *Submitted*.
[5] Neves A. Cellulose nitrate objects in collections: history of science and technology hand in hand with conservation of cultural heritage. Doctoral dissertation. Lisbon: Universidade Nova de Lisboa, Faculdade de Ciências e Tecnologia. *Forthcoming*.
[6] Callapez ME. Os plásticos em Portugal: a origem da indústria transformadora. Lisbon: Editorial Estampa; 2000.
[7] Webber TG, editor. Coloring of plastics. New York: John Wiley & Sons Inc.; 1979.
[8] Harris RM. Coloring technology for plastics. Norwich: Plastics Design Library; 1999.
[9] Müller A. Coloring of plastics. Munich: Carl Hanser Verlag; 2003.
[10] Charvat RA, editor. Coloring of plastics: fundamentals. New Jersey: John Wiley & Sons Inc., second ed.; 2004.
[11] Angelin EM, Ghirardello M, Babo S, Picollo M, Chelazzi L, Melo MJ, Nevin A, Valentini G, Comelli D. The multi-analytical in situ analysis of cadmium-based pigments in plastics. Microchem J. 2020; 157: 105004. DOI: 10.1016/j.microc.2020.105004.
[12] Angelin EM, França de Sá S, Picollo M, Nevin A, Callapez ME, Melo MJ. The identification of synthetic organic red pigments in historical plastics: developing an in situ analytical protocol based on Raman microscopy. J Raman Spectrosc. 2021; 52: 145-158. DOI: 10.1002/jrs.5985.
[13] Angelin EM, Babo S, Ferreira JL, Melo MJ. Raman microscopy for the identification of pearlescent pigments in acrylic works of art. J Raman Spectrosc. 2019; 50: 232-241. DOI: 10.1002/jrs.5431.
[14] Müller A. Colorants for polymer. In: Coloring of plastics. Munich: Carl Hanser Verlag; 2003. p. 61-210.
[15] Surgeon P. The environment and government regulations. In: Charvat RA, editor. Coloring of plastics: fundamentals. New Jersey: John Wiley & Sons Inc., second ed.; 2004. p. 358-379.

[16] Diário da República n.º 293/1998, Série I-A de 1998-12-21. URL: dec-lei/407/1998/12/21/p/dre/pt.
[17] Lavédrine B, Fournier A, Martin G, editors. Preservation of Plastic Artefacts in Museum Collections (POPART). Paris: Comité Des Travaux Historiques Et Scientifiques (CTHS); 2012.
[18] Angelin EM, França de Sá S, Soares I, Callapez ME, Ferreira JL, Melo MJ, Bacci M, Picollo M. Application of infrared reflectance spectroscopy on plastics in cultural heritage collections: a comparative assessment of two portable mid-Fourier transform infrared reflection devices. Appl Spectrosc. 2021; 75: 818-833. DOI: 10.1177/0003702821998777
[19] Bart JCJ. Additives in polymers – Industrial analysis and applications. Chichester: John Wiley & Sons Ltd; 2005.
[20] Hahladakis JH, Velis CA, Weber R, Iacovidou E, Purnell P. An overview of chemical additives present in plastics: migration, release, fate and environmental impact during their use, disposal and recycling. J Hazard Mater. 2018; 344: 179-199. DOI: 10.1016/j.jhazmat.2017.10.014.
[21] Hunt TP. Polymer additives: supercritical fluid chromatography. In: Wilson ID, editor. Encyclopedia of separation science. Academic Press; 2000. p. 3901-3906. DOI: 10.1016/B0-12-226770-2/03351-2.
[22] Micheluz A, Angelin EM, Almeida Lopes J, Melo MJ, Pamplona M. Discoloration of historical plastic objects: new insight into the degradation of β-naphthol pigment lakes. Polymers 2021; 13: 2278. DOI: 10.3390/polym13142278.
[23] Miliani C, Monico L, Melo MJ, Fantacci S, Angelin EM, Romani A, Janssens K. Photochemistry of artists' dyes and pigments: towards better understanding and prevention of colour change in works of art. Angew Chem Int Ed. 2018; 57: 7324-7334. DOI: 10.1002/anie.201802801.
[24] Angelin EM, Conceição Oliveira M, Nevin A, Picollo M, Melo MJ. To be or not to be an azo pigment: chemistry for the preservation of historical β-naphthol reds in cultural heritage. Dyes Pigm. 2021; 190: 109244. DOI: 10.1016/j.dyepig.2021.109244.
[25] Montalti M, Credi A, Prodi L, Gandolfi MT. Handbook of photochemistry. Boca Raton: Taylor & Francis, third ed.; 2006.
[26] Sousa MM., Miguel C, Rodrigues I, Parola AJ, Pina F, de Melo JSS, Melo MJ. A photochemical study on the blue dye indigo: from solution to ancient Andean textiles. Photochem Photobiol Sci. 2008; 7: 1353-1359. DOI: 10.1039/B809578G.
[27] Claro A. An interdisciplinary approach to the study of colour in Portuguese manuscript illuminations. Doctoral dissertation. Lisbon: Universidade Nova de Lisboa, Faculdade de Ciências e Tecnologia; 2009.
[28] França de Sá S, Marques da Cruz S, Callapez ME, Carvalho V. Plastics that made history – The contribution of conservation science for the history of the Portuguese Plastics Industry. Conservar Património 2020; 35: 85-100. DOI: 10.14568/cp2019017.
[29] Angelin EM, Cucci C, Picollo M. UV-Vis-NIR reflectance spectroscopy: a review of its application to the study of contemporary art materials. In: 3rd International Conference on Innovation in Art Research and Technology (InArt2018), Parma (Italy), 26-29 March 2018; Oral presentation.
[30] Angelin EM, Cucci C, Picollo M. UV-Vis-NIR reflectance spectroscopy: its application to the study of plastic heritage. In: Marchiafava V, Picollo M, editor. Colour and Colorimetry Multidisciplinary Contributions. Milano: Gruppo del Colore – Associazione Italiana Colore, Vol XVI B; 2020. p. 115-121.
[31] Cucci C, Delaney JK, Picollo M. Reflectance hyperspectral imaging for investigation of works of art: old master paintings and illuminated manuscripts. Acc Chem Res. 2016: 49(10): 2070-2079. DOI: 10.1021/acs.accounts.6b00048.
[32] Delaney JK, Picollo M. Reflectance hyperspectral imaging to support documentation and conservation of 2D artworks. J Am Inst Conserv. 2019; 58: 1-2. DOI: 10.1080/01971360.2019.1589001
[33] Cucci C, Bigazzi L, Picollo M. Fibre optic reflectance spectroscopy as a non-invasive tool for investigating plastics degradation in contemporary art collections: A methodological study on an expanded polystyrene artwork. J Cult Heritage. 2013; 14(4): 290-96. DOI: 10.1016/j.culher.2012.08.003.

[34] Toja F, Nevin A, Comelli D, Levi M, Cubeddu R, Toniolo L. Fluorescence and Fourier-transform infrared spectroscopy for the analysis of iconic Italian design lamps made of polymeric materials. Anal Bioanal Chem. 2011; 399: 2977-2986. DOI: 10.1007/s00216-010-4323-2.
[35] Toja F, Saviello D, Nevin A, Comelli D, Lazzari M, Levi M, Toniolo L. The degradation of poly(vinyl acetate) as a material for design objects: a multi-analytical study of the effect of dibutyl phthalate plasticizer. Part 1. Polym Degrad Stab. 2012; 97(11): 2441-2448. DOI: 10.1016/j.polymdegradstab.2012.07.018.
[36] Comelli D, Toja F, D'Andrea C, Toniolo L, Valentini G, Lazzari M, Nevin A: Advanced non-invasive fluorescence spectroscopy and imaging for mapping photo-oxidative degradation in acrylonitrile-butadiene-styrene: a study of model samples and of an object from the 1960s. Polym Degrad Stab. 2014; 107: 356-365. DOI: 10.1016/j.polymdegradstab.2013.12.030.
[37] Romani A, Clementi C, Miliani C, Favaro G. Fluorescence spectroscopy: a powerful technique for the noninvasive characterization of artwork. Acc Chem Res. 2010; 43(6): 837-846. DOI: 10.1021/ar900291y.
[38] Anglos D, Solomidou M, Zergioti I, Zafiropulos V, Papazoglou TG, Fotakis C. Laser-induced fluorescence in artwork diagnostics: an application in pigment analysis. Appl Spectros. 1996; 50(10): 1331-1334. DOI: 10.1366/0003702963904863.
[39] Dooley KA, Chieli A, Romani A, Legrand S, Miliani C, Janssens K, Delaney JK. Molecular fluorescence imaging spectroscopy for mapping low concentrations of red lake pigments: Van Gogh's painting *The Olive Orchard*. Angew Chem. 2020; 132(15): 6102-6109. DOI: 10.1002/ange.201915490.
[40] Picollo M, Aceto M, Vitorino T. UV-Vis spectroscopy. Phys Sci Rev. 2018; 4(4): 1-14. DOI: 10.1515/psr-2018-0008.
[41] Melo MJ, Claro A. Bright light: microspectrofluorimetry for the characterization of lake pigments and dyes in works of art. Acc Chem Res. 2010; 43(6): 857-866. DOI: 10.1021/ar9001894.
[42] Nevin A, Comelli D, Valentini G, Anglos D, Burnstock A, Cather S, Cubeddu R. Time-resolved fluorescence spectroscopy and imaging of proteinaceous binders used in paintings. Anal Bioanal Chem. 2007; 388(8): 1897-1905. DOI: 10.1007/s00216-007-1402-0.
[43] Nevin A, Echard JP, Thoury M, Comelli D, Valentini G, Cubeddu R. Excitation emission and time-resolved fluorescence spectroscopy of selected varnishes used in historical musical instruments. Talanta 2009; 80(1): 286-293. DOI: 10.1016/j.talanta.2009.06.063.
[44] Nevin A, Cesaratto A, Bellei S, D'Andrea C, Toniolo L, Valentini G, Comelli D. Time-Resolved Photoluminescence Spectroscopy and Imaging: New Approaches to the Analysis of Cultural Heritage and Its Degradation. Sensors 2014; 14(4): 6338-6355. DOI: 10.3390/s140406338.
[45] Comelli D, D'Andrea C, Valentini G, Cubeddu R, Colombo C, Toniolo L. Fluorescence lifetime imaging and spectroscopy as tools for nondestructive analysis of works of art. Appl Opt. 2004; 43: 2175-2183. DOI: 10.1364/AO.43.002175.
[46] Comelli D, Valentini G, Nevin A, Farina A, Toniolo L, Cubeddu R. A portable UV-fluorescence multispectral imaging system for the analysis of painted surfaces. Rev Sci Instrum. 2008; 79(8): 086112. DOI: 10.1063/1.2969257.
[47] Comelli D, Nevin A, Valentini G, Osticioli I, Castellucci EM, Toniolo L, Gulotta D, Cubeddu R. Insights into Masolino's wall paintings in Castiglione Olona: advanced reflectance and fluorescence imaging analysis. J Cult Herit. 2011; 12(1): 11-18. DOI: 10.1016/j.culher.2010.06.003.
[48] Comelli D, Artesani A, Nevin A, Mosca S, Gonzalez V, Eveno M, Valentini G. Time-resolved photoluminescence microscopy for the analysis of semiconductor-based paint layers. Materials 2017; 10(11): 1335. DOI: 10.3390/ma10111335.
[49] Whitmore PM, Bailie C, Connors SA. Micro-fading tests to predict the result of exhibition: progress and prospects. Stud Conserv. 2000; 45(sup1): 200-205. DOI: 10.1179/sic.2000.45.Supplement-1.200.

Appendices

A. Application of infrared reflectance spectroscopy on plastics in cultural heritage collections: a comparative assessment of two portable mid-Fourier transform infrared reflection devices

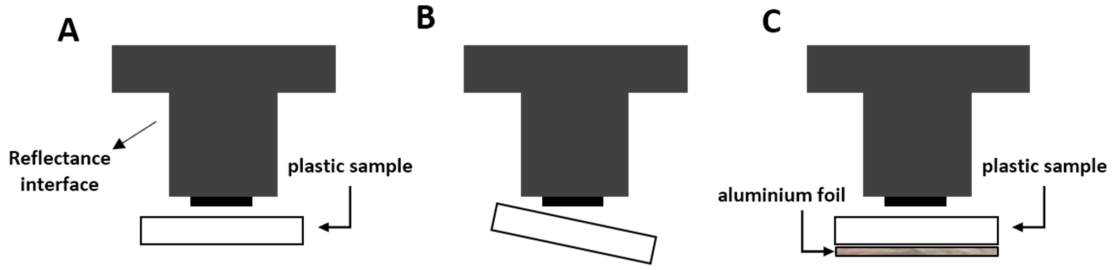

Figure A.1.: Schematic representation of the two tested sample positions in relation to the acquisition reflectance interface: parallel (A) and oblique (B); and presence (C) of the aluminum foil in the back of the sample.

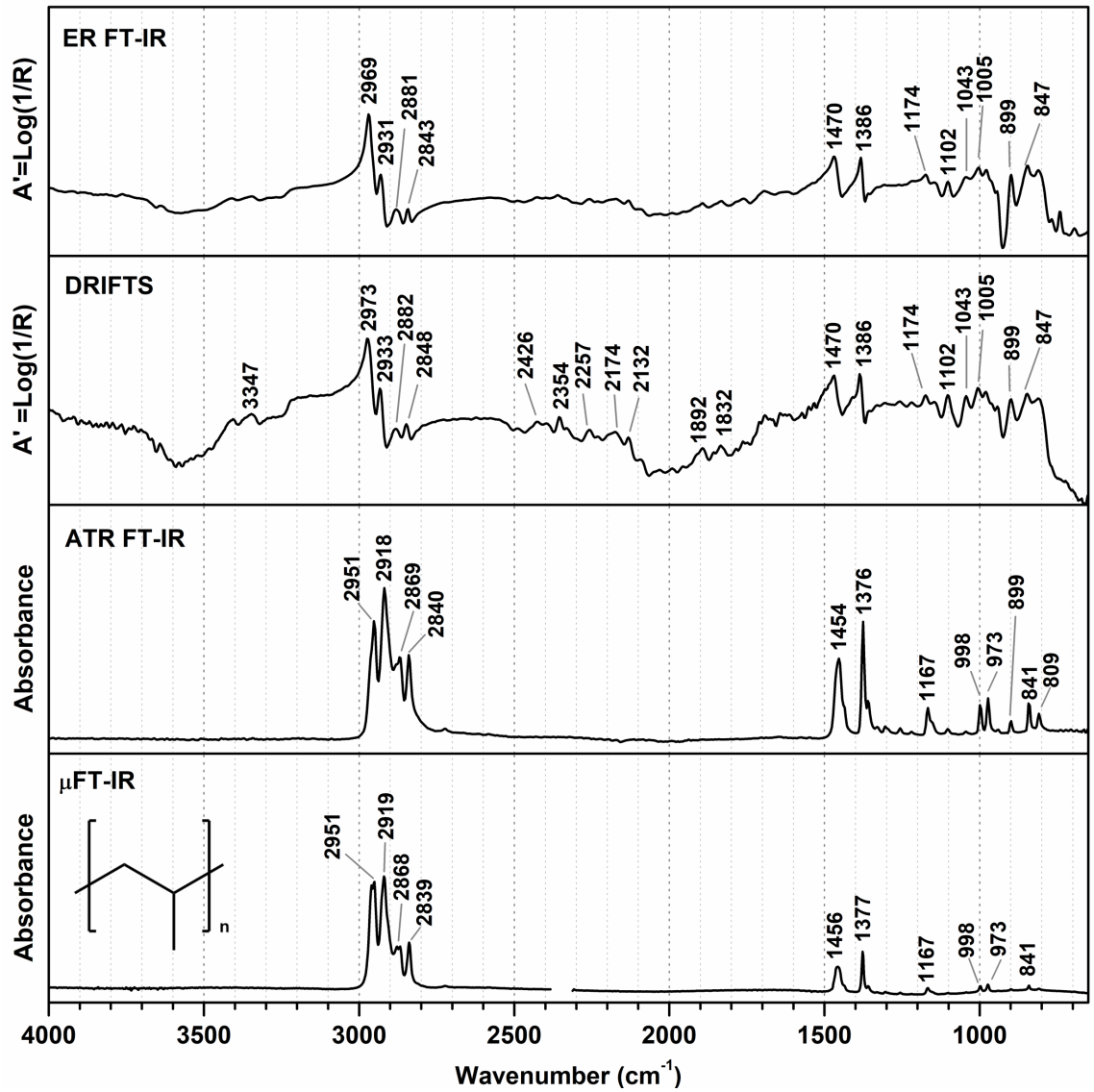

Figure A.2.: FT-IR spectra of the PP polymer reference using several acquisition modes. From bottom to top: μFT-IR, ATR FT-IR, DRIFTS and ER FT-IR.

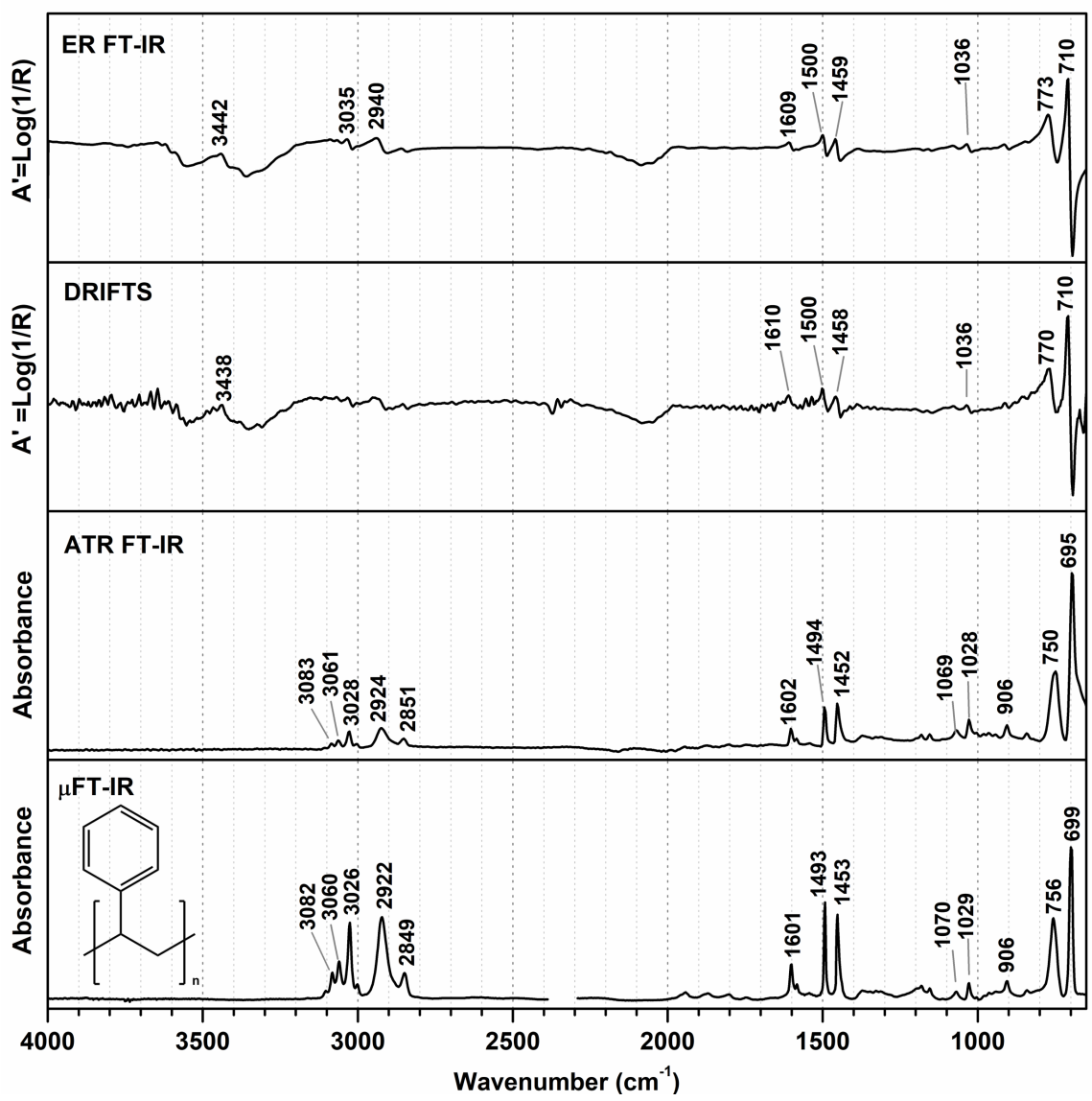

Figure A.3.: FT-IR spectra of the PS polymer reference using several acquisition modes. From bottom to top: μFT-IR, ATR FT-IR, DRIFTS and ER FT-IR.

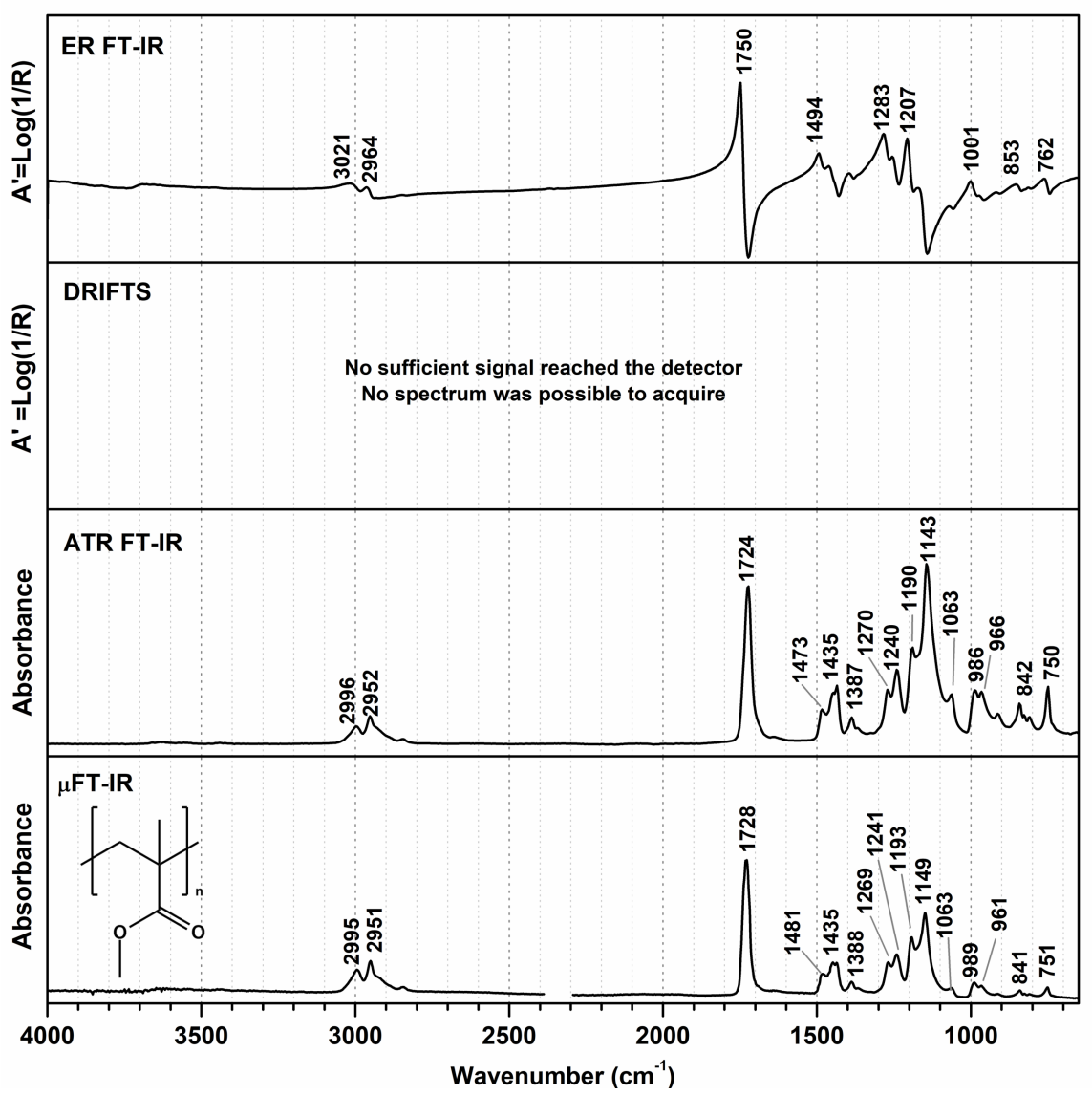

Figure A.4.: FT-IR spectra of the PMMA polymer reference using several acquisition modes. From bottom to top: μFT-IR, ATR FT-IR, DRIFTS and ER FT-IR.

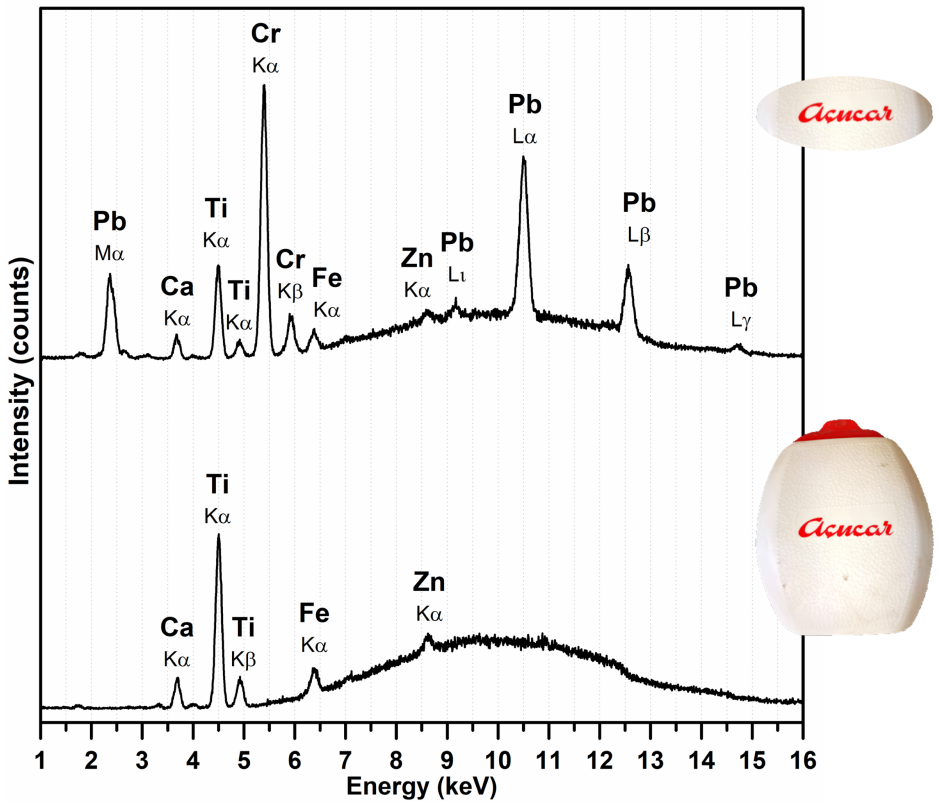

Figure A.5.: µEDXRF spectra of sugar container, white body (bottom) and red printed lettering '*Açúcar*' (up).

Table A.1.: Characteristic IR bands of the plastic references acquired in transmission mode (μFT-IR). Assignments from Noda et al. [1].

High density Polyethylene (HDPE)		**Polypropylene (PP)**		**Polystyrene (PS)**		**Polymethyl methacrylate (PMMA)**	
Frequency (cm^{-1})	**Assignments**	**Frequency (cm^{-1})**	**Assignments**	**Frequency (cm^{-1})**	**Assignments**	**Frequency (cm^{-1})**	**Assignments**
2918vs	$\nu_{as}(CH_2)$	2951vs	$\nu_{as}(CH_3)$	3082m	$\nu(CH)_{ar}$	2995m	$\nu(CH_3)$ α-methyl
2851s	$\nu_s(CH_2)$	2919vs	$\nu_{as}(CH_2)$	3060m		2951m	$\nu(CH_3)$ ester methyl
1468w	$\delta(CH_2)$	2868s	$\nu_s(CH_3)$	3026s		1728vs	ν(C=O)
718w	$\rho(CH_2)$	2839s	$\nu_s(CH_2)$	2922s	$\nu_{as}(CH_2)$	1481m	$\delta_{as}(CH_3)$ α-methyl
		1456s	$\delta(CH_2)$	2849m	$\nu_s(CH_2)$	1435m	$\delta_s(CH_2)$, δ(O-CH_3)
		1377s	$\delta_s(CH_3)$, $\omega(CH_2)$	1601m	ring quadrant stretch	1388w	$\delta_s(CH_3)$
		1167m	$\nu(CC)_b$, $\rho(CH_3)$, δ(CH)	1493s	ring semicircle stretch	1269m	ν(C-O)
		998w	$\rho(CH_3)$, (CH_3), δ(CH)	1453s	ring semicircle stretch, $\delta(CH_2)$	1241m	ν(C-O)
		973w	$\rho(CH_3)$, $\nu(CC)_b$	1029m	ring in-phase δ(CH)	1193s	ν(C-O)
		841w	$\rho(CH_2)$, ν(C-CH_3)	756s	mono-substituted ring in-phase ω(CH)	1149s	ν(C-O)
				699vs	mono-substituted ring out-of-plane bend	989w	ν(C-O-C)
						961w	$\nu(CC)_b$
						841w	$\nu(CC)_b$
						751w	$\nu(CC)_b$, ρ(CH)

Abbreviations: m = medium, s = strong, v = very, w = weak, δ = bending, ν = stretching, ρ = rocking, ω = wagging, $_{as}$ = asymmetric, $_s$ = symmetric, $_{ar}$ = aromatic, $_b$ = backbone chain

References

[1] Noda I, Dowrey AE, Haynes JL, Marcott C. Group frequency assignments for major infrared bands observed in common synthetic polymers. In: Mark JE, editor. Physical properties of polymers handbook. New York: Springer, second ed.; 2007. p. 395-406.

B. Raman microscopy for the identification of pearlescent pigments in acrylic works of art

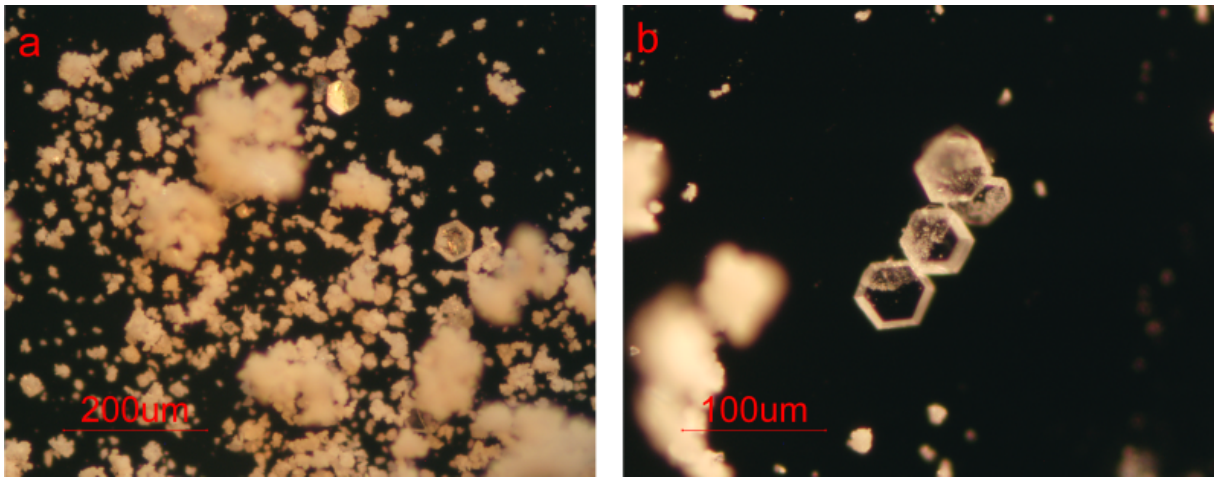

Figure B.1.: Microscopy images of synthetized crystals of plumbonacrite under reflected visible light in dark field (a-b).

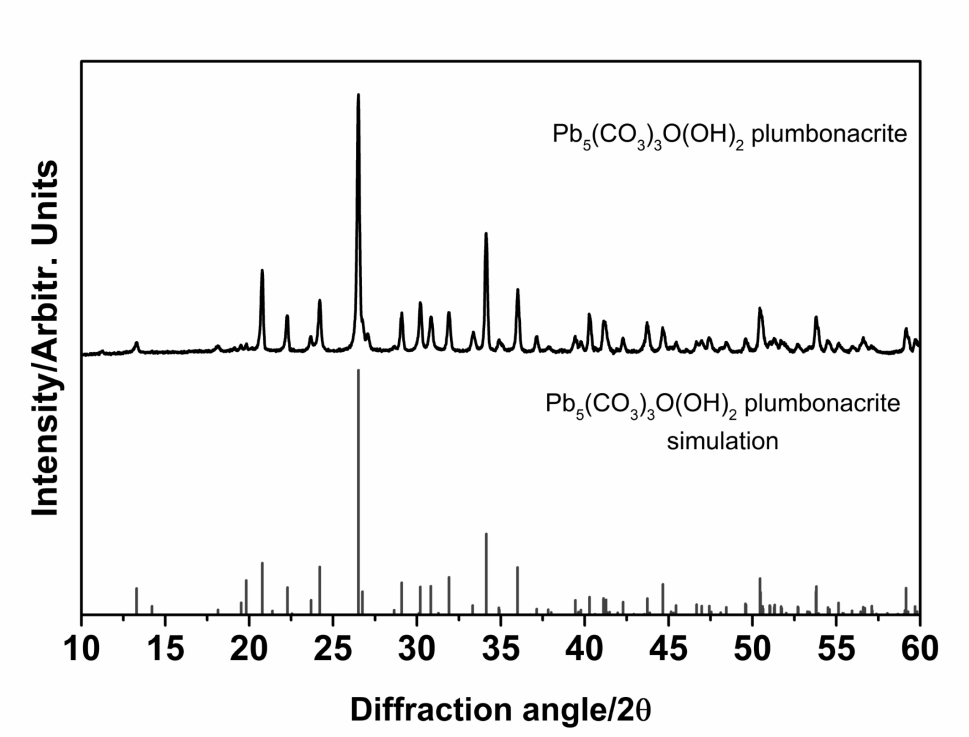

Figure B.2.: XRD patterns of the synthesized plumbonacrite $Pb_5(CO_3)_3O(OH)_2$ and plumbonacrite $Pb_5(CO_3)_3O(OH)_2$ X-ray diffraction simulation with lattice parameters published in literature (primitive unit cells with $a = 9.0921$ Å, $c = 24.923$ Å) [1].

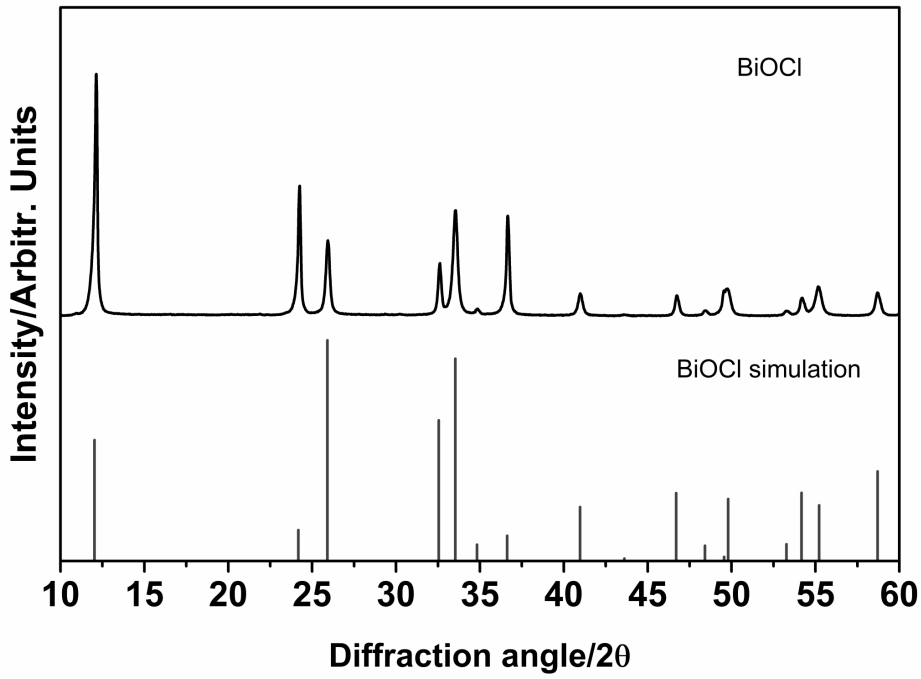

Figure B.3.: XRD patterns of synthesized bismuth oxychloride BiOCl and bismoclite BiOCl X-ray driffraction simulation with lattice parameters published in literature (primitive unit cells with $a = 3.887$ Å, $c = 7.354$ Å) [2].

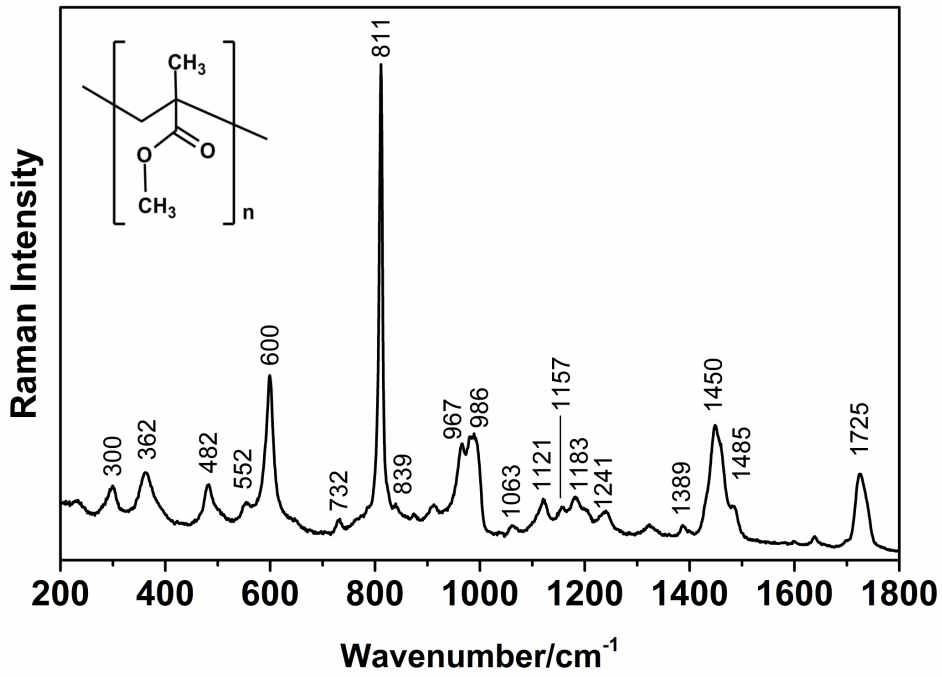

Figure B.4.: Vibrational spectrum of polymer PMMA collected in situ through Raman microscopy (632.8 nm excitation).

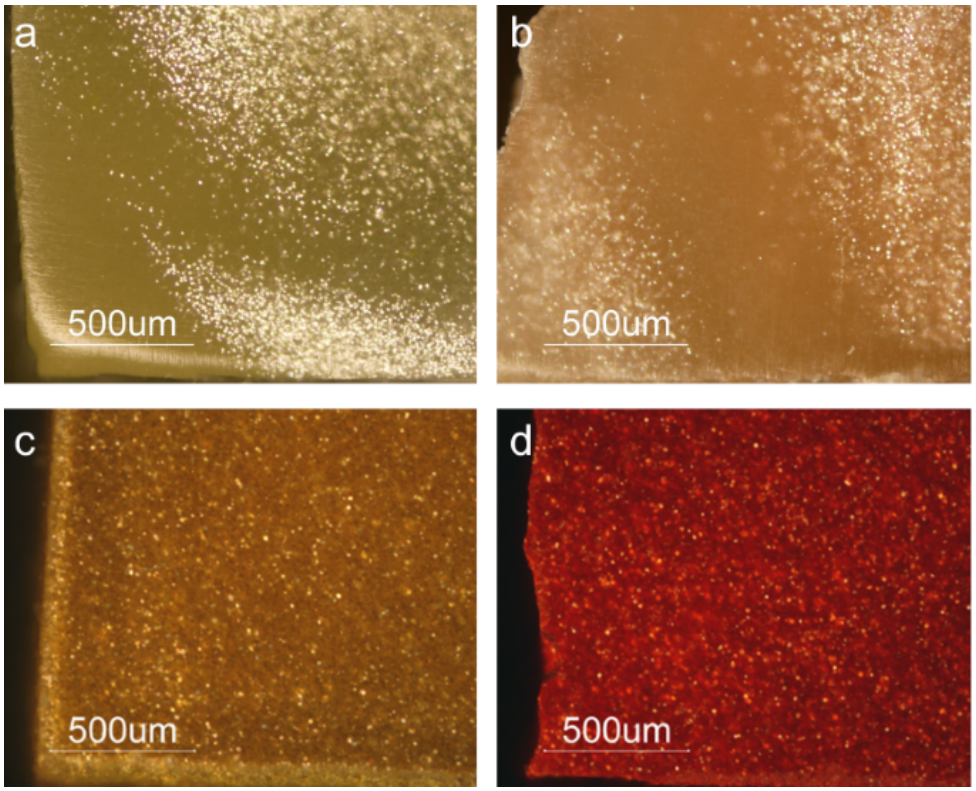

Figure B.5.: Microscopy images of the platelets in (a,c) yellow, (b) orange, (c) red pearlescent acrylic sheet probably made in 1960s (a-b) and 2000s (c-d) under reflected visible light in dark field.

References

[1] Krivovichev SV, Burns PC. Crystal chemistry of basic lead carbonates. II. Crystal structure of synthetic 'plumbonacrite'. Mineral Mag. 2000; 64(6): 1069-1075. DOI: 10.1180/002646100549887.

[2] Keramidas KG, Voutsas GP, Rentzeperis PI. The crystal structure of BiOCl. Z Kristallogr Cryst Mater. 1993; 205(1): 35-40. DOI: 10.1524/zkri.1993.205.Part-1.35.

C. The multi-analytical in situ analysis of cadmium-based pigments in plastics

Background: PMMA and Plásticos do Sado products

Plásticos do Sado was a small Portuguese company that produced acrylic sheets from c.1959-1960 until the beginning of the 21st c. It was founded by an Armenian entrepreneur who settled and started a business in Portugal producing acrylic sheets for the button industry. One of the particularities of this company was that the PMMA production was based on recycled monomer, which was also produced on the factory through chemical recycling. PMMA scrap was collected in Portugal and abroad, and depolymerization into MMA was carried out by pyrolysis in a molten lead bath reactor. The monomer was then purified in several steps of washing, decantation and distillation. The production of acrylic sheets would start by the preparation of a pre-polymerized syrup of PMMA by mixing the distilled MMA, an initiator, a release agent, and a plasticizer. When the syrup reached the desired viscosity, colorants and anti-UV agents could be added. To produce cast acrylic sheets, the pre-polymerized syrup was poured into glass molds, which were heated in water tanks where the polymerization would occur. After cooling, PMMA sheets were removed from the molds and both surfaces protected. Plásticos do Sado was a family business, with a small-scale production using basic technology [1]. In casting of PMMA, coloring must be done prior to polymerization, and as described above, the cadmium pigments were probably added as a powder to the pre-polymerized MMA syrup. During the polymerization free radicals are produced and colorants must be relatively inert; otherwise, they may flocculate, change color or affect the polymerization. The use of cadmium pigments allowed the successful production of colored acrylic sheets due to their chemical stability during the polymerization reactions [2]. The samples here studied were ceded by the last owner of Plásticos do Sado company.

Powder X-ray diffraction (PXRD)

High quality XRPD data of reference *(Cd,Hg)S* was recorded in a 0.3 mm glass capillary on a Bruker New D8 Da Vinci diffractometer (Cu-Kα_1 radiation = 1.54056Å, 40 kV x 40 mA), equipped with a Bruker LYNXEYE-XE detector, scanning range 2θ = 14-90°, 0.017° increments of 2θ and a counting time of 6 s/step. For Rietveld refinement was used the software TOPAS 6. (Bruker AXS, Copyright ©, 1999, 2016 Bruker AXS) with a shifted Chebyshev with nine coefficients to fit background and a Double Voigt approach to fit peak shape. The cif files of greenockite and barite were used as a starting point for Rietveld refinement. Barium sulfate was also characterized by XRPD analysis using a Barium sulfate purchased from Merck at the same condition in which was analyzed the pigment. In the greenockite structure the percentage of Hg in the site generally occupied by Cd results in 21($\pm$6)%. The final accordance parameters for Rietveld refinement result in Rwp = 4.37, Rp = 3.18 and GOF = 1.87; the refined diffraction pattern is shown **Figure C.6**.

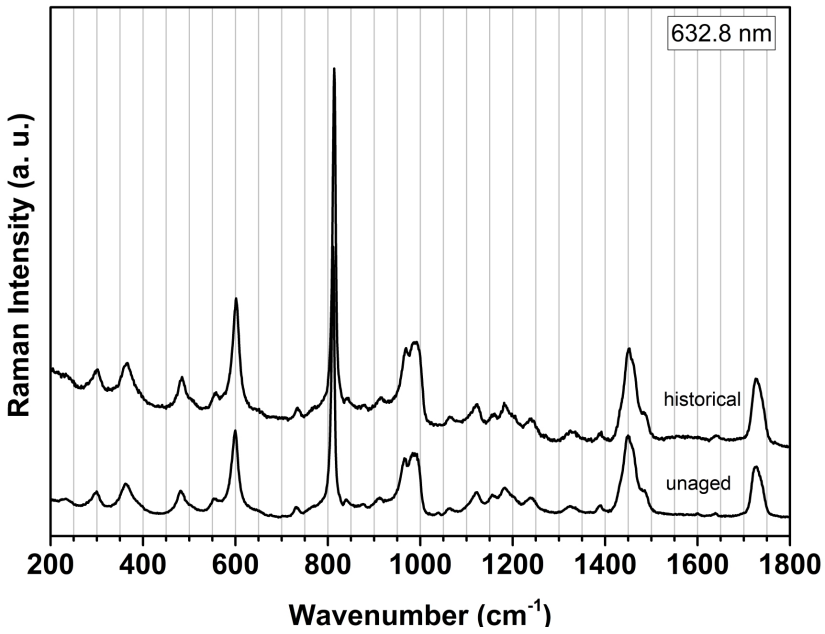

Figure C.1.: Raman spectra of historical (sample 355) and unaged (Paraglass, Portugal) PMMA (632.8 nm excitation).

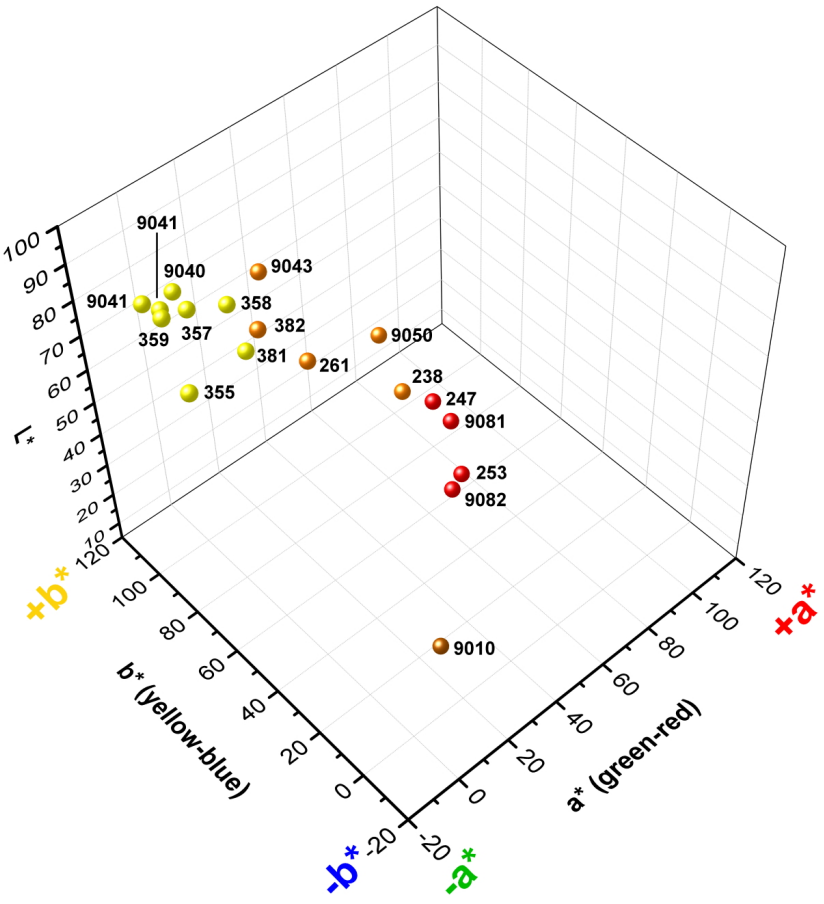

Figure C.2.: Color coordinates of historical acrylic samples in the CIELAB 76 color space.

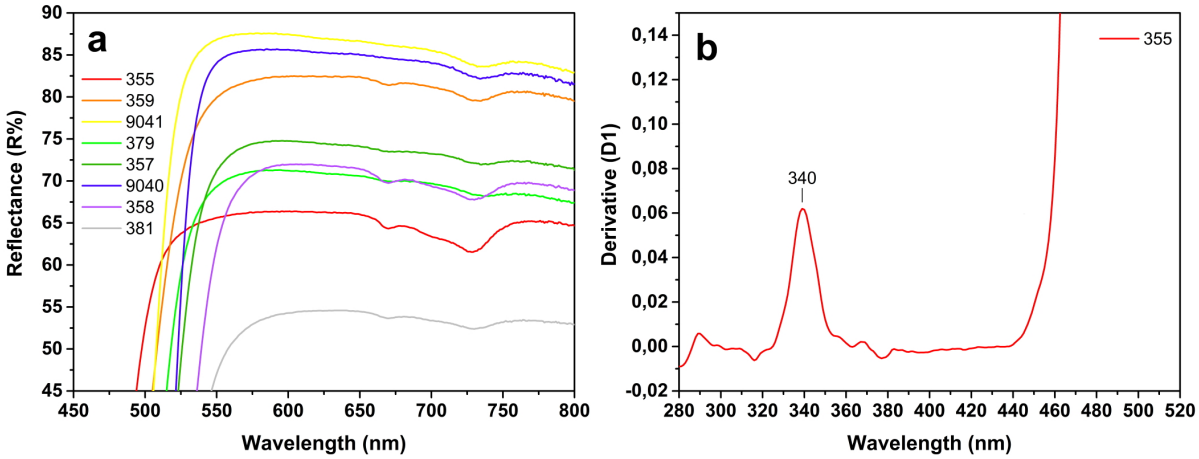

Figure C.3.: a) UV-Vis reflectance spectra of yellow acrylic samples highlighting very weak composite absorption bands in the 650-750 nm range, which indicate the presence of Co(II) in a pseudo tetrahedral sulfur coordination in ZnS; b) UV-Vis reflectance spectra of yellow acrylic sample 355. Inflection point of ZnS is identified (340 nm).

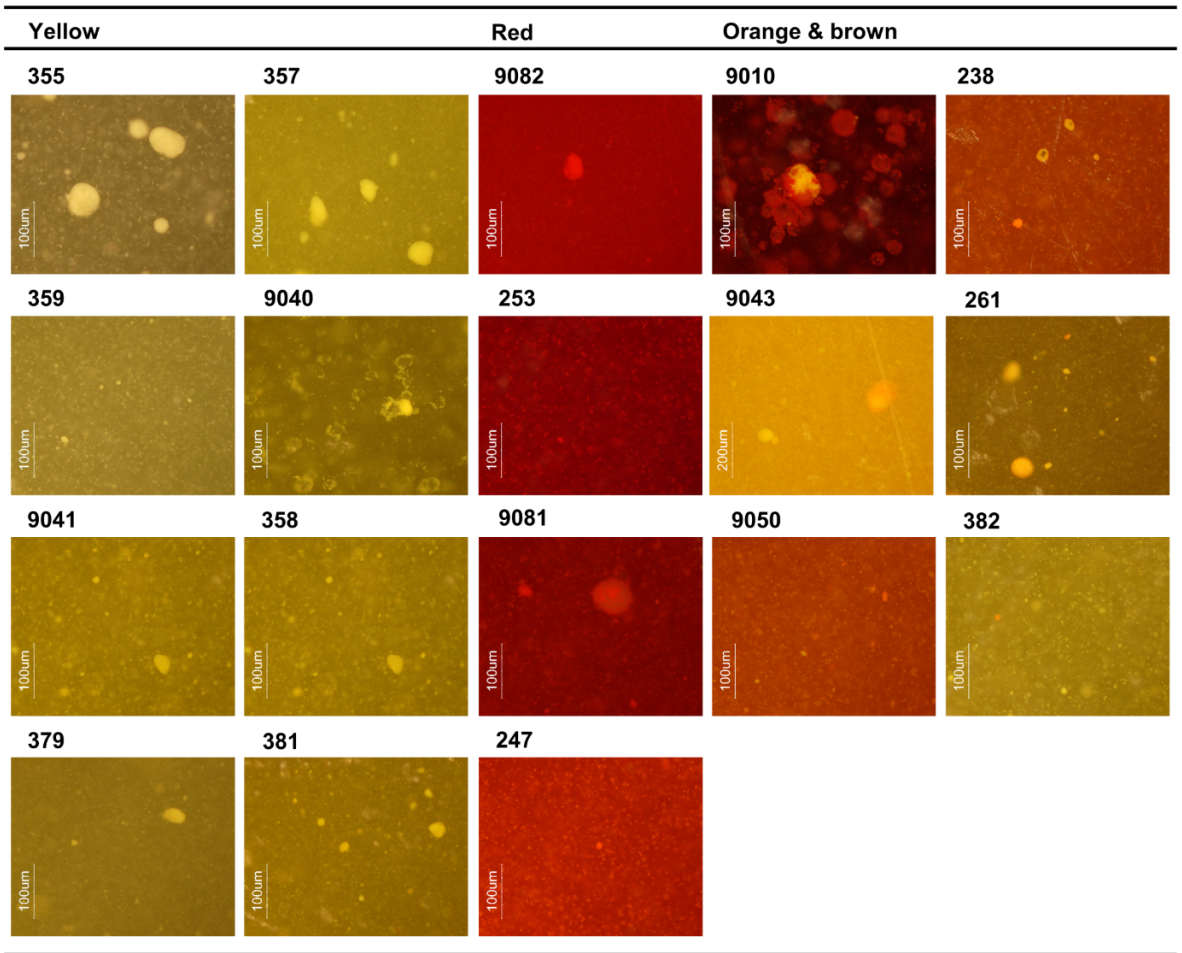

Figure C.4.: Microscopy images of the Cd-based pigment particles in yellow, red, orange and brown historical acrylic samples (dark field 10× and 20×).

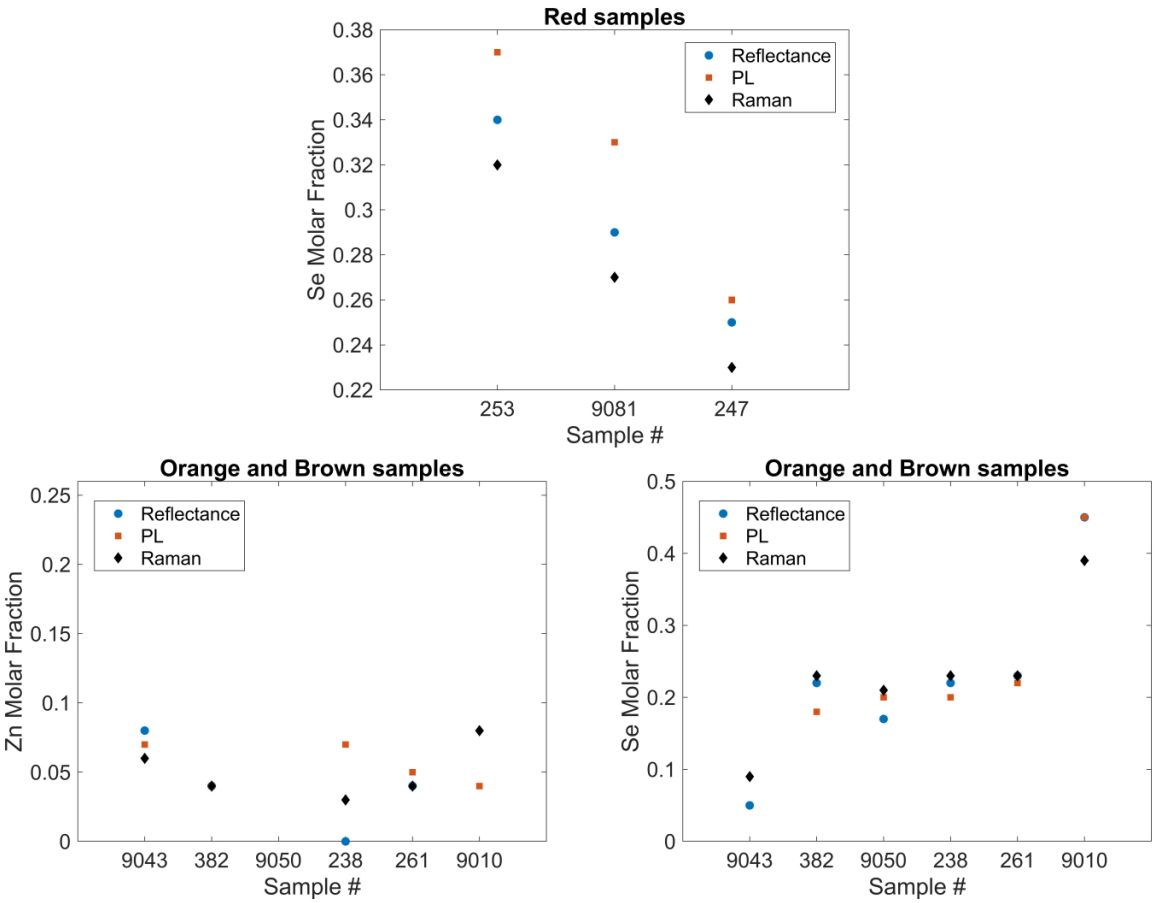

Figure C.5.: Extrapolated molar fractions of Se and Zn of the red, orange-brown acrylic samples obtained on the basis of reflectance (blue colored circles), PL (red colored squares) and μ-Raman (black colored diamonds) data.

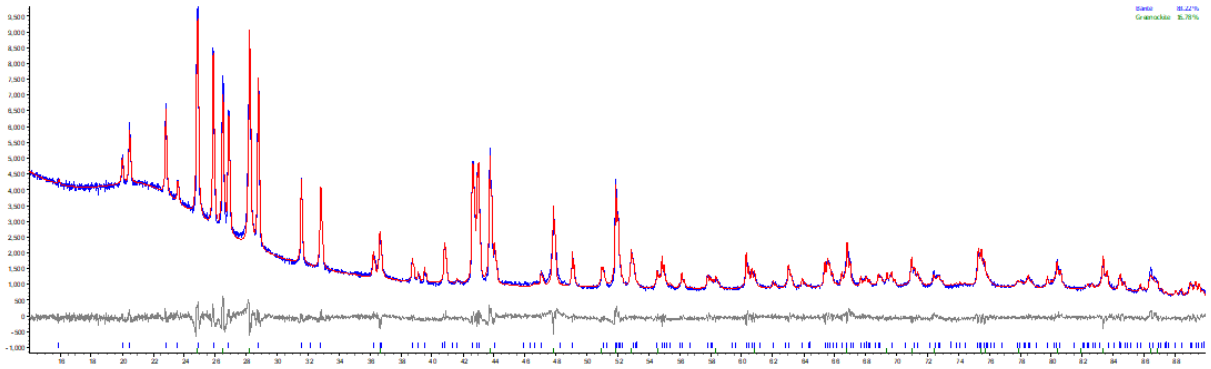

Figure C.6.: Rietveld refinement of pigment *(Cd,Hg)S* reference, difference (gray) between the experimental (blue) and calculated (red) powder pattern (x axis in 2Theta and y axis in counts).

Table C.1.: Raman bands (cm^{-1}) and assignments of historical (sample 355) and unaged (Paraglass, Portugal) PMMA (632.8 nm excitation).

Raman shift (cm^{-1})		
Unaged PMMA	**Historical PMMA**	**Mode[a]**
1726	1725	ν(C=O)
1485	1486	$\delta_{as}(CH_3)$
1452	1452	d(CH_2)
1388	1390	$\delta_s(CH_3)$
1238	1240	ν(C–C)
1182	1181	ν(C–C)
1156	1159	ν(C–O) + $\rho(CH_3)$
1122	1122	ν(C–O) + $\rho(CH_3)$
1063	1063	$\omega(CH_2)$
988	988	ν(C–C)
966	969	ν(C–C)
840	840	d(C=O) + $\rho(CH_3)$
812	813	ν_s(C-C)
730	732	d(O–C=O) + $\rho(CH_3)$
600	601	δ(O-C=O)
553	554	δ(O–C=O)
483	484	d(C–C)
363	365	d(C–C)
300	301	d(C–C)

Note. ν, stretching (a, symmetric; as, asymmetric); ρ, rocking; δ, bending (a, symmetric; as, asymmetric); τ, twisting; ω, wagging; d, deformation.
[a] [3]

Table C.2.: Assignments and long-wavelength optical phonon frequencies ($\Delta\nu$ in cm^{-1}) of reference *h-CdS* and CdS phase identified in the yellow acrylic samples (785 nm excitation).

Published work[a] CdS	**This work *h-CdS***	**352**	**355**	**357**	**358**	**359**	**379**	**381**	**9040**	**9041**	**Phonon frequency**
213	210s	213m	211m	210vs	211m	211vs	211s	210vs	210m	211s	Multi-phonon mode
235	232s		233vw	232s	235w,br	233m	233w	233s	233w	233w	TO modes (A_1/E_1)
242			242vw								
252*	248m	250vw	252vw	250m	250w	250w	252w	250m	248w	250vw	E_2
307	300s	301m	303m	302s	300m	301vs	303s	301m	301w	300s	LO modes (A_1/E_1)
323	321m	325vw		323w,br		323w		323w			Multi-phonon modes
331	335m		331vw							331vw	
344	342m	344w	345 vw	343m,br	344m	346 h	348 m	344w		346sh	
352		354w	354w,b			356m				358m	
367	360m		362vw	361w,br	366m		366sh	366sh			
560	558w,br			561w,br		561br,m				560w,br	
600	598m	597m	597m	589s	598m	597s	600s	597m	598w	597s	2LO mode

Note. Raman bands are indicated as very strong (vs), strong (s), medium (m), weak (w), very weak (vw), broad (b) and shoulder (sh).
* h-CdS specific Raman signature.
[a] [4]

Table C.3.: Assignments and long-wavelength optical phonon frequencies ($\Delta\nu$ in cm^{-1}) of α-*HgS*, cinnabar (632.8 nm excitation).

Published work[a]	**Published work**[b]	**Published work**[c]	**This work**	**Phonon frequency**
256	255	256	253	A_1
283	283	280	283	TO(E)
290	289	288	288	LO(E)
345	343	342	342	TO(E)
353	351	350	349	LO(E)

[a] [5]
[b] [6]
[c] [7]

References

[1] Babo S, Ferreira JL, Melo MJ, Ramos AM. Back to the origin: understanding the history of production and its influence on the properties of acrylic sheet. In: Bechthold T, editor. Future Talks 015 – Processes. The making of design and modern art materials, technologies and conservation strategies. Munich: Die NeueSammlung-The Design Museum; 2015. p. 160-170.

[2] Webber TG, editor. Coloring of plastics. New York: John Wiley & Sons Inc.; 1979.

[3] Angelin EM, Babo S, Ferreira JL, Melo MJ. Raman microscopy for the identification of pearlescent pigments in acrylic works of art. J Raman Spectrosc. 2019; 50: 232-241. DOI: 10.1002/jrs.5431.

[4] Chi TTK, Gouadec G, Colomban P, Wang G, Mazerolles L, Liem NQ. Off-resonance Raman analysis of wurtzite CdS ground to the nanoscale: structural and size-related effects. J Raman Spectrosc. 2011; 42: 1007-1015. DOI: 10.1002/jrs.2793.

[5] Zallen R, Lucovsky G, Taylor W, Pinczuk A, Burstein E. Lattice vibrations in trigonal HgS. Phys Rev B 1970; 1: 4058-4070. DOI: 10.1103/PhysRevB.1.4058.

[6] Nusimovici MA, Meskaoui A. Raman scattering by α-HgS (cinnabar). Phys Status Solidi B 1973; 58: 121-125. DOI: 10.1002/pssb.2220580112.

[7] Cardona M, Kremer RK, Siegle G, Muñoz A, Romero AH, Schmidt M. Electronic and phononic properties of cinnabar: *ab initio* calculations and some experimental results. Phys Rev B 2010; 82(8): 085210. DOI: 10.1103/PhysRevB.82.085210.

D. The identification of synthetic organic red pigments in historical plastics: developing an in situ analytical protocol based on Raman microscopy

Figure D.1.: Manufacturing brand stamps found for some of the plastic objects.

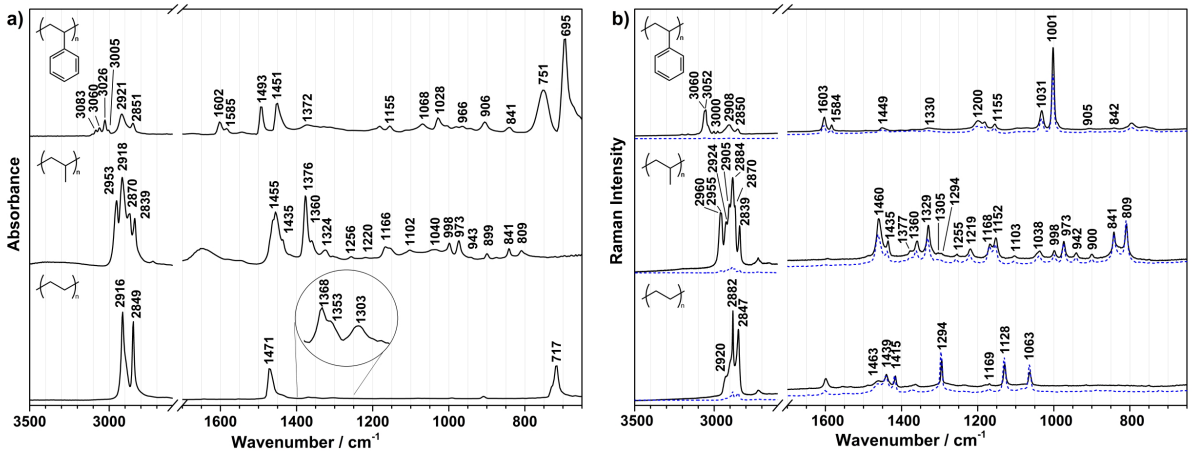

Figure D.2.: ATR-FTIR (a) and μ-Raman (b) spectra of PE (bottom), PP (middle), PS (top). Raman spectra are recorded with 632.8 (black, solid) and 785 laser lines (blue, dash).

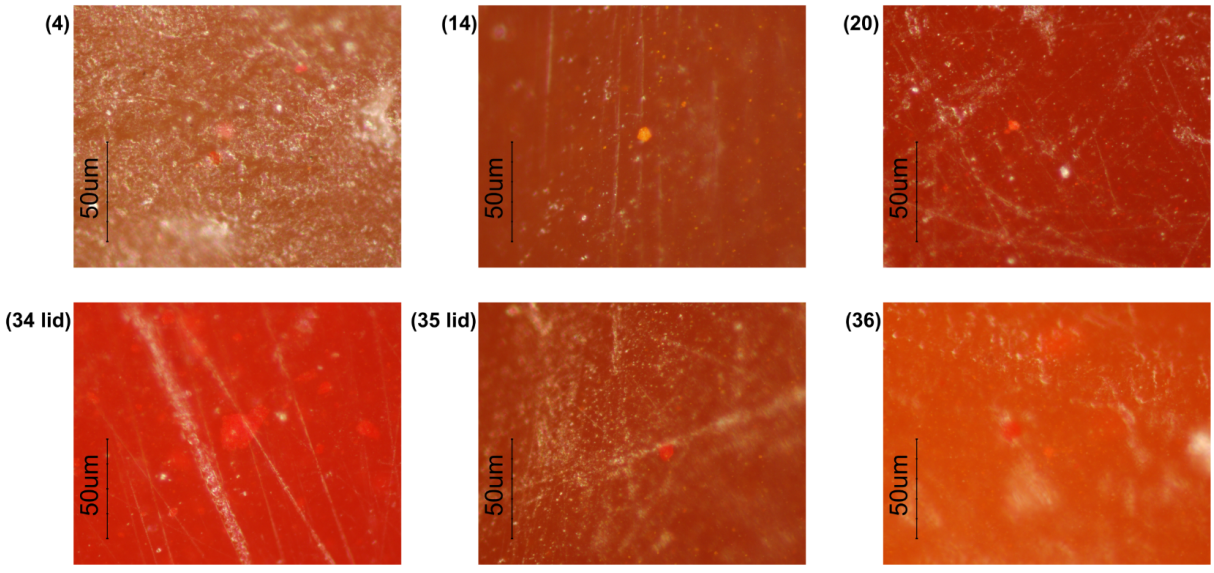

Figure D.3.: Microscopy images of the red particles/aggregates dispersed in the polymeric matrix under reflected visible light (dark field). Images were collected directly from the red plastic components (in situ). The number of the object is reported in parenthesis.

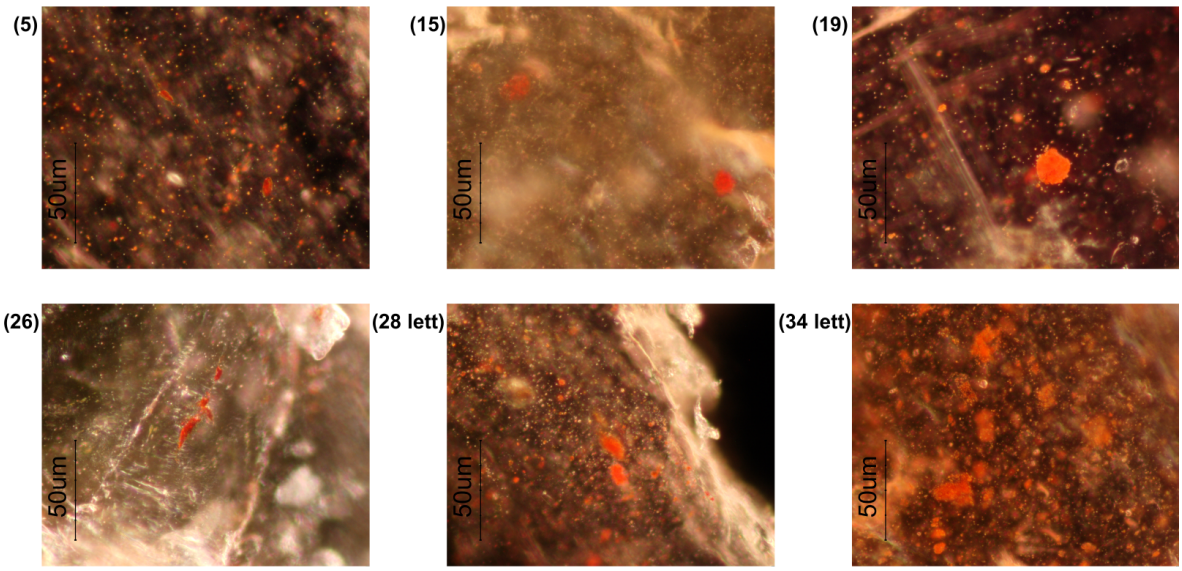

Figure D.4.: Microscopy images of the red particles/aggregates dispersed in the polymeric matrix under reflected visible light (dark field). Images of microsamples were collected from the red plastic components. The number of the object is reported in parenthesis.

Figure D.5.: Back-illuminated illuminated image of object n. 3 showing heterogeneous distribution of red pigment particles.

Table D.1.: Detailed description of the objects under study.

Object n.	Description	Manufacturing brand	Proposed date	Place of production
1	food container without lid, 3D fish decoration, printed lettering (namely parsley)	-	1950s –1970s	-
2	food container without lid, 3D fish decoration, printed lettering (namely parsley)	-	1950s –1970s	-
3	lid	-	1950s –1970s	-
4	sandal with heart decoration	-	1950s –1970s	-
5	sandal with butterfly decoration	-	1950s –1970s	-
6	food container with lid and printed lettering (garlic)	-	1950s –1970s	-
7	food container with lid and printed lettering (soda)	-	1950s –1970s	-
8	food container with lid and printed lettering (paprika)	-	1950s –1970s	-
9	food container with lid and printed lettering (pepper)	-	1950s –1970s	-
10	demijohn with lid	-	1950s –1970s	-
11	demijohn with lid	-	1950s –1970s	-
12	demijohn with lid	F.L.P. - Fábrica Leiriense de Plásticos	1956 – 1990s	Leiria, Portugal
13	bowl	-	1950s –1970s	-
14	drug container with lid and printed lettering (soap)	F.P. EDMAR - Plásticos Edmar	1955 – 1995	Leiria, Portugal
15	cup	F.L.P. - Fábrica Leiriense de Plásticos	1956 – 1990s	Leiria, Portugal
16	dish	-	1950s –1970s	-
17	food container with lid and printed pois, lettering (butter)	Plásticos Santo António	1955 – ?	Leiria, Portugal
18	food container with lid (sugar)	-	1950s –1970s	-
19	cup	-	1950s –1970s	-
20	food container with lid (sugar)	-	1950s –1970s	-
21	food container with lid (sugar)	-	1950s –1970s	-
22	drug container with lid and printed lettering (salt)	F.P. Lena - Fábrica de Plásticos do Lena	1961 – 2016	Leiria, Portugal
23	food container with lid and printed lettering (margarine)	-	1950s –1970s	-
24	drug container with lid and printed lettering (butter)	Plásticos Santo António	1955 – ?	Leiria, Portugal
25	demijohn with lid and ribbon	-	1950s –1970s	-
26	jar with lid and printed lettering (sugar)	-	1950s –1970s	-
27	jar with lid and printed lettering (pasta)	-	1950s –1970s	-
28	jar with lid and 3D lettering (chickpeas)	F.L.P. - Fábrica Leiriense de Plásticos	1956 – 1990s	Leiria, Portugal
29	jar with lid and 3D lettering (beans)	F.L.P. - Fábrica Leiriense de Plásticos	1956 – 1990s	Leiria, Portugal
30	jar with lid and printed lettering (flour)	Jalfe - Fábrica J. Alves de Freitas	Before 1963 – ?	Lisbon, Portugal
31	jar with lid and 3D lettering (chickpeas)	-	1950s –1970s	-
32	jar with lid	F.P.D. Dinis - Fábrica de Plásticos D.Dinis	1960 – ca1985	Leiria, Portugal
33	jar with lid and 3D lettering (rice)	F.P.D. Dinis - Fábrica de Plásticos D.Dinis	1960 – ca1985	Leiria, Portugal
34	jar with lid and 3D lettering (chickpeas)	-	1950s –1970s	-
35	food container with lid and printed lettering (rice)	-	1950s –1970s	-
36	bottle with lid	-	1950s –1970s	-

Table D.2.: Infrared and Raman bands assigned for polymers identified in historical objects.

Polyethylene (PE)				Polypropylene (PP)				Polystyrene (PS)			
Infrared (ν/cm^{-1})	Raman shift ($\Delta\nu$/cm^{-1})		Assignment [1,2]	Infrared (ν/cm^{-1})	Raman shift ($\Delta\nu$/cm^{-1})		Assignment [2,3]	Infrared (ν/cm^{-1})	Raman shift ($\Delta\nu$/cm^{-1})		Assignment [4,5]
	@632.8nm	@785nm			@632.8nm	@785nm			@632.8nm	@785nm	
2916vs	2920m	2884w	$\nu_{as}(CH_2)$	-	2960s	-	$\nu_{as}(CH_3)$	3083w	-	-	$\nu(CH)_{ar}$
-	2882vs	-		2953vs	2955s	-		3060w	3060s	3060vw	
2849vs	2847vs	2849w	$\nu_s(CH2)$	2918vs	2924s	2927w	$\nu_{as}(CH_2)$	3026m	3052s	3053vw	
1471m	1463w,br	1463w	$\delta(CH_2)$	-	2905s	2905w	$\nu(CH)$	3005w	3000w	3000vw	
-	1439	1441m		-	2884vs	2884w	$\nu_s(CH_3)$	2921s	2908m	2908vw	$\nu_{as}(CH_2)$
-	1415m	1419m	$\omega(CH_2)$	2870vs	2870s	2870vw	$\nu_s(CH_2)$	2851m	2850m	2851vw	$\nu_s(CH_2)$
1368vw	-	-	$\omega(CH_2)$	2839vs	2839s	2840vw		1602m	1603m	1603m	$\nu_{9B}(B_1)_{ar}$
1353vw	-	-		1455s	1460s	1462s	$\delta(CH_3)$, $\delta(CH_2)$	1585m	1584m	1585m	$\nu_{9A}(A_1)_{ar}$
1303vw	-	-		1435m	1435m	1438m	$\delta(CH_3)$	1493s	-	-	$\nu_{19A}(A_1)_{ar}$
-	1294s	1296vs	$\tau(CH_2)$	1376s	1377w	1377w	$\delta(CH_3)$, $\omega(CH_2)$, $\delta(CH)$, $\nu(CC)_b$	1451s	1449w,br	1450w,br	$\nu_{19B}(B_1)_{ar}$, $\delta(CH_2)$
-	1169w	1171w	$\rho(CH_2)$	1360m	1360m	1362m	$\delta(CH_3)$, $\delta(CH)$	1372m,br	-	-	
-	1128s	1129s	$\nu(CC)_b$, $\delta(CC)_b$	1324w	1329s	1330s	$\delta(CH)$, $\tau(CH_2)$	-	1330w,br	1330w,br	$\nu_{14}(B_1)_{ar}$
-	1063s	1064s	$\nu(CC)_b$	-	1305w	-	$\omega(CH_2)$, $\tau(CH_2)$	-	1199m	1200m	$\nu_{8A}(A_1)_{ar}$
717m	-	-	$\rho(CH_2)$	-	1294w	-	$\omega(CH_2)$, $\delta(CH)$, $\tau(CH_2)$	1155w	1155m	1156m	$\nu'_{15}(B_1)_{ar}$
				1256vw	1255w	1257w	$\delta(CH)$, $\tau(CH_2)$, $\rho(CH_3)$	1068w	-	-	$\nu'_{18B}(B_1)_{ar}$, $\nu(CC)_b$
				1220w	1219m	1222m	$\tau(CH_2)$, $\delta(CH)$, $\nu(CC)_b$	1028m	1031m	1031m	$\nu_{18A}(A_1)_{ar}$
				1166w	1168m	1169m	$\nu(CC)_b$, $\rho(CH_3)$, $\delta(CH)$	-	1001vs	1001vs	$\nu_1(A_1)$, $\nu_5(B_2)$, ν'_{13} (A_1)
				-	1152m	1153m	$\nu(CC)_b$, $\nu(C\text{-}CH_3)$, $\delta(CH)$, $\rho(CH_3)$	966w	-	-	$\nu_{17A}(A_2)_{ar}$
				1102vw	1103w	1103w	$\nu(CC)_b$, $\rho(CH_3)$, $\omega(CH_2)$, $\tau(CH)$, $\delta(CH)$	906m	905w	906ww	$\nu_{17B}(B_2)_{ar}$
				1040w	1038m	1038m	$\nu(C\text{-}CH_3)$, $\nu(CC)_b$, $\delta(CH)$	841w	842w	842w	$\nu_{10A}(A_2)_{ar}$
				998w	998m	998m	$\rho(CH_3)$, $\delta(CH)$, $\omega(CH_2)$	751s	-	-	$\nu_{10B}(B_2)_{ar}$
				973w	973m	973m	$\rho(CH_3)$, $\nu(CC)_b$	695vs	-	-	$\nu_{11}(B_2)_{ar}$
				943vw	942w	942w					
				899w	900w	900w	$\rho(CH_3)$, $\rho(CH_2)$, $\delta(CH)$				
				841w	841s	841s	$\rho(CH_2)$, $\nu(CC)_b$, $\nu(C\text{-}CH_3)$, $\rho(CH_3)$				
				809w	809s	809s	$\rho(CH_2)$, $\nu(CC)_b$, $\nu(C\text{-}CH_3)$				

Abbreviations: b = backbone chain, m = medium, s = strong, sh = shoulder, v = very, w = weak, δ = bending, ν = stretching, ρ = rocking, ω = wagging, τ = twisting, $_{as}$ = asymmetric, $_s$ = symmetric, $_{ar}$ = aromatic

* Normal modes (A_1, B_1, A_2, B_2) specify the assignments of the vibrations of the monosubstituted benzene. Their numbering follows the Wilson's notation [6].

Table D.3.: Molar fraction of Se content of PR 108 based on μ-Raman spectra acquired with 632.8 nm.

Object n.	**Plastic component**	**Se molar fraction (x)**
34	lettering	0.43
4		0.32
29	lid	0.32
28		0.30
20	lid	0.28
2	3D fish decoration	0.28
35	lid	0.23
	base	0.16
18	lid	0.13
23	lid	0.11
21	lid	0.11
14	lid	0.09

References

[1] Krimm S, Liang CY, Sutherland GBBM. Infrared spectra of high polymers. II. Polyethylene. J Chem Phys. 1956; 25(3), 549-562. DOI: 10.1063/1.1742963

[2] Noda I, Dowrey AE, Haynes JL, Marcott C. Group frequency assignments for major infrared bands observed in common synthetic polymers. In: Mark JE, editor. Physical properties of polymers handbook. New York: Springer, second ed.; 2007. p. 395-406.

[3] Andreassen E. Infrared and Raman spectroscopy of polypropylene. In: Karger-Kocsis J, editor. Polypropylene: an A-Z reference. Dordrecht: Springer, Polymer Science and Technology Series, Vol. 2; 1999. p. 320-328.

[4] Liang CY, Krimm S. Infrared spectra of high polymers. VI. Polystyrene. J Polym Sci. 1958; 27: 241-254. 10.1002/pol.1958.1202711520.

[5] Nyquist RA, Putzig CL, Leugers MA, McLachlan RD, Thill B. Comparison of the vibrational spectra and assignments for α-syndiotactic, β-syndiotactic, isotactic, and atactic polystyrene and toluene. Appl Spectrosc. 1992; 46(6): 981-987. DOI: 10.1366/0003702924124321.

[6] Wilson EB. The normal modes and frequencies of vibration of the regular plane hexagon model of the benzene molecule. Phys Rev. 1934; 45(10): 706-714. DOI: 10.1103/PhysRev.45.706.

E. To be or not to be an azo pigment: chemistry for the preservation of historical β-naphthol reds in cultural heritage

Table E.1.: UV-Vis absorbance spectra and experimental data for the ε_{max} calculation together with molecular structures & acronyms of the colorants studied in this work.

Colorant	Chemical formula	UV-Vis spectra	ε_{max} calculation
SY14 Sudan I	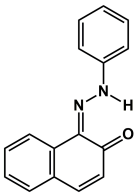	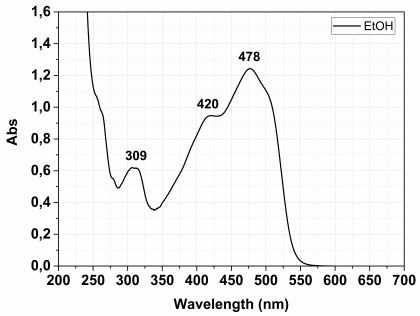	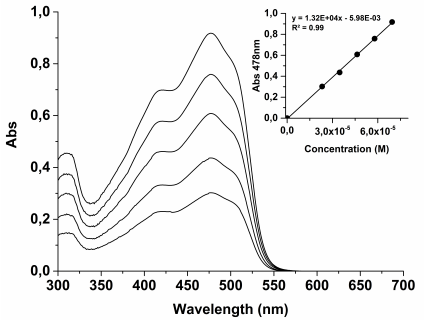
AO7 Orange II	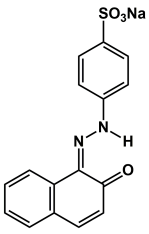	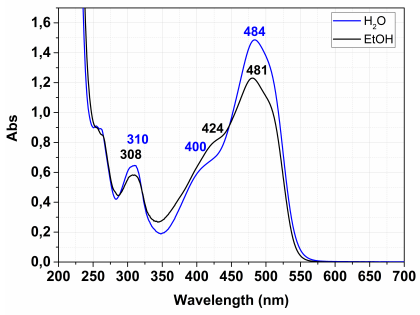	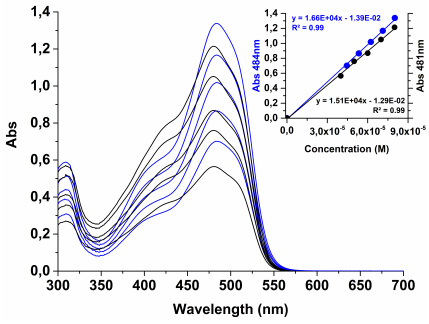
AO10 Orange G	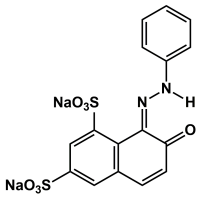	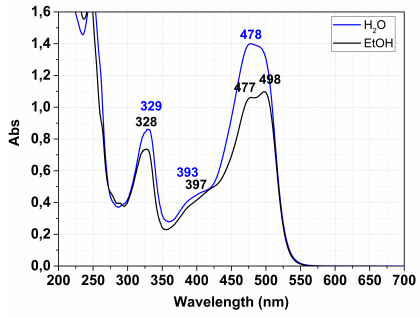	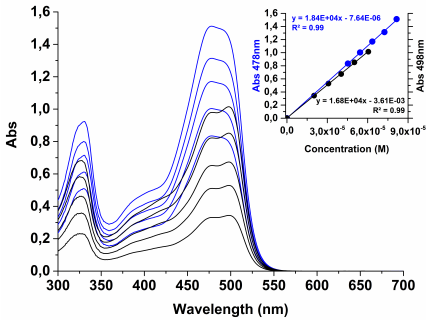
PR1 Para Red	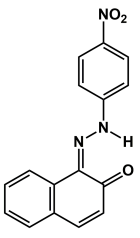	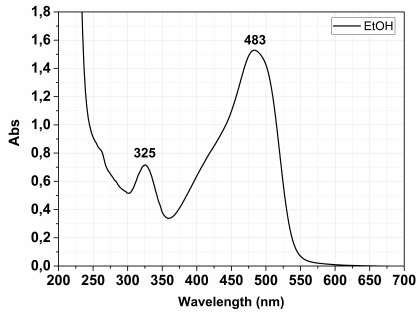	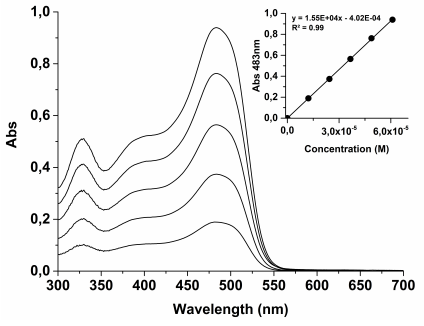

Colorant	Chemical formula	UV-Vis spectra	ε_{max} calculation
PR3 Toluidine Red	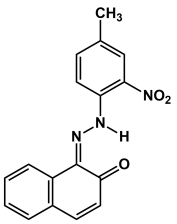	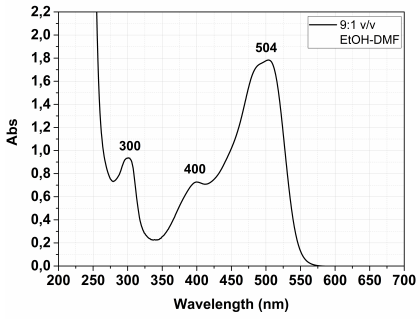	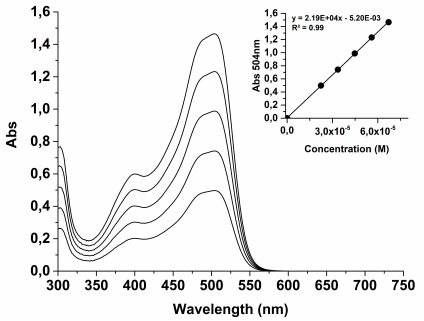
PR48:2 Permanent 2B	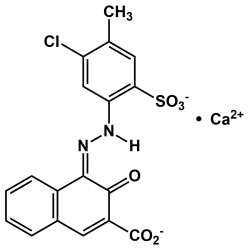	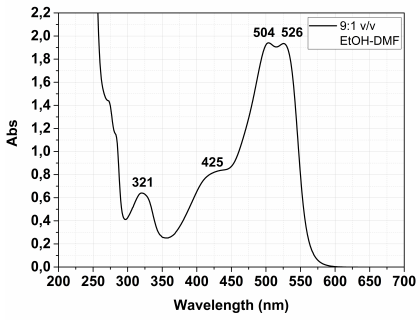	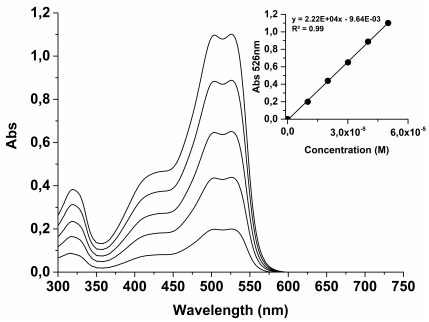
PR49:2 Lithol Red	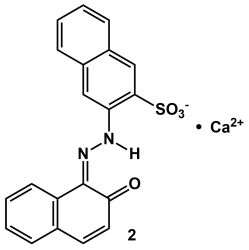	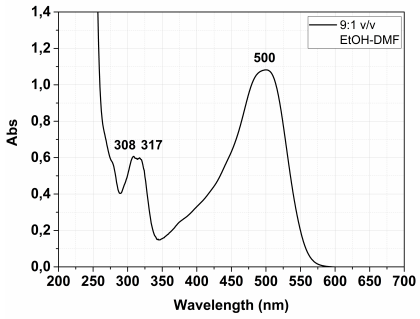	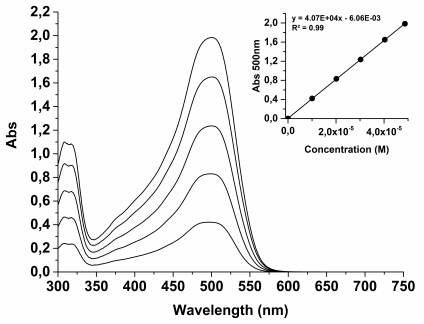
PR53:1 Red Lake C	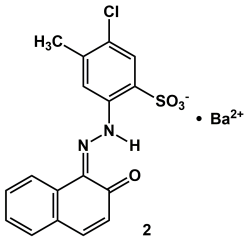	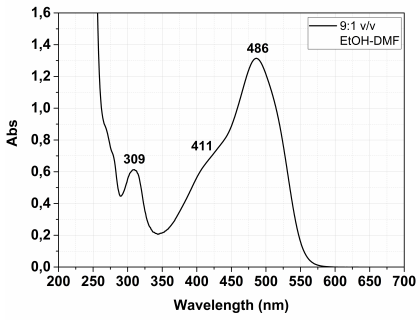	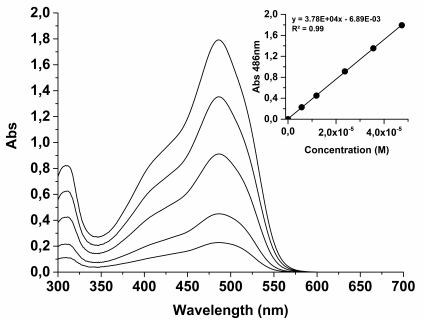

Colorant	Chemical formula	UV-Vis spectra	ε_{max} calculation
PR57:1 Lithol Rubine	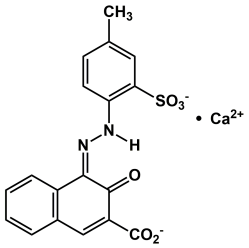	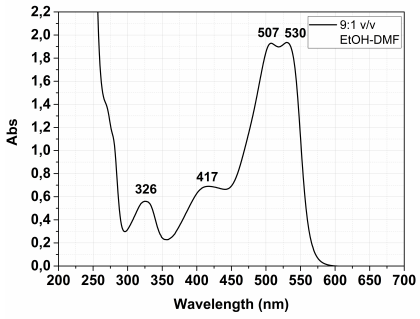	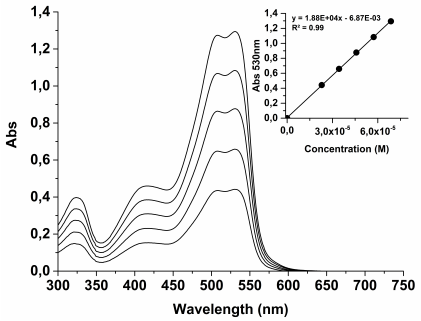

Table E.2.: Bond lengths and intramolecular distances in the hydrogen bonding involving the N(1)-N(2) bridge of the molecular structures of the colorants studied in this work.

Acronym / common name	Bond Lengths / Å			Intramolecular distances / Å		T / K and Ref
	C(2)-O[a]	N(1)-N(2)[b]	C(1)-N(2)	N(1)···O	N(1)-H···O	
SY14 / Sudan I	1.2773	1.2957	1.3471	2.5284	-	298 [2]
	1.284	1.306	1.348	-	-	300 [3]
AO10 / Orange G	1.271	1.299	1.342	2.542	1.818	123 [4]
PR1 / Para Red	1.259	1.345	1.331	2.472	-	293 [5]
	1.25	1.32	1.32	2.58	1.87	100 [6]
PR3 / Toluidine Red	1.228	1.318	1.309	2.585	-	293 [7]
PR49 / Lithol Red	1.275	1.303	1.333	2.51	1.93	298 [8][c]
	1.25	1.31	1.33	2.6	1.93	120 [9][c]
	1.23	1.30	1.36	2.59	1.90	120 [9][d]
	1.25	1.31	1.33	2.59	1.92	120 [9][d]
	1.267	1.312	1.337	-	-	[9][e]
	1.26	1.32	1.31	2.60	1.93	123 [9][f]
PR53 / Lake Red C	1.308	1.287	1.347	2.512	1.799	293 [10][e]
PR57:1 / Lithol Rubine	1.25	1.39	1.33	2.7	2	293 [11][g]
	1.25	1.39	1.34	2.6	1.9	293 [11][h]

[a] 1.20-1.25Å (for keto form), 1.31-1.36Å (for azo form) [1]. [b] 1.31-1.35 Å (for keto form), 1.28-1.31 Å (for azo form) [1]. [c] Na^{+} counterion. [d] Ba^{2+} counterion. [e] Ca^{2+} counterion. [f] Sr^{2+} counterion. [g] Trihydrate. [h] Monohydrate.

Published absorption maxima (λ_{max}) and respective molar absorption coefficients (ε_{max}) in various solvents

Determining molar absorption coefficients from absorption spectrophotometric experiments has potential for large errors [12], usually around 20%. Generally, good agreement between experimental ε_{max} and published values is observed (**Table E.3**) with a maximum percent variance of 20% for aqueous and ethanolic solutions. For only SY14, a discrepancy is found with one order of magnitude of difference. Hydrazone-azo dyes are known to have good color strength which corresponds to values of ε that are of the order of 10^4 [13]. Our values range between 15 000 and 16 000 $Mol^{-1}cm^{-1}$ and they are coherent with the molar absorption coefficient of chromophore azobenzene at its π-π* absorption maximum (ca 22 000 $Mol^{-1}cm^{-1}$) [14].

Table E.3.: Absorption maxima (λ_{max}) and respective molar absorption coefficients (ε_{max}) of the colorants studied in this work compared with literature data in various solvents at 298K.

Colorant	Solvent	λ_{max} / nm	ε_{max} / $Mol^{-1}cm^{-1}$	Ref
SY14	Toluene	476	7 400	[15]
	1,4-dioxane	476	9 200	[15]
		474	2 058	[16]
	EtOAc[a]	474	9 600	[15]
		473	2 232	[16]
	$CHCl_3$	475	9 800	[15]
		482	2 579	[16]
		482	17 400	[17]
	FMF[b]	473	7 600	[15]
		474	2 430	[16]
	DMSO[c]	480	2 331	[16]
	ACN[d]	473	10 200	[15]
		474	2 802	[16]
	MeOH[e]	473	10 400	[15]
	EtOH[f]	477	2 356	[16]
	EtOH	478	13 200	this work
AO7	H_2O	480	15 400	[18]
		483	19 430	[19]
		484	15 700	[20]
		486	20 700	[21]
	H_2O	484	16 600	this work
	EtOH[f]	481	15 100	
AO10	H_2O	480	20 900	[18]
	H_2O	478	18 400	this work
	EtOH[f]	498	16 800	
PR1	1,4-dioxane	486	15 001	[16]
	EtOAc[a]	482	14 943	[16]
	$CHCl_3$	492	17 638	[16]
		489	23 950	[17]
	DMF[b]	489	15 060	[16]
	DMSO[c]	498	13 390	[16]
	ACN[d]	483	15 792	[16]
		480	28 840	[22]
	MeOH[e]	480	28 183	[22]
	aq. H_2SO_4	550	19 054	[23]
	EtOH[f]	483	13 800	[16]
	EtOH[f]	483	15 500	this work

[a] Ethyl acetate. [b] Dimethylformamide. [c] Dimethyl sulfoxide. [d] Acetonitrile. [e] methanol. [f] Ethanol.

UV-Vis spectra of the main degradation compounds identified by LC-DAD analysis

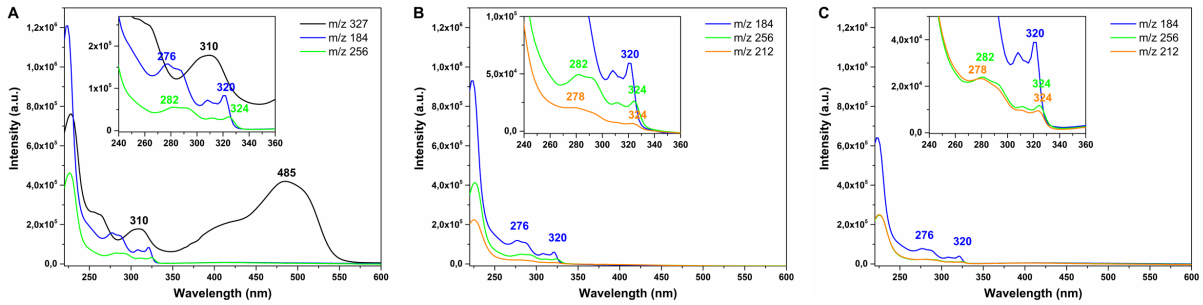

Figure E.1.: AO7 in ethanol, UV–Vis absorption spectra of compound with m/z 327 & t_R=23.3 min, recorded during LC-DAD analysis at 60h (A), 80h (B), 100h (C) of irradiation.

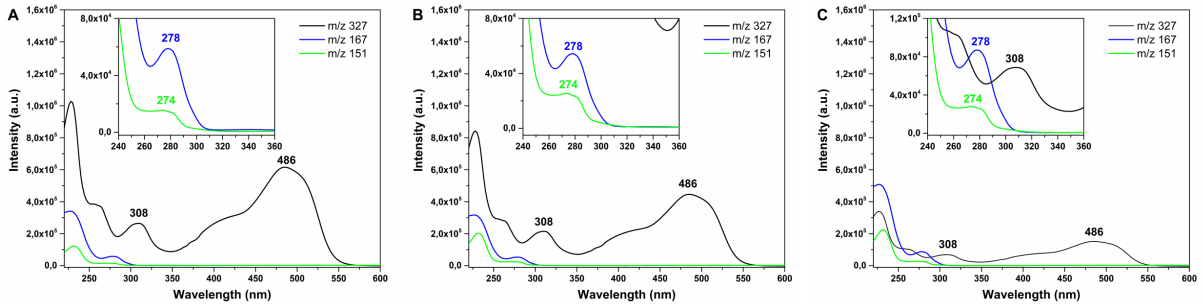

Figure E.2.: AO7 in water, UV-Vis absorption spectra of compound with m/z 327 & t_R=23.5 min, recorded during LC-DAD analysis at 60h (A), 80h (B), 100h (C) of irradiation.

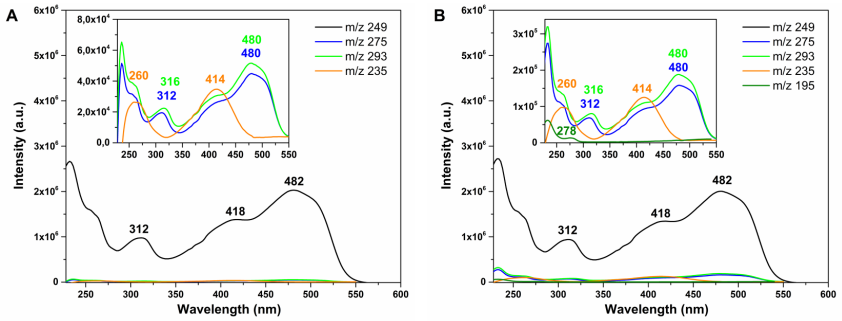

Figure E.3.: SY14 in ethanol, UV-Vis absorption spectra of compound with m/z 249, t_R=25.2 min, recorded during LC-DAD analysis at 80h (A), 100h (B) of irradiation.

LC-DAD-MS data (Table E.4), chromatograms profiles (Figures E.4-E.6), LC-HRMS/MS data (Table E.5) and proposed fragmentation pathways (Schemes E.7-E.15) for AO7, SY14 and their degradation products

Identification of degradation products by LC-DAD-MS and its characterization by LC-HRMS/MS analysis

LC-DAD-MS data obtained for colorants analyzed in this study and its irradiated solutions are summarized in **Table E.4**. Chromatogram profiles of the main degradation products identified for each colorant are shown in **Figures E.4-E.6**. Identification and structural characterization of the detected intermediates was further carried out by high efficiency liquid chromatography-high resolution tandem mass spectrometry accurate measurements. The MS/MS results are summarized in **Table E.5**. The proposed structures for the intermediates and final products (cf. **Tables 8.4-8.6** in the manuscript) are supported by the fragmentation patterns present in **Figures E.7** to **E.15**.

As mentioned in the experimental part, LC and the UHPLC analysis were performed at different flow rates and with different mobile phases B, leading to different retention times for the same eluted compounds.

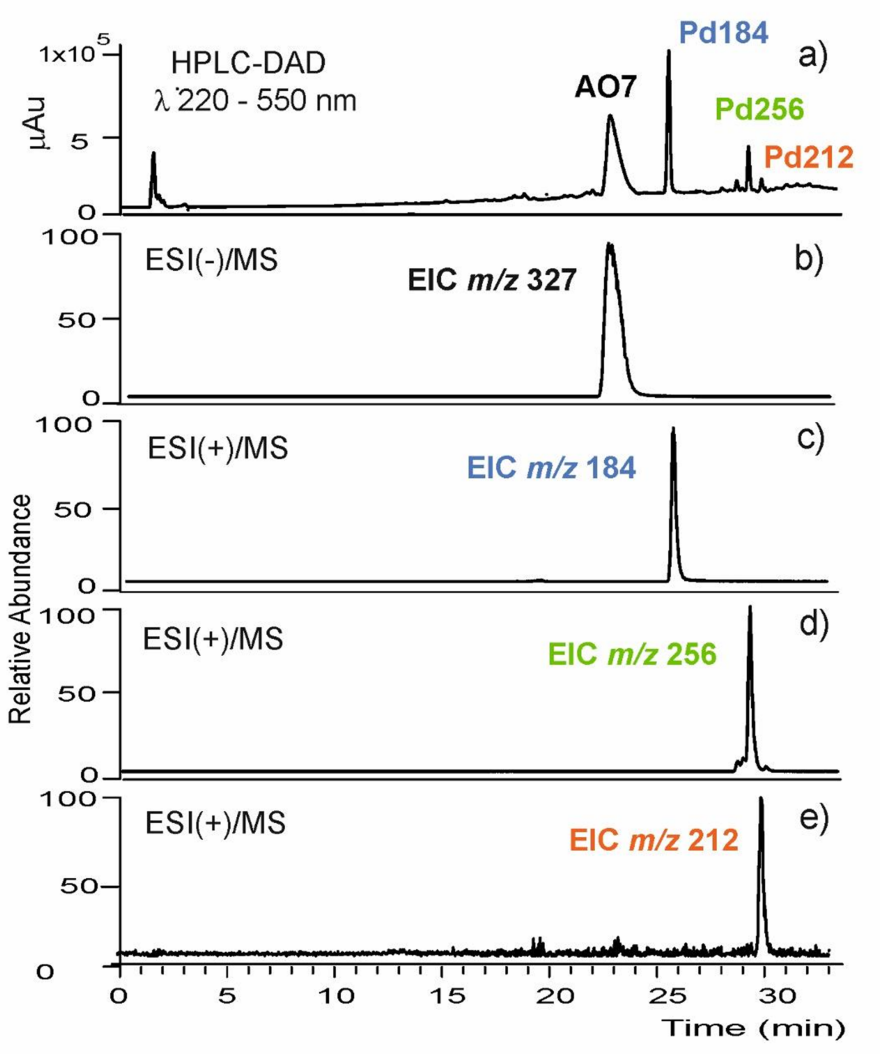

Figure E.4.: AO7 sample in ethanol at 60h, LC-DAD-MS analysis obtained in the ESI positive/negative mode: a) DAD chromatogram obtained between 220 and 550 nm; b) extracted ion chromatogram for the deprotonated molecule of AO7 *m/z* 327; c), d) and e) extracted ion chromatograms for the main degradation products with *m/z* 184, 256 and 212, respectively.

Table E.4.: LC-DAD-MS data for colorants and its irradiated solutions.

Compound	**Irradiation time / h**	t_R **/ min**	λ_{max} **/ nm**	**[M-H]$^-$**	**[M-H]$^+$**
AO7 / EtOH	0	23.3	228; 256; 310; 485	327	329
	20	23.3	228; 256; 310; 485	327	329
	40	23.3	228; 256; 310; 485	327	329
		26.2	223; 276; 320	-	184
	60	23.3	228; 256; 310; 485	327	329
		26.2	223; 276; 320	-	184
		28.9	226; 282; 324	-	256
	80	26.2	223; 276; 320	-	184
		28.9	226; 282; 324	-	256
		29.5	226; 278; 324	-	212
	100	26.2	223; 276; 320	-	184
		28.9	226; 282; 324	-	256
		29.5	226; 278; 324	-	212
AO7 / H_2O	0	23.5	228; 256; 308; 486	327	329
	20	23.5	228; 256; 308; 486	327	329
	40	23.5	228; 256; 308; 486	327	329
		10.7	226; 278	-	167
	60	23.5	228; 256; 308; 486	327	329
		10.7	226; 278	-	167
		10.2	232; 274	-	151
	80	23.5	228; 256; 308; 486	327	329
		10.7	226; 278	-	167
		10.2	232; 274	-	151
	100	23.5	228; 256; 308; 486	327	329
		10.7	226; 278	-	167
		10.2	232; 274	-	151
SY14 / EtOH	0	25.2	233; 312; 418; 482	247	249
	20	25.2	233; 312; 418; 482	247	249
	40	25.2	233; 312; 418; 482	247	249
	60	25.2	233; 312; 418; 482	247	249
	80	25.2	233; 312; 418; 482	247	249
		23.8	234; 312; 424; 480	-	275
		22.7	234; 316; 416; 480	-	293
		22.1	260; 414	-	235
	100	25.2	233; 312; 418; 482	247	249
		23.8	234; 312; 424; 480	-	275
		22.7	234; 316; 416; 480	-	293
		22.1	260; 414	-	235
		11.1	234; 278	193	195

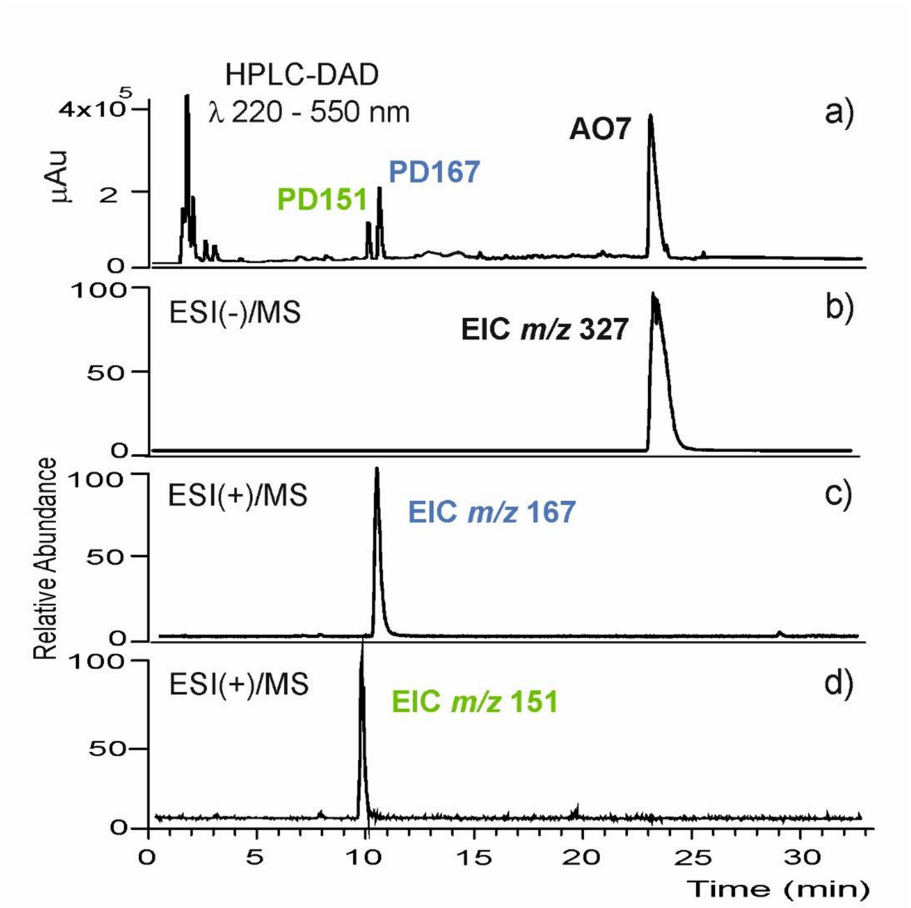

Figure E.5.: AO7 in water at 80h, LC-DAD-MS analysis obtained in the ESI positive/negative mode: a) DAD chromatogram obtained between 220 and 550 nm; b) extracted ion chromatogram for the deprotonated molecule of AO7 m/z 327; c) and d) extracted ion chromatograms for the main degradation products with m/z 167 and 151, respectively.

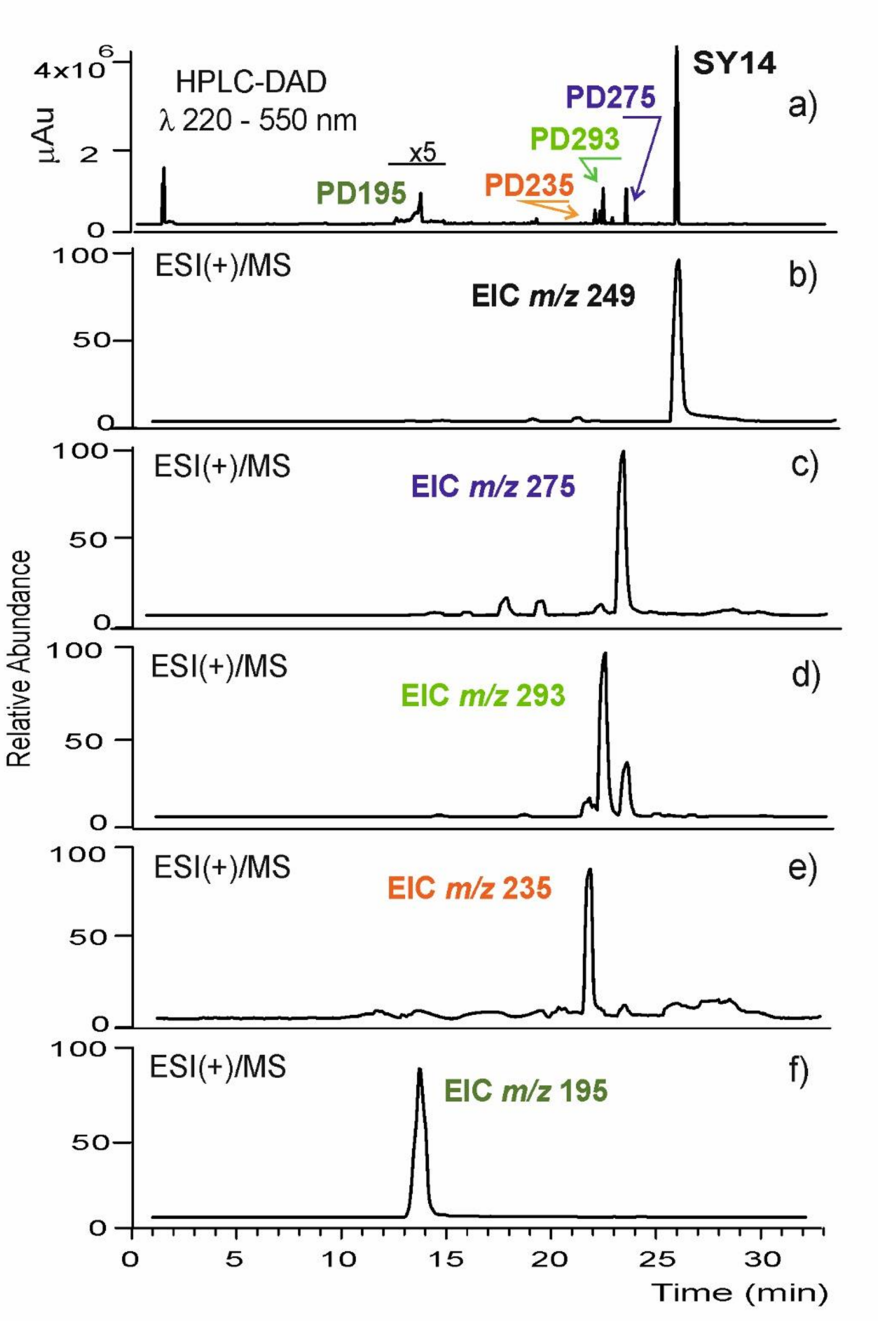

Figure E.6.: SY14 in ethanol at 100h, LC-DAD-MS analysis obtained in the ESI positive mode: a) DAD chromatogram obtained between 220 and 550 nm; b) extracted ion chromatogram for the protonated molecule of SY14 *m/z* 249; c), d), e) and f) extracted ion chromatograms for the degradation products with *m/z* 275, 293, 235 and 195, respectively.

Table E.5.: LC-ESI(±)-HRMS/MS identification of colorants and their degradation products.

Compound	t_R / min	Proposed structure	$[M\text{-}H]^-/[MH]^+/[M^+]$ [m/z (Δ ppm)]	MS/MS [(m/z) (Δ ppm) (attribution) (%)]	CODE DP
AO7 / EtOH	9.9	$C_{16}H_{12}N_2O_4S$	327.0438 (2.2)	247.0874 (1.0) $[C16H11N2O]^-$ (7)	AO7*
				219.0814 (0.7) $[C6H11O]^-$ (5)	
				170.9991 (2.9) $[C6H5NO3S]^{-\bullet}$ (70)	
				155.9882 (3.0) $[C6H4O3S]^{-\bullet}$ (55)	
				107.0373 (3.8) $[C6H5NO]^-$ (45)	
	11.3	$C_{12}H_9NO$	184.0756 (-1.0)	166.0655 (-2.0) $[C12H8N]^+$ (5)	DP184
				143.0491 (0.3) $[C10H7O]^+$ (10)	
				128.0620 (0.6) $[C10H8]^{+\bullet}$ (3)	
				115.0541 (1.1) $[C9H7]^+$ (80)	
	13.1	$C_{16}H_{18}NO_2^+$	256.1332 (-0.1)	212.0708 (-1.1) $[C13H10NO2]^+$ (15)	DP256
				210.0916 (-1.2) $[C14H12NO]^+$ (25)	
				168.0806 (-1.3) $[C12H10N]^+$ (5)	
				141.0698 (0.9) $[C11H9]^+$ (40)	
				128.0621 (0.2) $C10H8]^{+\bullet}$ (10)	
				115.0542 (0.5) $[C9H7]^+$ (50)	
	13.4	$C_{14}H_{14}NO^+$	212.1071 (-0.4)	197.0837 (-1.0) $[C13H11NO2]^{+\bullet}$ (15)	DP212
				196.0764 (1.6) $[C13H10NO2]^+$ (12)	
				168.0807 (0.5) $[C12H10N]^+$ (10)	
				128.0619 (1.1) $[C10H8]^{+\bullet}$ (50)	
				115.0543 (-0.6) $[C9H7]^+$ (20)	
AO7 / H_2O	5.9	$C_8H_6O_4$	167.0345 (-3.9)	149.0234 (-0.2) $[C8H5O3]^+$ (50)	DP167
				121.0287 (-2.5) $[C7H5O2]^+$ (60)	
				111.0439 (1.1) $[C6H7O2]^+$ (25)	
	5.8	$C_8H_6O_3$	151.0382 (4.9)	133.0289 (-3.9) $[C8H5O2]^+$ (60)	DP151
				105.0339 (-5.2) $[C7H5O2]^+$ (80)	
				95.0486 (5.7) $[C6H7O]^+$ (30)	
SY14 / EtOH	15.0	$C_{16}H_{12}N_2O$	249.1022 (-3.1)	232.1002 (-2.8) $[C16H12N2]^{+\bullet}$ (60)	SY14*[1]
				231.0927 (-4.6) $[C16H11N2]^+$ (20)	
				204.0814 (-3.2) $[C15H10N]^+$ (7)	
				174.0555 (-2.9) $[C10H8NO2]^+$ (10)	
				156.0447 (-1.9) $[C10H6NO]^+$ (100)	
				128.0498 (-2.5) $[C9H6N]^+$ (50)	
				101.0389 (-3.3) $[C8H5]^+$ (10)	
	13.9	$C_{18}H_{15}N_2O^+$	275.1184 (1.7)	258.1158 (-2.4) $[C18H14N2]^{+\bullet}$ (40)	DP275
				257.1082 (-3.5) $[C18H13N2]^+$ (20)	
				247.1238 (-3.3) $[C17H15N2]^+$ (5)	
				182.0609 (-5.0) $[C12H8NO]^+$ (35)	
				154.0655 (-2.4) $[C11H8N]^+$ (100)	
				127.0545 (-1.8) $[C10H7]^+$ (40)	
	13.1	$C_{18}H_{17}N_2O_2^+$	293.1290 (-1.5)	276.1263 (-2.0) $[C18H16N2O]^{+\bullet}$ (70)	DP293
				276.1263 (-2.0) $[C18H16N2O]^+$ (70)	

Compound	**t_R / min**	**Proposed structure**	**$[M\text{-}H]^-/[MH]^+/[M^+]$ [m/z (Δ ppm)]**	**MS/MS [(m/z) (Δ ppm) (attribution) (%)]**	**CODE DP**
				247.1236 (-2.6) $[C17H15N2]^+$ (5)	
				233.1062 (4.9) $[C16H13N2]^+$ (15)	
				200.0713 (3.5) $[C12H10NO2]^+$ (25)	
				182.0607 (-3.9) $[C12H8NO]^+$ (35)	
				172.0607 (-3.9) $[C11H10NO]^+$ (20)	
				130.0655 (-2.5) $[C9H8N]^+$ (50)	
				108.0684 (-1.6) $[C6H8N2]^+$ (40)	
	12.6	$C_{13}H_{14}O_4$	235.0974 (-2.9)	207.0656 (-0.4) $[C11H11O4]^+$ (30)	DP235
				179.0351 (-1.2) $[C9H7O4]^+$ (20)	
				133.0286 (-0.2) $[C8H5O2]^+$ (100)	
				105.0341 (-0.6) $[C7H5O]^+$ (25)	
	8.1	$C_{10}H_{10}O_4$	195.0663 (1.0)	177.0552 (-3.1) $[C10H9O3]^+$ (50)	DP195
				149.0237 (-2.4) $[C8H5O3]^+$ (100)	
				121.0287 (-2.3) $[C7H5O2]^+$ (25)	

* and *[1] : Product mass spectra in accordance with references [24] and [25], respectively.

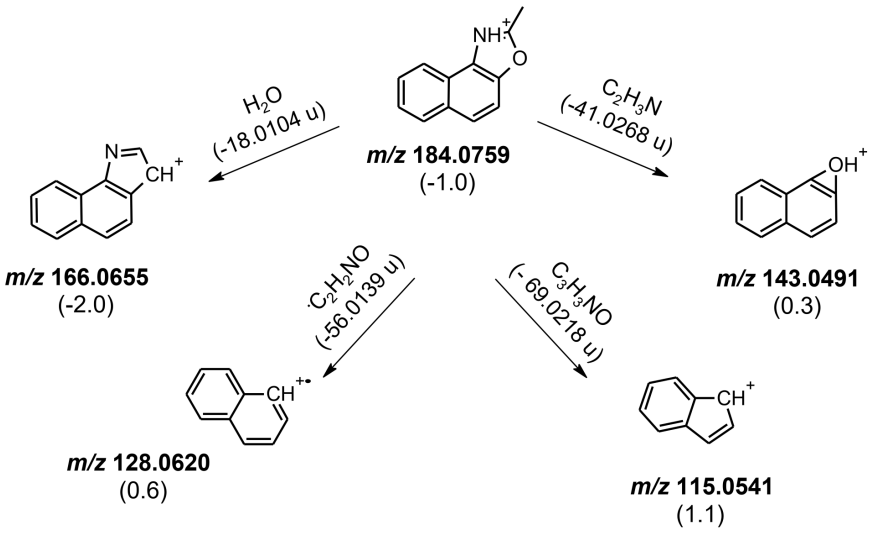

Figure E.7.: AO7 in ethanol, proposed fragmentation path for the precursor ion DP184 at t_R 11.3 min, identified at irradiation times of 40, 60, 80 and 100h.

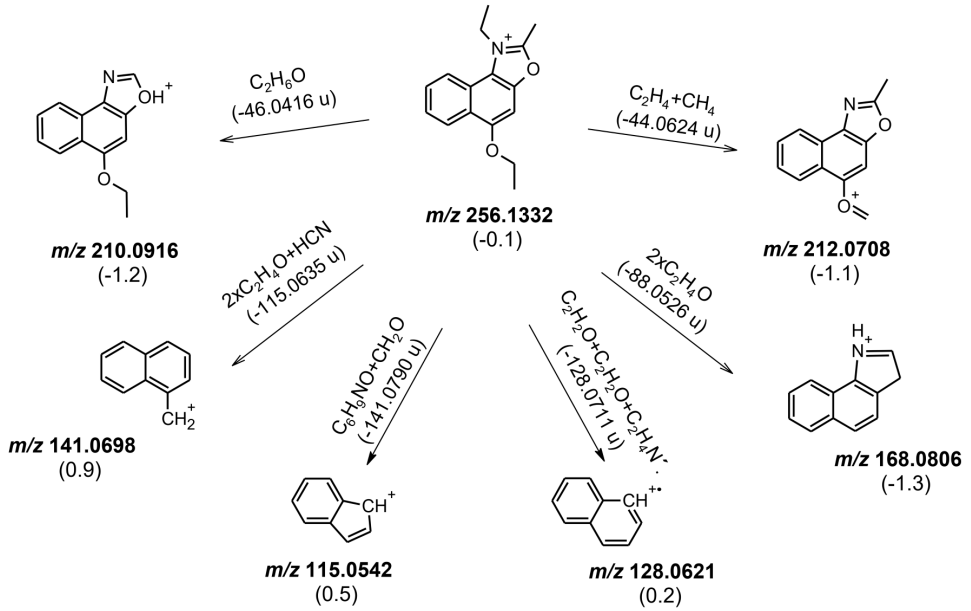

Figure E.8.: AO7 in ethanol, proposed fragmentation path for the precursor ion DP256 at t_R 13.1 min, identified at irradiation time of 60, 80 and 100h.

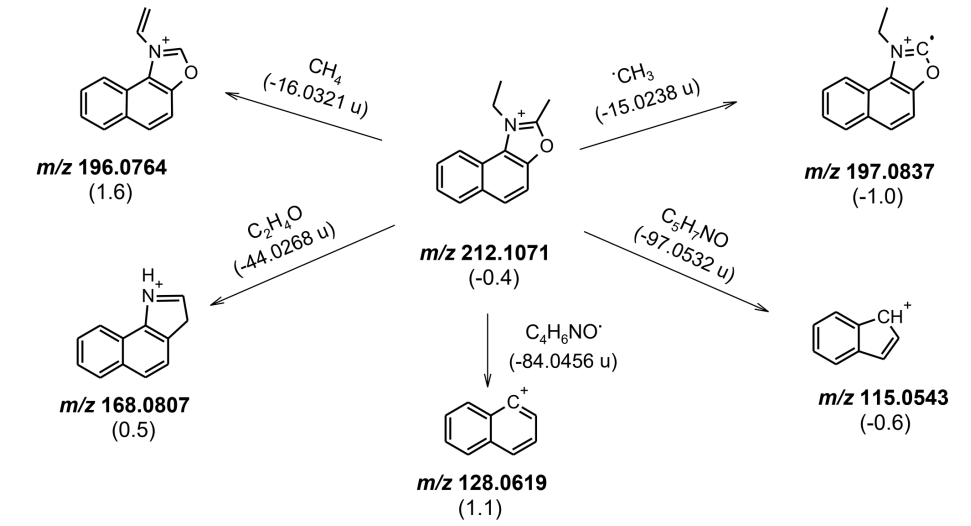

Figure E.9.: AO7 in ethanol, proposed fragmentation path for the precursor ion DP212 at t_R 13.4 min, identified at 60, 80 and 100h.

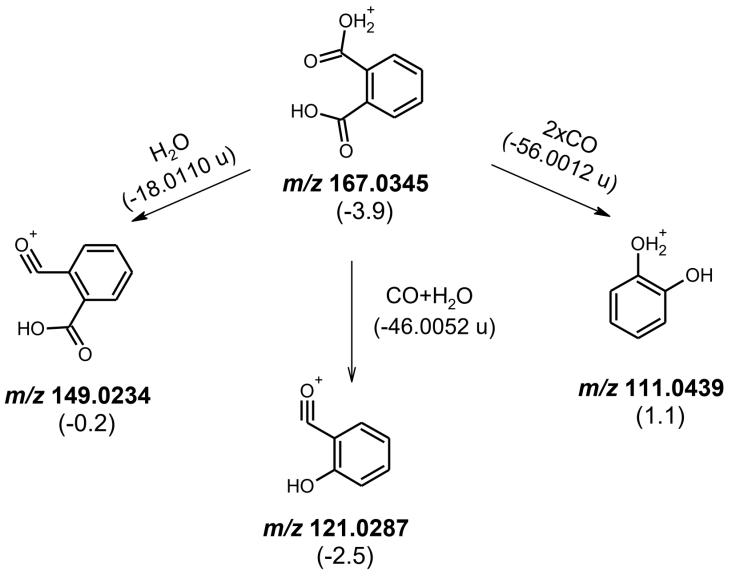

Figure E.10.: AO7 in aqueous solutions, proposed fragmentation path for the precursor ion DP167 (an isophthalic acid) at t_R 5.9 min, identified at irradiation times of 60, 80 and 100h.

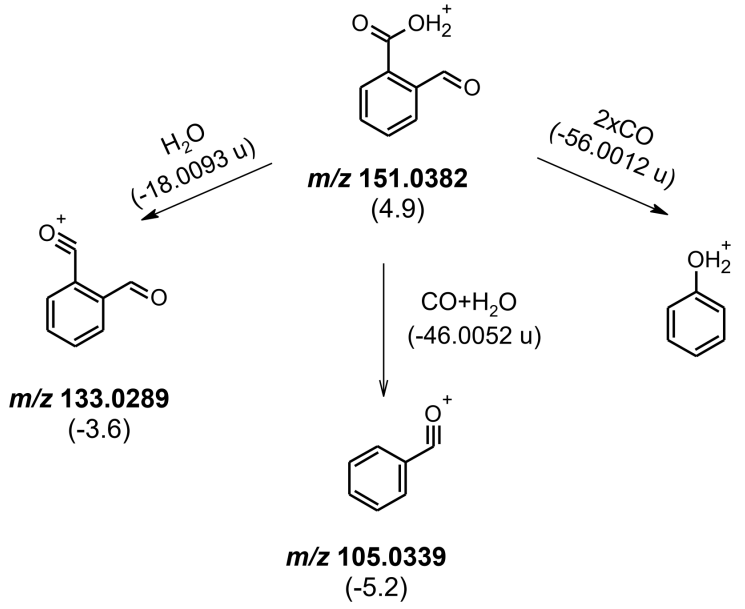

Figure E.11.: AO7 in aqueous solutions, proposed fragmentation path for the precursor ion DP151 (a carboxybenzaldeyde) at t_R 5.8 min, identified at irradiation times of 80 and 100h.

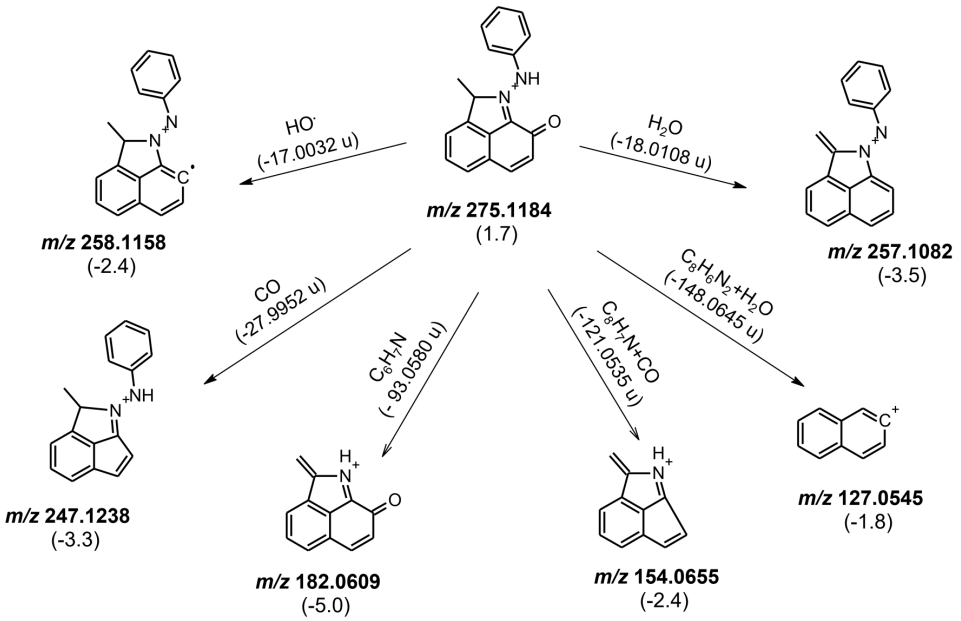

Figure E.12.: SY14 in ethanol, proposed fragmentation path for the precursor ion DP275 at t_R 13.9 min, identified at irradiation time of 80h.

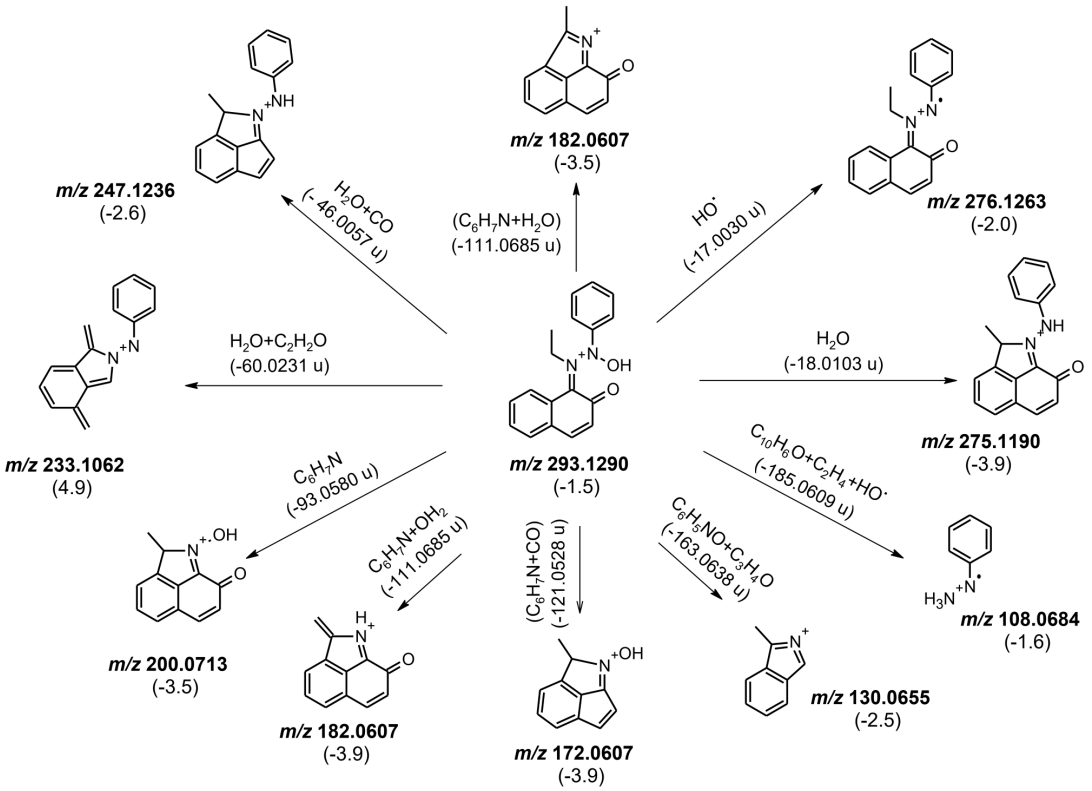

Figure E.13.: SY14 in ethanol, proposed fragmentation path for the precursor ion DP293 at t_R 13.1 min, identified at irradiation times of 80 and 100h.

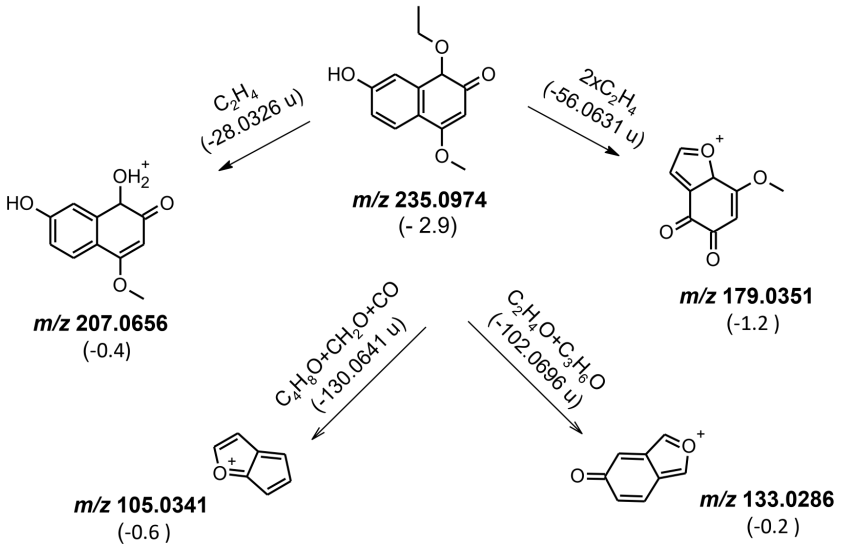

Figure E.14.: SY14 in ethanol, proposed fragmentation path for the precursor ion DP235 at t_R 12.6 min, identified at irradiation times of 80 and 100h.

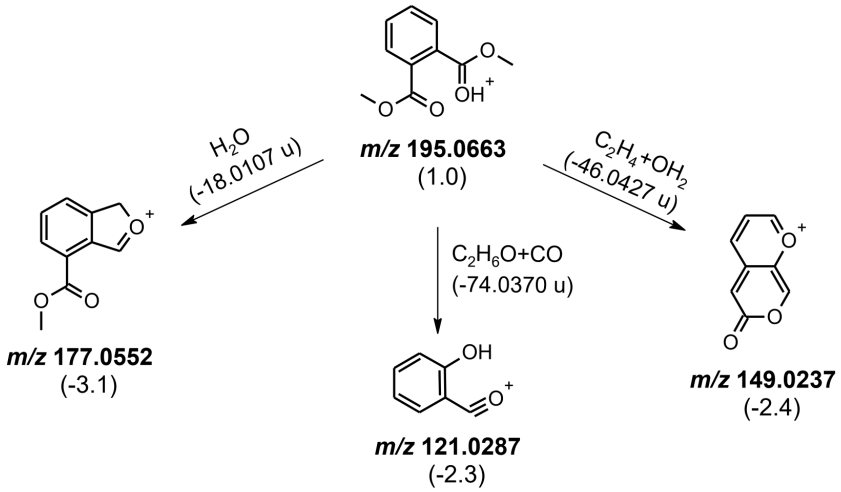

Figure E.15.: SY14 in ethanol, proposed fragmentation path for the precursor ion DP195 t_R 8.1 min, identified at irradiation time of 100h.

References

[1] Bertolasi V, Gilli P, Gilli G. Crystal Chemistry and Prototropic Tautomerism in 2-(1-Iminoalkyl)- phenols (or naphthols) and 2-Diazenyl-phenols (or naphthols). Curr Org Chem. 2009; 13(3): 250-268. DOI: 10.2174/138527209787314841.

[2] Ferreira GR, Garcia HC, Couri MRC, Dos Santos HF, de Oliveira LFC. On the Azo/Hydrazo Equilibrium in Sudan I Azo Dye Derivatives. J Phys Chem A 2013; 117: 642-649. DOI: 10.1021/jp310229h.

[3] Olivieri AC, Wilson RB, Paul IC, Curtin DY. Carbon-13 NMR and x-ray structure determination of 1-(arylazo)-2-naphthols. Intramolecular proton transfer between nitrogen and oxygen atoms in the solid state. J Am Chem Soc. 1989; 111: 5525-5532. DOI: 10.1021/ja00197a003.

[4] Kennedy AR, Kirkhouse JAB, Whyte L. Supramolecuar Motifs in s-Block Metal-Bound Sulfonated Monoazo Dyes: The Case of Orange G. Inorg Chem. 2006; 45: 2965-2971. DOI: 10.1021/ic0520115.

[5] Grainger CT, McConnell JF. The crystal structure of l-p-nitrobenzeneazo-2-naphthol (Para Red) from overlapped twin, crystal data. Acta Cryst. 1969; 25: 1962-1970. DOI: 10.1107/S0567740869005036.

[6] Bushuyev OS, Singleton TA, Barrett CJ. Fast, Reversible, and General Photomechanical Motion in Single Crystals of Various Azo Compounds Using Visible Light. Adv Mater. 2013; 25: 1796-1800. DOI: 10.1002/adma.201204831.

[7] Whitaker A. The crystal structure of C. I. Pigment Red 3, 4-methyl-2-nitrophenylazo-2-naphthol. Z Kristallogr. 1978; 147(1-2): 99-112. DOI: 10.1524/zkri.1978.147.1-2.99.

[8] Grzesiak-Nowak M, Oszajca M, Rafalska-Łasocha, Goszczycki, Ostrowska K, Łasocha W. Crystal structure studies of selected lithol red salts with the use of powder diffraction data. Dyes Pigm. 2019; 160: 252-25. DOI: 10.1016/j.dyepig.2018.08.002.

[9] Kennedy AR, Stewart H, Eremin K, Stenger S. Lithol Red: A Systematic Structural Study on Salts of a Sulfonated Azo Pigment. Chem Eur J. 2012; 18: 3064-3069. DOI: 10.1002/chem.201103027.

[10] Gorelik T, Schmidt MU, Brüning J, Beko S, Kolb U. Using Electron Diffraction to Solve the Crystal Structure of a Laked Azo Pigment. Cryst Growth Des. 2009; 9: 3898-3903. DOI: 10.1021/cg801099r.

[11] Bekö SL, Hammer SM, Schmidt MU. Crystal Structures of the Hydration States of Pigment Red 57:1. Angew Chem Int Ed. 2012; 51: 4735-4738. DOI: 10.1002/anie.201109082.

[12] Burnett RW. Accurate measurement of molar absorptivities. J Res Natl Bur Stand Sect A 1972; 76: 483-489. URL: nistpubs/jres/76A/jresv76An5p483.

[13] Hunger K. Important Chemical Chromophores of Dye Classes. In: Industrial Dyes: Chemistry, Properties, Applications. Weinheim: Wiley-VCH; 2003. p. 13-112.

[14] Zollinger H. Azo Dyes and Pigments. In: Color Chemistry: Synthesis, Properties, and Applications of Organic Dyes and Pigments. Zürich: Verlag Helvetica Chimica Acta; 2003. p. 165-245.

[15] Jadhav AG, Shinde SS, Sekar N. Red Emitting Monoazo Disperse Dyes with Phenyl(1H-benzoimidazol-5-yl) Methanone as Inbuilt Photostabilizing Unit: Synthesis, Spectroscopic, Dyeing and DFT Studies. J Fluoresc. 2018; 28: 639-653. DOI: 10.1007/s10895-018-2226-3.

[16] Satam MA, Raut RK, Sekar N. Fluorescent azo disperse dyes from 3-(1,3-benzothiazol-2-yl)naphthalen-2-ol and comparison with 2-naphthol analogs. Dyes Pigm. 2013; 96(1): 92-103. DOI: 10.1016/j.dyepig.2012.07.019.

[17] Aiken S, Gabbutt CD, Gillie LJ, Heywood JD, Jacquemin D, Rice CR, Heron BM. The Remarkable Hyperchromicity of Ketohydrazone Dyes and Pigment Lakes Derived from 4-Morpholino-2-naphthol. Eur J Org Chem. 2013; 36: 8097-8107. DOI: 10.1002/ejoc.201390103.

[18] Sugiura W, Yoda T, Matsuba T, Tanaka Y, Suzuki Y. Expression and characterization of the genes encoding azoreductases from Bacillus subtilis and Geobacillus stearothermophilus. Biosci Biotechnol Biochem. 2006; 70(7): 1655-1665. DOI: 10.1271/bbb.60014.

[19] Daneshvar N, Aleboyeh A, Khataee AR. The evaluation of electrical energy per order (E_{Eo}) for photooxidative decolorization of four textile dye solutions by the kinetic model. Chemosphere 2005; 59(6): 761-767. DOI: 10.1016/j.chemosphere.2004.11.012.

[20] Oakes J, Gratton P, Clark R, Wilkes I. Kinetic investigation of the oxidation of substituted arylazonaphthol dyes by hydrogen peroxide in alkaline solution. J Chem Soc Perkin Trans 2 1998; 12: 2569-2576. DOI: 10.1039/A806571C.

[21] Gautam J, Schott H. Interaction of Anionic Compounds with Gelatin I: Binding Studies. J Pharm Sci. 1994; 83(7): 922-930. DOI: 10.1002/jps.2600830703.

[22] Boga C, Degani J, Vecchio E, Fochi R, Forlani L, Todesco P. Arenediazonium *o*-Benzenedisulfonimides: Some Kinetics of Azo Coupling Reactions with Naphthols. Eur J Org Chem. 2002; 3837-3843. DOI: AID-EJOC3837%3E3.0.CO;2-X.

[23] Churkina LN, Belyaev EY, Kazak YY. Synthesis of Dyes from Aromatic C-Nitroso-N-hydroxytriazenes. Russ J Org Chem. 2001; 37: 680-682. DOI: 10.1023/A:1012495616858.

[24] Sabatini F, Degano I. Investigating the fragmentation pathways of β-naphthol pigments using liquid chromatography/electrospray ionization quadrupole time-of-flight mass spectrometry. Rapid Commun Mass Spectrom. 2020; 34: e8789. DOI: 10.1002/rcm.8789.

[25] Calbiani F, Careci M, Elviri L, Mangia A, Zagnoni I. Accurate mass measurements for the confirmation of Sudan azo-dyes in hot chilli products by capillary liquid chromatography-electrospray tandem quadrupole orthogonal-acceleration time of flight mass spectrometry. J Chrom A 2004; 1058(1-2): 127-135. DOI: 10.1016/j.chroma.2004.08.159.

F. Discoloration of historical plastic objects: new insight into the degradation of β-naphthol pigment lakes

Colorimetric measures

During color measurement significant differences with the 0h are indicated for both PE reference samples and historical lids. In detail, stepwise increase in the positive b* values of HDPE and LDPE samples was observed indicative of yellowing (**Figure F.2a,b**). The historical lids share the same tendency with their positive a* and b* coordinates decreasing towards more achromatic values as L* increases (**Figure F.2c,d**). This trend is easily explained because the red pigments of the historical samples faded. L*a*b* coordinates and total color variation between 0h and 770h of irradiation are reported in **Table F.3**. The most dramatic color change was observed for lid 1 and 2 ($\Delta E^*_{ab} > 45$). Lid 2 was partially discolored before irradiation, and its color faded completely with the photoaging **(Figure F.3**). Interestingly, it presents fading until 220h while after the only polymer contributes to color change with yellowing symptoms (**Figure F.2d**).

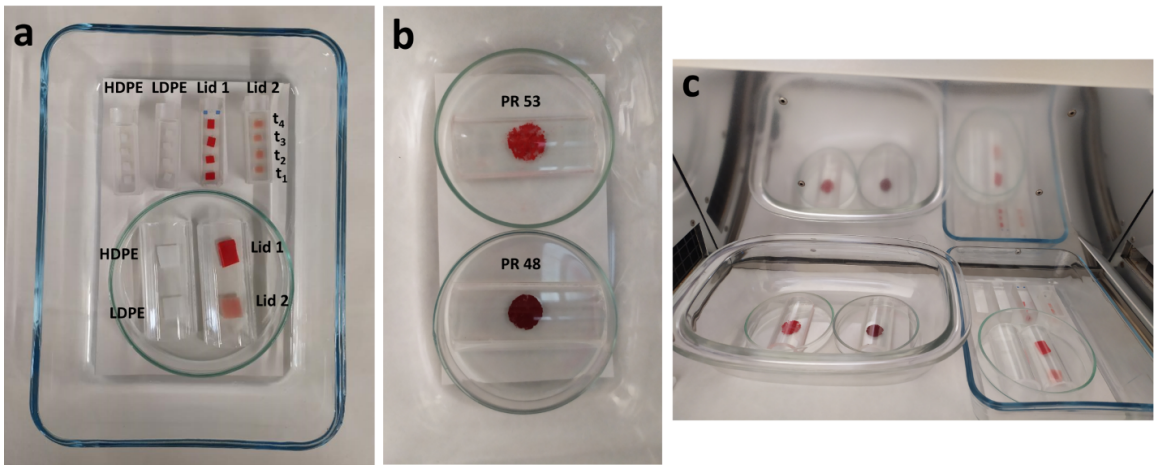

Figure F.1.: Arrangement of samples during the aging experiment. a) historical and polymer reference samples, b) pigment powders, c) all samples inside of the chamber.

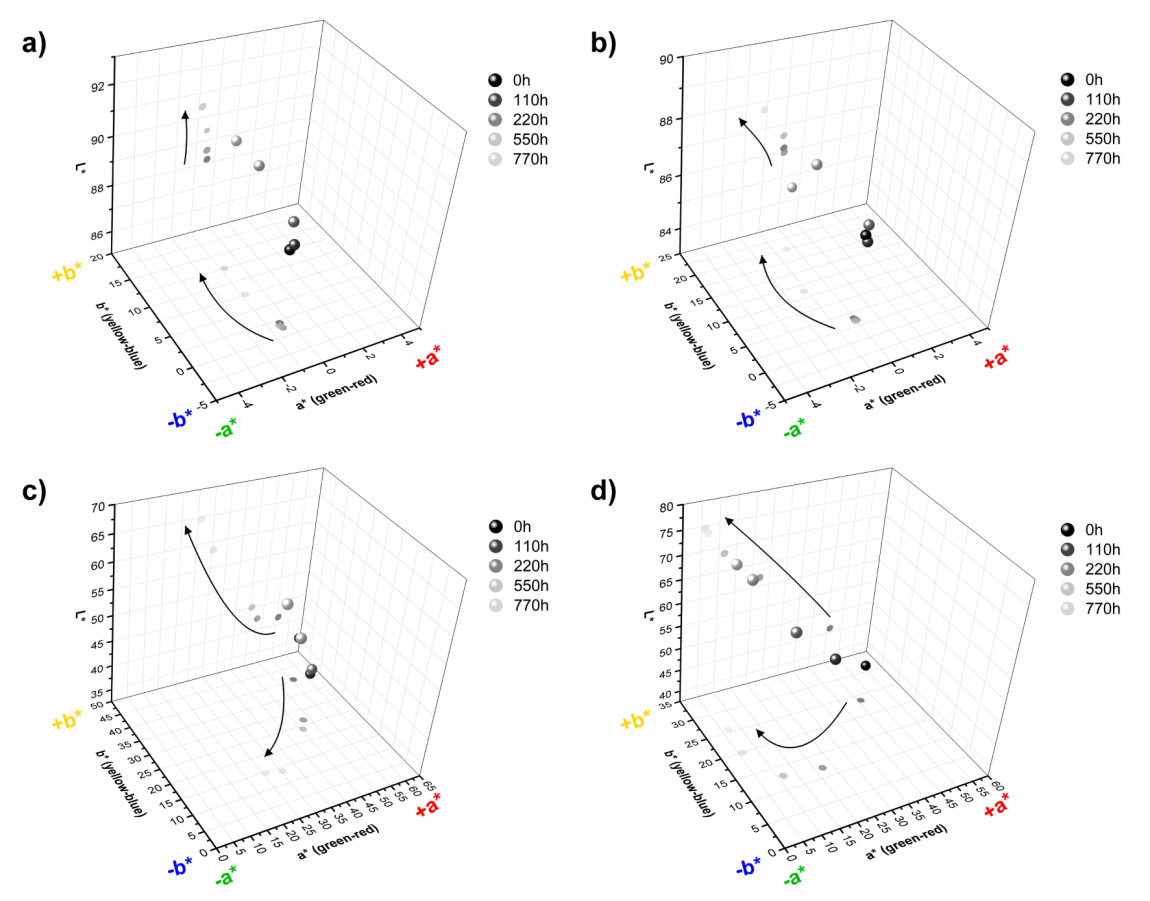

Figure F.2.: L*, a*, b* values in 3-dimensional CIELab76 Color Space during aging: (a) HDPE, (b) LDPE, (c) lid 1, (d) lid 2. Projections of the points along the L* vertical axis and a* and b* perpendicular horizontal axes are also reported. The arrows define the color change over time.

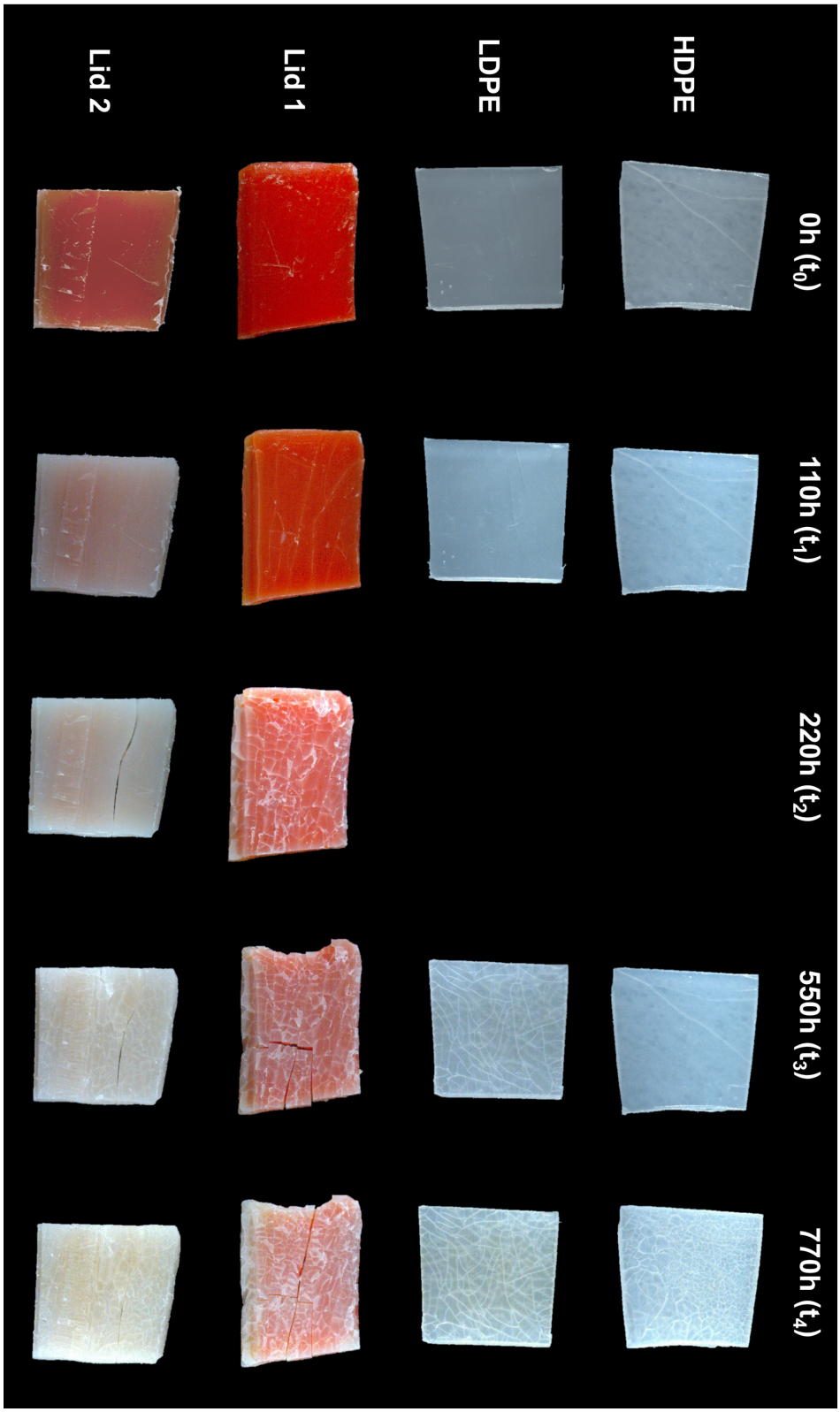

Figure F.3.: Stereomicroscope images of the plastic samples during the aging (25×). The pictures show the exposed areas.

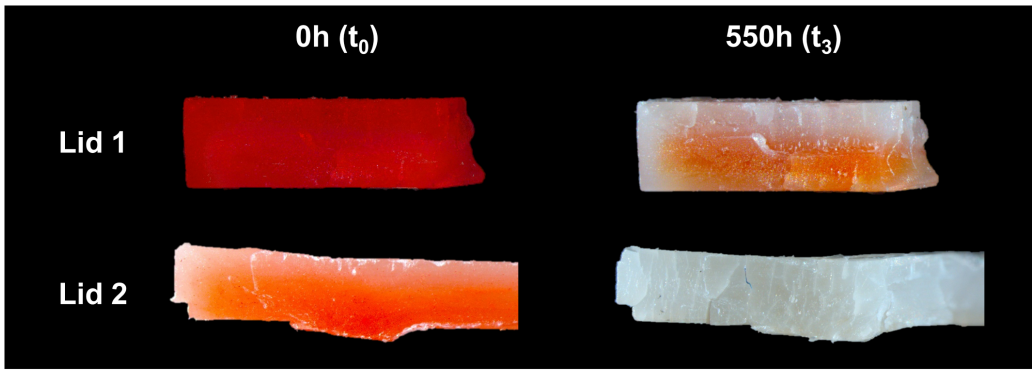

Figure F.4.: Stereomicroscope images taken from the side of the lids 1 and 2 at 0h and 550h (ca.1 mm thickness). The exposed areas correspond to the upper part of the sample.

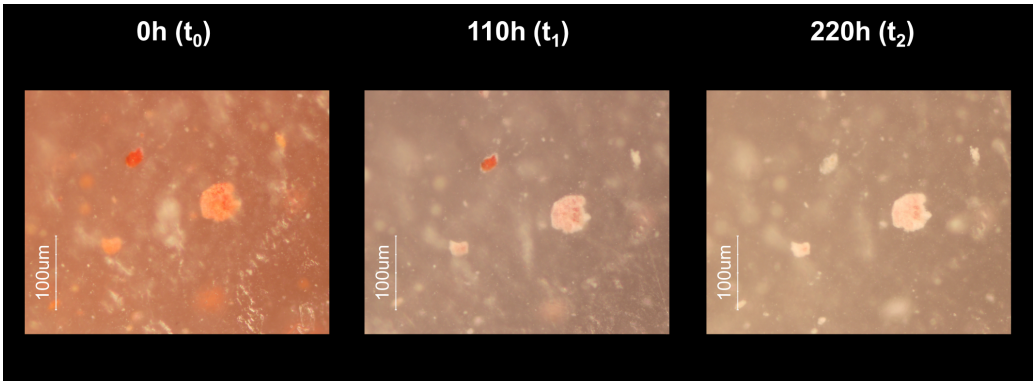

Figure F.5.: Microscopy images of the red particles/aggregates dispersed in the polymeric matrix under reflected visible light (dark field) of lid 2 sample. Images were collected directly from the sample in situ.

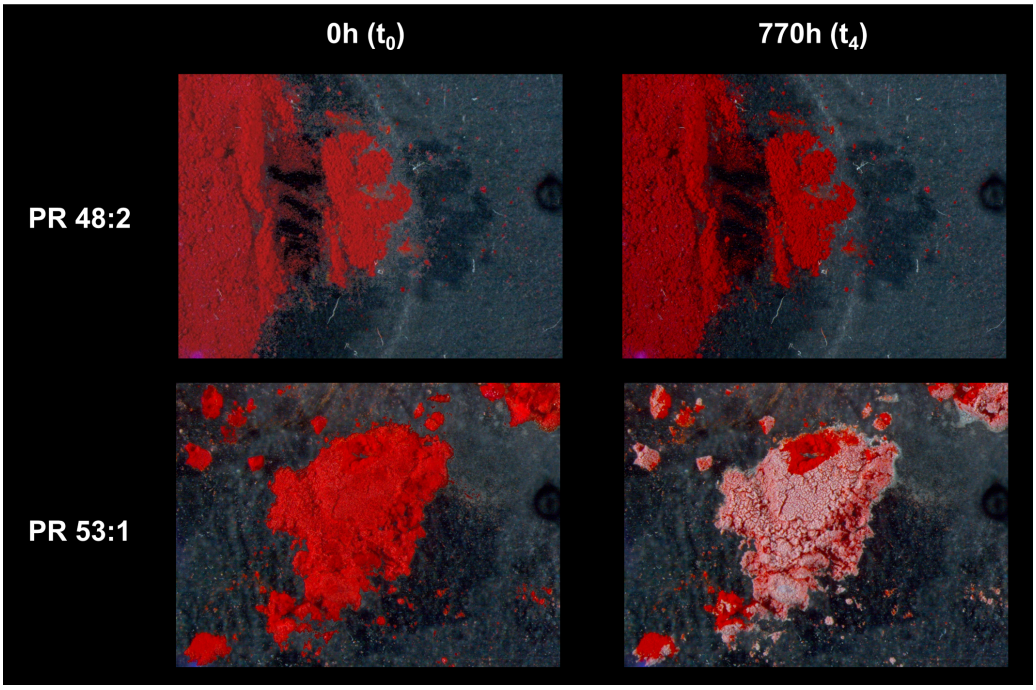

Figure F.6.: Stereomicroscope images of the pigment powders at 0h and 770h.

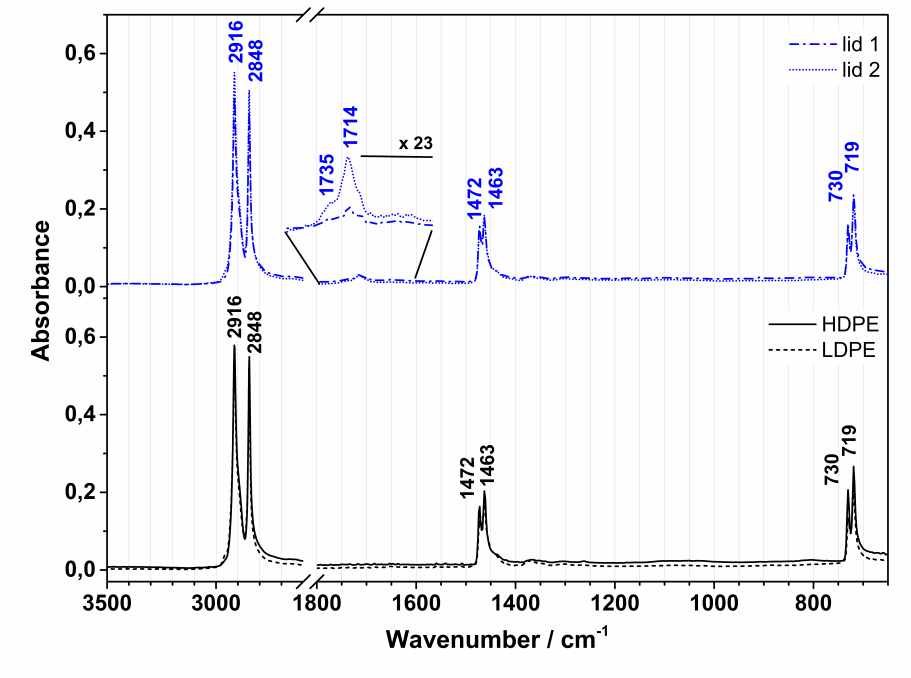

Figure F.7.: ATR-FTIR spectra of lid 1 and lid 2 samples (top, blue lines). Vibrational spectra of the polymer references HDPE and LDPE are reported for comparison (bottom, black lines).

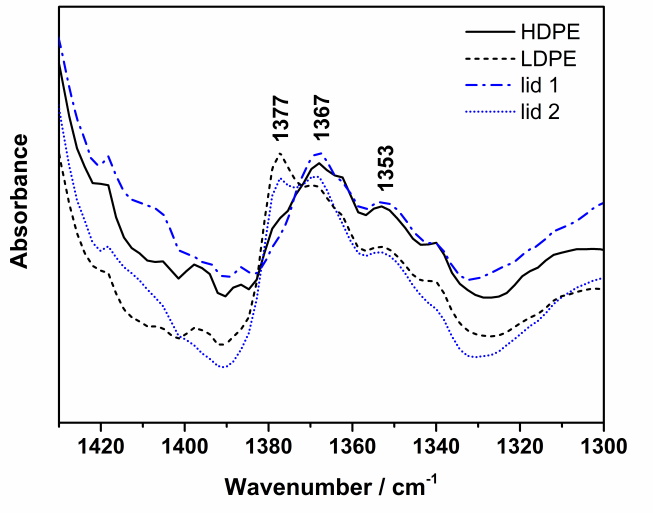

Figure F.8.: ATR-FTIR spectra of HDPE, LDPE, lid 1 and lid 2 samples at t_0 (detail of the interval 1300-1430 cm^{-1}).

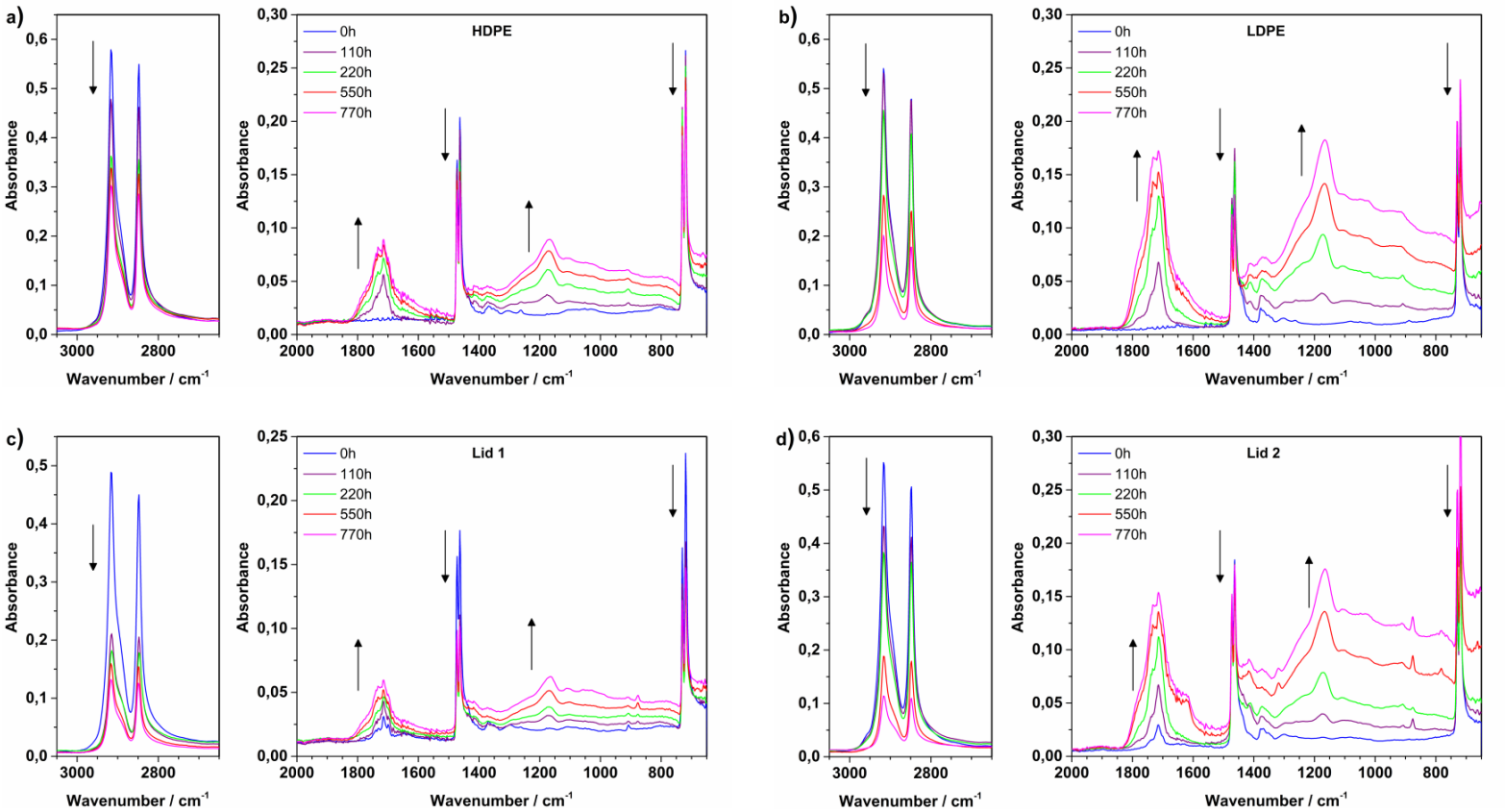

Figure F.9.: ATR-FTIR spectra of HDPE (a), LDPE (b), lid 1 (c) and lid 2 (d) samples over aging. The arrows' direction indicates the increase or decrease of IR bands intensity with increasing aging.

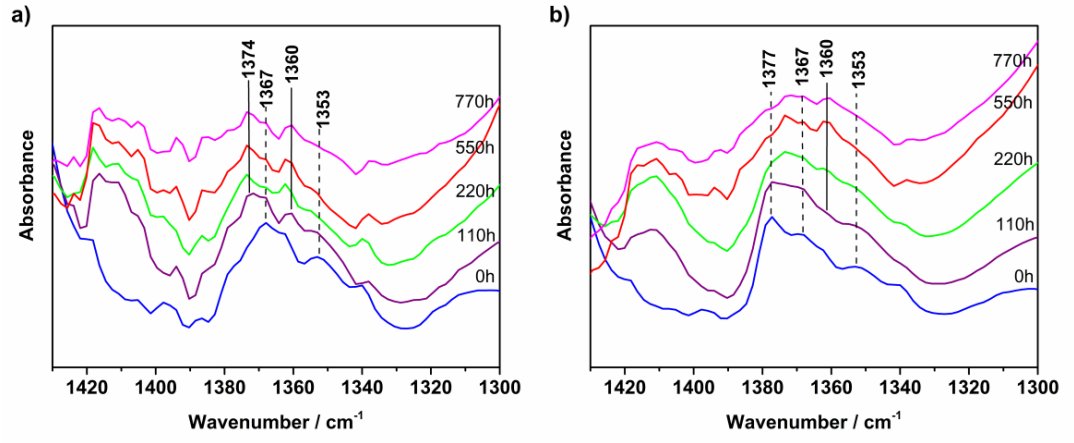

Figure F.10.: ATR-FTIR spectra of the (a) HDPE and (b) LDPE with magnification of the 1300-1430 cm^{-1} range over aging.

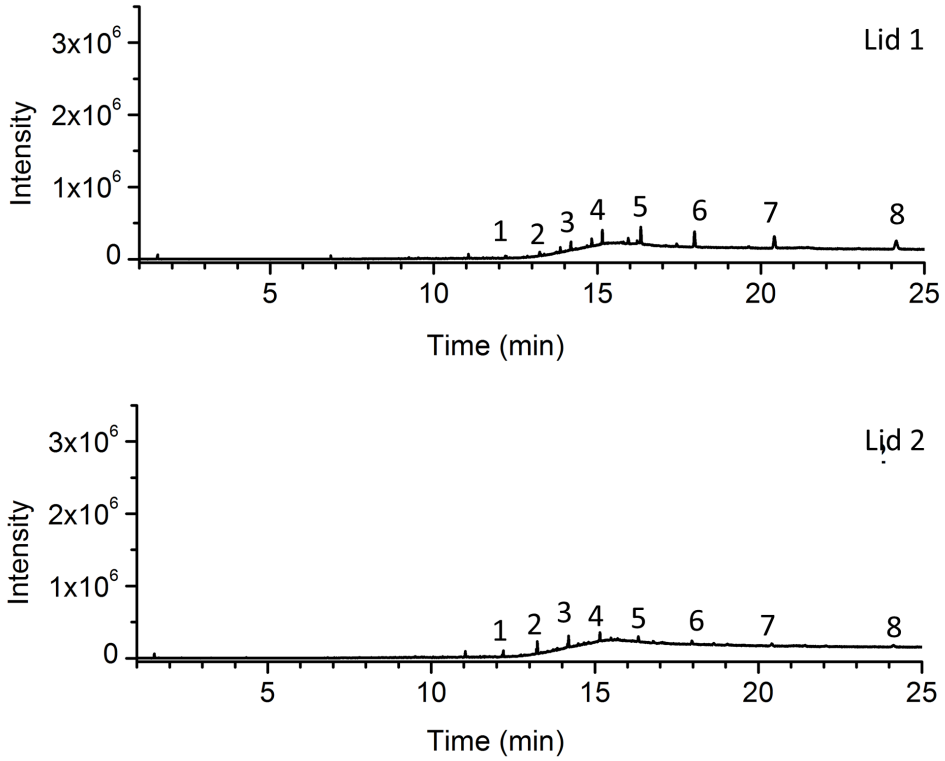

Figure F.11.: TD-chromatograms of lid 1 (up) and lid 2 (bottom). See **Table 9.2** for peak identification.

Figure F.12.: Historical sample presenting PR 53 not discolored. PS lid 3 on the bottom.

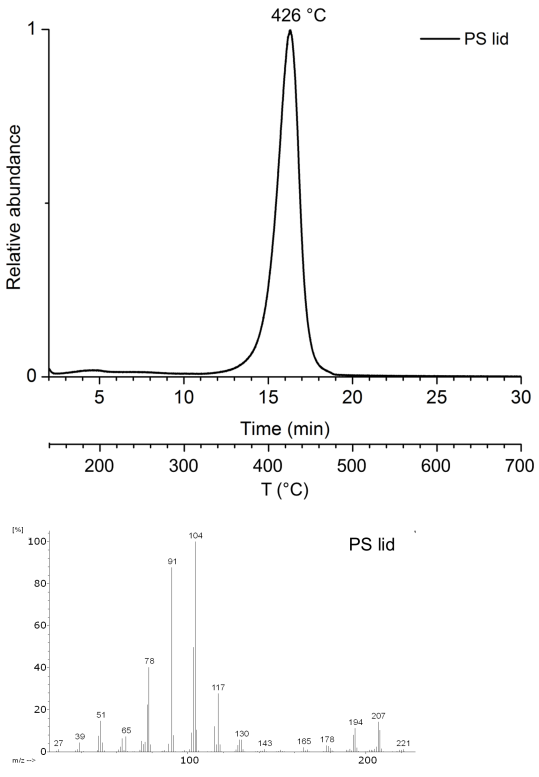

Figure F.13.: Top: normalized EGA-MS curves of the red PS lid 3 and bottom: related average mass spectrum.

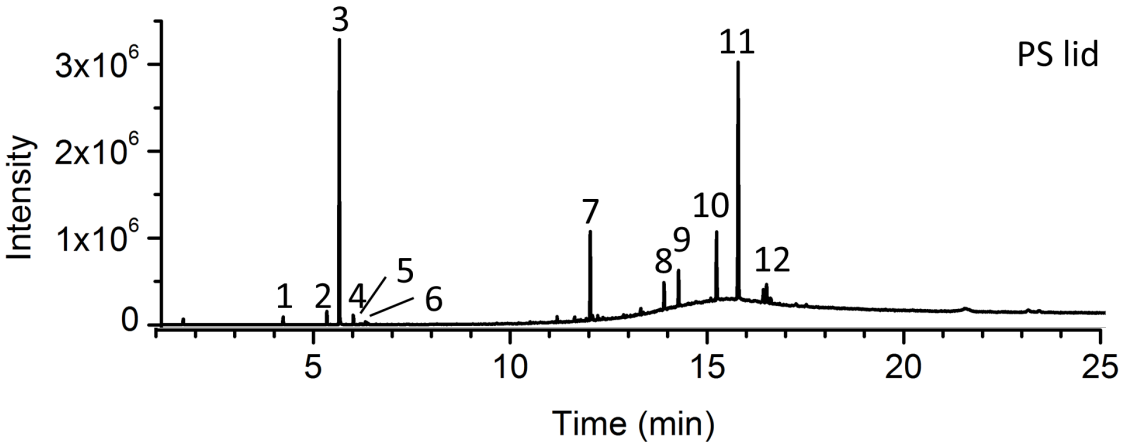

Figure F.14.: TD-chromatogram of the red PS lid 3. For the peaks identification, see **Table F.5**.

Table F.1.: Summary of multi-analytical analysis of polymer, red pigments and white pigments / fillers from [1].

Historical sample	Plastic polymer	Elemental composition	Red organic pigments	Red inorganic pigments	White pigments / fillers
Lid 1	PE	Ti, Ca, Zn, Fe, K, Cl, Si	PR 48:2	PR 101	-
Lid 2	PE	Ti, Ca, Zn, Fe, Ba	PR 53:1	-	PW (R)

Note. PR: Pigment Red, PW: Pigment White, R: rutile crystalline form.

Table F.2.: Molecular structures and acronyms of the synthetic organic pigments studied.

C.I. Generic name	Common name	C.I. Constitution number	Class[a]	Structure[b]
PR 48:2	Calcium Red 2B	15865:2	BONA pigment lake	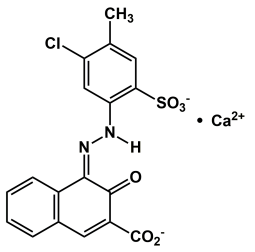
PR 53:1	Lake Red C	15585:1	β-naphthol pigment lake	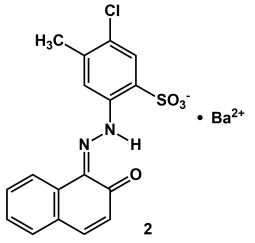

Note. PR: Pigment Red, [a] Classification of organic pigments based on the chemical structure as presented in [2]. [b] Colorants based on 1-arylhydrazone-2-naphthol skeleton, such as β-naphthol pigments, undergo a tautomeric rearrangement between hydrazone/keto and azo/enol forms. Molecular structures of the organic red pigment are depicted in the hydrazone/keto form which is accepted as the major tautomer [2].

Table F.3.: Colorimetric coordinates of HDPE, LDPE, lid 1 and lid 2 at each irradiation time. Total color difference ΔE^*_{ab} (CIE1976), ΔE_{00}(CIEDE2000) between 0h and 770h are reported.

	HDPE			LDPE			Lid 1			Lid 2		
	L*	a*	b*	L*	a*	b*	L*	a*	b*	L*	a*	b*
0h (t_0)	88.17	-0.41	2.04	86.14	-0.01	3.92	41.55	55.61	40.56	46.02	45.99	23.65
±	0.12	0.01	0.02	0.05	0.01	0.02	0.04	0.06	0.07	0.05	0.20	0.08
110h (t_1)	88.57	-0.44	1.28	85.96	0.03	3.53	42.37	47.87	26.59	61.87	22.12	12.04
±	0.06	0.02	0.01	0.01	0.01	0.01	0.03	0.15	0.23	0.05	0.01	0.06
220h (t_2)	89.42	-0.51	1.67	86.60	-0.06	3.40	45.08	45.54	23.89	68.67	11.51	12.92
±	0.51	0.01	0.03	0.07	0.01	0.01	0.02	0.05	0.06	0.29	0.10	0.06
550h (t_3)	90.43	-0.85	7.65	87.69	-1.14	11.20	58.45	30.51	13.74	74.59	5.97	19.97
±	0.80	0.01	0.04	0.25	0.02	0.04	0.09	0.08	0.16	0.24	0.01	0.32
770h (t_4)	90.45	-0.81	12.54	85.44	-0.41	20.07	64.62	25.87	14.74	73.47	6.81	25.67
±	0.08	0.04	0.15	0.16	0.01	0.04	0.06	0.05	0.14	0.28	0.04	0.97
$\boldsymbol{\Delta E^*_{ab}}$			**10.75**			**16.17**			**45.64**			**47.88**
$\boldsymbol{\Delta E_{00}}$			**8.04**			**10.50**			**25.74**			**33.94**

Table F.4.: List of pyrolysis products from the pigment powders PR 48:2 and PR 52:1 before (0h) and after aging (770h). Characteristic ions in mass spectra: molecular weight (M_w) bold, base peak underlined.

t_R / min	Compound	*m/z*	PR48 (0h)	PR48 (770h)	PR53 (0h)	PR53 (770h)
1.56	CO_2	28, **44**	x	x	x	x
1.60	Sulfur dioxide	32, 48, **64**	x	x	x	x
2.73	Benzene	39, 51, **78**	x	x	x	x
5.27	Styrene	51, 78, **104**	x	x	x	x
5.99	Toluene, o-chloro	39, 63, 91, **126**	x	x	x	x
6.24	Phenol	39, 66, **94**		x		x
6.25	Aniline	39, 66, **93**	x		x	
6.32	Benzonitrile	50, 76, **103**	x	x	x	x
7.05	Indene	39, 63, 89, 115, **116**	x	x	x	x
7.26	m-tolunitrile	39, 63, 90, **117**	x	x		
7.27	m-cresol	51, 77, 90, 107, **108**			x	x
7.30	p-toluidine	39, 53, 77, 89, 106, **107**	x	x		
7.36	m-toluidine	39, 53, 77, 89, 106, **107**			x	x
8.46	Quinoline	51, 63, 76, 102, **129**	x	x	x	x
8.51	Naphthalene	51, 63, 102, **128**	x	x	x	x
8.59	m-Chloroaniline	39, 65, 92, **127**	x	x		
9.09	3-Chloro-4-methylbenzonitrile	39, 63, 89, 116, **151**	x	x		
9.36	Phenol, 3-chloro-4-methyl	39, 51, 77, 107, **142**	x	x		
9.38	Phenol, 4-chloro-3-methyl	39, 51, 77, 107, **142**			x	x
9.49	p-Toluidine, 3-chloro-	51, 77, 106, 140, **141**	x	x		
9.56	m-Toluidine, 4-chloro	51, 77, 106, 140, **141**			x	x
9.67	Phthalic anhydride	50, 76, 104, **148**		x		x
9.95	1H-Indene-1,3(2H)-dione	50, 76, 104, **146**		x		
10.52	Similar to 4-Cyanocinnoline	50, 74, 100, 127, **155**	x	x		
10.90	Phthalimide	50, 76, 104, **147**		x		x
11.29	2,4-di-tert-Butylphenol	57, 163, 191, **206**	x			
11.47	β-Naphthol	89, 115, **144**	x	x	x	x
11.50	Similar to 4-quinoline carboxaldehyde	51, 75, 101, 129, **157**	x	x		
11.69	Unidentified	114, 140, 169	x	x		
11.70	Similar to 2-naphthalenamine	71, 115, **143**			x	x
12.48	Unidentified	114, 154, 183	x	x		
13.26	2-Naphthalenol, 1-amino	51, 77, 103, 130, **159**	x	x	x	x

t_R / min	Compound	*m/z*	PR48 (0h)	PR48 (770h)	PR53 (0h)	PR53 (770h)
15.76	Unidentified	189, 219, 234			x	x
16.16	Unidentified	94, 189, 218	x	x		
17.05	Similar to 2H-phenanthro [9,10-b]pyran	101, 202, **232**			x	x
17.13	Unidentified	202, 232	x	x		
17.19	Unidentified	115, 205, 268			x	x
17.50	Unidentified	189, 202, 218, 233, 268	x	x	x	x
17.72	Unidentified	94, 189, 252	x	x	x	x
17.83	Unidentified	76, 104, 192, 227, 236, 271		x		
17,88	Unidentified	114, 245	x	x	x	x
18.67	Unidentified	122, 244, 266	x	x		
18.75	9-Chloro-5,6-dihydronaphthol [1,2-c]cinnoline	101, 202, 231, **266**			x	x
18.77	8-Chloro-5,6-dihydronaphthol [1,2-c]cinnoline	101, 202, 231, **266**	x	x		
19.59	Unidentified	115, 127, 241, 270			x	x
20.22	Unidentified	121, 243, 278	x	x		
21.20	Unidentified	119, 239, 268			x	x
21.85	Unidentified	200, 231, 330			x	x

Table F.5.: Main volatile organic compounds detected in the red PS lid 3 (molecular weight, M_w, in bold and base peak underlined). Additives are marked in *italic*.

Peak number	Compound	*m/z*
1	Toluene	39, 65, 89, 91, **92**
2	Ethylbenzene	39, 51, 65, 77, 91, **106**
3	Styrene	39, 51, 63, 78, **104**
4	Isopropylbenzene	39, 51, 79, 91, 105, **120**
5	Allylbenzene	39, 51, 65, 78, 91, 103, 117, **118**
6	α-Methylstyrene	39, 51, 78, 91, 103, 117, **118**
7	3-Butene-1,3-diyldibenzene (styrene dimer)	39, 51, 65, 77, 91, 104, 115, 130, 193, **208**
8	*Drometrizol*	*39, 51, 66, 78, 93, 154, 168, 196, **225***
9	*Palmitic acid butyl ester*	*29, 43, 56, 73, 97, 129, 185, 239, 257, **312***
10	*Stearic acid butyl ester*	*29, 43, 56, 73, 97, 129, 185, 241, 267, 285, **340***
11	5-Hexene-1,3,5-triyltribenzene (styrene trimer)	65, 77, 91, 117, 194, 207, **312**
12	Isomers of styrene trimer	65, 77, 91, 129, 207, **312**

References

[1] Angelin EM, França de Sá S, Picollo M, Nevin A, Callapez ME, Melo MJ. The identification of synthetic organic red pigments in historical plastics: developing an in situ analytical protocol based on Raman microscopy. J Raman Spectrosc. 2021; 52: 145-158. DOI: 10.1002/jrs.5985.

[2] Hunger K, Schmidt MU. Industrial organic pigments: production, crystal structures, properties, applications. Weinheim: Wiley-VCH, fourth completely revised ed.; 2018.